DYNAMIC BEHAVIOUR OF GEOGRID REINFORCED SEGMENTAL BLOCK WALLS UNDER EARTHQUAKE LOADS

by

Ercüment Başbuğ

B.S. in Civil Engineering, İstanbul Technical University, 2003

M.S. in Civil Engineering, Boğaziçi University, 2005

M.S. in Acoustical Engineering, Denmark Technical University, 2006

Submitted to the Institute for Graduate Studies in
Science and Engineering in partial fulfillment of
the requirements for the degree of
Doctor of Philosophy

Graduate Program in Civil Engineering

Boğaziçi University

2011

To my wonderful parents,

Hale Başbuğ

Mehmet Bülent Başbuğ

And to my beloved brother,

Levent Başbuğ

ACKNOWLEDGEMENTS

This study has been, without a doubt, the hardest and at the same time the most meaningful challenge I have ever encountered in my professional life. Due to the nature of the PhD. study, it took several years to get to the level of completing this thesis. By that time, I have found myself surrounded by success and failure, harmony and disorder, happiness and sadness, hopefulness and desperateness, eagerness and anxiousness, wisdom and foolishness, love and hate, the best of times and the worst of times,briefly, by life itself. At the very end, when I look back, I feel no regrets and although a bit cliché but I must say (like Frank Sinatra song) “I did it my way”. Of course it is not I and myself only but a great number of people have contributed in different ways to my PhD. study and I owe my deepest gratitude to all of them, including those whose names are not mentioned here.

In the first place, it is my pleasure to extend my genuine gratitude to Prof. ErolGüler for his supervision, advice and guidance from the very early stage of my PhD. studies as well as giving me extraordinary experiences throughout the work. Above all and the most needed, he provided me unflinching encouragement and support in various ways. I am grateful to him for being my thesis advisor. It has been a privilege to work with a scientist and engineer like him. Once he told me “once an engineer, always an engineer!” I will always bear his advice on mind and cling onto his teachings and wisdom throughout my life.

Assoc. Prof. İsmail HakkıAksoy has made available his support in a number of ways starting from the very first years of my university studies. I have learnt so much from his teachings and advices. His contribution on my studies is beyond words and I am indebted to him more than he knows. Many heartfelt thanks to him.

I gratefully acknowledge Prof. Gökhan Baykal, for his teachings and help during my studies. He has triggered me to look into and analyze problems in different perspectives that I will benefit from for a long time to come. I feel lucky to be one of his students.

I am very grateful to Assoc. Prof. Ayşe Baykal for giving me the opportunity to work in the shaking table laboratory in Kandilli. Although it was not easy to make the arrangements,she made it possible. Also, she provided me such a pleasant working atmosphere. Many thanks for her efforts.

I would like to thank Mr. Ümit Özdemir for giving me an opportunity to work as an engineer in Tekfen Inc. Co. during my studies. I have learnt so much and gained a unique experience in the private sector by his help.

Many heartfelt thanks go in particular to (my big brother) Oktay Abi and Ahmet Abi in Kandilli Earthquake Research Laboratory. Both have helped me so much in this study. Without their incredible effort, I would not have accomplished this thesis. I will never forget their contribution.

I would like to thank all my friends who helped and supported me during my PhD. studies. Especially, my friends from Boğaziçi University Terzaghi Soil Mechanics Laboratory Öznur Selek, Elif Çiçek, Mustafa Koç, Hakkı Özhan and Arshiya Abadkon. They have helped me so much during the creation and writing part of this study. Many thanks to them. Of course, I owe my deepest gratitude to Anano Korkia, Tuğçe Önal who helped me more than they think of. I also would like to acknowledge Başak Doğan for her huge contribution on this study. Many heartfelt thanks to her.

And finally I would like to thank my parents Hale Başbuğ and Mehmet Bülent Başbuğ. From the very early days when I started writing this thesis I have been thinking how to thank them perfectly in the acknowledgements part of this thesis. However, it is not possible to find enough words for their support, encouragement and love that they gave me during my life. They provided me the best working environment and gave me the power to finish this thesis. They were the ones who made me believe that the soothing light at the end of tunnel was not the freight train coming on my way but the daylight instead. But most importantly, throughout my life they have made me feel special and loved. Mom and Dad, I thank you from the very bottom of my heart. It is an honor for me to dedicate this thesis to my wonderful parents Hale Başbuğ and Mehmet Bülent Başbuğ and to my beloved brother Levent Başbuğ.

ABSTRACT

DYNAMIC BEHAVIOUR OF GEOGRID REINFORCED SEGMENTAL BLOCK WALLS UNDER EARTHQUAKE LOADS

This study investigates the seismic performance of geogrid reinforced segmental block walls. For this purpose, shaking table tests were performed on four ½ reduced-scale geogrid reinforced segmental block walls at Bogazici University Kandilli Observatory and Earthquake Research Institute. The walls were instrumented by installing 9 accelerometers to measure the accelerations within the soil and facing blocks, 6 linear laser displacement sensors to measure the displacement of facing blocks. Additionally, the strain gages were installed on the three geogrid reinforcement layers to measure the reinforcement strains. The heights of the models were 1.9 m and each wall was excited with El Centro, Izmit and Sakarya earthquake motions. The effect of increasing horizontal base acceleration, reinforcement length and stiffness, backfill material type, facing batter (inclination) on measured parameters under seismic excitation are analyzed and presented.

The experimental work in this study helps to develop a better understanding of the tensile stress-strains generated in geogrid reinforcement and facing displacements of geogrid reinforced soil walls during construction and extreme seismic excitations. Additionally, whether the experimental results are in accordance with the current NCMA and FHWA design methodologies for reinforced soil retaining walls are investigated and conclusions are drawn. The results obtained from experiments, permanent displacements and geogrid reinforcement tensile loads obtained from experiments are compared with Newmark's displacement method and NCMA and FHWA design methodologies respectively.

The geogrid reinforced segmental block walls designed according to current specifications showed a very good resistance to earthquake loading conditions. They remained stable even under extreme lateral accelerations (peak lateral acceleration values

up to 0.97 g). All four wall configurations designed in this study showed very successful behavior. No stability problem occurred even under extreme lateral accelerations. The Geogrid Reinforced Segmental Block Walls showed minimal residual deformations and acceptable maximum deformations under extreme lateral earthquake accelerations.

ÖZET

GEOGRİD DONATILI İSTİNAT DUVARLARININ DEPREM YÜKLERİ ALTINDA DİNAMİK DAVRANIŞI

Bu çalışma geogrid donatılı istinat duvarlarının sismik performansını araştırmaktadır. Bu amaçla, Boğaziçi Üniversitesi Kandilli Rasathanesi ve Deprem Araştırması Enstitüsü'nde bulunan sarsma tablasında dört farklı ½ ölçekli geogrid donatılı istinat duvar modeli test edilmiştir. Her bir duvara zeminde ve cephe bloğundaki ivmeleri ölçebilmesi için 9 adet akselerometre ve cephe elemanlarındaki deplasmanları ölçebilmesi için ise 6 adet lazer deplasman sensörleriyerleştirilmiştir. Ayrıca geogrid donatılar üzerindeki çekme gerilmelerini ölçebilmek için üç adet donatı tabakasına gerinim pulları yerleştirilmiştir. Hazırlanan model duvarların yüksekliği 1.9 m.'dir ve her bir duvar El Centro, Izmit ve Sakarya deprem hareketleri ile sarsılmıştır. Artan yatay ivme, donatı uzunluğu ve rijitliği, dolgu malzemesi tipi ve duvar eğiminin ölçülen parametreler üzerine etkisi analiz edilmiş ve sunulmuştur.

Bu çalışmadaki deneysel çalışma inşaat sırasında ve aşırı sismik durumlarda geogrid donatılarda ortaya çıkan gerilmelerve cephe deplasmanları hakkında daha iyi bir yaklaşım sağlamaktadır. Ek olarak, deney sonuçlarının geogrid donatılı istinat duvarları için mevcut NCMA ve FHWA tasarım metodolojileri ile uygun olup olmadığı araştırılmışve sonuçlar ortaya konulmuştur. Deneylerden elde edilen kalıcı deformasyonlar ve donatı çekme gerilmeleri Newmark yerdeğiştirme metodu ve NCMA ve FHWA tasarım şartnameleri ile karşılaştırılmıştır.

Mevcut tasarım şartnamelerine uygun olarak tasarlananGeogrid donatılı istinat duvarları deprem yüklerine karşı çok iyi direnç göstermektedir.Duvarlar uygulanan aşırı yatay ivmelere (örnek olarak pik yatay ivmeler 0.97 g'ye kadar çıkmıştır) karşın stabil kalmayı başarmıştır. Bu çalışmada tasarlanmış dört duvar da sismik kuvvetler altında oldukça iyi performans göstermiştir. Yüksek yatay ivmeler uygulandığında bile duvarlarda

herhangi bir stabilite problemi oluşmamıştır. Geogrid donatılı duvarlarda aşırı deprem yükleri altında minimum kalıcı deformasyon ve kabul edilebilir maksimum deformasyon oluşmuştur.

TABLE OF CONTENTS

ACKNOWLEDGEMENTS iv
ABSTRACT vi
ÖZET viii
LIST OF FIGURES xv
LIST OF TABLES xxxv
LIST OF SYMBOLS xlvi
LIST OF ACRONYMS/ABBREVIATIONS xlviii
1. INTRODUCTION 1
2. SCOPE OF WORK, OBJECTIVES AND THESIS ORGANIZATION 3
2.1. Scope of Work and Objectives 3
2.2. Research Overview and Thesis Organization 4
3. GENERAL INFORMATION ABOUT GEOGRID-REINFORCED STRUCTURES AND SIMILAR STUDIES IN LITERATURE 6
3.1. Background and Description 6
3.1.1. Types of Geosynthetic Reinforced Soil Walls 10
3.1.2. Geogrid Reinforced Walls 11
3.1.3. Reinforcing Mechanisms 13
3.1.4. Performance of GRS-RWs 17
3.2. Design of GRS-RWs 20
3.2.1. Earth Pressure Concept 21
3.2.1.1. Static Lateral Earth Pressures 22
3.2.1.2. Seismic Earth Pressures 26
3.2.2. Seismic Design of Segmental Retaining Walls 30
3.2.2.1. Assumptions for the Seismic Design 30
3.2.2.2. Modes of Failure of GRS-RWs 31
3.2.2.3. Internal Stability 33
3.2.2.4. External Stability 36
3.2.2.5. Seismic Stability 37
3.2.2.6. Facing Stability 38
3.2.3. Retained Soil 38

3.2.4. Facing Design 41
3.3. Physical Model Tests Of GRS-RWs In Literature 43
3.3.1. Dynamic Centrifuge Tests 44
3.3.2. Shaking Table Tests On GRS-RWs 46
3.3.3. Seismic Analysis of GRS-RWs Using Finite Element Methods 50
4. METHODOLOGY 52
4.1. Introduction 52
4.2. Scaling Of The Model Walls 52
4.3.1. Shaking Table 53
4.3.2. Materials Used in the Tests 56
4.3.2.1. Steel Container Soil Box 56
4.3.2.2. Glass Covered Steel Frame 57
4.3.2.3. Rubber Sheets 58
4.3.2.4. Backfill-Sand 59
4.3.2.5. Backfill-Gravel 62
4.3.2.6. Granular Rubber Fill 64
4.3.2.7. Reinforcement Material- Geogrid 65
4.3.2.8. Facing Panels-Concrete Modular Blocks 66
4.3.2.9. Compactor 67
4.3.3. Instrumentation 68
4.3.3.1. Laser Sensors 70
4.3.3.2. Strain Gages 71
4.3.3.3. Accelerometers 72
4.3.4. Data Acquisition (DAQ) Systems 74
4.3.4.1. National Instruments' PCI-6229 M Data Acquisition System for Accelerometers and Laser Sensors 75
4.3.4.2. TDG Ai8b Data Acquisition System for Strain Gages 75
4.3.5. Construction Method of Walls 76
4.4. Wall Configurations and Reinforcement Layout 83
4.5. Dynamic Base Excitations and Shaking Sequence of Model Walls 87
4.6. Test Program 89
5. TEST RESULTS AND EVALUATION 90
5.1. General 90

5.2. Background and Description 90
5.2.1. Data Evaluation Method for Displacement Laser Sensors and Accelerometers..... 90
5.2.2. Data Evaluation Method for Strain Gages 93
5.3. Fundamental Frequency of the Wall..... 95
5.4. Acceleration Amplification 98
5.4.1. Test Results..... 98
5.4.2. Evaluation of the Results 119
5.4.2.1. Influence of Wall Inclination on Acceleration Amplification..... 120
5.4.2.2. Influence of Backfill Material on Acceleration Amplification 120
5.4.2.3. Influence of Reinforcement Type and Length on Acceleration Amplification..... 121
5.5. Horizontal Displacements of Wall Facing 122
5.5.1. Test Results..... 122
5.5.2. Evaluation..... 133
5.5.2.1. Influence of Wall Inclination on Horizontal Displacements of Wall Facings 134
5.5.2.2. Influence of Backfill Material on Horizontal Displacements of Wall Facings 134
5.5.2.3. Influence of Reinforcement Type and Length on Horizontal Displacements of Wall Facings..... 135
5.6. Verification of Strain Gages..... 135
5.6.1. Testing Procedure..... 135
5.6.2. Test Results..... 137
5.7. Strain Distrubution in Geogrid Reinforcements during and at the end of Construction of Wall 138
5.7.1. Test results 138
5.7.2. Evaluation of the Results 142
5.8. Strains and Tensile Loads Generated in Geogrid Layers 144
5.8.1. Test results of Strain Gage Readings 145
5.8.2. Evaluation of the Strain Gage Measurements 162

5.8.2.1. Influence of Wall Inclination on Strains generated on Reinforcement Layers 162
5.8.2.2. Influence of Backfill Material on Strains generated on Reinforcement Layers 163
5.8.2.3. Influence of Reinforcement Type on Strains generated on Reinforcement Layers 164
5.8.3. Tensile Loads in Geogrid Layers 164
5.8.4. Evaluation of Tensile Loads on Reinforcements 174
5.9. Observations 175
6. CALCULATION METHODS FOR PERMENANT DISPLACEMENTS AND GEOGRID REINFORCEMENT DESIGN TENSILE LOADS 179
6.1. Newmark's Displacement Method 179
6.1.1. Material Properties 179
6.1.2. Determination of Critical Accelerations 181
6.1.3. Calculation of Permenant Displacements 182
6.1.4. Seismic Data 184
6.1.5. The Results of the Analysis 185
6.1.6. Comparison of Measured and Calculated Total Wall Displacements 186
6.2. Comparison Of Measured And Design Tensile Loads On Geogrids During Earthquake 190
6.2.1. Design of GRS-RWs Considering Seismic Effects as Pseudo-Static Loading 190
6.2.1.1. FHWA Recommendation of Pseudostatic Loading in Extenal Stability Calculations 191
6.2.1.2. FHWA Recommendation of Pseudostatic Loading in Internal Stability Calculations 193
6.2.2. The Comparison Of Measured And Design Tensile Loads On Geogrid Reinforcement During The Earthquake Motion Applied On Model Walls 195
7. GENERAL CONCLUSIONS 202
APPENDIX A: ACCELERATION-TIME HISTORY GRAPHS OBTAINED FROM THE TESTS 206

APPENDIX B: FACE DISPLACEMENT-TIME HISTORY GRAPHS OBTAINED FROM THE TESTS 288
APPENDIX C: STRAIN-TIME HISTORY GRAPHS OBTAINED FROM THE TESTS. 329
APPENDIX D: EXCEL CALCULATION SHEETS FOR DETERMINING THE CRITICAL ACCELERATIONS AND WALL DISPLACEMENTS 370
APPENDIX E: EXCEL CALCULATION SHEETS FOR COMPARISON OF MEASURED STRESSES IN GEOGRID WITH STRESSES USED IN DESIGN METHODOLOGIES 380
REFERENCES 422

LIST OF FIGURES

Figure 3.1. Example of Retaining Wall Systems 7

Figure 3.2. Principal Elements of a GRS-RW 8

Figure 3.3. Geogrid reinforcement together with facing blocks. 12

Figure 3.4. A view of Geogrid-Reinforced Segmental Retaining Wall 12

Figure 3.5. Construction process of a Geogrid-Reinforced Soil Structure. 13

Figure 3.6. Reinforcing Mechanism of Reinforced Soil Retaining Structures. 14

Figure 3.7. Principal Stress Conditions of Reinforced Soil 15

Figure 3.8. Tensile forces in the reinforcements 17

Figure 3.9. Various Lateral Earth Pressure Distribution 23

Figure 3.10. Rankine Active earth pressure 24

Figure 3.11. Earth pressure acting on the wall-Coulomb Approach 25

Figure 3.12. Forces and geometry used in pseudo-static seismic analysis. 27

Figure 3.13. The acting locations of the static active and incremental dynamic active earth pressure forces 28

Figure 3.14. Modes of failure for reinforced SRW structures 32

Figure 3.15. Geometry & Forces Used to Calculate Reinforcement Loads for Reinforced SRW Structures 34

Figure 3.16. Reinforcement tensile load calculation using Bathurst and Cai method .. 34

Figure 3.17. Two-part wedge analysis: (a) free-body diagram (b) with reinforcement forces 35

Figure 3.18. Log-spiral analysis: (a)free-body diagram (b)with reinforcement forces . 35

Figure 3.19. External Stability Calculation Variable for GRS-RWs 36

Figure 3.20. Typical Examples of Measured lateral Earth Pressures and Tensions in ties just prior to wall failure 39

Figure 3.21. Effect of reinforcement stiffness on tension in reinforcement..... 40

Figure 3.22. Sources of horizontal deformations in reinforced soil..... 41

Figure 3.23. Facing Types of a reinforced soil wall..... 42

Figure 3.24. Modeling of Centrifuge 45

Figure 4.1. The achievable motion and 5 per cent Response Spectrum with payload of 10 tons 54

Figure 4.2. A view of shaking table at the Shaking Table Laboratory of Kandilli Observatory 55

Figure 4.3. A view from the Control Room 55

Figure 4.4. Steel container and glass-covered frame on the shaking table..... 56

Figure 4.5. Steel container soil box 57

Figure 4.6. Dimensions of Glass Covered Steel Frame 57

Figure 4.7. The glass covered steel frame attached to the steel container box..... 58

Figure 4.8. Rubber sheets are installed at the side walls of the soil box 59

Figure 4.9. Grain Size Distribution Curve for Sand..... 60

Figure 4.10. Direct Shear Results obtained from sand..... 60

Figure 4.11. Proctor Compaction Test Results..... 61

Figure 4.12. Grain Size Distribution Curve for Gravel 63

Figure 4.13. Correlation chart of relative density and internal friction angle 63

Figure 4.14. Granular rubber fill 64

Figure 4.15. The Polypropylene Geogrid 20/20 used in experiments 65

Figure 4.16. The dimensions of the blocks used in the study..... 66

Figure 4.17. Sand filled concrete modular blocks used in this study..... 67

Figure 4.18. Dynapac LF82 type of compactor employed in compaction..... 68

Figure 4.19. Location of Laser displacement transducers on steel frame 68

Figure 4.20. Typical Section of an Instrumented Wall..... 69

Figure 4.21. Front view of the locations of Accelerometers and Laser Displacement Transducers on the Wall..... 69

Figure 4.22. Top view of the Wall 70

Figure 4.23. A view of the laser sensors mounted inside the glass-covered frame 70

Figure 4.24. TML GFLA-6-50 Strain gages installed on geogrids 71

Figure 4.25. The location of strain gages on geogrid 72

Figure 4.26. Accelerometers mounted on facing 73

Figure 4.27. 3 Accelerometers embedded in on top of fill 73

Figure 4.28. National Instruments' PCI-6229 M DAQ System and Control Room ... 74

Figure 4.29. TDG Ai8b Data Acquisition System boxes used in the experiments 75

Figure 4.30. A view of the TDG Ai8b Data Acquisition System together with strain gage cables attached..... 75

Figure 4.31. The steel container soil box on shaking table 76

Figure 4.32. A view of bolted connection of steel container to the shaking table 77

Figure 4.33. The rubber sheets installed and compaction 78

Figure 4.34. Installation of geogrids with frictional connection to the facing blocks.. 79

Figure 4.35. Details of block and geogrid interface..... 79

Figure 4.36. Strain gage cables inside polymer pipes passing through previously drilled holes of the blocks 80

Figure 4.37. The top view of grouted and steel bar installed block 81

Figure 4.38. The constructed Geogrid Reinforced Wall 82

Figure 4.39. The glass covered steel frame while being attached to the steel container. 82

Figure 4.40. The steel container with glass covered steel frame on shaking table before shaking 83

Figure 4.41. Reinforcement Layout and instrumentation of the Wall 1 and Wall 2 ... 85

Figure 4.42. Reinforcement Layout and instrumentation of the Wall 3 and Wall 4 ... 86

Figure 4.43. Scaled original record of the El Centro earthquake and Response spectrum 88

Figure 4.44. Scaled original record of the Izmit earthquake and Response spectrum.. 88

Figure 5.1. Noise Influenced Accelerometer Data 91

Figure 5.2. 0.1 to 20 Hz. Bandpass Filtered Accelerometer Data 91

Figure 5.3. Noise Influenced Displacement Data..... 92

Figure 5.4. 0.1 to 20 Hz. Bandpass Filtered Displacement Data 92

Figure 5.5. The displacement-time history data where permanent facing displacement observed 93

Figure 5.6. Tensile force dominant strain gage data..... 94

Figure 5.7. Compressional force dominant strain gage data 94

Figure 5.8. Acceleration-time history data of Wall 3- El Centro 100% excitation together with the Fourier Amplitude Spectra..... 95

Figure 5.9. Peak Accelerations at base and wall facing for Wall 1 for all Dynamic Excitations 111

Figure 5.10. Peak Accelerations on top of backfill for Wall 1 for all Dynamic Excitations 112

Figure 5.11. Peak Accelerations at base and wall facing for Wall 2 for all Dynamic Excitations 113

Figure 5.12. Peak Accelerations on top of backfill for Wall 2 for all Dynamic Excitations 114

Figure 5.13. Peak Accelerations at base and wall facing for Wall 3 for all Dynamic Excitations 115

Figure 5.14. Peak Accelerations on top of backfill for Wall 3 for all Dynamic Excitations 116

Figure 5.15. Peak Accelerations at base and wall facing for Wall 4 for all Dynamic Excitations 117

Figure 5.16. Peak Accelerations on top of backfill for Wall 4 for all Dynamic Excitations 118

Figure 5.17. Peak Displacements at the wall facing for Wall 1 in base excitations a) El Centro Earthquake, b)Izmit Earthquake, c)Sakarya Earthquake Motions 125

Figure 5.18. Peak Displacements at the wall facing for Wall 2 in base excitations a) El Centro Earthquake, b)Izmit Earthquake, c)Sakarya Earthquake Motions 126

Figure 5.19. Peak Displacements at the wall facing for Wall 3 in base excitations a) El Centro Earthquake, b)Izmit Earthquake, c)Sakarya Earthquake Motions 127

Figure 5.20. Peak Displacements at the wall facing for Wall 4 in base excitations a) El Centro Earthquake, b)Izmit Earthquake, c)Sakarya Earthquake Motions 128

Figure 5.21 Horizontal Residual Facing Displacement on Top Modular block (@h=1.9m) as a function of Maximum Input Base Acceleration Amplitude for El-Centro Earthquake Motion 131

Figure 5.22. Horizontal Facing Displacement on Top Modular block as a function of Maximum Input Base Acceleration Amplitude for El-Centro Earthquake Motion 131

Figure 5.23. Horizontal Facing Displacement on Top Modular block as a function of Maximum Input Base Acceleration Amplitude for Izmit Earthquake Motion 132

Figure 5.24. Horizontal Facing Displacement on Top Modular block as a function of Maximum Input Base Acceleration Amplitude for Sakarya Earthquake Motion 132

Figure 5.25. View of the calibration tensile testing experimental set up 135

Figure 5.26. Test Apparatus 136

Figure 5.27. Strain-Time History graph for three strain gages installed on geogrid for verification 137

Figure 5.28. The strains generated at the midheight instrumented geogrid layer during construction of Wall 3 138

Figure 5.29. The strains generated at the bottom instrumented geogrid layer during construction of Wall 3 139

Figure 5.30. The strains generated at the midheight instrumented geogrid layer during construction of Wall 4 140

Figure 5.31. The strains generated at the bottom instrumented geogrid layer during construction of Wall 4 140

Figure 5.32. End of Construction Max. Tensile Strains at a) midheight b) bottom geogrid reinforcement for Wall 3 (aggregate backfill) 141

Figure 5.33. End of Construction Max. Tensile Strains at a) midheight b) bottom geogrid reinforcement for Wall 4 (sand backfill) 141

Figure 5.34. Post Construction Tensile Stresses on instrumented Geogrid layers together with failure surfaces for Wall 3 143

Figure 5.35. Post Construction Tensile Stresses on instrumented Geogrid layers together with failure surfaces for Wall 4 144

Figure 5.36. Max. Tensile Strains at top, mid-height and bottom Geogrid Layers with increasing base acceleration - Wall 1- El Centro Earthquake Motion... 150

Figure 5.37. Max. Tensile Strains at top, mid-height and bottom Geogrid Layers with increasing base acceleration - Wall 1- Izmit Earthquake Motion 151

Figure 5.38. Max. Tensile Strains at top, mid-height and bottom Geogrid Layers with increasing base acceleration - Wall 1- Sakarya Earthquake Motion 152

Figure 5.39. Max. Tensile Strains at top, mid-height and bottom Geogrid Layers with increasing base acceleration - Wall 2- El Centro Earthquake Motion... 153

Figure 5.40. Max. Tensile Strains at top, mid-height and bottom Geogrid Layers with increasing base acceleration - Wall 2- Izmit Earthquake Motion 154

Figure 5.41. Max. Tensile Strains top, mid-height and bottom Geogrid Layers with increasing base acceleration - Wall 2- Sakarya Earthquake Motion 155

Figure 5.42. Max. Tensile Strains at top, mid-height and bottom Geogrid Layers with increasing base acceleration - Wall 3- El Centro Earthquake Motion... 156

Figure 5.43. Max. Tensile Strains at top, mid-height and bottom Geogrid Layers with increasing base acceleration - Wall 3- Izmit Earthquake Motion 157

Figure 5.44. Max. Tensile Strains at top, mid-height and bottom Geogrid Layers with increasing base acceleration - Wall 3- Sakarya Earthquake Motion 158

Figure 5.45. Max. Tensile Strains at top, mid-height and bottom Geogrid Layers with increasing base acceleration - Wall 4- El Centro Earthquake Motion... 159

Figure 5.46. Max. Tensile Strains at top, mid-height and bottom Geogrid Layers with increasing base acceleration - Wall 4- Izmit Earthquake Motion 160

Figure 5.47. Max. Tensile Strains at bottom, mid-height and top Geogrid Layer with increasing base acceleration - Wall 4- Sakarya Earthquake Motion 161

Figure 5.48. Location of peak reinforcement tensile loads and internal failure surface a) El Centro, b) Izmit, c) Sakarya Earthquake motions for Wall 1 170

Figure 5.49. Location of peak reinforcement tensile loads and internal failure surface a) El Centro, b) Izmit, c) Sakarya Earthquake motions for Wall 2 171

Figure 5.50. Location of peak reinforcement tensile loads and internal failure surface a) El Centro, b) Izmit, c) Sakarya Earthquake motions for Wall 3 172

Figure 5.51. Location of peak reinforcement tensile loads and internal failure surface a) El Centro, b) Izmit, c) Sakarya Earthquake motions for Wall 4 173

Figure 5.52. A view from the top of the backfill of Unreinforced zone of Wall 4 prior to shaking 175

Figure 5.53. A view from the top of the backfill of unreinforced zone of Wall 4 after successive shaking 175

Figure 5.54. A view from the top of the backfill of reinforced zone behind the blocks of Wall 4 prior to shakings 176

Figure 5.55. A view from the top of the backfill of reinforced zone behind the blocks of Wall 4 after shakings 176

Figure 5.56. Tensile cracks observed in sand backfill 177

Figure 5.57. Overhanging of Geogrid after shakings 178

Figure 6.1. Calculation of permanent displacements (unidirectional displacement) using Newmark's method 180

Figure 6.2. The non-dimensionalized displacement in terms of d/(vm2/kmg) versus critical acceleration ratio of the displacement methods 181

Figure 6.3. Seismic Data of the El Centro 100% Earthquake 182

Figure 6.4. Seismic Data of the El Centro 150% Earthquake 183

Figure 6.5. Seismic Data of the El Centro 200% Earthquake 183

Figure 6.6. Seismic Data of the El Centro 250% Earthquake 183

Figure 6.7. Seismic Data of the El Centro 275% Earthquake 184

Figure 6.8. Forces considered in seismic external stability calculations: (a) for level backfill (b) for sloping backfill 192

Figure 6.9. Reinforcement tensile load calculation using FHWA method..... 195

Figure 6.10. Comparison Of Measured And Design Tensile Loads On a) top, b)midheight, c)lower Geogrid Reinforcement for Wall 1 196

Figure 6.11. Comparison Of Measured And Design Tensile Loads On a) top, b)midheight, c)lower Geogrid Reinforcement for Wall 2 197

Figure 6.12. Comparison Of Measured And Design Tensile Loads On a) top, b)midheight, c)lower Geogrid Reinforcement for Wall 3 199

Figure 6.13. Comparison Of Measured And Design Tensile Loads On a) top, b)midheight, c)lower Geogrid Reinforcement for Wall 4 200

Figure A.1. Accelerations Measured for Wall Configuration 1- El Centro 100% ... 206

Figure A.2. Accelerations Measured for Wall Configuration 1- El Centro 150% ... 208

Figure A.3. Accelerations Measured for Wall Configuration 1- El Centro 200% ... 210

Figure A.4. Accelerations Measured for Wall Configuration 1- Izmit 100%..... 212

Figure A.5. Accelerations Measured for Wall Configuration 1- Izmit 150%..... 214

Figure A.6. Accelerations Measured for Wall Configuration 1- Izmit 200%..... 216

Figure A.7. Accelerations Measured for Wall Configuration 1- Sakarya 100%..... 218

Figure A.8. Accelerations Measured for Wall Configuration 1- Sakarya 150%..... 220

Figure A.9. Accelerations Measured for Wall Configuration 1- Sakarya 200%..... 222

Figure A.10. Accelerations Measured for Wall Configuration 2- El Centro 100% ... 224

Figure A.11. Accelerations Measured for Wall Configuration 2- El Centro 150% ... 226

Figure A.12. Accelerations Measured for Wall Configuration 2- El Centro 200% ... 228

Figure A.13. Accelerations Measured for Wall Configuration 2- Izmit 100%..... 230

Figure A.14. Accelerations Measured for Wall Configuration 2- Izmit 150%..... 232

Figure A.15. Accelerations Measured for Wall Configuration 2- Izmit 200%..... 234

Figure A.16. Accelerations Measured for Wall Configuration 2- Sakarya 100%..... 236

Figure A.17. Accelerations Measured for Wall Configuration 2- Sakarya 150%..... 238

Figure A.18. Accelerations Measured for Wall Configuration 2- Sakarya 200%..... 240

Figure A.19. Accelerations Measured for Wall Configuration 3- El Centro 100% ... 242

Figure A.20. Accelerations Measured for Wall Configuration 3- El Centro 150% ... 244

Figure A.21. Accelerations Measured for Wall Configuration 3- El Centro 200% ... 246

Figure A.22. Accelerations Measured for Wall Configuration 3- El Centro 250% ... 248

Figure A.23. Accelerations Measured for Wall Configuration 3- Izmit 100%..... 250

Figure A.24. Accelerations Measured for Wall Configuration 3- Izmit 150%..... 252

Figure A.25. Accelerations Measured for Wall Configuration 3- Izmit 200%..... 254

Figure A.26. Accelerations Measured for Wall Configuration 3- Izmit 250%..... 256

Figure A.27. Accelerations Measured for Wall Configuration 3- Sakarya 100%..... 258

Figure A.28. Accelerations Measured for Wall Configuration 3- Sakarya 150%..... 260

Figure A.29. Accelerations Measured for Wall Configuration 3- Sakarya 200%..... 262

Figure A.30. Accelerations Measured for Wall Configuration 3- Sakarya 250%..... 264

Figure A.31. Accelerations Measured for Wall Configuration 4- El Centro 100% ... 266

Figure A.32. Accelerations Measured for Wall Configuration 4- El Centro 150% ... 268

Figure A.33. Accelerations Measured for Wall Configuration 4- El Centro 200% ... 270

Figure A.34. Accelerations Measured for Wall Configuration 4- El Centro 250% ... 272

Figure A.35. Accelerations Measured for Wall Configuration 4- El Centro 275% ... 274

Figure A.36. Accelerations Measured for Wall Configuration 4- Izmit 100%..... 276

Figure A.37. Accelerations Measured for Wall Configuration 4- Izmit 150%..... 278

Figure A.38. Accelerations Measured for Wall Configuration 4- Izmit 200%..... 280

Figure A.39. Accelerations Measured for Wall Configuration 4- Sakarya 100%..... 282

Figure A.40. Accelerations Measured for Wall Configuration 4- Sakarya 150%..... 284

Figure A.41. Accelerations Measured for Wall Configuration 4- Sakarya 200%..... 286

Figure B.1. Facing Displacements Measured for Wall Configuration 1- ElCentro 100% 288

Figure B.2. Facing Displacements Measured for Wall Configuration 1- El Centro 150% 289

Figure B.3. Facing Displacements Measured for Wall Configuration 1- ElCentro 200% 290

Figure B.4. Facing Displacements Measured for Wall Configuration 1- Izmit 100% 291

Figure B.5. Facing Displacements Measured for Wall Configuration 1- Izmit 150% 292

Figure B.6. Facing Displacements Measured for Wall Configuration 1- Izmit 200% 293

Figure B.7. Facing Displacements Measured for Wall Configuration 1- Sakarya 100% 294

Figure B.8. Facing Displacements Measured for Wall Configuration 1- Sakarya 150% 295

Figure B.9. Facing Displacements Measured for Wall Configuration 1- Sakarya 200% 296

Figure B.10. Facing Displacements Measured for Wall Configuration 2- El Centro 100% 297

Figure B.11. Facing Displacements Measured for Wall Configuration 2- El Centro 150% 298

Figure B.12. Facing Displacements Measured for Wall Configuration 2- El Centro 200% 299

Figure B.13. Facing Displacements Measured for Wall Configuration 2- Izmit 100% 300

Figure B.14. Facing Displacements Measured for Wall Configuration 2- Izmit 150% 301

Figure B.15. Facing Displacements Measured for Wall Configuration 2- Izmit 200% 302

Figure B.16. Facing Displacements Measured for Wall Configuration 2- Sakarya 100% 303

Figure B.17. Facing Displacements Measured for Wall Configuration 2- Sakarya 150% 304

Figure B.18. Facing Displacements Measured for Wall Configuration 2- Sakarya 200% 305

Figure B.19. Facing Displacements Measured for Wall Configuration 3- El Centro 100% 306

Figure B.20. Facing Displacements Measured for Wall Configuration 3- El Centro 150% 307

Figure B.21. Facing Displacements Measured for Wall Configuration 3- El Centro 200% 308

Figure B.22. Facing Displacements Measured for Wall Configuration 3- El Centro 250% 309

Figure B.23. Facing Displacements Measured for Wall Configuration 3- Izmit 100% 310

Figure B.24. Facing Displacements Measured for Wall Configuration 3- Izmit 150% 311

Figure B.25. Facing Displacements Measured for Wall Configuration 3- Izmit 200% 312

Figure B.26. Facing Displacements Measured for Wall Configuration 3- Izmit 250% 313

Figure B.27. Facing Displacements Measured for Wall Configuration 3- Sakarya 100% 314

Figure B.28. Facing Displacements Measured for Wall Configuration 3- Sakarya 150% 315

Figure B.29. Facing Displacements Measured for Wall Configuration 3- Sakarya 200% 316

Figure B.30. Facing Displacements Measured for Wall Configuration 3- Sakarya 250% 317

Figure B.31. Facing Displacements Measured for Wall Configuration 4- El Centro 100% 318

Figure B.32. Facing Displacements Measured for Wall Configuration 4- El Centro 150% 319

Figure B.33. Facing Displacements Measured for Wall Configuration 4- El Centro 200% 320

Figure B.34. Facing Displacements Measured for Wall Configuration 4- El Centro 250% 321

Figure B.35. Facing Displacements Measured for Wall Configuration 4- El Centro 275% 322

Figure B.36. Facing Displacements Measured for Wall Configuration 4- Izmit 100% 323

Figure B.37. Facing Displacements Measured for Wall Configuration 4- Izmit 150% 324

Figure B.38. Facing Displacements Measured for Wall Configuration 4- Izmit 200% 325

Figure B.39. Facing Displacements Measured for Wall Configuration 4- Sakarya 100% 326

Figure B.40. Facing Displacements Measured for Wall Configuration 4- Sakarya 150% 327

Figure B.41. Facing Displacements Measured for Wall Configuration 4- Sakarya 200% 328

Figure C.1. Strains Measured in Top, Midheight and Bottom Geogrids for Wall 1-El Centro 100% 329

Figure C.2. Strains Measured in Top, Midheight and Bottom Geogrids for Wall 1-El Centro 150% 330

Figure C.3. Strains Measured in Top, Midheight and Bottom Geogrids for Wall 1-El Centro 200% 331

Figure C.4. Strains Measured in Top, Midheight and Bottom Geogrids for Wall 1-Izmit 100%..... 332

Figure C.5. Strains Measured in Top, Midheight and Bottom Geogrids for Wall 1-Izmit 150%..... 333

Figure C.6. Strains Measured in Top, Midheight and Bottom Geogrids for Wall 1-Izmit 200%..... 334

Figure C.7. Strains Measured in Top, Midheight and Bottom Geogrids for Wall 1-Sakarya 100%..... 335

Figure C.8. Strains Measured in Top, Midheight and Bottom Geogrids for Wall 1-Sakarya 150%..... 336

Figure C.9. Strains Measured in Top, Midheight and Bottom Geogrids for Wall 1-Sakarya 200%..... 337

Figure C.10. Strains Measured in Top, Midheight and Bottom Geogrids for Wall 2-El Centro 100% 338

Figure C.11. Strains Measured in Top, Midheight and Bottom Geogrids for Wall 2-El Centro 150% 339

Figure C.12. Strains Measured in Top, Midheight and Bottom Geogrids for Wall 2-El Centro 200% 340

Figure C.13. Strains Measured in Top, Midheight and Bottom Geogrids for Wall 2-Izmit 100%..... 341

Figure C.14. Strains Measured in Top, Midheight and Bottom Geogrids for Wall 2-Izmit 150% 342

Figure C.15. Strains Measured in Top, Midheight and Bottom Geogrids for Wall 2-Izmit 200% 343

Figure C.16. Strains Measured in Top, Midheight and Bottom Geogrids for Wall 2-Sakarya 100% 344

Figure C.17. Strains Measured in Top, Midheight and Bottom Geogrids for Wall 2-Sakarya 150% 345

Figure C.18. Strains Measured in Top, Midheight and Bottom Geogrids for Wall 2-Sakarya 200% 346

Figure C.19. Strains Measured in Top, Midheight and Bottom Geogrids for Wall 3-El Centro 100% 347

Figure C.20. Strains Measured in Top, Midheight and Bottom Geogrids for Wall 3-El Centro 150% 348

Figure C.21. Strains Measured in Top, Midheight and Bottom Geogrids for Wall 3-El Centro 200% 349

Figure C.22. Strains Measured in Top, Midheight and Bottom Geogrids for Wall 3-El Centro 250% 350

Figure C.23. Strains Measured in Top, Midheight and Bottom Geogrids for Wall 3-Izmit 100% 351

Figure C.24. Strains Measured in Top, Midheight and Bottom Geogrids for Wall 3-Izmit 150% 352

Figure C.25. Strains Measured in Top, Midheight and Bottom Geogrids for Wall 3-Izmit 200% 353

Figure C.26. Strains Measured in Top, Midheight and Bottom Geogrids for Wall 3-Izmit 250%. 354

Figure C.27. Strains Measured in Top, Midheight and Bottom Geogrids for Wall 3-Sakarya 100%. 355

Figure C.28. Strains Measured in Top, Midheight and Bottom Geogrids for Wall 3-Sakarya 150%. 356

Figure C.29. Strains Measured in Top, Midheight and Bottom Geogrids for Wall 3-Sakarya 200%. 357

Figure C.30. Strains Measured in Top, Midheight and Bottom Geogrids for Wall 3-Sakarya 250%. 358

Figure C.31. Strains Measured in Top, Midheight and Bottom Geogrids for Wall 4-El Centro 100% 359

Figure C.32. Strains Measured in Top, Midheight and Bottom Geogrids for Wall 4-El Centro 150% 360

Figure C.33. Strains Measured in Top, Midheight and Bottom Geogrids for Wall 4-El Centro 200% 361

Figure C.34. Strains Measured in Top, Midheight and Bottom Geogrids for Wall 4-El Centro 250% 362

Figure C.35. Strains Measured in Top, Midheight and Bottom Geogrids for Wall 4- El Centro 275%. 363

Figure C.36. Strains Measured in Top, Midheight and Bottom Geogrids for Wall 4-Izmit 100%. 364

Figure C.37. Strains Measured in Top, Midheight and Bottom Geogrids for Wall 4-Izmit 150%. 365

Figure C.38. Strains Measured in Top, Midheight and Bottom Geogrids for Wall 4-Izmit 200%. 366

Figure C.39. Strains Measured in Top, Midheight and Bottom Geogrids for Wall 4-Sakarya 100%. 367

Figure C.40. Strains Measured in Top, Midheight and Bottom Geogrids for Wall 4-Sakarya 150%. 368

Figure C.41. Strains Measured in Top, Midheight and Bottom Geogrids for Wall 4-Sakarya 200%. 369

LIST OF TABLES

Table 2.1. Thesis Organization and Overview of the Chapters 5

Table 3.1. Recommended minimum factors of safety for design of GRS-RW Structures 32

Table 4.1. Scaling factors used in this study..... 53

Table 4.2. The properties of sand 59

Table 4.3. Test Results of Sand Cone Tests 62

Table 4.4. The properties of gravel used in the experiments 62

Table 4.5. Properties of Geogrids used in the experiments..... 65

Table 4.6. Properties of the Dynapac Compactor LF82 68

Table 4.7. Wall Configurations and model parameters used in this study 84

Table 4.8. Test Program 89

Table 5.1. Predominant frequencies evaluated according to the plotted acceleration response spectrums for each applied base excitation..... 97

Table 5.2. Acceleration amplification factors with the peak values of the accelerations and the time instances at the occurrences of the peaks for Wall 1 El Centro Earthquake 99

Table 5.3. Acceleration amplification factors with the peak values of the accelerations and the time instances at the occurrences of the peaks for Wall 1 Izmit Earthquake 100

Table 5.4. Acceleration amplification factors with the peak values of the accelerations and the time instances at the occurrences of the peaks for Wall 1 Sakarya Earthquake 101

Table 5.5. Acceleration amplification factors with the peak values of the accelerations and the time instances at the occurrences of the peaks for Wall 2 El Centro Earthquake 102

Table 5.6. Acceleration amplification factors with the peak values of the accelerations and the time instances at the occurrences of the peaks for Wall 2 Izmit Earthquake 103

Table 5.7. Acceleration amplification factors with the peak values of the accelerations and the time instances at the occurrences of the peaks for Wall 2 Sakarya Earthquake 104

Table 5.8. Acceleration amplification factors with the peak values of the accelerations and the time instances at the occurrences of the peaks for Wall 3 El Centro Earthquake 105

Table 5.9. Acceleration amplification factors with the peak values of the accelerations and the time instances at the occurrences of the peaks for Wall 3 Izmit Earthquake 106

Table 5.10. Acceleration amplification factors with the peak values of the accelerations and the time instances at the occurrences of the peaks for Wall 3 Sakarya Earthquake 107

Table 5.11. Acceleration amplification factors with the peak values of the accelerations and the time instances at the occurrences of the peaks for Wall 4 El Centro Earthquake 108

Table 5.12. Acceleration amplification factors with the peak values of the accelerations and the time instances at the occurrences of the peaks for Wall 4 Izmit Earthquake 109

Table 5.13. Acceleration amplification factors with the peak values of the accelerations and the time instances at the occurrences of the peaks for Wall 4 Sakarya Earthquake 110

Table 5.14. Summary of Maximum Acceleration Amplification factors observed together with locations 121

Table 5.15. Measured Horizontal Displacement of Wall Facing for Wall Configuration 1 and Wall Configuration 2 123

Table 5.16. Measured Horizontal Displacement of Wall Facing for Wall Configuration 3 and Wall Configuration 4 124

Table 5.17. Residual Displacements Measured on (@h=1.9m) Top Modular Blocks for Wall 1, 2, 3 and 4 129

Table 5.18. Residual Displacements Measured on (@h=1.65m) Modular Block for Wall 1, 2, 3 and 4 129

Table 5.19. Residual Displacements Measured on (@h=1.25m) Modular Block for Wall 1, 2, 3 and 4 129

Table 5.20. Residual Displacements Measured on (@h=0.95m) Modular Block for Wall 1, 2, 3 and 4 130

Table 5.21. Residual Displacements Measured on (@h=0.25m) Modular Block for Wall 1, 2, 3 and 4 130

Table 5.22. Measured Strains in Geogrid Reinforcement at the end of construction for Wall 3 and Wall 4 142

Table 5.23. Measured Peak Tensile Strains together with peak compressive strains for each base excitations applied on Wall 1 146

Table 5.24. Measured Peak Tensile Strains together with peak compressive strains for each base excitations applied on Wall 2 147

Table 5.25. Measured Peak Tensile Strains together with peak compressive strains for each base excitations applied on Wall 3 148

Table 5.26. Measured Peak Tensile Strains together with peak compressive strains for each base excitations applied on Wall 4 149

Table 5.27. Peak Average Tensile Forces on Geogrid Reinforcement for each base excitations applied on Wall 1 165

Table 5.28. Peak Average Tensile Forces on Geogrid Reinforcement for each base excitations applied on Wall 2 166

Table 5.29. Peak Average Tensile Forces on Geogrid Reinforcement for each base excitations applied on Wall 3 167

Table 5.30. Peak Average Tensile Forces on Geogrid Reinforcement for each base excitations applied on Wall 4 168

Table 6.1. Material Properties together with seismic data used in the experimented walls 185

Table 6.2. The measured and calculated values of permanent displacements for Wall 1 and Wall 2 187

Table 6.3. The measured and calculated values of permanent displacements for Wall 3 and Wall 4 188

Table D.1. Calculation of k_c for the external base sliding for Wall 1 370

Table D.2. Calculation of k_c for the internal base sliding for Wall 1 370

Table D.3. Calculation of k_c for the interface shear for Wall 1 371

Table D.4. Calculation of Displacements for Wall 1-El Centro 100% 371

Table D.5. Calculation of Displacements for Wall 1-El Centro 150% 371

Table D.6. Calculation of Displacements for Wall 1-El Centro 200% 372

Table D.7. Calculation of k_c for the external base sliding for Wall 2 372

Table D.8. Calculation of k_c for the internal base sliding for Wall 2..... 372

Table D.9. Calculation of k_c for the interface shear for Wall 2 373

Table D.10. Calculation of Displacements for Wall 2-El Centro 100% 373

Table D.11. Calculation of Displacements for Wall 2-El Centro 150% 373

Table D.12. Calculation of Displacements for Wall 2-El Centro 200% 374

Table D.13. Calculation of k_c for the external base sliding for Wall 3 374

Table D.14. Calculation of k_c for the internal base sliding for Wall 3..... 374

Table D.15. Calculation of k_c for the interface shear for Wall 3 375

Table D.16. Calculation of Displacements for Wall 3-El Centro 100% 375

Table D.17. Calculation of Displacements for Wall 3-El Centro 150% 375

Table D.18. Calculation of Displacements for Wall 3-El Centro 200% 376

Table D.19. Calculation of Displacements for Wall 3-El Centro 250% 376

Table D.20. Calculation of k_c for the external base sliding for Wall 4 376

Table D.21. Calculation of k_c for the internal base sliding for Wall 4..... 377

Table D.22. Calculation of k_c for the interface shear for Wall 4 377

Table D.23. Calculation of Displacements for Wall 4-El Centro 100% 377

Table D.24. Calculation of Displacements for Wall 4-El Centro 150% 378

Table D.25. Calculation of Displacements for Wall 4-El Centro 200% 378

Table D.26. Calculation of Displacements for Wall 4-El Centro 250% 378

Table D.27. Calculation of Displacements for Wall 4-El Centro 275% 379

Table E.1. Calculation of Tensile Load in Geogrids for Wall 1-El Centro 100% using a) NCMA Segmental Retaining Walls Seismic Design Manual b) FHWA Recommendations 380

Table E.2. Calculation of Tensile Load in Geogrids for Wall 1-El Centro 150% using a) NCMA Segmental Retaining Walls Seismic Design Manual b) FHWA Recommendations 381

Table E.3. Calculation of Tensile Load in Geogrids for Wall 1-El Centro 200% using a) NCMA Segmental Retaining Walls Seismic Design Manual b) FHWA Recommendations 382

Table E.4. Calculation of Tensile Load in Geogrids for Wall 1-Izmit 100% using a) NCMA Segmental Retaining Walls Seismic Design Manual b) FHWA Recommendations 383

Table E.5. Calculation of Tensile Load in Geogrids for Wall 1-Izmit 150% using a) NCMA Segmental Retaining Walls Seismic Design Manual b) FHWA Recommendations 384

Table E.6 Calculation of Tensile Load in Geogrids for Wall 1-Izmit 200% using a) NCMA Segmental Retaining Walls Seismic Design Manual b) FHWA Recommendations 385

Table E.7. Calculation of Tensile Load in Geogrids for Wall 1-Sakarya 100% using a) NCMA Segmental Retaining Walls Seismic Design Manual b) FHWA Recommendations 386

Table E.8. Calculation of Tensile Load in Geogrids for Wall 1-Sakarya 150% using a) NCMA Segmental Retaining Walls Seismic Design Manual b) FHWA Recommendations 387

Table E.9. Calculation of Tensile Load in Geogrids for Wall 1-Sakarya 200% using a) NCMA Segmental Retaining Walls Seismic Design Manual b) FHWA Recommendations 388

Table E.10. Comparison of Calculated and Measured Seismic Induced Tensile Loads in Geogrids for Wall 1 389

Table E.11. Calculation of Tensile Load in Geogrids for Wall 2-El Centro 100% using a) NCMA Segmental Retaining Walls Seismic Design Manual b) FHWA Recommendations 389

Table E.12. Calculation of Tensile Load in Geogrids for Wall 2-El Centro 150% using a) NCMA Segmental Retaining Walls Seismic Design Manual b) FHWA Recommendations 390

Table E.13. Calculation of Tensile Load in Geogrids for Wall 2-El Centro 200% using a) NCMA Segmental Retaining Walls Seismic Design Manual b) FHWA Recommendations 391

Table E.14. Calculation of Tensile Load in Geogrids for Wall 2-Izmit 100% using a) NCMA Segmental Retaining Walls Seismic Design Manual b) FHWA Recommendations 392

Table E.15. Calculation of Tensile Load in Geogrids for Wall 2-Izmit 150% using a) NCMA Segmental Retaining Walls Seismic Design Manual b) FHWA Recommendations 393

Table E.16. Calculation of Tensile Load in Geogrids for Wall 2-Izmit 200% using a) NCMA Segmental Retaining Walls Seismic Design Manual b) FHWA Recommendations 394

Table E.17. Calculation of Tensile Load in Geogrids for Wall 2-Sakarya 100% using a) NCMA Segmental Retaining Walls Seismic Design Manual b) FHWA Recommendations 395

Table E.18. Calculation of Tensile Load in Geogrids for Wall 2-Sakarya 150% using a) NCMA Segmental Retaining Walls Seismic Design Manual b) FHWA Recommendations 396

Table E.19. Calculation of Tensile Load in Geogrids for Wall 2-Sakarya 200% using a) NCMA Segmental Retaining Walls Seismic Design Manual b) FHWA Recommendations 397

Table E.20. Comparison of Calculated and Measured Seismic Induced Tensile Loads in Geogrids for Wall 2 398

Table E.21. Calculation of Tensile Load in Geogrids for Wall 3-El Centro 100% using a) NCMA Segmental Retaining Walls Seismic Design Manual b) FHWA Recommendations 398

Table E.22. Calculation of Tensile Load in Geogrids for Wall 3-El Centro 150% using a) NCMA Segmental Retaining Walls Seismic Design Manual b) FHWA Recommendations 399

Table E.23. Calculation of Tensile Load in Geogrids for Wall 3-El Centro 200% using a) NCMA Segmental Retaining Walls Seismic Design Manual b) FHWA Recommendations 400

Table E.24. Calculation of Tensile Load in Geogrids for Wall 3-El Centro 250% using a) NCMA Segmental Retaining Walls Seismic Design Manual b) FHWA Recommendations 401

Table E.25. Calculation of Tensile Load in Geogrids for Wall 3-Izmit 100% using a) NCMA Segmental Retaining Walls Seismic Design Manual b) FHWA Recommendations 402

Table E.26. Calculation of Tensile Load in Geogrids for Wall 3-Izmit 150% using a) NCMA Segmental Retaining Walls Seismic Design Manual b) FHWA Recommendations 403

Table E.27. Calculation of Tensile Load in Geogrids for Wall 3-Izmit 200% using a) NCMA Segmental Retaining Walls Seismic Design Manual b) FHWA Recommendations 404

Table E.28. Calculation of Tensile Load in Geogrids for Wall 3-Izmit 250% using a) NCMA Segmental Retaining Walls Seismic Design Manual b) FHWA Recommendations 405

Table E.29. Calculation of Tensile Load in Geogrids for Wall 3-Sakarya 100% using a) NCMA Segmental Retaining Walls Seismic Design Manual b) FHWA Recommendations 406

Table E.30. Calculation of Tensile Load in Geogrids for Wall 3-Sakarya 150% using a) NCMA Segmental Retaining Walls Seismic Design Manual b) FHWA Recommendations 407

Table E.31. Calculation of Tensile Load in Geogrids for Wall 3-Sakarya 200% using a) NCMA Segmental Retaining Walls Seismic Design Manual b) FHWA Recommendations 408

Table E.32. Calculation of Tensile Load in Geogrids for Wall 3-Sakarya 250% using a) NCMA Segmental Retaining Walls Seismic Design Manual b) FHWA Recommendations 409

Table E.33. Comparison of Calculated and Measured Seismic Induced Tensile Loads in Geogrids for Wall 3 410

Table E.34. Calculation of Tensile Load in Geogrids for Wall 4-El Centro 100% using a) NCMA Segmental Retaining Walls Seismic Design Manual b) FHWA Recommendations 410

Table E.35. Calculation of Tensile Load in Geogrids for Wall 4-El Centro 150% using a) NCMA Segmental Retaining Walls Seismic Design Manual b) FHWA Recommendations 411

Table E.36. Calculation of Tensile Load in Geogrids for Wall 4-El Centro 200% using a) NCMA Segmental Retaining Walls Seismic Design Manual b) FHWA Recommendations 412

Table E.37. Calculation of Tensile Load in Geogrids for Wall 4-El Centro 250% using a) NCMA Segmental Retaining Walls Seismic Design Manual b) FHWA Recommendations 413

Table E.38. Calculation of Tensile Load in Geogrids for Wall 4-El Centro 275% using a) NCMA Segmental Retaining Walls Seismic Design Manual b) FHWA Recommendations 414

Table E.39. Calculation of Tensile Load in Geogrids for Wall 4-Izmit 100% using a) NCMA Segmental Retaining Walls Seismic Design Manual b) FHWA Recommendations 415

Table E.40. Calculation of Tensile Load in Geogrids for Wall 4-Izmit 150% using a) NCMA Segmental Retaining Walls Seismic Design Manual b) FHWA Recommendations 416

Table E.41. Calculation of Tensile Load in Geogrids for Wall 4-Izmit 200% using a) NCMA Segmental Retaining Walls Seismic Design Manual b) FHWA Recommendations 417

Table E.42. Calculation of Tensile Load in Geogrids for Wall 4-Sakarya 100% using a) NCMA Segmental Retaining Walls Seismic Design Manual b) FHWA Recommendations 418

Table E.43. Calculation of Tensile Load in Geogrids for Wall 4-Sakarya 150% using a) NCMA Segmental Retaining Walls Seismic Design Manual b) FHWA Recommendations 419

Table E.44. Calculation of Tensile Load in Geogrids for Wall 4-Sakarya 200% using a) NCMA Segmental Retaining Walls Seismic Design Manual b) FHWA Recommendations 420

Table E.45. Comparison of Calculated and Measured Seismic Induced Tensile Loads in Geogrids for Wall 4 421

LIST OF SYMBOLS

a	Maximum ground acceleration coefficient
a_m	Maximum horizontal acceleration coefficient in reinforced soil wall
c	Cohesion of soil
C	Reinforcement effective unit parameter
C_c	Coefficient of curvature
C_u	Coefficient of uniformity
e	Eccentricity
E	Modulus of Elasticity
F_T	Total force applied by the retained fill on the back of reinforced zone
H	Wall Height
K_A	Activecoefficient of earth pressure
K_{AE}	Total seismic earth pressure coeffiecient
K_{ar}	Earth pressure coefficient calculated for reinforced zone
K_P	Passive coefficient of earth pressure
k_c	Critical acceleration
k_h	Horizontal seismic coefficient
k_v	Vertical seismic coefficient
L	ReinforcementLength
L_a	Length of reinforcement in front of critical surface
L_e	Length of embedment in the resisting zone
P_A	Active static earth pressure resultant force
P_{AE}	Total dynamic active earth force
P_d	Driving force
P_I	Inertia force acting on the active zone
P_{IR}	Inertia force
P_R	Resisting force
R_c	Coverage ratio
q_{ult}	Ultimate bearing capacity
S_v	Spacing between reinforcement layers
t	Time

T_a	Allowable tensile force per unit width of reinforcement
T_{max}	Maximum tension force per unit width of wall
W_a	Weight of active zone
W_R	Weight of reinforced zone
v_m	Peak ground velocity
z	Depth
α	Scale correction factor
β	Angle of backfill slope
γ	Unit weight
γ_f	Unit weight of retained fill
ϕ	Internal friction angle
δ	Interface friction angle
ε	Strain
ε_{ult}	Ultimate strain
λ	Scalingfactor
μ	Soil-reinforcement friction coefficient
P	Soil-reinforcement friction angle
σ_1	Vertical principal stress
σ_3	Lateral confining stress
σ_H	Horizontal stress
σ_V	Vertical stress
τ	Shear stress
Ψ	Seismic inertia angle
ΔK_{dyn}	Incremental dynamic active earth pressure coefficient
ΔP_{dyn}	Incremental dynamic component of P_{AE}
$\Delta\sigma_H$	Incremental of horizontal stress due to horizontal surcharge

LIST OF ACRONYMS/ABBREVIATIONS

AASHTO	American Association of State Highway and Transportation Officials
FHWA	Federal Highway Administration
FS	Factor of safety
GRS-RW	Geosynthetic-ReinforcedSoil Retaining Wall
HDPE	High Density Polyethylene
NCMA	National Concrete Masonry Association
PET	Polyester
PGA	Peak ground acceleration
PP	Polypropylene

1.INTRODUCTION

It is only after major earthquakes that, people and the media become more sensitive about earthquake resistant structures and discuss deeply about design and construction methods of such structures. And after a while it is all forgotten. However, it should always be kept in mind that; Turkey has confronted major earthquakes in the past and will confront major earthquakes in the future as well.In geotechnical engineering, designing and construction of earthquake resistant reinforced earth structures are among one of the most challenging and yet not deeply assessed subjects.

When compared with the conventional gravity walls, Geosynthetic-Reinforced Soil Retaining Walls (GRS-RWs) offer cost-efficiency, higher performance, aesthetic appearance and much more durability. Because of these advantages, they are widely constructed in place of the conventional gravity walls (Koseki *et. al*., 2006). Specifically, the use of segmental retaining walls that include dry-stacked concrete block units as the facia system together with extensible sheets of polymeric materials (geosynthetics) that internally reinforce the retained soils and anchor the facia has gained wide popularity. The distinguishing feature of these structures is the facing that is constructed using mortarless modular concrete block units that are stacked to form a wall batter into the retained soils (typically 3° to 15° from vertical). In practice, such walls are routinely designed using limit-equilibrium analysis andearthquake loads are considered using pseudo-static methods (AASHTO, 1996; FHWA, 1996).

The seismic design methodologies for GRS-RWs are largely based on the results of numerical modelingof reinforced structures constructed with inextensible reinforcement although the related empirical rules developed from these types of structures may not be applicable to nominal identical walls constructed with geosynthetic reinforcement. To help improve these kinds of inadequacies of the current seismic design methods and to gain a better insight into dynamic behavior of a Geosynthetic-Reinforced Soil Retaining wall (GRS-RW) under earthquake loads, a large number of numerical and experimental tests must be available.

Due to the constraints in laboratory environment and difficulties in examining the behavior of a full-scale prototype model of a reinforced soil retaining wall under dynamic excitations, scaled-models of the prototypes are constructed and centrifuge and shaking table tests are applied by the utilization of scaling laws. Scaling laws provided by the dimensional analysis is a compacting technique for reducing the number and complexity of experimental variables. Based on the scaling laws, similarity is achieved between the model and prototype.

To improve the performance of GRS-RWs and to increase confidence in their use, especially for permanent or critical structures, reliable information on their face deformations and stress-strain distributions in reinforcement layers, is necessary. Furthermore, overly conservative designs are also uneconomical, so considerable cost savings can result from improved design procedures.

2. SCOPE OF WORK, OBJECTIVES AND THESIS ORGANIZATION

2.1. Scope of Work and Objectives

Because of advantages such as cost-efficiency, higher performance, aesthetic appearance and much more durability, Geosynthetic Reinforced Soil Retaining Walls are widely constructed and becoming widespread. In practice, such walls are routinely designed using limit-equilibrium analysis and earthquake loads are considered using pseudo-static methods (AASHTO, 1996; FHWA, 2010). Increasing popularity of such wall systems makes the seismic performance of Geogrid Reinforced Soil Walls to be of great concern. A reliabledatabase is needed for conducting analysis and examining/improving design procedures.Shaking table tests were conducted by Ling *et al.* (2005) and Leshchinsky *et al.* (2008). Leshchinsky demonstrates that although Limit Equilibrium analysis shows a FS≈1 for an acceleration of 0.39g, for a 2.8 m high geogrid reinforced slope having geocell facing and sand backfill, no failure was observed even for an acceleration of 0.8g.

The seismic design methodologies for GRS-RWs are largely based on the results of numerical modeling of reinforced structures constructed with inextensible reinforcement although the related empirical rules developed from these types of structures may not be applicable to nominal identical walls constructed with geosynthetic reinforcement. To help improve these kinds of inadequacies of the current seismic design methods and to gain a better insight into dynamic behavior of a Geosynthetic-Reinforced Soil Retaining wall (GRS-RW) under earthquake loads, a large number of numerical and experimental tests must be available.

This study investigates the dynamic performance of four 1/2 reduced-scale Geogrid-Reinforced Soil Retaining Block Wallmodels that were tested on a shaking table. The effect of increasing horizontal base acceleration, reinforcement length and stiffness, backfill material type, facing batter(inclination) on measured parameters under seismic excitation are analyzed and presented. The walls were instrumented by installing 9 accelerometers to measure the accelerations within the soil and facing blocks, 6 linear laser

displacement sensors to measure the displacement of facing blocks. Additionally, the strain gages were installed on the geogrid reinforcement to measure the reinforcement strains. The heights of the models were 1.9 m and each wall was excited with scaled El Centro, Izmit and Sakarya earthquake motionsto compare the effects of different earthquake motions on the walls. Comprehensive seismic design methodologies of GRS-RWs proposed by the NationalConcrete Masonry Association (NCMA) and The Federal Highway Administration (FHWA) are used to calculate the permanent displacements on structures and reinforcement tensile loads on reinforcements under earthquake loading and the results are compared with the obtained results from experiments.

The majorcomponent of this research has been the construction, instrumentation and monitoring of four 1/2 reduced-scale geogrid reinforced soil retaining walls.

The principal objectives of the experimental work are:

- How GRS walls perform and behave with different and increasing seismic excitations(even at extreme seismic excitations).
- The influence of reinforcement stiffness and length on performance of GRS walls under seismic loading.
- The influence of backfill material on performance of GRS walls under seimic loading.
- Develop a better understanding of the stress-strains generated in geogrid reinforcement and facing of georid reinforced soil walls during construction and at extreme seismic excitations.
- Whether the experimental results are in accordance with the current NCMA and FHWA design methodologies for reinforced soil retaining walls.

2.2. Research Overview and Thesis Organization

The Table 2.1.shown below summarizes the thesis organization andpresents an overview of the chapters.

Table 2.1. Thesis Organization and Overview of the Chapters

Chapter No./Name	Overview
Chapter 1 /Introduction	A general introduction to the subject.
Chapter 2 / Scope Of Work, Objectives and Research Approach	Scope and objective of the study is summarized. Research overview and thesis organization are presented.
Chapter 3 / General Information About Geogrid-Reinforced Structures And Similar Studies In Literature	Reinforced Soil Structures, their composition, history and their usage areas are explained briefly.. The methods to investigate the behavior of these kinds of structures and conventional design methods are defined. Similar studies in literature are summarized and presented.
Chapter 4 / Methodology	Herein, the methodology regarding the experimental work is presented. The scaling factors used for the experiments, preparation of test set-up, the materials used in the experiments, instrumentation of all electronic devices together with their properties and capabilities, construction method of walls are all explained in detail in this chapter.
Chapter 5 / Test Results and Evaluation	The results and evaluation of acceleration amplification, horizontal displacements on wall facing and Strain/stress Distribution in Geogrid Reinforcements during and at the end of Construction of Wall Strains and Tensile Loads generated in Geogrid Layers during Earthquake motion are presented in detail.
Chapter 6 / Calculation Methods For Displacement, Inclination Of Failure Surface And Geogrid Tensile Loads.	In this chapter, the permanent displacements on structures due to seismic loading and reinforcement tensile loads are calculated using the seismic design methodologies of GRS-RWs proposed by the National Concrete Masonry Association (NCMA) and The Federal Highway Administration (FHWA). The calculated results are compared with the measured experimental results. Also, the inclination of failure surface is calculated.
Chapter 7 /General Conclusions	The general conclusions drawn from this study is presented in this chapter.
Appendices	The acceleration vs. time, horizontal displacement vs. time and strain vs. time plots obtained from experiments are presented. The excel charts used in the calculations are also given.

3. GENERAL INFORMATION ABOUT GEOGRID-REINFORCED STRUCTURES AND SIMILAR STUDIES IN LITERATURE

3.1. Background and Description

Construction of soil retaining structures began when lifestyle of humankind changed to sedentary life. First applications of soil retaining structures were defensive walls and religious monuments. (Kerisel, 1992). The demand of increasing size, especially the height, in soil retaining structures made people quickly realize that the most important concern was the earth pressure generated by the mass of backfill soil. The problem was first solved by resisting the lateral earth pressure externally by employing materials like rocks or huge stones, whose mass and volume were greater than those of the backfill soil mass. It is also found out that reinforcing backfill soil can decrease the earth pressure as well.

Most of historical structures have proof of practices of reinforced soil in retaining structures. When ziggurats were constructed by people from Middle East more than 3000 years ago, using woven reed mats as reinforcement can be shown as an example of the proof of these applications. The mats were laid horizontally inside the fill soil providing planar tensile reinforcement, which resembles the applications of today (Jones, 1997).

As shown in Figure 3.1., soil retaining structures can be divided into two major groups:

- Externally stabilized soil retaining system
- Internally stabilized soil retaining system

In conventional earth retaining systems, which can be classified as externally stabilized soil retaining systems; outer structural walls made up of high stiff substance and/or large unit weight that locates the backfill keep backfill soils.

Internally stabilized soil retaining systems which are called as reinforced soil systems are constructed by stabilizing the soil mass with adding extra tensile reinforcing elements like geosynthetics, steel straps or soil nails towards inner parts of backfill soil. In most cases, soil and these layered reinforcements often lengthen outwards the potential failure surface.

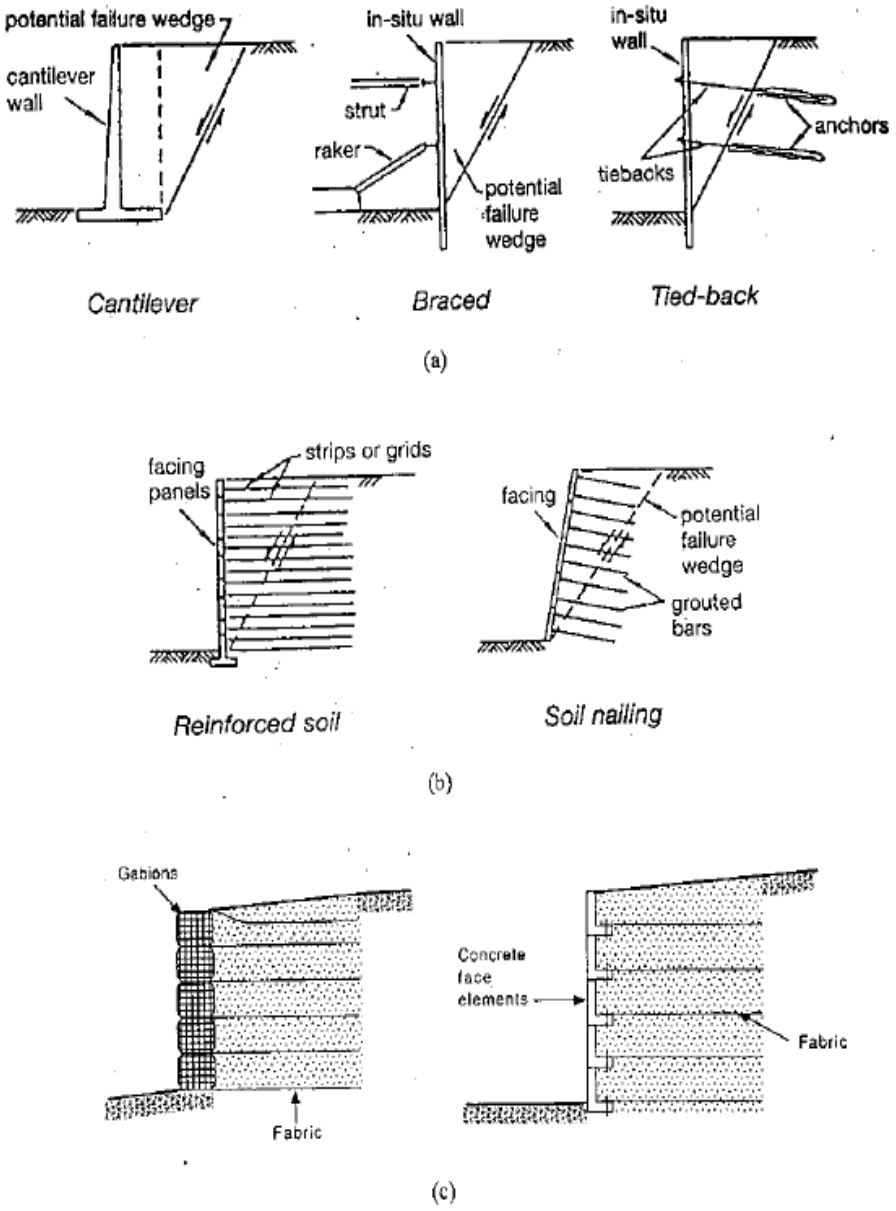


Figure 3.1. Example of Retaining Wall Systems (Jones, 1997)

Reinforced Earth concept was invented in France by Henri Vidal during the 1960s.Vidal developed the system by introducing reinforcing strips to granular fill to form the Reinforced Earth composite material that is capable of retaining earth and slopes, and supporting large applied loads. The use of textiles for reinforcement was not contemplated until the development of synthetic polymer-based materials. it was not until the late 1960s and early 1970s that the advances in synthetic fabric and geotextile developments led to the construction of reinforced soil structures. Nowadays, the use of geosynthetics as earth reinforcement in a wide variety of applications including retaining structures, embankment walls in highways, bridge abutments, railway crossings, river walls, and many industrial and military applications.

Geosynthetic Reinforced Soil Retaining Wall, henceforth shall be designated as GRS-RW, is an internally stabilized soil system with geosynthetic inclusion. In GRS-RWs Geosynthetic material is used as reinforcement in soil.

As shown in Figure 3.2., retained backfill soil, foundation soil, facing unit, mechanically stabilized soil mass and reinforcement are the components of GRS-RWs.

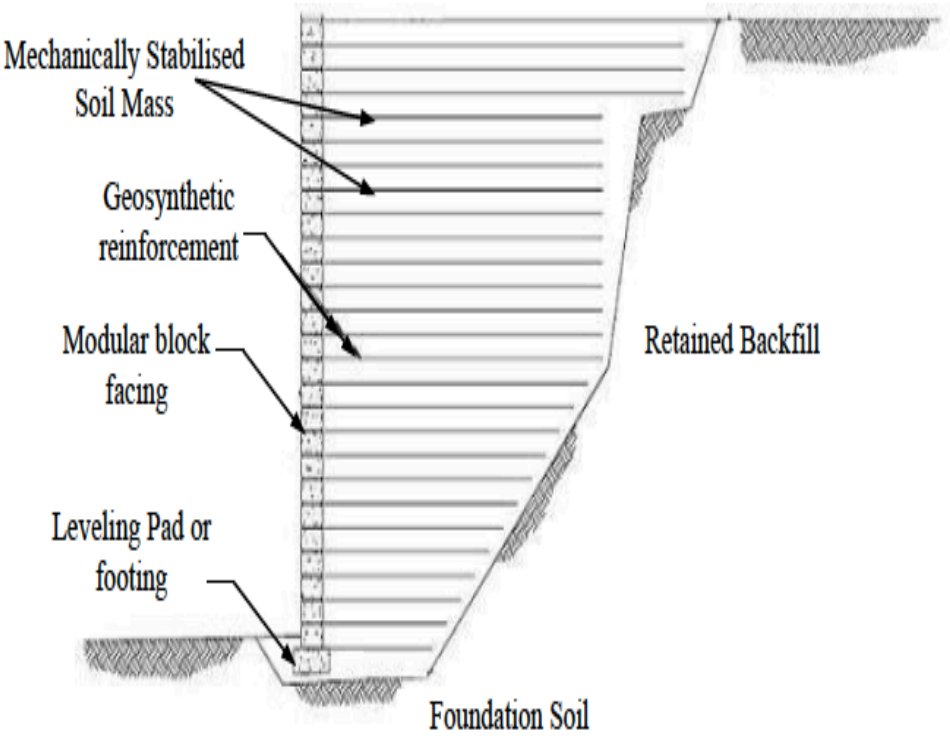


Figure 3.2. Principal Elements of a GRS-RW (Kasay, 2007)

The terminology used in GRS-RWs is as follows;

- *Retained backfill:* Retained backfill is a fill material and it is selected to comply with some requirements. The requirements of retained backfill, whose location is between the mechanically stabilized soil mass and the natural soil, are as follows: i-i- For the essential interaction between soil and reinforcement, the angle of surface resistance to relative motion (friction angle) should be sufficiently high.ii-Creep sensitiveness should be low enough so that unreasonable deformations will be prevented.iii-In order to prevent adverse effects to the reinforcements or compaction efforts, maximum grain size should not be too large. iv-During compaction, moisture content should be limited so that the operation can be easier.v- There should not be unreasonable corrosiveness. Also, all backfill materials should not contain any organic and harmful materials.

- *Reinforcement:* Reinforcement can be identified as an inclusion where soil-inclusion stress transfer occurs permanently along itself. Steel strips and geotextile or geosynthetic sheets can be counted as the most popular reinforcing elements. Geosynthetic is a common term for the materials, so geotextiles, geomembranes, geonets and geogrids, which are several types of elastic synthetic materials used in geotechnical engineering, can be counted in the content of geosynthetics.

- *Facing Unit:*Facing units are parts of reinforced soil system used to avoid the soil to disentangle between reinforcements. Precast concrete modular blocks, concrete panels, metal sheets and plates, gabions, welded wire mesh, shotcrete, wood lagging and panels and wrapped sheets of geosynthetics are amongst the most commonly used facing unit types. Modular-block units are typically joined to geosynthetic reinforcement layers by the use of mechanical and/or frictional devices such as polymeric pins, inserts, clips, concrete shear keys. Besides, the global stability of GRS-RWs is reinforced by the dead weight of the modular blocks.

- *Mechanically stabilized soil mass* is a comprehensive term which comprises both reinforced fill (and reinforced earth as it is sometimes called) and multi-anchored mass. The term "reinforced fill" is used when multiple layers of inclusions, carry out

the task of reinforcement in soils placed as fill. "Reinforced Earth" is a trademark for a specific reinforced soil system. On the other hand, the term "multi-anchored soil mass" is used when multiple layers of inclusions act anchored tendons in soils placed as fill.

- Foundation soil is the soil underneath the mechanically stabilized soil mass and the retained backfill that carries the whole system. Indubitably it is essential that the the design manual criteria are met by the foundation soil. Before the implementation of the reinforced earth structures, some important factors need to be investigated, such as the bearing capacity, settlement potential and position of the ground water levels. Correspondingly, weak foundation soil characteristics may be improved before the application in order to satisfy the adequate bearing capacity and/or limiting total and/or differential settlements (FHWA, 2009).

One of the main factors that geosynthetics are used in reinforced earth has been its economics. The earth reinforcement technique is employed in bridge abutments, retaining structures, seawalls, damns, and industrial bulk storage facilities. They are flexible and they can large differential settlements. Elemental construction helps to adapt to difficult topography and allows the use of relatively less manpower (Selek, 2005).

3.1.1. Types of Geosynthetic Reinforced Walls

Generally, the retaining walls can be grouped in two major categories, namely the conventional retaining walls and the mechanically stabilized earth walls. The conventional walls can be categorized as gravity retaining wall, cantilever retaining wall, crib wall, sheet pile wall and so on, whereas the mechanically stabilized earth walls have been used in constructions where the soil reinforcements may be galvanized metal strips, geotextiles, geogrids or geocomposites.

In this study, the seismic performance of geogrid reinforced segmental walls is investigated and for brevity, in the following section information about the geogrid reinforced soil retaining walls shall be given.

3.1.2. Geogrid Reinforced Walls

Geogrid reinforced walls are gravity retaining walls with an expanded width created by the placement of geogrid behind a column of segmental facing units. The combination of segmental units and geosynthetic layers act together creating a coherent mass to resist the destabilizing forces generated by the retained soil and applied surcharge loadings. The reinforced soil concept has got a huge momentum with the development of Geogrids. These plastic products, specifically engineered for soil reinforcement, provide civil engineers with factory-controlled characteristics, uniform behavior, very limited variability and very high durability. Geogrids allow the construction of reinforced soil slopes and walls in a much more reliable, fast, safe and economic way than with the natural materials used in the past.

The properties of the geogrid reinforcing elements play an important role in producing cost-effective designs. Commercially available geogrids are polyester (PET), high density polyethylene (HDPE), polypropylene (PP) or steel (strips, mesh panels or ladders) Polypropylene and polyethene are planar and high-modulus of elasticity products Geogrids include mesh or net-like regular open network of intersecting ribs integrally connected at the junction. Ribs are tensile-resistant elements, which can be linked by extrusion, bonding or interlacing. Stiff netlike materials with openings are known as 'aperture' composes geogrids. Apertures are large enough to enable the interlock with the surrounding soil or rock for performing the function of reinforcement and/or segregation (Das, 2004). As an example, the geogrid reinforcement together with facing blocks are shown in Figure 3.3.

By placing geogrid sheets in the soil the strength of the soil can be improved significantly. Also by using a facing system, soil raveling between the reinforcing elements can be prevented. This allows very steep slopes and vertical walls to be safely constructed. The use of segmental retaining walls that include dry-stacked concrete block units as the facia system together with extensible sheets of geogrids that internally reinforce the retained soils and anchor the facia has gained wide popularity.



Figure 3.3.Geogrid reinforcement together with facing blocks

The distinguishing feature of these structures is the facing column that is constructed using mortarless modular concrete block units that are stacked to form a wall batter into the retained soils (typically 3° to 15° from vertical). A simple illustration of a segmental retaining wall with concrete facing system can be seen in Figure 3.4. Typical view from construction process of a Geogrid-Reinforced Soil Structure can be seen in Figure 3.5.

The economic benefits of these systems over conventional reinforced concrete gravity wall structures and mechanically stabilized soil retaining walls that use inextensible (steel) reinforcement) and selected backfills have been demonstrated in several of the references cited in an earlier paper by Bathurst and Simac (1994).



Figure 3.4. A view of Geogrid-Reinforced Segmental Retaining Wall



Figure 3.5. Construction process of a Geogrid-Reinforced Soil Structure (Kasay, 2007)

3.1.3. Reinforcing Mechanisms

The basic concept of Reinforced Earth retaining system, which was founded in 1960 by Henri Vidal as an alternative type of soil retaining structure, is to transfer shear forces that generate inside the soil mass to closely spaced reinforcement as yielding of the soil commences (Mitchell and Villet, 1987).

The discrete system and the composite material approaches have been widely used to explain the reinforcing mechanisms. According to discrete system approach; friction and adhesion provide the transfer of additional shear forces of unstable soil mass to the reinforcement that is shown in Figure 3.6.Friction is the component of shear resistance that is proportional to the normal stress acting on the shear plane. Adhesion is the shear resistance between different materials (soil and reinforcements) and is independent of normal stress (Hausmann, 1990). Internal shear transformation results that soil mass stays at its stable state and lateral pressure generated by the reinforced soil mass is also reduced due to the existence of reinforcement.

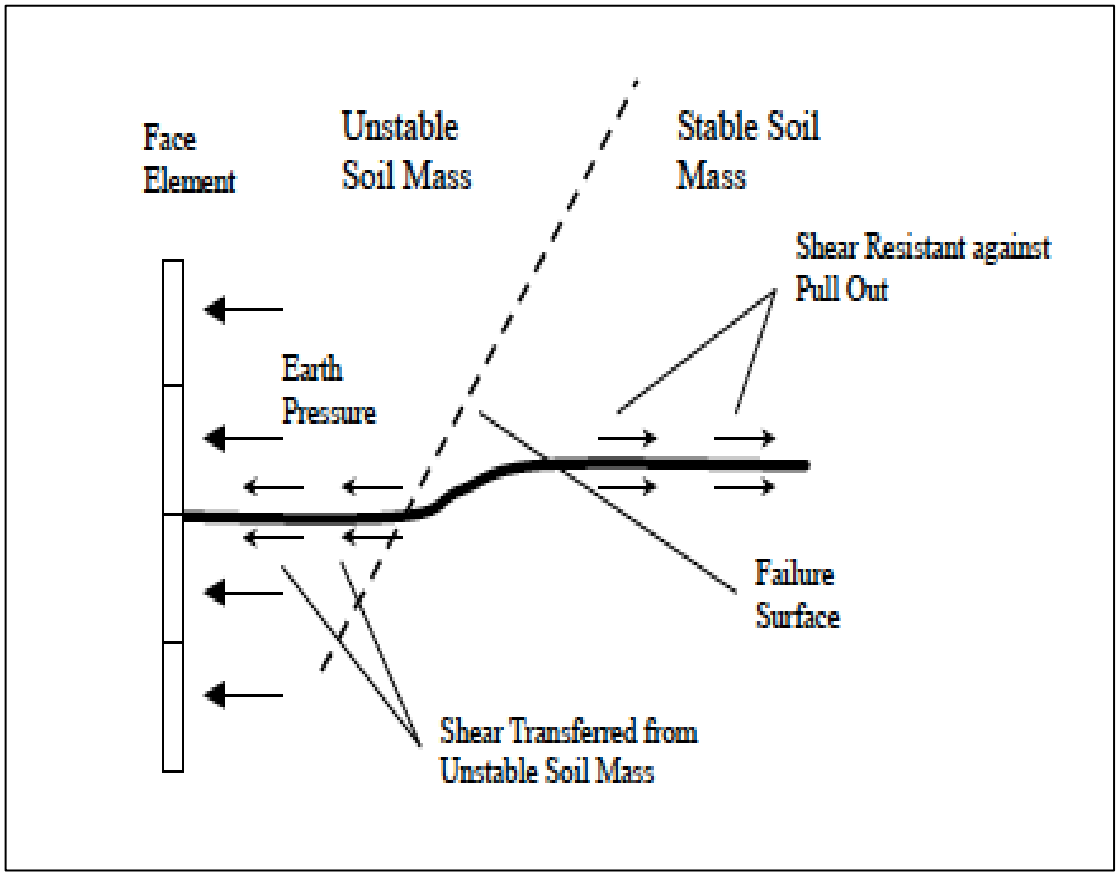


Figure 3.6. Reinforcing Mechanism of Reinforced Soil Retaining Structures (Hausmann, 1990)

A Mohr-Coulomb failure criterion is represented in Figure 3.7.to summarize the composite approach on the reinforcing mechanism.

- Mohr Circle 0:Under initial condition, it represents a reinforced soil composite element at its initial condition. Assume that this element has reinforcement inserted in the horizontal plane, and a pair of principal stresses (vertical and horizontal stresses, where vertical stress is the major principal stress) are applied to it. When the vertical stress increases, the Mohr circle moves to higher stress levels. The greater the vertical stress on to the reinforcement, the higher stress levels can be reached by the Mohr Circle.
- Mohr Circle 1: Failure condition of the unreinforced soil is represented with Mohr Circle 1.
- Mohr Circle 2: Failure condition of the reinforced soil is represented with Mohr Circle 2.

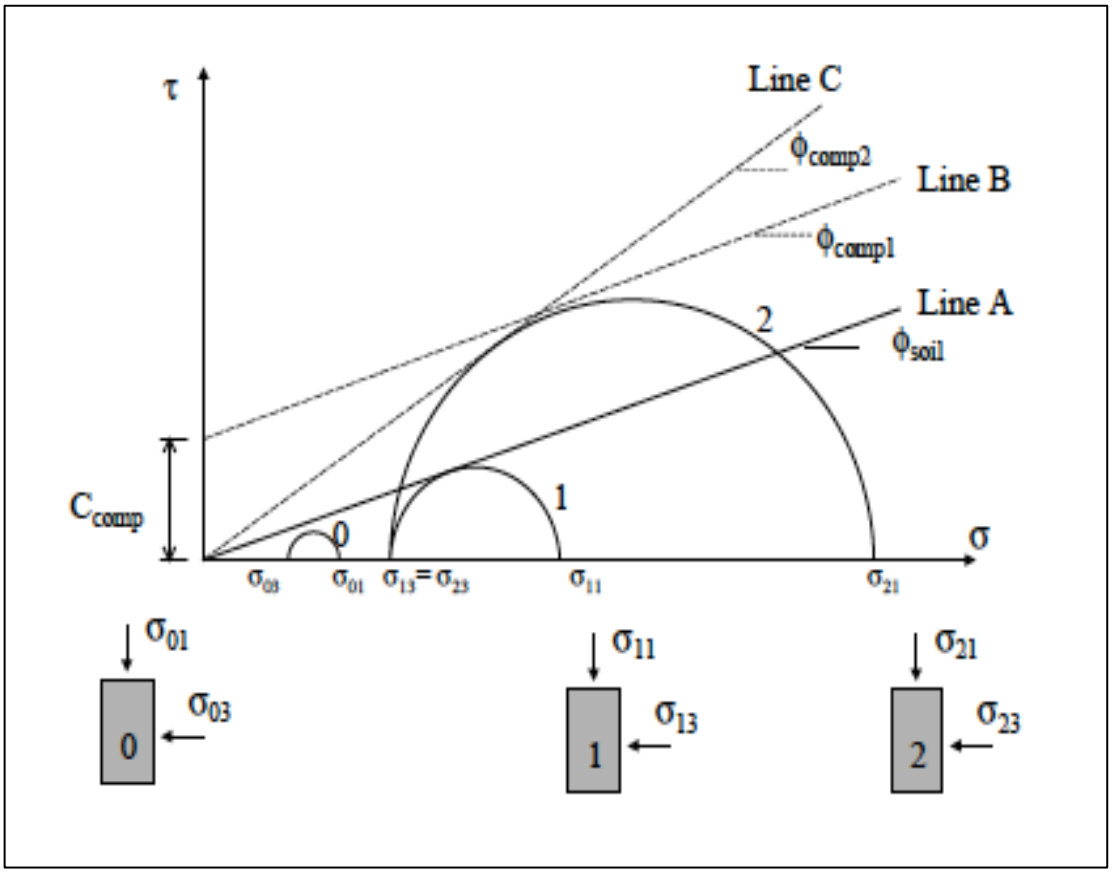


Figure 3.7. Principal Stress Conditions of Reinforced Soil (Hausmann, 1990)

The difference between σ_{21} and σ_{11} is the additional vertical stresses that soil can bear with the aid of the reinforcement. Line A is the failure envelope of the unreinforced soil. Lines B and C are two hypothetical failure envelopes that are used to define the failure of the reinforced soil composite.

There are two hypotheses represented with Lines B and C.

- Hypothesis for Line B: Reinforced soil has the same friction angle like soil. Cohesion (c) is additionally provided from the reinforcement to the composite.

- Hypothesis for Line C:Reinforced soil composite has higher friction angle because of the existence of the reinforcement

Equation 3.1 represents the formulas for Line B and Line C respectively.

$$\tau = c + \sigma \cdot \tan \varphi \quad (3.1)$$

where,

φ= maximum angle of shear resistance of the soil.

τ= maximum overall shear stress provided by the soil.

c= cohesion of soil (for Line B)

The variation of the tensile forces along the reinforcement and the location of the maximum force has been established both experimentally, through instrumented models and full-scale structures, and theoretically, using numerical analysis.

As shown in Figure 3.8, the maximum tensile force in the reinforcement is generally located some distance behind the facing. In order to create a maximum force at that location, the shear stresses exerted by the fill on the reinforcement must be in oppositedirections on the two sides of the peak force as shown.

The locus of the points of maximum tensile force, called the maximum tensile forcesline, thus separates the reinforced fill into two zones: i- An active zone between the facing and the maximum tensile forces line, where theshear stresses on the reinforcements are directed towards the wall face.ii-A resistant zone behind the maximum tensile forces line, where the shear stresseson the reinforcement are directed away from the wall face.

With inextensible reinforcements (Figure 3.8b), the maximum tensile forces line can be modeled by a bilinear failure surface which is vertical in the upper part of the wall. The state of stress is assumed to be at rest at the top and decreases to the active state in the lower part of the wall (the at rest state at the top of the wall has been attributed to both construction stresses and the restraint provided by the reinforcements against lateral yielding). With extensible reinforcements (Figure 3.8c), the maximum tensile forces line coincides with the Coulomb or Rankine active failure plane, and the stresses in the fill correspond to the active earth pressure condition. The location of the maximum tensile forces line may also vary due to external factors such as the shape of the structure and surcharge conditions (FHWA, 2001).

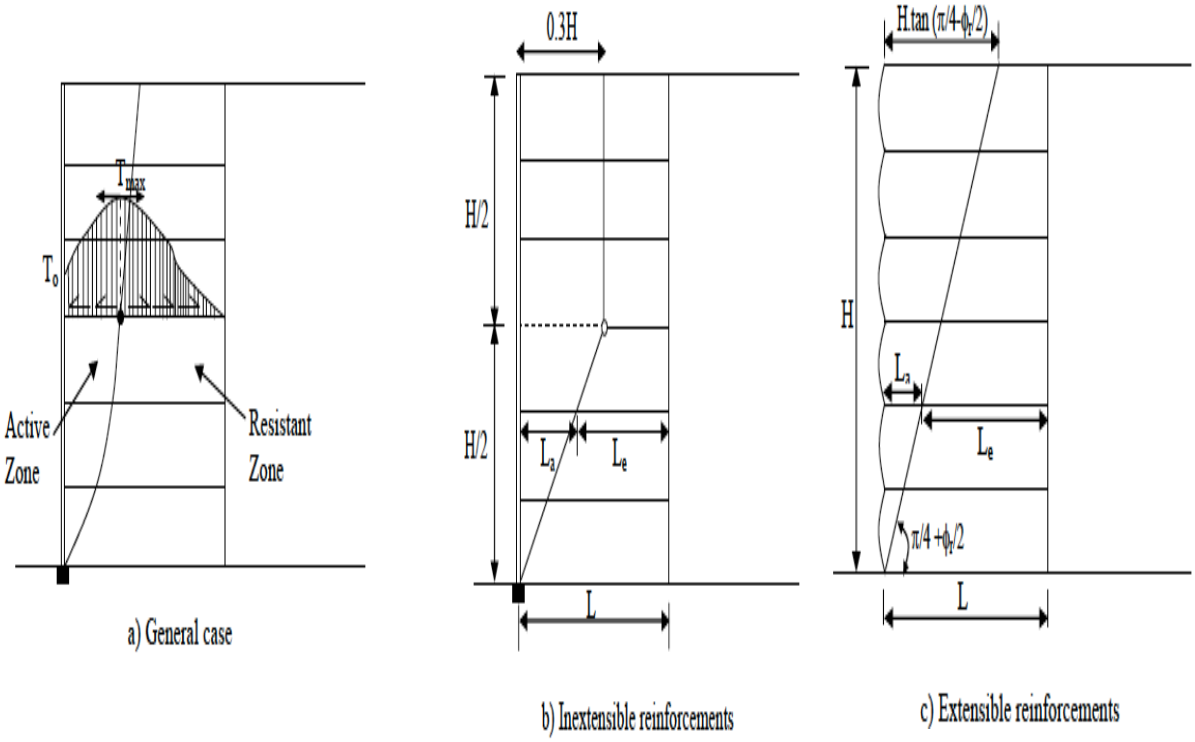


Figure 3.8. Tensile forces in the reinforcements (FHWA, 2001)

3.1.4. Performance of GRS-RWs

Reinforced soil structures are counted as an alternative against the gravity types of walls. These consist of bridge abutments, wing walls, right-of-way restricted areas in order not to construct embankment or excavation with stable side slopes. Reinforced soil structures are especially suitable for economical construction in steep sided regions, grounds that have lack of slope stability, and areas with poor foundation soils.

Reinforced Earth is especially appropriate for construction in seismically active areas as a coherent and yet flexible gravity mass. The structure is able to provide the high degree of structural damping which is necessary to absorb the large energy releases caused by the earthquakes.

When compared to conventional reinforced concrete retaining structures, reinforced soil walls have important advantages at sites with poor foundation conditions because

reinforced soil walls have flexibility; so they can undergo large displacements. Below, the advantages and disadvantages of reinforced soil structures are summarized.

The advantages of reinforced soil structures are;

- The construction can be fast and easy without using large equipment.
- Special talent is not needed for the construction of these type of structures, ordinary craftsman can construct them as well.
- Only little preparations for site are needed.
- For the operations on site, do not require wide spaces in front of the structure.
- Restriction of right-of-way with construction or excavation of steeper slopes.
- Since reinforced soil structures have a tolerance to deformations, they do not need any inflexible foundation supports. With these kind of reinforcements located on the base, constructing on soils which have low-bearing capacity is feasible. Otherwise, in additionto the need of preliminary consolidation, whole construction process should be observed very carefully.
- The opportunity to construct much vertical gradients allows less amount of matter to be used. Also working with low-value materials is not impossible. Therefore, the combination of these means a low-priced and cost-effective approach at work.
- Improved stability is provided by reinforced soil structures like the reinforcement ensures in the factor of safety, even in seismic areas.

On the other hand, the disadvantages of reinforced soil structures can be stated as follows:

- Comparatively large space behind the wall face is necessary so that wall has enough width considering internal and external stability.
- Granular fill is required mostly at the present time
- Drainage system for ground nailing is generally necessary, but its construction and maintenance may be difficult (FHWA, 2001).

Inspections made by Sandri (1994) by observing the performances of geosynthetic reinforced soil retaining structures during recent earthquakes, provide satisfactoryresults.

The survey after Northridge Earthquake dated on 17 January 1994 showed that retaining wall structures, which are placed between 23 and 113 km of the earthquake epicenter and have wall heights over 4.5 m, has no visual damage except 2 structures named Valencia and Gould Walls on which tension cracks within and behind the reinforced soil mass were observed. All of the facing columns were unharmed although at one site peak horizontal ground accelerations of value 0.5g were estimated.

White and Holtz (1996) conducted a similar survey on three geosynthetic reinforced walls and four geosynthetic reinforced slopes after the same earthquake. This survey disclosed no visual evidence of distress.

Stewart *et al.* (1994) indicated that no movement was observed in the slope indicator measurements at the toe of a 24 m high geogrid reinforced slope which was estimated to have sustained peak horizontal ground accelerations of 0.2g. However, some cracks were developed in the backfill of some unreinforced crib walls and unreinforced segmental walls because of the limited flexibility of the concrete crib walls.

Eliahu and Watt (1991) and Collin *et al.* (1992) also conveyed similar surveys on good performance of several geosynthetic reinforced soil walls and slopes during the 1989 Loma Prieta earthquake, which was recorded as 7.1 Richter magnitude. In addition, Tatsuoka*et al.* (1995, 1996) reported after the 1995 Great Hanshin Earthquake, in Kobe, Japan, that a movement of moved 260 mm at the top and 100 mm at ground level occurred in the 6.2 m high geosynthetic reinforced soil retaining wall with a full height rigid facing construction but no damage was observed despite the fact that the peak ground acceleration at the site have been as great as 0.7g. The phenomenon of tilting of the wall is associated with the shrinking of the reinforcement lengths due to site constraints. Following the same earthquake in Japan, Nishimura *et al.* (1996) made a survey on 10 geogrid reinforced soil walls and steepened slopes. Despite the though peak ground acceleration range changing between 0.3 to 0.7g, all structured survived the 18 earthquake. Nishimura *et al.* calculated critical accelerations for these structures by use of GRB (1990) and PWRI (1992) methods of analysis and they concluded that predicted critical acceleration coefficient (k_h) values were as low as 0.1. Following the results of stability calculations using these methods, they drew the conclusions that the length of reinforcement layers at the top of the reinforced soil

structures should be increased so that the critical failure volumes generated under even modest horizontal seismic accelerations can be captured (Bathurst and Alfaro, 2000).

3.2. Design of GRS-RWs

Geogrids or geotextiles are used as the reinforcing element to construct GRS-RW to increase the bearing capacity and slope stability, thereby providing resistance to erosion and reducing the settlement and lateral deformation. In Turkey the latter is commonly used for the construction of GRS-RWs in an economic sense. However the use of Geogrid reinforced soil retaining structures is increasing day by day.

In the design of GRS-RW walls, limit equilibrium analysis has been employed. It is based on the application of global factors of safety against failure. The design methods which use this approach differ in the assumptions dealing with stress distributions, failure surfaces, safety factors, and the inclination of the reinforcement at the failure surface. The complex soil geosynthetic-facing interaction mechanism, which actually takes place, is not modeled with these methods.

The evaluations for global factors of safety in limit equilibrium analysis include the forces due to reinforcement by geosynthetics in the examination of test-bodies which are assumed to be at the verge of failure. 2 approaches are commonly used in the definition of safety factors in limit equilibrium analysis (Claybourn and Wu, 1993).

The definitions of the factor of safety in these two approaches are as follows:

- The ratio of forces or moments resisting to the forces or moments tending to cause Instability are defined as factor of safety.
- With the application of factor of safety, the strength parameters are reduced.

For the design of reinforced soil walls, the most common used methods since middle of 1990s are stated as follows (Rowe and Ho, 1993):Bromsmethod, Murray method, Forest Service method, Collin method, TC method, Jewel method, Bonaparte *et al*.method,

Simac*et al.* method, Coherent Gravity method, Rugger method, Schmertman*et al.* method and Leschchinsky and Perry method.

The first nine methods are known as 'Tie-Back Wedge' methods while the rest are called as 'Slope Stability' methods on the basis that methods one through nine may be considered as stress methods base on lateral earth pressure whereas the remaining three employ stresses analysis on a failure surface with using the common approaches in conventional slope stability analysis.

General design guides which have been regularly used in the current practice are stated as follows:

- National Concrete Masonry Association (NCMA) design manual ,
- Federal Highway Association (FHWA) design and construction guidelines ,
- AASHTO guidelines for design,
- Eurocode7,
- Deutsches Institut für Bautechnik design method,
- British Standards Institution, BS 8006 code of practice.

3.2.1. Earth Pressure Concept

Lateral earth pressure is required to be determined for the retaining wall design. Lateral earth pressure is the pressure that is developed by the backfill. Lateral force composes of most of the forces acting on the retaining wall.

The determination of the lateral earth pressure acting against retaining wall requires knowledge of following soil parameters for the assessment of a particular wall design and its overall stability by a qualified engineer:

- soil unit weight
- angle of friction (for sands)
- cohesion and plasticity indices (for clays)
- water table location

Additional analysis with assumptions must be incorporated to support static equilibrium equations which are not enough to determine the forces and the pressures on the wall. ‘Limit-equilibrium analysis’ is an approach performed to solve equilibrium equations with the assumption that a ‘limit’ or failure state exists along some surface and shear forces acting on it corresponds to the shear strength of the material. According to the analysis, if the assumed failure does not occur as a matter of fact, then factor of safety or strength mobilization factor is applied to the material strength. Deformations have an influence of causing failure and they are not included directly in the limit equilibrium analysis.

The static gravitational pressure which exists before the earthquake motion and transient dynamic pressures that occur during the earthquake motion are included in total lateral earth pressure which affects seismic reaction of retaining walls as well (Kasay, 2007).

3.2.1.1. Static Lateral Earth Pressures.The minimum horizontal pressure condition, or active earth pressure, occurs under the conditions that a wall rotates about its base and away from the backfill an amount on the order of 0.001 to 0.003 radian(a top deflection of 0.001 to 0.003h, where h denotes the wall height). Parallel to the movement of the wall, the horizontal stresses in the soil get smaller and the vertical stresses caused by the backfill weight are handled by the increasing shear stresses until the shear pressure is imminent. When the wall is moved toward the backfill, horizontal stresses get bigger and shear stresses change direction, i.e. first they decrease and then they increase till a maximum at failure.

Since both shear stress and vertical stress components display resistance against the horizontal stress component along the shear planes, higher horizontal stresses can be created compared to those for the active pressure case. To develop the maximum possible horizontal stress, or passive pressure, it is necessary to have larger wall rotations than for the active case, as much as 0.02 to 0.2 radians.

The Rankine (1857) and Coulomb (1776) approaches on static earth pressure are greatly used in many practices.

The most common lateral earth pressure distribution for internal stability design of GRS

structures among the distributions as shown in Figure 3.9 is the classical Rankine earth pressure distribution which was proposed by Steward et al (1977). The distribution assumes a triangular shape lateral earth pressure distribution (Figure 3.9. a). Most of well-known design methods, like FHWA (Federal Highway Administration) and NCMA (National Concrete and Masonry Association) methods, still widely use the classical Rankine earth pressure distribution.

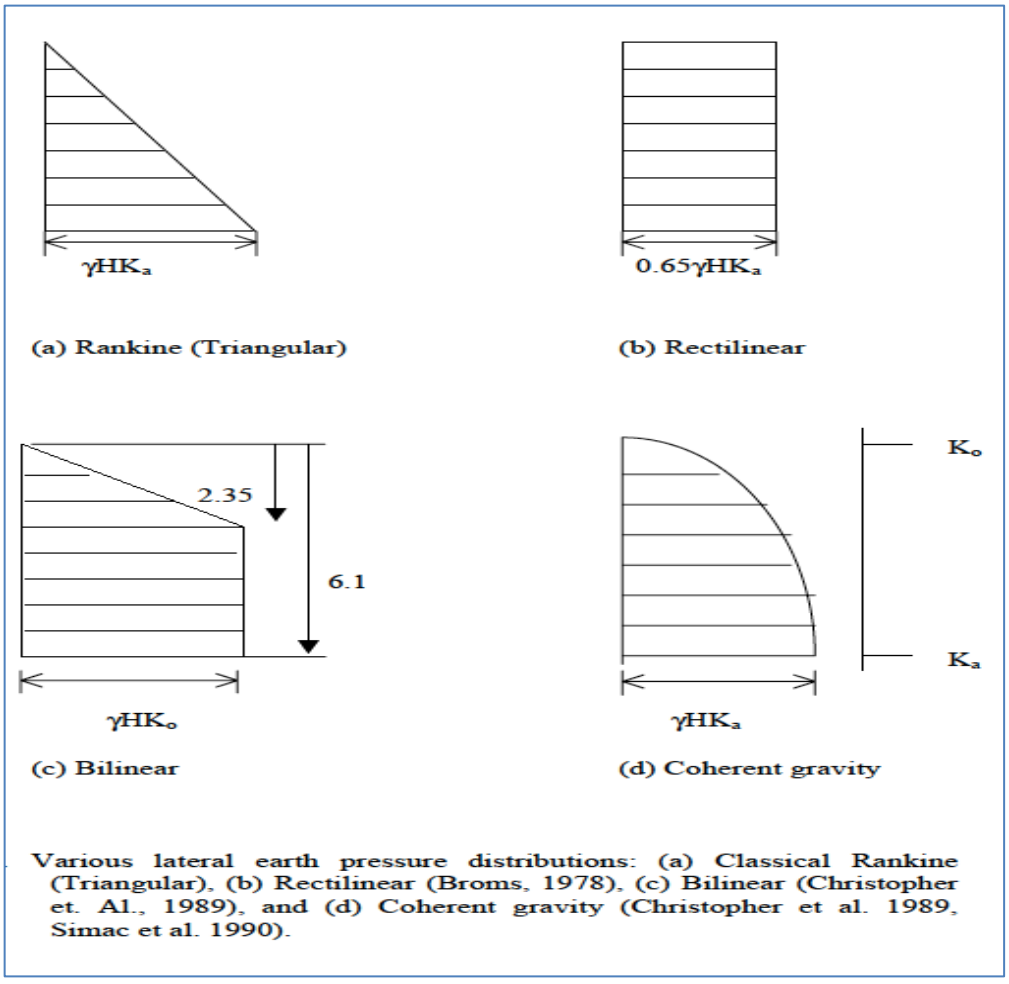


Figure 3.9. Various Lateral Earth Pressure Distrubution (Holtz, 2002)

For dry homogenous cohesionless backfill, Rankine's theory predicts a triangular active pressure distribution oriented parallel to the backfill surface (Figure 3.10). The active earth pressure resultant, PA, acts at a point located H/3 above the base of a wall of height, H, with magnitude of

$$P_A = \frac{1}{2} K_A \gamma H^2 \tag{3.2}$$

In the case of cohesionless backfill inclined at an angle β with the horizontal, infinite slope solutions can be used to compute K_A as:

$$K_A = \cos\beta \frac{\cos\beta - \sqrt{\cos^2\beta - \cos^2\phi}}{\cos\beta + \sqrt{\cos^2\beta - \cos^2\phi}} \quad \text{for } \beta \leq \phi \tag{3.3}$$

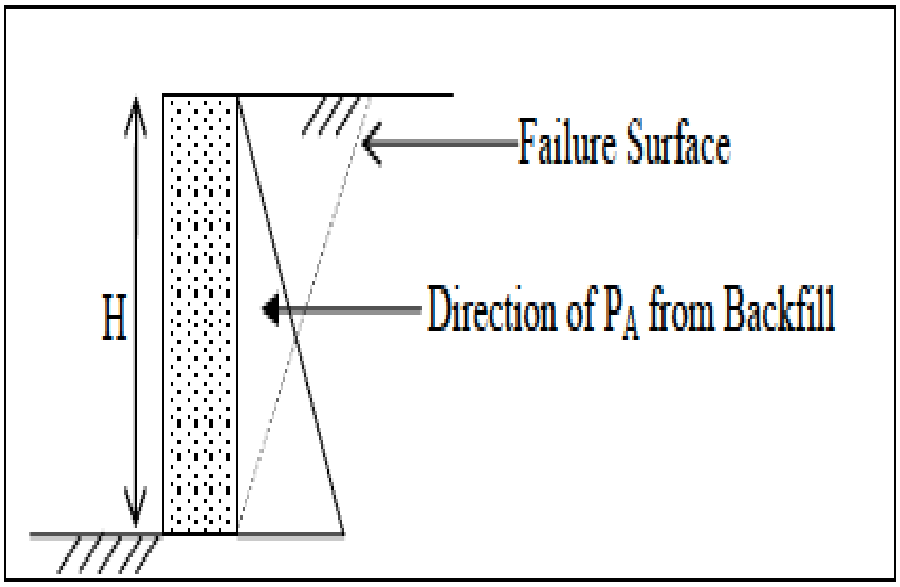


Figure 3.10.RankineActive earth pressure

The angle of the shear plane with respect to horizontal is (45 + φ/2), measured from the heel of the wall.

The Coulomb theory provides a method of analysis that gives the resultant horizontal force on a retaining system for any slope of wall, wall friction, and slope of backfill provided β≤φ. A wide range of earth pressure problems can be solved using the force polygon technique implied in Coulomb's method. The closed-form solution for the minimum active earth force for a general case including dry, cohesionless material, inclined rough wall, and sloping backfill is presented in Figure 3.11.

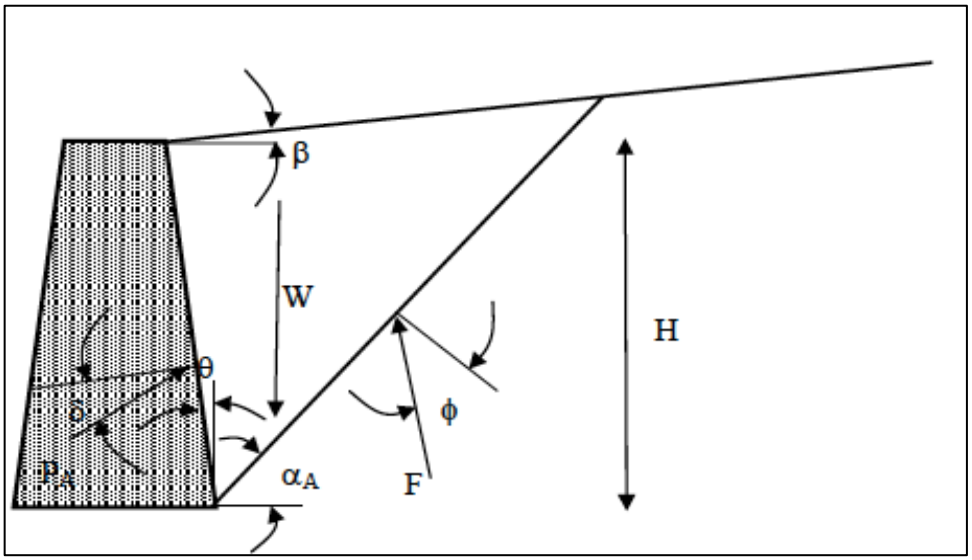


Figure 3.11. Earth pressure acting on the wall-Coulomb Approach

Under the minimum active earth pressure conditions, the active thrust on a wall with the geometry as shown in the previous Figure 3.11 is obtained from force equilibrium. For the critical failure surface, the active thrust on a wall retaining cohesionless soil can be expressed as:

$$P_A = \frac{1}{2} K_A \gamma H^2 \tag{3.4}$$

$$K_A = \frac{\cos^2(\phi - \theta)}{\cos^2\theta \cos(\delta + \theta)\left[1 + \sqrt{\frac{\sin(\delta + \phi)\sin(\phi - \beta)}{\cos(\delta + \theta)\cos(\beta - \theta)}}\right]^2} \tag{3.5}$$

in which δ is the angle of interface friction between the wall and the soil; β is the backslope angle (from horizontal) and θ is the wall inclination.

The related formulas regarding the Coulomb and Rankine can be found in Earth Pressure Theory and Application prepared by State of California Department of Transportation (1990).

In contrast to Rankine theory, Coulomb theory can be used to predict soil thrust on walls with irregular backfill slopes, concentrated loads on the backfill surface, and seepage forces. Coulomb wedge theory calculates less earth pressure than Rankine theory for a

level backslope whereas the values converge under backslope conditions when $\delta = \beta$. Coulomb theory calculates a unique failure angle for every design condition whereas application of Rankine theory to reinforced soil structures fixes the internal failure plane at $45 + \varphi/2$. If the shoring system is vertical and the backfill slope and wall friction angles are zero, Coulomb's equation will be the same as Rankine's for a level ground motion (State of California Department of Transportation, 1990).

3.2.1.2. Seismic Earth Pressures In 1929, regarding the evaluation of the active earth pressure at high seismic load levels, Mononobe and Okabe proposed a method called Mononobe-Okabe Method in which pseudo-static and limit equilibrium conditions were assumed. This approach is the most famous one to evaluate the active earth pressures and commonly used although it has some drawsbacks. Therefore the method has an important role in assessment of the peak dynamic force on a retaining wall.

There are 3 fundamental assumptions made for Mononobe-Okabe Method (M-O Method) (Steedman, 1997).

- The wall has already deformed outwards for the minimum earth pressure to be generated.
- A soil wedge, which has planar sliding surface along the base of the wall, is located on the spot of failure with amobilized maximum shear strength.
- It is supposed that accelerations are uniform along the backfill at the instant of failure since the soil located after the wall acts like a rigid substance.

The Mononobe-Okabe theory incorporates the effect of earthquakes through the use of a constant horizontal acceleration in units of g, $a_h = k_h.g$, and a constant vertical accelerationin units of g, $a_v = k_v.g$, acting on the soil mass comprising Coulomb's active wedge (or passive wedge) within the backfill as shown in Figures 3.13. The term k_h is the fraction ofhorizontal acceleration (horizontal inertial coefficient or seismic coefficient), $k_v$is the fraction of vertical acceleration (vertical inertial coefficient or seismic coefficient), and g is the acceleration of gravity.

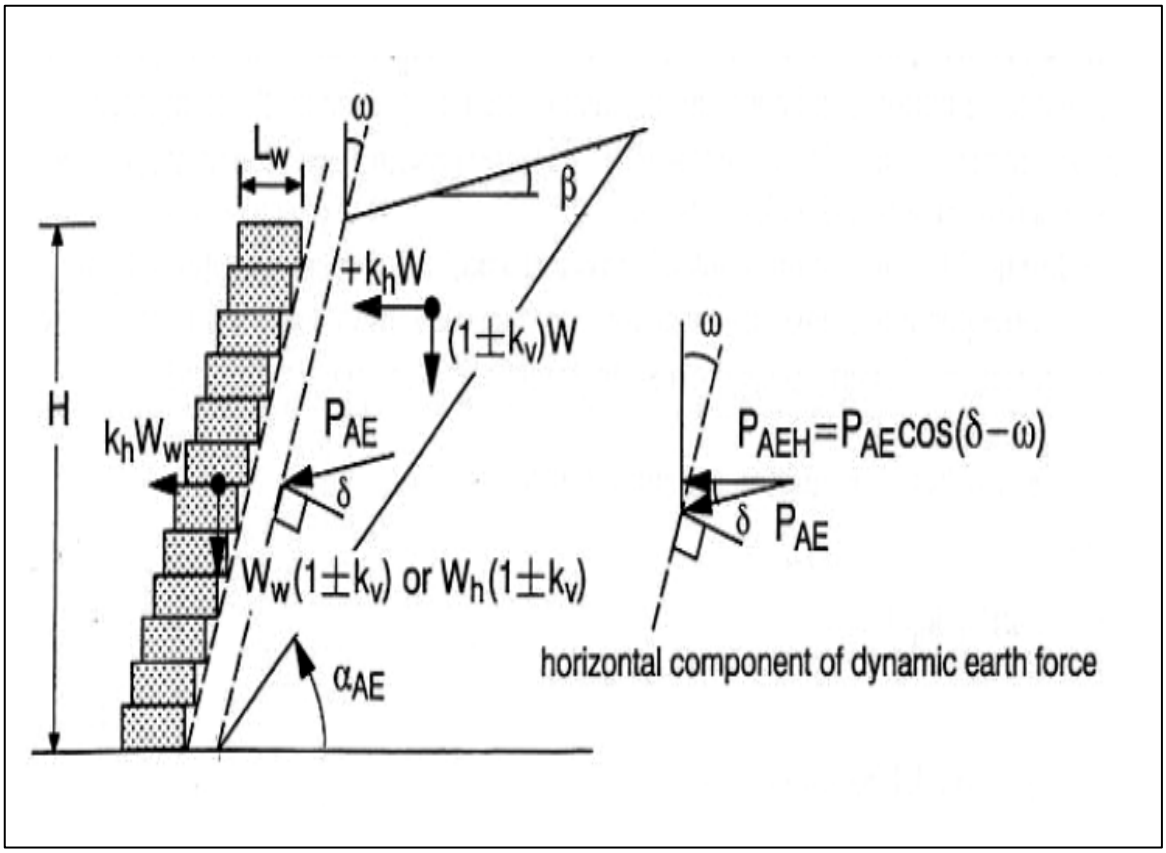


Figure 3.12.Forces and geometry used in pseudo-static seismic analysis.

In Figure 3.12, positive a_v values act downward, and positive a_h values act to the left. The acceleration of the mass in the directions of positive horizontal and positive vertical accelerations result in the inertial forces k_h.W and k_v.W as shown in the figure, where W is the weight of soil wedge. These inertial forces act opposite to the direction in which the mass is accelerating. This type of analysis is described as a pseudo static method of analysis, wherethe effect of the earthquake is modeled by an additional set of static forces, k_h.W and k_v.W.

The total dynamic active earth force, P_{AE}, imparted by dry backfill soil is calculated as (Seed and Whitman 1970):

$$P_{AE} = \frac{1}{2} K_{AE} [\gamma_t (1 - k_v)] H^2 \qquad (3.6)$$

where: γ= unit weight of the soil; and H = height of the wall. The dynamic earth pressure coefficient, K_{AE} , can be calculated as follows:

$$K_{AE} = \frac{\cos^2(\phi - \psi - \theta)}{\cos\psi \cos^2\theta \cos(\psi + \theta + \delta)\left[1 + \sqrt{\frac{\sin(\phi + \delta)\sin(\phi - \psi - \beta)}{\cos(\delta + \psi + \theta)\cos(\beta - \theta)}}\right]^2} \quad (3.7)$$

where: ϕ= peak soil friction angle; ω= total wall inclination (positive in a clockwise direction from the vertical); δ= mobilized interface friction angle assumed to act at the back of the wall; β= backslope angle (from horizontal); and Ψ= seismic inertia angle given by:

$$\psi = \tan^{-1}\left[\frac{k_h}{(1 - k_v)}\right] \quad (3.8)$$

Further details can be found inAASHTO/FHWA guidelines.The position of the dynamic earth force, P_{AE}, acting against gravity retaining walls has been shown to be variable and to depend on the magnitude of ground acceleration. A general range for the point of application of the dynamic force increment has been reported to be H = 0.4H to 0.7H above the toe of the wall (Seed and Whitman 1970). This range compares favorably to measured values of m ranging from 0.3 to 0.5 reported by Ichihara and Matsuzawa (1973) from the results of shake table tests on small-scalegravity wall models. (Ebling and Morrison 1993). The acting locations of the static active and incremental dynamic active earthpressure forces are shown in Figure 3.13.

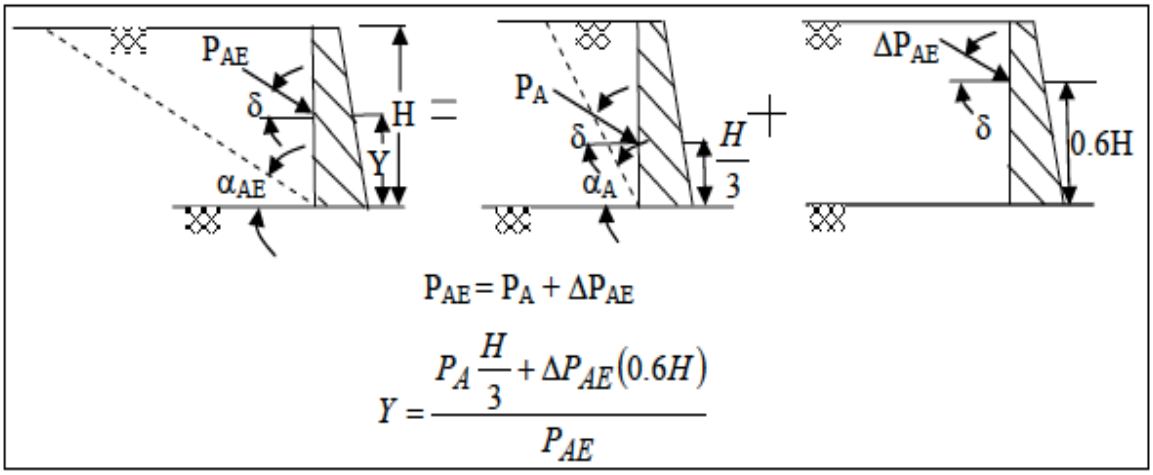


Figure 3.13. The acting locations of the static active and incremental dynamic active earthpressure forces

Current AASHTO/FHWA guidelines use an equation proposed by Segrestin and Bastick (1988) that relates k_h to a_{max}(am) according to;

$$k_h = \frac{\left(1.45 - \frac{a_{\max}}{g}\right) a_{\max}}{g} \tag{3.9}$$

where$a_{max}$is the peak base acceleration. This formula results in $k_h > a_m/g$ for $a_m < 0.45g$. Insome practices, it is also advised to take k_h= PGA/g in which PGA represents the peakground acceleration. Generally, the selection of k_h for design is based on engineeringjudgment, experience and in some instances local regulations. As the value of thehorizontal pseudo-static coefficient increases, the inclination of the failure surfacedecreases resulting smaller values of α_{AE}.

For all external and facing stability calculations for conventional SRW structures and for all external stability and internal stability for GR-SRW structures, $k_h$recommended is calculated from (NCMA):

$$k_h = \frac{PGA}{2g} \tag{3.10}$$

In this study, the criteria of the NCMA's Segmental Retaining Walls – Seismic Design Manual (1998) is used as a guide. For the seismic design of conventional gravity structures and external stability of reinforced segmental retaining walls the peak horizontal ground acceleration may be reduced by 50 per cent as recommended by AASHTO (1996) guidelines for the free-standing conventional SRW structures and reinforced SRW structures, which are typically able to tolerate lateral deformations of this magnitude provided they are not seated on piles and/or constrained from moving laterally by connected structures. Hence, using the AASHTO approach, the horizontal seismic coefficient for all external stability and internal sliding stability calculations for GR-SRW structures (NCMA) is estimated according to Equation 3.10, $k_{h(ext)}$ = PGA/2.

3.2.2. Seismic Design of Segmental Retaining Walls

Herein, a method of analysis and design for conventional and geosynthetic-reinforced segmental retaining walls (GRSRWs) under seismic loading shall be described briefly. The methodology extends the approach for structures under static loading to simple structures that may be required to resist additional dynamic loads due to earthquakes. The seismic design method described briefly her can be found in detail in NCMA Seismic Design Manual for Segmental Retaining Walls (1998) which adopts a pseudo-static approach and uses the Mononobe-Okabe (M-O) method to calculate dynamic earth forces. The methodology adopts many of the recommendations contained in AASHTO (2002) / FHWA (2001) guidelines for the design and analysis of mechanically stabilized earth (MSE) structures subjected to earthquake loads. However, the NCMA *Design Manual* goes beyond the AASHTO/ FHWA publications by addressing the unique stability requirements of SRWs that are constructed with a dry-stacked column of modular block units.

Seismic or dynamic load induced properly designed reinforced GRSRW will in general perform well due to their flexible nature and enhanced ductility. When an GRSRW requires seismic analysis, that evaluation should be performed in addition to the static analysis to satisfy all static and seismic safety factors (NCMA TEK, 2010).

3.2.2.1. Assumptions for the Seismic Design. The NCMA seismic design can be applied only when the following criteria are followed:

- SRW structures are free-standing and able to displace horizontally at the base and yield laterally through the height of the wall.
- Reinforced and retained soils are cohesionless, unsaturated, and homogeneous. Soil strength is described by the Mohr- Coulomb failure criterion. The apparent cohesive strength component reported under Mohr-Coulomb failure criterion is ignored for conservatism.
- Vertical ground acceleration is zero (kv= 0).
- Geometry is limited to infinite or broken-backslope, and constant horizontal slope angle.

- Live surcharges are ignored at the top of the soil surface behind the facing column given their transient nature.
- Retained and reinforced soils are placed to a depth corresponding to the full height of the SRW facing units
- Cap units are ignored in the stability analysis and assumed to be securely attached such that they cannot be dislodged during ground shaking.
- The stabilizing influence of the wall embedment is ignored with the exception of bearing capacity analyses.
- No permanent surcharge or footing load exists within the active failure wedge.
- Global stability involving failure of soil volumes beyond the base of the SRW unit column and/or geosynthetic reinforced fill zone is not considered.
- SRW structures are built on competent foundations for which excessive settlement, squeezing or liquefaction are not potential sources of instability (NCMA TEK, 2010).

In cases where Mononobe-Okabe formulation leads to unrealistic results, it is suggested that numerical procedures using the same principles are of Mononbe-Okabe formulation be utilized. These include the Culmann method, Coulomb's trial wedge method, or limit equilibrium slope stability programs that are outside of the scope of NCMA Design Manual.

3.2.2.2. Modes of Failure of GRS-RWsStability analyses for GRSRW systems under static and seismic loading conditions involve separate calculations to establish factors of safety against external, internal, facing and internal compound modes of failure (Figure 3.14).

Minimum recommended factors of safety (FS) of static and seismic design of geosynthetic reinforced SRW structures are given in Table 3.1. In general, Factor of safety for seismic design are taken as 75% of the values recommended for statically loaded structures following AASHTO / FHWA practice.

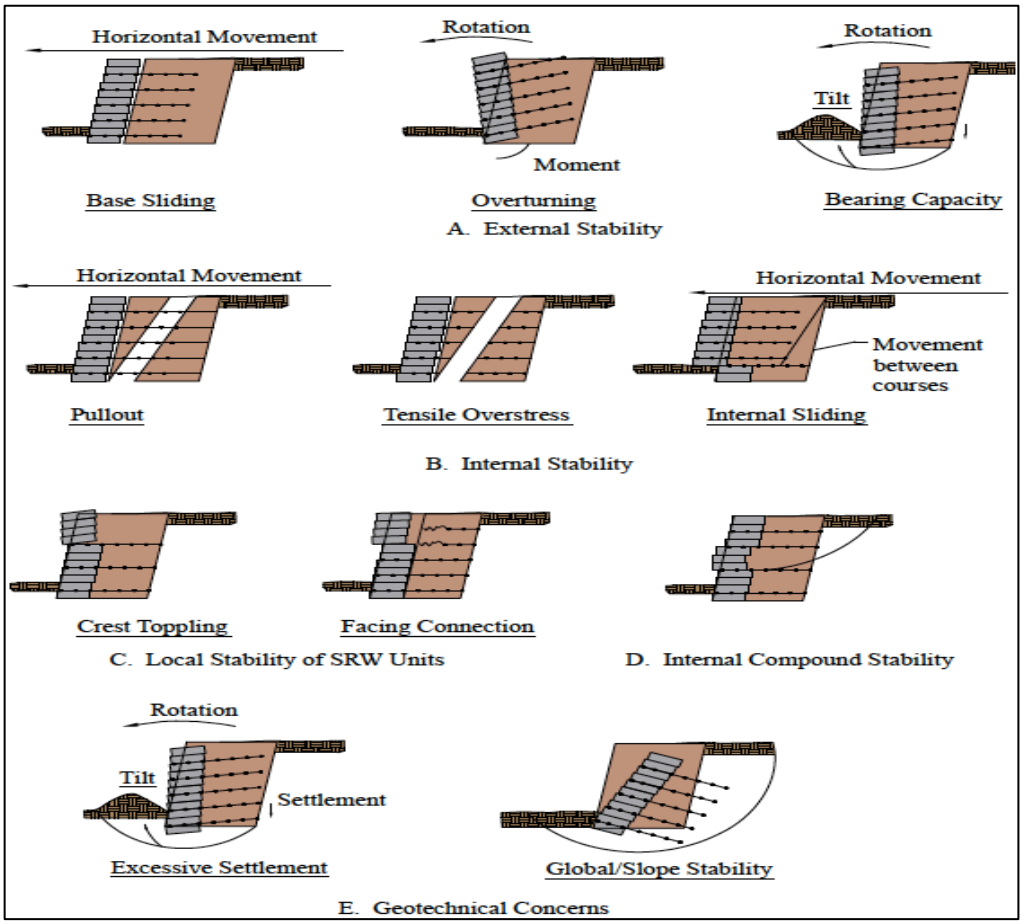


Figure 3.14. Modes of failure for reinforced SRW structures (NCMA TEK, 2010)

Table 3.1. Recommended minimum factors of safety for design of GRS-RW Structures (NCMA TEK, 2010)

Failure Modes: Wall Design	Static	Seismic
Base sliding, FS_{sl}	1.5	1.1
Overturning, FS_{ot}	1.5/2.0	1.1/1.5
Internal sliding, $FS_{sc}/FS_{sl(i)}$	1.5	1.1
Tensile overstress, FS_{to}	1.5	1.1
Pullout, FS_{po}	1.5	1.1
Connection, FS_{cs}	1.5	1.1
Internal compound stability, F_{com}	1.3	1.1
Failure Modes: Geotechnical Concerns	**Static**	**Seismic**
Bearing capacity, FS_{bc}	2.0	1.5
Global stability, FS_{gl}	1.3—1.5	1.1

In this study for the experimented retaining wall, base sliding, internal sliding and column shear failure mechanisms, which are the most governing modes corresponding to external, internal and facing types respectively, are presented briefly.

3.2.2.3. Internal Stability. Different from the conventional system in which backfill soil properties are the major internal stability design concern, the reinforced soil system has a much more complicated internal stability design. Internal stability design of the reinforced soil retaining structure involves consideration of:

- The strength properties of backfill and reinforcement material,
- The reinforcement arrangement,
- Interaction between soil and reinforcement,
- Interaction between facing element and soil,
- Durability of the reinforcement, and
- Connection between facing units and reinforcement (especially for systems with segmental facing structures).

Internal stability is calculated for the integrity of reinforced zone as a monolithic composite including geosynthetic reinforcement, soil and facing units. Coulomb lateral earth pressure theory is used for calculation of tensile forces which are to be withstood by horizontal reinforcement. Figure 3.14 shows tensile overstress, pullout and internal sliding failures which are considered separately. Also, these 3 modes of failure are independent of the properties of facing units and the connection between the geosynthetic and facing units. NCMA Manual consists of whole design procedure for internal stability (NCMA, 1998).

The contributory area approach used for the static stability analysis of SRWs is extended to the dynamic loading case (Figure 3.15). In this method, the reinforcement layers are modeled as tie-backs with the tensile force *Fi* in layer *n* equal to the earth pressure integrated over the contributory area *Ac(n)* at the back of the facing column plus the corresponding wall inertial force increment.

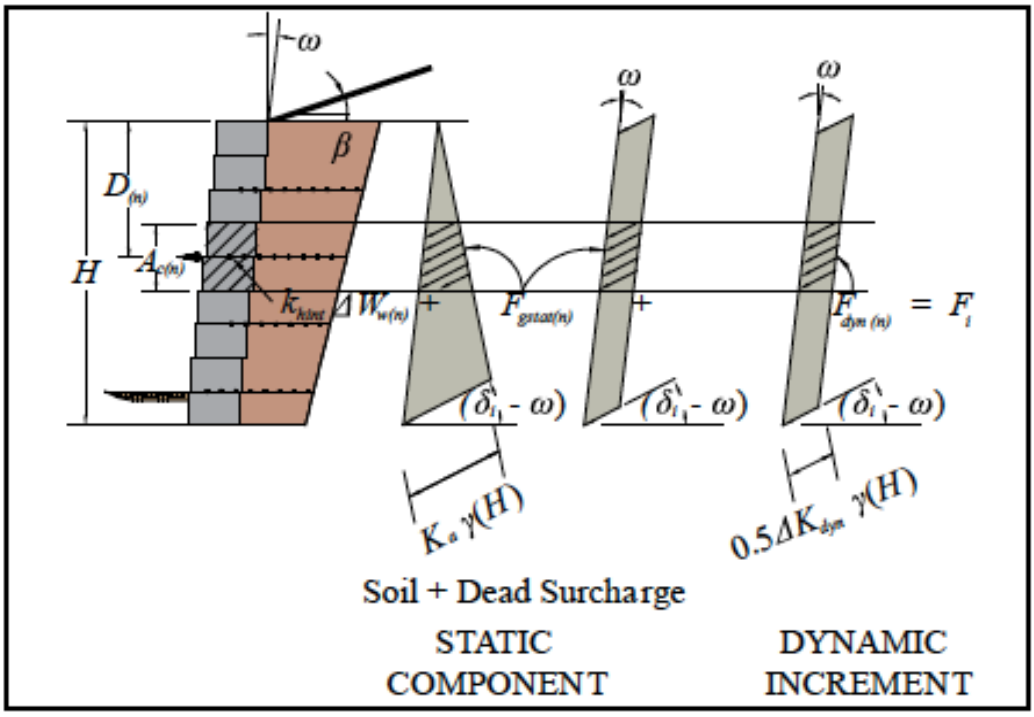


Figure 3.15.Geometry & Forces Used to Calculate Reinforcement Loads for Reinforced SRW Structures (NCMA TEK, 2010)

For internal stability calculations, each reinforcement layer is required to carry the part of the assumed internal pressure distribution applied to the area S_v in Figure 3.16. Tensile strength, facing connection strength and pullout capacity of the reinforcement layer should be adequate. Various methods used are presented in Figures 3.17 to 3.18.

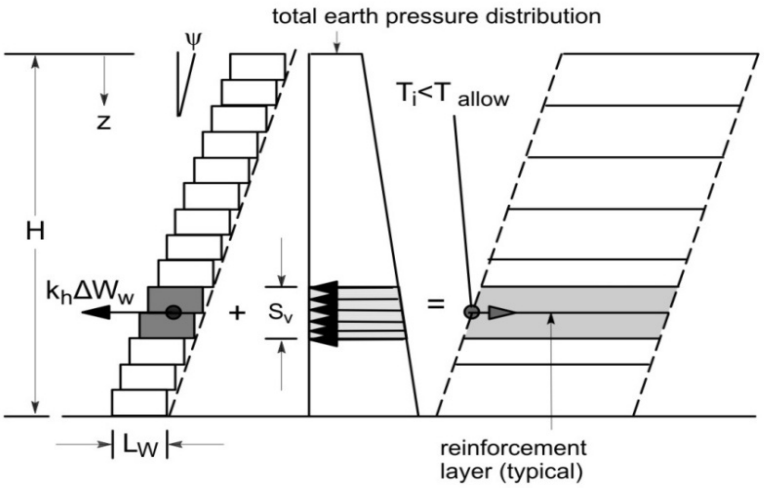


Figure 3.16. Reinforcement tensile load calculation using Bathurst and Cai method (Bathurst and Alfaro, 1997)

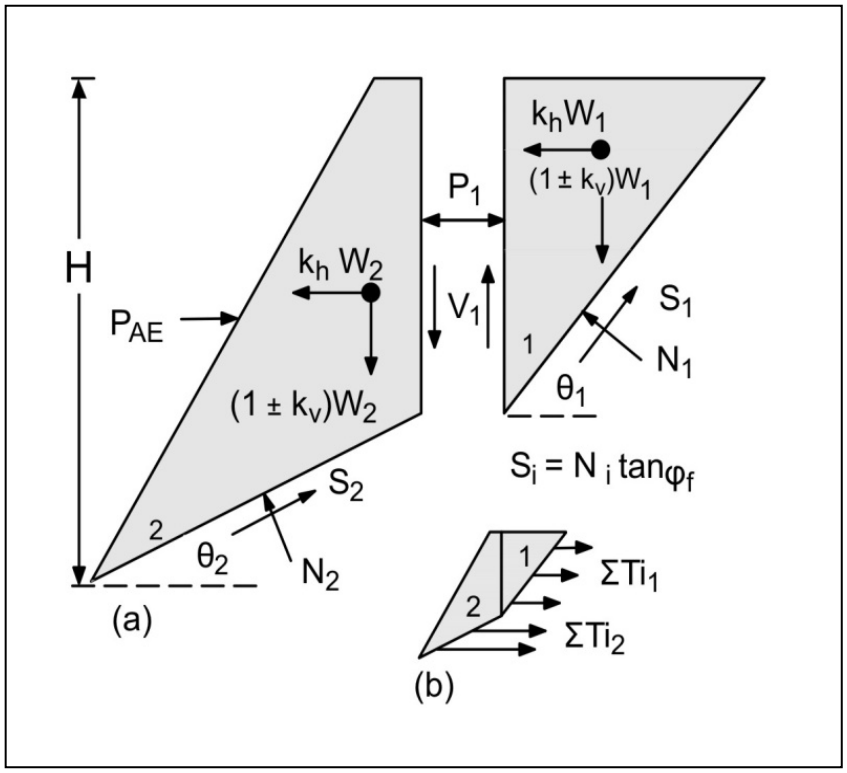


Figure 3.17. Two-part wedge analysis: (a) free-body diagram (b) with reinforcement forces (Bathurst and Alfaro, 1997)

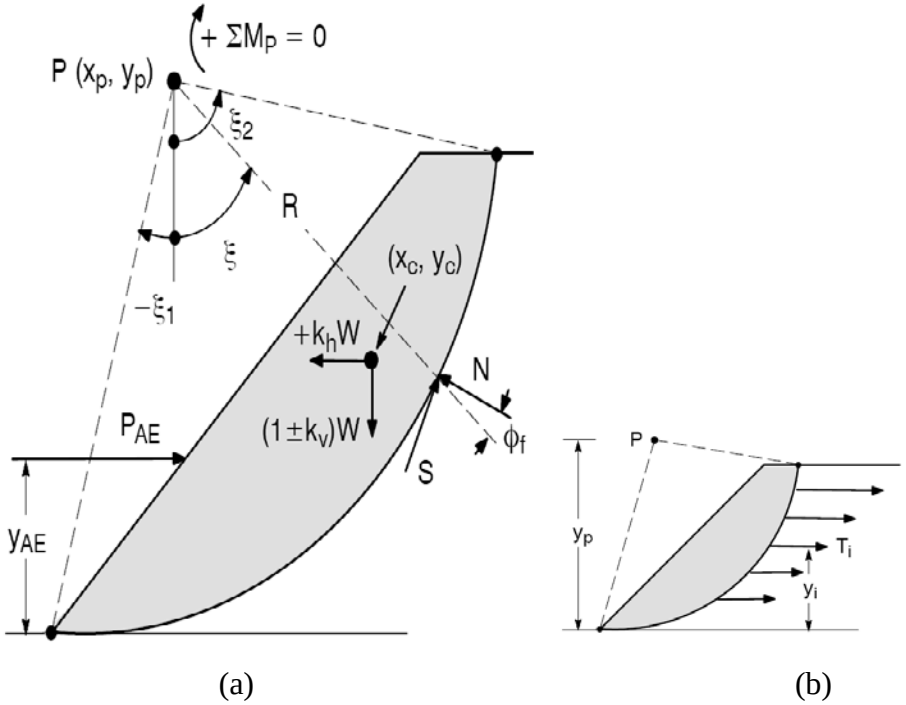


Figure 3.18. Log-spiral analysis: (a) free-body diagram (b) with reinforcement forces (Bathurst and Alfaro, 1997)

3.2.2.4. External Stability.All reinforced soil retaining walls, whether reinforced by steel or geosynthetics, have the same external stability concerns as conventional retaining structures.

External stability design of retaining structures basically includes analyses of:

- Friction between retaining structures and foundation soil--possibility of base slidingfailure,
- Bearing capacity of foundation soil and creep of the foundation soil--possibility ofoverturning, and excessive settlement, and
- Overall slope stability

External stability calculations are similar to those for conventional static conditions, with the addition of the inertial force due to wall weight and the dynamic earth increment. Dynamic earth pressure, shown in Figure 3.19, is used to calculate the destabilizing forces in otherwise conventional expressions for the factor of safety against sliding along the foundation surface, overturning about the toe, and bearing capacity failure of the foundations soils. By convention, only half of the dynamic earth force increment is applied when calculating external seismic forces on conventional and reinforced SRWs.

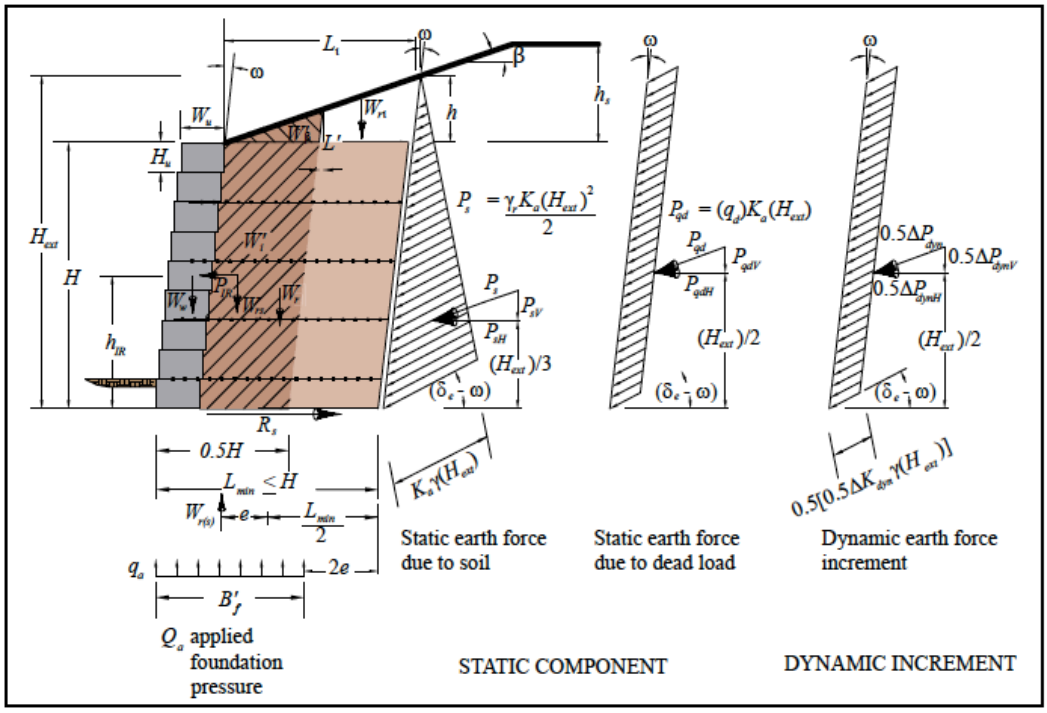


Figure 3.19. External Stability Calculation Variable for GRS-RWs (NCMA TEK, 2010)

3.2.2.5. Seismic Stability.Important public concerns were demonstrated by seismic stability and the performance of reinforced soil structures following the disastrous failuresof major civil engineering structures in recent earthquakes of which the 1994 Northridge earthquake in California and the 1995 Kobe earthquake in Japan can be given as two examples. This concern, when combined with the broadening applications of geosynthetics in permanent and important structures, results in the need of some design procedures which may guarantee stability or tolerable displacement under seismic loading. In other words, even if the reinforced soil structure survives an earthquake, the induced permanent displacement should stay below a serviceable limit. Regarding metal strip reinforced soil structures, Richardson & Lee (1975) proposed the first seismic design procedure based on M-O Method (Mononobe, 1926; Okabe, 1926). With taking pull-out failure, but not external stability, into consideration, the total reinforcement length was defined same as static design. Parallel with the theoretical study, small-scale shaking table test series were conducted. Also, this approach is extended with the seismic design procedure which was proposed by Bathurst &Cai (1995) so that planar reinforcement is involved. Also, the seismic design procedure can be found in FHWA Manual (Christopher *et al.*, 1990). These design procedures address stability whereas permanent displacements are not addressed. A pseudo-static limit equilibrium approach was proposed to design reinforced slopes (Bonaparte *et al.* , 1986) Two part wedge mechanism was used to assess internal stability (Jewell et al 1984) while the external stability was examined through direct sliding analysis. Several design charts show necessary properties of geosynthetics for the resistance of these failure modes; such as length and strength. Also, permanent displacement is not taken into account in this approach. Shaking table tests and pseudo – static limit equilibrium analysis were used for the seismic studies on reinforced soil structures that were widely managed in Japan. (e.g. Koga &Washida, 1992; Murata *et al.*, 1994; Yamanouchi & Fukuda, 1993).For design of highway and railway dikes in Japan, procedures are recently used and they are developed by two main Japanese agencies called ‘the Japan Railway Technical Research Institute’ and ‘Public Works Research Institute’. In these procedures, two different methodologies were used for designing reinforced slopes and walls. The design procedures for walls can be counted as an extension of two part wedge mechanism which was used in static analysis conducted by Jewell et al in 1984. (Ling *et al.*, 2005).

3.2.2.6. Facing Stability. Facing stability calculations are similar to those used for the static analysis with the addition of the dynamic load. To evaluate the connection strength, the connection capacity at each reinforcement elevation is compared to the tensile force *Fi* already determined. The crest toppling is evaluated, determining the static, inertial and dynamic forces acting on the unreinforced top blocks. Only half of the dynamic load $\Delta P_{dyn}$is used to mirror the external overturning analysis. Interface shear and connection failure are the two governing criteria for the facing design and more information can be found in NCMA design manual.

3.2.3. Retained Soil

Soil retaining walls require high quality backfill in terms of durability, drainage and friction including. In order to avoid pore pressures and cohesive bond effects, free draining and non-plastic backfill is generally used as the backfill.

When cohesive soil is used as backfill material, it should be ascertained that it is possible to determine the pore water pressures and soil-reinforcing bond strength. Density and angle of friction of the backfill are important where they depend on type and density of the soil to a great degree.

The ranking of numerous retained soils for permanent walls using the Unified Soil Classification is SW, SP, GW, GP and any of these as a borderline classification that is dual designated with GM or SM. there is a limitation of 12% passing sieve No.200 for the fines in the soil. This limitation guarantees that seeping water washes the possible migration of fines and that the geotextile sheets traps it, as well as that the creation of permeability liners is prevented. In general, the permeability of the retained soil should be greater than 10^{-3} cm/sec. Since the utilization of Gravel requires special attention, it is not preferred much although it is highly permeable and strong. Particularly in the cases that the gravel has angular edges, it might be dangerous for the rupture of the geotextile sheets during construction. GP and GW can be preferred over SP and SW when the puncture resistanceof the geotextile is high. Plasticity index (PI) should be smaller than or equal to six. Also, there should not be any shale, soft and organic matter or other harmful

substances in the soil, since these materials enhance corrosion and cause excessive settlement [RSS-U.S. Department of Transportation, 1990).

Deformations within the reinforced and unreinforced zone and also movements due to the construction and foundation cause horizontal soil movement s whose magnitude varies with some parameters stated as follows: compaction effort, reinforcement extensibility, reinforcement density (horizontal and vertical spacing), reinforcement length, facing type, reinforcement facing connection details, strength and deformation characteristics of both backfill and foundation soil, surcharge intensity location of strip surcharge loading and construction practice (Rowe and Ho, 1993).

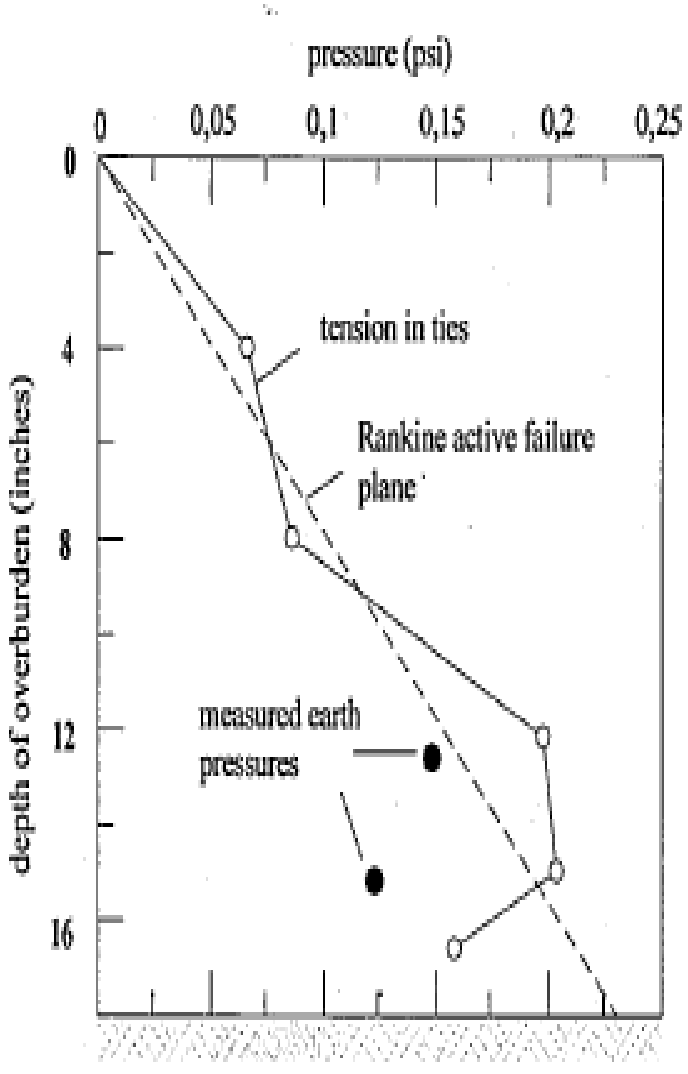


Figure 3.20. Typical Examples of Measured lateral Earth Pressures and Tensions in ties just prior to wall failure (Lee *et al.*, 1973)

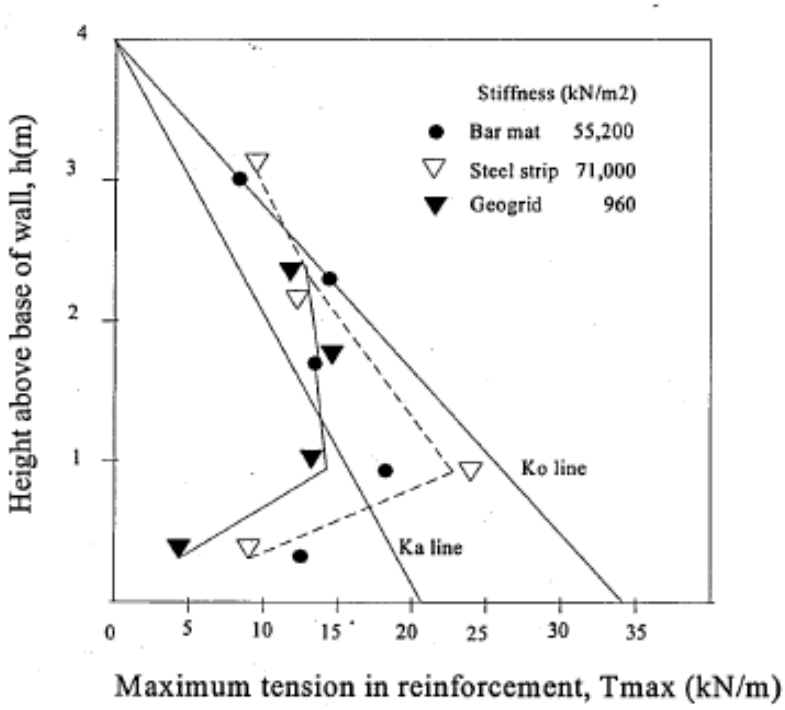


Figure 3.21. Effect of reinforcement stiffness on tension in reinforcement (Rowe and Ho, 1993)

Horizontal movements, which generally come from the active zone (area OAB) as shown in Figure 3.22, can be determined by finding total magnitude of strains along the reinforcement layers (if strain compatibility between the soil and reinforcement is maintained and reinforcement is attached to the facing). Area OBCE: is called transition zone which has less movement. Line OD is a line called zero force line that originates from toe inclined at angle Ø to the horizontal. Under the OD line, only less movement can be expected (Rowe and Ho, 1993).

Soil movement within the reinforcement zone is controlled by some parameters of the reinforcement and the fill such as reinforcement density and stiffness, and shear strength of the fill.As the reinforcement stiffness and reinforcement density get higher the strain in the soil is reduced, and as the shear strength of fill gets larger the force in the reinforcement that is needed to maintain equilibrium gets less, which results in less deformation. The reduction in the deformation of the reinforced zone, which is caused by the increase in the shear strength of the fill, also results in a reduction in horizontal movement. The amount of horizontal deformation caused by the construction depends on three criteria, namely the compaction effort, the connection between the facing panels and

whether there is any local temporary support provided during the construction of the layer of interest. In the generation of horizontal movement, strength and stiffness of the foundation have important role. When these parameters are below the desired values, it is suitable to provide higher stiffness reinforcement close to the base or to increase the density of the reinforcement (Rowe and Ho, 1993).

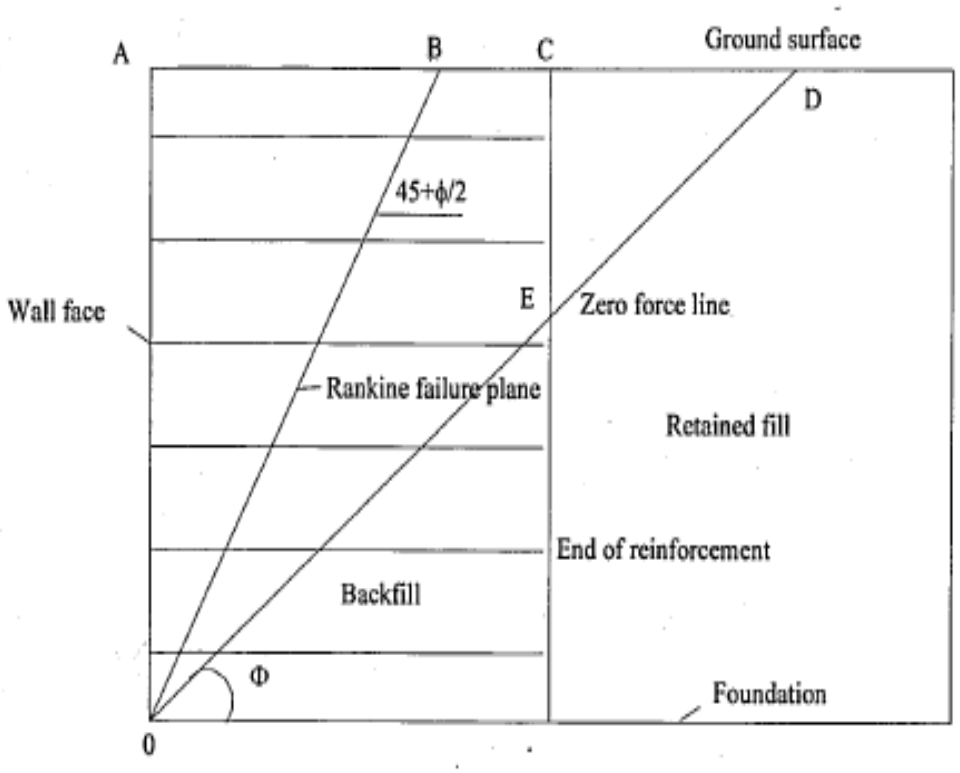


Figure 3.22. Sources of horizontal deformations in reinforced soil (Rowe and Hoe, 1993)

3.2.4. Facing Design

The facing design of a reinforced soil retaining wall is the only visible part of the structure that it controls the aesthetics of the wall with providing various colors and finishing. Additionally, it protects the structure against erosion and backfill sloughing and provides drainage paths.

Some of facing types that affect settlement tolerancesare stated as; segmental precast concrete panels, cast in place concrete panels, shotcrete or full-height precast panels, metallic facings, welded wire grids, fabric facings, plastic grids, gabion facings, post-construction facing. Some of these facing types can be seen in Figure 3.23. (Tatsuoka,

1993). In this study precast concrete facing elements are utilized in construction of geogrid reinforced retaining walls.

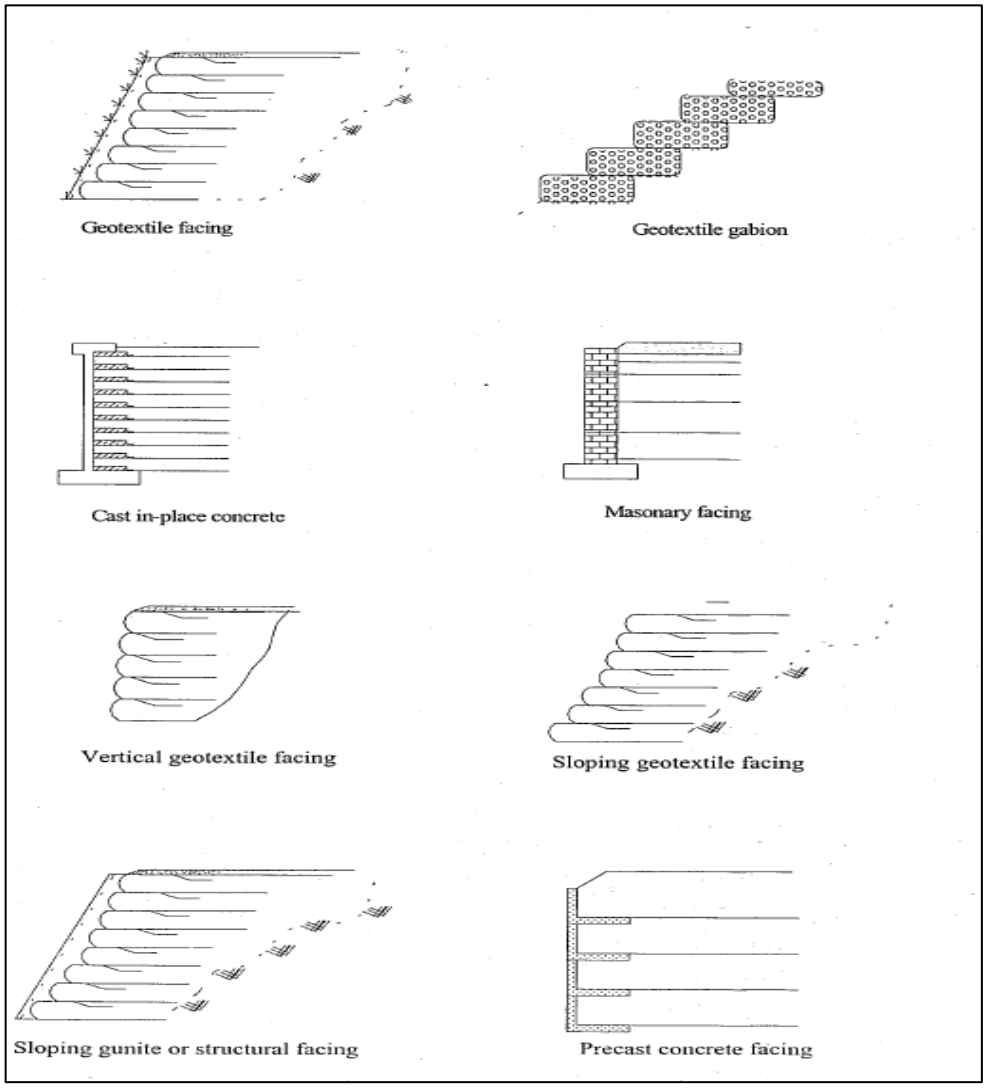


Figure 3.23. Facing Types of a reinforced soil wall

One of the most commonly preferred types of facing is segmental wall systems using dry-stacked columns of interlocking modular concrete units, which first appeared in the mid 80's in North America. In the construction of the segmental retaining walls no mortar or concrete footings are used. Rather, the retaining walls are just stacked on a shallow, granular leveling pad, which creates walls that are easy and economical to install. The walls have structural stability however they still keep the flexibility to tolerate minor earth movement without damage. Generally the performance of the geosynthetic-reinforced segmental retaining walls was good in different seismic events both in United States and

Japan. According to a survey conducted by Sandri in 1994, only two of the 11 structures that fall within the 23-113 km of the epicenter had tension cracks within and behind the reinforced soil mass following the Northridge earthquake, which had a moment magnitude if 6.7. Even though peak horizontal accelerations as great as 0.5g were estimated on site, facing of the walls were intact (Barthaust and Simac, 1994).

Variable batter (wall tiltback) is permitted by some segmental systems that batter of the facing into the fill can be increased in direct proportion to the height of the wall. Ratios of batter vary from one in six to one in ten typically.

3.3. Physical Model Tests of GRS-RWs in Literature

In order to find out how GRS structures behavein seismic motions, physical model tests have been carried out. It is possible to execute the seismic model tests by using either laboratory shaking tables or dynamic centrifuges. Full-scale model is preferred over the reduced-scale model, since the full-scale model is not associated with problems such as similitude and boundary effects often encountered in reduced-scale model and in centrifuge testing. Bathurst *et al.* (2002), Nova-Roessig and Sitar (2006), and Sabermahani et al (2009) reported the reviews of the physical model tests. According to the model tests, there are two important conclusions:

- Horizontal displacement of segmental block facing wall can greatly be reduced by implementing wall batter to 8° from vertical (Bathurst et al, 2002).

- Model tests have also revealed that seismic deformation is inversely proportional to the initial relative density of backfill while acceleration amplification is directly proportional to it. In other words, as the relative density increases, acceleration amplification increases but seismic deformation decreases.

Regarding the effects of input wave form, the researches condcted by Koseki et al (2003) show the comparison of the observed critical seismic coefficients against overturning with using the irregular input motion and sinusoidal input motion. According to the study, the coefficient with a sinusoidal input motion is less than the one with using

the irregular input motion, where a sinusoidal input wave is more destructive than an irregular input motion which was stated differently in this research.

El- Emam and Bathurst (2005, 2007) found (the experiments conducted on shaking table) that wall facing displacement varies based on properties of reinforcement and mass of facing panel. The results of the experiments show that increasing length, quantity and stiffness of reinforcement with decreasing mass of facing panel cause a decrease in wall facing displacement. According to studies of Sabermahani *et al.* (2009) on GRS wall, the controlling parameter in seismic deformation is the reinforcement stiffness rather than reinforcement ultimate tensile strength. Zarnani and Bathurst (2007) also found from another shaking table tests that geofam panel application behind the wall could reduce the dynamic earth loads.

3.3.1. Dynamic Centrifuge Tests

To maintain similitude between prototypes and small models many (but not all) of the difficulties associated with scaling can be avoided if the stresses at corresponding points in the model and the prototype are the same. One way that this can be achieved is by using a geotechnical centrifuge to increase the local equivalent gravitational field in order to balance the decrease in stresses that would otherwise result from the chosen linear scale.

In a centrifuge device, soil models placed at the end of a centrifuge arm, which is located at a distance r from the axis of the centrifuge, can be rotated at a rotational speed, $\omega = \sqrt{ng/r}$, so that they are subjected to an inertial radial acceleration field, which, as far as the model is concerned, feels like a gravitational acceleration field but N times stronger than Earth's gravity. Soil held in a model container has a free unstressed surface and within the soil body the magnitude of stress increases with depth at a rate related to the soil density and the strength of the acceleration field. If the same soil is used in the model as in the prototype and if a careful model preparation procedure is adopted whereby the model is subjected to a similar stress history ensuring that the packing of the soil particles is replicated, then for the centrifuge model subjected to an inertial acceleration field of n times Earth's gravity the vertical stress at depth $h_m$will be identical to that in the

corresponding prototype at depth hp where $h_p = nh_m$. This is the basic scaling law of centrifuge modeling, that stress similarity is achieved at homologous points by accelerating a model of scale *n* to *n* times Earth's gravity.

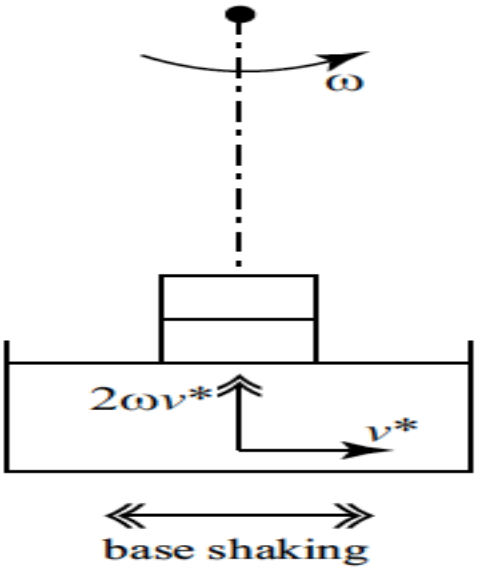


Figure 3.24.Modeling of Centrifuge (Muir, 2004)

A shaking table can be placed on the end of the arm while the centrifuge is spinning, which can send pressure and shear waves up through the model on the shaking table. This creates the same effect as the waves generated up through the soil during a real earthquake. Using this procedure both the static and dynamic behavior of the reinforced soil structures can be investigated. (Kasay, 2007)

It has been proven that the centrifugal modeling technique is greatly useful for the simulation of the stress level with using reduced scale models. If the acceleration is increased by 'n' times the gravity, the stress-strain behavior of the centrifuge model, whose dimension is n times smaller than prototype, is preserved based on the scaling rules. While the time is decreased by n times, the frequency has to be increased by n times for dynamic events in a centrifuge. Several researchers have performed tests and reports the applications of centrifugal modeling techniques to reinforced soil retaining walls and slopes. However, static conditions restrict the tests.For the analysis of the behavior of Geosynthetic Reinforced Soil Retaining Wall, Ling *et al.* (2004) conducted centrifuge tests in which dynamic finite element procedure is used together with an advanced generalized plasticity soil model and bounding surface geosynthetic model. The first analysis of the

construction behavior of a full-scale wall was conducted after conducting 5 shaking table tests in a centrifuge. The parameters for the sandy backfill soil are marked so that they can be read in the desired units in the results of monotonic and cyclic tests. The presented results are wall facing deformations strains in the geogrid reinforcement layers, lateral earth pressures acting at the facing blocks, and vertical stresses at the foundation.

The results of the centrifugal shaking table tests are compared with below items:

- The response of the walls subject to 20 cycles of sinusoidal wave having a frequency of 2 Hz and of acceleration amplitude of 0.2.
- The acceleration in the backfill,
- Strain in the geogrid layers,
- Facing deformation

As a conclusion, the results of the study are given as:

- The finite element procedure could simulate the construction behavior like dynamic behavior according to the comparison of numerical and experimental results. Therefore, the results show that geosynthetic model and the generalized plasticity model for granular soil were appropriate to describe the monotonic and cyclic behaviors of soil and reinforcement, especially under cyclic loading.
- It is also confirmed during the analysis that reinforcement length and spacing are important parameters to make wall deformations and strains in the reinforcements smaller.
- The effect of the reinforcement layout to the amplification of acceleration was around 1.5 for the 7.5 m height of the wall which seems to be very small (Ling et al, 2004).

3.3.2. Shaking Table Tests On Grs-Rws

Model tests are especially important when the prototype behavior is complicated and not easily understandable. Model tests are executed on a small-scale representation of the prototype system where the boundary conditions are replicated. By the help of this setup,

the model tests are employed to learn more about the effects of various parameters and processes that lead to the failure of prototype at a real time.

It is possible to distinguish to categories of model tests, namely model tests performed under gravitational field of earth (generally called shaking table tests) and model tests performed underhigher gravitational field (centrifuge tests). Both categories have certain benefits and restrictions. The advantages of shaking table tests can be listed as the well-controlled large amplitude, multi-axis input motions and easier experimental measurements. Therefore it is beneficial to use the shaking table tests if the goal is to understand the basic failure mechanisms or to validate the numerical model.

The necessary system for reproducing actual earthquake data is a six degree of freedom shaking table which is very expensive and complicated electro-hydraulic system and needs high maintenance and operational costs. However, when the response and failure mechanism of earth structures such as embankment, retaining wall, quay wall are considered as important, the adequate one is single horizontal translational degree of freedom shaking table. (Prasad*et al.*,2004)

Ling reported review of several significant shaking table tests (Ling *et al.*2003) Richardson led the way of performing small scale and full-scale shaking table tests on RE walls with using metallic reinforcement (Richardson and Lee 1975; Richardson *et al.* 1977) Additionally, Futaki have tested 6 m high RE wall and 5m high multi anchor earth wall in Japan. (Futaki et al 1996, Futaki et al 2001) The literature includes the reports of the results of these various smallscale shaking table tests on GRS walls. The main country for these tests was generally Japan due to the availability of test facilities and requirements of earthquake – resistant design. Two main Japanese agencies, Japan Railway ~JR! Technical Research Institute (Murata *et al.* 1994) and Public Works Research Institute (Matsuo *et al.* 1998) conducted a series of the most notable model tests to establish design specifications with 2.5 m and 1m high, respectively. However, the results were deviated by especially 1m high wall unless modeling of the soil was appropriate. In the JR Wall, a geogrid that had strength of one-third of the prototype was used and the tested walls which are of back-to-back type had a rigid full-height facing, which is to say a tall embankment supported on either side by a wall. The reinforcement had a length of 40% of the wall

height and similar to field construction a couple of layers were tied to the wall on the opposite side. Shaking applied on the wall by the use of both sinusoidal waves and real earthquake motions. The results obtained in the study were use to verify limit design procedures.

After the 1995 Kobe earthquake an additional study was conducted on the same class of soils by Koseki *et al.* (2003). Several small shaking table tests (~1 m high, 2.4 m long, 1.4 m wide and acted as models of a 6 m full-scale wall) were conducted on MB–GRS walls in Canada, for which the study of Bathurst *et al.* (1997, 2002) can be given as examples. Concrete blocks with dimensions 100 mm by 160 mm by 34 mm were employed as facing and the walls were externally supported during construction. The block-geogrid interface was frictional while the connection between the blocks was either frictional or fixed. The input acceleration was increased gradually by using a frequency of 5 Hz until it was about 0.35*g*.

The following conclusion can be derived from the reported performance of RE walls. Amplitudes of lateral displacement which are greater than 50mm, corresponding to an earthquake with horizontal acceleration of 0.4 *g*, are excessive for civil engineering practices. It may create consequences such as dislocating a bridge deck resting directly on the reinforce soil.

It is noteworthy to mention that the results obtained from metallic reinforcements may not be valid for reinforcement such as MB–GRS walls, where the wall facing improves the performance in terms of deformation and acceleration response.

It has been reported that a rigid facing JR wall with geogrid reinforcement had better performance compared to that having discrete wall panels. This is due to the fact that the JR wall utilized geosynthetic reinforcement, its full-height cast-in-place concrete facing made it a rigid system that is different from MB–GRS walls. (Ling, 2003)

Few studies have been conducted to investigate the influence length, stiffness and number of layers (i.e. vertical distance between layers) on the response of reinforced soil walls to earthquake loading. The study of Bathurst and Hatami (1998) has shown that the

magnitude of the wall lateral displacement and the magnitude and distribution of reinforcement loads under both static and dynamic loading conditions is highly dependent on the length, stiffness and number of reinforcement layers.

Following the study of Sakaguchi*et al.* (1992) where they carried out reduced-scale shaking table tests on 1.5 m-high reinforced soil models with wrapped-face and lightweight modular block configurations, it was understood that the maximum lateral wall displacement decreased by increasing the number of reinforcement layers. Sinusoidal loading were used to excite the model walls (similar to the accelerogram used in the current study) with accelerations up to 0.7 g, and a predominant frequency of 4 Hz. Bathurst and Hatami (1999) have also reached similar results after using a numerical model of a 3 m-high wall with a hinged toe.

Kosek*et al.* (1998) conducted shaking table tests on 0.5 m-high conventional and reinforced soil retaining model walls, where the reinforced soil model walls were propped panel type and 10 phosphor bronze reinforcement strips were employed to model the reinforcement. In this study the reinforcement length to wall height ratio was L/H 1/4 0.4. During this study it was observed that when the length of the top reinforcement layer was increased by a factor of four and the fourth layer by a factor of 2.25, the critical acceleration (i.e. acceleration corresponding to a lateral displacement equal to 5% of the wall height) increased by about 20%. On the other hand, the shaking table test results reported by Sakaguchi (1996) and the numerical modeling results for walls subjected to simulated seismic shaking that are reported by Bathurst and Hatami (1998) suggested that there may be diminishing benefit from uniform reinforcement lengths exceeding L/H 1/4 1.

Another significant parameter that has impact on the response of reinforced soil walls under static and earthquake loading is the reinforcement stiffness. According to the study of Bathurst and Hatami (1998) which was carried on using dynamic numerical experiments, the tensile loads in all reinforcement layers increase as the reinforcement stiffness increases. The results of the study of Saunders and Bathurst (2002) conducted on instrumented full-scale walls under static loading conditions have pointed out that the restrained toe of a metallic wire mesh reinforced soil wall attracted a bigger portion of the earth force compared to the toe of a nominally identical geosynthetic reinforced wall.

Allen *et al.* (2003) and Bathurst *et al.* (2005) have proposed a working stress method which is based on a back analysis of a large database and which takes into account the stiffness of the reinforcement layer and their distribution in the calculation of static design loads. They have investigated the impact of reinforcement properties on the response of reinforced soil retaining walls to simulated seismic loading by the help of the results of a series of reduced-scale reinforced soil retaining wall models built on a shaking table, where the model walls were constructed with different reinforcement length, vertical spacing and stiffness values. By the use of a stepped-amplitude harmonic excitation record applied at the model base, all models were loaded to failure. In the paper by El-Emam and Bathurst (2004) background information for experimental design, equipment and instrumentation of the models in this test program can be found. Likewise the paper El-Emam and Bathurst (2005) explains the influence of facing geometry, facing mass and facing toe boundary condition on wall response (El Amam and Bathurst, 2007).

3.3.3. Seismic Analysis of GRS-RWs Using Finite Element Methods.

Numerical investigation on seismic response of GRS wall has economical advantage over those from the physical model tests. However, it has the drawback of extreme idealism, which is not the case with physical model tests. Despite this, compared to the conventional limit equilibrium approach, numerical solutions are much more rigorous since they satisfy force-equilibrium condition, strain-compatibility condition, and essential material laws. It is possible to obtain both the qualitative and quantitative performances can be from numerical investigations.

Some programs and the researches related with geosynthetic reinforced walls are as follows:

- FLAC (FLAC 1995): It is the dynamic finite-difference program that performed firstly by Bathurst and Hatami (1998) and used to perform a parametric analysis of geosynthetic reinforced propped panel walls to.
- Bathurst and Hatami (1998) showed that current assumptions for the distribution of the dynamic increment of reinforcement load for inextensible reinforcement may not apply to relatively extensible polymeric reinforcement.

- The American Association of State Highway Transportation Officials (AASHTO) adopted inappropriate and unconservative existing pseudostatic design methods which have been based on a limited amount of physical and numerical modeling of steel strip reinforcement walls
- DYN3D: It is the program used by Bachus et al. (1993) for the simulation of the blast response of GRS walls constructed with incremental concrete panel facings.
- Dynamic finite-element modelling of geosynthetic reinforced segmental retaining walls was used by Cai and Bathurst (1995) subject to ‘‘scaled’’ earthquake loads. The modified TARA-3 code was used together with hysteretic soil and reinforcement models.
- Finite-element parametric analysis: It is used by Segrestin and Bastick (1988) to test reinforced earth retaining wall systems, which used inextensible reinforcement (steel strips). Due to the lack of similar parametric data for extensible reinforced structures, the Federal Highway Administration (FHWA) (1996) and AASHTO (1996) has performed this study to design GRS walls with extensible reinforcement.

4. METHODOLOGY

4.1. Introduction

In this chapter, the methodology regarding the four 1/2 reduced-scale Geogrid-Reinforced Soil Retaining Block Wall models is presented.

Firstly, information about the scaling of the model walls shall be explained. Afterwards, detailed information about the test set-up shall be presented. The shaking table, the materials, instrumentation and data acquisition systems utilized in the tests shall be introduced and explained in detail respectively. Accordingly, the construction method of the walls shall be presented in order to fully cover the experimental process of the study.

Later on, model configurations of four 1/2 reduced-scale Geogrid-Reinforced Soil Retaining Block Walls together with reinforcement layout are explained and illustrated. The dynamic excitations applied on model walls and shaking sequence are presented. Lastly, test program summarizes essential details and objectives of the four test walls constructed in this study.

4.2. Scaling of the Model Walls

For the four model walls tested in this study, model size is devised based on the dimensions of the test facility available. The constraints of the shaking table limit the weight of the model to be tested to 100 kN. Therefore in order to simulate a higher wall, scaled models are used. To evaluate the results obtained from model tests and link the results to its full size prototype, scaling laws are used. Scaling laws provided by the dimensional analysis is a compacting technique for reducing the number and complexity of experimental variables. Based on the scaling laws, similarity is achieved between the model and prototype.

In Table 4.1. the most common scale factors used in this study can be seen. These scale factors are in agreement with the ones proposed by Iai and Sugano (1999) and Jakrapiyanun and Ashford (2003).

Table 4.1. Scaling factors used in this study

Quantity	Theorotical Ratio (Prototype/Model)	Study
Length	N	2
Density	1	1
Stress	N	2
Strain	1	1
Acceleration	1	1
Frequency	$N^{-0.5}$	$1/\sqrt{2}$
Time	$N^{-0.5}$	$1/\sqrt{2}$
Stiffness	N^2	4

It should be noted that, Rankine active coefficient, K_a, the angle of friction of the soil, φ_{soil}, and the strain, ε, are already dimensionless parameters and dimensional analysis can not provide information regarding them.

This study features reduced-scaled modular block walls subjected to varying dynamic base excitations, facing inclination and backfill materials. However, it is important to state that scaling, gravity and stress-level effects could possibly affect the obtained results of the reduced-scale models. Therefore, these walls may not represent response of real world field conditions.

4.3. Test Setup

4.3.1. Shaking Table

In the present study, a computer-controlled servo-hydraulic single degree of freedom (horizontal) large shaking table facility at the Shaking Table Laboratory of Kandilli

Observatory and Earthquake Research Institute (KOERI) in Kandilli-Istanbul/Turkey was used to simulate the horizontal shaking action, associated with seismic conditions. ANCO Engineering, Inc manufactured the ANCO R-148 uniaxial shaking table, which comprises a loading platform of 3 m x3 m size and payload capacity of 10 tons.

Shaking is provided by a digitally controlled servo-hydraulic actuator with ± 12 cm stroke and has dual 3-stage Moog servo-valve rated at 200 GPM each. The Moog servo-valve and GS actuator are controlled by a GS2000 analog control servo-loop, servo-controller. The servo-controller accepts the displacement table program signals from the digital control system and seeks to control the actuator to match this signal.

The shaking table can be operated over an acceleration range of to 2g and frequency range 0 to 50 Hz with a 24 cm peak-to peak displacement. Maximum velocities are 1.2 m/s. In Figure 4.1. below, the achievable motion and 5 per cent Response Spectrum for R-148 shaking table with payload of 10 tons is shown. A view of shaking table at the Shaking Table Laboratory of Kandilli Observatory and Earthquake Research Institute (KOERI) in Kandilli-Istanbul/Turkey can be seen in Figure 4.2.

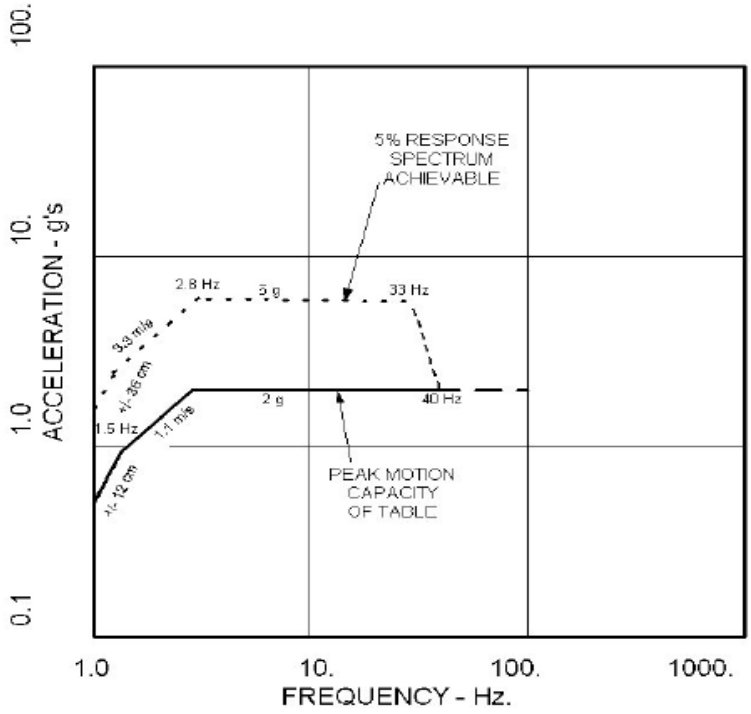


Figure 4.1. The achievable motion and 5 per cent Response Spectrum with payload of 10 tons



Figure 4.2. A view of shaking table at the Shaking Table Laboratory of Kandilli Observatory

A dedicated control room housing the control system includes a Data Physics 550 WIN digital data control and acquisition system to facilitate testing under both constant amplitude and pseudo-random conditions. Data Physics 550 WIN Compaq PC-based system is a 16 channel data acquisition and control system which is composed of anti-aliasing filters, amplifier, a UPS for safe operation, the COMPAQ control PC and Monitor, the Gardner System servo-controller, and the emergency hydraulic power supply/dump valve e-stops. The picture of the control room and WIN Compaq PC-based system is a 16-channel data acquisition and control system can be seen below in Figure 4.3.



Figure 4.3. A view from the Control Room

4.3.2. Materials Used in the Tests

In this section, the materials used in the tests shall be presented in detail.

4.3.2.1. Steel Container Soil Box. The major problems associated with laboratory model studies are scaling and boundary effects, especially in studies related to earthquake engineering. In this study, a steel container soil box was constructed to accommodate the geogrid-reinforced soil retaining wall. The steel container soil box used for the tests is rectangular in cross-section, with inside dimensions 1,9m (height) x 2,8 m (length) x 0,53 m (width), with a design weight of approximately 4 tons, designed to be installed on the shaking table. Since the payload of shaking table is 10 tons, the fabricated steel container was dimensioned as to maximize the width and depth of the wall as mentioned above.

Furthermore, an outside glass-covered frame with dimensions 1,9m (height) x 1 m (length) x 0,53 m (width) was designed and attached to the steel container soil box to make visual observation possible. Also, the laser displacement sensors were installed inside the glass-covered frame to measure the facing displacements in various heights. Since the laser displacement sensors were fixed to the glass frame, it was possible to read the relative displacements of the wall directly.

The steel container and glass-covered frame installed on the shaking table can be seen in Figure 4.4. The dimensions can be seen in Figure 4.5.



Figure 4.4. Steel container and glass-covered frame on the shaking table

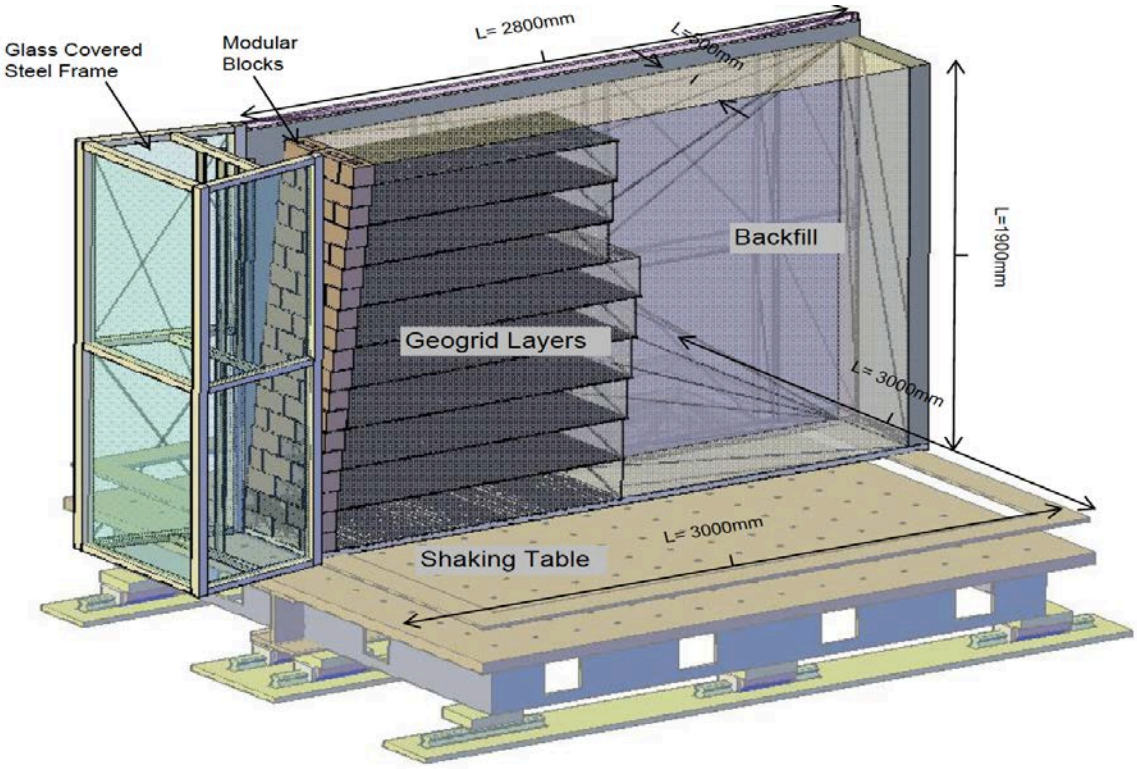


Figure 4.5. Steel container soil box

4.3.2.2. Glass Covered Steel Frame. In the tests, a glass covered steel frame is attached to the front of the steel container soil box by bolted connection. The dimensions of the frame can be seen in Figure 4.6.

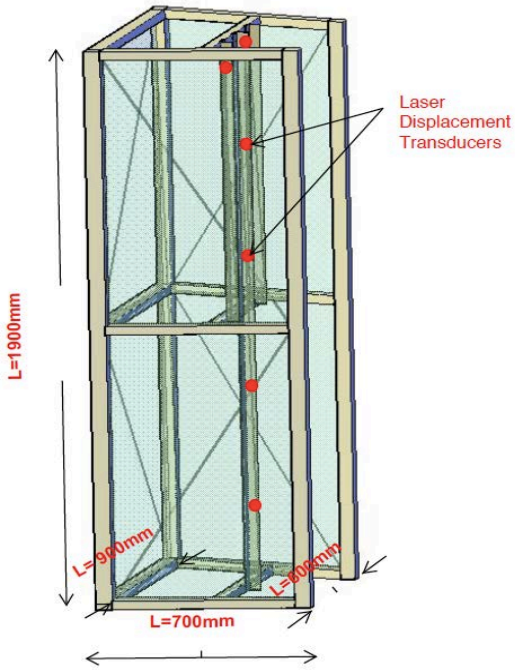


Figure 4.6. Dimensions of Glass Covered Steel Frame

The glass-covered frame worked as a containment of the backfill in case of a possible collapse of the front wall during shaking. The glass on the steel frame is a high strength glass that can endure the impact of facing elements. The steel frame is designed from lightweight steel since the overall system should not have excessed the weight limit of the shaking table. The glass-covered steel frame weighs approximately 150 kg. Moreover, the glass cover makes the visual observations possible during experiments. Also, most importantly the laser displacement sensors were attached inside the steel frame for an accurate reading of the front facing displacements during dynamic excitations. Since the frame and container work as a unibody system, the relative displacement data obtained from the laser sensors are accurate. The procedure and details of the laser displacement sensor installation are explained in more detail in section 4.3.3.1. The glass covered steel frame attached to the steel container box can be seen in Figure 4.7. below.



Figure 4.7. The glass covered steel frame attached to the steel container box

4.3.2.3. Rubber Sheets. The frictionless sliding between the greased sidewalls and backfill was obtained by placing 6 mm thick rubber sheets. Those rubber sheets were used in each wall configuration. Rubber sheets were not only helpful on eliminating the side effects of the friction phenomena but also the rubber sheet would follow the deformation of the

backfill without significant resistance. The rubber sheets installed till the mid height of the wall can be seen in the Figure 4.8. below.



Figure 4.8. Rubber sheets are installed at the side walls of the soil box.

4.3.2.4. Backfill-Sand. In this study, in one of the wall configurations (Wall 4); commercially available well graded sand was used as a backfill material. The properties obtained from mechanical grain size tests are summarized in in Table 4.2. Grain size distribution curve can be seen in Figure 4.9.

Table 4.2. The properties of sand

Unit Weight of Sand, γ_{sand}	15
Max. Dry Unit Weight of Sand	18.9
Coefficient of Uniformity, C_u	3,3
Coefficient of Curvature, C_c	1,48

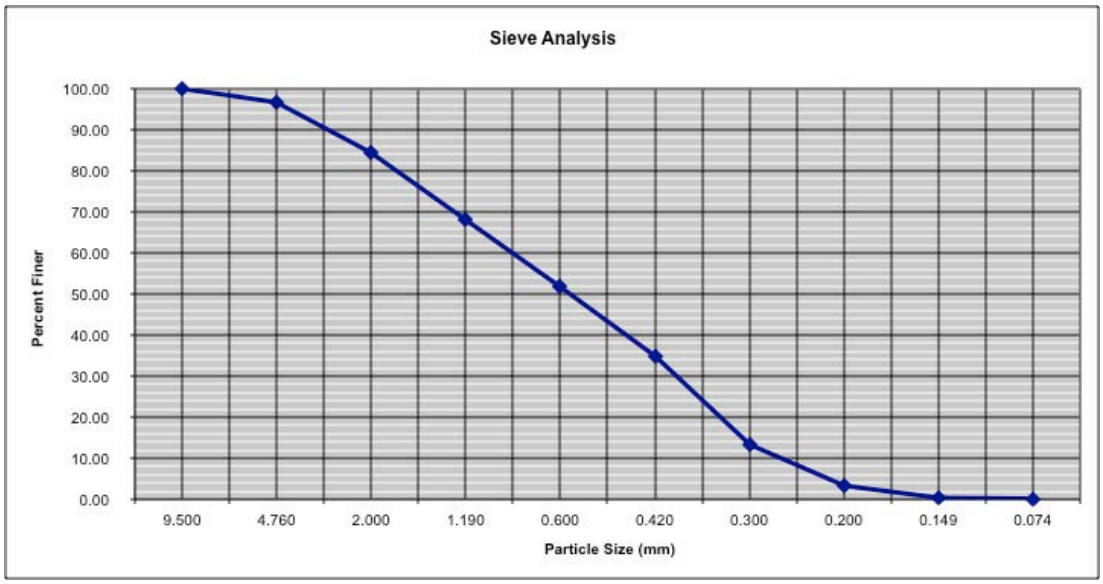


Figure 4.9. Grain Size Distribution Curve for Sand

Also, for determining the stress-strain relationship, direct shear tests were conducted on sand. Two different normal stresses 100 and 200 kPa are applied on 6cm x 6 cm x 2cm (width, length, height) specimens with a loading rate of 0.00138 kN/div and strain rate of 0.5 mm/min. As a result $Ø_{sand}$ is found to be 34°.

The normal stress vs. the shear stress graph obtained from direct shear test can be seen in Figure 4.10.

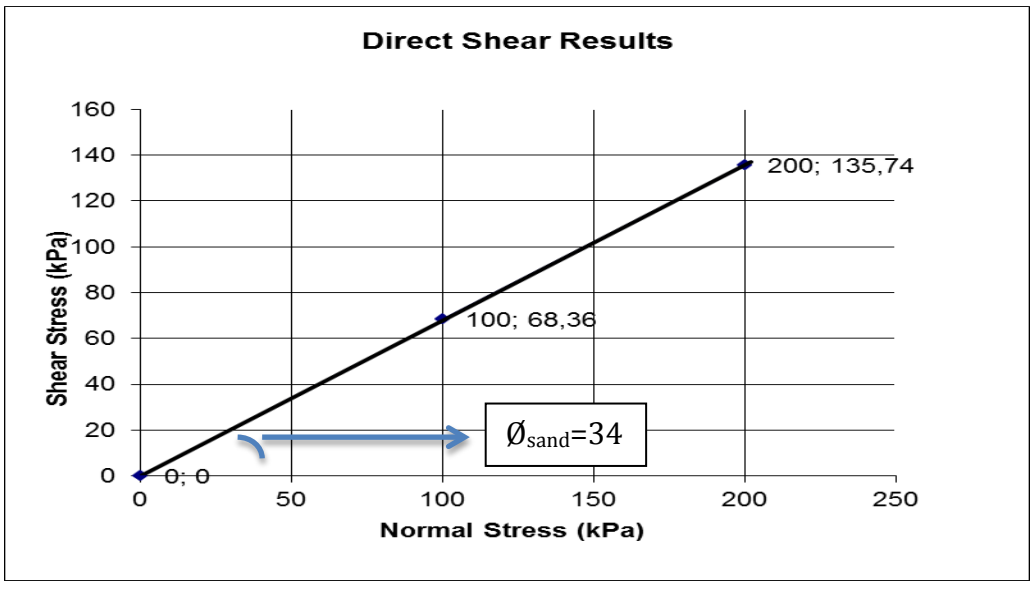


Figure 4.10. Direct Shear Results obtained from sand

Following the completion of shaking test of the sand backfill wall, soil specimens were sampled from four different locations (the top @h=1.80 m., midheight @h=1.30 m., @h=0.8 m. and bottom layers @h=0.2 m.) of the sand backfill. Sand cone tests are conducted on the specimens to determine in-situ dry unit weight. In the Sand Cone Method, as done in this study, a hole is excavated in the area where the soil has been compacted and the dry weight of the soil can be obtained by determining the weight of the moist soil and the moisture content. The volume for the hole excavated is calculated by reintroducing the sand into the hole and then the dry unit weight of compaction is calculated by dividing the dry weight of the soil by the volume of the hole.

The Proctor compaction test is a laboratory method of experimentally determining the optimal moisture content at which a given soil type will become most dense and achieve its maximum dry density. The proctor compaction tests are also conducted on sand. The results can be seen on Figure 4.11. As a result of proctor compaction test, the maximum dry density is found γ_{dry}= 18.9 kN/m^3 and optimum water content is found w_n= 4.6%. The relative density (Dr) of the sand is found to be 43% which is equivalent to medium dense in relative density scale.

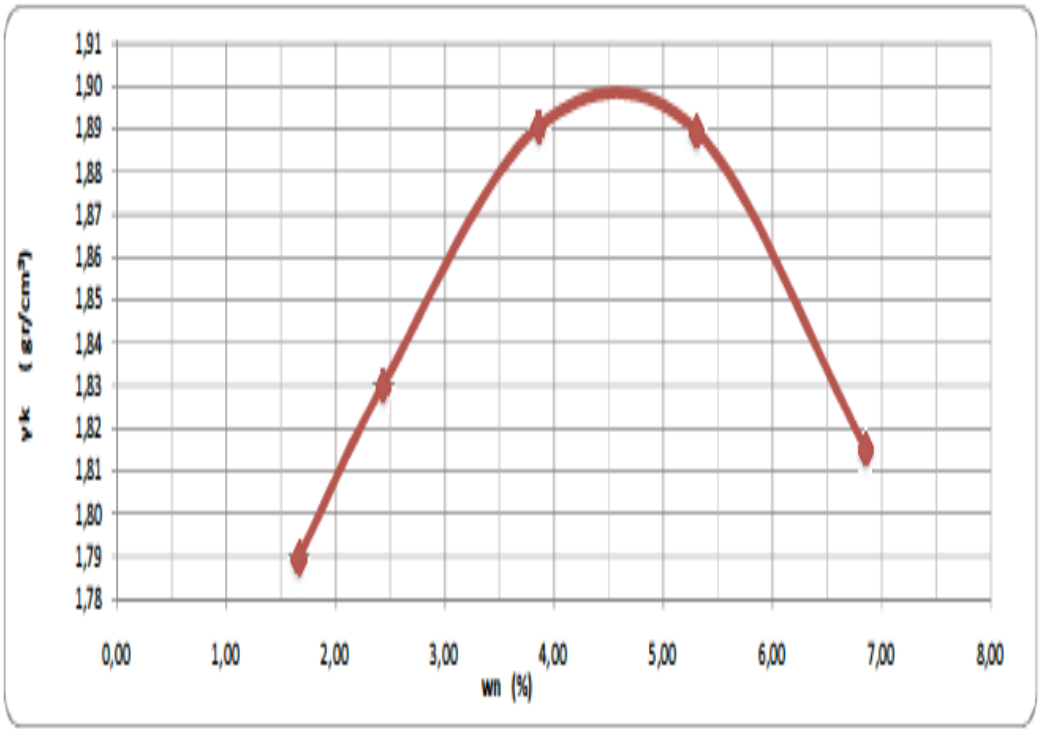


Figure 4.11. Proctor Compaction Test Results

The test results of the sand cone tests are summarized and can be seen in Table 4.3.

Table 4.3. Test Results of Sand Cone Tests

Test Parameters	LAYERS			
	top @h=1.80 m	midheight @h=1.30 m.	midheight @h=0.80 m.	bottom @0.2m
Sand Weight In Funnel (gr)	1560	1560	1560	1560
Sand Weight Before Test (gr)	5000 g	5000 g	5000 g	5000 g
Sand Weight After Test (gr)	2618 g	2690 g	2593 g	2539 g
Sand Weight In Hole (gr)	822 cm^3	750 cm^3	847 cm^3	901 cm^3
Hole Volume (cm3)	578 cm^3	528 cm^3	596 cm^3	634 cm^3
Wet Soil Weight Taken Hole (gr)	1087 g	1012 g	1114 g	1178 g
Wet Unit Weight (gr/cm3)	1.879 g/cm^3	1.917 g/cm^3	1.869 g/cm^3	1.858 g/cm^3
Wet Sample+Tare (gr)	736.00 g	755.00 g	700.00 g	786.00 g
Dry Sample+Tare	728.00 g	743.00 g	690.00 g	778.00 g
Water Weight (gr)	8 cm^3	12 cm^3	10 cm^3	8 cm^3
Tare(gr)	424 g	424 g	424 g	424 g
Dry Soil Weight(gr)	304 cm^3	319 cm^3	266 cm^3	354 cm^3
Water Contents (%)	3%	4%	4%	2%
Dry Unit Weight	1.83 g/cm^3	1.85 g/cm^3	1.80 g/cm^3	1.82 g/cm^3
Compaction Percent	95%	96%	96%	97%

4.3.2.5. Backfill-Gravel. Commercially available Gravel No.1 is used for the Wall 1, 2 and 3. Mechanical grain tests are conducted on the gravel and according to ASTM D-2487-98 standards the material is found to be poorly graded gravel. The properties of the gravel is given in Table 4.4. and the grain size distribution is shown in Figure 4.12.

Table 4.4. The properties of gravel used in the experiments

Unit Weight of Gravel, γ_{gravel}	17,5
Coefficient of Uniformity, C_u	3,05
Coefficient of Curvature, C_c	0,95

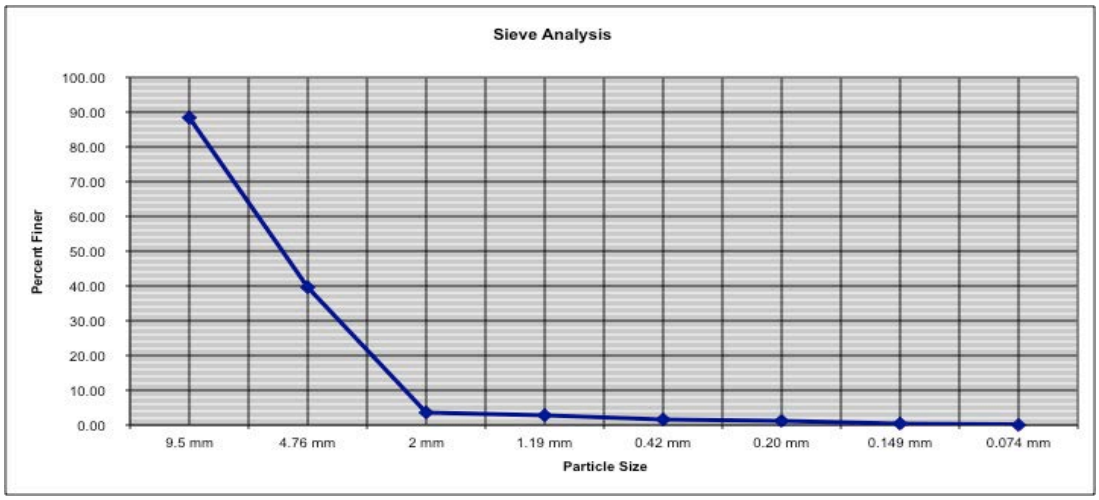


Figure 4.12. Grain Size Distribution Curve for Gravel

For evaluation of the approximate internal friction angle; the correlation chart (proposed by Schmertmann (1978)) between relative density and internal friction angle is utilized. The chart is shown in Figure 4.13. By taking into account the values of 16 kN/m and 20 kN/m as typical minimum and maximum dry unit weights of gravel, and placing those values in equation 4.1. the angle of internal friction values are evaluated to be 40°.

$$D_r = \frac{\gamma_{k\max}}{\gamma_k}\frac{\gamma_k - \gamma_{k\min}}{\gamma_{k\max} - \gamma_{k\min}} \qquad (4.1)$$

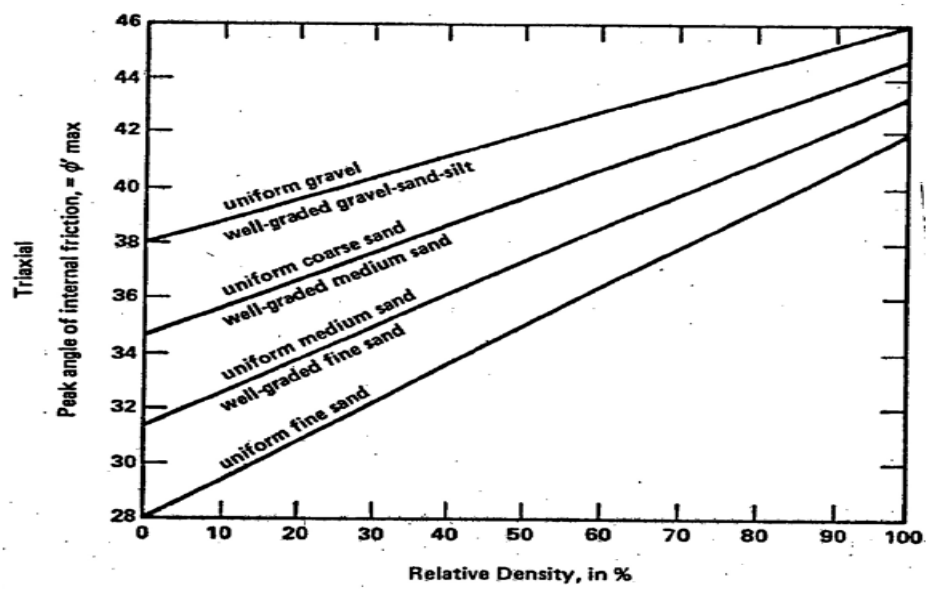


Figure 4.13. Correlation chart of relative density and internal friction angle (Schmertmann, 1978 (FHWA))

4.3.2.6. Granular Rubber Fill. In order to absorb the possible reflecting of earthquake waves from the backside of the steel container soil box, granular rubber was used in this study. 5cm. wide granular rubber was placed at the backside of the fill in each test. The details of the granular fill properties can be found in Kasay (2007). The granular rubber fill material placed in the steel container can be seen in the Figure 4.14.



Figure 4.14. Granular rubber fill

4.3.2.7. Reinforcement Material - Geogrid. In geogrid reinforced retaining wall design, geogrid reinforcements with an ultimate tensile strength of 45 kN/m is utilized commonly in practice. Due to model scale effects, two types of geogrids were used in this study. A low strength Huesker- Frornit Polypropylene Geogrids 20/20 was used as reinforcement in every layer in Wall-1 and Wall-2. Since the prototype design for Wall 3 and Wall 4 was taken from a design made for a real project, the geogrid reinforcement were ½ scaled versions of the real wall. In Wall-3 and Wall-4 Polypropylene Geogrids 20/20 were used only on the top half portion of the wall. Huesker Fortrac- Polyester geogrids 45/15-20 were placed on the lower portion till the mid height of the Wall-3 and Wall-4.

Table 4.5 summarizes the properties of the geogrids. The Elasticity Moduli of the geogrids are calculated according to the data sheets provided by the manufacturer. The Polypropylene Geogrid 20/20 used in experiments can be seen in Figure 4.15. The arrangement scheme of the reinforcement is given in Figure 4.41 and 4.42.

Table 4.5. Properties of Geogrids used in the experiments

Properties	**Polypropylene Geogrid 20/20-40T**	**Polyester Geogrid (PET) 45/15-20**
Mass per Unit Area	~ 190 g/m2	~ 230 g/m²
Mesh Size (mm)	40 x 40	20 x 20
Ultimate Tensile Strength (kN/m)	22	45
Tensile Strength %2 strain (kN/m)	8	10.5
Tensile Strength %3 strain (kN/m)	15	13
Tensile Strength %5 strain (kN/m)	20	18
Strain at Nominal Tensile strength (%)	7	12
Elasticity Modulus (kN/m)	405	310



Figure 4.15. The Polypropylene Geogrid 20/20 used in experiments

According to the scaling laws proposed by Iai (1999), the relationship between prototype-scale reinforcement stiffness (J_p) and model scale stiffness (J_m) can be calculated as $J_p = J_m \lambda^2$, where $1/\lambda$ is the model scale (equal to 1/2 in this study). In reduced-scale models, the stiffness of the Polypropylene Geogrid 20/20-40T geogrid (J_m = 15 kN/m at 3% strain) is equivalent to reinforcement at prototype scale (J_p = 60 kN/m at 3% strain). The stiffness of the Polyester Geogrid (PET) 45/15-20 geogrid (J_m = 13 kN/m at 3% strain) is equivalent to to reinforcement at prototype scale (J_p = 52 kN/m at 3% strain). Although the PET 45/15-20 has a higher ultimate tensile stress, Polypropylene Geogrid 20/20-40T is stiffer in 2% to 5% strain working conditions.

4.3.2.8. Facing Panels-Concrete Modular Blocks. Segmental block walls consist of concrete blocks manufactured to provide a mortarless facing system and geogrids, which are connected to the facing blocks and extend horizontally, back into the engineered backfill soil to create a composite structure. Mostly the concrete blocks used in such design are hollow. In practice, hollow concrete modular blocks are filled with soil during installations. This improves the stability of the facing by increasing the interblock shear resistance and friction between geogrid and facing element.

In this study, as facing blocks, ½ scaled versions of hollow blocks used in Turkey as facing elements were utilized. The dimensions of these model blocks were 100 mm x 100 mm x 200 mm (height, depth, width). The dimensions of the blocks can be seen in Figure 4.16. Special steel molds are prepared for producing the concrete modular blocks. Gravel and sand were filled in the hollow part accordingly to the backfill material used. Sand filled concrete modular blocks used in this study can be seen in Figure 4.17.

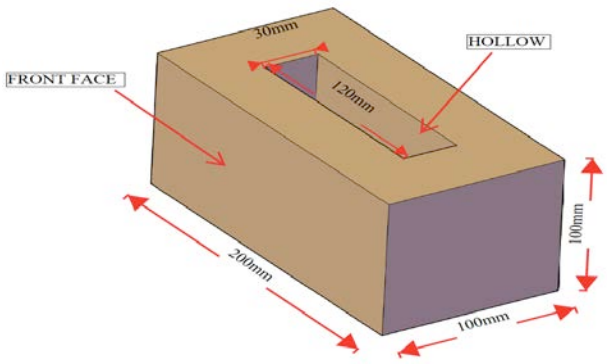


Figure 4.16. The dimensions of the blocks used in the study



Figure 4.17. Sand filled concrete modular blocks used in this study

4.3.2.9. Compactor. In order to achieve the compaction, both gravel and sand backfills were compacted at each 10 cm. by a commercially available Dynapac LF82 type of compactor Figure 4.18. The properties of the compactor are given below in Table 4.6.



Figure 4.18. Dynapac LF82 type of compactor employed in compaction

Table 4.6. Properties of the Dynapac Compactor LF82

Net Weight	62 kg
Plate Dimensions	W400 mm x L510 mm
Frequency	92 Hz
Amplitude	0.8 mm
Centrifugal Force	10 kN
Engine	Honda GX120
Engine output	2.9 kW / 3600 rpm

4.3.3. Instrumentation

The walls constructed were instrumented with sensors such as laser sensors, strain gages and accelerometers at various locations. The details about the sensors and installation procedures are given for each type separately. To compare the accelerations and displacements obtained from various tests, accelerometers and laser displacement sensors were placed at identical locations in all tests. Since the reinforcement length was variable for different tests the locations of the strain gages vary in each tests. Great care was taken in installing the sensors and wiring during construction. Figure 4.19 to Figure 4.22. show the location of sensors and abbreviations used in this study. Please refer to Figure 4.41 and Figure 4.42. for the detailed dimensions of the sensors.

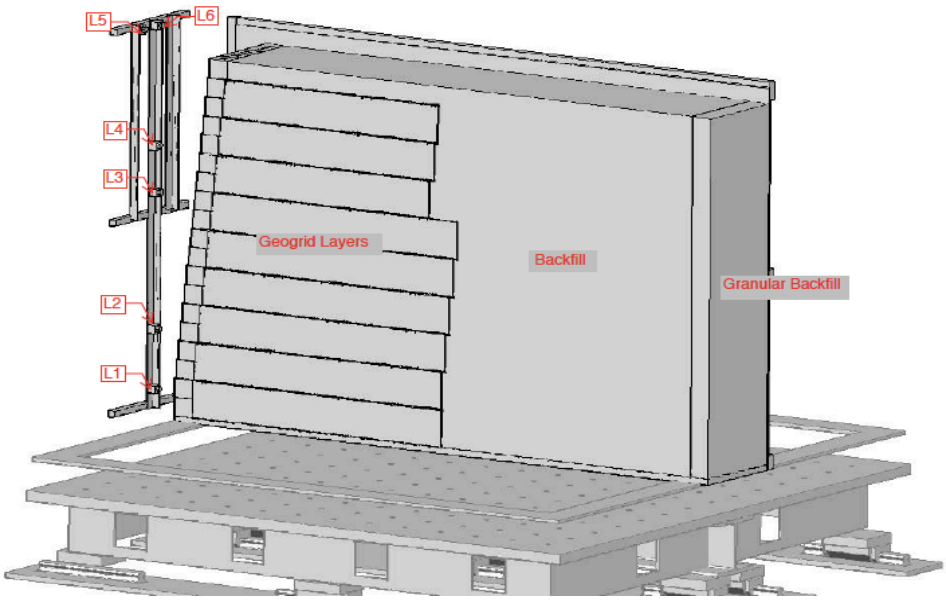


Figure 4.19. Location of Laser displacement transducers on steel frame

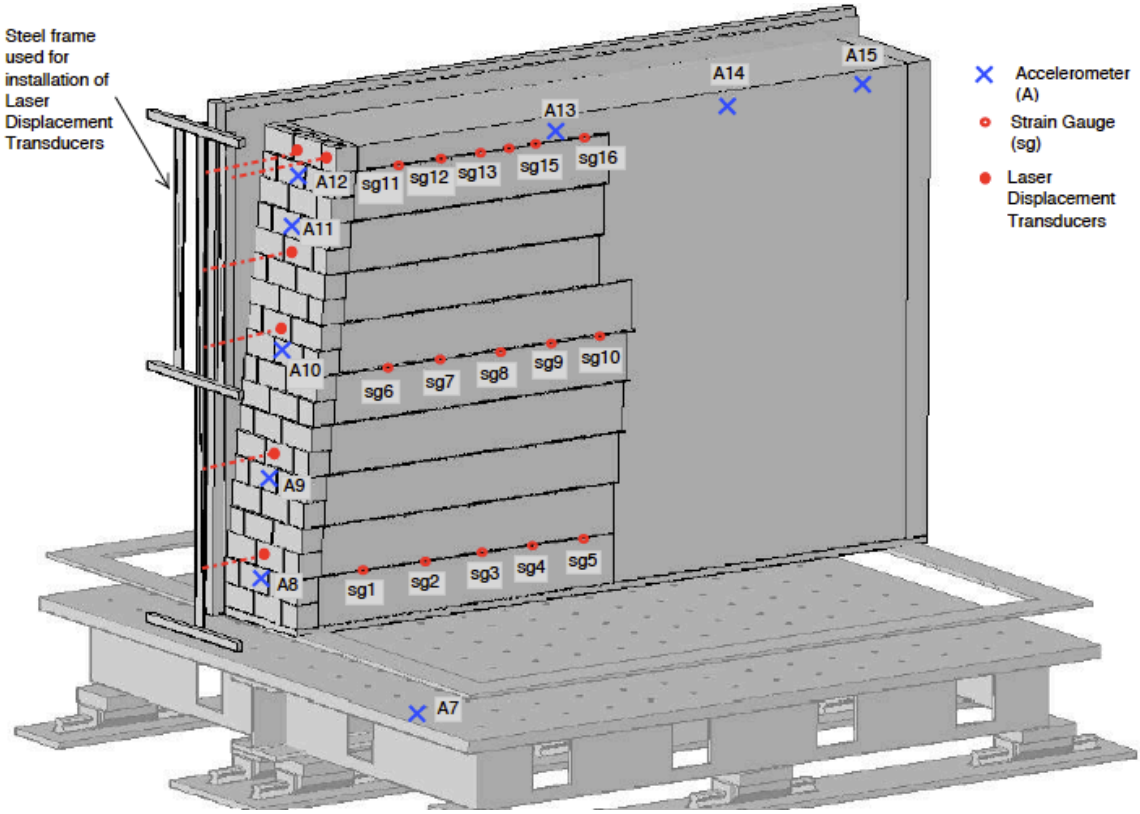


Figure 4.20. Typical Section of an Instrumented Wall

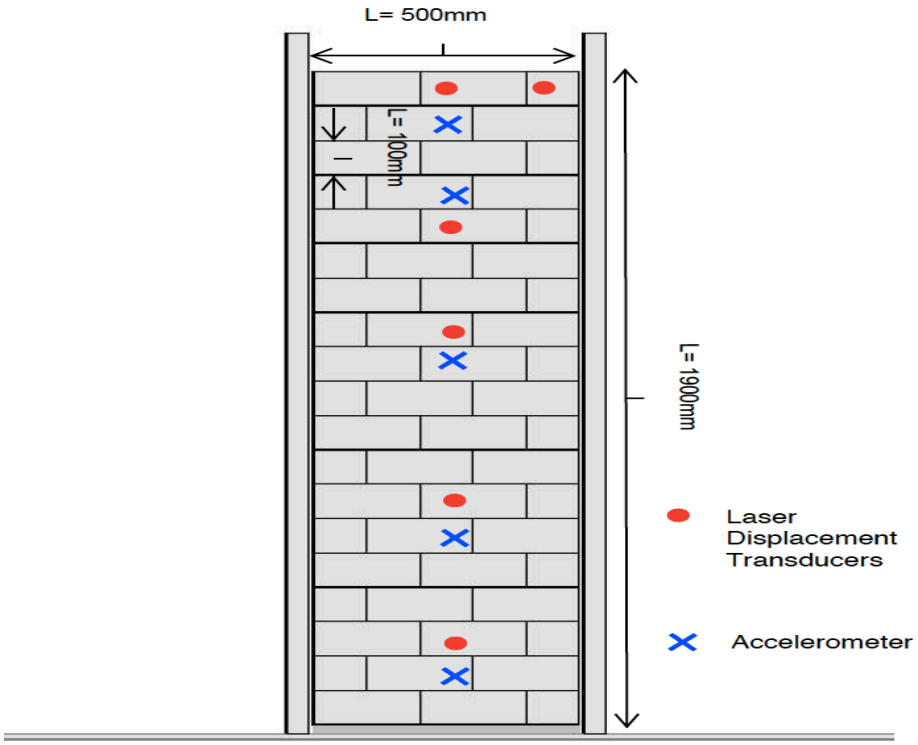


Figure 4.21. Front view of the locations of Accelerometers and Laser Displacement Transducers on the Wall

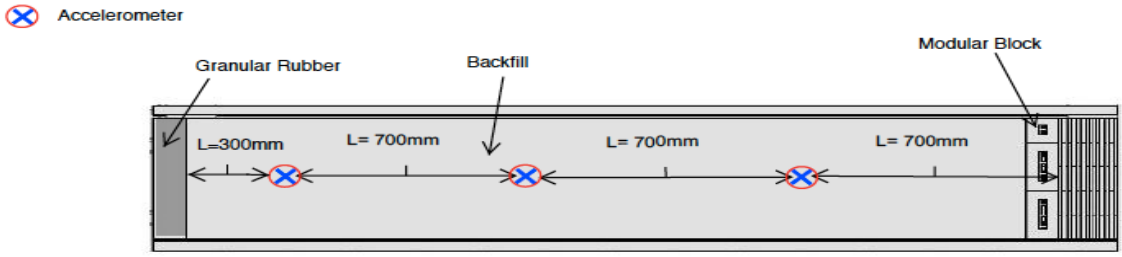


Figure 4.22. Top view of the Wall

4.3.3.1. Laser Sensors. Six 40 cm range laser displacement transducers were used at different elevations to measure the displacements at the wall face. The laser sensors are mounted to glass covered steel frame. Since the glass covered frame is attached to the steel container soil box, the attached systems act as a unibody that allows the laser displacement sensors accurately measure the displacements on the facing during dynamic excitation.

The Laser Displacement Sensors were of type ODSL8-V/4-400-S-12 from Leuze Electronic. They have a displacement measurement range from 2 to 40 cm with 0.1 mm of precision measurement ability. In tests they were adjusted as 5ms (200 Hz) of measurement time of 5 ms (and a response time of up to 20 ms. In Figure 4.23. the laser sensors mounted inside the glass covered frame is shown.



Figure 4.23. A view of the laser sensors mounted inside the glass-covered frame

4.3.3.2. Strain Gages . One of the most important part of this study was to measure the local strains in geogrids during dynamic excitation. For that reason, TML GFLA-6-50 strain gages which have a 2.09 ±1% gage factor are used for the tests to measure the strains on the geogrids. These gages are produced especially for plastic materials and configured to minimize the effect of gage tightening. The gages have 6 mm of gage length with a 120 ±0.3Ω of gage resistance. Gage material is Cu-Ni alloy.

The following procedures are followed in strain gage installation.

- In order to bond the strain gages to geogrids, the most appropriate strain gage, which is TML GFLA-6-50, is selected.
- Grease, dirt, etc. have been gently wiped off from the bonding surface of the geogrid to increase the bonding of the strain gages and to create a smooth flat surface.
- Strain gages and terminals are installed on geogrids using Cyanoacrylate based CN adhesive.
- The lead wires are soldered to the strain gages through connecting terminals
- Finally, the gage resistances are checked using a voltmeter.

The gages are installed on the middle portion of geogrids. The strain gages are protected by AW106 epoxy resin where the lead wires are protected by flexible tubes. The strain gages installed can be seen in Figure 4.24.

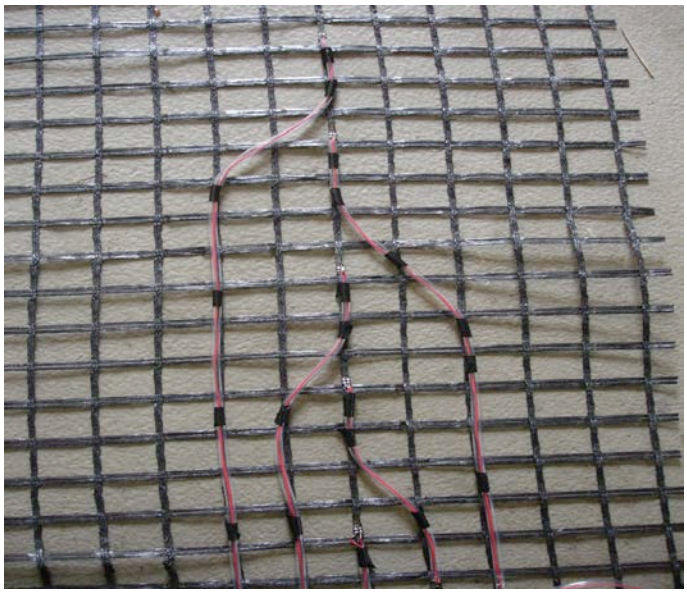


Figure 4.24. TML GFLA-6-50 Strain gages installed on geogrids.

Considering the total number of 16 available channels on TDG ai8b Data Acquisition System, a total of three geogrid layers were instrumented with strain gages. For the layout plan of strain gages please refer to Figure 4.41 and 4.42. Below in Figure 4.25. location of strain gages on a single geogrid reinforcement is illustrated.

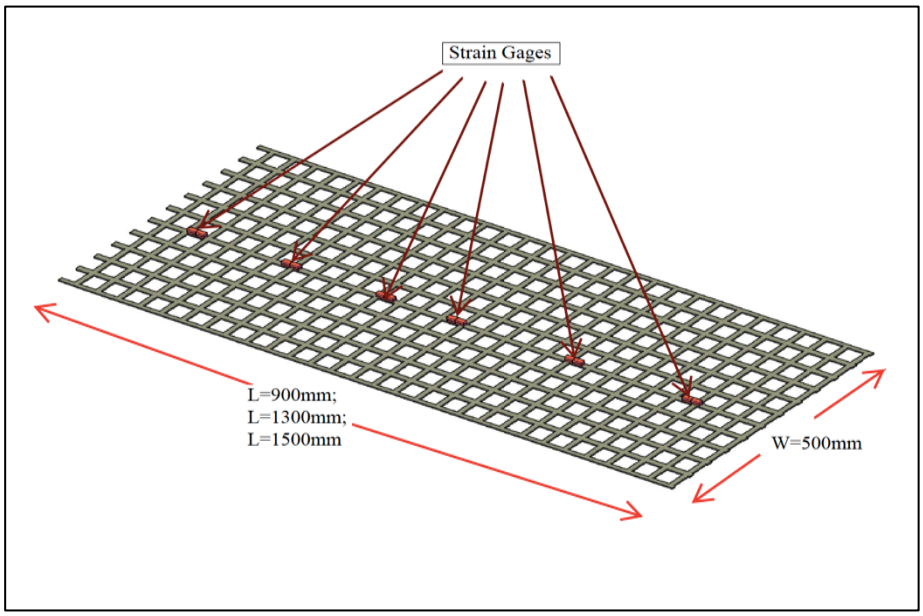


Figure 4.25. The location of strain gages on geogrid

4.3.3.3. Accelerometers. Since there are a limited number of channels available in Data Acquisition system, a total of 9 accelerometers were installed in each test at the front face of the blocks and on top of the fill. 1 accelerometer was fixed to the shaking table to record the base acceleration, 5 accelerometers were mounted on facing and the remaining three were embedded in on top of the fill by excavating the soil to the top reinforcement layer level. A flexible bag protected the accelerometers installed on top of the fills. Please refer to Figure 4.41 and 4.42. for the location of the accelerometers.

Accelerometers were manufactured by “PCB Piezotronics Inc.” and Model no is “3801G3FB3G”. They are of capacitive type, which have +/- 3g acceleration measurement capacity, an average of 1000mV/g sensitivity and a frequency range of 0 to 100 Hz.

A general view of the accelerometers mounted on facing and on top of the fill can be seen in Figure 4.26. and Figure 4.27.



Figure 4.26. Accelerometers mounted on facing



Figure 4.27. 3 Accelerometers embedded in on top of fill

4.3.4. Data Acquisition (DAQ) Systems

In this study, two different types of Data Acquisition Systems (DAQs) are utilized for sensors. Laser sensors and accelerometers are connected to National Instruments' PCI-6229 M DAQ. Strain gages are connected to TDG ai8b DAQ system.

4.3.4.1. National Instruments' PCI-6229 M Data Acquisition System. The testing facilities included a National Instruments' PCI-6229 M Data Acquisition System. It is utilized for connection of accelerometers and laser sensors. It allows working with 16 analog input channels that have 16-bit of resolution and 250 kS/s (250000 samples per second) of sampling rate. The VI Logger DAQ software, SCB-68 noise-shielded connector blocks and SHC68-68-EPM cables were the other accessories used in this DAQ system (Figure 4.28). 200 sample per second rate is adjusted for the laser sensor and accelerometer data.



Figure 4.28. National Instruments' PCI-6229 M DAQ System and Control Room

4.3.4.2. TDG Ai8b Data Acquisition System for Strain Gages. For strain gage measurements two TDG Ai8b Data Acquisition System boxes each having 8 channels were used in experiments (Figure 4.29). So, 16 strain gages were connected to the TDG Ai8b DAQ systems. Special cables are used to construct a quarter-Wheatstone Bridge. A gateway device is used as a converter for serial to USB with this device DAQ can be

connected to any computer having a USB port. The TDG takes maximum 8 samples per second with 16 bits of resolution. Each channel has 8 different gain settings within a ±10 V range.



Figure 4.29. TDG Ai8b Data Acquisition System boxes used in the experiments

Information such as gage factor, calibration coefficient and channel gain are entered to TDG Ai8b Testbasic software and the strain data is automatically read from the software. A view of the TDG Ai8b Data Acquisition System together with strain gage cables attached can be seen in Figure 4.30.



Figure 4.30. A view of the TDG Ai8b Data Acquisition System together with strain gage cables attached

4.3.5. Construction Method of Walls

Herein, the construction method of the walls shall be explained. Please refer to Section 4.3.2. for more detailed information on the materials used and instrumentation process in the construction.

The steel container soil box that weighs almost 4 tons was transported onto the shaking table by a crane and was bolted at 10 different locations to the shaking table to secure a tight connection. The steel container soil box on shaking table and a view of bolted connections are shown in Figure 4.31. and Figure 4.32. respectively.

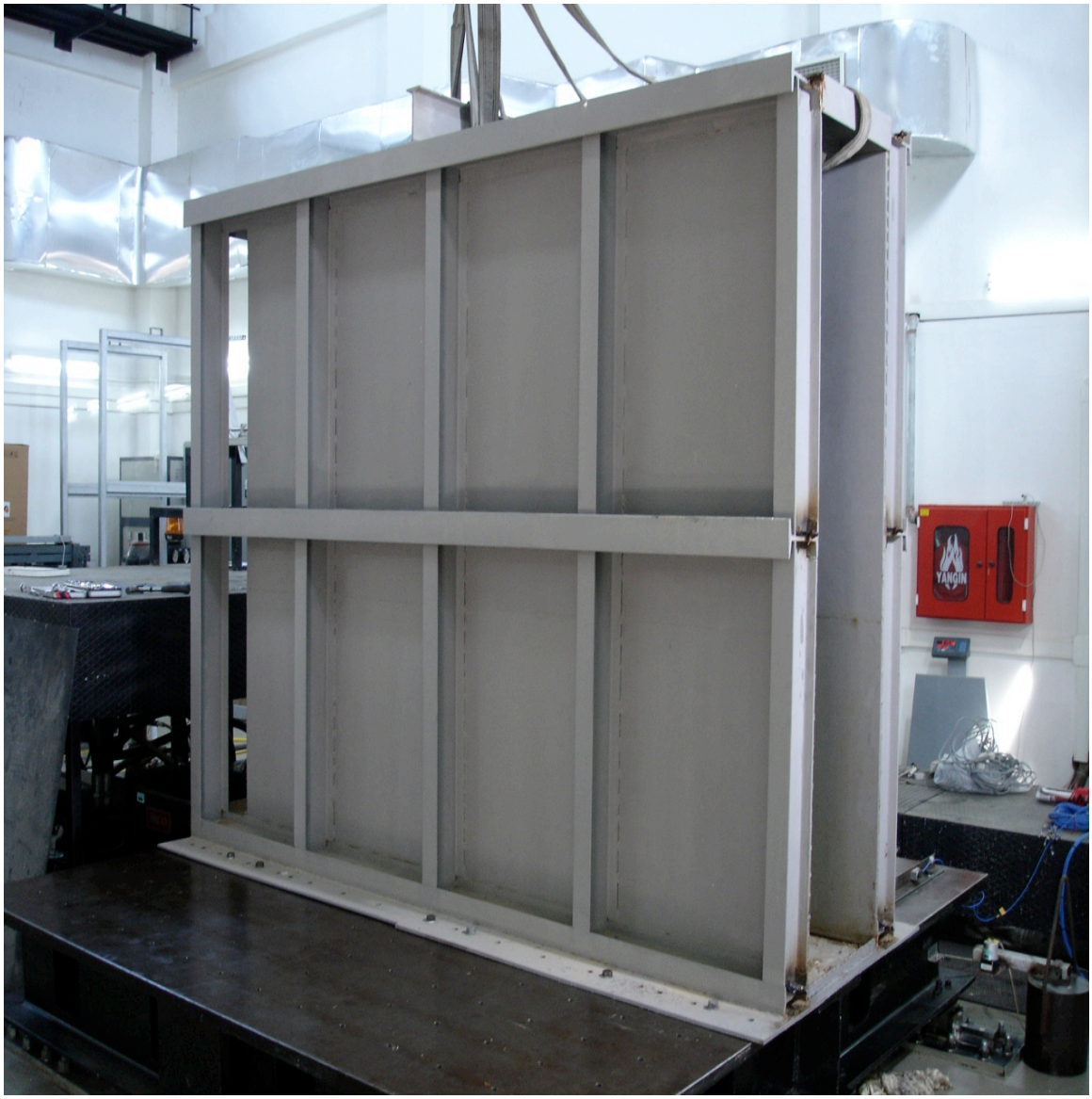


Figure 4.31. The steel container soil box on shaking table



Figure 4.32. A view of bolted connection of steel container to the shaking table

Inner sidewalls of the soil box were lubricated and rubber sheets were placed in. At this point, the rubber sheets were attached to the inner sidewalls by strong tapes and as the construction progressed and backfill soil added in, the tapes were removed. Please refer to Section 4.3.2.3. for detail information on the rubber sheets used in this study.

Following the rubber sheet placement, the filling of the steel container with backfill material took place in construction sequence. Soil was placed in plastic bags and transported to the soil box. The compaction of soil was achieved by a hand-operated compactor inside the steel container soil box at each 20 cm. The compaction level was based on past and field experience. Two advancements –forward and back- along the steel container were enough for the compaction. In order to have a constant compacted zone throughout the layer, in places where some swelling observed, the compaction was achieved by hammer. Same compaction method is applied to the two different types of backfill materials (aggregate and sand) that were used in this study. Granular rubber fill was also placed during these application processes. Please refer to Section 4.3.2.3. and Section 4.3.2.9. for detailed information on rubber sheets and compaction. In Figure 4.33. below, the rubber sheets installed and compaction effort can be seen.



Figure 4.33. The rubber sheets installed and compaction

The sequence of block placement and installation of reinforcement placement followed the previous study by Guler and Enunlu (2009) and field experience.

In this study, both vertical and 6° inclined facings were constructed. In order to simulate segmental retaining structures, hollow concrete facing blocks are placed vertically on the facing with vertical alignment and an inclination of 6° from the vertical. As facing blocks, scaled versions of hollow building blocks used in Turkey as facing elements were used. The dimensions of these model blocks were 100 mm x 100 mm x 200 mm (height, depth, width). The hollow part of the model blocks was filled with sand to increase the interconnection. Please refer to Section 4.3.2.8. for the details of the facing blocks used in this study.

Two different types of geogrid reinforcements with varying lengths were utilized in this study. Detailed information on geogrid specifications and configurations can be found in Section 4.4.

In this study, geogrid reinforcements were horizontally placed with a vertical spacing of 0,2 m., in other words a reinforcement was placed for every two rows of model blocks. No intermediate reinforcement layers were placed during the experiments. The interconnection between the facing blocks and geogrid reinforcement was purely frictional as can be seen in Figure 4.34. Details of geogrid and modular block interface are illustrated in Figure 4.35.



Figure 4.34. Installation of geogrids with frictional connection to the facing blocks

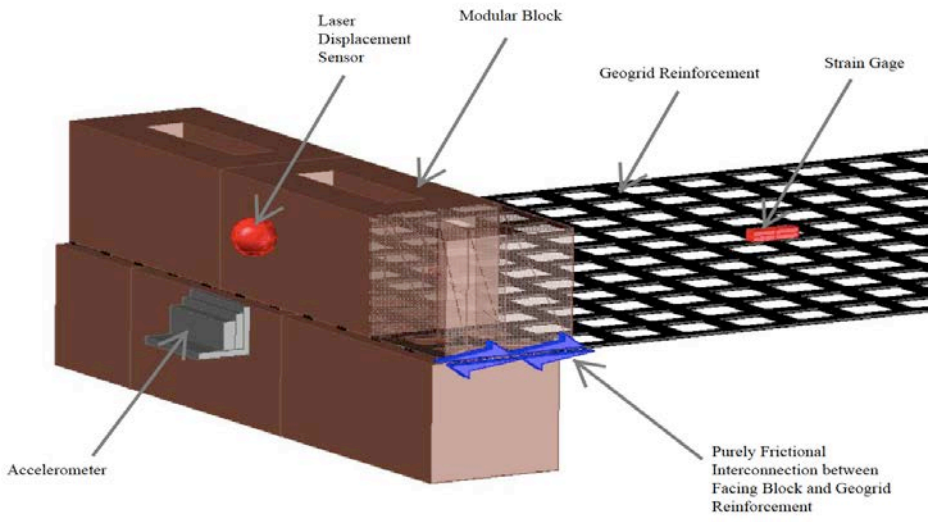


Figure 4.35. Details of block and geogrid interface

The strain gage installed geogrids were placed gently on the backfill and the strain gage cables in flexible polymer pipes were connected to the Data Acquisition System by passing those cables through the previously drilled holes on the facing blocks. Please refer to Section 4.3.3.2. for strain gage installation and details.



Figure 4.36. Strain gage cables inside polymer pipes passing through previously drilled holes of the blocks

The facing wall toe was restricted by welding a piece of steel plate at the bottom part of the container.

The construction scheme can be summarized as filling the backfill soil, compacting of the soil, filling the inside of the modular blocks with sand and then laying down of the geotextile layers and then putting the blocks on top of each other.

Since the uppermost two block levels were the most unstable ones during dynamic excitations, the hollow part of the upper two layers with blocks were filled with concrete grout and two Ø12 construction steel rebars were installed on each block on top to increase

the stability. The top view of grouted and steel bar installed block from the top of the wall can be seen in Figure 4.37.



Figure 4.37. The top view of grouted and steel bar installed block

Finally, when the wall is constructed on the steel container soil box, the glass covered steel frame which hosts the laser displacement sensors is lifted by crane and attached to the container by bolt connections at 6 different locations. That concludes the wall construction process. Please refer to Section 4.3.2.2. for details on glass covered steel frame. The constructed wall can be seen in Figure 4.38. Figure 4.39. shows the glass covered steel frame whie being attached to the steel container. Figure 4.40. shows the final view of the steel container with glass covered steel frame on shaking table before shaking.



Figure 4.38. The constructed Geogrid Reinforced Wall



Figure 4.39. The glass covered steel frame while being attached to the steel container.



Figure 4.40. The steel container with glass covered steel frame on shaking table before shaking.

4.4. Wall Configurations and Reinforcement Layout of Model Walls

A total of four 2 m. high wall models at 1/2 scale comprise the experimental portion of this study. The four walls were constructed with different facing batter (inclination), backfill material and reinforcement strength and length. Also, three different recorded earthquake motions (El Centro, Izmit and Sakarya Earthquakes) were applied on each model. Since the model is a 1:2 scaled model, the natural periods are decreased by $1/\sqrt{2}$. On later stages of the experiment the peak acceleration values of the earthquakes were doubled and tripled meaning that almost 1 g peak acceleration values are applied on the models. Table 4.7. summarizes the wall configurations and model parameters used in this study.

In Table 4.7. where base excitations applied on the walls are stated, it should be noted that abbreviation Earthquake 100% stands for the original scaled earthquake motions are applied on the models where Earthquake 150%, 200%, 250%, 275% abbreviations stands for the earthquake peak accelerations are multiplied by 1.5, 2, 2.5 and 2.75 respectively.

The geogrid reinforcement layout and instrumentations for the four test walls are shown in Figure 4.41. and 4.42. respectively.

Table 4.7. Wall Configurations and model parameters used in this study

Properties	Wall Configuration 1	Wall Configuration 2	Wall Configuration 3	Wall Configuration 4
Base Excitations Applied	El Centro Earthquake 100%, 150%, 200%; Izmit Earthquake 100%, 150%, 200%; Sakarya Earthquake 100%, 150%, 200%	El Centro Earthquake 100%, 150%, 200%; Izmit Earthquake 100%, 150%, 200%; Sakarya Earthquake 100%, 150%, 200%	El Centro Earthquake 100%, 150%, 200%, 250%; Izmit Earthquake 100%, 150%, 200%, 250%; Sakarya Earthquake 100%, 150%, 200%, 250%	El Centro Earthquake 100%, 150%, 200%, 250%, 275%; Izmit Earthquake 100%, 150%, 200%; Sakarya Earthquake 100%, 150%, 200%
Backfill Material	Gravel	Gravel	Gravel	Sand
Facing Inclination	Vertical	6° Inclined	6° Inclined	6° Inclined
Reinforcement Length	0.90 m. (throughout the height of the wall)	0.90 m. (throughout the height of the wall)	1.30 m. (from midheight till upper portion of wall); 1.50 m. (from lower portion till midheight of wall)	1.30 m. (from midheight till upper portion of wall); 1.50 m. (from lower portion till midheight of wall)
L/H Ratio	0.47 (throughout the height of the wall)	0.47 (throughout the height of the wall)	0.70 (from midheight till upper portion of wall); 0.80 (from lower portion till midheight of wall)	0.70 (from midheight till upper portion of wall); 0.80 (from lower portion till midheight of wall)
Ultimate Tensile Strength of Reinforcement (kN/m)	20	20	20 (from midheight till upper portion of wall); 45 (from lower portion till midheight of wall)	20 (from midheight till upper portion of wall); 45 (from lower portion till midheight of wall)
Vertical Reinforcement Spacing (m)	0.2	0.2	0.2	0.2

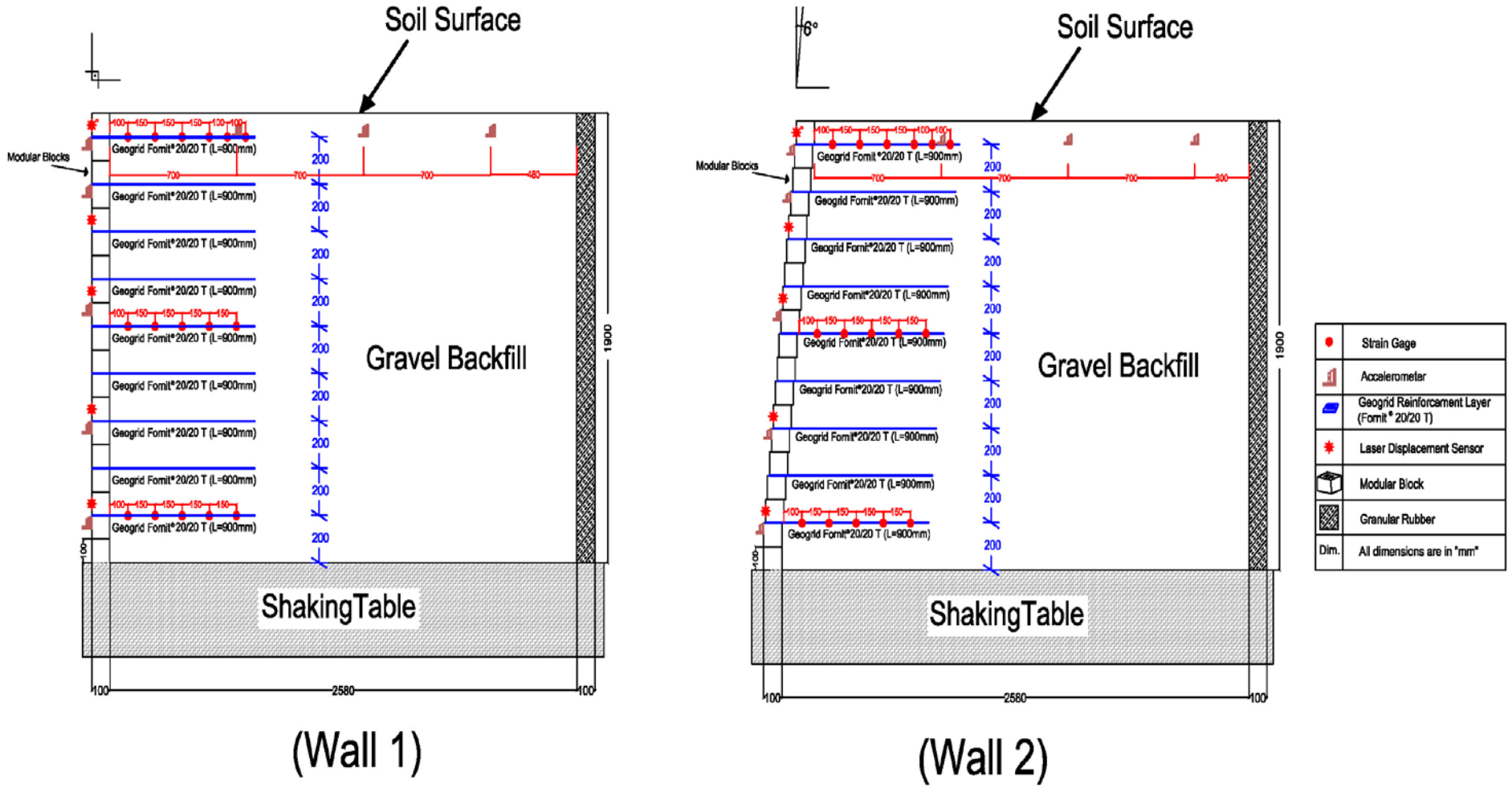


Figure 4.41. Reinforcement Layout and instrumentation of the Wall 1 and Wall 2

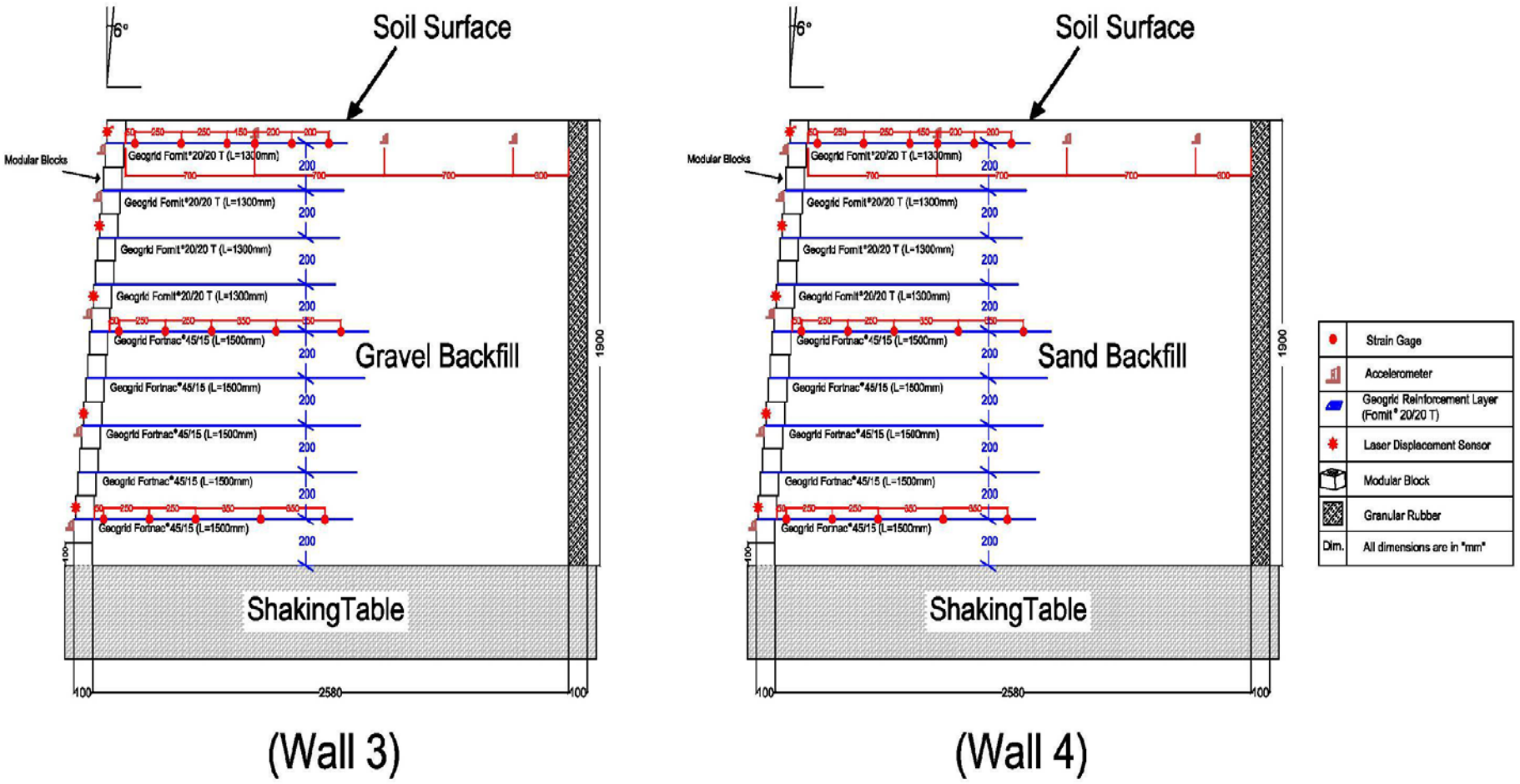


Figure 4.42. Reinforcement Layout and instrumentation of the Wall 3 and Wall 4

In Walls 1 and 2 the reinforcement length was *L*=90 cm throughout the height of the wall. The height of the wall was H= 190 cm. The length of the reinforcement *L* was measured from the front end of the block. The Wall 1 has a vertical facing where Wall 2 has a 6° inclined facing. Both in Wall 1 and Wall 2 the same geogrid reinforcement was used throughout the height of the walls.

Based on the design of a real project, geogrid length of Walls 3 and 4 was increased to L=150 cm for the lower part and L=130 cm. for the upper part of the walls. It should be kept in mind that in Wall 3 and 4 the top geogrid layers were less stronger and shorter (*L*=130 cm) than the geogrid used in lower portion of the wall.

The modification of reinforcement length and spacing was implemented based on the experience on previous studies.

The vertical spacing between consecutive reinforcement layers were *D*=20 cm for all wall configurations. No intermediate reinforcement layers were installed in the walls.

4.5. Dynamic Base Excitations and Shaking Sequence of Model Walls

Three different recorded earthquake motions (El Centro, Izmit and Sakarya Earthquakes) were applied on each model. . Since the model is a 1:2 scaled model, the natural periods are decreased by $1/\sqrt{2}$.

The period of the motion for each earthquake lasted 18.75 seconds for El-Centro, 28 seconds for Izmit and 20 seconds for Sakarya in which the peak accelerations were 0.4 g for El Centro and lower peak accelerations for other two earthquakes. On each model the earthquake peak accelerations were doubled and in some cases almost tripled. Please refer to Table 4.7. for the excitations applied on each wall configuration.

For each test, firstly the original normal scaled versions of the earthquake excitations were applied on shaking table. After the normal scaled versions are completed the increased scaled excitations are run. The test was stopped for about 10 minutes after each excitation since the strain gage data were needed to be set to zero values.

As an example, the scaled versions of El-Centro 100%, Izmit 100% Earthquake motion applied on the shaking table and response spectrums are given in Figure 4.43.. and Figure 4.44. respectively. The data regarding the accelerations and response spectrum can be found in Appendix .A for each test.

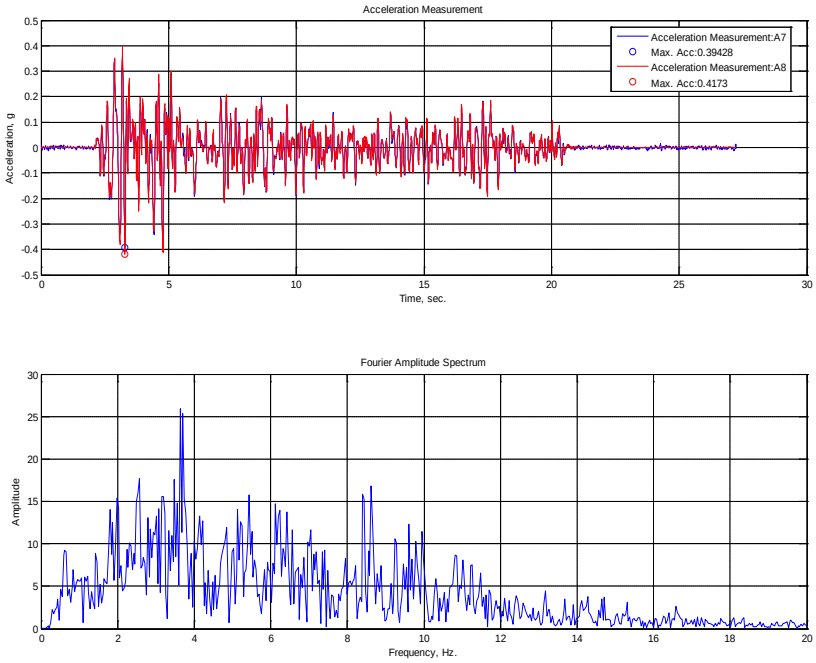


Figure 4.43. Scaled original record of the El Centro earthquake and Response spectrum

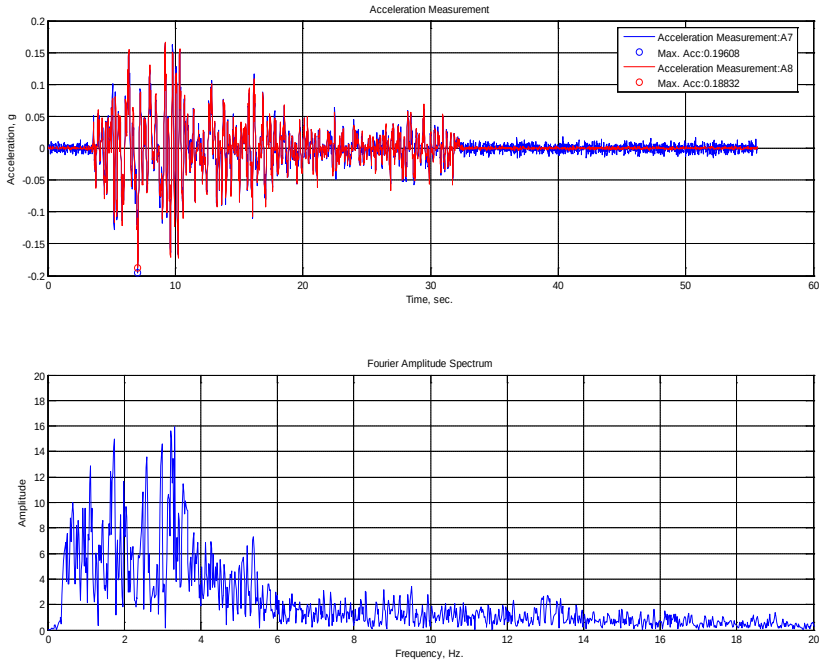


Figure 4.44. Scaled original record of the Izmit earthquake and Response spectrum

4.6. Test Program

Table 4.8. summarizes essential details and objectives of the four test walls constructed in this study.

Table 4.8. Test Program

Wall Configuration	Description	Objectives/Variables
Wall 1	Geogrid reinforced soil wall with vertical modular block facing and a weak biaxial polypropylene (PP) geogrid placed at 0.2 m vertical spacing in gravel backfill.	Influence of facing batter and increasing horizontal base acceleration on facing deformation / acceleration amplification / reinforcement strains are investigated.
Wall 2	Geogrid reinforced soil wall with 6° inclined modular block facing and a weak biaxial polypropylene (PP) geogrid placed at 0.2 m vertical spacing in gravel backfill.	Reference Wall for Wall 1 and Wall 3
Wall 3	Geogrid reinforced soil wall with 6° inclined modular block facing and a strong polyester (PET) geogrid placed at 0.2 m vertical spacing in gravel backfill.	Influence of reinforcement type and length and increasing horizontal base acceleration on facing deformation/acceleration amplification/ reinforcement strains are investigated. Reference Wall for Wall 4.
Wall 4	Geogrid reinforced soil wall with 6° inclined modular block facing and a strong polyester (PET) geogrid placed at 0.2 m vertical spacing in sand backfill.	Influence of backfill material and increasing horizontal base acceleration on facing deformation/acceleration amplification/ reinforcement strains are investigated.

5. TEST RESULTS AND EVALUATION

5.1. General

In this chapter, firstly the data evaluation method of test results shall be presented. The results, evaluation and assessment of acceleration amplification, horizontal displacements on wall facing and strain/stress distribution in geogrid reinforcements during and at the end of construction of the model walls are presented with related figures and tables. Lastly, the strains and tensile loads generated in geogrid layers during earthquake motion and observations made in the experiments are presented and evaluated in detail.

5.2. Test Data Evaluation Method

5.2.1. Data Evaluation Method for Displacement Laser Sensors and Accelerometers

The data from displacement laser sensors and accelerometers were collected at a high sampling rate (200 sample per second) so as to avoid aliasing errors and to capture the peak values of dynamic wall response during base excitation. National Instruments' PCI-6229 M Data Acquisition System was used for both instruments.

Since the time-history data obtained from accelerometers were noise influenced all acceleration- time-history data were filtered between 0,1 Hz and 20 Hz to obtain accurate and correct results. In data evaluation, the filtered data were taken into account. As an example, the raw acceleration data of El Centro 100% earthquake motion obtained from the accelerometer mounted on shaking table is shown in Figure 5.1. In Figure 5.2., the filtered accelerometer data can be seen. The evaluation and assessment of accelerometer data were based on the filtered data.

Due to large amount of data collected, please refer to Appendix A. for all of the output on acceleration-time history curves obtained from tests.

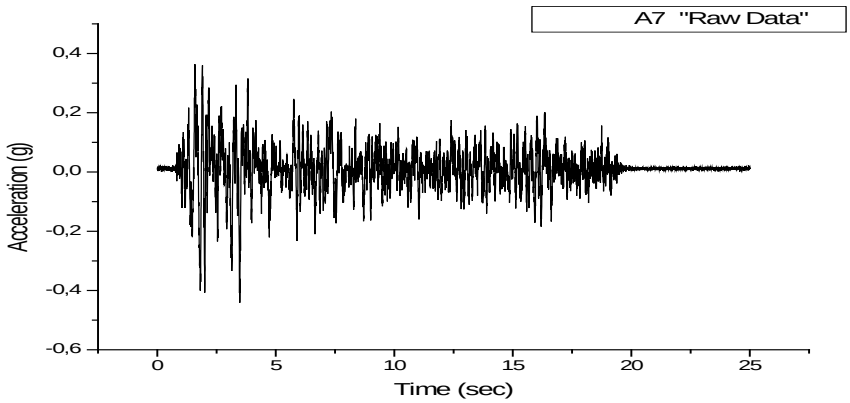


Figure 5.1. Noise Influenced Accelerometer Data

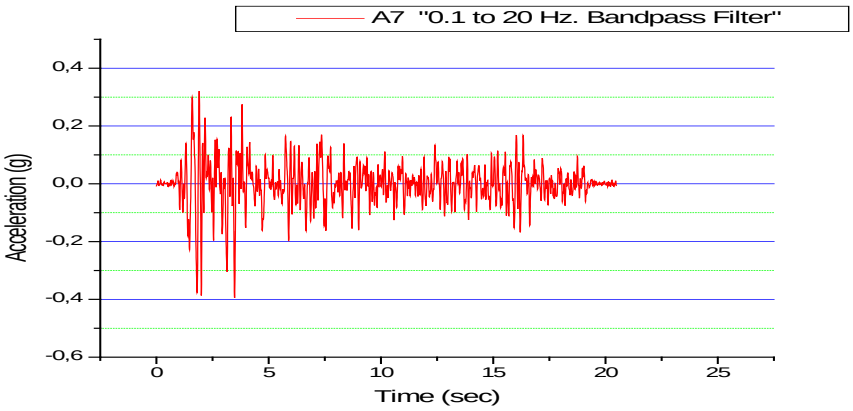


Figure 5.2. 0.1 to 20 Hz. Bandpass Filtered Accelerometer Data

The raw displacement-time history data obtained from laser displacement sensors can be seen in Figure 5.3. As seen on the related figure, there are many sudden and big increments of displacement shifts that are caused by the noise. In order to prevent this, all displacement- time-history data were filtered between 0,1 Hz and 20 Hz and undisturbed diagrams were obtained as shown in Figure 5.4. The evaluation and assessment of displacement data were based on the filtered data.

As can be seen in Figure 5.3. and Figure 5.4. no residual displacement of the front facing is observed in the diagrams. However, in some tests permanent displacements are observed on the front facing of the walls. As an example; the front facing displacement-time history data where permanent displacement observed is presented in Figure 5.5.

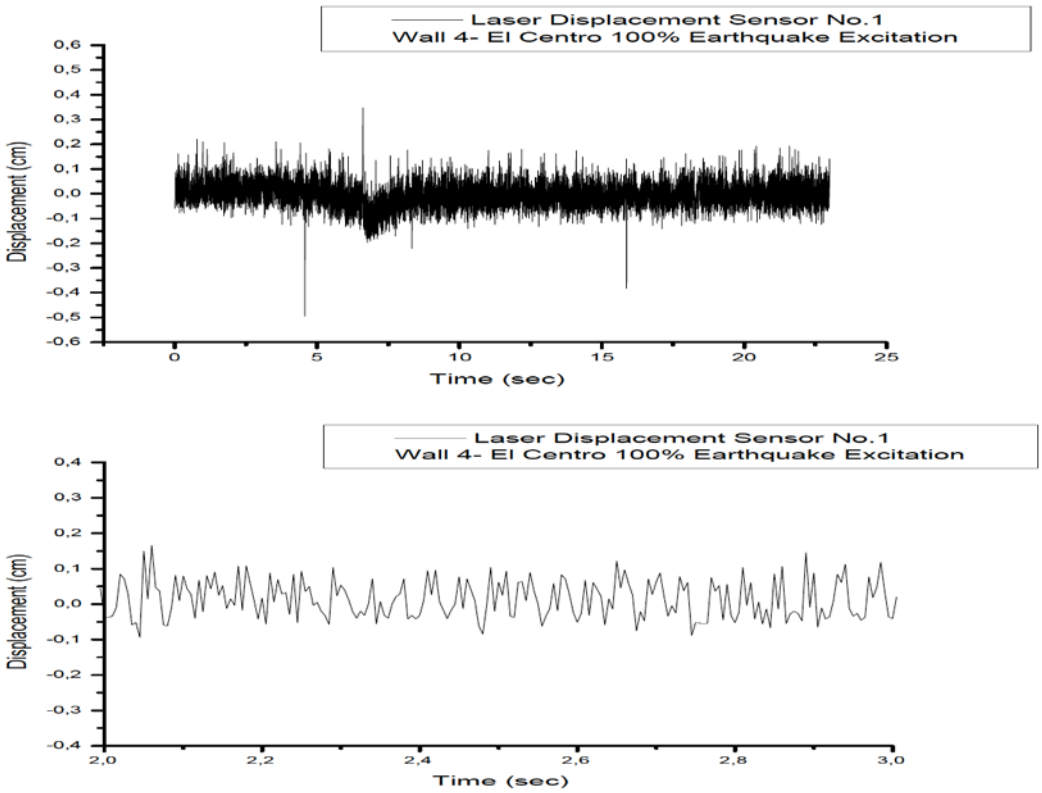


Figure 5.3. Noise Influenced Displacement Data

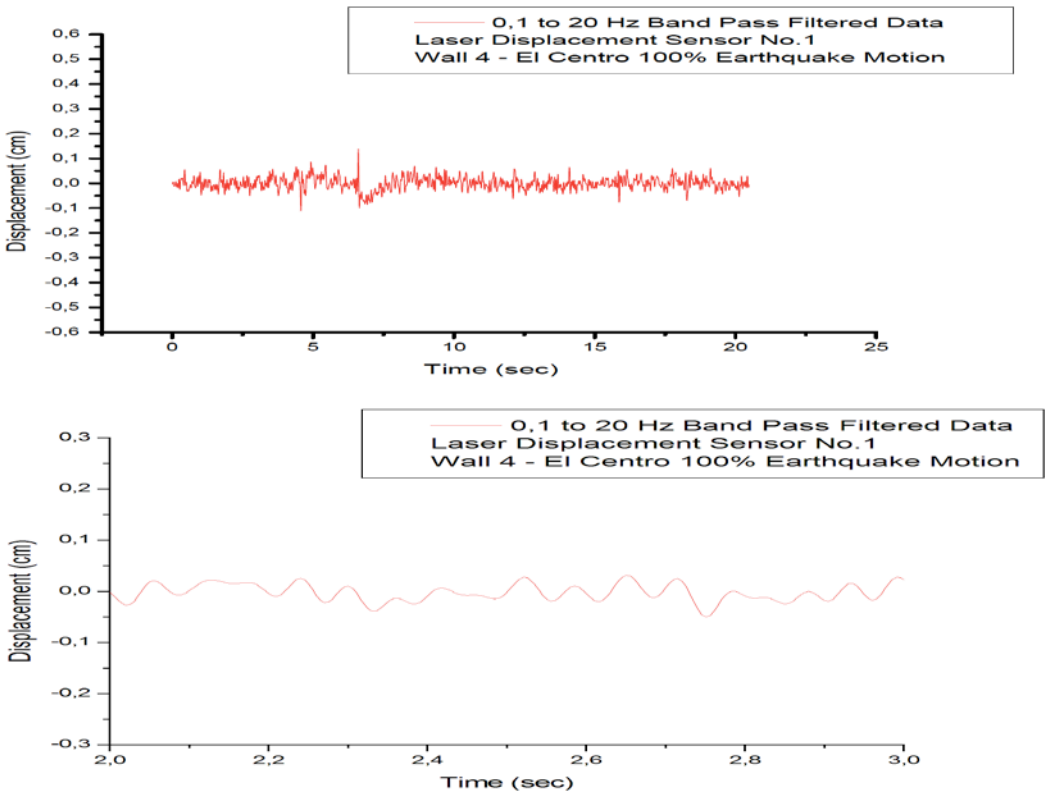


Figure 5.4. 0.1 to 20 Hz. Bandpass Filtered Displacement Data

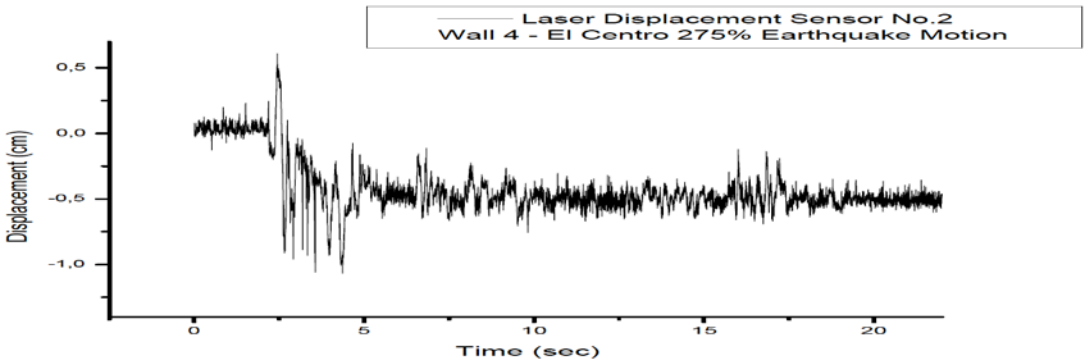


Figure 5.5. The displacement-time history data where permanent facing displacement observed

Due to large amount of data collected, please refer to Appendix B. for all of the output on facing displacement-time history curves.

5.2.2. Data Evaluation Method for Displacement Laser Sensors and Accelerometers

Since the data acquisition systems used for strain data were different from the ones used for accelerometer and laser displacement data, the sampling rates differed. 8 sample per second sampling rate is applied for strain data. Due to low sampling rate and clarity of the strain data, no filters were applied on those data. The data are analyzed using OriginLab and Matlab computer programs.

As an example, the strain gage data of El Centro 100% earthquake motion obtained from the differemt strain gages mounted on the same geogrid reinforcement is shown in Figure 5.6. and Figure 5.7. both figures demonstrates that both tensile and compressional forces are active during the earthquake motion which acts as pressure waves propagating through the media.

In the plots presented in the following sections, the commencement point of the strain data and acceleration and displacement data of the base acceleration have been manually adjusted due to usage of different Data Acquisition systems. So, unless told otherwise the wall response values are referenced to the peak features of the each applied seismic excitation.

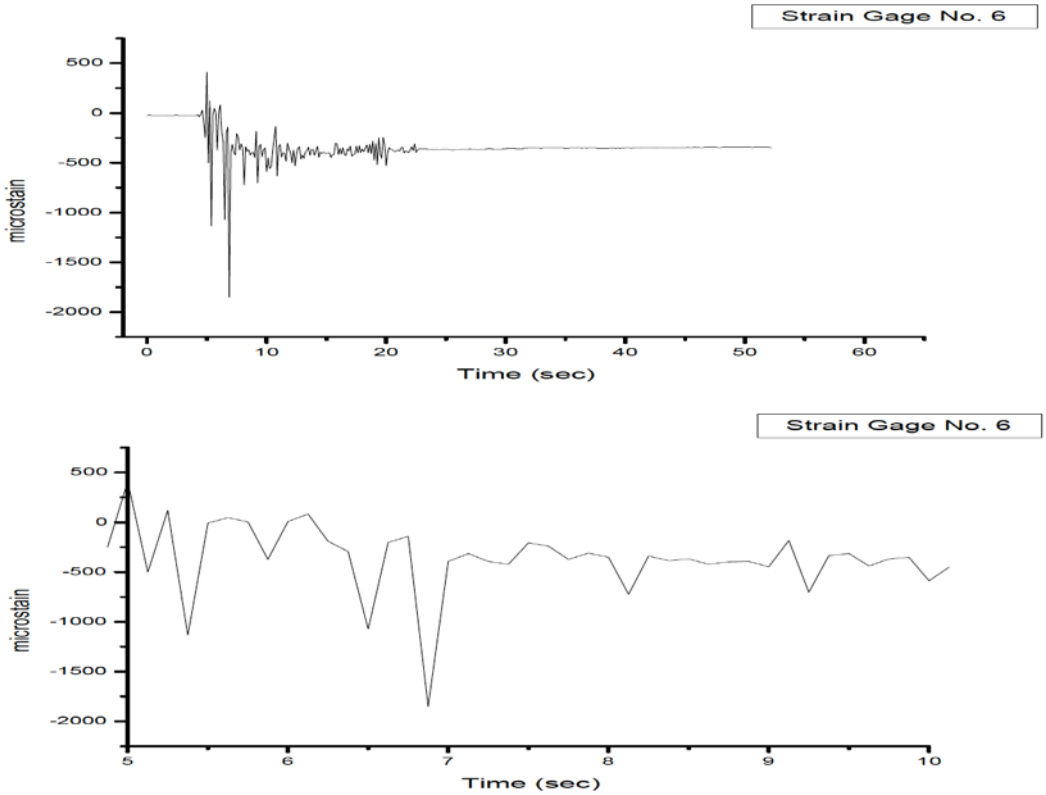


Figure 5.6. Tensile force dominant strain gage data

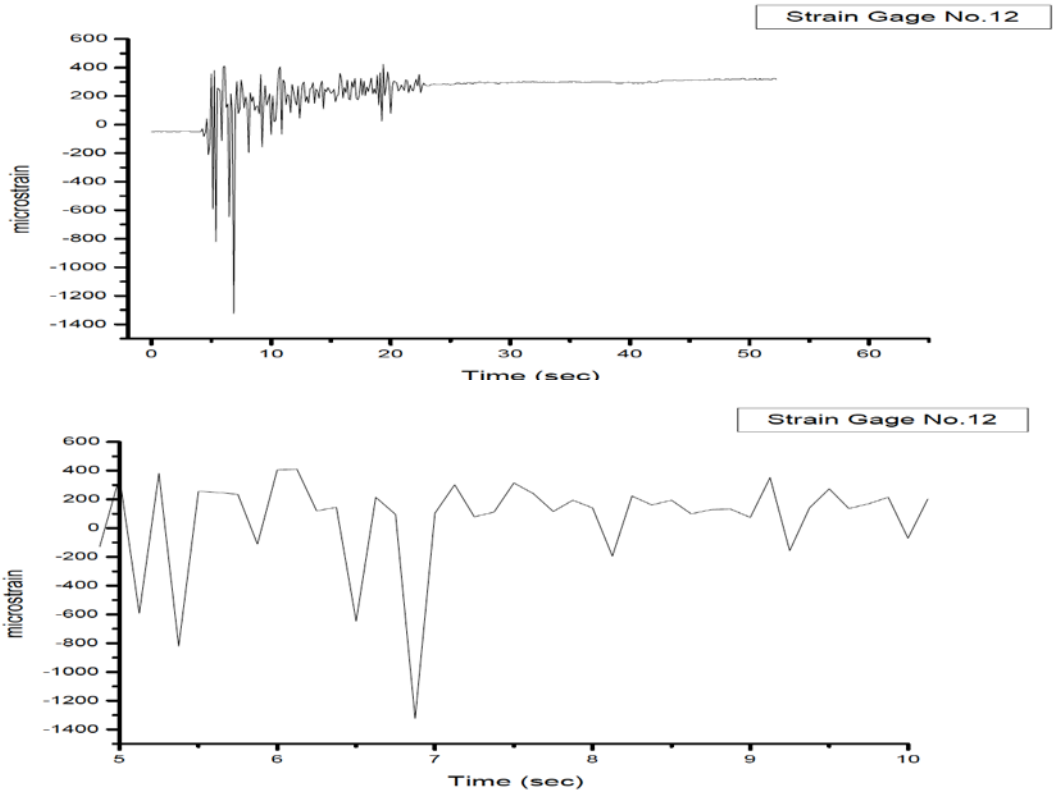


Figure 5.7. Compressional force dominant strain gage data

Due to large amount of data collected, please refer to Appendix C. for all of the output on strain-time history curves.

5.3. Fundamental Frequency of the Walls

The acceleration-time history data obtained from the experiments were used for to find out the predominant frequencies of the each wall configuration. Fast Fourier Transform is applied on each acceleration-time history data to plot the acceleration response spectra by using MATLAB computer program. The predominant frequencies are determined by reading the peak values on the acceleration response spectra. As an example, The Fourier Amplitude Spectra plotted related to table acceleration-time history data of Wall 3- El Centro 100% excitation can be seen in Figure 5.8.

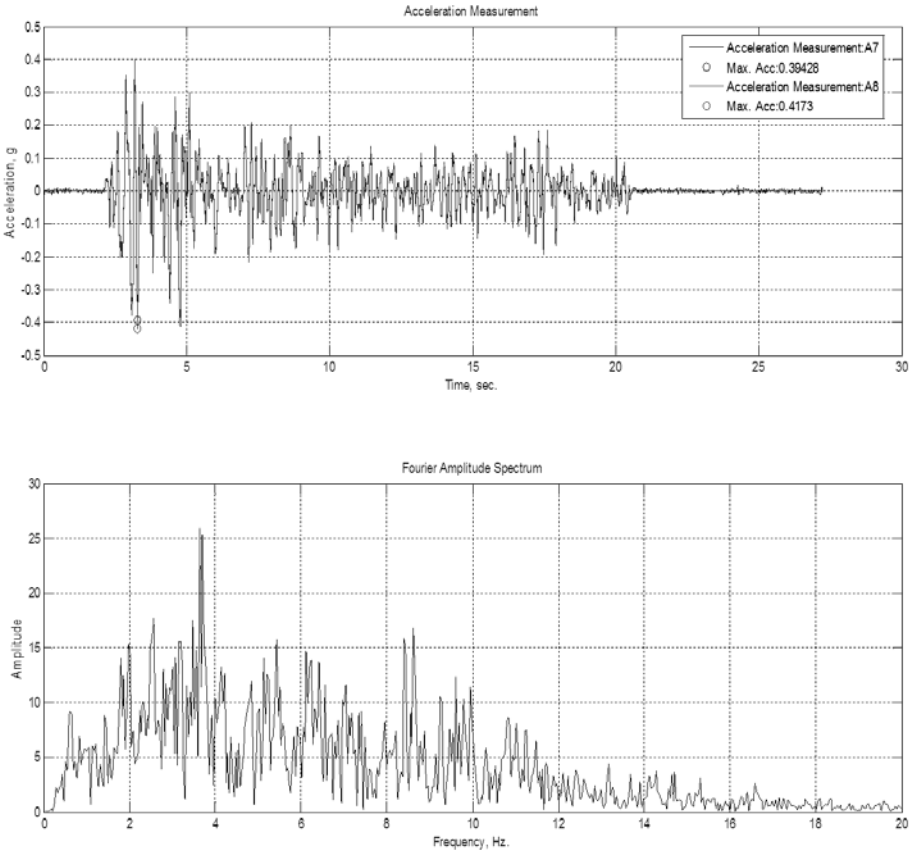


Figure 5.8.Acceleration-time history data of Wall 3- El Centro 100% excitation together with the Fourier Amplitude Spectra

Due to large amount of data collected, please refer to Appendix A.for all Fourier Amplitude Spectra plotted according to the acceleration-time history data.

The fundamental frequency is defined as the lowest frequency of a periodic waveform. Wu (1994) suggested the empirical Formula 5.1. to find out the fundamental frequency of vibration for a two dimensional, linear elastic mediumof width “B” and height “H”, which contained by two rigid vertical boundaries, a rigid base and subjected to horizontal base excitation.

$$f_{11}=\frac{1}{4H}\sqrt{\frac{G}{Q}}\sqrt{1+\left(\frac{2}{1-\nu}\right)\left(\frac{H}{B}\right)^2)} \qquad (5.1)$$

Where f_{11} is frequency in Hz corresponding to the first mode shape of the medium in both the horizontal and vertical directions, G is the shear modulus; Q is density and ν is the Poisson ratio of the soil medium.

The fundamental frequency of the wall with soil layer height H = 1.9 m and B = 2.8 m. ($\gamma_{approx.}$ = 17 kN/m^2. Q= 1.73 gr/cm^3. G = 11220 kN/m^2 for E=29180 kN/m^2) is found to be f_{11}=16 Hz.

Below in Table 5.1, a summary of the predominant frequencies for each experiment is presented.

Even when the peak amplitudes of the applied earthquake records (El-Centro, Izmit and Sakarya) are doubled and almost tripled, the predominant frequencies of the scaled records of the earthquakes cannot attain the calculated empirical fundamental frequency of the models (16 Hz).

As a result, a resonant behavior was not expected and observed during the experiments.

Table 5.1. Predominant frequencies evaluated according to the plotted acceleration response spectrums for each applied base excitation.

WALL 1, WALL 2 , WALL3 AND WALL 4														
Accelerometers \ Dynamic Excitations		EL CENTRO EARTHQUAKE 100%	EL CENTRO EARTHQUAKE 150%	EL CENTRO EARTHQUAKE 200%	EL CENTRO EARTHQUAKE 250%	EL CENTRO EARTHQUAKE 275%	IZMIT EARTHQUAKE 100%	IZMIT EARTHQUAKE 150%	IZMIT EARTHQUAKE 200%	IZMIT EARTHQUAKE 250%	SAKARYA EARTHQUAKE 100%	SAKARYA EARTHQUAKE 150%	SAKARYA EARTHQUAKE 200%	SAKARYA EARTHQUAKE 250%
Location of Accelerometers	Accelerometer No.	Predominant Frequency (fdom) (Hz)	Predominant Frequency (fdom) (Hz)	Predominant Frequency (fdom) (Hz)	Predominant Frequency (fdom) (Hz)	Predominant Frequency (fdom) (Hz)	Predominant Frequency (fdom) (Hz)	Predominant Frequency (fdom) (Hz)	Predominant Frequency (fdom) (Hz)	Predominant Frequency (fdom) (Hz)	Predominant Frequency (fdom) (Hz)	Predominant Frequency (fdom) (Hz)	Predominant Frequency (fdom) (Hz)	Predominant Frequency (fdom) (Hz)
SHAKING TABLE	Accelerometer 1 (Base Input)	3.75	3.75	3.75	3.75	3.75	3.2	3.2	3.2	3.2	1.23	1.23	1.23	1.23
WALL FACE	Accelerometer 2 (@h= 0,15 m)	3.85	3.85	3.85	3.85	3.85	3.23	3.23	3.23	3.23	1.25	1.25	1.25	1.25
	Accelerometer 3 (@h= 0,55 m)	3.86	3.86	3.86	3.86	3.86	3.3	3.3	3.3	3.3	1.28	1.28	1.28	1.28
	Accelerometer 4 (@h= 1,05 m)	3.88	3.88	3.88	3.88	3.88	3.32	3.32	3.32	3.32	1.28	1.28	1.28	1.28
	Accelerometer 5 (@h= 1,55 m)	3.9	3.9	5.12	5.12	5.12	3.4	3.4	3.4	3.45	1.35	1.35	1.35	1.35
	Accelerometer 6 (@h= 1,75 m)	3.91	3.91	5.13	5.13	5.13	3.4	3.4	3.4	3.47	1.35	1.35	1.35	1.35
BACKFILL	Accelerometer 7 (@80 cm. from face block)	3.92	3.92	3.92	3.95	3.95	3.42	3.42	3.42	3.42	1.4	1.4	1.4	1.4
	Accelerometer 8 (@160 cm. from face block)	3.93	3.93	3.93	3.93	3.95	3.45	3.45	3.45	3.45	1.44	1.44	1.44	1.44
	Accelerometer 9 (@240 cm. from face block)	3.93	3.93	5.09	5.12	5.2	3.48	3.48	3.48	3.48	1.45	1.45	1.45	1.45

5.4. Acceleration Amplification

The acceleration responses measured with accelerometers are investigated to understand the acceleration amplification behavior of the wall systems constructed since the distribution and magnitude of peak accelerations on structure and in the backfill soil is of interest in pseudo static seismic design methods.

The maximum acceleration amplification factor is described as the ratio of the maximum acceleration in the structure to the peak input base acceleration. The peak accelerations for each accelerometer on shaking table, in the front end of the blocks, in the reinforced and un-reinforced zone of the backfill soil are used for the calculation of acceleration amplification. The amplification factor is calculated as the ratio of maximum acceleration on the facing blocks and at the top of backfill, to the maximum acceleration at the shaking table for the certain time instance.

5.4.1. Test Results

In this section the results obtained from accelerometer measurements shall be summarized. All acceleration-time history curve plots are given in Appendix A. In the Tables 5.2.through 5.13. acceleration amplification factors together with the peak values of the accelerations and the time instances at the occurrences of the peaks are compiled and presented for each wall configurations and base excitations. The results show that maximum accelerations occurred when the base acceleration was at its peak. The yellow highlighted values are the maximum acceleration values observed at front face of wall and on top of backfill respectively. The red highlighted values represent that the acceleration amplification value is below 1 meaning that the acceleration observed is lower than the base input acceleration. However this phenomenon has occurred only in few experiments and can be ignored.The observed time instances of the maximum base accelerations may differ in each test due to the manual commencing of the shaking table tests by an operator. The maximum accelerations for each accelerometer in the front end of the blocks and on top of the backfill (when the base acceleration was at its peak) are shown in the Figures 5.9 though 5.16. in order to compare the different effects of the wall configurations. The base excitation amplitudes for each applied earthquake motion are given in the figures.

Table 5.2. Acceleration amplification factors with the peak values of the accelerations and the time instances at the occurrences of the peaks for Wall 1 El Centro Earthquake

WALL CONFIGURATION 1									
Accelerometers \ Dynamic Excitations		EL CENTRO EARTHQUAKE 100%			EL CENTRO EARTHQUAKE 150%			EL CENTRO EARTHQUAKE 200%	
Location of Accelerometers	Accelerometer No.	Time Instance (sec.)	Peak Acceleration (g)	Amplification Factor	Time Instance (sec.)	Peak Acceleration (g)	Amplification Factor	Time Instance (sec.)	Peak Acceleration (g)	Amplification Factor
SHAKING TABLE	Accelerometer 1 (Base Input)	4.79	-0.39		2.14	-0.558		1.93	-0.74	
WALL FACE	Accelerometer 2 (@h= 0,15 m)	4.79	-0.396	1.015	2.14	-0.565	1.013	1.93	-0.787	1.064
	Accelerometer 3 (@h= 0,55 m)	4.8	-0.417	1.069	2.33	0.595	1.066	1.94	-0.75	1.014
	Accelerometer 4 (@h= 1,05 m)	4.81	-0.437	1.121	2.24	0.653	1.17	2.05	0.866	1.17
	Accelerometer 5 (@h= 1,55 m)	4.81	-0.477	1.223	2.25	0.727	1.303	2.06	0.965	1.304
	Accelerometer 6 (@h= 1,75 m)	4.81	-0.472	1.21	2.225	0.713	1.278	2.06	0.884	1.195
BACKFILL	Accelerometer 7 (@80 cm. from face block)	4.81	-0.488	1.251	2.225	0.742	1.33	2.06	0.924	1.249
	Accelerometer 8 (@160 cm. from face block)	4.81	-0.471	1.208	2.225	0.734	1.315	2.06	0.943	1.274
	Accelerometer 9 (@240 cm. from face block)	4.81	-0.448	1.149	2.24	0.677	1.213	2.05	1.051	1.42

Table 5.3. Acceleration amplification factors with the peak values of the accelerations and the time instances at the occurrences of the peaks for Wall 1 Izmit Earthquake

WALL CONFIGURATION 1										
Accelerometers \ Dynamic Excitations		IZMIT EARTHQUAKE 100%			IZMIT EARTHQUAKE 150%			IZMIT EARTHQUAKE 200%		
Location of Accelerometers	Accelerometer No.	Time Instance (sec.)	Peak Acceleration (g)	Amplification Factor	Time Instance (sec.)	Peak Acceleration (g)	Amplification Factor	Time Instance (sec.)	Peak Acceleration (g)	Amplification Factor
SHAKING TABLE	Accelerometer 1 (Base Input)	10.29	-0.179		5.86	-0.272		5.42	-0.368	
WALL FACE	Accelerometer 2 (@h= 0,15 m)	7.73	-0.187	1.045	5.86	-0.261	0.96	5.43	-0.336	0.913
	Accelerometer 3 (@h= 0,55 m)	7.74	-0.196	1.095	5.87	-0.271	0.996	5.43	-0.339	0.921
	Accelerometer 4 (@h= 1,05 m)	7.74	-0.212	1.184	5.87	-0.29	1.066	5.43	-0.342	0.929
	Accelerometer 5 (@h= 1,55 m)	7.74	-0.221	1.235	5.87	-0.299	1.099	7.99	-0.355	0.965
	Accelerometer 6 (@h= 1,75 m)	7.74	-0.225	1.257	5.87	-0.307	1.129	7.99	-0.364	0.989
BACKFILL	Accelerometer 7 (@80 cm. from face block)	7.74	-0.223	1.246	5.87	-0.302	1.11	7.99	-0.362	0.984
	Accelerometer 8 (@160 cm. from face block)	7.74	-0.215	1.201	5.87	-0.292	1.074	5.44	-0.348	0.946
	Accelerometer 9 (@240 cm. from face block)	7.74	-0.209	1.168	5.87	-0.287	1.055	5.44	-0.34	0.924

Table5.4. Acceleration amplification factors with the peak values of the accelerations and the time instances at the occurrences of the peaks for Wall 1 Sakarya Earthquake

WALL CONFIGURATION 1										
Accelerometers \ Dynamic Excitations		SAKARYA EARTHQUAKE 100%			SAKARYA EARTHQUAKE 150%			SAKARYA EARTHQUAKE 200%		
Location of Accelerometers	Accelerometer No.	Time Instance (sec.)	Peak Acceleration (g)	Amplification Factor	Time Instance (sec.)	Peak Acceleration (g)	Amplification Factor	Time Instance (sec.)	Peak Acceleration (g)	Amplification Factor
SHAKING TABLE	Accelerometer 1 (Base Input)	7.75	-0.223		9.59	-0.31		7.81	-0.379	
WALL FACE	Accelerometer 2 (@h= 0,15 m)	7.74	-0.223	1	9.59	-0.311	1.003	7.81	-0.393	1.037
	Accelerometer 3 (@h= 0,55 m)	7.75	-0.229	1.027	9.6	-0.317	1.023	7.81	-0.398	1.05
	Accelerometer 4 (@h= 1,05 m)	7.75	-0.247	1.108	9.6	-0.329	1.061	7.81	-0.399	1.053
	Accelerometer 5 (@h= 1,55 m)	7.75	-0.259	1.161	9.61	-0.335	1.081	9.08	0.395	1.042
	Accelerometer 6 (@h= 1,75 m)	7.75	-0.265	1.188	9.61	-0.346	1.116	9.08	0.399	1.053
BACKFILL	Accelerometer 7 (@80 cm. from face block)	7.75	-0.259	1.161	9.61	-0.341	1.1	9.08	0.399	1.053
	Accelerometer 8 (@160 cm. from face block)	7.75	-0.248	1.112	9.61	-0.338	1.09	7.81	-0.39	1.029
	Accelerometer 9 (@240 cm. from face block)	7.75	-0.242	1.085	9.61	-0.331	1.068	7.81	-0.38	1.003

Table 5.5. Acceleration amplification factors with the peak values of the accelerations and the time instances at the occurrences of the peaks for Wall 2 El Centro Earthquake

WALL CONFIGURATION 2										
Accelerometers \ Dynamic Excitations		EL CENTRO EARTHQUAKE 100%			EL CENTRO EARTHQUAKE 150%			EL CENTRO EARTHQUAKE 200%		
Location of Accelerometers	Accelerometer No.	Time Instance (sec.)	Peak Acceleration (g)	Amplification Factor	Time Instance (sec.)	Peak Acceleration (g)	Amplification Factor	Time Instance (sec.)	Peak Acceleration (g)	Amplification Factor
SHAKING TABLE	Accelerometer 1 (Base Input)	1.73	-0.429		1.83	-0.577		1.79	0.735	
WALL FACE	Accelerometer 2 (@h= 0,15 m)	1.73	-0.436	1.016	1.84	-0.597	1.035	1.9	0.743	1.011
	Accelerometer 3 (@h= 0,55 m)	1.74	-0.448	1.044	2.04	-0.621	1.076	3.14	-0.842	1.146
	Accelerometer 4 (@h= 1,05 m)	1.74	-0.472	1.1	1.95	-0.679	1.177	2.01	-0.883	1.201
	Accelerometer 5 (@h= 1,55 m)	1.75	-0.509	1.186	1.96	0.785	1.36	1.93	1.044	1.42
	Accelerometer 6 (@h= 1,75 m)	3.24	-0.509	1.186	1.96	0.837	1.451	1.94	1.14	1.551
BACKFILL	Accelerometer 7 (@80 cm. from face block)	1.75	-0.512	1.193	1.96	0.742	1.286	1.92	0.903	1.229
	Accelerometer 8 (@160 cm. from face block)	1.75	-0.524	1.221	1.96	0.758	1.314	1.92	0.944	1.284
	Accelerometer 9 (@240 cm. from face block)	3.23	-0.521	1.214	1.95	0.806	1.397	1.92	1.337	1.819

Table5.6. Acceleration amplification factors with the peak values of the accelerations and the time instances at the occurrences of the peaks for Wall 2 Izmit Earthquake

WALL CONFIGURATION 2										
Dynamic Excitations / Accelerometers		IZMIT EARTHQUAKE 100%			IZMIT EARTHQUAKE 150%			IZMIT EARTHQUAKE 200%		
Location of Accelerometers	Accelerometer No.	Time Instance (sec.)	Peak Acceleration (g)	Amplification Factor	Time Instance (sec.)	Peak Acceleration (g)	Amplification Factor	Time Instance (sec.)	Peak Acceleration (g)	Amplification Factor
SHAKING TABLE	Accelerometer 1 (Base Input)	5.58	-0.201		6.07	-0.288		8.4	-0.347	
WALL FACE	Accelerometer 2 (@h= 0,15 m)	5.59	-0.209	1.04	6.07	-0.28	0.972	7.97	0.342	0.986
	Accelerometer 3 (@h= 0,55 m)	5.59	-0.217	1.08	6.07	-0.291	1.01	7.97	0.364	1.049
	Accelerometer 4 (@h= 1,05 m)	5.59	-0.235	1.169	6.07	-0.296	1.028	7.98	0.379	1.092
	Accelerometer 5 (@h= 1,55 m)	5.59	-0.257	1.279	6.08	-0.317	1.101	7.98	0.405	1.167
	Accelerometer 6 (@h= 1,75 m)	5.6	-0.279	1.388	6.08	-0.327	1.135	7.98	0.418	1.205
BACKFILL	Accelerometer 7 (@80 cm. from face block)	5.59	-0.259	1.289	6.08	0.311	1.081	7.98	0.413	1.19
	Accelerometer 8 (@160 cm. from face block)	5.59	-0.264	1.313	6.08	0.312	1.083	7.98	0.419	1.207
	Accelerometer 9 (@240 cm. from face block)	5.59	-0.271	1.348	6.08	0.304	1.056	7.98	0.405	1.167

Table5.7. Acceleration amplification factors with the peak values of the accelerations and the time instances at the occurrences of the peaks for Wall 2 Sakarya Earthquake

WALL CONFIGURATION 2										
Accelerometers / Dynamic Excitations		SAKARYA EARTHQUAKE 100%			SAKARYA EARTHQUAKE 150%			SAKARYA EARTHQUAKE 200%		
Location of Accelerometers	Accelerometer No.	Time Instance (sec.)	Peak Acceleration (g)	Amplification Factor	Time Instance (sec.)	Peak Acceleration (g)	Amplification Factor	Time Instance (sec.)	Peak Acceleration (g)	Amplification Factor
SHAKING TABLE	Accelerometer 1 (Base Input)	7.68	-0.235		7.64	-0.319		9.4	-0.419	
WALL FACE	Accelerometer 2 (@h= 0,15 m)	7.69	-0.244	1.038	7.64	-0.32	1.003	9.4	-0.398	0.95
	Accelerometer 3 (@h= 0,55 m)	7.69	-0.243	1.034	7.64	-0.322	1.009	9.4	-0.43	1.026
	Accelerometer 4 (@h= 1,05 m)	7.69	-0.246	1.047	7.65	-0.332	1.041	10.69	0.424	1.012
	Accelerometer 5 (@h= 1,55 m)	7.69	-0.27	1.149	7.66	-0.338	1.06	10.69	0.441	1.053
	Accelerometer 6 (@h= 1,75 m)	7.69	-0.276	1.174	11.36	-0.354	1.11	10.69	0.452	1.079
BACKFILL	Accelerometer 7 (@80 cm. from face block)	7.69	-0.268	1.14	7.65	-0.342	1.072	10.69	0.452	1.079
	Accelerometer 8 (@160 cm. from face block)	7.69	-0.269	1.145	7.65	-0.34	1.066	10.69	0.454	1.084
	Accelerometer 9 (@240 cm. from face block)	7.69	-0.263	1.119	11.35	-0.331	1.038	10.69	0.441	1.053

Table 5.8. Acceleration amplification factors with the peak values of the accelerations and the time instances at the occurrences of the peaks for Wall 3 El Centro Earthquake

WALL CONFIGURATION 3													
Accelerometers \ Dynamic Excitations		EL CENTRO EARTHQUAKE 100%			EL CENTRO EARTHQUAKE 150%			EL CENTRO EARTHQUAKE 200%			EL CENTRO EARTHQUAKE 250%		
Location of Accelerometers	Accelerometer No.	Time Instance (sec.)	Peak Acceleration (g)	Amplification Factor	Time Instance (sec.)	Peak Acceleration (g)	Amplification Factor	Time Instance (sec.)	Peak Acceleration (g)	Amplification Factor	Time Instance (sec.)	Peak Acceleration (g)	Amplification Factor
SHAKING TABLE	Accelerometer 1 (Base Input)	1.6	-0.405		1.44	-0.58	1.043	1.45	0.728	1.28	1.3	-0.903	1.051
WALL FACE	Accelerometer 2 (@h= 0,15 m)	1.6	-0.423	1.044	1.44	-0.605	1.14	1.36	-0.932	1.196	1.42	0.949	1.186
	Accelerometer 3 (@h= 0,55 m)	1.6	-0.42	1.037	1.36	0.661	1.236	1.46	0.871	1.24	1.43	1.071	1.179
	Accelerometer 4 (@h= 1,05 m)	1.61	-0.457	1.128	1.36	0.717	1.278	1.47	0.903	1.422	1.44	1.065	1.327
	Accelerometer 5 (@h= 1,55 m)	1.61	-0.48	1.185	1.37	0.741	1.309	1.48	1.035	1.516	1.46	1.198	1.618
	Accelerometer 6 (@h= 1,75 m)	1.61	-0.494	1.22	1.37	0.759	1.307	1.47	1.104	1.352	1.46	1.461	1.45
BACKFILL	Accelerometer 7 (@80 cm. from face block)	1.61	-0.486	1.2	1.37	0.758	1.078	1.48	0.984	1.271	1.45	1.309	1.45
	Accelerometer 8 (@160 cm. from face block)	1.61	-0.402	0.993	1.37	0.625	1.302	1.47	0.925	1.683	1.44	1.309	1.852
	Accelerometer 9 (@240 cm. from face block)	1.61	-0.455	1.123	1.36	0.755	1.043	1.47	1.225	1.28	1.44	1.672	1.051

Table5.9. Acceleration amplification factors with the peak values of the accelerations and the time instances at the occurrences of the peaks for Wall 3 Izmit Earthquake

WALL CONFIGURATION 3													
Dynamic Excitations / Accelerometers		IZMIT EARTHQUAKE 100%			IZMIT EARTHQUAKE 150%			IZMIT EARTHQUAKE 200%			IZMIT EARTHQUAKE 250%		
Location of Accelerometers	Accelerometer No.	Time Instance (sec.)	Peak Acceleration (g)	Amplification Factor	Time Instance (sec.)	Peak Acceleration (g)	Amplification Factor	Time Instance (sec.)	Peak Acceleration (g)	Amplification Factor	Time Instance (sec.)	Peak Acceleration (g)	Amplification Factor
SHAKING TABLE	Accelerometer 1 (Base Input)	4.92	-0.195		7.65	-0.264		8.8	-0.365		4.4	-0.431	
WALL FACE	Accelerometer 2 (@h= 0,15 m)	4.92	-0.188	0.964	7.22	0.262	0.992	8.8	-0.356	0.975	6.54	0.447	1.037
	Accelerometer 3 (@h= 0,55 m)	4.92	-0.198	1.015	7.22	0.274	1.038	7.65	0.38	1.041	6.54	0.464	1.077
	Accelerometer 4 (@h= 1,05 m)	4.93	-0.208	1.067	7.22	0.29	1.098	7.65	0.437	1.197	7.15	0.499	1.158
	Accelerometer 5 (@h= 1,55 m)	4.93	-0.223	1.144	7.22	0.301	1.14	7.66	0.417	1.142	7.7	0.549	1.274
	Accelerometer 6 (@h= 1,75 m)	7.48	-0.238	1.221	7.05	-0.315	1.193	8.08	-0.442	1.211	7.7	0.602	1.397
BACKFILL	Accelerometer 7 (@80 cm. from face block)	4.93	-0.223	1.144	7.22	0.305	1.155	7.66	0.42	1.151	7.7	0.555	1.288
	Accelerometer 8 (@160 cm. from face block)	4.93	-0.181	0.928	7.22	0.246	0.932	7.66	0.337	0.923	7.14	0.407	0.944
	Accelerometer 9 (@240 cm. from face block)	4.93	-0.206	1.056	7.22	0.295	1.117	7.66	0.404	1.107	7.14	0.49	1.137

Table 5.10. Acceleration amplification factors with the peak values of the accelerations and the time instances at the occurrences of the peaks for Wall 3 Sakarya Earthquake

WALL CONFIGURATION 3													
Accelerometers / Dynamic Excitations		SAKARYA EARTHQUAKE 100%			SAKARYA EARTHQUAKE 150%			SAKARYA EARTHQUAKE 200%			SAKARYA EARTHQUAKE 250%		
Location of Accelerometers	Accelerometer No.	Time Instance (sec.)	Peak Acceleration (g)	Amplification Factor	Time Instance (sec.)	Peak Acceleration (g)	Amplification Factor	Time Instance (sec.)	Peak Acceleration (g)	Amplification Factor	Time Instance (sec.)	Peak Acceleration (g)	Amplification Factor
SHAKING TABLE	Accelerometer 1 (Base Input)	7.44	-0.228		7.68	-0.334		7.41	-0.365		6.67	-0.499	
WALL FACE	Accelerometer 2 (@h= 0,15 m)	7.44	-0.227	0.996	7.68	-0.328	0.982	7.42	-0.356	0.975	6.68	-0.506	1.014
	Accelerometer 3 (@h= 0,55 m)	7.44	-0.24	1.053	8.53	-0.333	0.997	7.42	0.38	1.041	7.98	0.533	1.068
	Accelerometer 4 (@h= 1,05 m)	7.44	-0.245	1.075	8.53	-0.339	1.015	7.43	0.437	1.197	7.98	0.583	1.168
	Accelerometer 5 (@h= 1,55 m)	7.45	-0.263	1.154	11.4	-0.362	1.084	7.42	0.417	1.142	7.98	0.605	1.212
	Accelerometer 6 (@h= 1,75 m)	4.57	-0.286	1.254	11.4	-0.399	1.195	7.41	-0.442	1.211	7.98	0.626	1.255
BACKFILL	Accelerometer 7 (@80 cm. from face block)	7.45	-0.264	1.158	11.4	-0.368	1.102	7.42	0.42	1.151	7.98	0.606	1.214
	Accelerometer 8 (@160 cm. from face block)	7.45	-0.212	0.93	11.39	-0.308	0.922	7.83	0.337	0.923	7.98	0.474	0.95
	Accelerometer 9 (@240 cm. from face block)	7.45	-0.248	1.088	11.39	-0.359	1.075	7.83	0.404	1.107	7.98	0.565	1.132

Table 5.11. Acceleration amplification factors with the peak values of the accelerations and the time instances at the occurrences of the peaks for Wall 4 El Centro Earthquake

WALL CONFIGURATION 4																
Accelerometers \ Dynamic Excitations		EL CENTRO EARTHQUAKE 100%			EL CENTRO EARTHQUAKE 150%			EL CENTRO EARTHQUAKE 200%			EL CENTRO EARTHQUAKE 250%			EL CENTRO EARTHQUAKE 275%		
Location of Accelerometers	Accelerometer No.	Time Instance (sec.)	Peak Acceleration (g)	Amplification Factor	Time Instance (sec.)	Peak Acceleration (g)	Amplification Factor	Time Instance (sec.)	Peak Acceleration (g)	Amplification Factor	Time Instance (sec.)	Peak Acceleration (g)	Amplification Factor	Time Instance (sec.)	Peak Acceleration (g)	Amplification Factor
SHAKING TABLE	Accelerometer 1 (Base Input)	3.3	-0.41		1.64	-0.609		4.06	-0.752		1.47	0.93		2.12	-0.982	
WALL FACE	Accelerometer 2 (@h= 0,15 m)	3.3	-0.411	1.002	1.55	0.603	0.99	3.97	0.77	1.024	1.48	0.963	1.035	2.23	1.015	1.034
	Accelerometer 3 (@h= 0,55 m)	1.82	-0.43	1.049	1.56	0.655	1.076	3.98	0.871	1.158	1.49	1.146	1.232	2.25	1.189	1.211
	Accelerometer 4 (@h= 1,05 m)	1.72	0.455	1.11	1.57	0.692	1.136	4	0.87	1.157	1.51	1.073	1.154	2.27	1.119	1.14
	Accelerometer 5 (@h= 1,55 m)	1.83	-0.489	1.193	1.58	0.788	1.294	4.02	1.002	1.332	1.53	1.118	1.202	2.028	1.205	1.227
	Accelerometer 6 (@h= 1,75 m)	1.83	-0.487	1.188	1.58	0.768	1.261	4.02	1.062	1.412	1.54	1.225	1.317	2.3	1.249	1.272
BACKFILL	Accelerometer 7 (@80 cm. from face block)	1.83	-0.479	1.168	1.58	0.802	1.317	4.02	0.947	1.259	1.2	0.986	1.06	1.96	1.072	1.092
	Accelerometer 8 (@160 cm. from face block)	1.83	-0.468	1.141	1.57	0.812	1.333	4.02	1.09	1.449	1.2	1.002	1.077	1.95	1.098	1.118
	Accelerometer 9 (@240 cm. from face block)	1.83	-0.448	1.093	1.56	0.755	1.24	4	1.256	1.67	1.51	1.486	1.598	2.27	1.484	1.511

Table 5.12. Acceleration amplification factors with the peak values of the accelerations and the time instances at the occurrences of the peaks for Wall 4 Izmit Earthquake

WALL CONFIGURATION 4										
Dynamic Excitations / Accelerometers		IZMIT EARTHQUAKE 100%			IZMIT EARTHQUAKE 150%			IZMIT EARTHQUAKE 200%		
Location of Accelerometers	Accelerometer No.	Time Instance (sec.)	Peak Acceleration (g)	Amplification Factor	Time Instance (sec.)	Peak Acceleration (g)	Amplification Factor	Time Instance (sec.)	Peak Acceleration (g)	Amplification Factor
SHAKING TABLE	Accelerometer 1 (Base Input)	8.02	-0.198		6.76	0.29		6.18	0.337	
WALL FACE	Accelerometer 2 (@h= 0,15 m)	7.41	-0.186	0.939	7.19	-0.273	0.941	7.19	-0.332	0.985
	Accelerometer 3 (@h= 0,55 m)	7.41	-0.196	0.99	6.76	0.286	0.986	7.2	-0.351	1.042
	Accelerometer 4 (@h= 1,05 m)	7.41	-0.212	1.071	7.19	-0.296	1.021	7.2	-0.366	1.086
	Accelerometer 5 (@h= 1,55 m)	7.41	-0.239	1.207	7.18	-0.307	1.059	7.2	-0.373	1.107
	Accelerometer 6 (@h= 1,75 m)	7.41	-0.256	1.293	4.04	-0.313	1.079	7.2	-0.383	1.136
BACKFILL	Accelerometer 7 (@80 cm. from face block)	7.41	-0.243	1.227	7.18	-0.309	1.066	7.2	-0.377	1.119
	Accelerometer 8 (@160 cm. from face block)	7.41	-0.235	1.187	4.04	-0.301	1.038	7.19	-0.366	1.086
	Accelerometer 9 (@240 cm. from face block)	7.41	-0.225	1.136	6.76	0.287	0.99	7.19	-0.348	1.033

Table 5.13.Acceleration amplification factors with the peak values of the accelerations and the time instances at the occurrences of the peaks for Wall 4 Sakarya Earthquake

WALL CONFIGURATION 4										
Accelerometers / Dynamic Excitations		SAKARYA EARTHQUAKE 100%			SAKARYA EARTHQUAKE 150%			SAKARYA EARTHQUAKE 200%		
Location of Accelerometers	Accelerometer No.	Time Instance (sec.)	Peak Acceleration (g)	Amplification Factor	Time Instance (sec.)	Peak Acceleration (g)	Amplification Factor	Time Instance (sec.)	Peak Acceleration (g)	Amplification Factor
SHAKING TABLE	Accelerometer 1 (Base Input)	7.78	-0.215		8	-0.31		9.67	0.453	
WALL FACE	Accelerometer 2 (@h= 0,15 m)	7.79	-0.218	1.014	8	-0.323	1.042	9.67	0.46	1.015
	Accelerometer 3 (@h= 0,55 m)	7.78	-0.222	1.033	8	-0.331	1.068	9.67	0.485	1.071
	Accelerometer 4 (@h= 1,05 m)	5.93	-0.225	1.047	8	-0.353	1.139	9.67	0.488	1.077
	Accelerometer 5 (@h= 1,55 m)	5.93	-0.236	1.098	8	-0.366	1.181	9.68	0.488	1.077
	Accelerometer 6 (@h= 1,75 m)	5.93	-0.241	1.121	8	-0.367	1.184	9.4	0.498	1.099
BACKFILL	Accelerometer 7 (@80 cm. from face block)	5.93	-0.235	1.093	8	-0.369	1.19	9.68	0.494	1.091
	Accelerometer 8 (@160 cm. from face block)	5.93	-0.232	1.079	8	-0.366	1.181	9.68	0.493	1.088
	Accelerometer 9 (@240 cm. from face block)	5.93	-0.224	1.042	8.01	-0.344	1.11	9.68	0.474	1.046

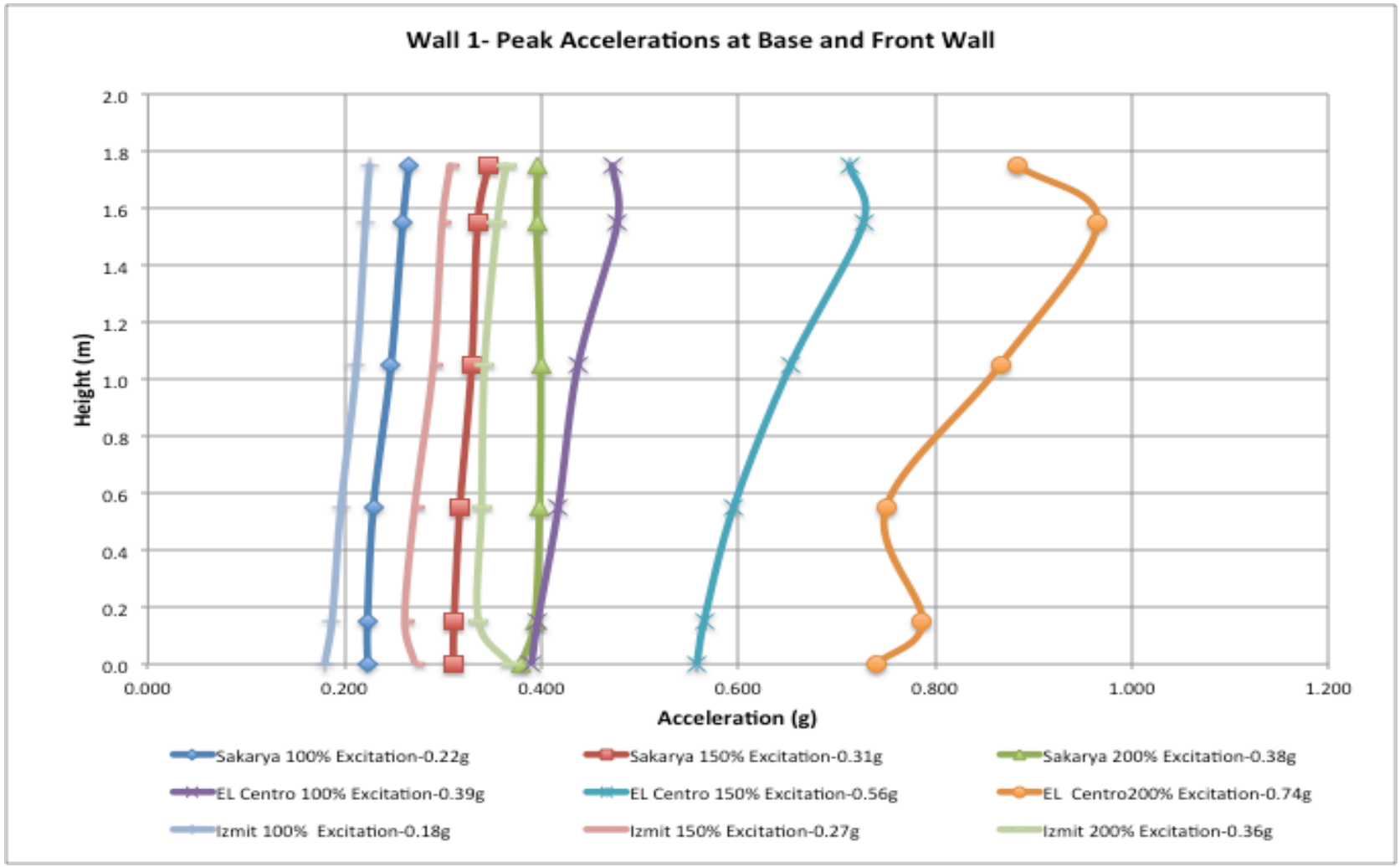


Figure 5.9. Peak Accelerations at base and wall facing for Wall 1 for all Dynamic Excitations

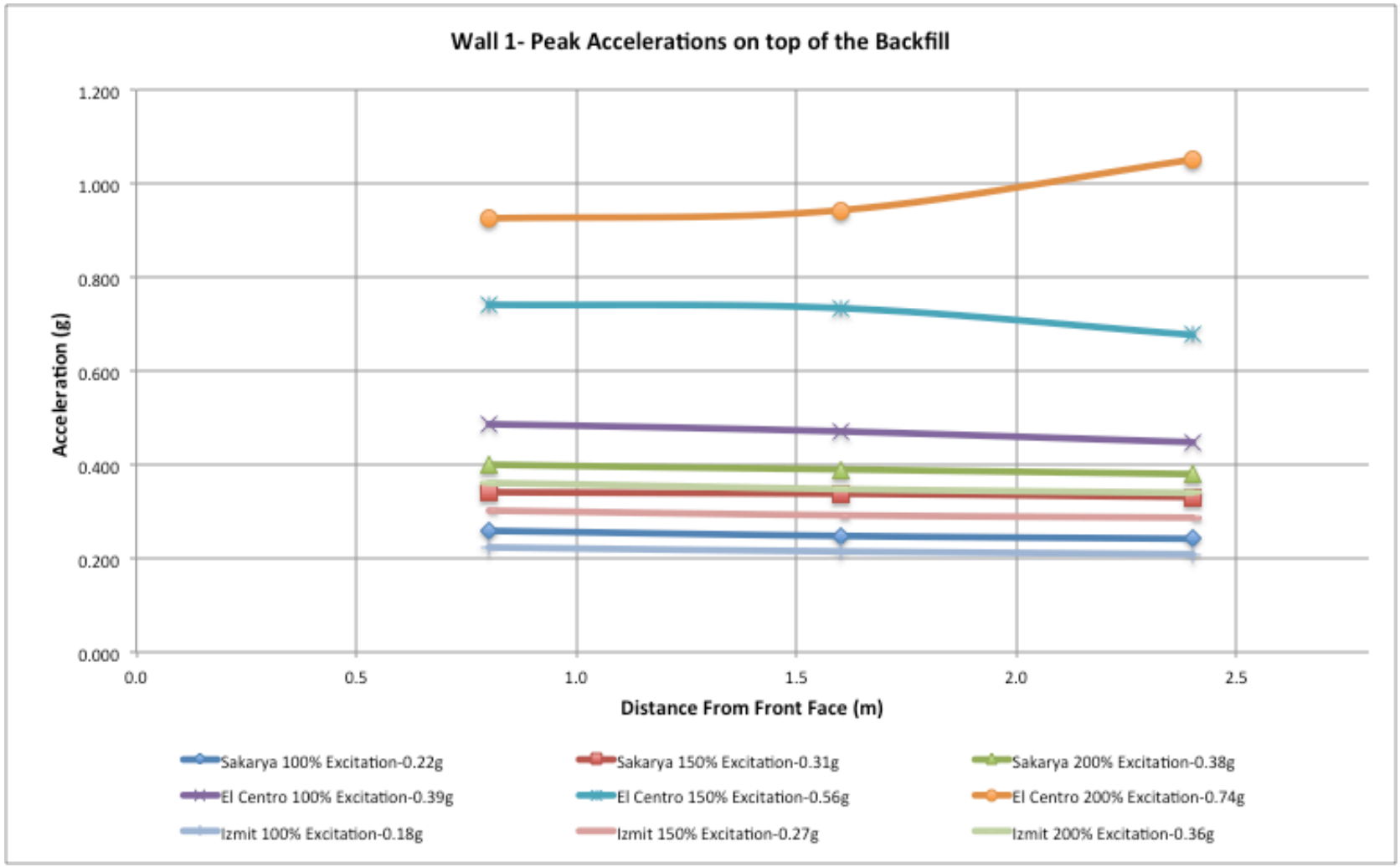


Figure 5.10. Peak Accelerations on top of backfill for Wall 1 for all Dynamic Excitations

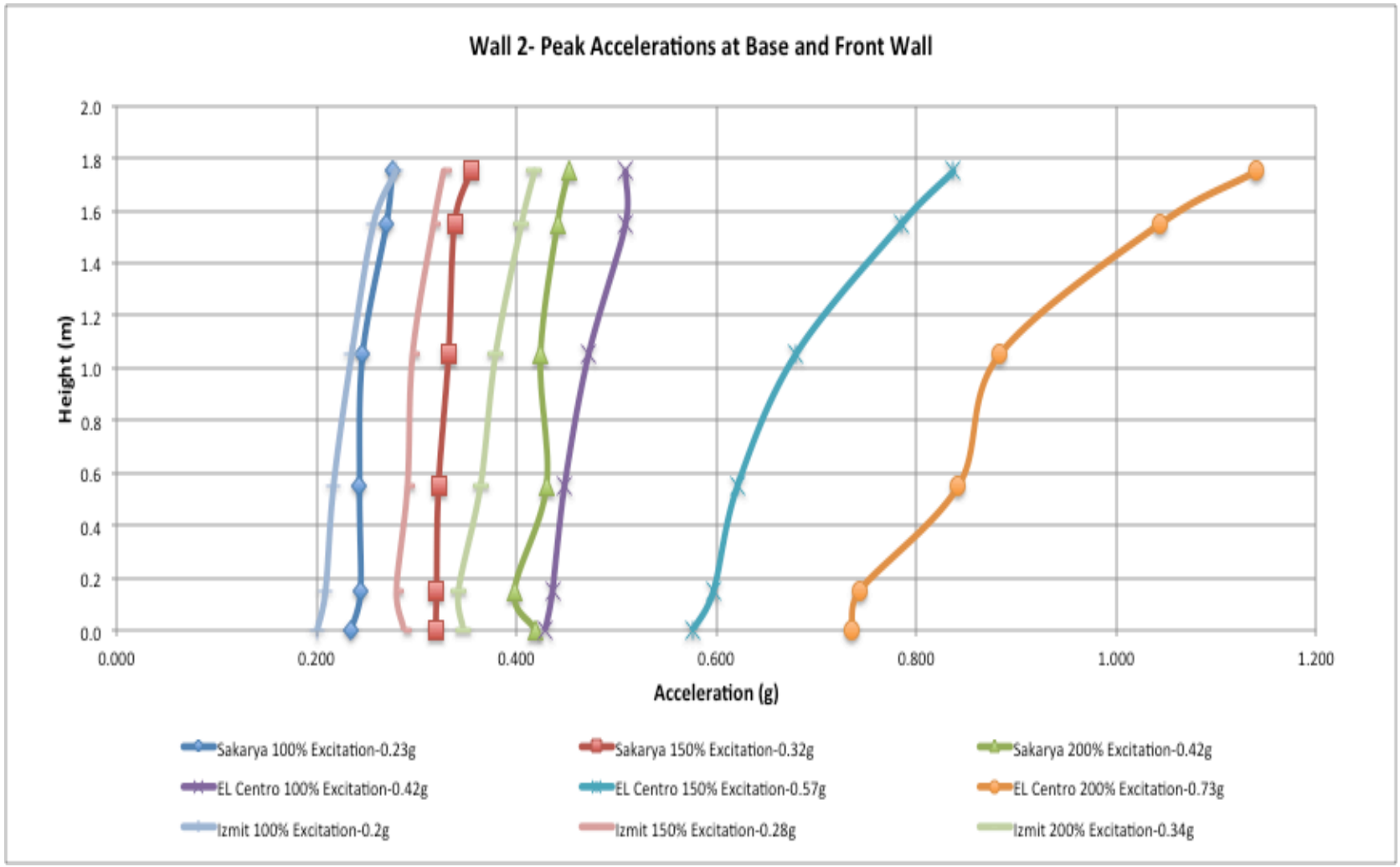


Figure 5.11. Peak Accelerations at base and wall facing for Wall 2 for all Dynamic Excitations

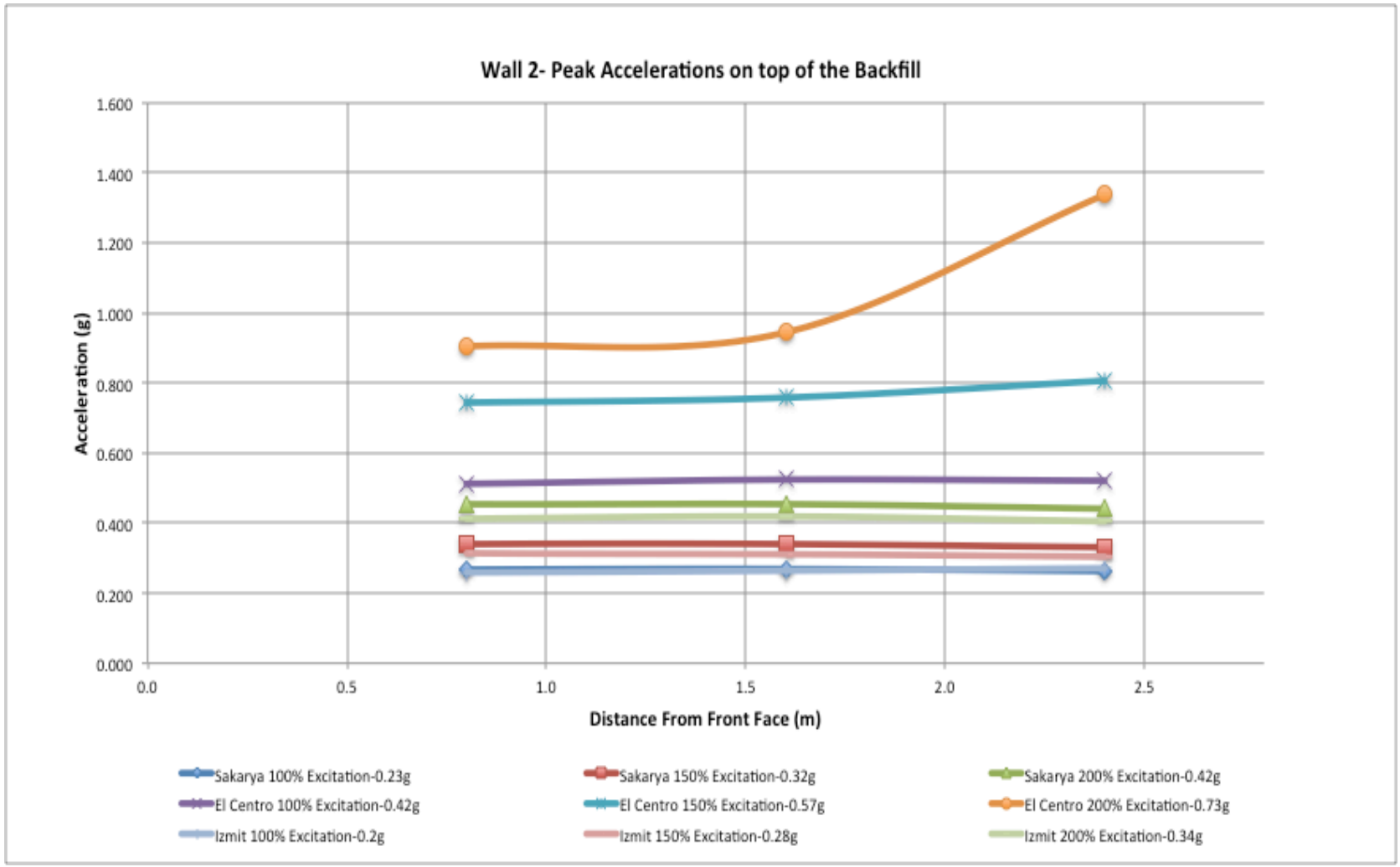


Figure 5.12. Peak Accelerations on top of backfill for Wall 2 for all Dynamic Excitations

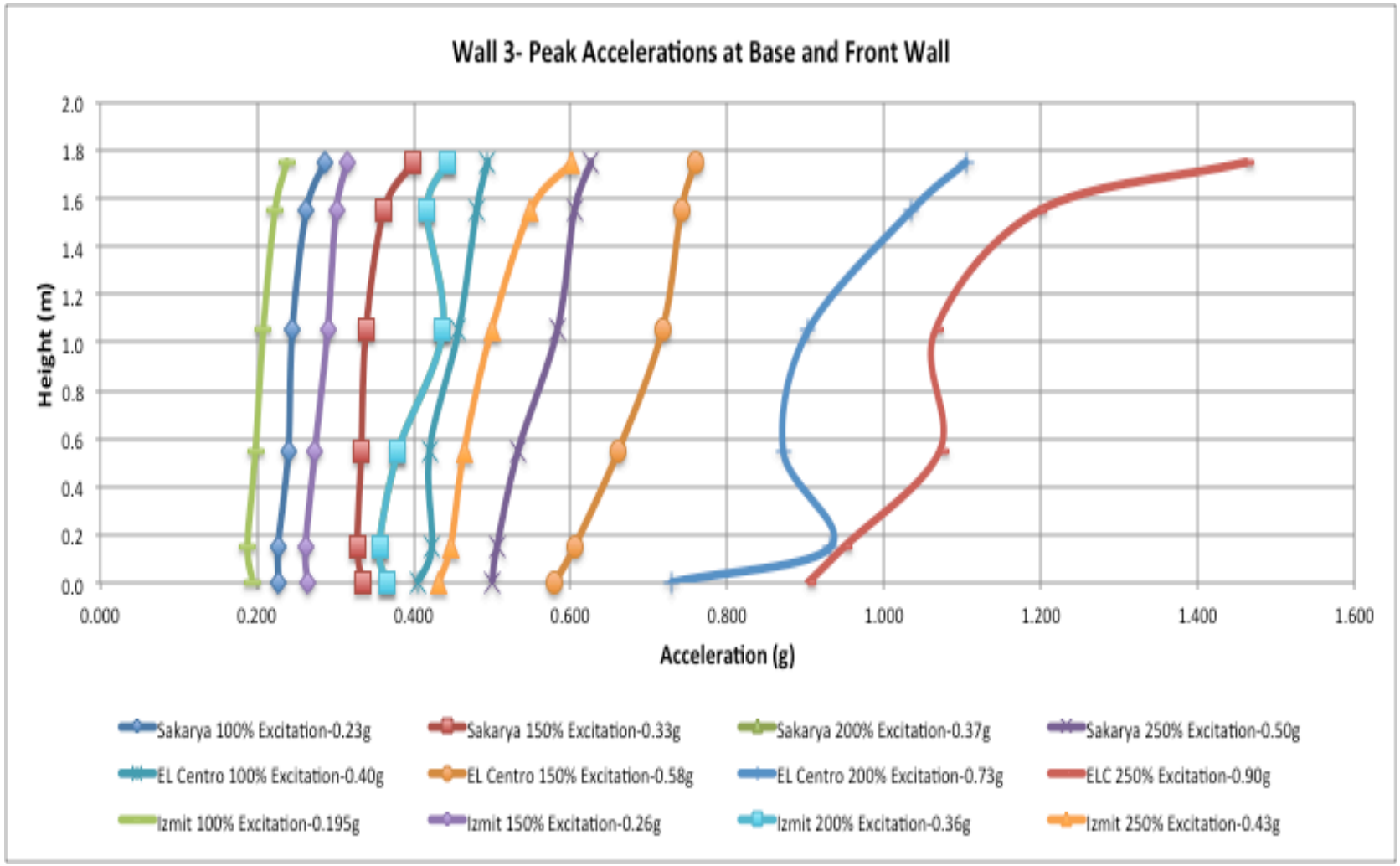


Figure 5.13. Peak Accelerations at base and wall facing for Wall 3 for all Dynamic Excitations

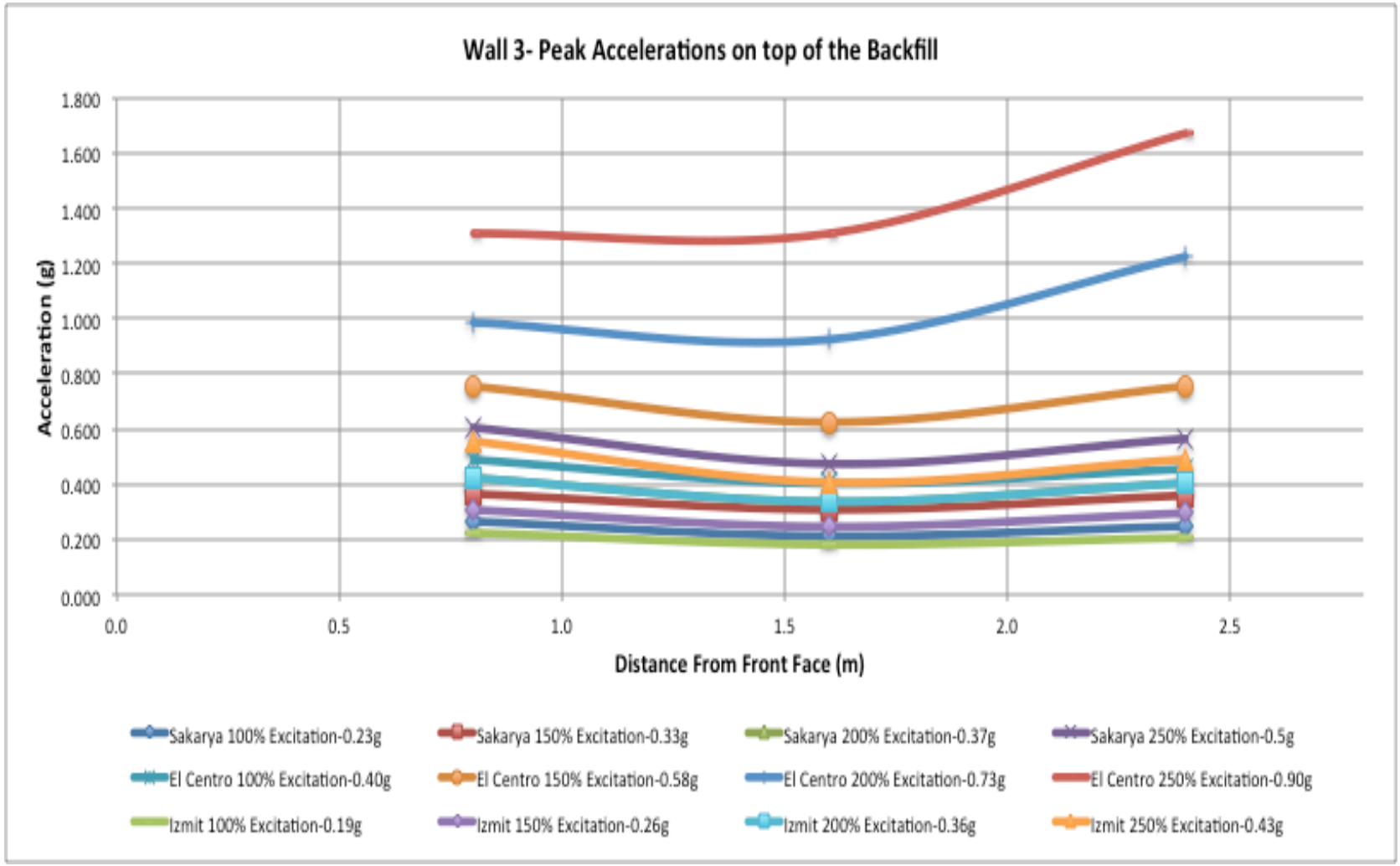


Figure 5.14. Peak Accelerations on top of backfill for Wall 3 for all Dynamic Excitations

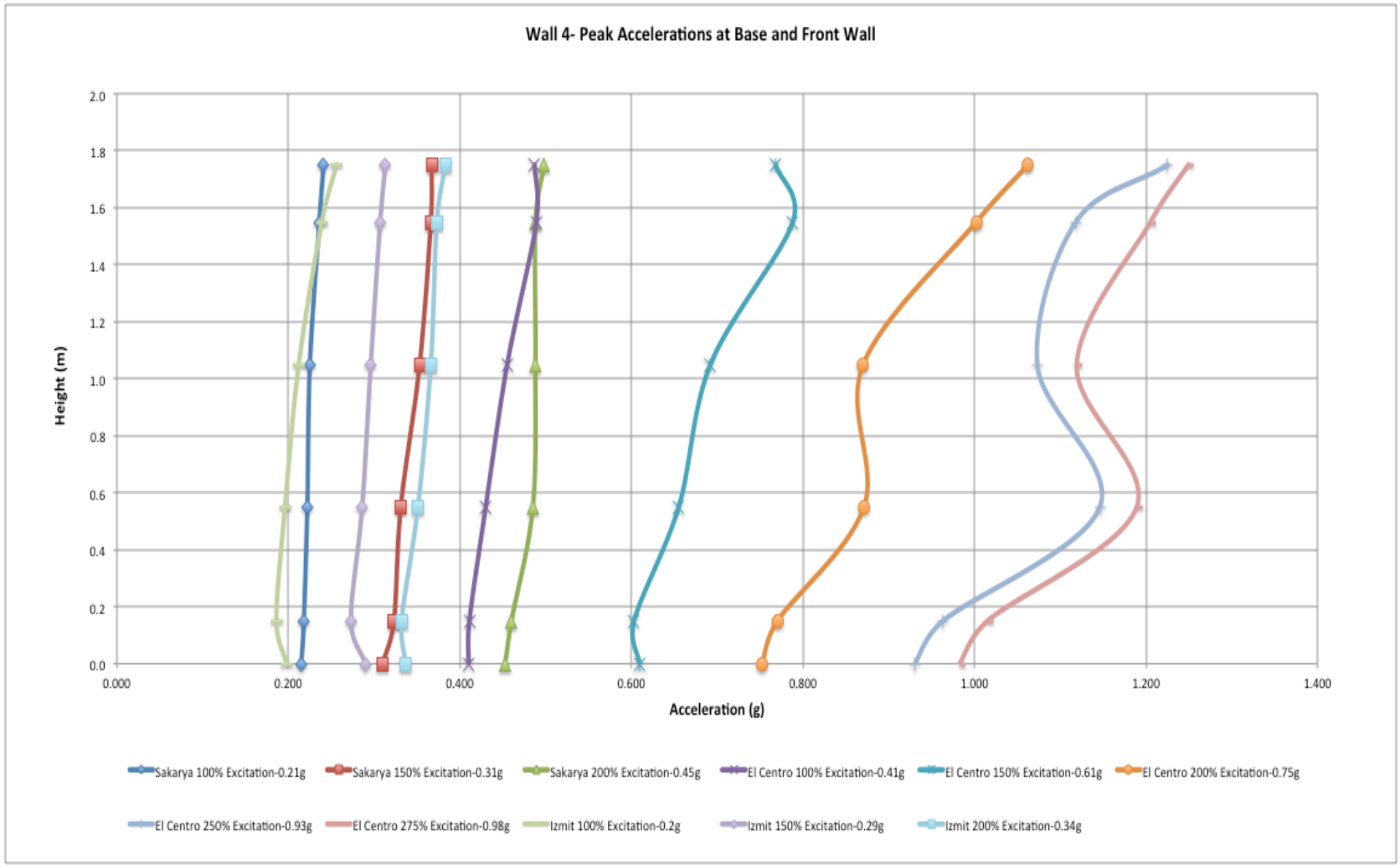


Figure 5.15. Peak Accelerations at base and wall facing for Wall 4 for all Dynamic Excitations

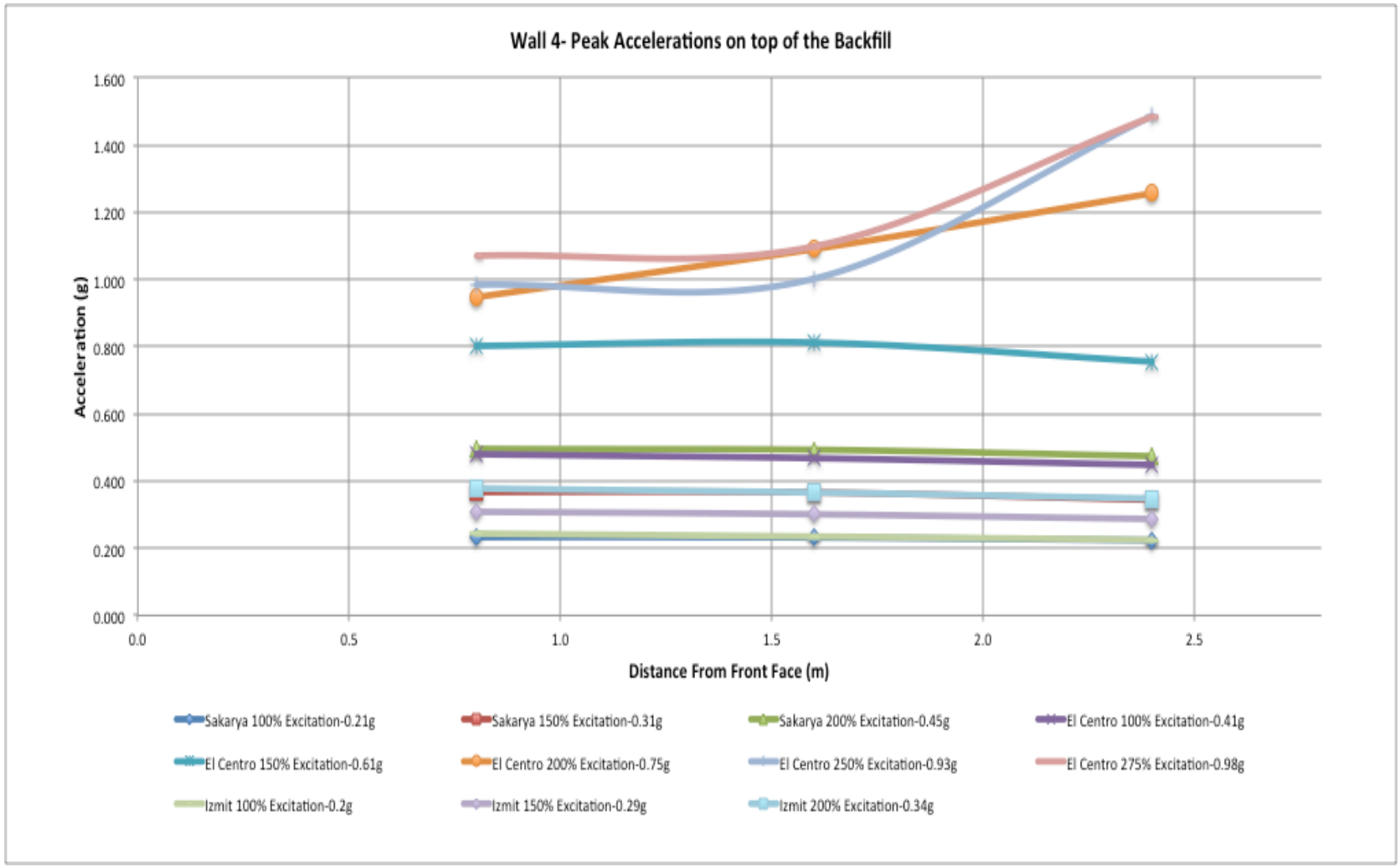


Figure 5.16. Peak Accelerations on top of backfill for Wall 4 for all Dynamic Excitations

5.4.2. Evaluation of the Results

The maximum acceleration amplification factors are evaluated as a summary in Table 5.14. The maximum amplification factor observed was 1.618 at 1.55 m. height of the facing panel and 1.852 at the backfill for Wall 3. On wall face, the maximum acceleration amplification factors tend to increase with the increase in height of wall. However, as seen on Table 5.14., the highest values of acceleration amplification factors for Wall 1, Wall 3 and Wall 4 occurs at 1.55 m. of the wall face where for Wall 2 it occurs at 1.75m (top of the facing).

Almost all acceleration amplification factors were relatively small (between 1.0 and 1.5) but tend to increase significantly after an input base acceleration of 0.56 g (corresponding to El Centro 150% base excitation) is applied on the models.This acceleration value may be referred to as critical acceleration value sincethe in each acceleration vs. wall height curveat this point corresponds to a sharp decrease in the slope of the plots. Nevertheless, it is understood that this definition may besubject to interpretation for a particular data set.Please refer to Section 6.1. for the calculation of the critical acceleration of the walls.El-Emam and Barthust(2005) report that this may be due to the shear stiffness reduction of the backfill material with accumulatingpermanent deformation. From elastic theoryand a single degree of freedom system with constant frequency of input motion (ω) and constant mass (m), the response ratio R (i.e. amplification factor) increases as the stiffness K of the structure decreases for a frequency ratio $\omega / \omega_n < 1$ (here ω_n is the structure fundamental frequency). Amplification factors with increasing amplitude of base excitation has been also reported by Matsuo et al. (1998) for shaking table models with extensible soil reinforcement.

From the measurements it is understood that the lower portion of the wall the accelerations measured are close to the table acceleration.The amplification factors observed in this study increased significantlywhen the input base acceleration amplitudeexceeded a certain value of acceleration (may be referred to as critical acceleration) amplitude for each wall.

Additionally, when the top of the backfill is considered, as the input base

acceleration increased the unreinforced region of the backfill tend to increase the amplification more than the reinforced zone.

5.4.2.1. Influence of Wall Inclination on Acceleration Amplification. Wall 1 and Wall 2 is compared in order to understand the effect of wall inclination on acceleration amplification. The following results can be drawn:

- Regarding Wall 1 and Wall 2 (same backfill and reinforcement type with different wall facing type), less maximum Acceleration amplification factors (1.304 at wall face and 1.42 at backfill)are observed for the vertical facing type (Wall 1). In the inclined wall type (Wall 2) the maximum acceleration amplification factors observed at 1.75m. of the wall face.Based on a comparison of results for Walls 1 and 2, there was little influence of wall inclination onthe measured acceleration amplification factors for the entire range of base excitations.

5.4.2.2. Influence of Backfill Material on Acceleration Amplification.In order to comprehend the influence of backfill material (sand and gravel) on acceleration amplification, Wall 3 and Wall 4 is compared and the general conclusions drawn are:

- Generally for the gravel backfill models, as the input base acceleration increased, the higher acceleration amplification factors were observed both on the front wall and on top of the backfill. In Wall 4 (sand backfill) when an input base acceleration value of above 0.75 g is applied, the max. acceleration amplification factors decreased. So, for Wall 4 the maximum acceleration amplification observed was at El Centro 200% excitation.

- When Wall 3 and Wall 4 compared (same reinforcement type and wall facing type with different backfill type), the Wall 3 (gravel backfill) has higher maximum acceleration amplification factor values than Wall 4(sand backfil). Stiff soils are strong and tend to amplify the accelerations, loose soils are ideal dampers and they decrease the acceleration amplification (Ling *et al.,* 2005). In this case, gravel is stiffer than sand and it is normal for the gravel backfill model to have higher amplification values than sand backfill model.

- In Wall 4, the maximum accelerations on the facing occur at the top. However, for El

Centro 200%, 250% and 275% excitations, the peak accelerations tend to increase significantly @h=0.55 m. which is almost the ¼ height of the wall meaning that the earthquake motion is effective at that part after 0.75g. On the other hand, in the gravel backfill wall model (Wall 3) maximum accelerations on the facing are observed at the top level even after the base excitation accelerations reach up to values of 0.90g.

5.4.2.3. Influence of Reinforcement Type and Length on Acceleration Amplification.When Wall 2 and Wall 3 are compared, the magnitude of acceleration amplification factorsdecreased with increasing length and tensile strength of reinforcement meaning that the Wall 3 that has longer and stronger reinforcement tend to prevent the vibration more.

Table 5.14. Summary of Maximum Acceleration Amplification factors observed together with locations

Wall Configuration and Dynamic Excitation in which the Max. Acc. Amplification Factor Observed	**Location**		**Max. Acceleration Amplification Factor**	
	Wall Face	**Backfill**	**Wall Face**	**Backfill**
Wall 1- El Centro 200%	@h=1.55 m	@L=2.40 m from front face	1.304	1.42
Wall 2- El Centro 200%	@h=1.75 m	@L=2.40 m from front face	1.551	1.819
Wall 3- El Centro 250%	@h=1.55 m	@L=2.40 m from front face	1.618	1.852
Wall 4- El Centro 200%	@h=1.55 m	@L=2.40 m from front face	1.412	1.67

5.5. Horizontal Displacements of Wall Facing

For all wall configurations, the time responses of horizontal wall facing displacements to each applied base excitations is given in Appendix B. In this section, the maximum displacements and residual displacements occurred when the peak base excitationsapplied, are compared for the four different wall configurations with different input base acceleration amplitudes. The positive (+) displacement values represent the inwards movement of the wall where the negative (-) displacement values represent the outwards movement of the wall. The two laser displacement sensors located on the top blocks give almost the same displacement values meaning that the top block system works as a whole. Additionally, the maximum lateral displacements and residual displacements (at the end of shakings) at the top of the wall facing as a function of peak base acceleration amplitude are shown and compared.

5.5.1. Test Results

In the plots and tables presented in this section, the wall response features are referenced to peak values that occurred during each applied base acceleration. Hence, the values are not time coincident.

The laser sensor measurements on front facing of the wall are compiled and presented in the Table 5.15. and Table 5.16.In Figures5.17.through 5.20.peak displacements observed in both outwards and inwards directions at wall facings are plotted for each wall configuration and dynamic excitation typesto compare the influence of changing wall parameters. The data obtained from laser displacement sensors that are attached to the steel frame are consistent since as the base input acceleration increases, the wall deformations increase. For the tests with base accelerations above 0.4 g (corresponding to El-Centro 100% motion), the face displacements through the outwards direction become more dominant. However, below 0.4 g the outwards and inwards motion of the blocks show similar behavior. The detailed evaluation of the test results are presented in the following section.

Table 5.15. Measured Horizontal Displacement of Wall Facing for Wall Configuration 1 and Wall Configuration 2

WALL CONFIGURATION 1

Lasers / Dynamic Excitations		EL CENTRO EARTHQUAKE 100%		EL CENTRO EARTHQUAKE 150%		EL CENTRO EARTHQUAKE 200%		IZMIT EARTHQUAKE 100%		IZMIT EARTHQUAKE 150%		IZMIT EARTHQUAKE 200%		SAKARYA EARTHQUAKE 100%		SAKARYA EARTHQUAKE 150%		SAKARYA EARTHQUAKE 200%	
Laser No.	Location of Laser Sensors (m)	Peak Displacement ("+" direction) (mm)	Peak Displacement ("-" direction) (mm)	Peak Displacement ("+" direction) (mm)	Peak Displacement ("-" direction) (mm)	Peak Displacement ("+" direction) (mm)	Peak Displacement ("-" direction) (mm)	Peak Displacement ("+" direction) (mm)	Peak Displacement ("-" direction) (mm)	Peak Displacement ("+" direction) (mm)	Peak Displacement ("-" direction) (mm)	Peak Displacement ("+" direction) (mm)	Peak Displacement ("-" direction) (mm)	Peak Displacement ("+" direction) (mm)	Peak Displacement ("-" direction) (mm)	Peak Displacement ("+" direction) (mm)	Peak Displacement ("-" direction) (mm)	Peak Displacement ("+" direction) (mm)	Peak Displacement ("-" direction) (mm)
Laser No. 1	@h=0.25	1.6	-1.7	2	-3.2	1.1	-7.3	1.6	-1.2	1.7	-1.2	1.6	-1.5	1.6	-1.5	1.6	-1.6	1.6	-1.3
Laser No. 2	@h=0.95	1.3	-0.7	1.2	-1.4	1.7	-3.7	1.3	-0.8	1.3	-0.7	1.3	-0.8	1.4	-0.7	1.3	-0.7	1.3	-1
Laser No. 3	@h=1.25	1.8	-1.3	1.9	-2.8	3.9	-5	1.6	-0.9	1.6	-0.9	1.6	-1	1.7	-0.9	1.7	-1.1	1.8	-1.1
Laser No. 4	@h=1.65	1.4	-1.7	2.4	-4.3	4.1	-6.7	1.6	-0.8	1.6	-0.9	1.5	-0.8	1.5	-0.8	1.4	-0.8	1.7	-0.9
Laser No. 5	@h=1.9	1.6	-1.7	2.4	-5.3	4.3	-9.6	1.6	-1	1.5	-1.1	1.6	-1.2	1.5	-1.1	1.6	-1.1	1.7	-1.9
Laser No. 6	@h=1.9	1.6	-1.7	1.8	-4.7	4.2	-9	1.6	-0.9	1.5	-1.1	1.6	-1.2	1.5	-1.3	1.5	-1.2	1.8	-1.7

WALL CONFIGURATION 2

Lasers / Dynamic Excitations		EL CENTRO EARTHQUAKE 100%		EL CENTRO EARTHQUAKE 150%		EL CENTRO EARTHQUAKE 200%		IZMIT EARTHQUAKE 100%		IZMIT EARTHQUAKE 150%		IZMIT EARTHQUAKE 200%		SAKARYA EARTHQUAKE 100%		SAKARYA EARTHQUAKE 150%		SAKARYA EARTHQUAKE 200%	
Laser No.	Location of Laser Sensors (m)	Peak Displacement ("+" direction) (mm)	Peak Displacement ("-" direction) (mm)	Peak Displacement ("+" direction) (mm)	Peak Displacement ("-" direction) (mm)	Peak Displacement ("+" direction) (mm)	Peak Displacement ("-" direction) (mm)	Peak Displacement ("+" direction) (mm)	Peak Displacement ("-" direction) (mm)	Peak Displacement ("+" direction) (mm)	Peak Displacement ("-" direction) (mm)	Peak Displacement ("+" direction) (mm)	Peak Displacement ("-" direction) (mm)	Peak Displacement ("+" direction) (mm)	Peak Displacement ("-" direction) (mm)	Peak Displacement ("+" direction) (mm)	Peak Displacement ("-" direction) (mm)	Peak Displacement ("+" direction) (mm)	Peak Displacement ("-" direction) (mm)
Laser No. 1	@h=0.25	1.5	-0.9	1.5	-1	2.4	-1.6	1.4	-0.9	1.6	-0.9	1.7	-0.9	1.9	-0.8	1.6	-0.8	1.6	-0.9
Laser No. 2	@h=0.95	1.5	-0.8	2.5	-5	2.2	-6.3	1.4	-0.8	1.5	-0.7	1.4	-0.9	1.3	-0.9	1.2	-0.8	1.4	-1.2
Laser No. 3	@h=1.25	3.9	-3.2	3.8	-8.5	5.1	-21.9	2.2	-3.1	2.2	-2.5	2.2	-2.8	2.4	-3.4	2.4	-2.9	2.5	-3.6
Laser No. 4	@h=1.65	1.7	-1.8	2.1	-6.6	4.3	-12.3	1.4	-1	1.4	-1.3	1.3	-1.2	1.3	-1	1.5	-1.2	1.5	-1.3
Laser No. 5	@h=1.9	1.3	-2.5	2.5	-8.2	3.9	-14.1	1.6	-1	1.8	-1.2	1.9	-1.3	1.9	-1.1	1.7	-1.5	1.8	-1.7
Laser No. 6	@h=1.9	1.8	-3	2.7	-8.4	5.1	-13.6	1.5	-0.8	1.5	-1.1	1.6	-1.1	1.7	-0.9	1.7	-1.5	1.7	-1.6

Table 5.16. Measured Horizontal Displacement of Wall Facing for Wall Configuration 3 and Wall Configuration 4

WALL CONFIGURATION 3

Lasers / Dynamic Excitations		EL CENTRO EARTHQUAKE 100%		EL CENTRO EARTHQUAKE 150%		EL CENTRO EARTHQUAKE 200%		EL CENTRO EARTHQUAKE 250%		IZMIT EARTHQUAKE 100%		IZMIT EARTHQUAKE 150%		IZMIT EARTHQUAKE 200%		IZMIT EARTHQUAKE 250%		SAKARYA EARTHQUAKE 100%		SAKARYA EARTHQUAKE 150%		SAKARYA EARTHQUAKE 200%		SAKARYA EARTHQUAKE 250%	
Laser No.	Location of Laser Sensors (m)	Peak Displacement ("+" direction) (mm)	Peak Displacement ("-" direction) (mm)	Peak Displacement ("+" direction) (mm)	Peak Displacement ("-" direction) (mm)	Peak Displacement ("+" direction) (mm)	Peak Displacement ("-" direction) (mm)	Peak Displacement ("+" direction) (mm)	Peak Displacement ("-" direction) (mm)	Peak Displacement ("+" direction) (mm)	Peak Displacement ("-" direction) (mm)	Peak Displacement ("+" direction) (mm)	Peak Displacement ("-" direction) (mm)	Peak Displacement ("+" direction) (mm)	Peak Displacement ("-" direction) (mm)	Peak Displacement ("+" direction) (mm)	Peak Displacement ("-" direction) (mm)	Peak Displacement ("+" direction) (mm)	Peak Displacement ("-" direction) (mm)	Peak Displacement ("+" direction) (mm)	Peak Displacement ("-" direction) (mm)	Peak Displacement ("+" direction) (mm)	Peak Displacement ("-" direction) (mm)	Peak Displacement ("+" direction) (mm)	Peak Displacement ("-" direction) (mm)
Laser No. 1	@h=0.25	1.6	-1.1	1.5	-3.3	3.4	-4.8	2.7	-7.8	1.9	-1.1	2	-1.1	1.8	-1.2	2.5	-1.5	1.7	-0.8	2.3	-1	2.1	-1.2	2.3	-1.7
Laser No. 2	@h=0.95	2.1	-1.7	1.4	-5.1	2.6	-9	4	-24	1.4	-1.1	1.4	-1.3	1.4	-1.4	1.6	-1.7	1.5	-1.3	1.5	-1.6	1.5	-1.4	1.7	-2.1
Laser No. 3	@h=1.25	2.3	-1.7	2.6	-6.4	4.7	-10.3	6.5	-14.5	2	-1.5	2	-1.2	1.8	-1.7	2.5	-3	1.6	-1.4	2.1	-1.5	2.4	-2.4	2.8	-3.7
Laser No. 4	@h=1.65	1.7	-0.8	2.7	-4.6	4.6	-9.8	7.1	-15.6	1.8	-0.7	1.8	-0.9	1.7	-1.6	2.2	-2	1.7	-0.8	1.9	-1	1.6	-1.7	2.8	-2.9
Laser No. 5	@h=1.9	1.9	-1.1	2.9	-4.3	5.2	-15	9.4	-26.3	1.7	-0.9	1.7	-1	2	-2	2.6	-2.7	1.8	-0.9	1.8	-1.6	2.2	-2.5	3.2	-4
Laser No. 6	@h=1.9	2.2	-1.3	2	-7.5	6.5	-13.3	9.7	-23.5	2.2	-1	1.8	-1.5	1.7	-2.3	2.9	-2.7	1.7	-1	1.8	-2.1	2.3	-2.5	3.4	-3.7

WALL CONFIGURATION 4

Lasers / Dynamic Excitations		EL CENTRO EARTHQUAKE 100%		EL CENTRO EARTHQUAKE 150%		EL CENTRO EARTHQUAKE 200%		EL CENTRO EARTHQUAKE 250%		EL CENTRO EARTHQUAKE 275%		IZMIT EARTHQUAKE 100%		IZMIT EARTHQUAKE 150%		IZMIT EARTHQUAKE 200%		SAKARYA EARTHQUAKE 100%		SAKARYA EARTHQUAKE 150%		SAKARYA EARTHQUAKE 200%	
Laser No.	Location of Laser Sensors (m)	Peak Displacement ("+" direction) (mm)	Peak Displacement ("-" direction) (mm)	Peak Displacement ("+" direction) (mm)	Peak Displacement ("-" direction) (mm)	Peak Displacement ("+" direction) (mm)	Peak Displacement ("-" direction) (mm)	Peak Displacement ("+" direction) (mm)	Peak Displacement ("-" direction) (mm)	Peak Displacement ("+" direction) (mm)	Peak Displacement ("-" direction) (mm)	Peak Displacement ("+" direction) (mm)	Peak Displacement ("-" direction) (mm)	Peak Displacement ("+" direction) (mm)	Peak Displacement ("-" direction) (mm)	Peak Displacement ("+" direction) (mm)	Peak Displacement ("-" direction) (mm)	Peak Displacement ("+" direction) (mm)	Peak Displacement ("-" direction) (mm)	Peak Displacement ("+" direction) (mm)	Peak Displacement ("-" direction) (mm)	Peak Displacement ("+" direction) (mm)	Peak Displacement ("-" direction) (mm)
Laser No. 1	@h=0.25	3.5	-4.9	1.6	-8.9	2.9	-10.7	4.7	-10.2	2.9	-10.1	2.3	-1.4	2.3	-1.5	2.3	-1.7	2.4	-1.4	2.3	-1.6	2.8	-2
Laser No. 2	@h=0.95	1.9	-1.7	1.2	-6.9	4.3	-7.8	5.2	-12.8	6.1	-10.6	1.7	-1.1	2.1	-1.2	2	-1.5	1.7	-1.1	2.1	-1.4	2.2	-1.7
Laser No. 3	@h=1.25	0.8	-3.2	7.2	-8	7	-13	8	-16	9	-20	1.4	-2	1.1	-2.6	0.8	-3	1.6	-2.4	2.7	-1.6	2.7	-2.5
Laser No. 4	@h=1.65	2.6	-1.8	3.6	-11.3	6.6	-12.9	7.3	-15.8	8	-20.6	1.8	-1.2	2	-1.5	2	-1.3	2	-1.6	2	-1.2	2.6	-1.7
Laser No. 5	@h=1.9	2.4	-1.4	3.6	-7.5	7.5	-16.6	11.4	-31.9	15.1	-31.2	2	-1.5	2.3	-1.9	1.6	-2.3	2.1	-1.5	1.9	-1.7	2.2	-2.4
Laser No. 6	@h=1.9	2.2	-2.2	4.7	-6.8	10.7	-15.1	12.1	-29.1	14.1	-36.2	1.6	-0.8	1.8	-0.7	1	-1.9	1.5	-1	1.9	-1	1.7	-0.9

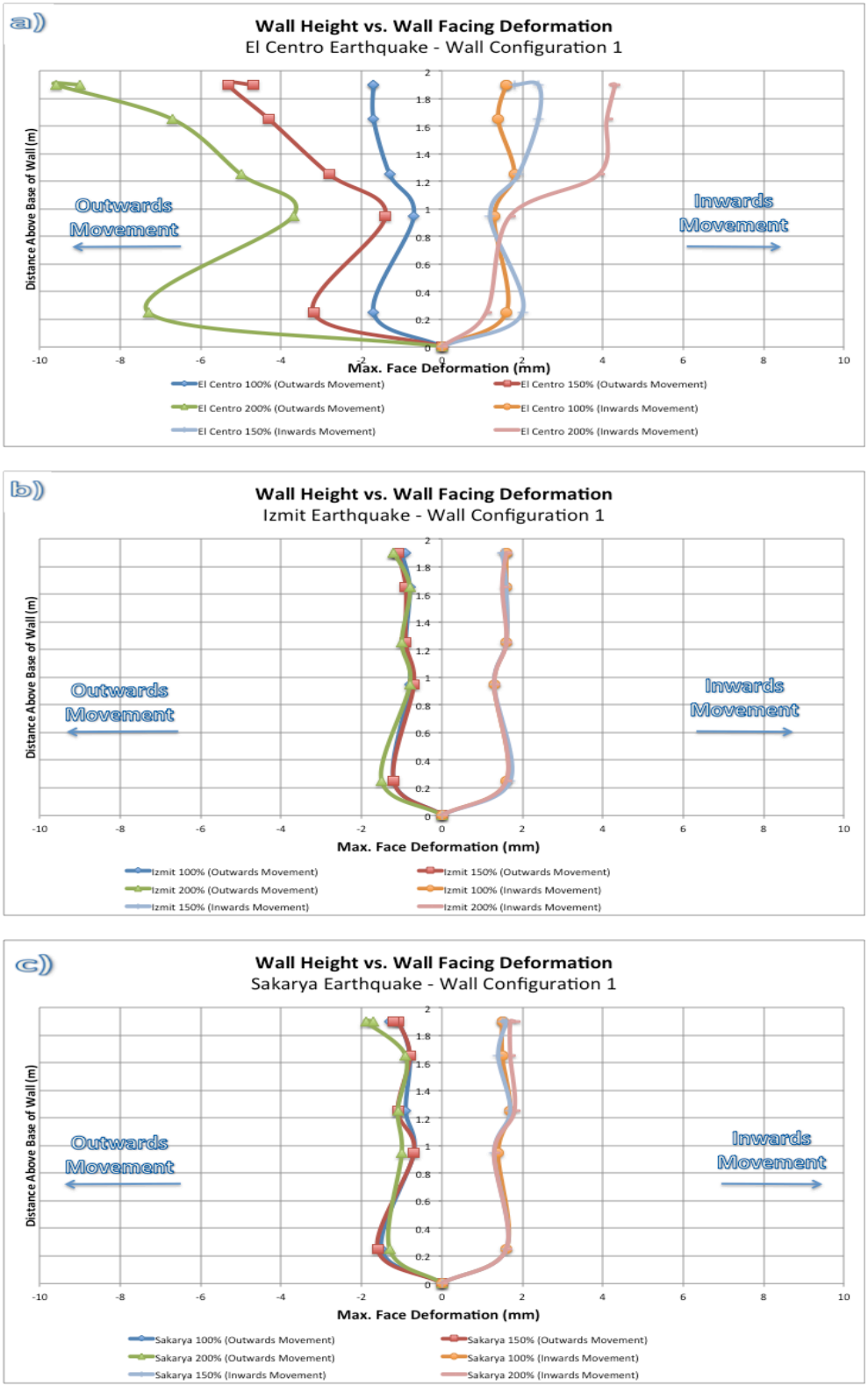


Figure 5.17. Peak Displacements at the wall facing for Wall 1 in base excitations a) El Centro Earthquake, b)Izmit Earthquake, c)Sakarya Earthquake Motions

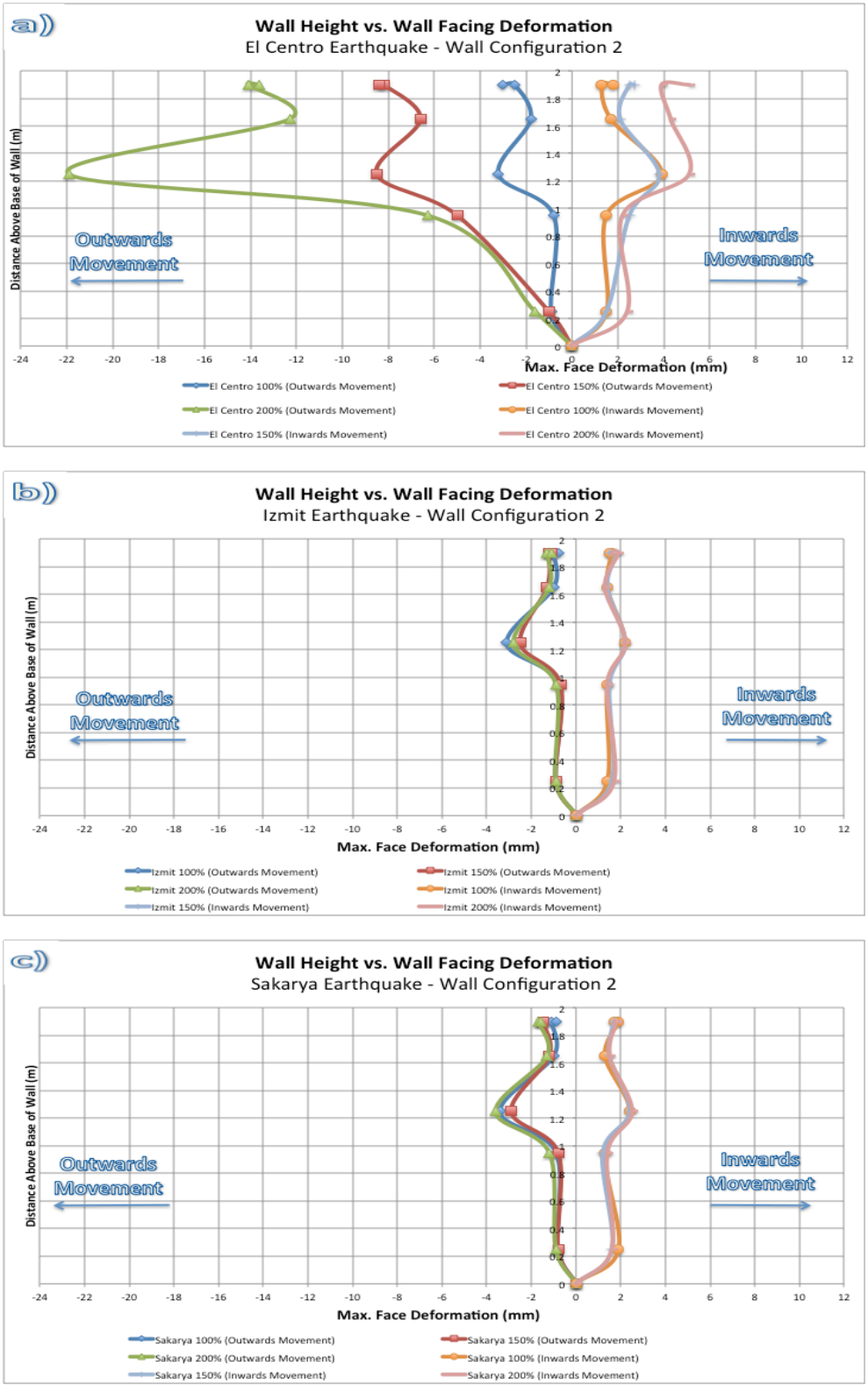


Figure 5.18. Peak Displacements at the wall facing for Wall 2 in base excitations a) El Centro Earthquake, b)Izmit Earthquake, c)Sakarya Earthquake Motions

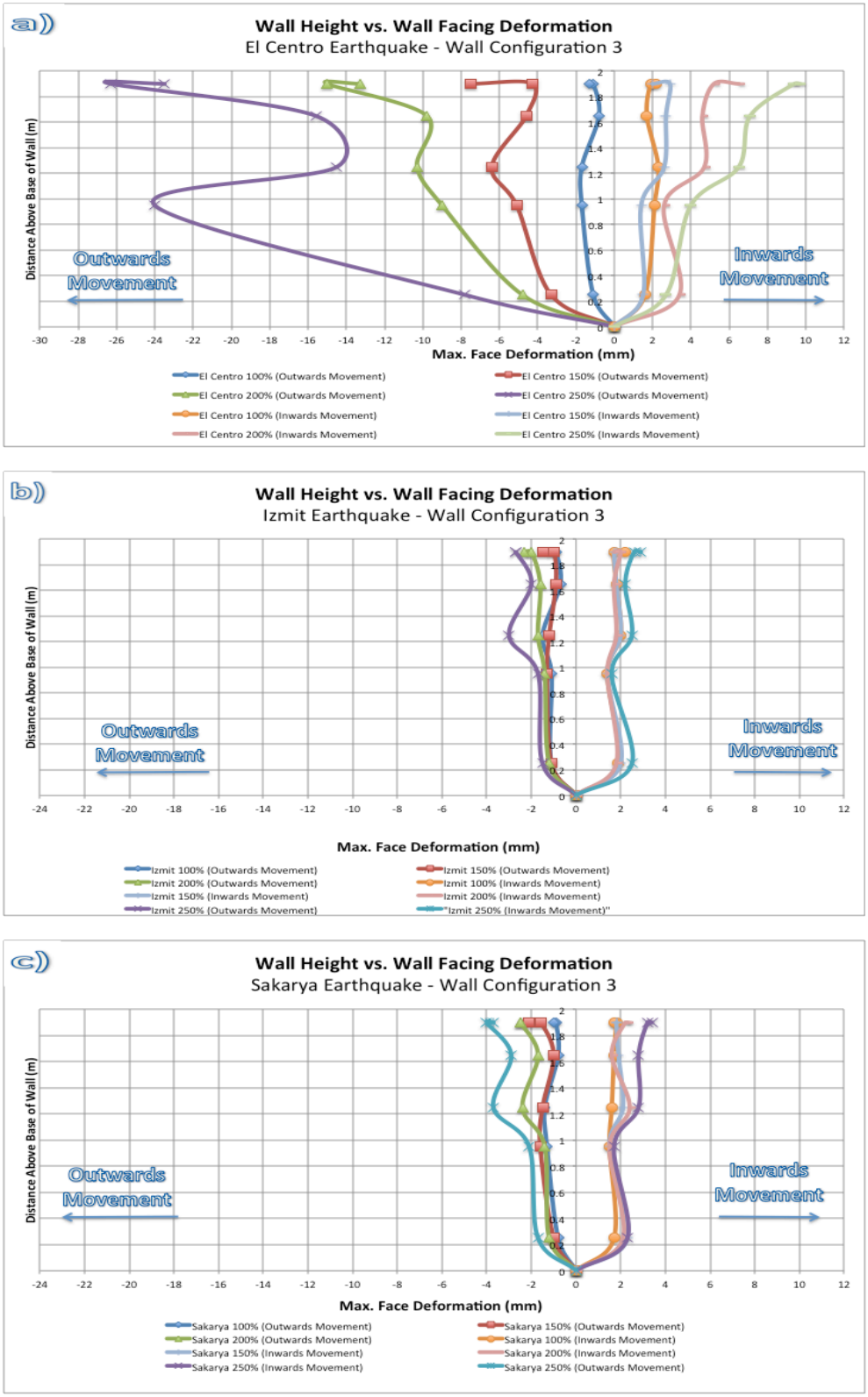


Figure 5.19.Peak Displacements at the wall facing for Wall 3 in base excitations a) El Centro Earthquake, b)Izmit Earthquake, c)Sakarya Earthquake Motions

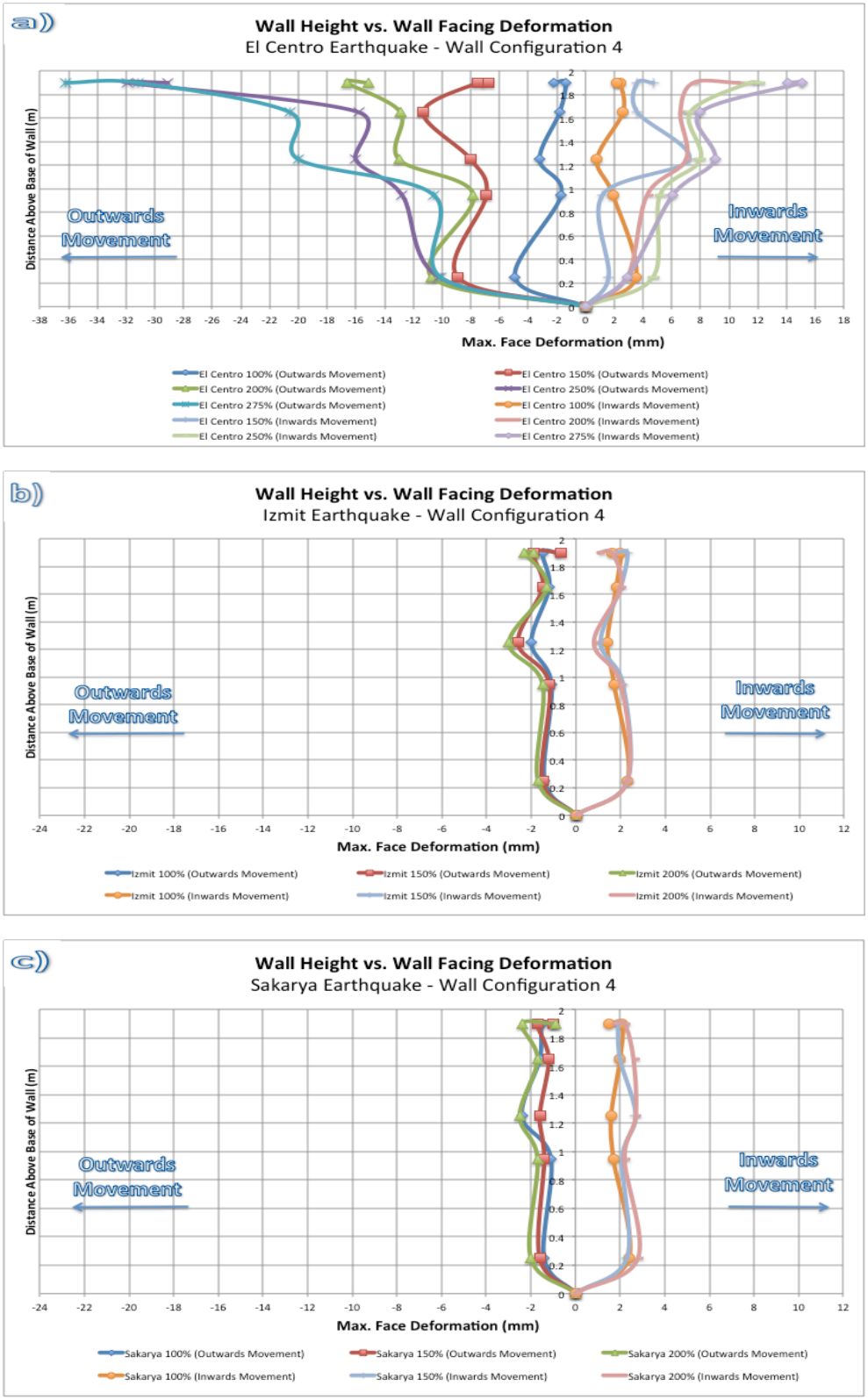


Figure 5.20. Peak Displacements at the wall facing for Wall 4 in base excitations a) El Centro Earthquake, b)Izmit Earthquake, c)Sakarya Earthquake Motions

Since the Sakarya and Izmit Earthquake motion base excitations resulted almost no residual displacements, the measured residual displacements on facing for Wall 1, 2, 3 and 4 are presented together with El-Centro Earthquake motion in Table 5.17 through Table 5.21. For each wall configuration and laser displacement transducer location, the maximum residual displacement values together with corresponding base acceleration values are highlighted in yellow in the following tables. The residual face deformations on top modular block as a function of base acceleration amplitude (for El-Centro Earthquake) are given in Figure 5.21.In these graphs, the minimum acceleration values that gives residual displacement to the structure can be observed.

Table 5.17 Residual Displacements Measured on(@h=1.9m) Top Modular Blocksfor Wall 1, 2, 3 and 4

		WALL 1	**WALL2**	**WALL3**	**WALL 4**
Dynamic Excitation Applied	**Max. Input Base Acceleration Amplitude (g)**	**Residual Displacement (mm)**	**Residual Displacement (mm)**	**Residual Displacement (mm)**	**Residual Displacement (mm)**
El Centro 100%	0.43	0	0	0.5	0.8
El Centro 150%	0.61	1	2	3.6	2.4
El Centro 200%	0.76	3.7	5.5	5.9	4.6
El Centro 250%	0.93	–	–	6.8	5
El Centro 275%	0.98	–	–	–	4.6

Table 5.18. Residual Displacements Measured on (@h=1.65m) Modular Block for Wall 1, 2, 3 and 4

		WALL 1	**WALL2**	**WALL3**	**WALL 4**
Dynamic Excitation Applied	**Max. Input Base Acceleration Amplitude (g)**	**Residual Displacement (mm)**	**Residual Displacement (mm)**	**Residual Displacement (mm)**	**Residual Displacement (mm)**
El Centro 100%	0.43	0	0	0	0
El Centro 150%	0.61	1.5	3	1.5	3
El Centro 200%	0.76	2	6	3.5	6
El Centro 250%	0.93	–	–	5	6.5
El Centro 275%	0.98	–	–	–	7

Table 5.19. Residual Displacements Measured on (@h=1.25m) Modular Block for Wall 1, 2, 3 and 4

		WALL 1	WALL2	WALL3	WALL 4
Dynamic Excitation Applied	**Max. Input Base Acceleration Amplitude (g)**	**Residual Displacement (mm)**	**Residual Displacement (mm)**	**Residual Displacement (mm)**	**Residual Displacement (mm)**
El Centro 100%	0.43	0	0	0	0
El Centro 150%	0.61	1.5	2.5	4	2.5
El Centro 200%	0.76	1.5	9	6	5.5
El Centro 250%	0.93	–	–	7	6
El Centro 275%	0.98	–	–	–	6.5

Table 5.20. Residual Displacements Measured on (@h=0.95m) Modular Blockfor Wall 1, 2, 3 and 4

		WALL 1	WALL2	WALL3	WALL 4
Dynamic Excitation Applied	**Max. Input Base Acceleration Amplitude (g)**	**Residual Displacement (mm)**	**Residual Displacement (mm)**	**Residual Displacement (mm)**	**Residual Displacement (mm)**
El Centro 100%	0.43	0	0	1.5	1
El Centro 150%	0.61	0	1.5	4	5
El Centro 200%	0.76	1.5	3	5.5	4
El Centro 250%	0.93	–	–	5.5	5
El Centro 275%	0.98	–	–	–	6

Table 5.21. Residual Displacements Measured on (@h=0.25m) Modular Blockfor Wall 1, 2, 3 and 4

		WALL 1	WALL2	WALL3	WALL 4
Dynamic Excitation Applied	**Max. Input Base Acceleration Amplitude (g)**	**Residual Displacement (mm)**	**Residual Displacement (mm)**	**Residual Displacement (mm)**	**Residual Displacement (mm)**
El Centro 100%	0.43	0	0	0	0
El Centro 150%	0.61	0	0	3	2
El Centro 200%	0.76	1	0	3.5	2.5
El Centro 250%	0.93	–	–	4	3.5
El Centro 275%	0.98	–	–	–	5

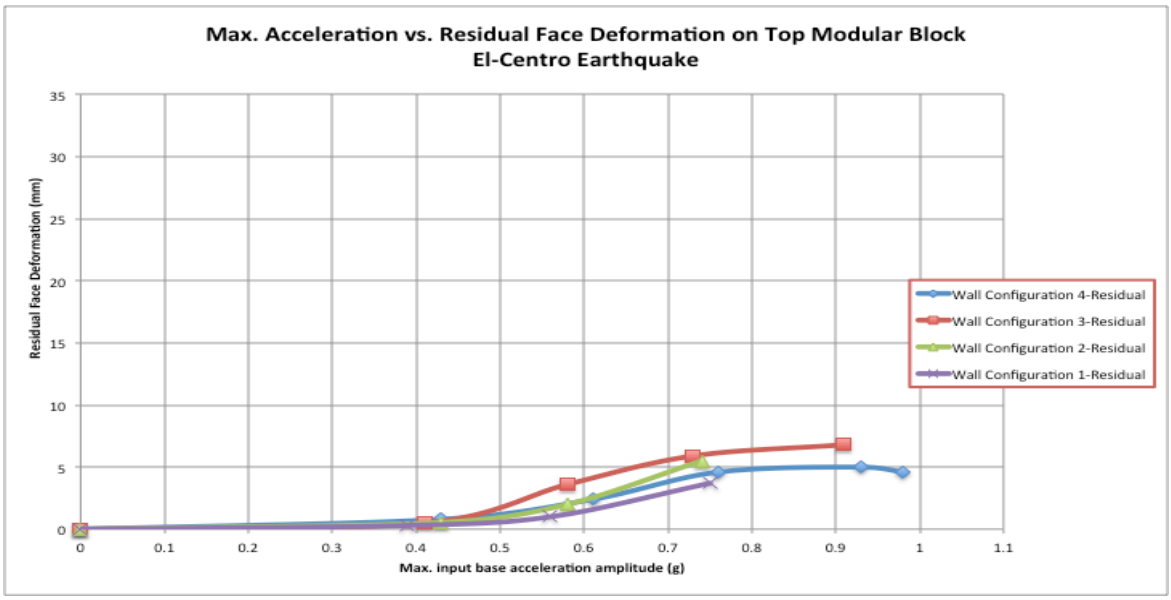


Figure 5.21. Horizontal Residual Facing Displacement on Top Modular block (@h=1.9m) as a function of Maximum Input Base Acceleration Amplitude for El-Centro Earthquake Motion

In order to compare the influence of different earthquake motions on wall facing displacement, the maximum lateral displacements as a function of peak base acceleration amplitude regarding the top modular block, are shown in Figures 5.22.through Figure 5.24.for model walls.

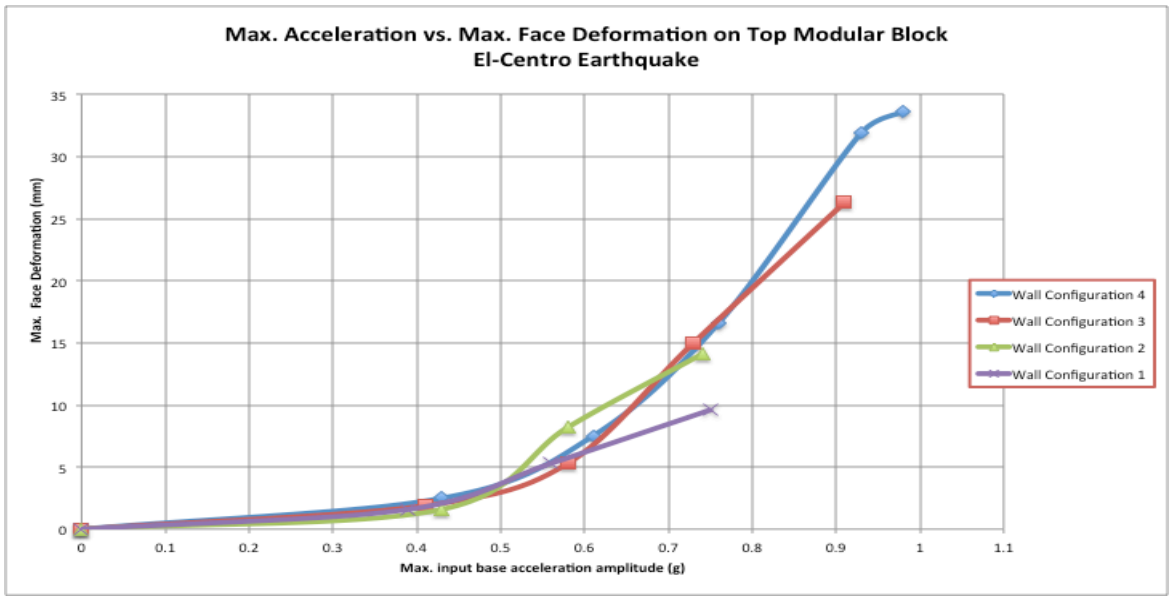


Figure 5.22. Horizontal Facing Displacement on Top Modular block as a function of Maximum Input Base Acceleration Amplitude for El-Centro Earthquake Motion.

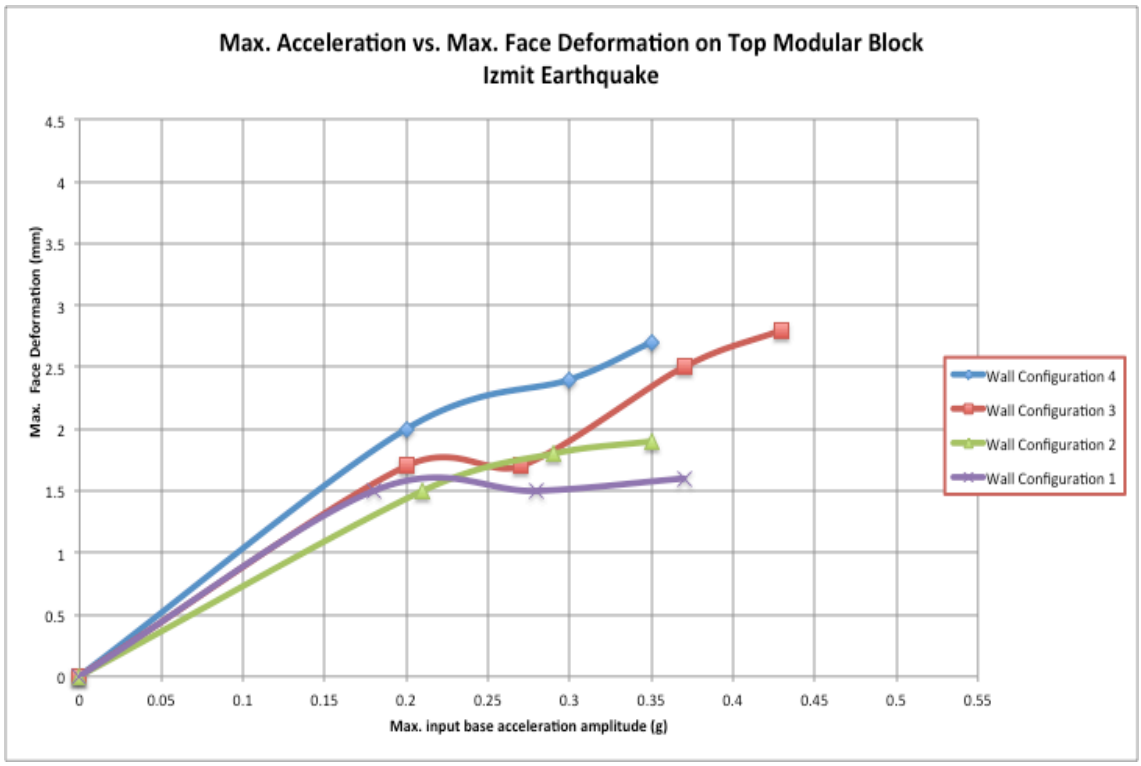


Figure 5.23. Horizontal Facing Displacement on Top Modular block as a function of Maximum Input Base Acceleration Amplitude for Izmit Earthquake Motion

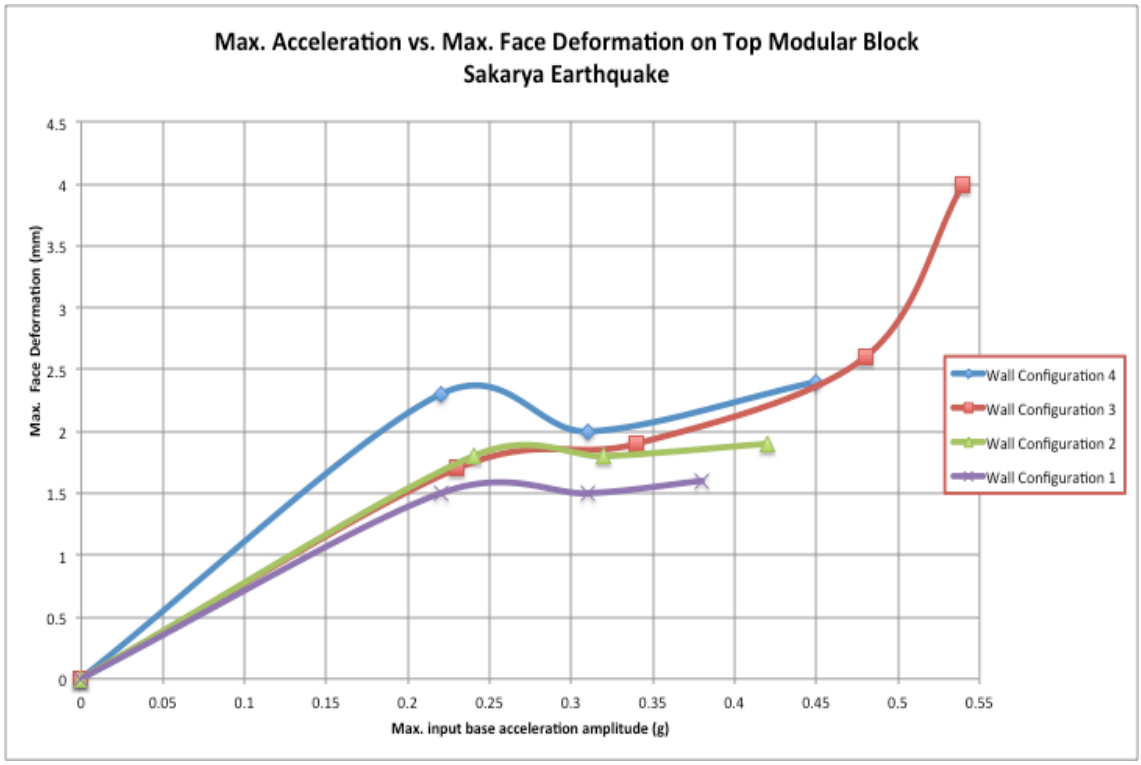


Figure 5.24. Horizontal Facing Displacement on Top Modular block as a function of Maximum Input Base Acceleration Amplitude for Sakarya Earthquake Motion

5.5.2. Evaluation of the Results

When the related tables and figures are observed, the following conclusions may be drawn regarding the wall face displacement:

- The walls in fact behave almost elastically and the residual displacements observed on the front of the wall were very small under the design earthquake accelerations.
- For all wall types, as the base acceleration increases, the wall facing displacement increases in both directions. However, with increasing base acceleration, the facing blocks tend to move on the outwards direction and have larger displacement values than the inwards direction.
- No failure on the facing of was observed even up to almost 1g. peak acceleration values were applied on model walls.
- For all wall types, residual displacements are observed only on the top block and only for El-Centro earthquake motion. Although the Izmit 200%, Sakarya 200% and Sakarya 250% earthquake excitations generate a higher maximum peak acceleration value than El-Centro 100% earthquake motion, no residual displacements are observed for Izmit and Sakarya Earthquake motions. That may be because of the wide frequency content of the El-centro-earthquake applied on the models.
- For the same applied dynamic excitations, the largest deformations occurred at Wall 2 (shorter reinforcement). Also, when more than 0,75 g is applied on the Wall 3 and Wall 4, the Wall 3 (gravel backfill) showed a slightly better behavior.
- For Wall 1, Wall3 and Wall4 the maximum face deformations occurred at the top block. However for Wall 2, the maximum face deformations occur at h=1.25 m of front facing. Wall 2 has inclined facing and weak reinforcement with respect to other wall models. Since the top blocks are grouted, the top blocks could not move as independently as the middle sections.
- Even under extreme accelerations applied on walls, the residual displacements remained minimal.
- The residual displacements occur at peak lateral acceleration values higher than 0.5 g. The highest residual displacement values are observed at Wall 3.
- No residual displacements are observed for Izmit and Sakarya Earthquake motions. This may be due to the acceleration to initiate permenantdisplacements is observed to

be around 0.5 g. The Sakarya and Izmit Earthquake motions applied on the models were unable to attain such peak acceleration amplitudes.

5.5.2.1. Influence of Wall Inclination on Horizontal Displacements of Wall Facings.Wall 1 and Wall 2 are compared in order to understand the effect of wall inclination on horizontal displacements of wall facings. The following results can be drawn:

- In terms of maximum facingdeformations Wall 1 and Wall 2 showed similar behavior and the results showed no significant difference. At some acceleration values at various heights of the wall (ie .El Centro 200% @h=1.25m. on front face) the inclined wall model (Wall2) showed higher displacement values. This result is unexpected since pseudo-static earth pressure theory predicts a decrease in lateral earth forces with increasing wall inclination towards the backfill soil. However as the face deformation values of wall 1 and wall 2 are close that might be due to small measurement errors.
- The Figure 5.18. and Figure 5.19.show that for the same reinforcement type (Wall 1 and Wall 2), inclined wall facing resulted a reduction in lateral diplacements at the lower portions of the wall however on mid-height and top portions of the wall a 47% increase in the wall maximum lateral displacement at an input base acceleration of 0.76 g is observed.
- The residual displacements had lower values in Wall 1 (vertical facing) than the Wall 2 (inclined facing). However, since the values are small, it might be said that both wall configurations showed almost the same behavior in terms of residual displacements on wall facings.

5.5.2.2. Influence of Backfill Material on Horizontal Displacements of Wall Facings. In order to comprehend the influence of backfill material (sand and gravel) on horizontal displacements of wall facings, Wall 3 and Wall 4 are compared. It can be stated that at low lateral accelerations (below 0.70 g base acceleration amplitudes), the backfill material has no significant effect on the maximum face deformations. However, when more than 0,7 g is applied on the Wall 3 and Wall 4, the Wall 3 (gravel backfill) showed slightly lower face deformationvalues than Wall 4. This may be due to the better interlocking of gravel material and geogrid.

5.5.2.3. Influence of Reinforcement Type and Length onHorizontal Displacements of Wall Facings. When Wall 2 and Wall 3 are compared in order to comprehend the influence of reinforcement type and length, the following conclusions may be drawn from the measurements:

- Increasing the reinforcement length and to wall height ratio,L/H from 0.47 to 0.7 and tensile strength, reduced the maximum wall deformations, especially at the top layers.
- When Wall 2 and Wall 3 compared, it is seen that although Wall 3 has stronger reinforcement (in terms of ultimate stress at rapture), less facing deformations observed in Wall 2. This is due to the higher reinforcement stiffness of Wall 2 reinforcement. Under seismic load conditions, the reinforcement stiffness becomes a key parameter.

5.6. Verification of Strain Gages

5.6.1. Testing Procedure

Please refer to Section 4.3.3.2.for more detailed information on installation procedure of the strain gages on georids. Huesker- Fortrac Polypropylene Geogrid 20/20 was selected to validate the strain gages under tensile loading. A 20 cm wide by 40 cm long geogrid sample is instrumented with 3 (TML-GFLA-6-50)strain gauges along the centre line strand. The test arrangement is shown and illustrated in Figure 5.25. andFigure 5.26. respectively.



Figure 5.25. View of the calibration tensile testing experimental set up

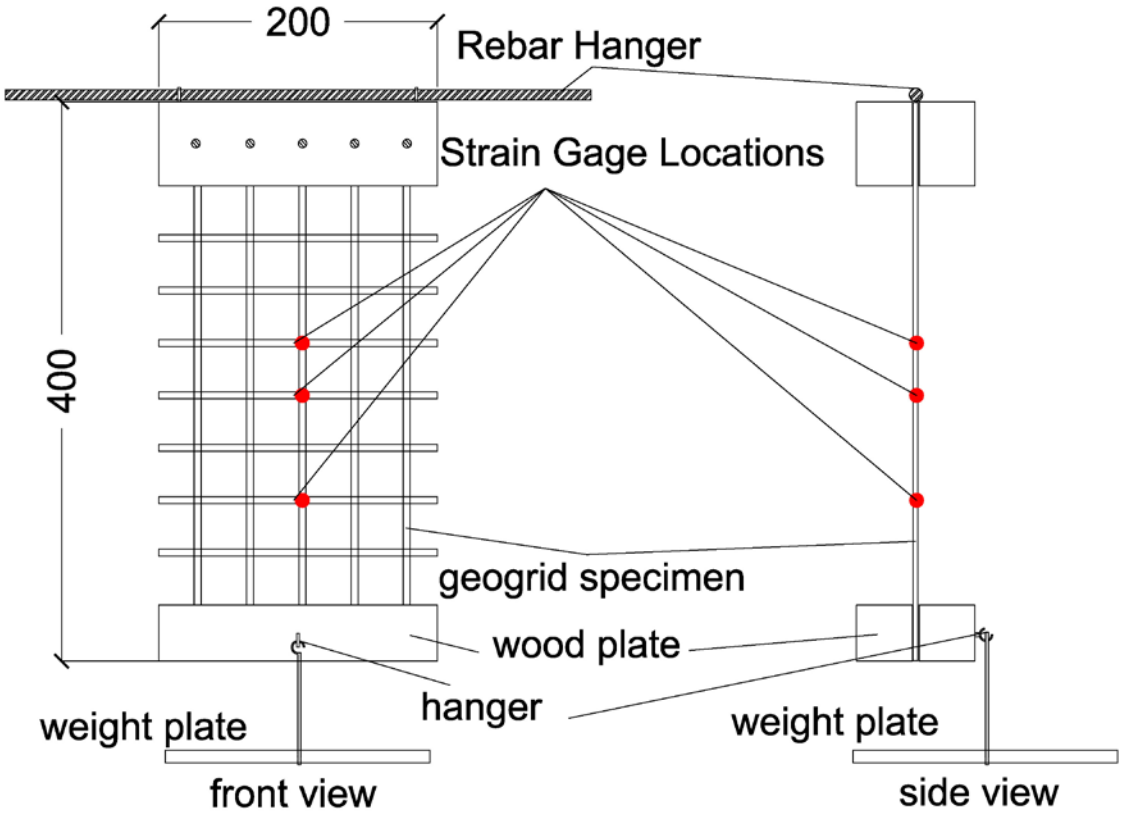


Figure 5.26. Test Apparatus

A simple arrangement for clamping the geogrid sample without slip at its ends was employed for the calibration test. The clamps were manufactured from hard wood which is considered to be the least detrimental material for the geotextile at the boundaries of the clamps. The wood plates clamped together at the bottom acted as a rigid beam to distribute the tensile force uniformly over the width of the geogrid. The dimensions of the jaws were 40x60x200 mm. which allowed testing of 200 mm wide geotextile specimen. Two hooks are mounted on the top of the clamp to hang the set up and one hook is mounted at the end of the jaw to hang the weights. The clamps were tightened using steel bolts. A total offive bolts were used on each clamp to distribute the loads uniformly over the width of the specimen.

The tensile load was applied to the geogrid by placing weights on the hangers in an approximately uniform fashion. Prescribed loads were applied by placing weights on the hangers and the corresponding strain gauge readings were recorded with the use of a computerized data acquisition system. The calibration test was stopped at a tensile load level of about 1 kN.

5.6.2. Test Results

The readings on three strain gages which were installed on the center line strand are shown all together in a single strain-time history plot in Figure 5.27.below. Sudden escalations in strains observed in strain-time history plot represent the placing of 10 kg. weights on the hangers.

When the scaling laws are applied to the explained test apparatus, it is seen that a tensile load of 100 kg (approx. 1kN) should result a tensile strain of 1.75 % on the Huesker- Fortrac Polypropylene Geogrid 20/20 specimen.

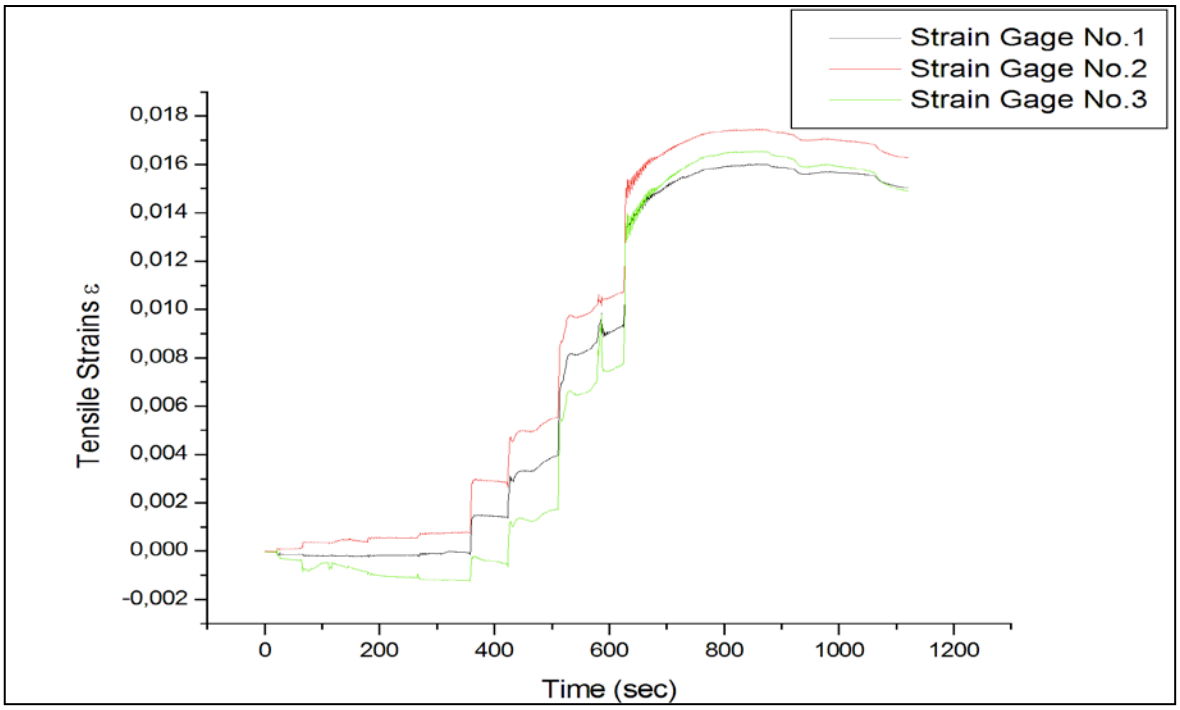


Figure 5.27. Strain-Time History graph for three strain gages installed on geogrid for verification.

As can be seen from the figure, three different total strains are obtained from the gages, which were mounted on different locations on geogrid. Although the tensile strain readings were a bit lower than the theoretical value (the readings were approx. ε=1.70% for strain gage No.1, ε=1.60% for Strain gage No.2 and ε=1.58% for Strain gage No.3 for an applied total load of 100 kg.).However, it can be concluded that the stain gages on geogrids work well under tensile loading.

5.7. Strain Distrubution in Geogrid Reinforcements during and at the end of Construction of Wall

The axial strains in two reinforcement layers (bottom and mid-height) are measured during and at the end of construction of test Wall 3 and Wall 4. The strain gage readings are taken at 10 second intervals. It should be noted that the construction phase of the wall was rapid and the end of construction strain values are obtained when the strain gage readings reached a stable state at the end of construction.

5.7.1. Test Results

The strains generated in the midheight and bottom reinforcement layer during the construction of the Wall 3 can be seen in Figure 5.28 and Figure 5.29 respectively.

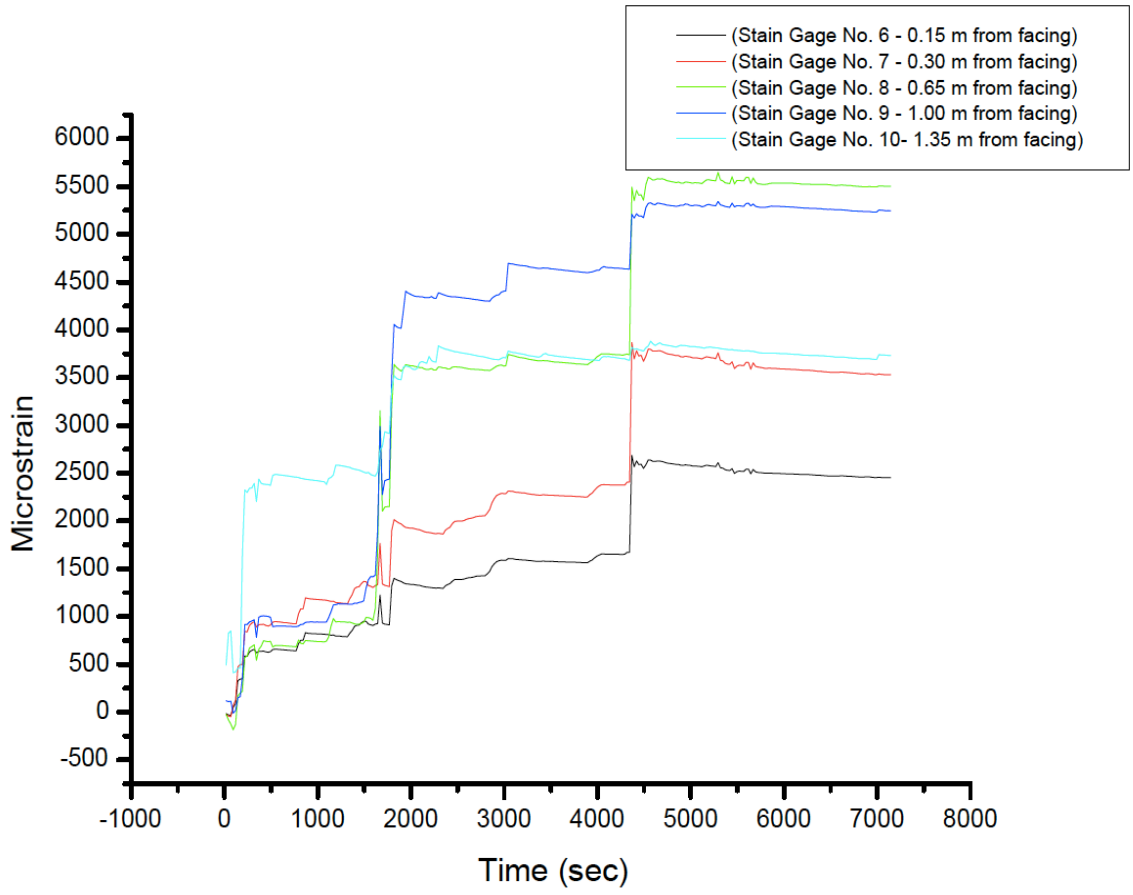


Figure 5.28. The strains generated at the midheight instrumented geogrid layer during construction of Wall 3

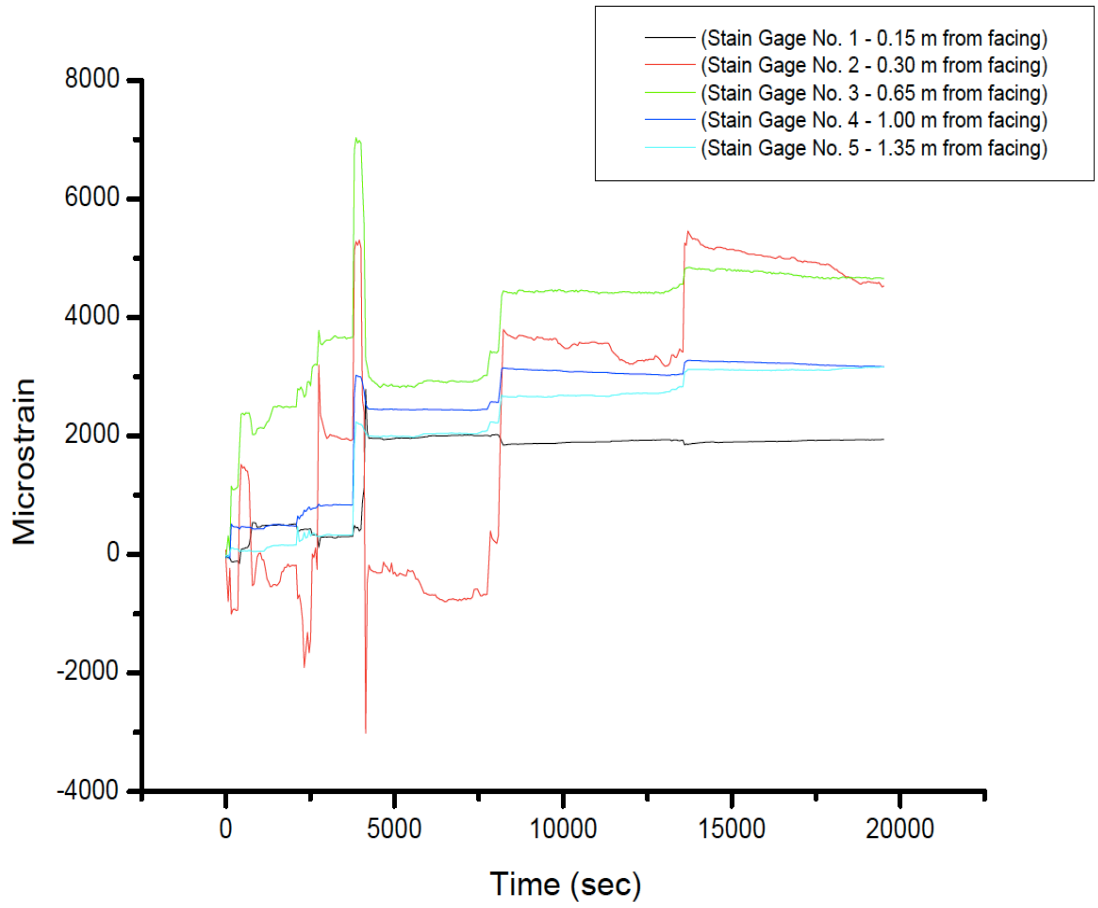


Figure 5.29. The strains generated at the bottom instrumented geogrid layer during construction of Wall 3

As can be seen from Figure 5.29. during the construction phase, at the bottom reinforcement layer, compressive strains ("-" sign in the figure)are generated at some locations of bottom reinforcement on the geogrid reinforcement as well as tensile strains. In the midheightgeogrid reinforcement, no compressive strains have occurred during construction.

The strains generated in the bottom and mid-height reinforcement layer during the construction of the Wall 4 can be seen in Figure 5.30 and Figure 5.31.respectively.

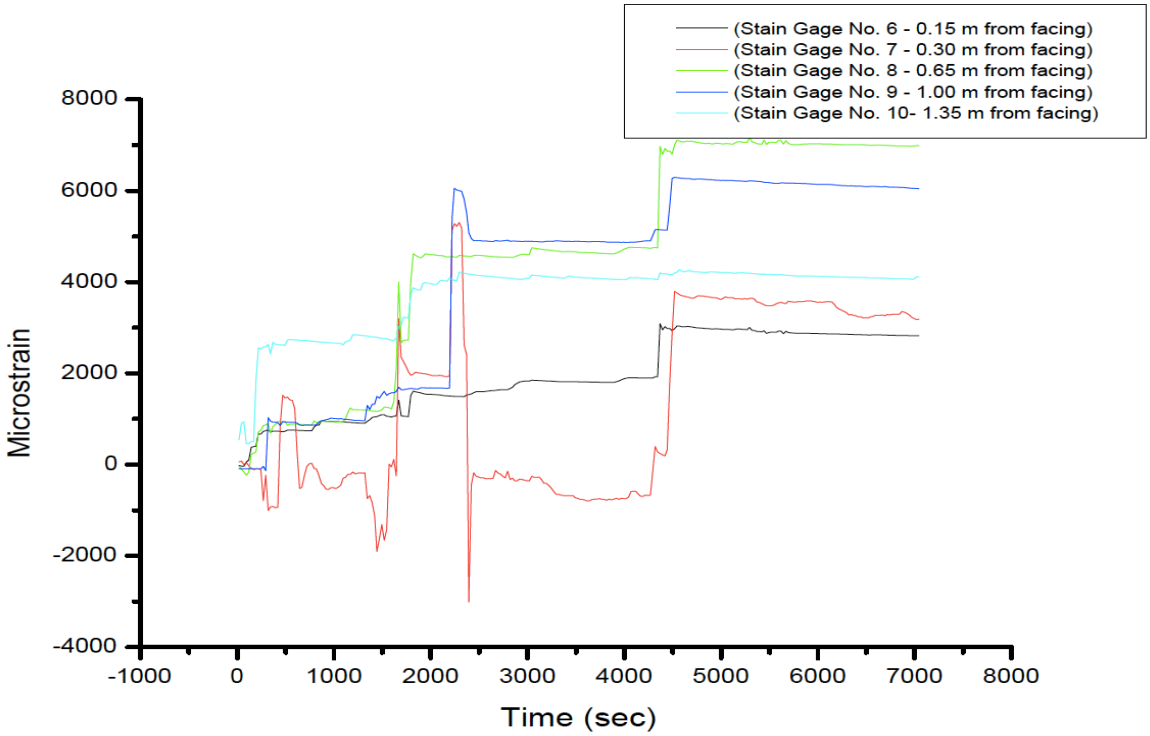


Figure 5.30. The strains generated at the midheight instrumented geogrid layer during construction of Wall 4

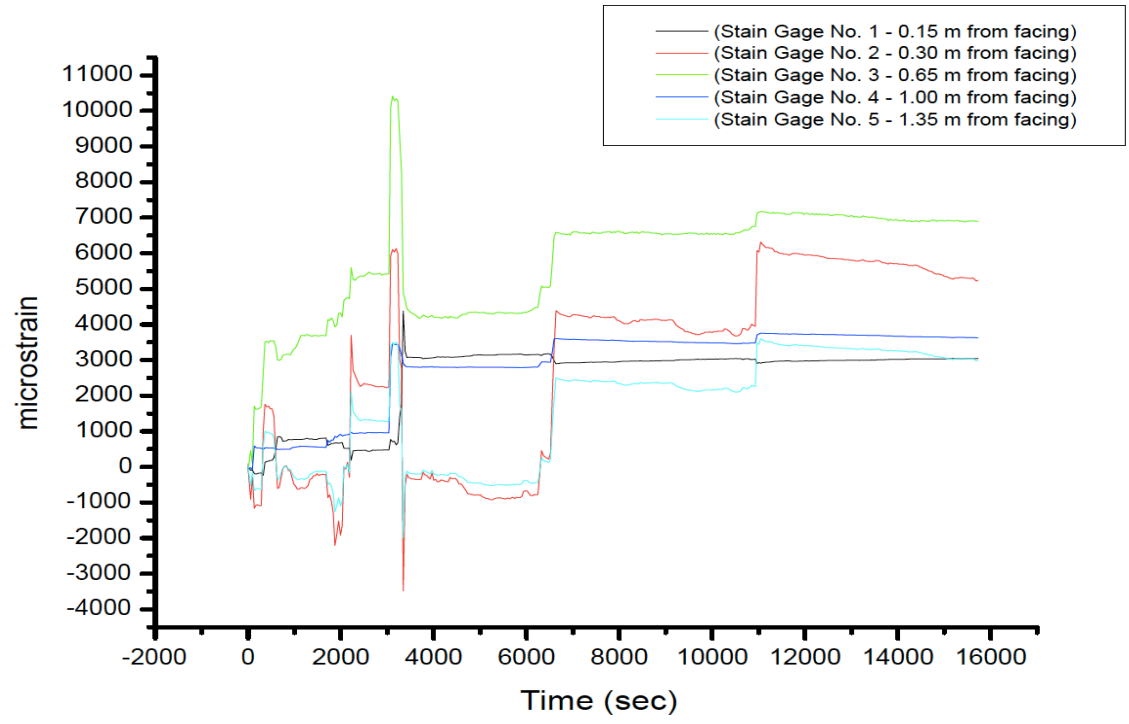
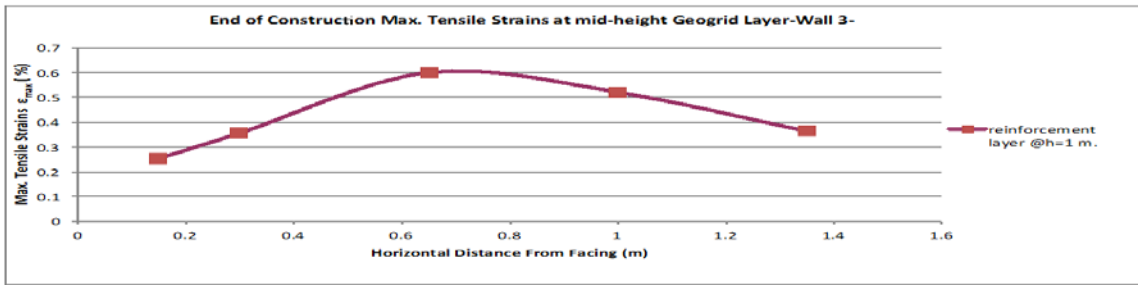
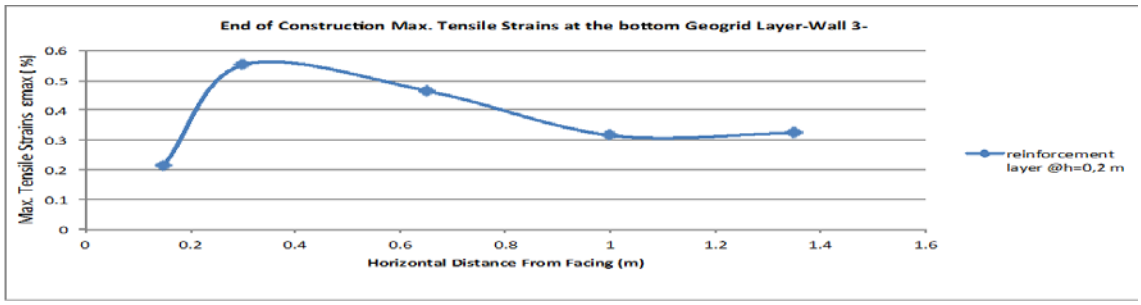


Figure 5.31. The strains generated at the bottom instrumented geogrid layer during construction of Wall 4

Figure 5.32. and Figure 5.33.show the distribution of strains in selected reinforcement layers at the end of construction of Wall 3 and Wall 4 respectively.

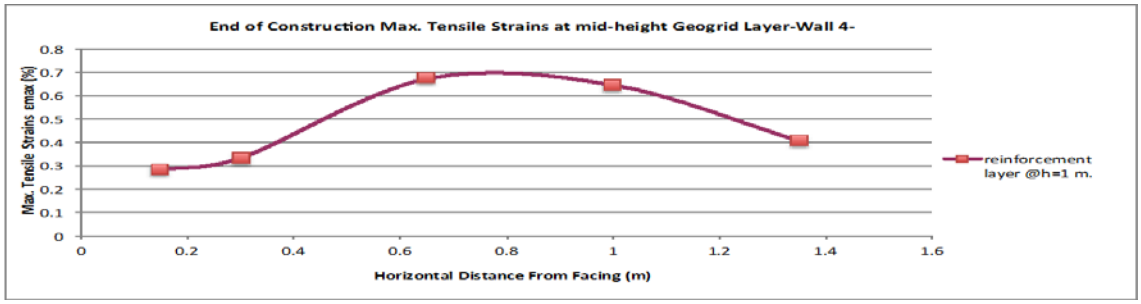


(a)

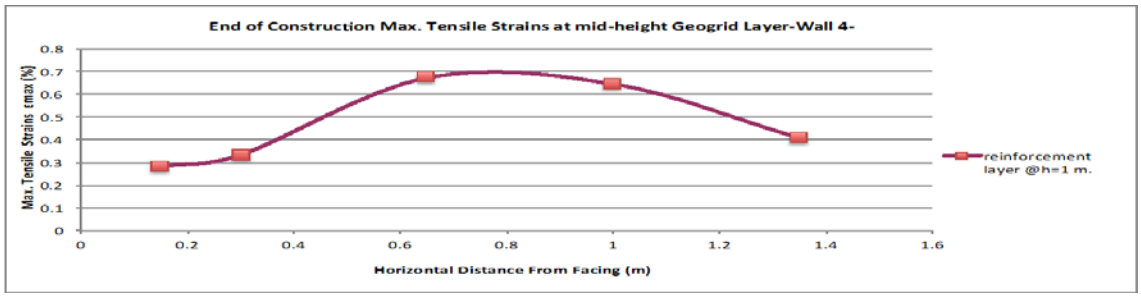


(b)

Figure 5.32.End of Construction Max. Tensile Strains at a) midheight b) bottom geogrid reinforcement for Wall 3 (aggregate backfill)



(a)



(b)

Figure 5.33. End of Construction Max. Tensile Strains at a) midheight b) bottom geogrid reinforcement for Wall 4 (sand backfill)

The peak strains obtained from the measurements are summarized in Table 5.22.

Table 5.22. Measured Strains in Geogrid Reinforcement at the end of construction for Wall 3 and Wall 4

Reinf. And Gages / Wall Configuration		WALL 3	WALL 4
Height of Reinforcement Layer from Base (m)	Strain Gage Horizontal Distance From Facing (m)	Measured Strains From Strain Gages (%)	Measured Strains From Strain Gages (%)
@h=0.25 m	0.15	0.21	0.33
	0.3	0.55	0.62
	0.65	0.47	0.60
	1	0.32	0.43
	1.35	0.32	0.36
@h=1 m	0.15	0.25	0.28
	0.3	0.36	0.33
	0.65	0.60	0.67
	1	0.52	0.65
	1.35	0.36	0.41

5.7.2. Evaluation of the Results

As can be seen from the related figures and tables, the strain gage readings obtained from the model walls are below 1% strain value. However peak strain magnitudes are observed on both Wall 3 and Wall 4 configurations. Bathurst (2002) reports that the reliability of strain gage readings at low strain levels (below 1%) corresponding to the end of construction are sufficient.

At the end of construction, Figure 5.32 and Figure 5.33. show that at the bottom layer the measured peak strains are located close to the facing and at mid-height reinforcement layer the peak strains are located in the middle section.

There are slight differences in the magnitudes of the strain values for the Wall 3 and Wall 4. Sand backfill model (Wall 4) has slightly larger peak strain values than gravelbackfill model (Wall 3).

At the bottom layer the strain gage readings at the closest distance to wall facing are expected to have a peak, however the peak occurs at the 30 cm. away from the facing. This may due to the occurrence of the peak strains between these two locations. Since there is no strain gage installed between those regions it is likely that the “real” peak strain readings might have been missed out.

An internal failure surface is obtained by joining the locus points of maximum stresses. The stresses are found by multiplying the strains with the corresponding Elasticity Moduli of geogrids. Wall 3 and Wall 4 through the reinforced zone a potential internal failure surface can be predicted. The measured failure surface and the potentialRankine failure surfaces are drawn by connecting the toe to the center points of the regions wherethe highest strains are measured. Since the strain gages installed on the top geogrid layer did not take any readings, the predicted critical surface was considered to pass linearly up to the top layer. The tensile stresses obtained at the end of construction together with potential Rankine Failure Surface are shown in Figure 5.34 and Figure 5.35 for Wall 3 and Wall 4 respectively. Measured and Rankine failure surface show good agreement.

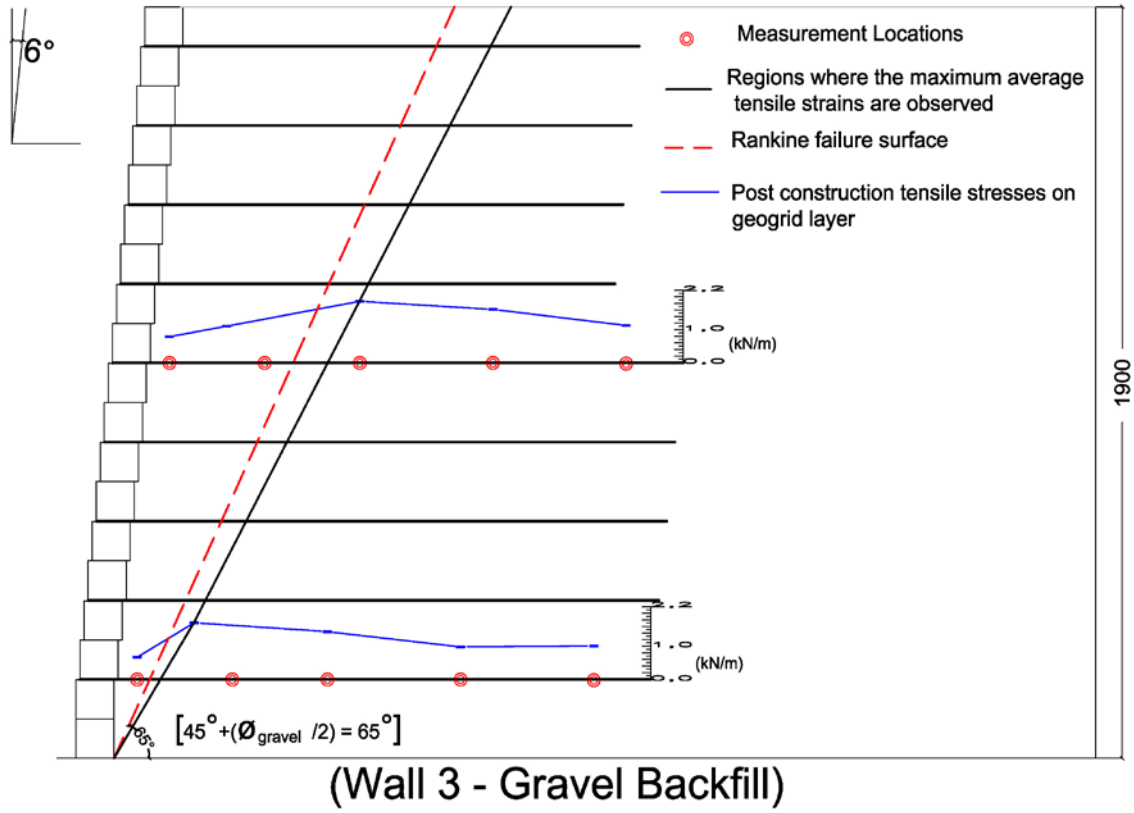


Figure 5.34. Post Construction Tensile Stresses on instrumented Geogridlayers together with failure surface for Wall 3

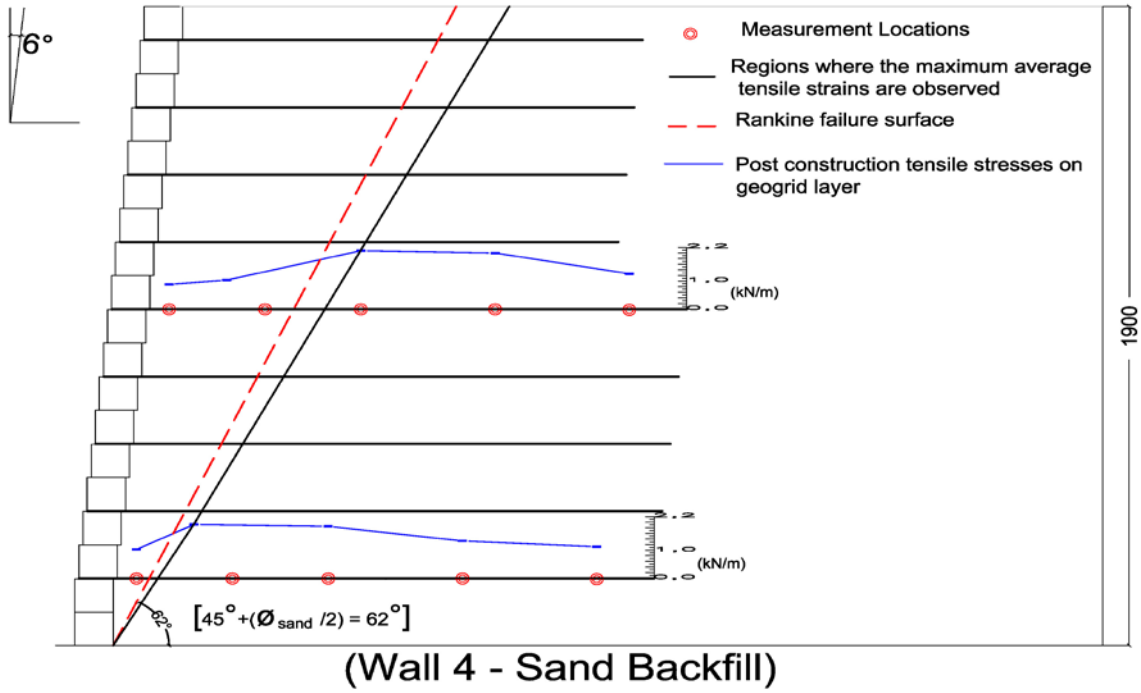


Figure 5.35. Post Construction Tensile Stresses on instrumented Geogridlayers together with failure surface for Wall 4

Integrated strain gauge readings do not account for movementsof the soil mass due to deformations behind and below the wall localizedsagging of the face or soil down-drag behind stiff wall facings.The review of physical data from a database of well-instrumented wall structureshas allowed the writers to comment on the reliability of the strain data, both qualitativelyand quantitatively. One possible use of this data is to estimate the mean andspread of reinforcement loads and compare estimated values to predicted values usingcurrent and proposed design methods for the internal stability of geosynthetic reinforcedsoil walls (Allen and Bathurst 2002). For that purpose in this study the strain gage readings under seismic motion are converted to tensile stresses and compared with the NCMA and FHWA pseudo static methods that is presented in Section 6.2.

5.8. Strains and Tensile Loads in Geogrid Layers During and Post Earthquake Motion

For all wall configurations and for each applied base excitation, the strain-time history plots obtained from strain gage readings on geogrids is given in Appendix A. It should be noted that Data Acquisition System used for strain gage readings was operated

during the dynamic excitations. As a result the dynamic strains are measured and evaluated. Please refer to Section 4.4.for strain gage locations.

Since the Data acquisition systems used for accelerometers and strain gages were different and the acceleration and strain measurements commenced at not exactly the same time, the acceleration-time history plot and the strain-time history plots did not coincide. However it is observed that the peak strains occurred when the base acceleration was at its peak value.

In this section, the maximum stains generated during the peak base accelerations are compared for the four different wall configurations with different input base acceleration amplitudes. It is of importance to note that, during the base excitations not only tensile strains did generate but also compressive strains occurred on the geogrids. However in this study, the tensile strains are presented. Additionally, the maximum tensile loads generated on the geogrids are presented.

5.8.1. Test Results of Strain Gage Readings

In the Tables 5.23 through 5.26 measured peak tensile strains together with measured peak compressive strains are compiled and presented for each wall configurations and base excitations. Additionally, the location of the strain gages and instrumented geogrid layer locations are presented in these tables. The yellow highlighted values represent the maximum tensile strain values and the red highlighted values represent the maximum compressive strain values observed at bottom, midheight and top strain gage instrumented geogrid layers respectively. In the tables the strain values are presented in micro strain(με) and as negative "-" signed.

It should be kept in mind that after each successive shaking the backfill soil got stiffer and that might have affected the measured values. In the evaluation of the test results, the compaction due to earthquake dynamic excitations is ignored.

Table 5.23. Measured Peak Tensile Strains together with peak compressive strains for each base excitations applied on Wall 1

WALL CONFIGURATION 1																				
Reinf. And Gages \ Base Excitation			El-Centro 100%		El-Centro 150%		El-Centro 200%		Izmit 100%		Izmit 150%		Izmit 200%		Sakarya 100%		Sakarya 150%		Sakarya 200%	
Height of Reinforcement Layer from Base (m)	Strain Gage No.	Strain Gage Horizontal Distance From Facing (m)	Measured Peak Tensile Strains From Strain Gages (με)	Measured Peak Compressive Strains From Strain Gages (με)	Measured Peak Tensile Strains From Strain Gages (με)	Measured Peak Compressive Strains From Strain Gages (με)	Measured Peak Tensile Strains From Strain Gages (με)	Measured Peak Compressive Strains From Strain Gages (με)	Measured Peak Tensile Strains From Strain Gages (με)	Measured Peak Compressive Strains From Strain Gages (με)	Measured Peak Tensile Strains From Strain Gages (με)	Measured Peak Compressive Strains From Strain Gages (με)	Measured Peak Tensile Strains From Strain Gages (με)	Measured Peak Compressive Strains From Strain Gages (με)	Measured Peak Tensile Strains From Strain Gages (με)	Measured Peak Compressive Strains From Strain Gages (με)	Measured Peak Tensile Strains From Strain Gages (με)	Measured Peak Compressive Strains From Strain Gages (με)	Measured Peak Tensile Strains From Strain Gages (με)	Measured Peak Compressive Strains From Strain Gages (με)
@h=0.2 m	Strain Gage No.1	0.2	-7912.24	1075.94	-11717.00	4339.20	-14743.22	8224.95	-1830.13	1220.09	-2627.76	1986.34	-4582.12	2944.41	-2113.62	1527.92	-3848.53	2689.83	-7178.28	5122.37
	Strain Gage No.2	0.35	-1969.79	-	-4445.61	733.06	-14630.13	2899.29	-127.09	305.02	-227.60	268.98	-574.94	435.56	-229.19	152.79	-413.82	310.37	-1446.11	1132.50
	Strain Gage No.3	0.5	-2002.89	-	-1359.70	603.00	-976.71	1480.49	-482.95	152.51	-682.80	372.44	-993.08	383.30	-611.17	127.33	-786.26	455.20	-1202.18	906.00
	Strain Gage No.4	0.65	-347.61	182.08	-1761.69	11.82	-7536.09	298.15	-177.93	355.86	-124.15	393.13	-383.30	209.07	-254.65	331.05	-289.67	331.06	-470.42	261.35
	Strain Gage No.5	0.8	-1572.52	314.50	-1950.87	756.70	-3475.04	1038.40	-813.39	686.30	-910.40	1117.31	-1689.99	1393.80	-789.42	993.15	-1220.77	1427.68	-2264.99	1864.26
@h=1 m	Strain Gage No.6	0.2	-1849.77	409.68	-3070.08	1124.21	-4157.40	2094.19	-467.36	285.61	-752.86	448.52	-1288.86	794.51	-623.14	350.52	-1308.17	565.98	-2003.28	1217.85
	Strain Gage No.7	0.35	-2271.87	33.11	-4529.49	851.32	-6886.83	2063.20	-421.92	201.22	-560.64	336.39	-913.68	419.32	-493.32	233.68	-827.62	357.74	-1217.85	710.41
	Strain Gage No.8	0.5	-7030.80	641.42	-13523.18	3464.59	-12735.56	7630.51	-1499.43	759.45	-2093.07	1164.00	-2829.32	1836.19	-1798.02	869.80	-2904.67	1463.01	-1637.04	3040.22
	Strain Gage No.9	0.65	-6269.38	914.54	-10014.10	3965.89	-13561.88	7679.58	-1616.28	876.29	-2274.62	1302.83	-3416.38	1973.01	-1895.39	973.66	-2974.08	1692.61	-4412.51	3287.31
	Strain Gage No.10	0.8	-5760.37	562.79	-9658.15	3274.75	-12133.98	6372.96	-1402.07	499.81	-1906.19	923.73	-2895.53	1549.29	-1538.38	688.05	-2557.59	1254.77	-3737.39	2696.03
@h=1.8 m	Strain Gage No.11	0.15	-1667.69	-	-1426.77	139.41	-3137.41	960.59	0.00	0.00	0.00	0.00	0.00	0.00	0.00	0.00	0.00	0.00	0.00	0.00
	Strain Gage No.12	0.25	-1324.22	422.10	-2948.47	551.73	-3362.07	462.22	-266.13	298.59	-464.53	304.35	-776.85	300.15	-415.43	246.66	-710.15	234.94	-1522.31	220.62
	Strain Gage No.13	0.4	-1311.81	-	-2752.69	186.87	-2548.66	581.00	-155.79	136.31	-266.97	122.81	-432.56	97.11	-285.61	84.38	-421.82	90.77	-564.80	291.22
	Strain Gage No.14	0.55	-2036.00	120.01	-4185.39	605.12	-3173.57	945.10	-506.30	285.51	-736.85	315.03	-1107.89	353.11	-642.62	214.20	-987.80	293.67	-1336.99	833.96
	Strain Gage No.15	0.7	-2102.21	136.56	-3170.94	993.70	-3217.47	1848.89	-584.20	259.54	-838.30	352.40	-1257.97	432.56	-746.47	214.20	-1142.65	336.39	-1244.33	1367.88
	Strain Gage No.16	0.8	-1522.86	82.76	-2545.05	768.26	-1843.72	1624.23	-499.81	181.75	-635.40	299.01	-900.44	370.77	-571.21	207.71	-864.99	293.67	-1023.70	1010.46

Table 5.24. Measured Peak Tensile Strains together with peak compressive strains for each base excitations applied on Wall 2

WALL CONFIGURATION 2																				
Reinf. And Gages / Base Excitation			El-Centro 100%		El-Centro 150%		El-Centro 200%		Izmit 100%		Izmit 150%		Izmit 200%		Sakarya 100%		Sakarya 150%		Sakarya 200%	
Height of Reinforcement Layer from Base (m)	Strain Gage No.	Strain Gage Horizontal Distance From Facing (m)	Measured Peak Tensile Strains From Strain Gages (με)	Measured Peak Compressive Strains From Strain Gages (με)	Measured Peak Tensile Strains From Strain Gages (με)	Measured Peak Compressive Strains From Strain Gages (με)	Measured Peak Tensile Strains From Strain Gages (με)	Measured Peak Compressive Strains From Strain Gages (με)	Measured Peak Tensile Strains From Strain Gages (με)	Measured Peak Compressive Strains From Strain Gages (με)	Measured Peak Tensile Strains From Strain Gages (με)	Measured Peak Compressive Strains From Strain Gages (με)	Measured Peak Tensile Strains From Strain Gages (με)	Measured Peak Compressive Strains From Strain Gages (με)	Measured Peak Tensile Strains From Strain Gages (με)	Measured Peak Compressive Strains From Strain Gages (με)	Measured Peak Tensile Strains From Strain Gages (με)	Measured Peak Compressive Strains From Strain Gages (με)	Measured Peak Tensile Strains From Strain Gages (με)	Measured Peak Compressive Strains From Strain Gages (με)
@h=0.2 m	Strain Gage No.1	0.2	-8723.33	2946.40	-12580.15	4800.31	-17495.37	9816.70	-2953.98	1120.47	-4034.75	2462.23	-5627.63	4390.60	-3310.49	1044.08	-4986.53	3082.96	-7892.60	4547.40
	Strain Gage No.2	0.35	-3525.75	678.66	-6869.40	2305.57	-16971.12	6681.56	-560.24	585.70	-372.44	434.51	-818.88	1358.99	-967.68	-	-165.53	393.13	-1916.53	1115.07
	Strain Gage No.3	0.5	-2300.84	1026.28	-8311.85	2033.63	-14956.38	5119.07	-916.75	178.26	-889.71	496.58	-1254.45	1097.65	-1426.05	-	-972.48	1055.24	-1602.92	1777.15
	Strain Gage No.4	0.65	-1158.70	165.53	-4492.91	212.82	-6188.13	627.04	-534.77	25.47	-62.07	268.98	-261.35	209.08	-789.42	-	-103.45	289.67	-574.96	243.92
	Strain Gage No.5	0.8	-844.19	711.77	-2234.63	1253.29	-5129.37	914.86	-1069.54	127.33	-993.17	869.02	-1254.45	1289.30	-1273.26	152.79	-827.64	1138.01	-1080.23	1742.30
@h=1 m	Strain Gage No.6	0.2	-1365.61	430.37	-3992.59	703.00	-6290.32	1621.64	-350.52	175.26	-512.59	347.07	-719.24	758.95	-382.97	136.31	-624.72	453.85	-988.72	878.37
	Strain Gage No.7	0.35	-1005.58	103.45	-1506.86	326.29	-2499.61	650.72	-214.20	129.82	-315.03	224.26	-485.37	308.88	-272.62	110.35	-336.39	309.69	-609.12	238.35
	Strain Gage No.8	0.5	-5541.04	773.84	-7727.12	1530.59	-9277.98	3578.98	-1096.99	298.59	-1361.56	443.18	-1884.14	908.98	-986.64	292.10	-1708.63	635.40	-2802.85	728.30
	Strain Gage No.9	0.65	-5441.73	1046.97	-9233.98	2254.36	-10483.88	4147.08	-1148.92	636.12	-1788.72	715.49	-2519.55	1469.36	-1207.34	480.34	-2082.39	977.12	-3460.51	1182.93
	Strain Gage No.10	0.8	-6273.51	1680.11	-10616.25	2906.93	-11976.40	4178.06	-1979.77	902.26	-3038.16	1062.55	-3988.91	2325.39	-1908.37	817.87	-3411.91	1575.14	-4996.55	2154.00
@h=1.8 m	Strain Gage No.11	0.15	0.00	0.00	0.00	0.00	0.00	0.00	0.00	0.00	0.00	0.00	0.00	0.00	-454.37	32.46	0.00	0.00	0.00	0.00
	Strain Gage No.12	0.25	-1589.07	277.26	-2212.84	347.05	-1967.66	581.00	-376.48	110.35	-576.66	42.72	-683.94	92.66	-454.37	32.46	-539.28	112.13	-865.13	176.56
	Strain Gage No.13	0.4	-1216.63	364.16	-1735.26	726.73	-1353.10	1208.48	-395.96	123.33	-501.91	133.49	-564.80	282.40	-467.36	25.96	-427.16	224.26	-697.40	269.25
	Strain Gage No.14	0.55	-3004.33	595.90	-4505.75	1026.33	-2902.44	2522.85	-720.51	292.10	-939.75	245.62	-1023.70	498.61	-675.07	175.26	-859.65	331.05	-1403.63	375.18
	Strain Gage No.15	0.7	-1357.33	662.11	-1741.20	2459.03	-2194.90	2817.22	-850.33	259.64	-1206.72	266.97	-1381.11	441.25	-928.22	175.26	-1137.30	389.78	-1721.43	454.63
	Strain Gage No.16	0.8	-2354.64	1224.91	-4034.11	2088.25	-2355.00	2778.48	-889.28	110.35	-1137.30	224.26	-1306.10	573.63	-908.75	149.29	-1126.63	459.19	-1650.81	662.09

Table 5.25. Measured Peak Tensile Strains together with peak compressive strains for each base excitations applied on Wall 3

WALL CONFIGURATION 3																								
Reinf. And Gages \ Base Excitation			El-Centro 100%		El-Centro 150%		El-Centro 200%		El-Centro 250%		Izmit 100%		Izmit 150%		Izmit 200%		Izmit 250%		Sakarya 100%		Sakarya 150%		Sakarya 200%	
Height of Reinforcement Layer from Base (m)	Strain Gage No.	Strain Gage Horizontal Distance From Facing (m)	Measured Peak Tensile Strains From Strain Gages (με)	Measured Peak Compressive Strains From Strain Gages (με)	Measured Peak Tensile Strains From Strain Gages (με)	Measured Peak Compressive Strains From Strain Gages (με)	Measured Peak Tensile Strains From Strain Gages (με)	Measured Peak Compressive Strains From Strain Gages (με)	Measured Peak Tensile Strains From Strain Gages (με)	Measured Peak Compressive Strains From Strain Gages (με)	Measured Peak Tensile Strains From Strain Gages (με)	Measured Peak Compressive Strains From Strain Gages (με)	Measured Peak Tensile Strains From Strain Gages (με)	Measured Peak Compressive Strains From Strain Gages (με)	Measured Peak Tensile Strains From Strain Gages (με)	Measured Peak Compressive Strains From Strain Gages (με)	Measured Peak Tensile Strains From Strain Gages (με)	Measured Peak Compressive Strains From Strain Gages (με)	Measured Peak Tensile Strains From Strain Gages (με)	Measured Peak Compressive Strains From Strain Gages (με)	Measured Peak Tensile Strains From Strain Gages (με)	Measured Peak Compressive Strains From Strain Gages (με)	Measured Peak Tensile Strains From Strain Gages (με)	Measured Peak Compressive Strains From Strain Gages (με)
@h=0.2 m	Strain Gage No.1	0.15	-9515.91	3214.10	-12685.82	4840.63	-16444.92	9227.29	-17431.62	9780.93	-3602.71	1366.54	-4503.24	2748.13	-6433.44	5019.27	-9650.16	7528.91	-3781.13	1192.51	-5983.83	3699.55	-7177.04	4135.13
	Strain Gage No.2	0.4	-10138.18	1951.48	-14053.42	4716.74	-20190.83	7949.16	-23017.55	9062.04	-3784.89	3956.93	-4731.15	5519.68	-6758.76	11216.65	-10138.14	16824.98	-4052.60	--	-6291.96	14943.39	-7231.20	4207.25
	Strain Gage No.3	0.65	-8844.75	3945.16	-9819.62	2402.53	-15334.84	5248.61	-15334.84	5248.61	-3552.59	690.78	-4440.80	2478.60	-6344.00	5551.00	-9516.00	8326.50	-3707.82	--	-5901.53	6403.81	-6635.31	7356.54
	Strain Gage No.4	1	-5906.98	843.86	-7815.86	370.22	-12797.62	1296.77	-12797.62	1296.77	-2771.83	131.99	-3464.77	15014.01	-4318.79	3455.03	-6478.19	5182.54	-2968.86	--	-4607.58	12901.25	-5306.35	2251.18
	Strain Gage No.5	1.35	-3021.69	2547.69	-3513.60	1970.59	-5977.78	1066.18	-7591.78	1354.04	-1128.04	134.29	-1410.07	1233.81	-2014.31	2070.27	-3021.47	3105.41	-1265.10	151.81	-1872.83	2575.15	-2257.81	3641.62
@h=1 m	Strain Gage No.6	0.15	-2297.73	724.13	-3501.16	616.47	-8399.77	1849.86	-7807.72	2012.83	-857.71	428.86	-1072.17	725.95	-1531.75	1616.33	-2297.63	2424.49	-920.81	327.75	-1424.84	1035.14	-1642.04	1458.77
	Strain Gage No.7	0.4	-3818.34	392.83	-5563.16	1204.62	-10282.28	2676.79	-10487.92	2730.32	-1425.61	864.01	-1781.90	1268.47	-2545.49	1619.86	-3818.23	2429.79	-1529.48	619.08	-2368.70	2180.72	-2731.36	1068.79
	Strain Gage No.8	0.65	-6258.53	874.04	-8987.45	1780.24	-13781.03	5316.02	-13091.98	5050.22	-2195.98	597.72	-2920.30	950.53	-4172.16	2012.80	-6258.24	3019.20	-2354.28	696.99	-3859.16	1435.13	-4204.42	1092.48
	Strain Gage No.9	1	-5037.49	969.19	-8288.79	2023.60	-12317.60	4872.44	-13672.53	5408.40	-2012.80	1114.43	-2500.88	1000.35	-3358.05	1958.36	-5037.07	2937.54	-2155.18	857.44	-3320.02	1557.86	-3707.82	1267.47
	Strain Gage No.10	1.35	-2925.25	783.41	-5475.70	1499.35	-10613.15	3702.48	-9976.36	3480.33	-1092.66	497.97	-1365.69	477.63	-1951.70	1137.77	-2927.55	1706.66	-1167.97	500.56	-1813.24	837.10	-2087.92	900.10
@h=1.8 m	Strain Gage No.11	0.15	0.00	0.00	0.00	0.00	-4858.01	344.30	-6072.51	430.37	-1092.66	497.97	-797.06	59.04	0.00	0.00	0.00	0.00	0.00	0.00	0.00	0.00	0.00	0.00
	Strain Gage No.12	0.4	-1708.02	298.01	-2926.58	458.99	-4025.42	1188.61	-4750.00	1402.56	-637.62	186.89	-797.06	59.04	-1138.43	154.24	-1707.64	231.36	-678.66	48.48	-1050.87	218.50	-1205.04	245.93
	Strain Gage No.13	0.65	-1751.95	524.39	-2517.68	1054.41	-3756.95	3355.42	-4545.91	4060.06	-654.01	203.71	-817.55	217.43	-1168.04	584.02	-1752.06	876.03	-698.05	38.78	-1078.30	566.11	-1232.95	476.01
	Strain Gage No.14	0.8	-1727.06	342.56	-2693.97	613.64	-3901.81	3391.52	-4799.23	4171.57	-644.91	261.45	-806.15	210.70	-1152.07	561.14	-1728.11	841.71	-688.60	178.77	-1066.00	410.51	-1203.15	321.60
	Strain Gage No.15	1	-1793.23	874.75	-3354.97	4738.09	-5123.44	6576.09	-6558.00	8417.39	-614.90	187.76	-817.13	180.78	-1097.64	350.68	-1646.46	526.03	-659.39	124.50	-1082.91	371.14	-1171.23	309.33
	Strain Gage No.16	1.2	-1915.33	996.37	-2206.16	1142.01	-3293.11	3885.30	-4182.25	4934.33	-687.45	85.30	-859.27	169.43	-1227.71	539.20	-1841.56	808.79	-685.29	112.58	-1142.59	465.70	-1227.54	492.33

Table 5.26. Measured Peak Tensile Strains together with peak compressive strains for each base excitations applied on Wall 4

WALL CONFIGURATION 4																								
Base Excitation / Reinf. And Gages			El-Centro 100%		El-Centro 150%		El-Centro 200%		El-Centro 250%		El-Centro 275%		Izmit 100%		Izmit 150%		Izmit 200%		Sakarya 100%		Sakarya 150%		Sakarya 200%	
Height of Reinforcement Layer from Base (m)	Strain Gage No.	Strain Gage Horizontal Distance From Facing (m)	Measured Peak Tensile Strains From Strain Gages (με)	Measured Peak Compressive Strains From Strain Gages (με)	Measured Peak Tensile Strains From Strain Gages (με)	Measured Peak Compressive Strains From Strain Gages (με)	Measured Peak Tensile Strains From Strain Gages (με)	Measured Peak Compressive Strains From Strain Gages (με)	Measured Peak Tensile Strains From Strain Gages (με)	Measured Peak Compressive Strains From Strain Gages (με)	Measured Peak Tensile Strains From Strain Gages (με)	Measured Peak Compressive Strains From Strain Gages (με)	Measured Peak Tensile Strains From Strain Gages (με)	Measured Peak Compressive Strains From Strain Gages (με)	Measured Peak Tensile Strains From Strain Gages (με)	Measured Peak Compressive Strains From Strain Gages (με)	Measured Peak Tensile Strains From Strain Gages (με)	Measured Peak Compressive Strains From Strain Gages (με)	Measured Peak Tensile Strains From Strain Gages (με)	Measured Peak Compressive Strains From Strain Gages (με)	Measured Peak Tensile Strains From Strain Gages (με)	Measured Peak Compressive Strains From Strain Gages (με)	Measured Peak Tensile Strains From Strain Gages (με)	Measured Peak Compressive Strains From Strain Gages (με)
@h=0.2 m	Strain Gage No.1	0.15	-9990.90	1358.60	-14015.88	5190.55	-18419.69	10275.99	-19693.27	11098.06	-21366.85	11920.14	-4586.21	3057.48	-6369.68	4814.88	-7493.42	4815.17	-4769.34	3447.71	-6597.48	4611.14	-10490.73	7486.11
	Strain Gage No.2	0.4	-12456.08	-	-15884.16	2619.21	-23911.33	4738.57	-26780.69	5307.20	-28215.37	5591.52	-5717.39	13721.77	-7940.79	9384.58	-9342.15	7077.38	-5944.12	3962.74	-8257.48	6193.11	-13077.40	10241.36
	Strain Gage No.3	0.65	-8295.97	-	-12687.86	5626.79	-15859.94	24040.36	-17763.13	26925.20	-22203.91	33656.50	-4528.84	1430.16	-6294.27	3433.24	-7399.81	2856.07	-4960.17	1033.37	-6541.67	3787.28	-10367.38	7813.13
	Strain Gage No.4	1	-6868.60	3597.83	-9088.91	61.00	-13540.62	535.71	-13269.81	525.00	-19633.90	776.79	-3733.19	7466.37	-5185.00	16419.17	-6097.11	3325.69	-3880.46	5044.58	-5389.59	6159.54	-8539.47	4744.15
	Strain Gage No.5	1.35	-4391.81	878.36	-5368.00	2082.14	-9149.97	2734.16	-9515.97	2843.53	-12169.47	3636.43	-2015.92	1700.93	-2799.88	3436.22	-3280.06	2705.20	-2096.53	2637.57	-2911.70	3405.21	-4804.80	3954.72
@h=1 m	Strain Gage No.6	0.15	-2671.06	591.58	-4075.00	1492.20	-7439.15	3747.30	-9373.33	4721.60	-9968.46	5021.39	-1227.04	749.86	-1703.11	1014.62	-2002.42	1234.36	-1271.26	715.08	-1767.01	764.50	-2805.24	1705.38
	Strain Gage No.7	0.4	-5061.72	73.76	-7734.50	1453.70	-11951.04	3580.38	-12070.56	3616.18	-13863.21	4153.24	-1537.05	733.05	-2086.15	1251.69	-2793.52	1282.05	-1599.47	757.65	-2162.50	934.76	-3909.39	2280.48
	Strain Gage No.8	0.65	-6122.82	558.59	-9594.73	2458.14	-16584.22	9936.44	-17413.43	10433.26	-20232.74	12122.45	-2598.47	1316.11	-3483.50	1937.26	-4098.62	2659.95	-2358.06	1140.72	-3344.61	1684.60	-5123.42	9514.94
	Strain Gage No.9	1	-7268.89	1060.35	-9268.47	3670.59	-15486.87	8769.63	-15796.60	8945.02	-20597.53	11663.60	-3090.65	1675.65	-4292.36	2458.52	-5049.71	2916.29	-3210.77	1649.37	-4465.07	2541.16	-7070.42	5267.45
	Strain Gage No.10	1.35	-2926.27	285.90	-6837.08	2318.22	-9022.70	4738.86	-12180.65	6397.47	-16331.09	8577.34	-1343.84	479.06	-1866.51	904.50	-2194.99	1174.46	-1397.15	624.89	-1940.28	951.92	-3064.42	2210.57
@h=1.8 m	Strain Gage No.11	0.15	0.00	0.00	0.00	0.00	0.00	0.00	0.00	0.00	0.00	0.00	0.00	0.00	0.00	0.00	0.00	0.00	0.00	0.00	0.00	0.00	0.00	0.00
	Strain Gage No.12	0.4	-1951.53	622.05	-2317.59	433.67	-6219.22	855.02	-7027.71	966.18	-8022.79	1102.98	-895.93	1005.20	-1244.24	815.19	-1463.72	565.53	-931.80	553.26	-1289.46	426.59	-2049.33	297.00
	Strain Gage No.13	0.65	-2439.96	-	-2927.37	198.73	-5610.79	1279.06	-6340.19	1445.34	-7294.03	1662.78	-1119.95	979.96	-1555.49	715.53	-1829.81	410.77	-1164.27	343.99	-1615.91	347.73	-2561.88	1320.97
	Strain Gage No.14	0.8	-2146.53	126.52	-3293.19	476.12	-6344.23	1889.33	-6788.33	2021.59	-6788.33	2021.59	-985.49	555.92	-1368.62	585.13	-1951.55	622.01	-1024.91	341.64	-1421.77	422.69	-2732.73	1704.58
	Strain Gage No.15	1	-2866.21	186.19	-4024.34	1261.13	-7318.66	4205.71	-8270.31	4752.45	-9734.08	5593.59	-1106.67	491.85	-1537.00	646.13	-2149.85	739.25	-1150.30	330.09	-1594.04	469.27	-3010.12	3309.00
	Strain Gage No.16	1.2	-1951.87	106.08	-2560.47	772.92	-5245.83	4621.32	-7658.91	6747.13	-8865.45	7810.03	-895.84	325.76	-1244.34	585.57	-1463.59	602.66	-930.17	338.24	-1294.04	439.34	-2049.60	2023.09

Through Figure 5.36 through Figure 5.47 the peak tensile strains at bottom, midheight and top geogrid layers with increasing base accelerations for all wall configurations and applied base excitations are presented.

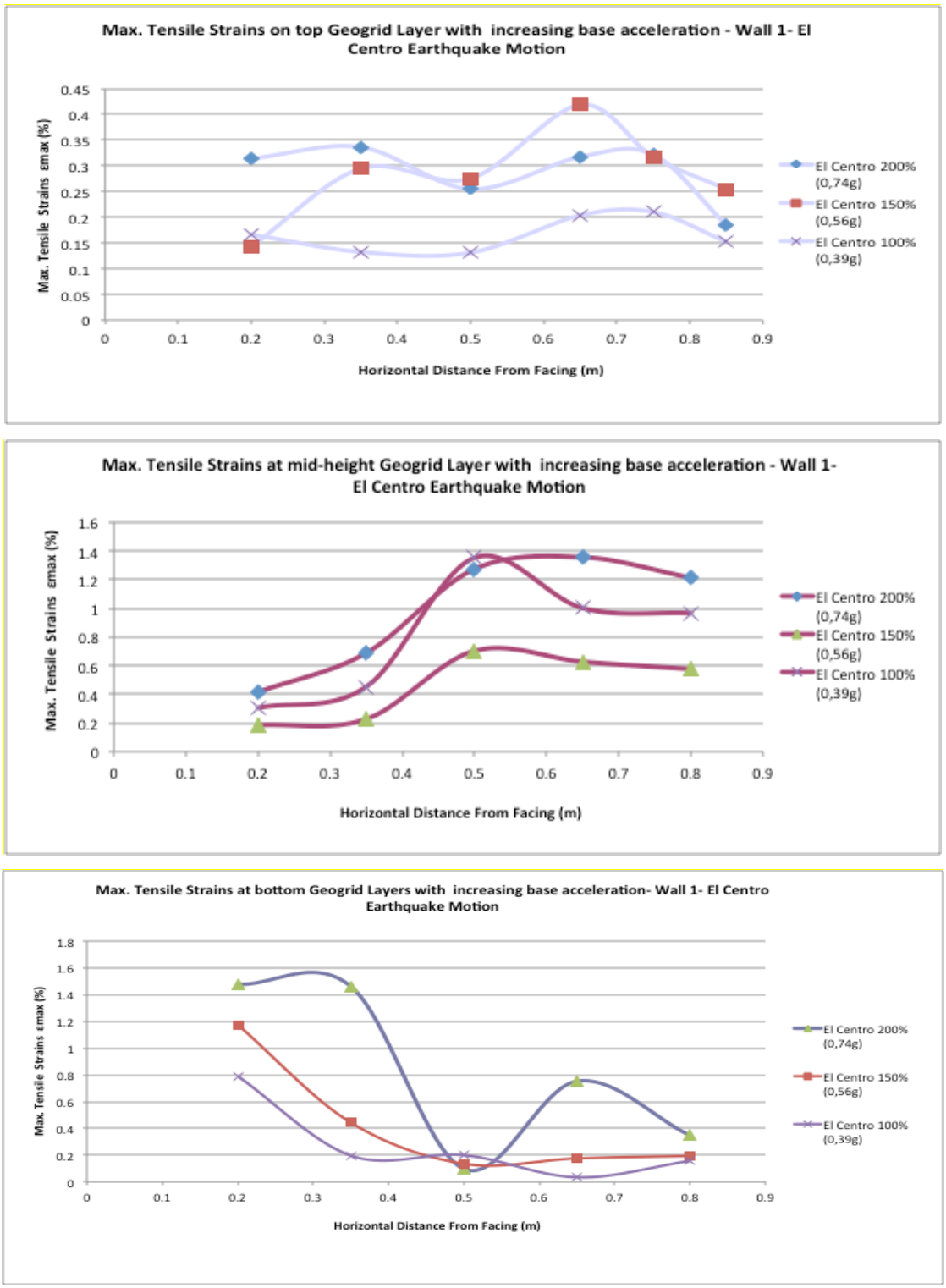


Figure 5.36. Max. Tensile Strains at top, mid-height and bottom Geogrid Layers with increasing base acceleration - Wall 1- El Centro Earthquake Motion

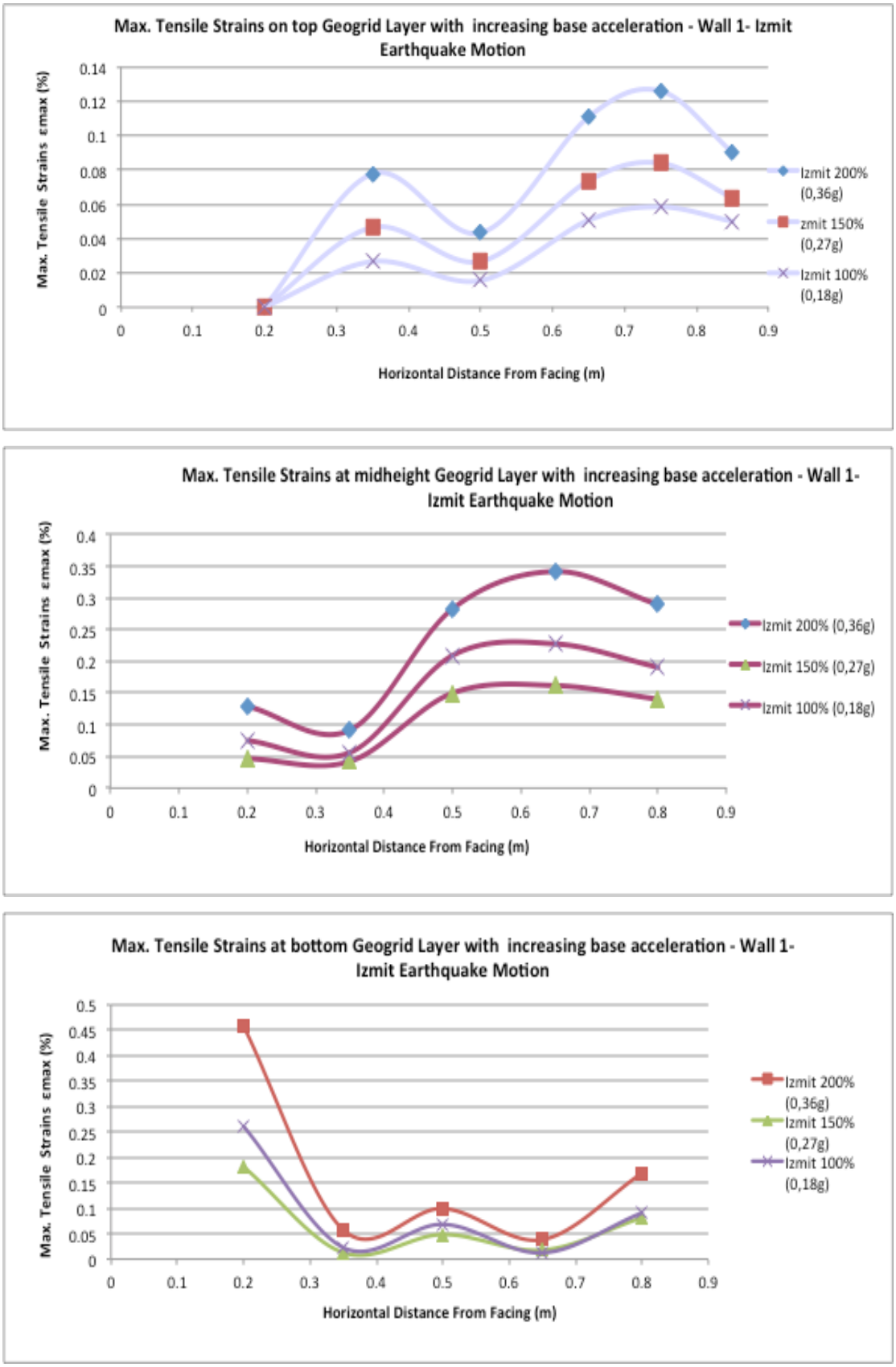


Figure 5.37. Max. Tensile Strains at top, mid-height and bottom Geogrid Layers with increasing base acceleration - Wall 1- Izmit Earthquake Motion

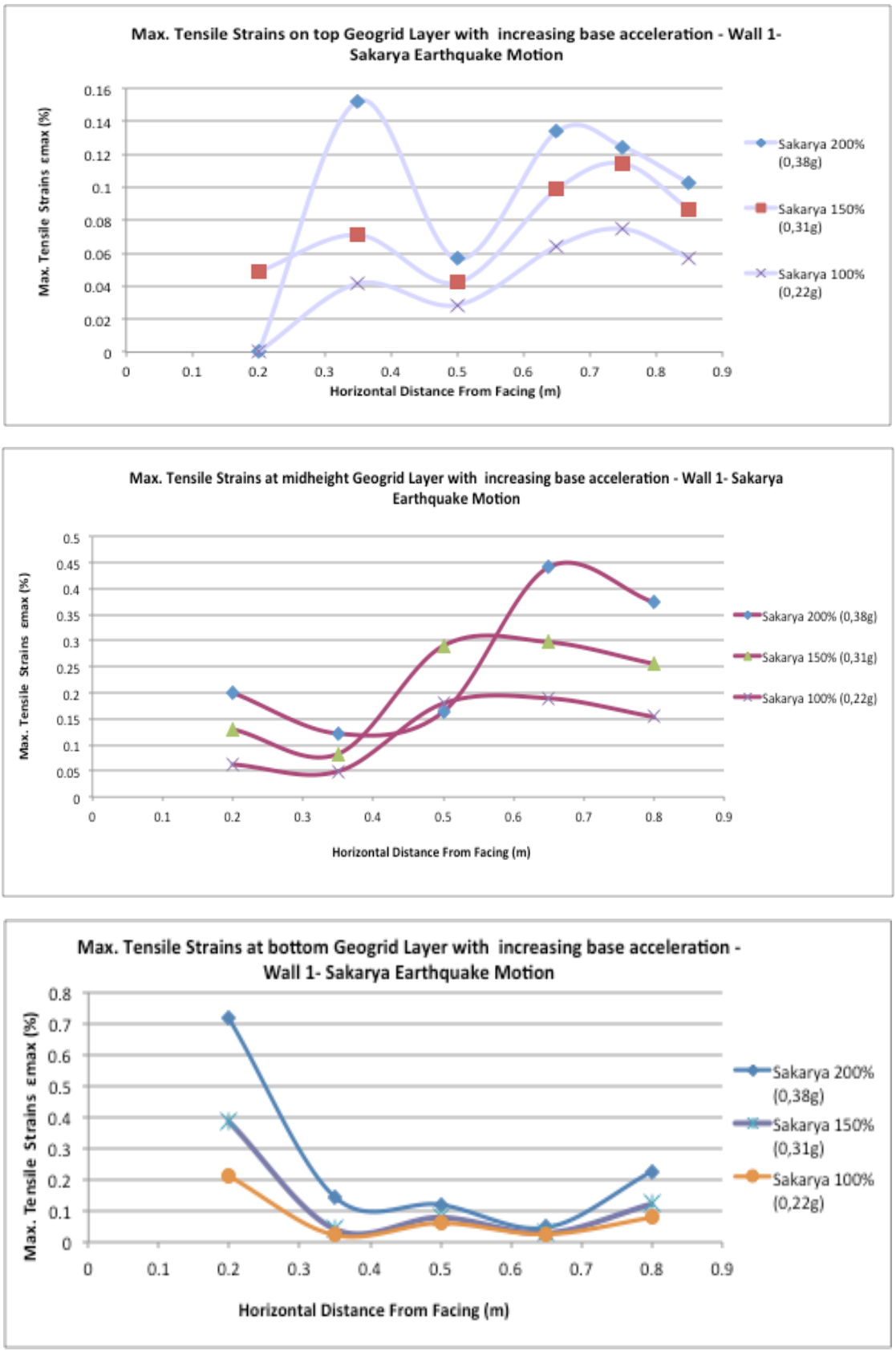
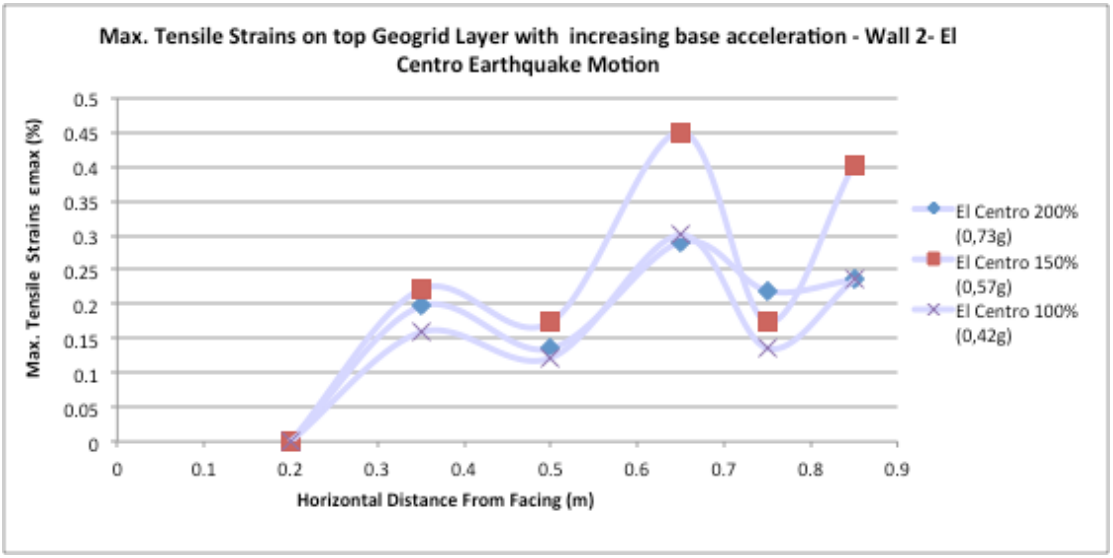
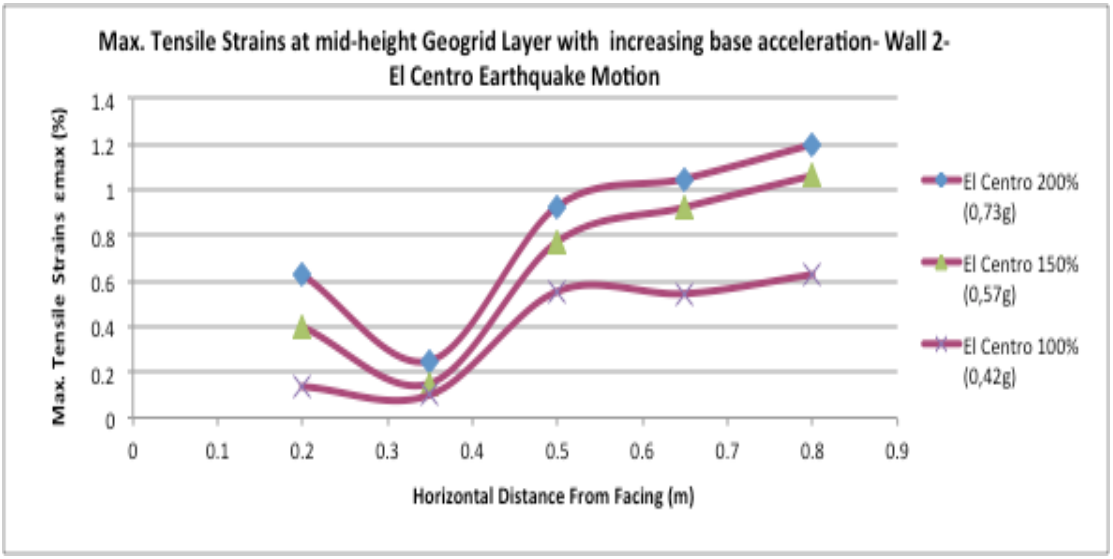


Figure 5.38. Max. Tensile Strains at top, mid-height and bottom Geogrid Layers with increasing base acceleration - Wall 1- Sakarya Earthquake Motion





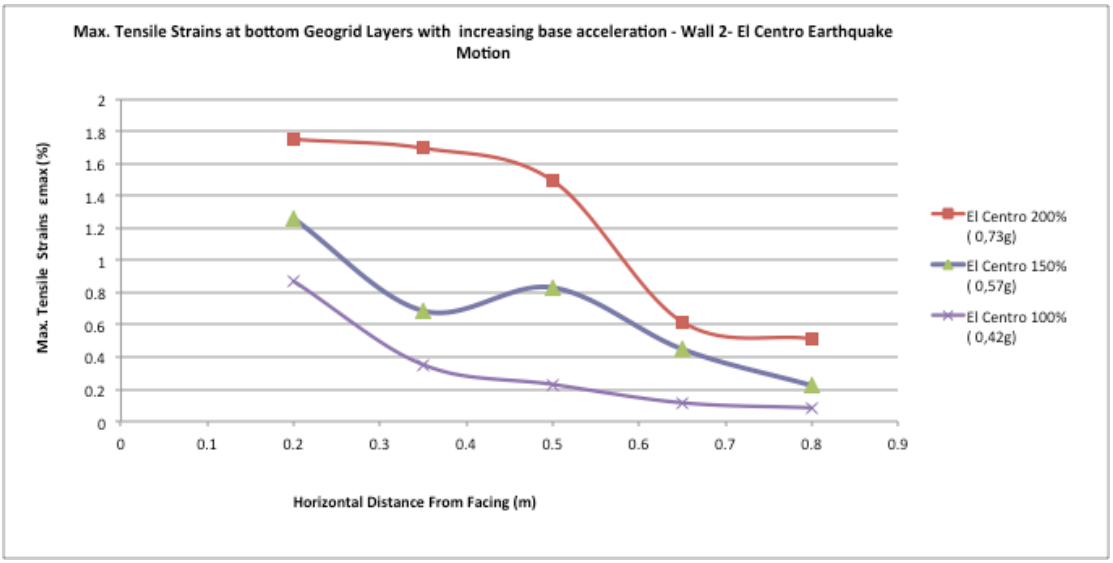


Figure 5.39.. Max. Tensile Strains at top, mid-height and bottom Geogrid Layers with increasing base acceleration - Wall 2- El Centro Earthquake Motion

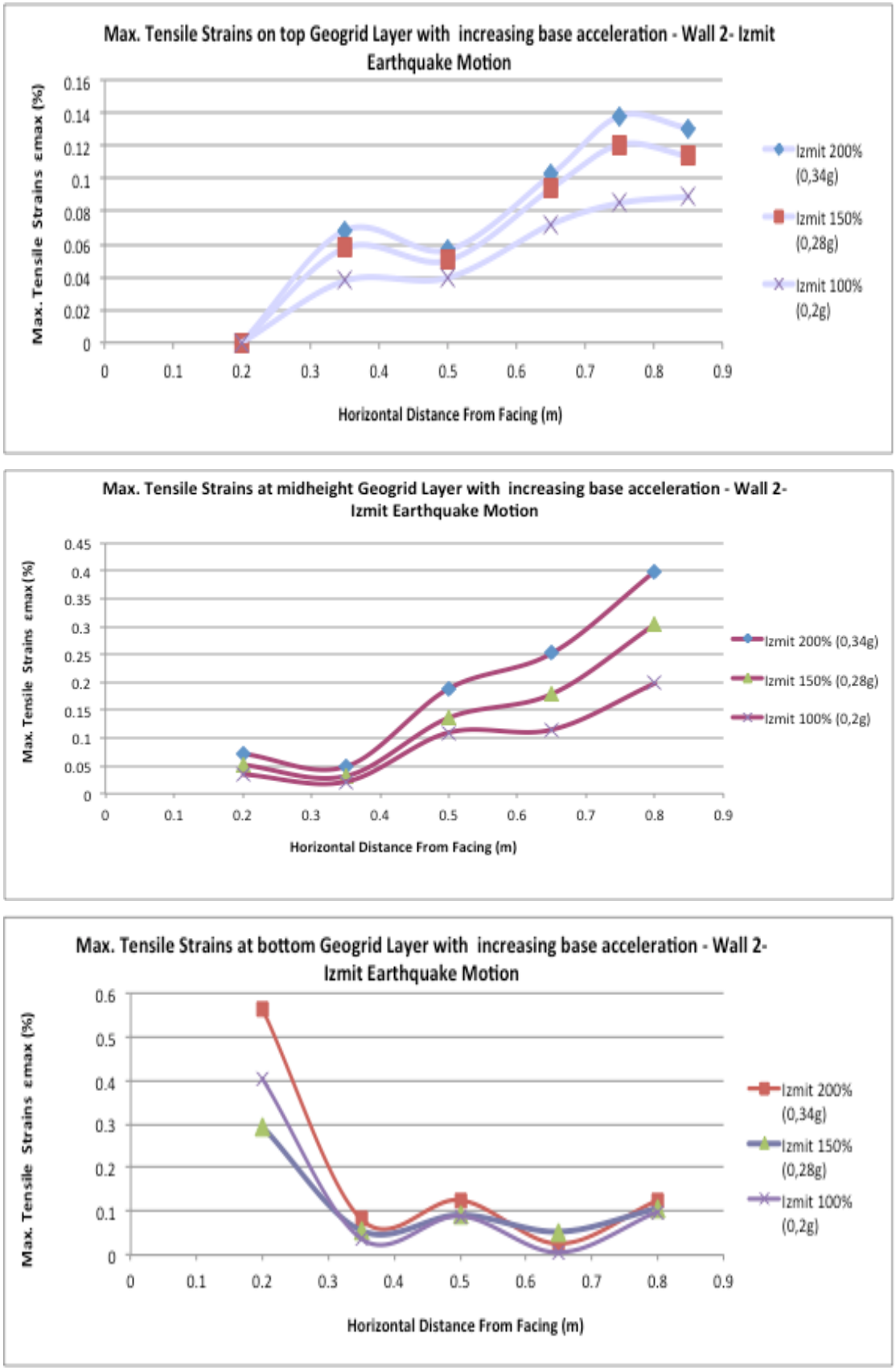
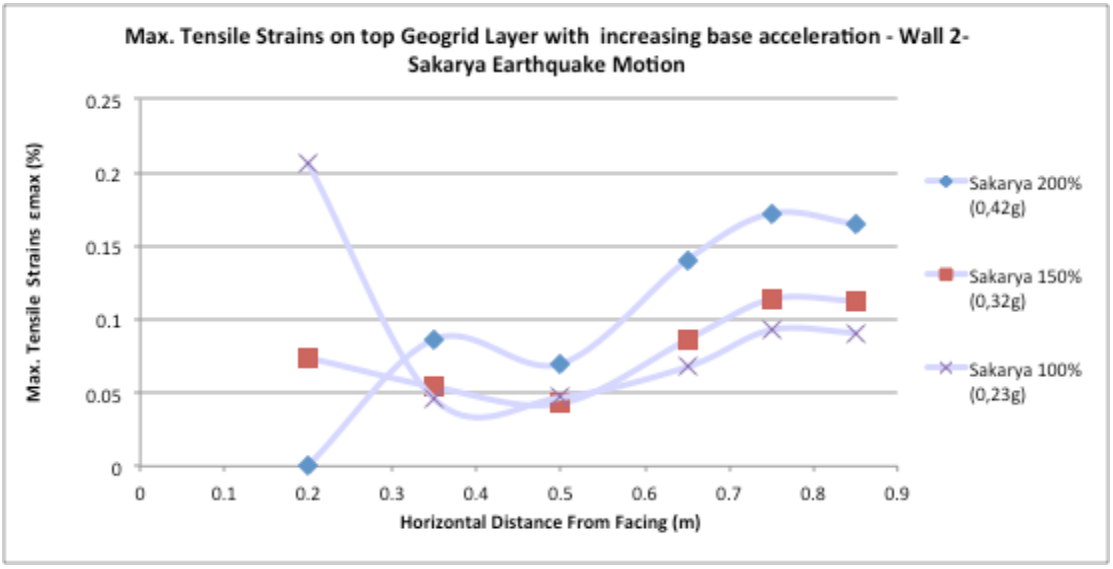
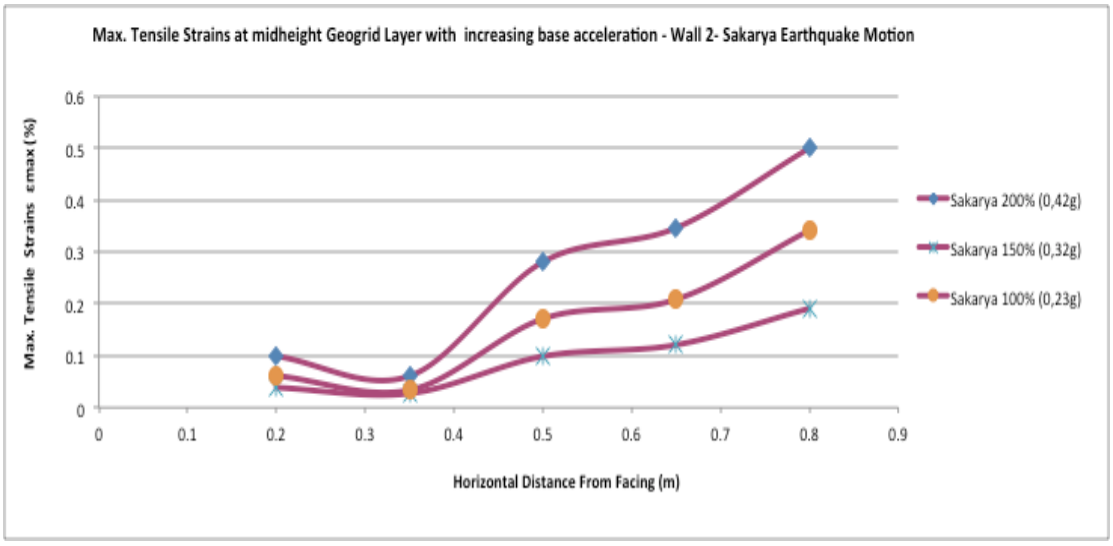


Figure 5.40. Max. Tensile Strains at top, mid-height and bottom Geogrid Layers with increasing base acceleration - Wall 2- Izmit Earthquake Motion





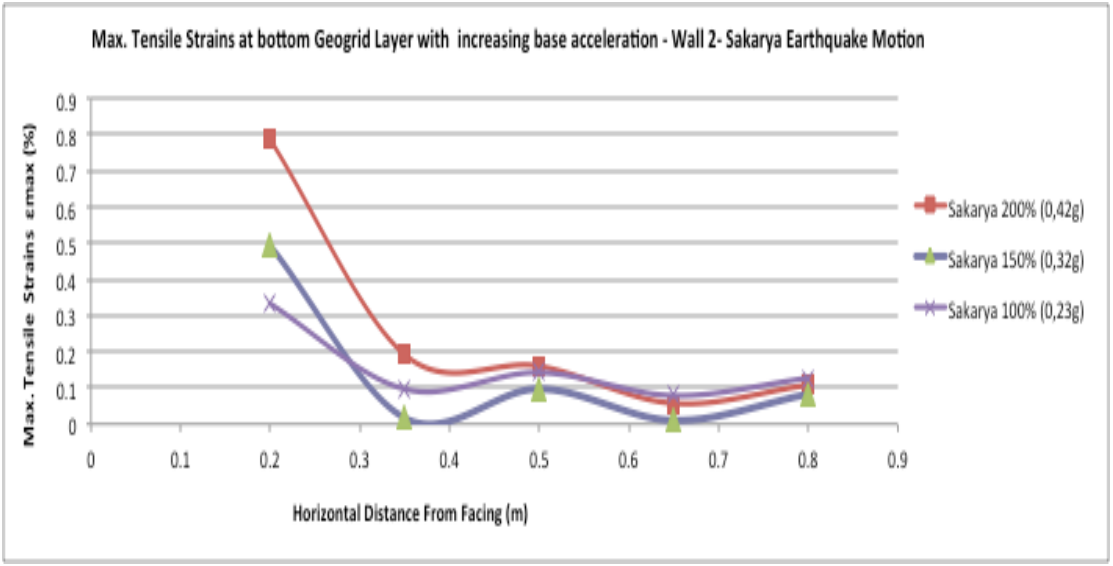


Figure 5.41. Max. Tensile Strains top, mid-height and bottom Geogrid Layers with increasing base acceleration - Wall 2- Sakarya Earthquake Motion

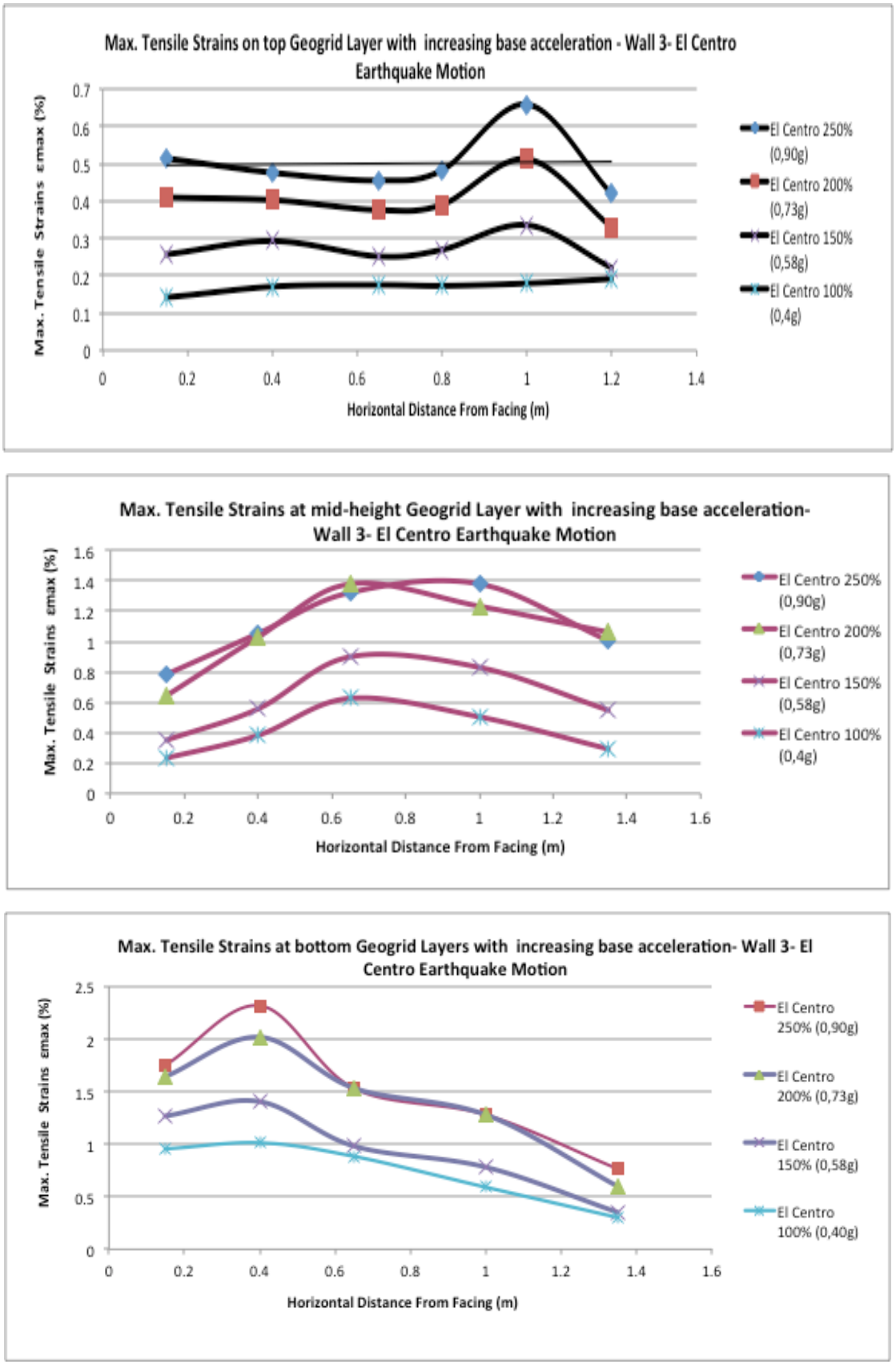
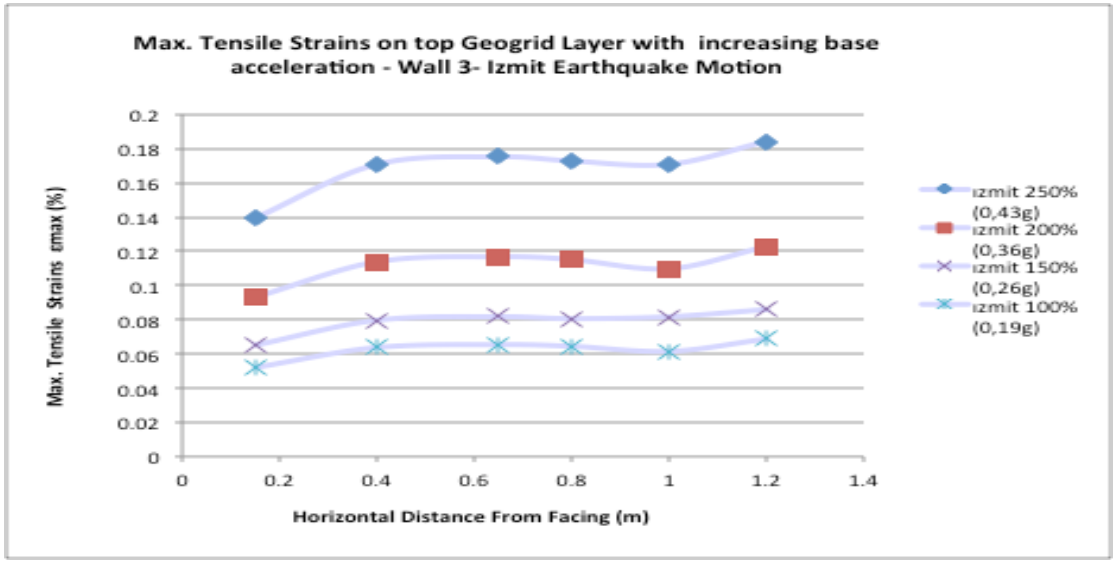
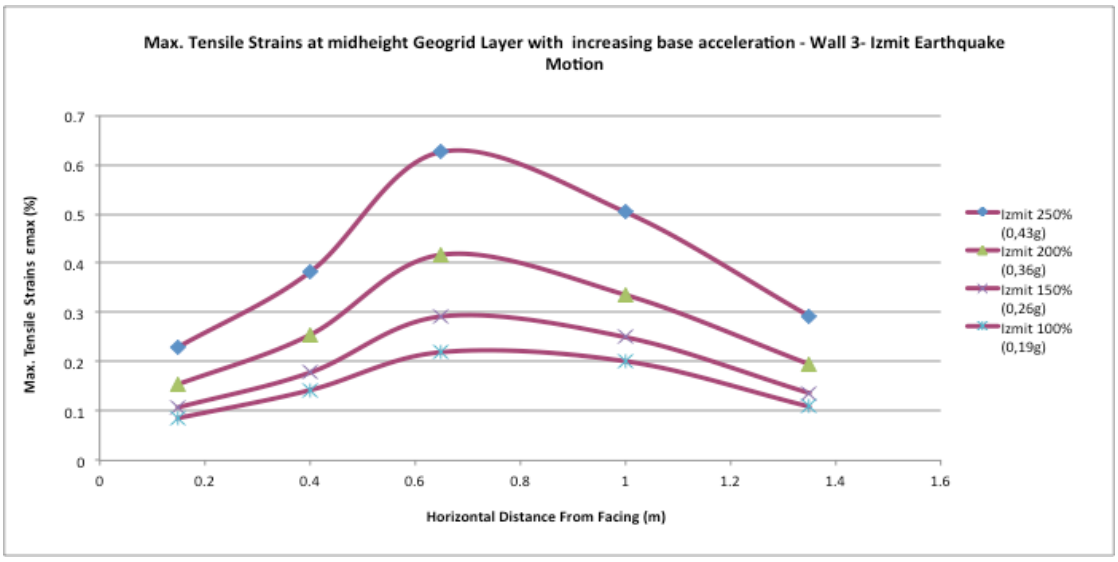


Figure 5.42. Max. Tensile Strains at top, mid-height and bottom Geogrid Layers with increasing base acceleration - Wall 3- El Centro Earthquake Motion





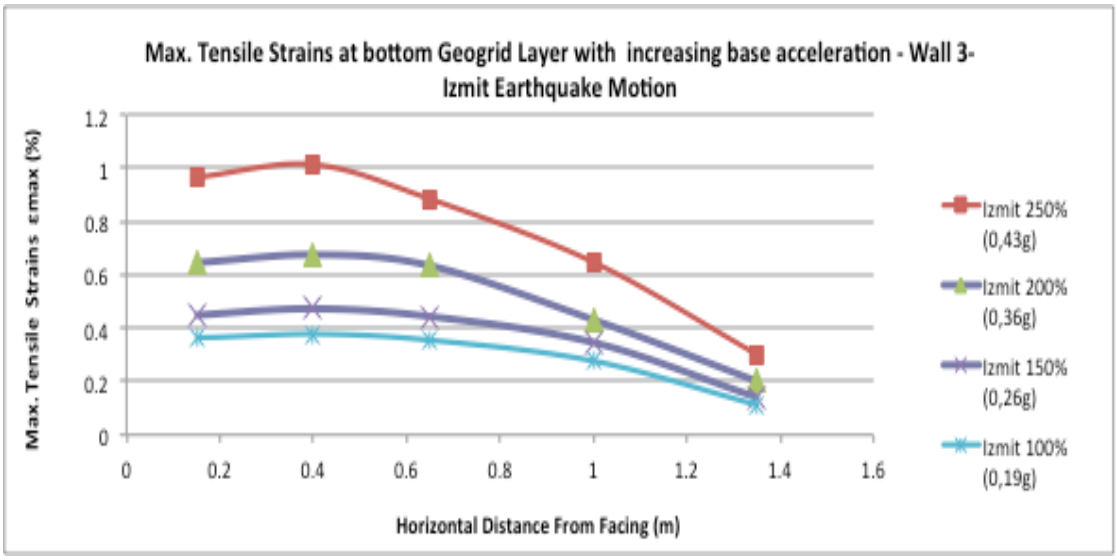
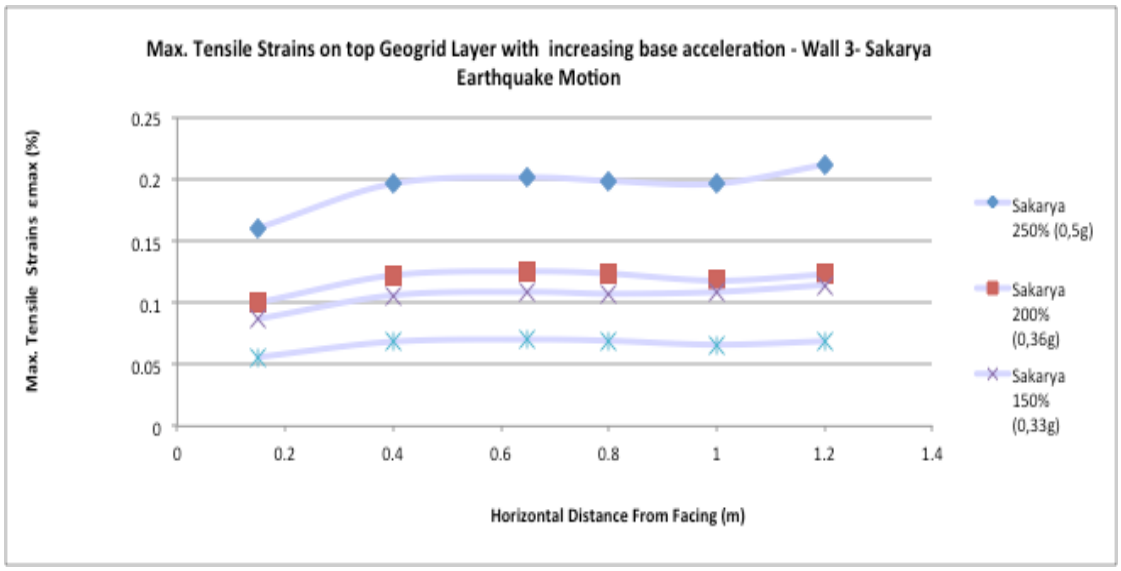
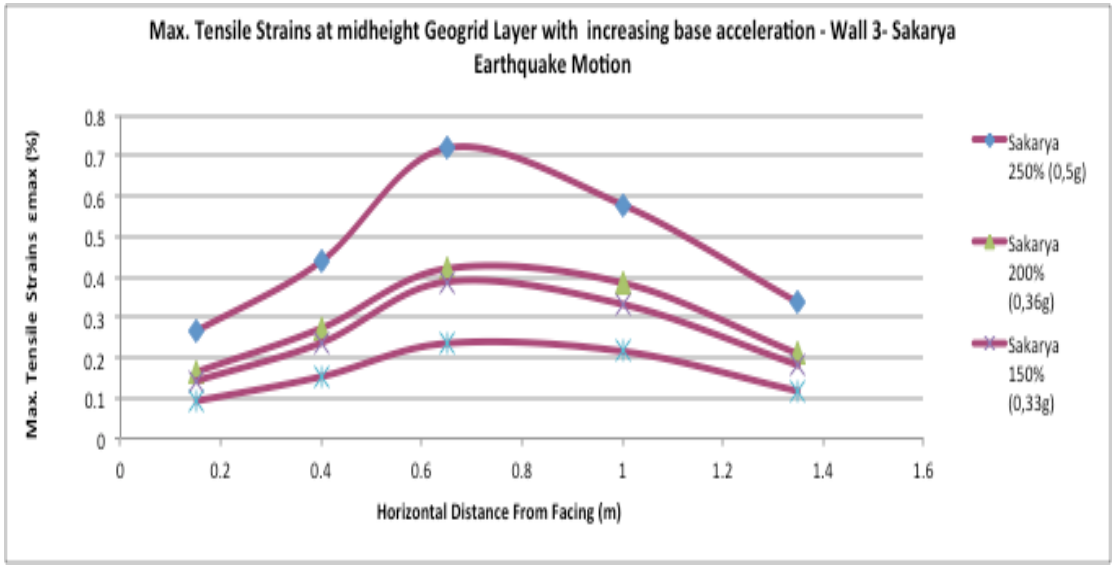


Figure 5.43. Max. Tensile Strains at top, mid-height and bottom Geogrid Layers with increasing base acceleration - Wall 3- Izmit Earthquake Motion





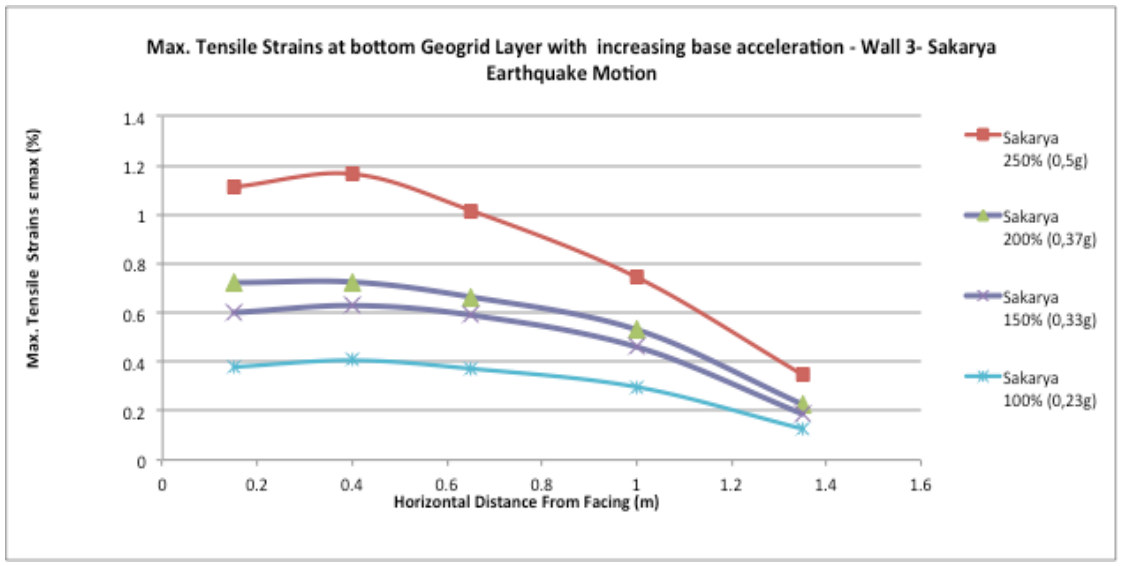


Figure 5.44. Max. Tensile Strains at top, mid-height and bottom Geogrid Layers with increasing base acceleration - Wall 3- Sakarya Earthquake Motion

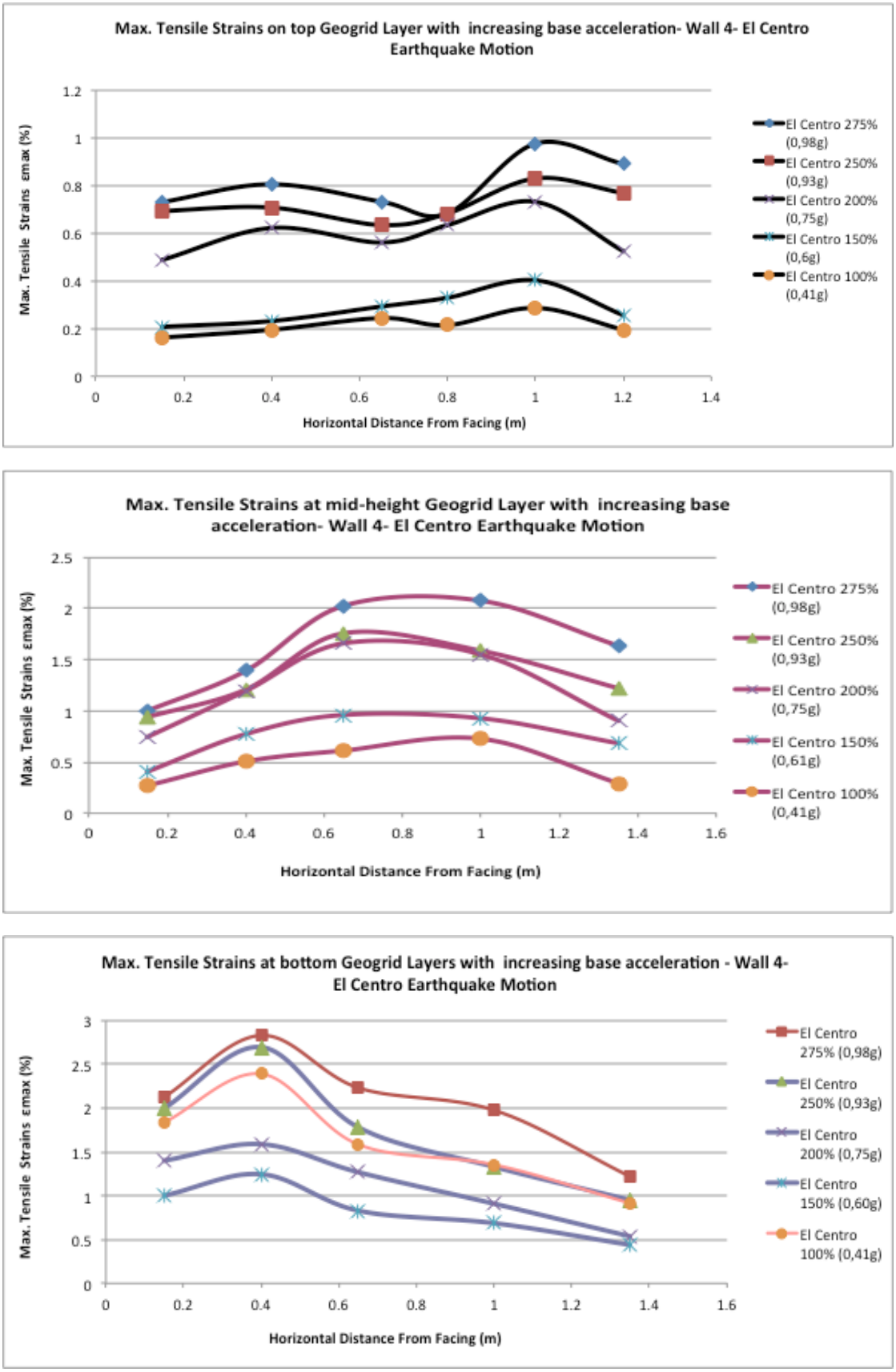
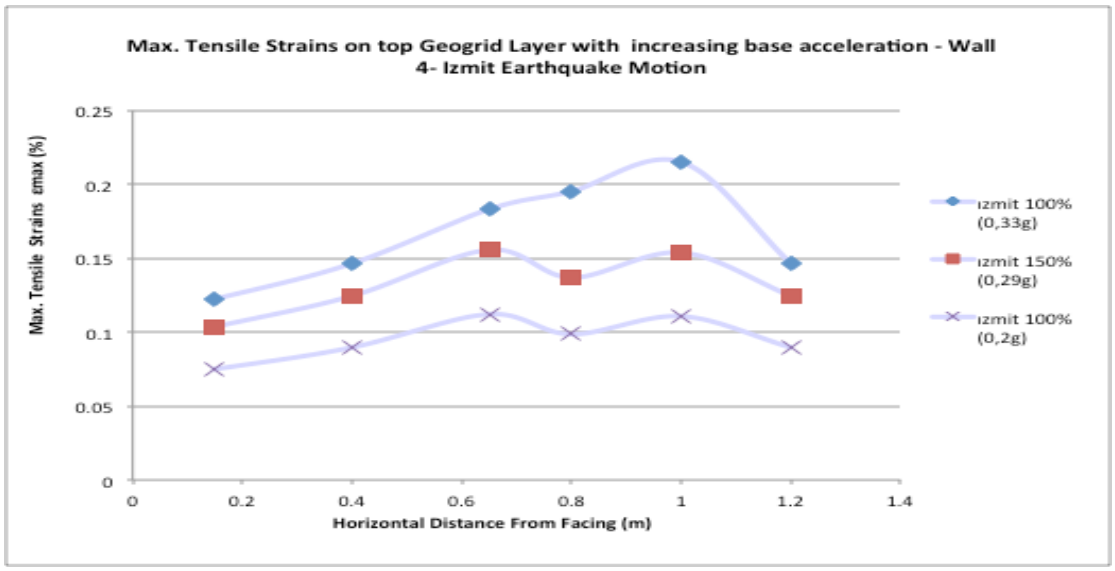
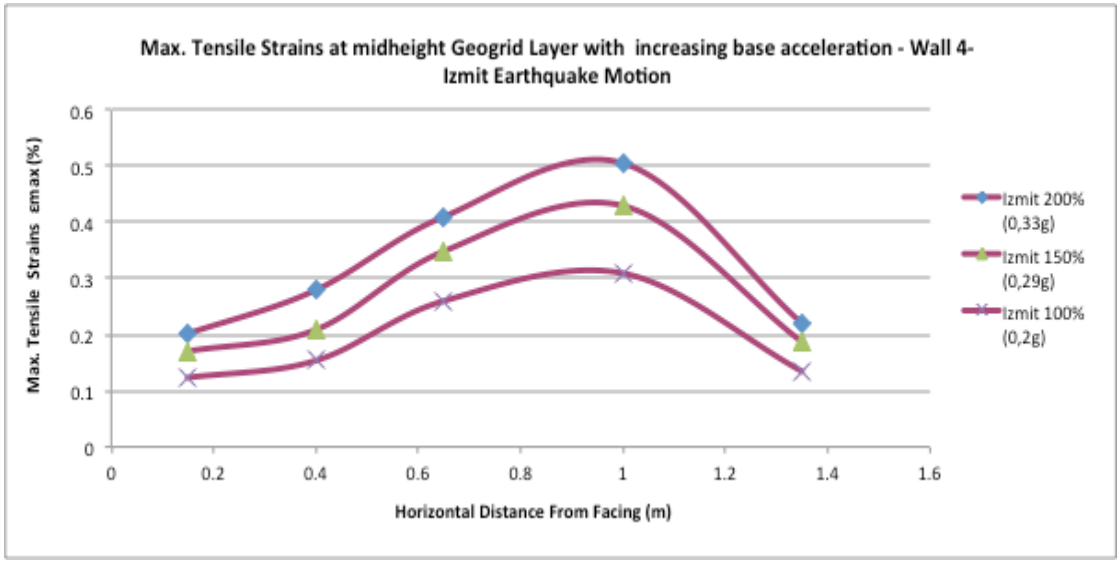


Figure 5.45. Max. Tensile Strains at top, mid-height and bottom Geogrid Layers with increasing base acceleration - Wall 4- El Centro Earthquake Motion





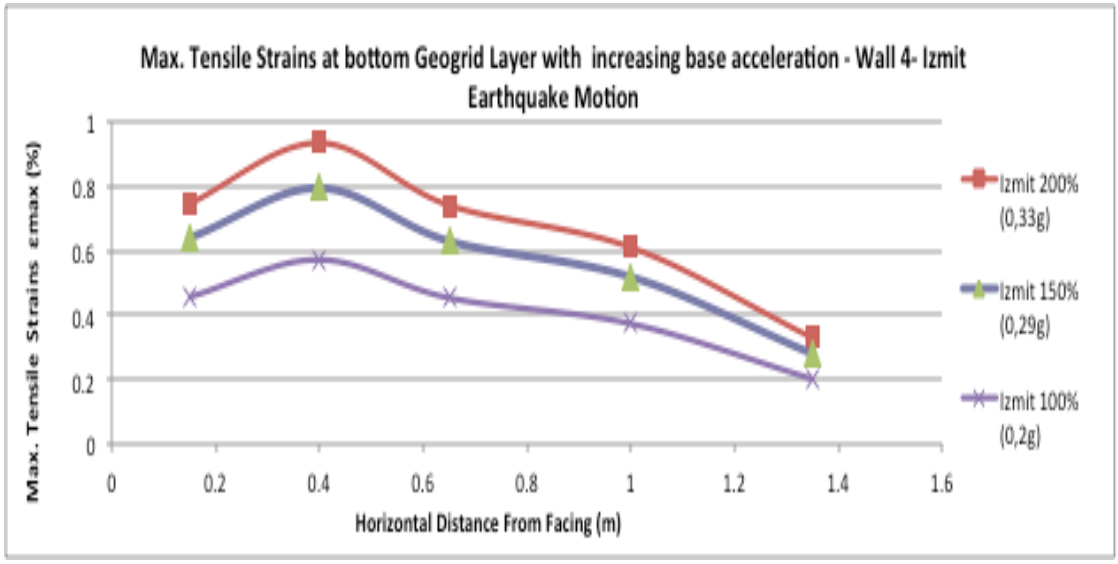
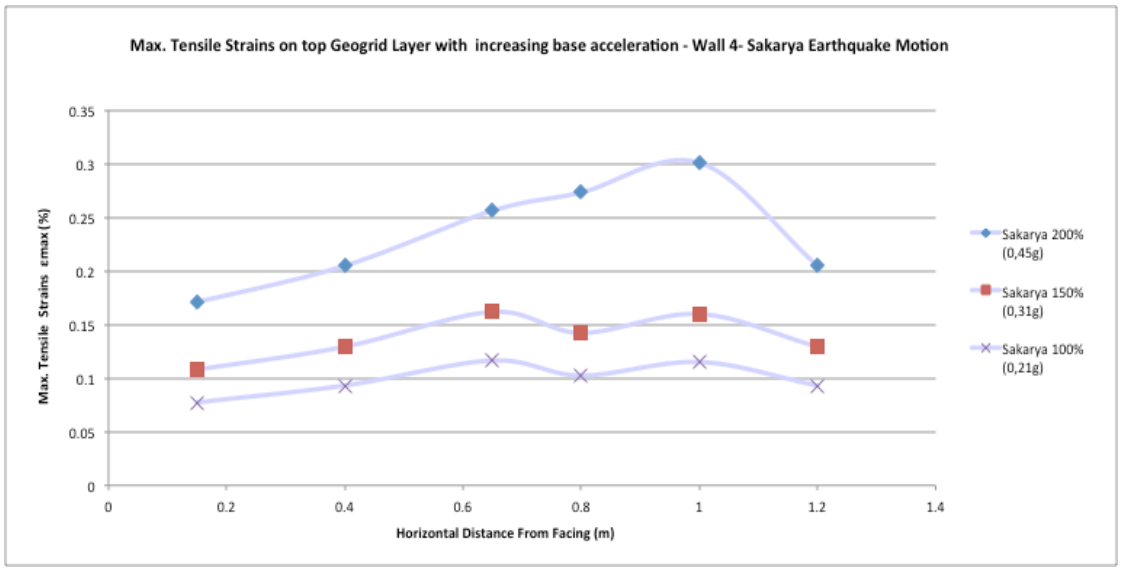
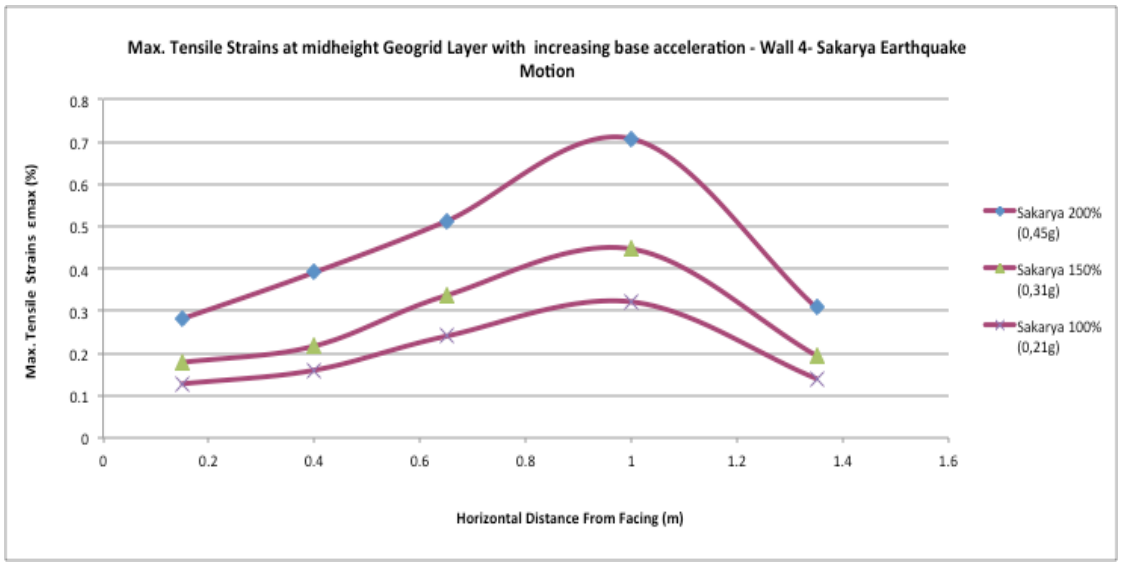


Figure 5.46.. Max. Tensile Strains at top, mid-height and bottom Geogrid Layers with increasing base acceleration - Wall 4- Izmit Earthquake Motion





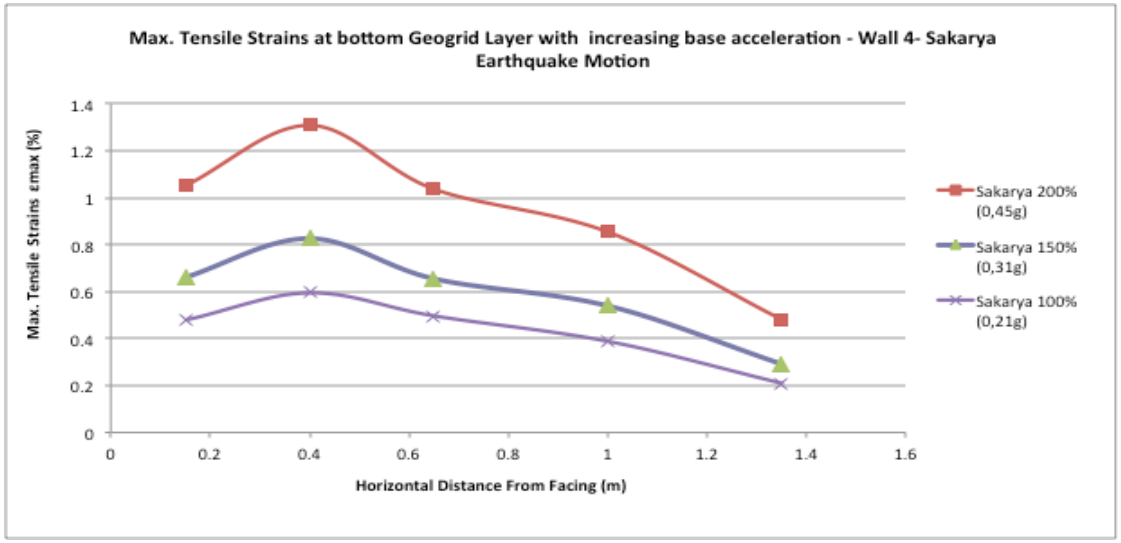


Figure 5.47. Max. Tensile Strains at bottom, mid-height and top Geogrid Layer with increasing base acceleration - Wall 4- Sakarya Earthquake Motion

5.8.2. Evaluation of the Strain Gage Measurements

The following conclusions may be drawn from the strain gage measurements;

- Strain gages on geogrids performed well under earthquake loading conditions.

- For all wall types and earthquake motions applied; as can be seen in the strain-time history plots presented in Appendix C. in some regions, opposite tensile and compression curves are observed due to the generation of compressional and tensional zones caused by the pressure waves propogating through the soil during base exacitations.

- Mostly, the peak tensile strains and peak compressional strains are observed to be at the very close location on the geogrid reinforcement. This may be due to the propogation of the pressure waves which generate compression and tension on different regions in soil. As an example; the strain gage measurement on midheightgeogrid layer where the gage is installed 15 cm. from the facing, indicate that while the other regions of the geogrid reinforcement undergo compressional forces, that particular region mentioned endure compressional forces. As the distance to the failure surface increases, the strains diminish.

- The top reinforcement layer experienced the lowest strains among the instrumented layers. The strains generated on the top reinforcement had no peaks as the other layers meaning that the earthquake loads were distributed almost equally at the top reinforcement.

- The maximum average strains observed at the bottom reinforcement level are higher than the mid-height and top level reinforcement strains.Low strain values were measured at locations situated far from the critical failure surface as expected.

5.8.2.1. Influence of Wall Inclination on Strains generated on Reinforcement Layers.Wall 1 and Wall 2 are compared in order to understand the effect of wall inclination onreinforcement layers and it can be stated that the wall batterhad no significant effect on

the strains generated on the geogrid reinforcements since the measured strain levels were close. However, in Wall 1 (vertical wall facing), the strains on top reinforcement layer are slightly higher than Wall 2.

- For Wall 1 and Wall 2 at the bottom layer the peak average strains near the wall facing (close to failure surface) increases dramatically with the increasing amplitude of base excitations. However, on midheight and top level geogrids with increasing base excitation amplitudes, the strain measurements tend to have a flat curve rather than a peaked curve. This may be due to the short reinforcement length of the wall configurations and the occurrence of the failure surface outside of the reinforced area.

- For Wall 1 and Wall 2; the peak strains are generated very close (20 cm. away from the front facing) to the facing at the bottom geogrid layer. Where for Wall 3 and Wall 4 the peak strains generated at the second strain gage location (40 cm. away from the front facing). This may be due to usage of different geogrid types (PolypropleneGeogrid 20/20 for Wall 1 and Wall 2 and PET Geogrid 45/15-20 for Wall 3 and Wall 4). For the weaker reinforcement the peak strains at the bottom geogrid layer occurred at very close distance to the facing. It can be stated that the high tensile load near the wall base is a result of both high overburden stress and restraining effect due to the geogrid reinforcements (Ling, 2005).

5.8.2.2. Influence of Backfill Material on Strains generated on Reinforcement Layers.In order to comprehend the influence of backfill material (sand and gravel) on strains generated on reinforcement layers, Wall 3 and Wall 4 are compared and the general conclusions drawn are:

- For Wall 3 and Wall 4 the strains observed on bottom, midheight and top level geogrids, the strain measurements tend to have a peaked curve with increasing base excitation amplitudes. As an example, when stain distribution the geogrid layer for wall 4 is observed, the El Centro 275% base excitation have a more ‘peaked’ strain distribution behavior than El (Centro 100% base excitation (especially at the bottom layer).

- The Wall 4 (sand backfill model) experienced higher strains on reinforcements than Wall 3 at each instrumented reinforcement layer confirming that the gravel backfill showed good performance against the dynamic increment pressure distribution during the earthquake loading proposed by the pseudo static approach of FHWA.

5.8.2.3. Influence of Reinforcement Type on Strains generated on Reinforcement Layers.When Wall 2 and Wall 3 are compared; the stronger reinforced wall (Wall 3) has experienced higher strains compared to the weakerreinforced wall(Wall 2).This is due to the difference in the stiffness of the geogrids. Wall 3 has less stiff geogrid reinforcement arrangement and as a result of this the strains generated in the geogrids are higher compared to the Wall 2. A 20% reduction in the reinforcement stiffness resulted in a 15% increase in the measured strains. Moreover, the strains generated on the reinforcement might have been affected since the mesh size of the reinforcement used in Wall 2 has larger openings than the Wall 3 reinforcement and the interlocking behavior of the geogrids on the gravel is different.

5.8.3. Tensile Loads in Geogrid Layers

The results of tensile strain measurements are converted to tensile loads by multiplying the corresponding strain values with the geogridElasticity Modulus that is available in the manufacturer's data sheet. Please refer to Section 4.3.2.7. for the properties of the geogrids used in this study.

In the Tables 5.27.through 5.30. measured peak tensile stresses are compiled and presented for each wall configurations and base excitations. The yellow highlighted values represent the highest tensile load observed at the reinforcement.

The maximum tensile force in the reinforcement is generally located some distance behind the facing. In order to create a maximum force at that location, the shear stresses exerted by the fill on the reinforcement is in opposite directions on the two sides of the peak force.

Table 5.27. Peak Average Tensile Forces on Geogrid Reinforcement for each base excitations applied on Wall 1

WALL CONFIGURATION 1										
Base Excitation / Reinf. And Gages		El-Centro 100%	El-Centro 150%	El-Centro 200%	Izmit 100%	Izmit 150%	Izmit 200%	Sakarya 100%	Sakarya 150%	Sakarya 200%
Height of Reinforcement Layer from Base (m)	Measurement Location- Horizontal Distance From Facing (m)	Measured Tensile Forces on Geogrids (kN/m)	Measured Tensile Forces on Geogrids (kN/m)	Measured Tensile Forces on Geogrids (kN/m)	Measured Tensile Forces on Geogrids (kN/m)	Measured Tensile Forces on Geogrids (kN/m)	Measured Tensile Forces on Geogrids (kN/m)	Measured Tensile Forces on Geogrids (kN/m)	Measured Tensile Forces on Geogrids (kN/m)	Measured Tensile Forces on Geogrids (kN/m)
@h=0.2 m	0.2	3.24	4.80	6.04	0.75	1.08	1.88	0.87	1.58	2.94
	0.35	0.81	1.82	6.00	0.05	0.09	0.24	0.09	0.17	0.59
	0.5	0.82	0.56	0.40	0.20	0.28	0.41	0.25	0.32	0.49
	0.65	0.14	0.72	3.09	0.07	0.05	0.16	0.10	0.12	0.19
	0.8	0.64	0.80	1.42	0.33	0.37	0.69	0.32	0.50	0.93
@h=1 m	0.2	0.76	1.26	1.70	0.19	0.31	0.53	0.26	0.54	0.82
	0.35	0.93	1.86	2.82	0.17	0.23	0.37	0.20	0.34	0.50
	0.5	2.88	5.54	5.22	0.61	0.86	1.16	0.74	1.19	0.67
	0.65	2.57	4.11	5.56	0.66	0.93	1.40	0.78	1.22	1.81
	0.8	2.36	3.96	4.98	0.57	0.78	1.19	0.63	1.05	1.53
@h=1.8 m	0.15	0.68	0.59	1.29	0.00	0.00	0.00	0.00	0.20	0.00
	0.25	0.54	1.21	1.38	0.11	0.19	0.32	0.17	0.29	0.62
	0.4	0.54	1.13	1.04	0.06	0.11	0.18	0.12	0.17	0.23
	0.55	0.83	1.72	1.30	0.21	0.30	0.45	0.26	0.41	0.55
	0.7	0.86	1.30	1.32	0.24	0.34	0.52	0.31	0.47	0.51
	0.8	0.62	1.04	0.76	0.20	0.26	0.37	0.23	0.35	0.42

Table 5.28. Peak Average Tensile Forces on Geogrid Reinforcement for each base excitations applied on Wall 2

WALL CONFIGURATION 2										
Base Excitation / Reinf. And Gages		El-Centro 100%	El-Centro 150%	El-Centro 200%	Izmit 100%	Izmit 150%	Izmit 200%	Sakarya 100%	Sakarya 150%	Sakarya 200%
Height of Reinforcement Layer from Base (m)	Measurement Location- Horizontal Distance From Facing (m)	Measured Tensile Forces on Geogrids (kN/m)	Measured Tensile Forces on Geogrids (kN/m)	Measured Tensile Forces on Geogrids (kN/m)	Measured Tensile Forces on Geogrids (kN/m)	Measured Tensile Forces on Geogrids (kN/m)	Measured Tensile Forces on Geogrids (kN/m)	Measured Tensile Forces on Geogrids (kN/m)	Measured Tensile Forces on Geogrids (kN/m)	Measured Tensile Forces on Geogrids (kN/m)
@h=0.2 m	0.2	3.58	5.16	7.17	1.21	1.65	2.31	1.36	2.04	3.24
	0.35	1.45	2.82	6.96	0.23	0.15	0.34	0.40	0.07	0.79
	0.5	0.94	3.41	6.13	0.38	0.36	0.51	0.58	0.40	0.66
	0.65	0.48	1.84	2.54	0.22	0.03	0.11	0.32	0.04	0.24
	0.8	0.35	0.92	2.10	0.44	0.41	0.51	0.52	0.34	0.44
@h=1 m	0.2	0.56	1.64	2.58	0.14	0.21	0.29	0.16	0.26	0.41
	0.35	0.41	0.62	1.02	0.09	0.13	0.20	0.11	0.14	0.25
	0.5	2.27	3.17	3.80	0.45	0.56	0.77	0.40	0.70	1.15
	0.65	2.23	3.79	4.30	0.47	0.73	1.03	0.50	0.85	1.42
	0.8	2.57	4.35	4.91	0.81	1.25	1.64	0.78	1.40	2.05
@h=1.8 m	0.15	0.00	0.00	0.00	0.00	0.00	0.00	0.84	0.30	0.00
	0.25	0.65	0.91	0.81	0.15	0.24	0.28	0.19	0.22	0.35
	0.4	0.50	0.71	0.55	0.16	0.21	0.23	0.19	0.18	0.29
	0.55	1.23	1.85	1.19	0.30	0.39	0.42	0.28	0.35	0.58
	0.7	0.56	0.71	0.90	0.35	0.49	0.57	0.38	0.47	0.71
	0.8	0.97	1.65	0.97	0.36	0.47	0.54	0.37	0.46	0.68

Table 5.29. Peak Average Tensile Forces on Geogrid Reinforcement for each base excitations applied on Wall 3

WALL CONFIGURATION 3													
Base Excitation / Reinf. And Gages		El-Centro 100%	El-Centro 150%	El-Centro 200%	El-Centro 250%	Izmit 100%	Izmit 150%	Izmit 200%	Izmit 250%	Sakarya 100%	Sakarya 150%	Sakarya 200%	Sakarya 250%
Height of Reinforcement Layer from Base (m)	Measurement Location- Horizontal Distance From Facing (m)	Measured Tensile Forces on Geogrids (kN/m)	Measured Tensile Forces on Geogrids (kN/m)	Measured Tensile Forces on Geogrids (kN/m)	Measured Tensile Forces on Geogrids (kN/m)	Measured Tensile Forces on Geogrids (kN/m)	Measured Tensile Forces on Geogrids (kN/m)	Measured Tensile Forces on Geogrids (kN/m)	Measured Tensile Forces on Geogrids (kN/m)	Measured Tensile Forces on Geogrids (kN/m)	Measured Tensile Forces on Geogrids (kN/m)	Measured Tensile Forces on Geogrids (kN/m)	Measured Tensile Forces on Geogrids (kN/m)
@h=0.2 m	0.15	2.85	3.81	4.93	5.24	1.08	1.35	1.93	2.90	1.13	1.80	2.16	3.33
	0.4	3.04	4.22	6.06	6.96	1.14	1.42	2.03	3.04	1.22	1.89	2.18	3.50
	0.65	2.65	2.95	4.60	4.60	1.07	1.33	1.90	2.65	1.12	1.77	1.99	3.05
	1	1.77	2.34	3.84	3.84	0.83	1.04	1.30	1.94	0.89	1.38	1.59	2.23
	1.35	0.91	1.05	1.79	2.29	0.34	0.42	0.60	0.91	0.38	0.56	0.68	1.04
@h=1 m	0.15	0.69	1.05	1.92	2.34	0.26	0.32	0.46	0.69	0.28	0.43	0.49	0.79
	0.4	1.15	1.67	3.08	3.16	0.43	0.53	0.76	1.15	0.46	0.71	0.82	1.32
	0.65	1.88	2.70	4.14	3.97	0.66	0.88	1.25	1.88	0.71	1.17	1.26	2.16
	1	1.51	2.49	3.70	4.14	0.60	0.75	1.01	1.51	0.65	1.00	1.16	1.74
	1.35	0.88	1.64	3.18	3.02	0.33	0.41	0.59	0.88	0.35	0.55	0.63	1.01
@h=1.8 m	0.15	0.00	0.00	1.68	2.11	0.21	0.27	0.38	0.57	0.23	0.36	0.41	0.66
	0.4	0.70	1.20	1.65	1.95	0.26	0.33	0.47	0.70	0.28	0.43	0.50	0.81
	0.65	0.72	1.03	1.54	1.87	0.27	0.34	0.48	0.72	0.29	0.45	0.51	0.83
	0.8	0.71	1.11	1.60	1.98	0.26	0.33	0.47	0.71	0.28	0.44	0.51	0.81
	1	0.74	1.38	2.10	2.70	0.25	0.34	0.45	0.70	0.27	0.45	0.48	0.81
	1.2	0.79	0.91	1.35	1.72	0.28	0.35	0.50	0.76	0.28	0.47	0.50	0.87

Table 5.30. Peak Average Tensile Forces on Geogrid Reinforcement for each base excitations applied on Wall 4

WALL CONFIGURATION 4												
Base Excitation / Reinf. And Gages		El-Centro 100%	El-Centro 150%	El-Centro 200%	El-Centro 250%	El-Centro 275%	Izmit 100%	Izmit 150%	Izmit 200%	Sakarya 100%	Sakarya 150%	Sakarya 200%
Height of Reinforcement Layer from Base (m)	Measurement Location- Horizontal Distance From Facing (m)	Measured Tensile Forces on Geogrids (kN/m)	Measured Tensile Forces on Geogrids (kN/m)	Measured Tensile Forces on Geogrids (kN/m)	Measured Tensile Forces on Geogrids (kN/m)	Measured Tensile Forces on Geogrids (kN/m)	Measured Tensile Forces on Geogrids (kN/m)	Measured Tensile Forces on Geogrids (kN/m)	Measured Tensile Forces on Geogrids (kN/m)	Measured Tensile Forces on Geogrids (kN/m)	Measured Tensile Forces on Geogrids (kN/m)	Measured Tensile Forces on Geogrids (kN/m)
@h=0.2 m	0.15	3.00	4.21	5.53	6.00	6.41	1.38	1.91	2.25	1.43	1.99	3.15
	0.4	3.74	4.77	7.17	8.09	8.49	1.72	2.38	2.80	1.78	2.48	3.92
	0.65	2.49	3.81	4.76	5.34	6.70	1.36	1.89	2.22	1.49	1.96	3.11
	1	2.06	2.73	4.06	3.99	5.93	1.12	1.56	1.83	1.16	1.62	2.56
	1.35	1.32	1.61	2.75	2.85	3.66	0.60	0.84	0.99	0.63	0.87	1.44
@h=1 m	0.15	0.80	1.22	2.23	2.82	3.00	0.37	0.51	0.60	0.38	0.53	0.84
	0.4	1.52	2.32	3.59	3.62	4.17	0.46	0.63	0.84	0.48	0.65	1.17
	0.65	1.84	2.88	4.98	5.27	6.08	0.78	1.05	1.23	0.72	1.01	1.54
	1	2.18	2.78	4.65	4.76	6.22	0.93	1.29	1.52	0.96	1.34	2.12
	1.35	0.88	2.05	2.71	3.66	4.90	0.40	0.56	0.66	0.42	0.58	0.92
@h=1.8 m	0.15	0.00	0.00	0.00	0.00	0.00	0.00	0.00	0.00	0.00	0.00	0.00
	0.4	0.80	0.95	2.55	2.90	3.30	0.37	0.51	0.60	0.38	0.53	0.84
	0.65	1.00	1.20	2.30	2.60	3.00	0.46	0.64	0.75	0.48	0.66	1.05
	0.8	0.88	1.35	2.60	2.80	2.80	0.40	0.56	0.80	0.42	0.58	1.12
	1	1.18	1.65	3.00	3.40	4.00	0.45	0.63	0.88	0.47	0.66	1.23
	1.2	0.80	1.05	2.15	3.15	3.65	0.37	0.51	0.60	0.38	0.53	0.84

Through Figure 5.48.to Figure 5.51. location of peak reinforcement tensile loads and internal failure surface for each Wall configurations are illustrated in scale. Internal failure surface is obtained by joining the locus points of maximum tensile forces which is called the maximum tensile forces line. This line separates the reinforced zone into two;

- An active zone between the facing and the maximum tensile forces line, where the shear stresses on the reinforcements are directed towards the wall face.
- A resistant zone behind the maximum tensile forces line, where the shear stresses on the reinforcement are directed away from the wall face.

The curve graphs set on the reinforcements on the figure denote the locations of strain measurements. The tensile loads in the graps are given in kN/m. These tensile loads corroborate the locations of peak strain recorded by strain gages.

Internal critical surfaces illustrated in thefollowing figures are drawn by connecting the toe to the highly tensile stressed regions of the lower, midheight and upper geogrids. The obtained critical surfaces are compared with potentialRankine failure surface and FHWA 2001 proposal of maximum tensile force lines (Please refer to Section 3.1.3 and 3.2.3. for information on FHWA proposal on maximum tensile forces line and potential Rankine failure surface).

The comparison of measured and design tensile loads on geogrid reinforcement during the earthquake motion applied on model walls shall be given in Section 6.2.

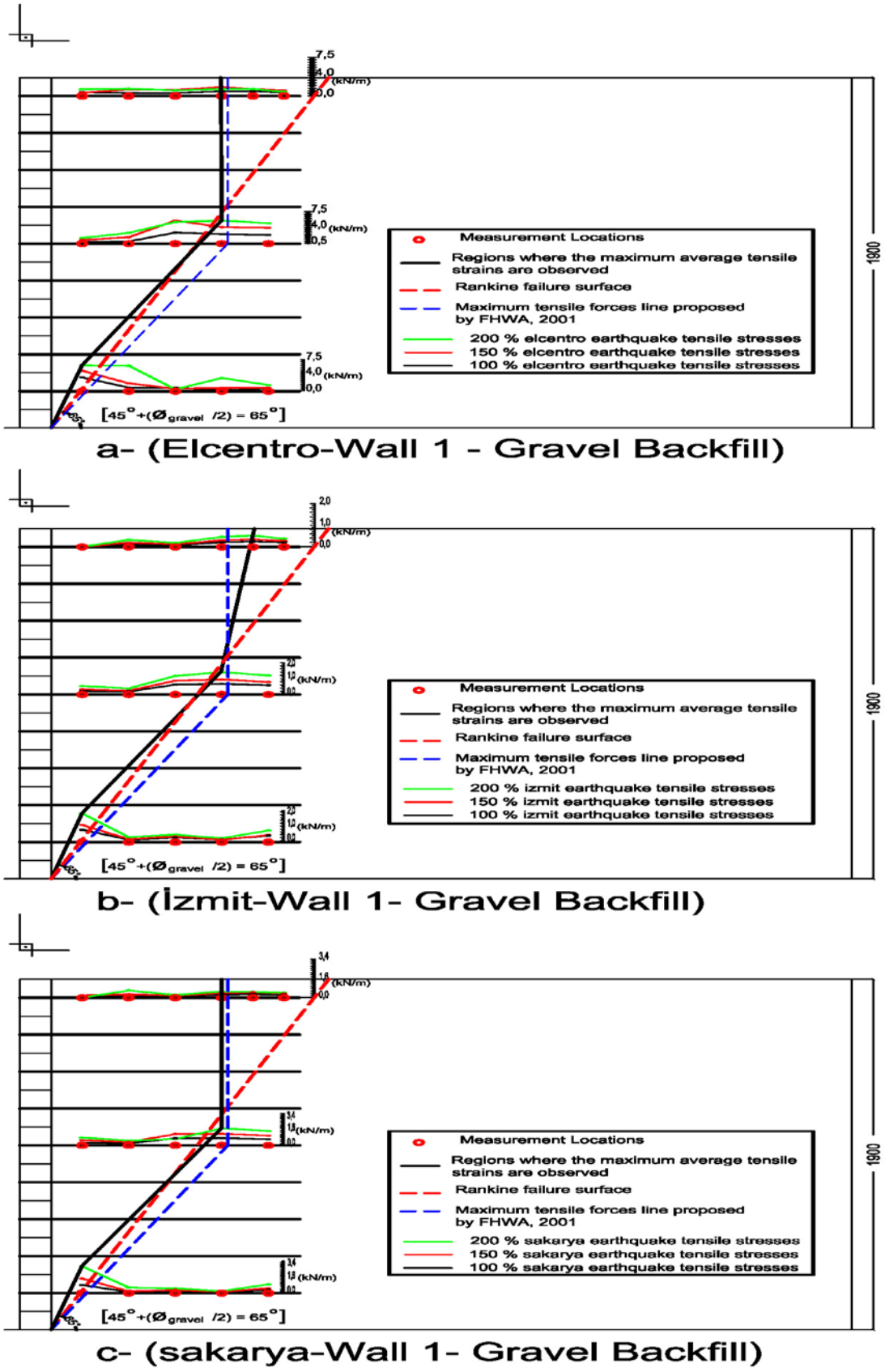


Figure 5.48. Location of peak reinforcement tensile loads and internal failure surface a) El Centro, b) Izmit, c) Sakarya Earthquake motions for Wall 1

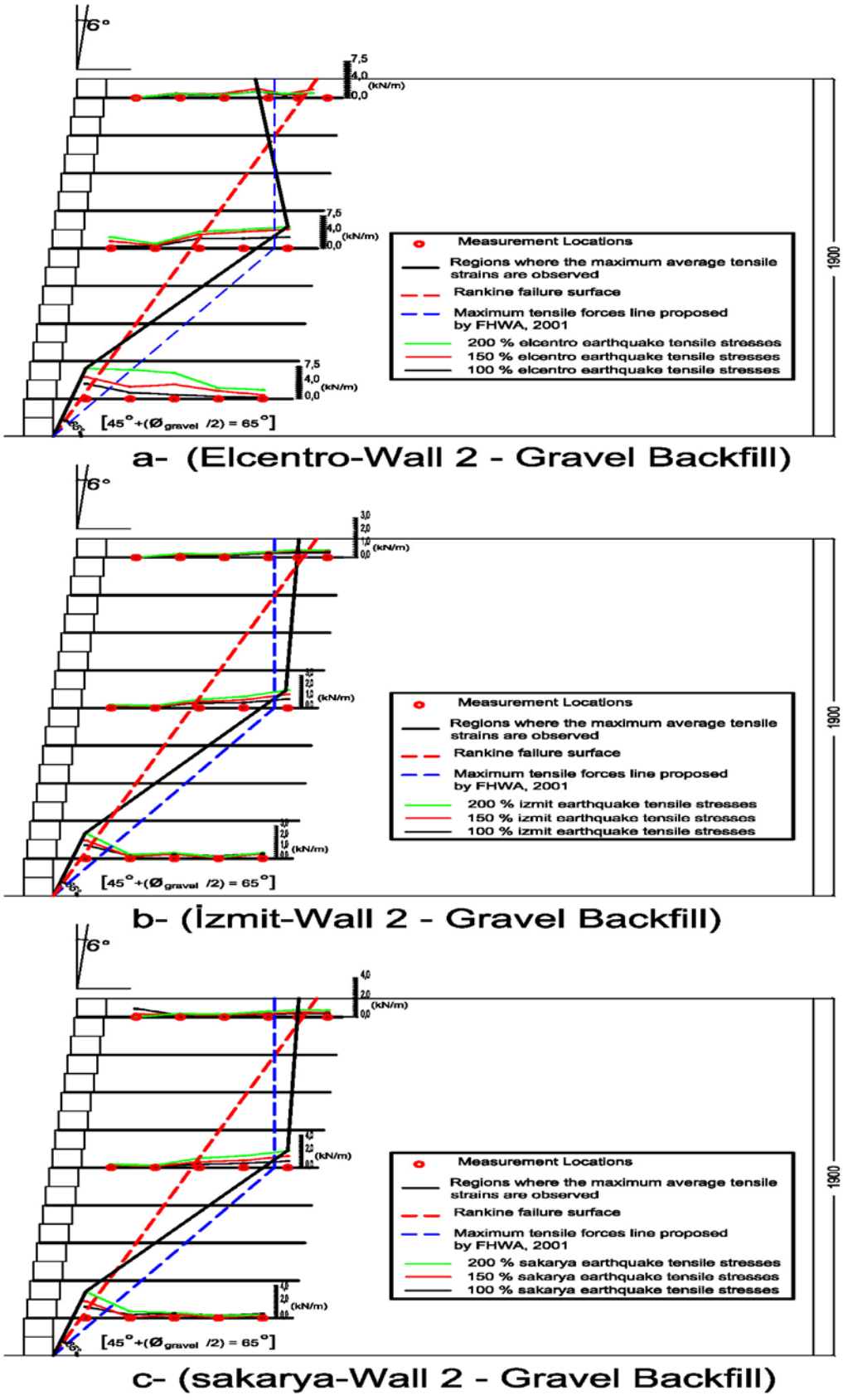


Figure 5.49. Location of peak reinforcement tensile loads and internal failure surface a) El Centro, b) Izmit, c) Sakarya Earthquake motions for Wall 2

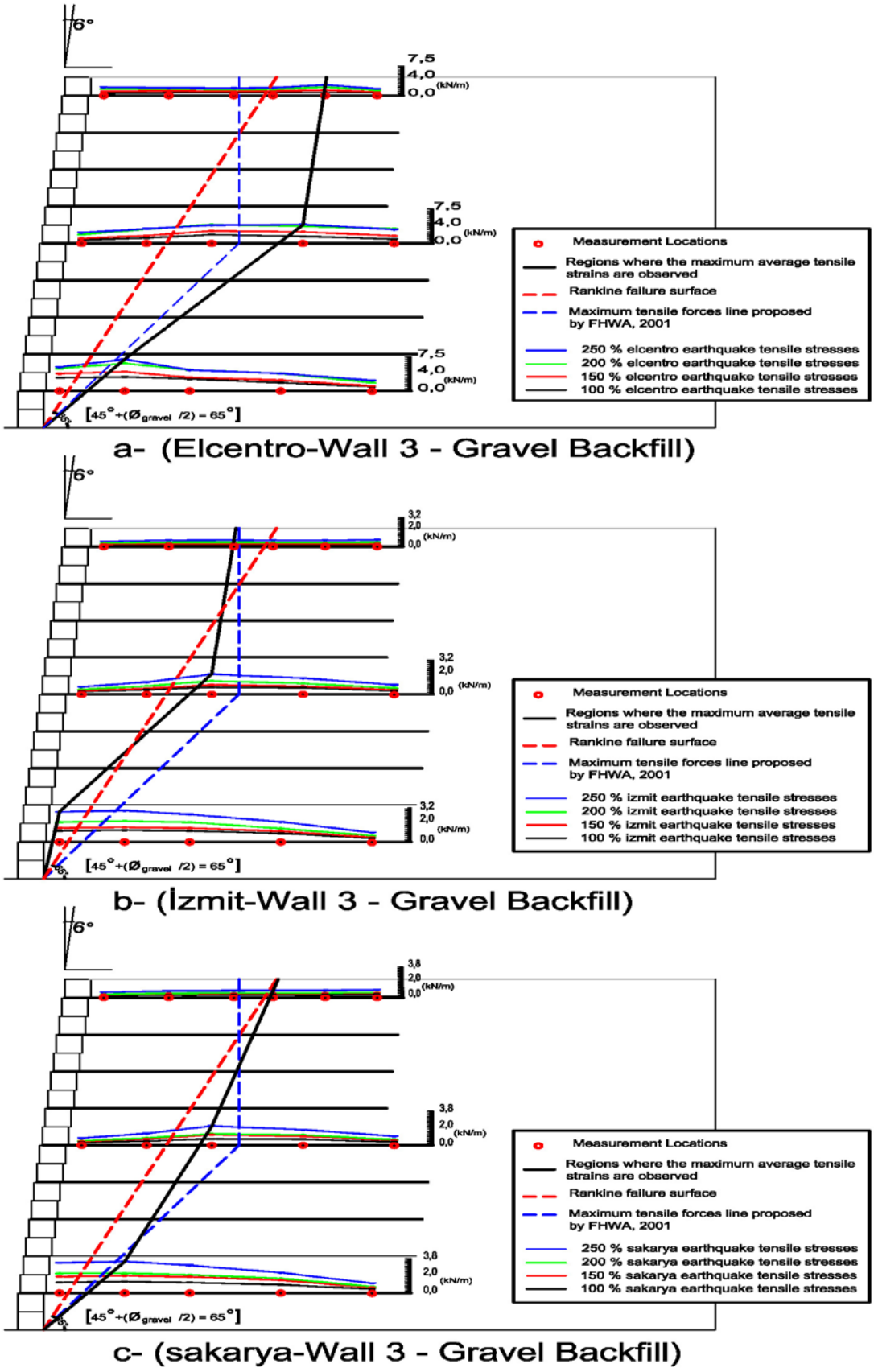


Figure 5.50. Location of peak reinforcement tensile loads and internal failure surface a) El Centro, b) Izmit, c) Sakarya Earthquake motions for Wall 3

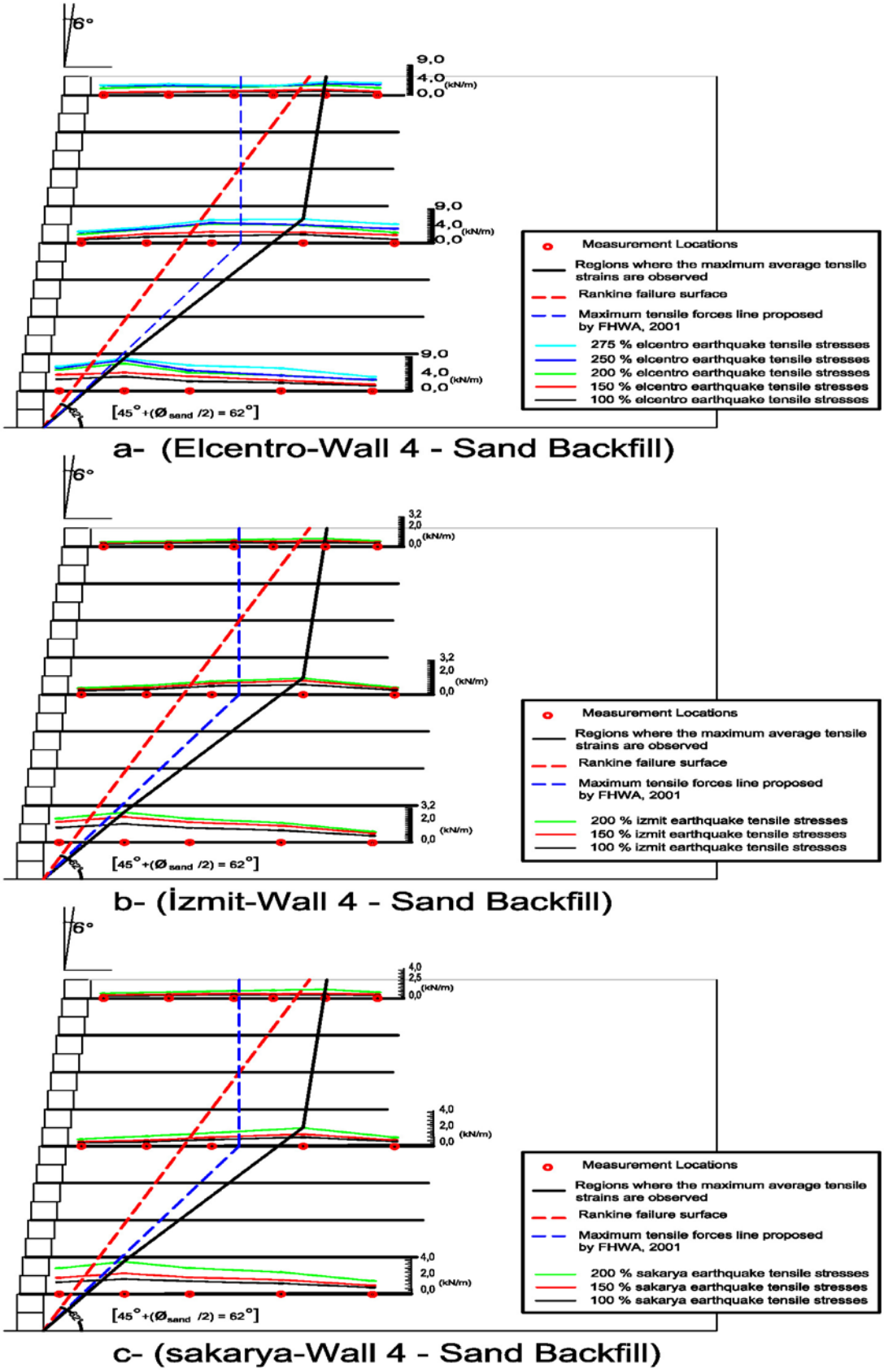


Figure 5.51. Location of peak reinforcement tensile loads and internal failure surface a) El Centro, b) Izmit, c) Sakarya Earthquake motions for Wall 4

5.8.4. Evaluation of Tensile Loads on Reinforcements

The critical surfaces obtained by measurements are in good agreement with the potential Rankine failure surface and maximum tensile forces line proposed by FHWA. In Wall 1 and Wall 2 the measured critical surface is between the Rankine surface and FHWA proposal. In Wall 3 and Wall 4 since longer reinforcement is utilized, the critical surface is shifted towards the back of the backfill. However, it should be stated that, the critical surface presented here is just an approximation of the maximum tensile stresses on the reinforcement and in some cases, the peak tensile stresses were not that obvious.

As the seismic loads increase the tensile stresses increase. This may be explained as the tensile load on reinforcement is proportional to the magnitude of the seismic loads.

For all wall types and earthquake motions applied; Measured results shows that the reinforcement near the wall base experiences the highest tensile load. High tensile loads are generated on the mid-height geogrid layer as well. The top reinforcement layer experiences less tensile load when compared to the other strain gage instrumented layers.

For Wall 3, as the magnitude of the acceleration increases the tensile forces line has been shifted towards the back of the wall meaning the reinforcements show good performance against the seismic dynamic increment due to earthquake loading.

When Wall 2 and Wall 3 are compared; the tensile loads generated in stronger reinforced wall (Wall 3) is lower compared to the weaker reinforced wall (Wall 2). This is due to the difference in the stiffness of the geogrids. Wall 3 has less stiff geogrid reinforcement arrangement and as a result of this the tensile loads in the geogrids are lower compared to the Wall 2. A 20% reduction in the reinforcement stiffness resulted in a 23% reduction in the measured values of tensile loads generated in the reinforcement. Numerical modeling of reinforced soil walls (Rowe and Ho, 1997; Bathurst and Hatami, 1998; Hatami et al., 2001) and results of instrumented reinforced soil walls in the field under loading conditions (Allen and Bathurst, 2002) have clearly demonstrated that reinforcement stiffness (rather than tensile strength at rupture) is a key parameter to accurately predict reinforcement loads under typical operational conditions.

5.9. Observations

After each successive shaking, visual observations are made on the wall and top of the fill. No failure was observed on the walls even when extreme seismic motions are applied (ie. El Centro 275% - 0.98 g). Because the top two rows of modular blocks were grouted no toppling of the blocks were observed during the earthquake motions.So it can be stated that geogrid reinforced walls showed good sperformance under seismic loads. Figure 5.52. and Figure 5.53.shows a view from the top of the backfill of Unreinforced zone of Wall 4 prior to and after the shakings, respectively.



Figure 5.52. A view from the top of the backfill of Unreinforced zone of Wall 4 prior to shaking



Figure 5.53. A view from the top of the backfill of unreinforced zone of Wall 4 after successive shaking

As can be seen from Figure 5.53. large settlements occurred at Wall 4 the unreinforced zone after successive shakings.

Figure 5.54and Figure 5.55.showa closer view of settlement behind the blocks prior to and after the shakings.



Figure 5.54. A view from the top of the backfill of reinforced zone behind the blocks of Wall 4 prior to shakings



Figure 5.55. A view from the top of the backfill of reinforced zone behind the blocks of Wall 4 after shakings

As can be seen from Figure 5.55.thesettlements occurred at Wall 4 on the reinforced zone after successive shakings is less than the settlements occurred at unreinforced zone.

Also, in sand backfilled models tensile cracks are observed at peak acceleration values of 1 g. The tensile cracks observed at the top ofthe model can be seen in Figure 5.56. No tensile cracks were observed on gravel backfilled models.



Figure 5.56.Tensile cracks observed in sand backfill

Lastly, after shakings (especially after peak acceleration values of 0.4 g and above is applied on the walls), some geogrid reinforcement was observed to be overhung at the block-reinforcement connection as seen on Figure 5.57. This may be due to different settlements of reinforced and unreinforced zone.

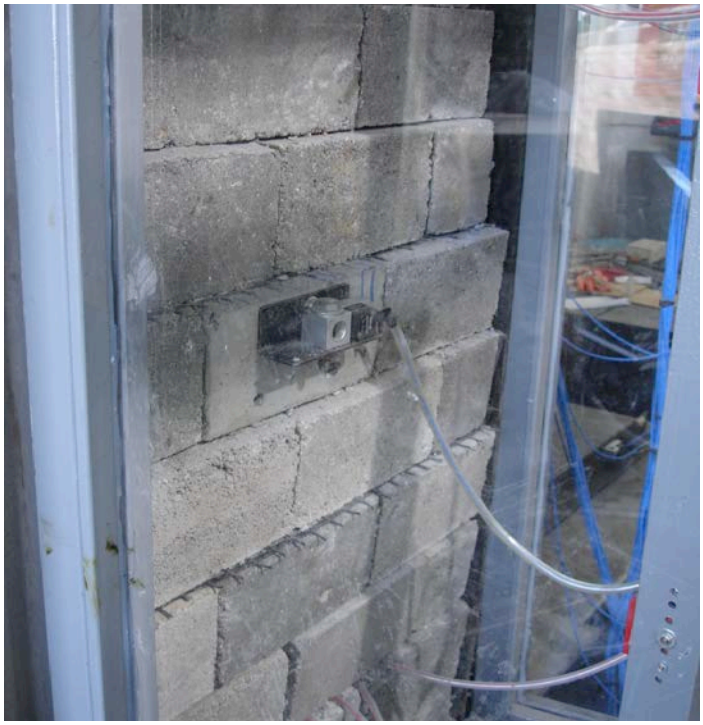


Figure 5.57. Overhanging of Geogrid after shakings

6. CALCULATION METHODS FOR PERMENANT DISPLACEMENTS AND GEOGRID REINFORCEMENT DESIGN TENSILE LOADS

6.1. Calculation of Permanent Displacements

Permanent displacements are assumed to accumulate each time the critical acceleration, a_c is exceeded by the horizontal input (ground) acceleration. In this section, permanent displacements associated with three sliding mechanisms are investigated; (1) external sliding along the base of total structure; (2) internal sliding along a reinforcement layer and through the facing column; and (3) block interface shear between facing column units. A pseudo-static method based on Mononobe - Okabe earth pressure theory and NCMA's Segmental Retaining Wall – Seismic Design Manual is used to determine the value of critical acceleration associated with each potential failure mechanism.

The permanent displacement of a geosynthetic-reinforced soil structure due to horizontal sliding/shear mechanisms can be estimated using one of the two general approaches;

- Newmark's sliding block displacement method
- Bathurst and Cai's empirical method

The details of these methods are given in the following.

6.1.1. Newmark's Sliding Block Displacement Method

The permanent displacement of a geosynthetic-reinforced segmental soil retaining wall due to the sliding or shear mechanisms can be estimated using Newmark's double integration method, based on sliding block theory.

Newmark's sliding block theory has been widely used to establish empirical

relationships between the expected permanent displacement and characteristic seismic parameters of the input earthquake by integrating existing acceleration records. According to Newmark's theory, a potential sliding body is treated as a rigid-plastic monolithic mass under the action of seismic forces. Permanent displacement of the mass takes place whenever the seismic force induced on the body (plus the existing static force) overcomes the available resistance along, a potential sliding/shear surface.

Newmark's method requires that the critical acceleration, a_c, to initiate sliding or shear failure be determined for each translation failure mechanism. The value of a_c can be determined by searching for values of k_h that give a factor of safety of unity in pseudo-static factor of safety expressions. The critical acceleration is then applied to the horizontal ground acceleration record at the site and double integration is performed to calculate cumulative displacements, as illustrated in Figure 6.1. where g is the gravitational constant, a(t) is the horizontal ground acceleration function with time t, $a_m = k_m$ g is the peak value of a(t), and $a_c = k_c g$ is the critical horizontal acceleration of the sliding block.(Bathurst,Cai 1996)

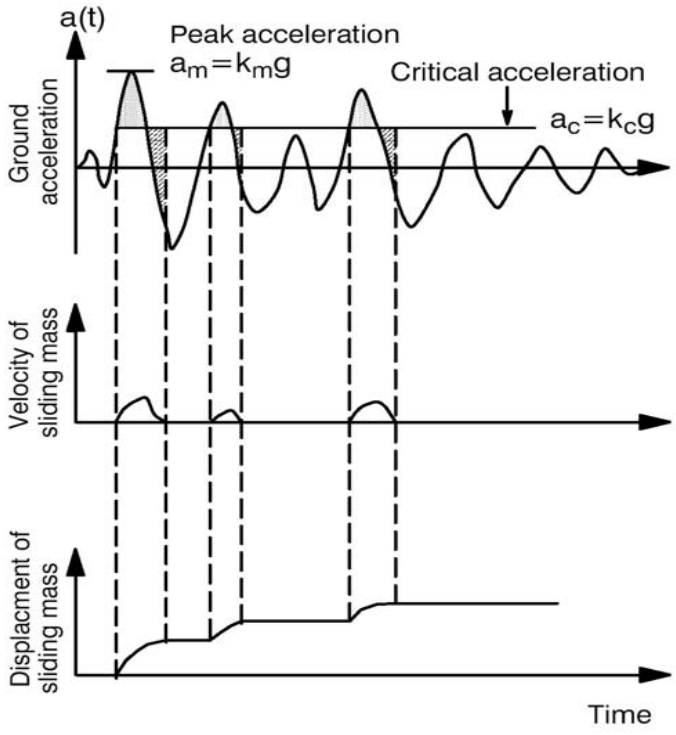


Figure 6.1. Calculation of permanent displacements (unidirectional displacement) using Newmark's method

6.1.2. Empirical Displacement Methods

Most of the displacement based methods in the literature have been created based on Newmark's sliding block theory. Thecritical acceleration ratio, which is the ratio of the critical acceleration, kcg, of the slidingblock to the peak horizontal acceleration, $k_m g$, of the earthquake, has been shown to be animportant parameter that affects the magnitude of the permanent displacement. Thus, the seismic displacement of a potential sliding soil mass computed using Newmark's theory has been traditionally correlated with the critical acceleration ratio k_c/k_m, and other representative characteristic seismic parameters, such as the peak ground acceleration, $k_m g$, the peak ground velocity, v_m, and the predominant period, T, of the acceleration spectrum (e.g. Newmark, 1965; Sarma, 1975) Based on nondimensionalized displacement terms, several writers have reformulated existing displacement methods according to the characteristic seismic parameters. The category in this study shall be utilizing the peak ground acceleration ($k_m g$) and peak ground velocity (v_m).

In the calculation of permanent displacements, Newmark's double integration method and Bathurst and Chai's mean upper bound methods are utilized. The non-dimensionalized displacement in terms of $d/(v_m^2/k_m g)$ versus critical acceleration ratio of the displacement methods can be seen in Figure 6.2. below.

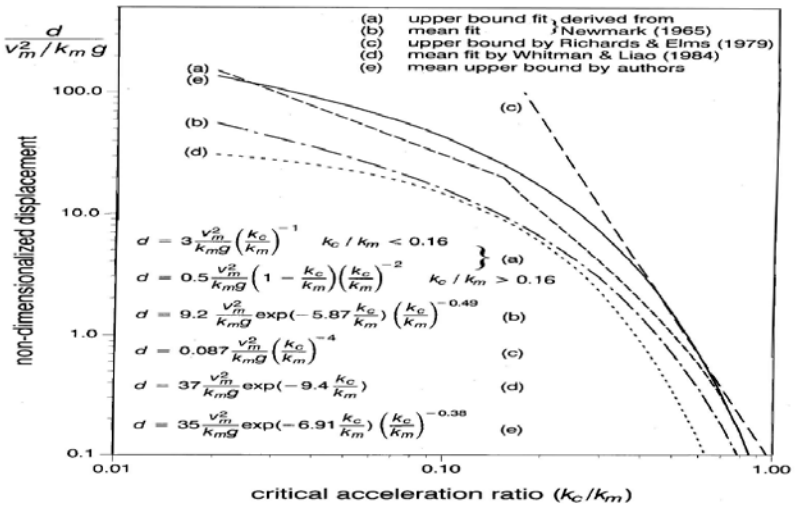


Figure 6.2.The non-dimensionalized displacement in terms of $d/(v_m^2/k_m g)$ versus criticalacceleration ratio of the displacement methods (Chai and Bathurst, 1996)

In this study, NCMA's Segmental Retaining Walls – Seismic Design Manual is used to calculate the critical acceleration andNewmark's displacement method and Barthaust and Chai's displacement method is used to calculate the permanent displacements.

6.1.3. Seismic Data

Since no permanent displacements were observed on test walls for applied Sakarya and Izmit earthquake motions, the application of the sliding-block and empirical methods to estimate wall deformations and comparison with the measured results will be based on El-Centro Earthquake records.

For the calculation of displacements, applied El-Centro 100%, 150%, 200%, 250%, 275% earthquake motions are utilized. The following Figure 6.3. through Figure 6.7. illustrate the applied velocity of the earthquakes mentioned. The computer programmeSeismoSignal Ver. 4.1.2. is utilized for the calculation of the velocities.

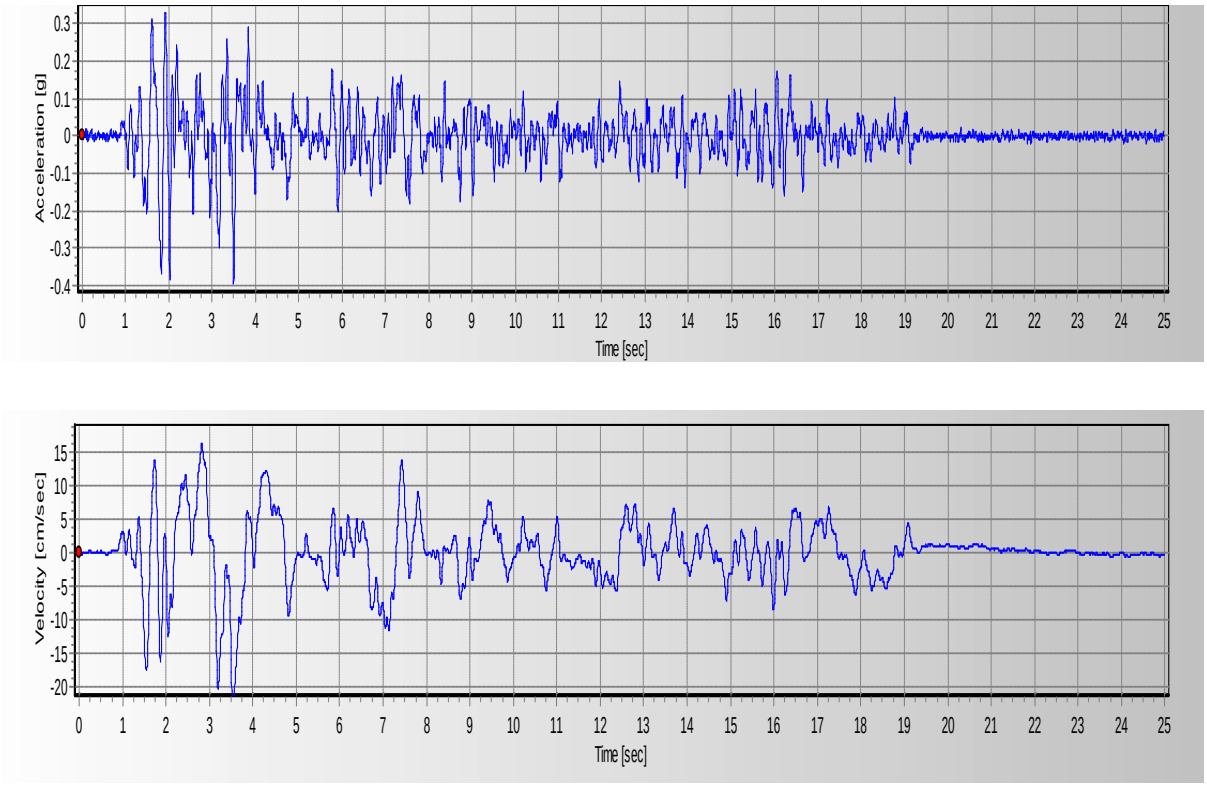


Figure 6.3. Seismic Data of the El Centro 100% Earthquake

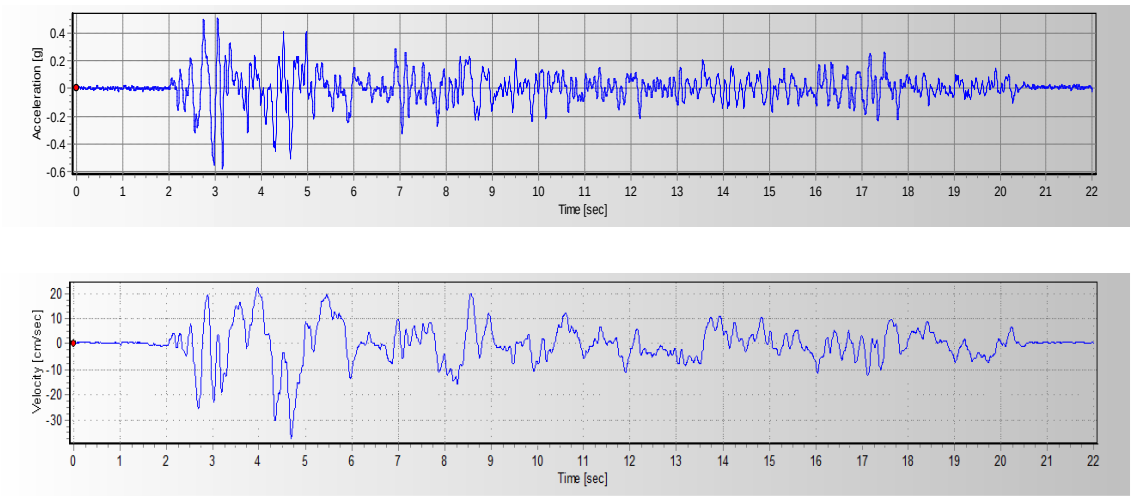


Figure 6.4. Seismic Data of the El Centro 150% Earthquake

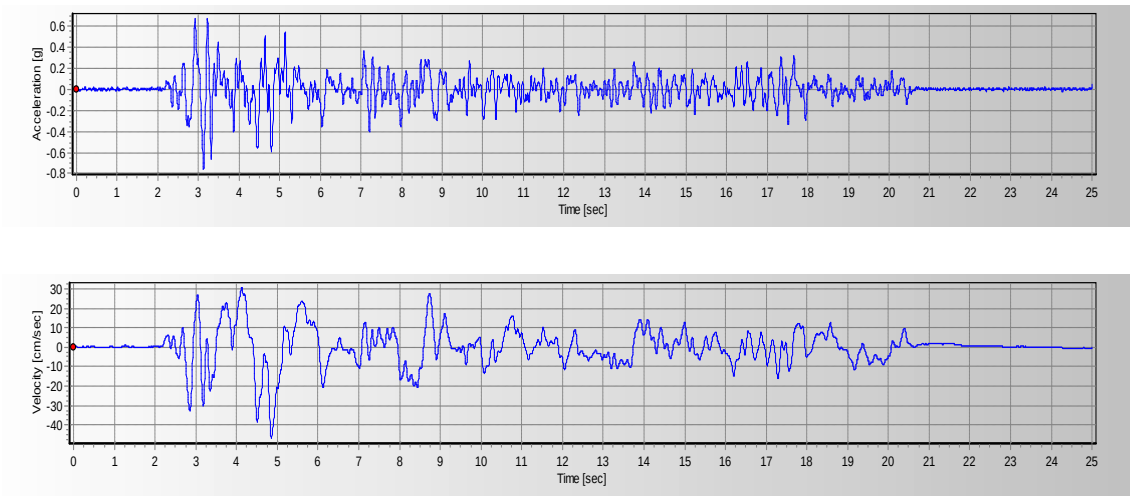


Figure 6.5. Seismic Data of the El Centro 200% Earthquake

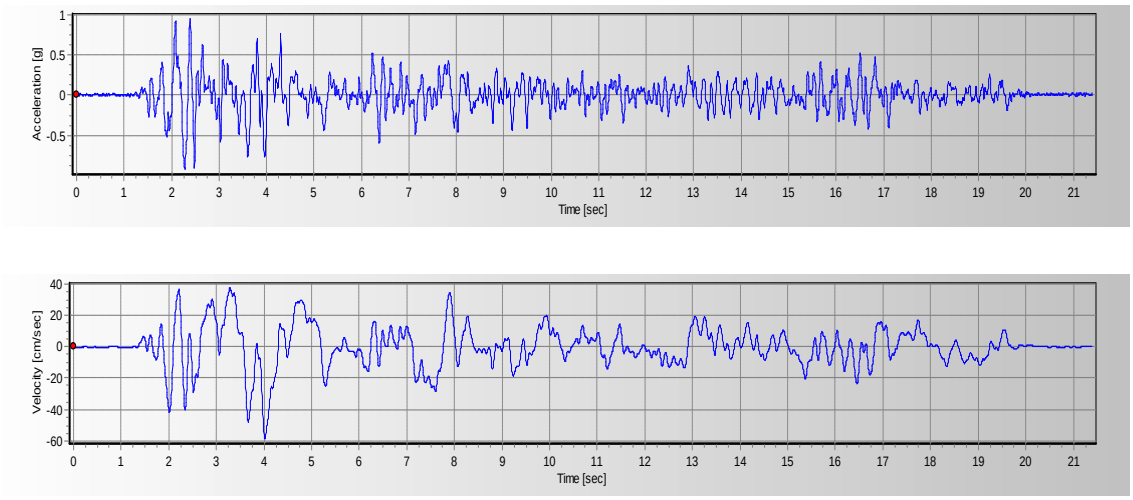


Figure 6.6. Seismic Data of the El Centro 250% Earthquake

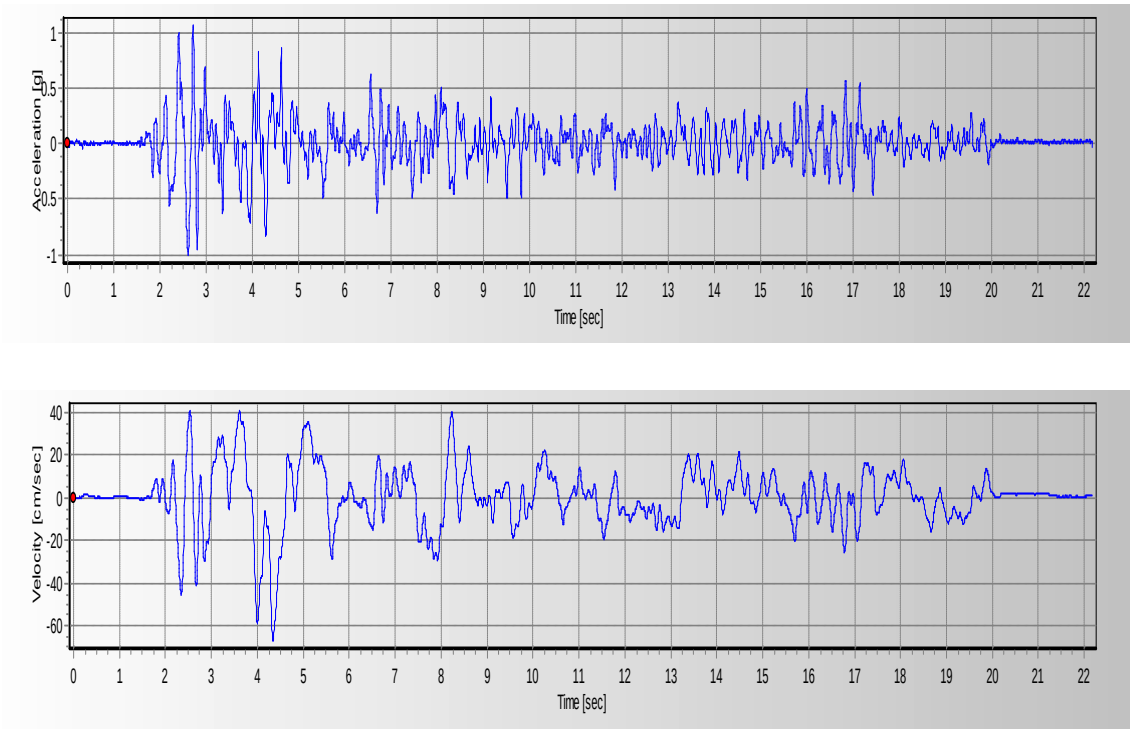


Figure 6.7. Seismic Data of the El Centro 275% Earthquake

It should be noted that the use of El Centro 150%, 200%, 250% and 275% meaning that $k_h=k_m$ values get as high as 1g in pseudostatic analysis represents a very extreme loading. However, the permanent displacements on the tested walls were observed at peak ground accelerations values above 0.4 g.

6.1.4. Material Properties

The material properties for the calculation of permanent displacements of the Wall1, 2, 3 and 4 are shown in the Table 6.1. below.

Since the interface shear-capacity data was not available, the charts proposed by Barthaust and Chai (1996) is used for the calculation of the data.

Table 6.1. Material Properties together with seismic data used in the experimented walls

		WALL 1	WALL 2	WALL 3	WALL 4
Input Data	**Properties**	**Values**	**Values**	**Values**	**Values**
Backfill Soil	Friction Angle (ϕb)	40°	40°	40°	34°
	Unit Weight(γb) (kN)	17.5	17.5	17.5	15
	Mobilized interface friction angle (δb)	40°	40°	40°	34°
Reinforced Soil	Friction Angle (ϕr)	40°	40°	40°	34°
	Unit Weight(γr) (kN)	17.5	17.5	17.5	15
	Mobilized interface friction angle (δb)	26.4	26.4	26.4	22.6
Geogrid	Ultimate Strength (Tult) (kN)	20	20	40	40
	Ultimate Strain (εult)	7%	7%	12%	12%
Soil-Geogrid	Coefficient of Direct Sliding	1	1	1	1
Segmental Block	Height (Hw)	0.1 m	0.1 m	0.1 m	0.1 m
	Depth (Dw)	0.1 m	0.1 m	0.1 m	0.1 m
	Length (Lw)	0.2 m	0.2 m	0.2 m	0.2 m
	Unit Weight(γw)	21 kN/m3	21 kN/m3	21 kN/m3	21 kN/m3
	Block-Geogrid Interface Shear (au)	6 kN/m	6 kN/m	8 kN/m	8 kN/m
	Block-Geogrid Interface Shear (λu)	30°	30°	24°	24°
Wall	Height (H)	1.9 m	1.9 m	1.9 m	1.9 m
	Setback (ω)	0°	6°	6°	6°
	Backslope Angle (β)	0°	0°	0°	0°
	Reinforcement Spacing	0.2 m	0.2 m	0.2 m	0.2 m
	Reinforcement Length/Height of Wall (L/H)	0.47	0.47	0.7	0.7
Seismic Data (El-Centro Earthquake 100%)	Peak Ground Acceleration (am)	0.39 g	0.42 g	0.41 g	0.41 g
	Peak Ground Velocity (vm)	24. 54 cm/sec	24. 98 cm/sec	24. 85 cm/sec	24. 85 cm/sec
Seismic Data (El-Centro Earthquake 150%)	Peak Ground Acceleration (am)	0.55 g	0.57 g	0.58 g	0.6 g
	Peak Ground Velocity (vm)	37.54 cm/sec	37.70 cm/sec	37.86 cm/sec	38.34 cm/sec
Seismic Data (El-Centro Earthquake 200%)	Peak Ground Acceleration (am)	0.74 g	0.73 g	0.73 g	0.75 g
	Peak Ground Velocity (vm)	46.97 cm/sec	46.95 cm/sec	46.95 cm/sec	46.97 cm/sec
Seismic Data (El-Centro Earthquake 250%)	Peak Ground Acceleration (am)	-	-	0.9 g	0.93 g
	Peak Ground Velocity (vm)	-	-	58.79 cm/sec	59.02 cm/sec
Seismic Data (El-Centro Earthquake 275%)	Peak Ground Acceleration (am)	-	-	-	0.98 g
	Peak Ground Velocity (vm)	-	-	-	66.69 cm/sec

6.1.5. Calculation of Total Wall Displacements

It is important to state that since the displacement methods are formulated based on different Earthquake data. The selection of material properties and earthquake data plays a crucial role in determining the permanent displacements on structure. For this reason, the calculated values of permanent displacements represents order of magnitude estimates rather than accurate estimates.

In the calculation of total wall displacements; firstly the critical acceleration coefficient (kc) are determined iteratively for any given set of output parameters setting the Factor of Safety values of three sliding mechanisms ((1) external sliding along the base of total structure; (2) internal sliding along a reinforcement layer and through the facing column; and (3) block interface shear between facing column) to unity. Later, thenon-dimensionalized displacement in terms of d/(vm^2/kmg) are calculated for theChai and Barthaust, 1996).

The related formulas can be found in NCMA's Segmental Retaining Walls – Seismic Design Manual and Barthaus and Chai's paper regarding the seismic induced permenant displacements of geosynthetic-reinforced segmental walls. For brevity, the calculations are made with excel computer programme and the calculation sheets for each wall are given in Appendix D.

The total wall displacement at the wall face at each elevation from the initial static position is calculated by adding layer displacement to the cumulative displacement below that layer. The layer displacement is taken as the larger of the facing shear displacement or internal sliding of that layer.

6.1.6. Comparison of Measured and Calculated Total Wall Displacements

As stated earlier, the calculation sheets for the total wall displacements are given in Appendix D. Herein this section,Table 6.2. and Table 6.3. presentthe comparison of the measured permanent displacement results together with calculated values. It should be kept in mind that this section deals with only the calculation of permanent displacements of reinforcedsegmental retaining walls related to external sliding, internal sliding, and block interface shear failure. These are only mechanisms that can be treated using conventional sliding block methods. The remaining failure mechanisms can be evaluated using a pseudo-static limit-equilibrium approach.

Table 6.2.The measured and calculated values of permanent displacements for Wall 1 and Wall 2.

	WALL 1								
	El Centro 100%			**El Centro 150%**			**El Centro 200%**		
	Calculated Total Displacement		Measured Residual	Calculated Total Displacement		Measured Residual	Calculated Total Displacement		Measured Residual
	d (Newmark) (cm)	d (Bathurst and Cai) (cm)	Displacements (cm)	d (Newmark) (cm)	d (Bathurst and Cai) (cm)	Displacements (cm)	d (Newmark) (cm)	d (Bathurst and Cai) (cm)	Displacements (cm)
Base Sliding	0,00	0,00	--	0,42	0,41	--	1,53	1,79	--
Layer 1 (@h=0.2m)	0,00	0,00	0	0,42	0,41	0	1,54	1,90	0
Layer 2 (@h=0.4m)	0,00	0,00	--	0,42	0,41	--	1,80	2,19	--
Layer 3(@h=0.6 m)	0,00	0,00	--	0,42	0,41	--	2,06	2,48	--
Layer 4 (@h=0.8 m)	0,00	0,00	--	0,42	0,41	--	2,30	2,75	--
Layer 5(@h=1 m)	0,00	0,00	0	0,42	0,41	0,15	2,68	3,13	0,3
Layer 6(@h=1.2m)	0,00	0,00	0	0,42	0,41	0,25	3,04	3,51	0,9
Layer 7(@h=1.4 m)	0,00	0,00	--	0,42	0,41	--	3,41	3,87	--
Layer 8 (@1.6 m)	0,00	0,00	0	0,46	0,55	0,3	4,51	4,98	0,6
Layer 9 (@h=1.8 m)	0,00	0,00	0	1,06	1,13	0,2	7,53	8,77	0,55

	WALL 2								
	El Centro 100%			**El Centro 150%**			**El Centro 200%**		
	Calculated Total Displacement		Measured Residual	Calculated Total Displacement		Measured Residual	Calculated Total Displacement		Measured Residual
	d (Newmark) (cm)	d (Bathurst and Cai) (cm)	Displacements (cm)	d (Newmark) (cm)	d (Bathurst and Cai) (cm)	Displacements (cm)	d (Newmark) (cm)	d (Bathurst and Cai) (cm)	Displacements (cm)
Base Sliding	0,00	0,00	--	0,20	0,22	--	1,23	1,36	--
Layer 1 (@h=0.2m)	0,00	0,00	0	0,20	0,22	0	1,24	1,48	0,1
Layer 2 (@h=0.4m)	0,00	0,00	--	0,20	0,22	--	1,24	1,48	--
Layer 3(@h=0.6 m)	0,00	0,00	--	0,20	0,22	--	1,24	1,48	--
Layer 4 (@h=0.8 m)	0,00	0,00	--	0,20	0,22	--	1,24	1,48	--
Layer 5(@h=1 m)	0,00	0,00	0	0,20	0,22	0	1,47	1,74	0,15
Layer 6(@h=1.2m)	0,00	0,00	0	0,20	0,22	0,15	1,75	2,05	0,15
Layer 7(@h=1.4 m)	0,00	0,00	--	0,20	0,22	--	2,08	2,38	--
Layer 8 (@1.6 m)	0,00	0,00	0	0,20	0,22	0,15	2,76	3,04	0,2
Layer 9 (@h=1.8 m)	0,00	0,00	0	0,34	0,41	0,1	3,83	4,15	0,37

Table 6.3.The measured and calculated values of permanent displacements for Wall 3 and Wall 4.

	WALL 3											
	El Centro 100%			El Centro 150%			El Centro 200%			El Centro 250%		
	Calculated Total Displacement		Measured Residual	Calculated Total Displacement		Measured Residual	Calculated Total Displacement		Measured Residual	Calculated Total Displacement		Measured Residual
	d (Newmark) (cm)	d (Bathurst and Cai) (cm)	Displacements (cm)	d (Newmark) (cm)	d (Bathurst and Cai) (cm)	Displacements (cm)	d (Newmark) (cm)	d (Bathurst and Cai) (cm)	Displacements (cm)	d (Newmark) (cm)	d (Bathurst and Cai) (cm)	Displacements (cm)
Base Sliding	0,00	0,00	--	0,00	0,00	--	0,27	0,28	--	0,34	0,36	--
Layer 1 (@h=0.2m)	0,00	0,00	0	0,00	0,00	0,3	1,01	1,00	0,35	1,26	1,25	0,4
Layer 2 (@h=0.4m)	0,00	0,00	--	0,00	0,00	--	1,47	1,46	--	1,84	1,82	--
Layer 3(@h=0.6 m)	0,00	0,00	--	0,00	0,00	--	1,93	1,91	--	2,42	2,39	--
Layer 4 (@h=0.8 m)	0,00	0,00	--	0,00	0,00	--	2,40	2,36	--	2,99	2,95	--
Layer 5(@h=1 m)	0,00	0,00	0,15	0,00	0,00	0,4	2,98	2,93	0,55	3,72	3,66	0,55
Layer 6(@h=1.2m)	0,00	0,00	0	0,00	0,00	0,4	3,55	3,48	0,6	4,44	4,35	0,7
Layer 7(@h=1.4 m)	0,00	0,00	--	0,00	0,00	--	4,12	4,03	--	5,14	5,04	--
Layer 8 (@1.6 m)	0,00	0,01	0	0,03	0,13	0,15	5,40	5,36	0,35	6,75	6,70	0,5
Layer 9 (@h=1.8 m)	0,00	0,01	0	0,32	0,43	0,36	7,98	8,48	0,59	9,98	10,60	0,68

	WALL 4														
	El Centro 100%			El Centro 150%			El Centro 200%			El Centro 250%			El Centro 275%		
	Calculated Total Displacement		Measured Residual	Calculated Total Displacement		Measured Residual	Calculated Total Displacement		Measured Residual	Calculated Total Displacement		Measured Residual	Calculated Total Displacement		Measured Residual
	d (Newmark) (cm)	d (Bathurst and Cai) (cm)	Displacements (cm)	d (Newmark) (cm)	d (Bathurst and Cai) (cm)	Displacements (cm)	d (Newmark) (cm)	d (Bathurst and Cai) (cm)	Displacements (cm)	d (Newmark) (cm)	d (Bathurst and Cai) (cm)	Displacements (cm)	d (Newmark) (cm)	d (Bathurst and Cai) (cm)	Displacements (cm)
Base Sliding	0,00	0,00	--	0,51	0,50	--	1,66	1,99	--	2,07	2,48	--	2,24	2,68	--
Layer 1 (@h=0.2m)	0,00	0,00	0	0,51	0,50	0,2	3,08	3,53	0,25	3,85	4,41	0,35	4,16	4,76	0,5
Layer 2 (@h=0.4m)	0,00	0,00	--	0,60	0,65	--	4,09	4,55	--	5,11	5,68	--	5,52	6,14	--
Layer 3(@h=0.6 m)	0,00	0,00	--	0,68	0,79	--	5,09	5,57	--	6,37	6,96	--	6,88	7,52	--
Layer 4 (@h=0.8 m)	0,00	0,00	--	0,83	0,98	--	6,10	6,60	--	7,63	8,25	--	8,24	8,91	--
Layer 5(@h=1 m)	0,00	0,00	0,1	1,07	1,24	0,5	7,32	7,88	0,4	9,15	9,84	0,5	9,88	10,63	0,6
Layer 6(@h=1.2m)	0,00	0,00	0	1,32	1,51	0,25	8,55	9,16	0,55	10,68	11,45	0,6	11,54	12,37	0,65
Layer 7(@h=1.4 m)	0,00	0,00	--	1,57	1,77	--	9,78	10,46	--	12,23	13,08	--	13,21	14,12	--
Layer 8 (@1.6 m)	0,00	0,00	0	1,94	2,14	0,3	12,18	13,36	0,6	15,23	16,70	0,65	16,44	18,04	0,7
Layer 9 (@h=1.8 m)	0,00	0,00	0	2,56	2,74	0,24	15,96	18,49	0,46	19,95	23,11	0,5	21,54	24,96	0,46

Both calculated and measured values state that, the top portions of the walls are the least stable portion as the seismic forces increase. In the experiments since the top two blocks were grouted, the residual displacements measured on (@h=1.65 m.) corresponding to 8 thgeogrid layer is observed to have the largest displacement. Additionally, the base sliding in the models were restricted by placing a welded metal plate on the toe of walls. So,no base sliding was observed during the experiments.

In order to eliminate the unquantifiable errors in the calculation, base acceleration at each geogrid elevation is taken as the amplified accelerations that aremeasured.

For critical acceleration ratios below 1 ($(k_c/k_m)<1$), the calculated displacement values and measured values show no residual displacements. When the base acceleration values exceed 0.58 g (corresponding to El Centro 150% earthquake motion) the residual displacements are observed on walls. As can be seen from the comparison of measured and calculated theoretical Newmark and Bathurst and Cai analysis of permanent displacements, the theorotical calculations are in good agreement with the measurements at El Centro 150% earthquake motions for each wall type. However, past 0.73 g base acceleration amplitudes, the calculated values over-estimate the permanent displacement values especially on the top portion of the wall. This may be due to the over estimation of critical acceleration values in the empirical formulas for the high lateral acceleration amplitudes.

As an example; when the critical acceleration values for the top portion of the wall 1 – El Centro 200% earthquake motion is back-calculated from the Newmarkformulas stated in Figure 6.2 and it is seen that an almost 50% of overestimation of critical acceleration at top portion of the wall is found. However, further detailed investigation is needed on this subject.

Additionally, as stated earlier, no accurate results but instead order-of estimates should be expected from the calculations since the methods have been formulated based on different earthquake data.

6.2. Comparison Of Measured And Design Tensile Loads On Geogrids During Earthquake

The calculations for the additional geogrid stresses due to earthquake loading for the instrumented geogrid layers are made with excel computer programme (according to specifications of FHWA (2001 and 2009) and NCMA) and the relevant data sheets are given in Appendix E. The material properties are taken from Table 6.1. Detailed description of the methods can be found in the NCMA and FHWA design books. Herein, a brief summary on Design of GRS-RWs Considering Seismic Effects as Pseudo-Static Loading shall be presented and later the comparison of measured and design tensile load on geogrid reinforcement during the earthquake motion applied on model walls shall be given.

6.2.1. Design of GRS-RWs Considering Seismic Effects as Pseudo-Static Loading

When designing GRS-RWs with granular backfill materials, numerous methods are utilized in order to determine the geometry and reinforcement properties of external and internal stability. Working stress analyses, limit equilibrium analyses, and deformation evaluations are the must have approaches of a complete design analysis (Elias *et al.*, 2001).

Commonly used FHWA (Elias *et al.*, 2001) design method for GRS-RWs proposes the Coulomb stress analysis for external stability calculations whereas a Rankine failure surface is considered for internal stability. The recommendations for external and internal stability calculations can be found in detail in FHWA and NCMA design books. Herein, a summary of seismic external and internal analysis recommended by FHWA shall be presented.

6.2.1.1. FHWA Recommendation of Pseudostatic Loading in External Stability Calculations. Following the static external stability of the GRS wall is ensured; the external stability with effects of seismic loading case is considered (Figure 6.8). The most commonly used method for the seismic analysis and design of GRS walls is the pseudo-static method. In this method, pseudo-static forces related to the ground acceleration are added to the conventional static limit equilibrium analysis.

The retained fill exerts a dynamic thrust, P_{AE}, on the GRS wall in addition to the static force during an earthquake motion. The reinforced soil mass is also subjected to a horizontal inertia force, P_{IR}, proposed in FHWA manuals as

$$P_{IR} = MA_m g \tag{6.1}$$

where: M = Mass of the active portion of the reinforced wall section assumed at a base width of $0.5H$, as shown in Figure 6.8.

A_m = maximum horizontal acceleration coefficient in the reinforced soil wall

$$A_m = (1.45 - A)A \tag{6.2}$$

where: A = maximum ground acceleration coefficient

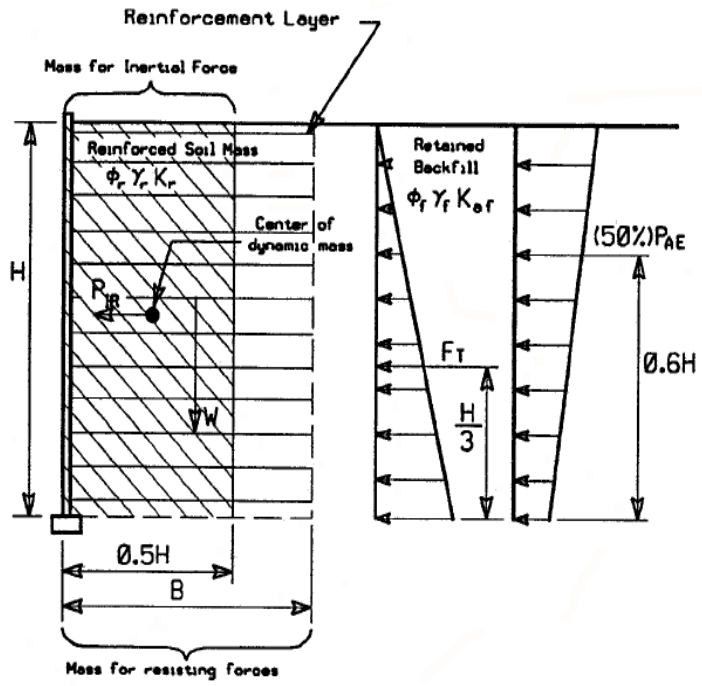
For horizontal backslope condition, the seismic thrust, P_{AE}, is suggested in FHWA recommendations as:

$$P_{AE} = 0.375 A_m \gamma_f H^2 \tag{6.3}$$

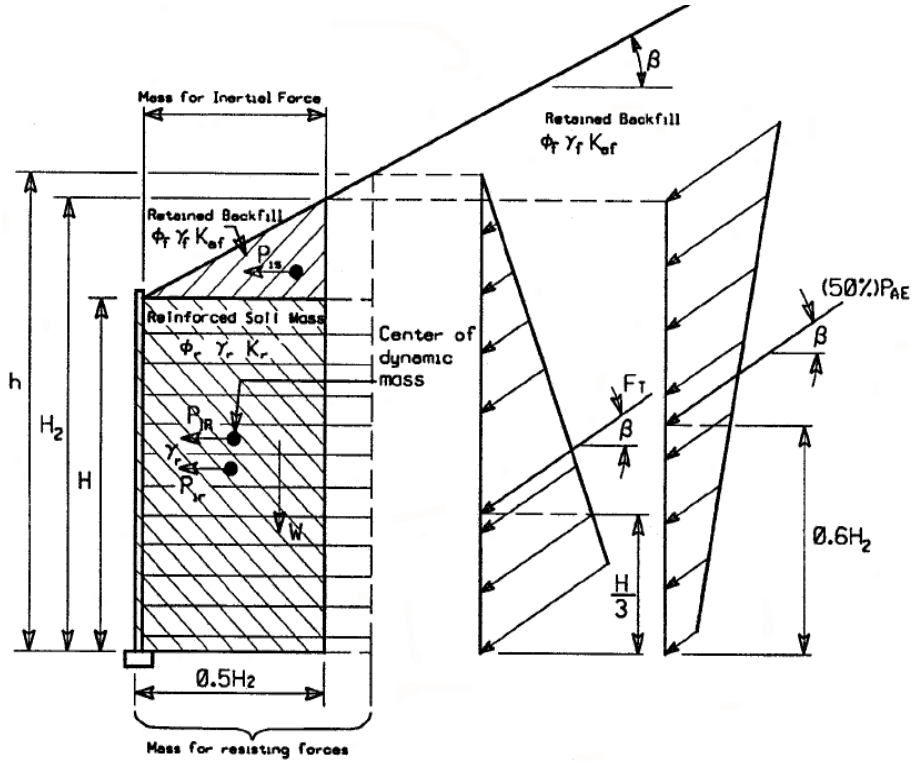
FHWA suggests adding the full inertia force P_{IR} and fifty per cent of the seismic thrust P_{AE} to the static forces. For sloping backfill condition, the seismic thrust, P_{AE}, can be calculated using the Mononobe-Okabe method:

$$P_{AE} = 0.5\gamma_f (H_2)^2 \Delta K_{AE} \tag{6.4}$$

where: $$H_2 = H + \frac{0.5H \tan\beta}{1 - 0.5\tan\beta}$$



(a)



(b)

Figure 6.8. Forces considered in seismicexternalstabilitycalculations: (a) forlevelbackfill (b) forslopingbackfill (Elias*et al.*, 2001)

K_{AE}, the total seismic earth pressure coefficient, is calculated based on the general Mononobe-Okabe expression:

$$K_{AE} = \frac{\cos^2(\varphi - \xi - 90 + \theta)}{\cos\xi \cos^2(90-\theta)\cos(\beta + 90 - \theta + \xi)\left[1 + \sqrt{\frac{\sin(\varphi+\beta)\sin(\varphi-\xi-\beta)}{\cos(\beta+90-\theta+\xi)\cos(\beta-90+\theta)}}\right]^2} \quad (6.5)$$

where: ξ = seismic inertia angle

$$\xi = \tan^{-1}\left(\frac{k_h}{1 \pm k_v}\right) \quad (6.6)$$

where: k_h = horizontal seismic coefficient

k_v = vertical seismic coefficient

As computed in the static case, the seismic external analysis is concluded by completing sliding stability, eccentricity and bearing capacity checks with the pseudo-static forces added. Computed factors of safety greater than 75 per cent of the static factors of safety and eccentricity falling within $L/3$ is considered as acceptable. (Selek, 2011)

FHWA suggests that a length of reinforcement should be greater than 0.7*H*. In the experimented Wall 1 and Wall 2, although the wall reinforcement length / wall height ratio (L/H) were below the FMWA agreement, no failure was observed at those walls.

6.2.1.2. FHWA Recommendation of Pseudostatic Loading in Internal Stability Calculations. In order to check the internal stability under seismic loading, FHWA recommends the addition of dynamic increments calculated at each reinforcement layer to T_{max} (the maximum tension force per unit width of wall) calculated by Equation 6.7.

$$T_{\max} = \sigma_H s_v \quad (6.7)$$

where: $\sigma_H = K_{ar}\sigma_v + \Delta\sigma_H$

K_{ar} = earth pressure coefficient calculated for reinforced zone
$\Delta\sigma_h$ = increment of horizontal stress due to any horizontal concentrated surcharge
σ_v = total vertical stress including soil self-weight and effects of any surcharge loads present
s_v = reinforcement spacing

as shown in Figure 6.9. The inertia force P_I considered in internal stability calculations and the dynamic increment in tensile force, T_{md}, resulting from the inertia force are calculated by using:

$$P_I = A_M W_A \tag{6.8}$$

where: W_A = weight of active zone

$$T_{md} = P_I \frac{L_{ei}}{\sum_{i=1}^{n} L_{ei}} \tag{6.9}$$

$$T_{total} = T_{\max} + T_{md} \tag{6.10}$$

In the updated recommendations of FHWA (2009), T_{md} is calculated by distributing the inertial force equally to the reinforcements.

More detailed information on the tensile calculation methods canbe found in FHWA and NCMA design books.

The Figure 6.9. shown below illustrates the reinforcement tensile load calculation using FHWA method.

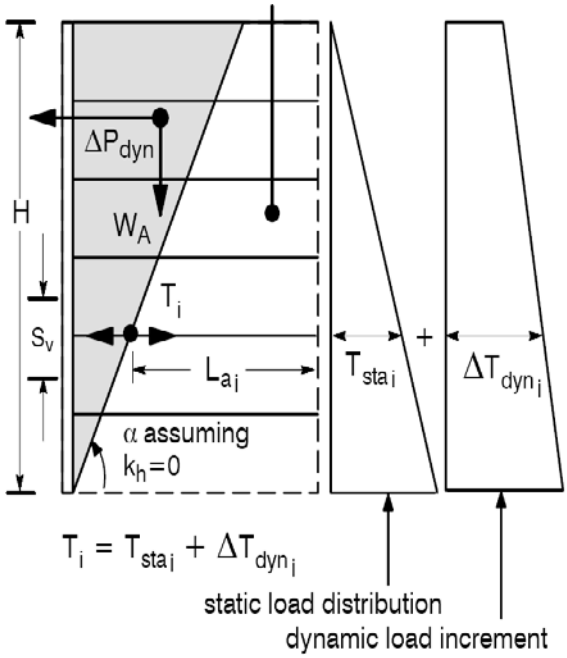
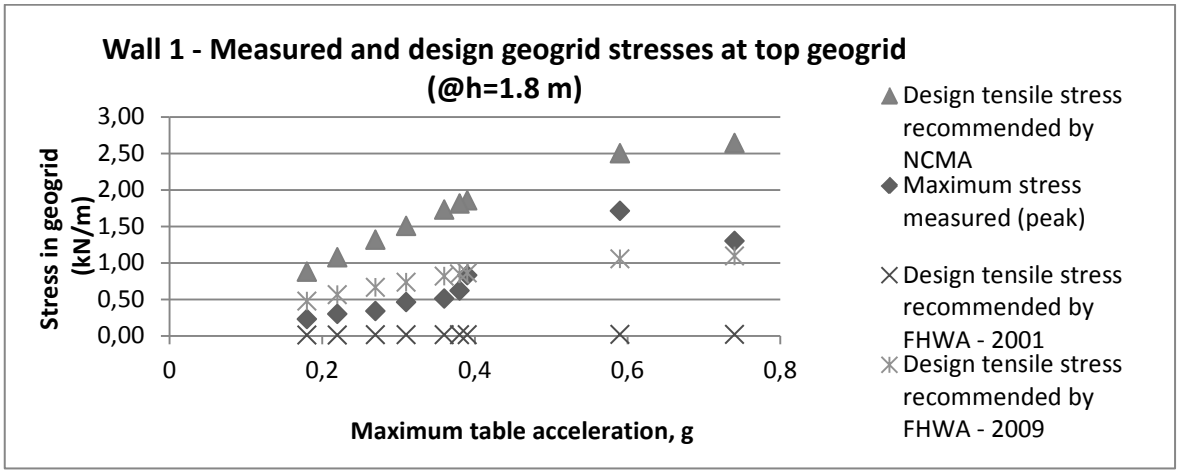


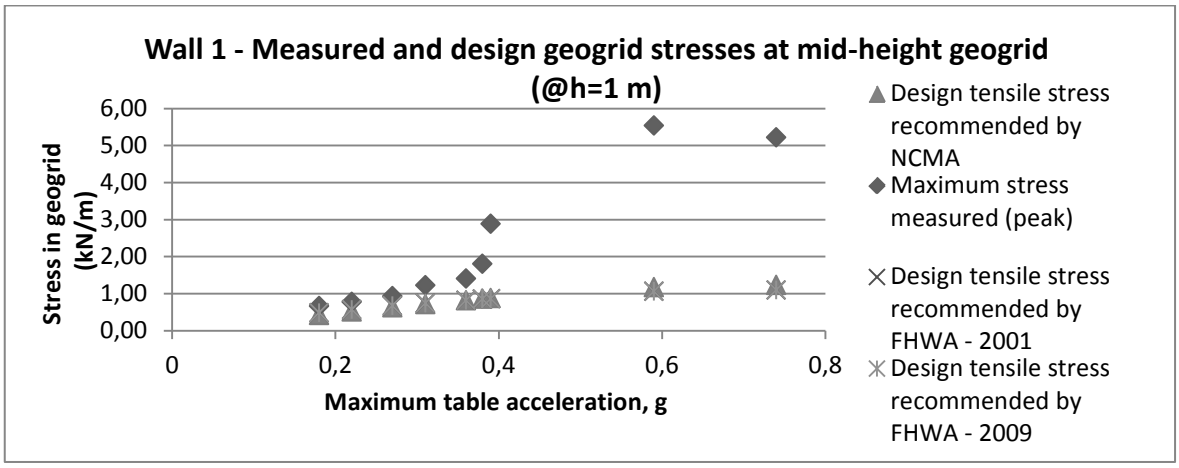
Figure 6.9. Reinforcement tensile load calculation using FHWA method (Bathurst and Alfaro, 1996)

6.2.2. The Comparison Of Measured And Design Tensile Loads On Geogrid Reinforcement During The Earthquake Motion Applied On Model Walls

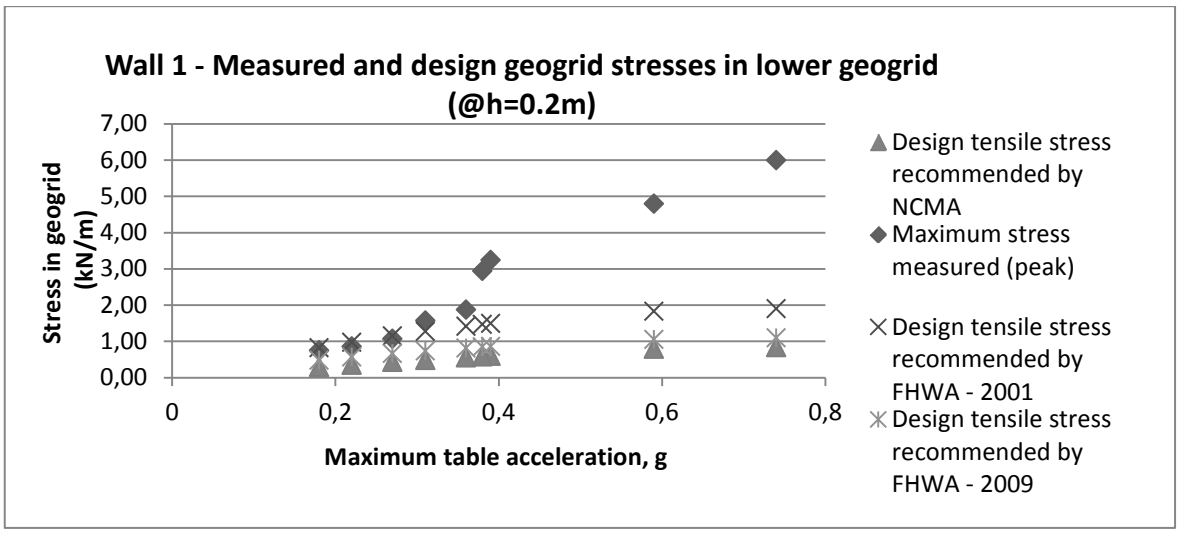
The calculations for the additional geogrid stresses due to earthquake loading for the instrumented geogrid layers are made in accordance with the FHWA (2001 and 2009) and NCMA methods. It should be noted that, in FHWA (2009) method the inertial force equally distributed to the reinforcement layers where in FHWA (2001) method and in NCMA method the dynamic increment is added to the inertia of the facing blocks and the inertial force on the reinforcement layer increases with the increasing height of the reinforcement from the base. The values recommended by FHWA and NCMA design manuals are compared with the measured values (by strain gages) at the most stressed regions of the geogrids in lower, midheight and upper partfor Wall 1, 2, 3 and 4. The graphs obtained from the calculations and comparison of measured and design tensile loads for Wall 1 and Wall 2 are shown in Figure 6.10 and Figure 6.11 respectively. The maximum stresses measured on instrumented geogrid layers are taken as a reference in the comparison. As mentioned earlier, please refer to Appendix E. for the excel data sheets utilized in calculations.



a)

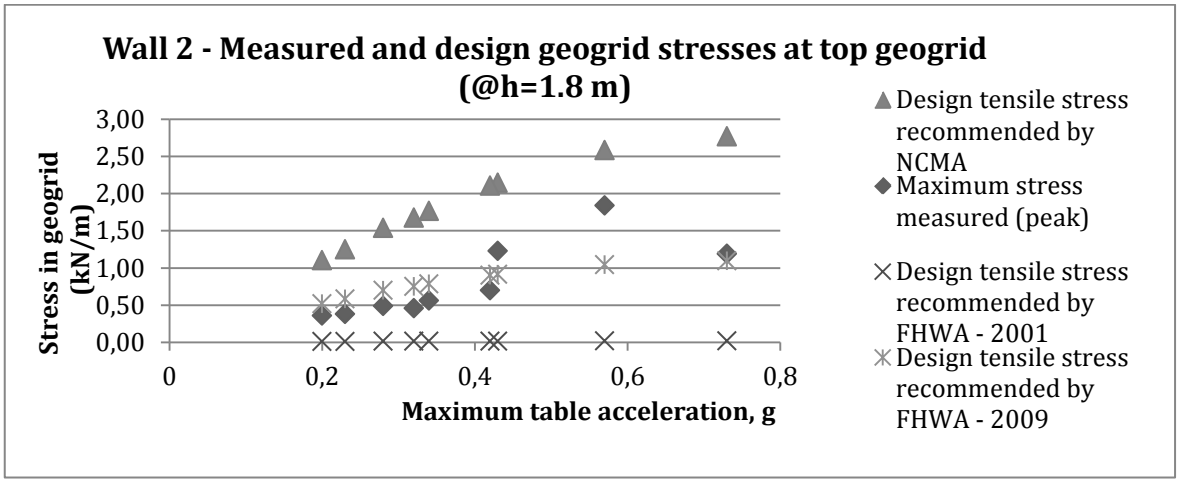


b)

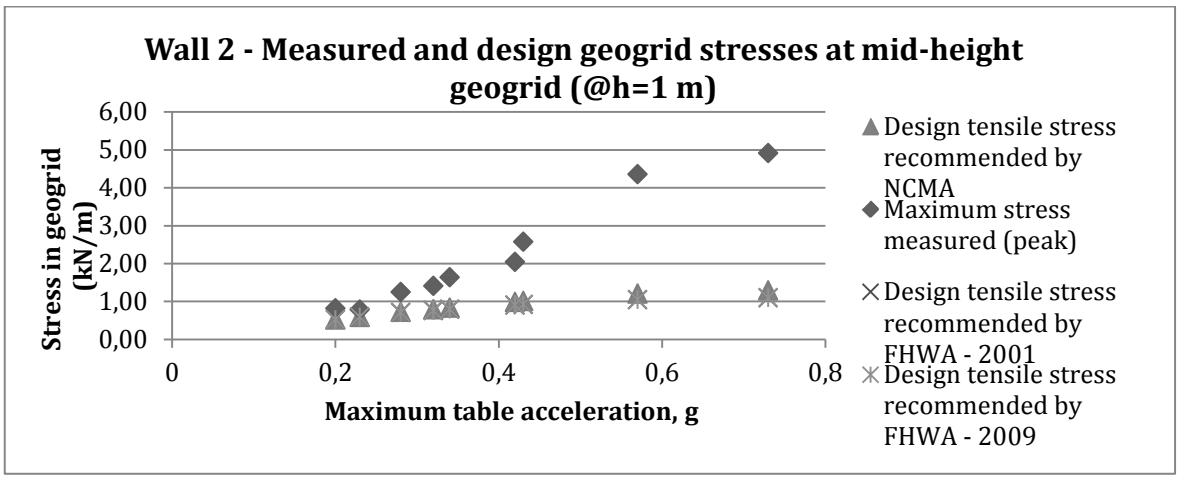


c)

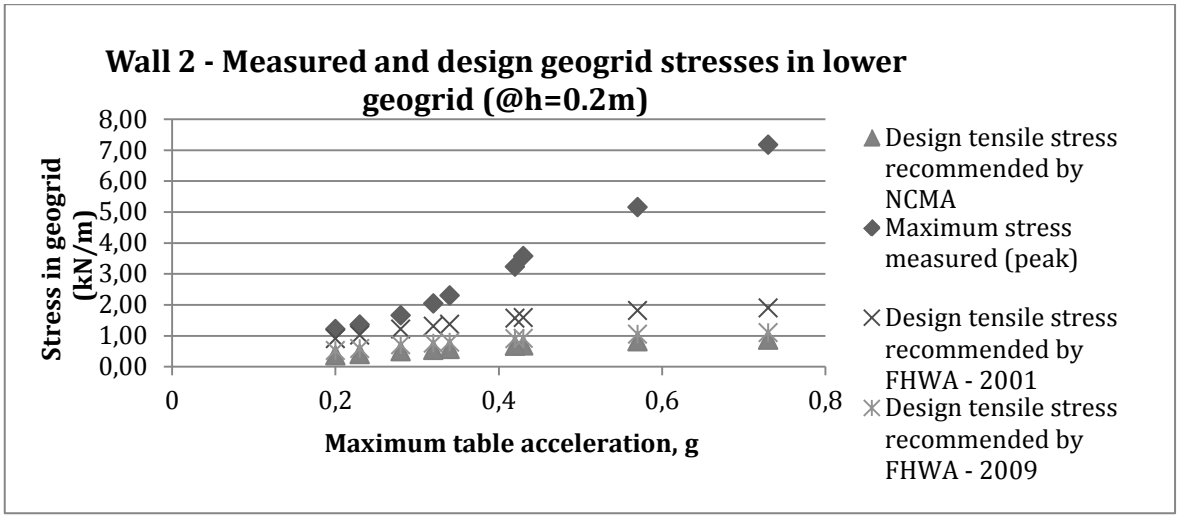
Figure 6.10. Comparison Of Measured And Design Tensile Loads On a) top, b)midheight, c)lower Geogrid Reinforcement for Wall 1



a)



b)



c)

Figure 6.11. Comparison Of Measured And Design Tensile Loads On a) top, b)midheight, c)lower Geogrid Reinforcement for Wall 2

For all types it can be stated that as the base acceleration increases the stresses in geogrids increase linear fashion.

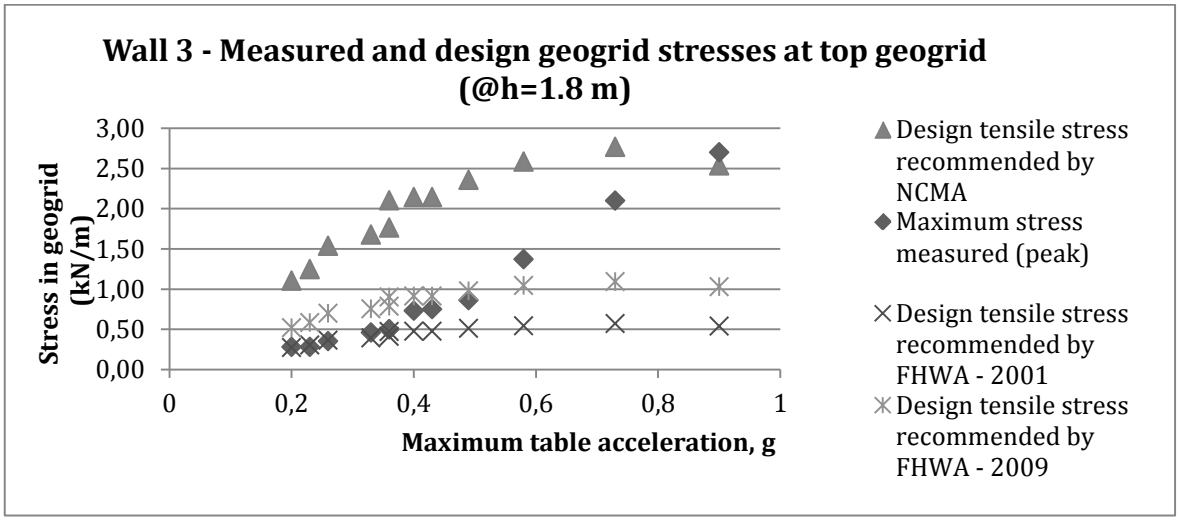
For Wall 1; the measured and calculated seismic induced stresses on lower and midheightgeogrids show good correlation up to El Centro 150% earthquake baseexcitation that corresponds to a base acceleration amplitude of 0.59 g. Past that acceleration amplitude, the measured stresses are observed to be much higher than the design stresses. This may be due to the fact that, when a threshold limit of base acceleration amplitude (i.e. 0.5 g) is exceeded on the structure, the seismic induced stresses on geogrids tend to increase significantly and the current methodologies are inadequate to predict the bottom and midheightreinforcement stresses under extreme seismic activity. The measured seismic induced tensile stresses show a linearly increasing behavior with the increasing base acceleration amplitude.

At top geogrid layer, the measured values are observed to be lower than the NCMA approach for all base excitation amplitudes. The measured stresses on top geogrid layer are observed to be between the FHWA 2001 and FHWA 2009 design stresses. According to the measurements, NCMADesign methodology for top reinforcement seems to be conservative; however even at extreme seismic motion the methodologies show good prediction of the measured stresses.

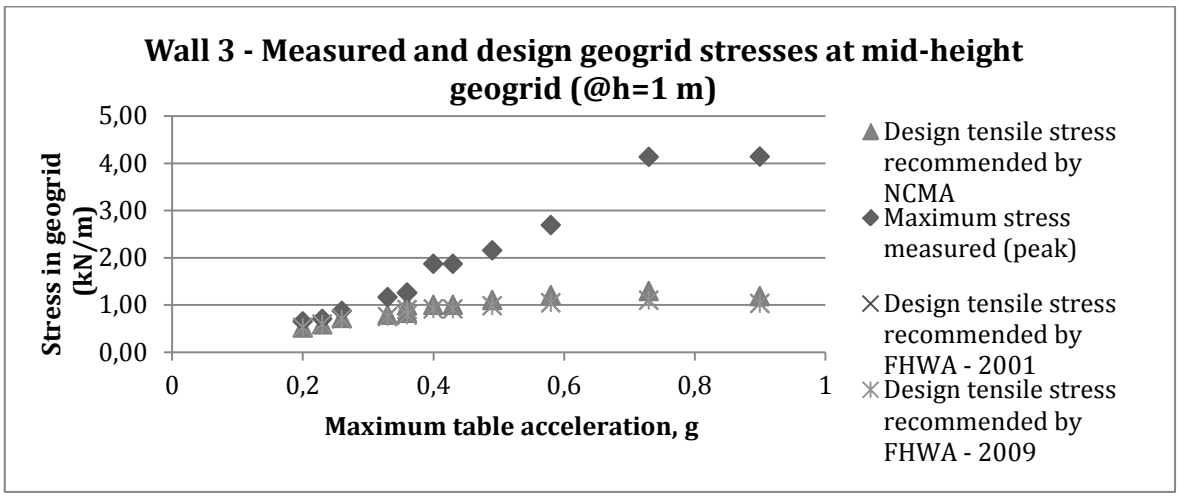
Even though the Wall 1 is under designed in terms of reinforcement length ($L/H<0.7$) that is proposed by FHWA methodologies, the design method proposed stresses are sufficient in predicting the reinforcement stresses up to acceleration amplitudes of 0.59 g. However, the FHWA 2009 and NCMA design methodologies over estimate the stresses on top reinforcement layer.

For Wall 2; the same comments made for Wall 1 applies. However the stresses measured on reinforcements are slightly higher than the Wall 1 reinforcement stresses due to differences base excitation values and wall batter.

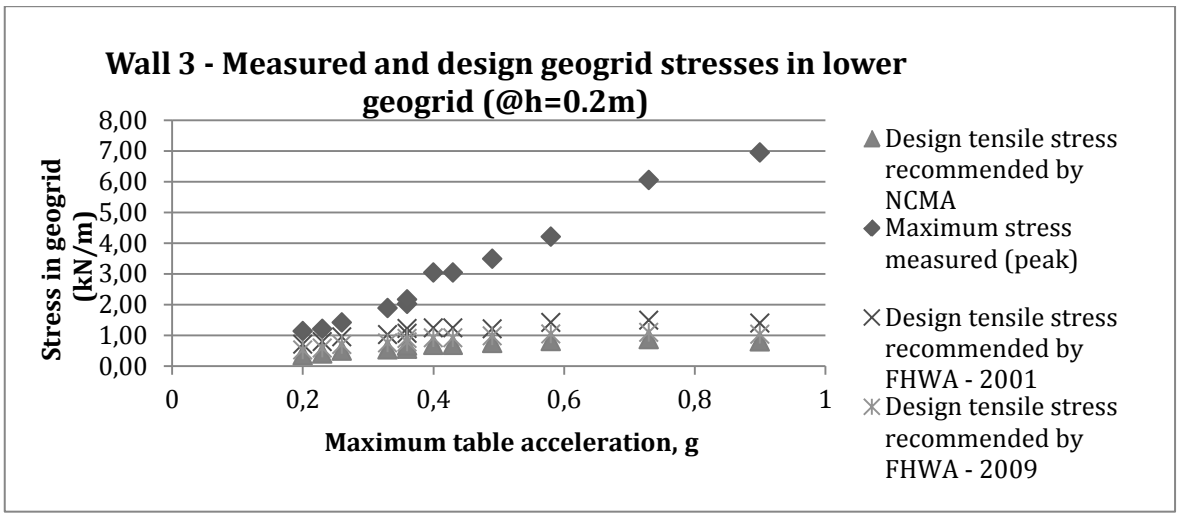
The graphs obtained from the calculations and comparison of measured and design tensile loads for Wall 3 and Wall 4 are shown in Figure 6.12 and Figure 6.13 respectively.



a)

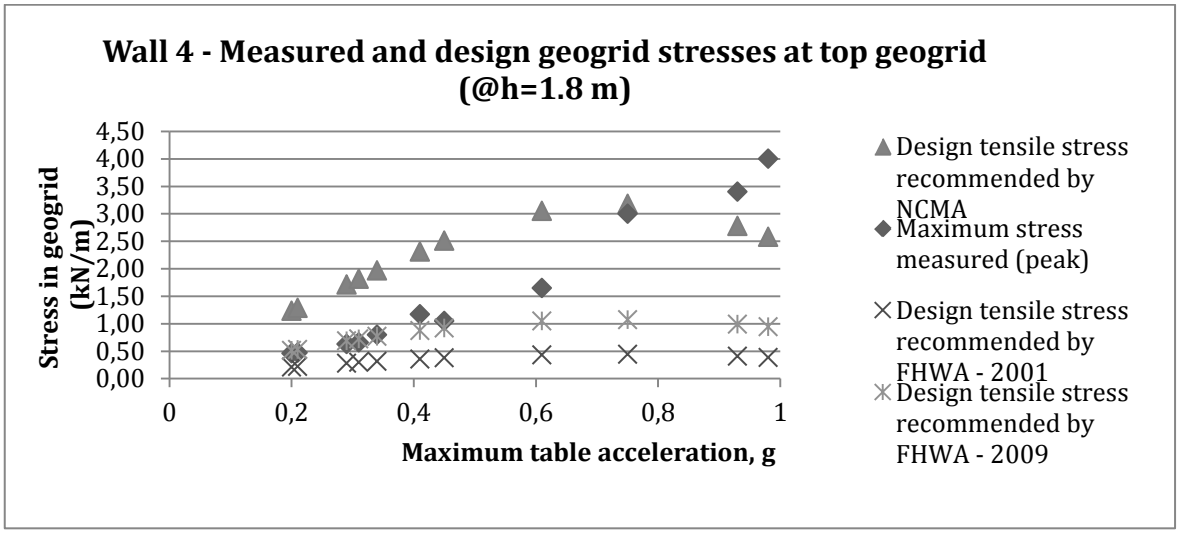


b)

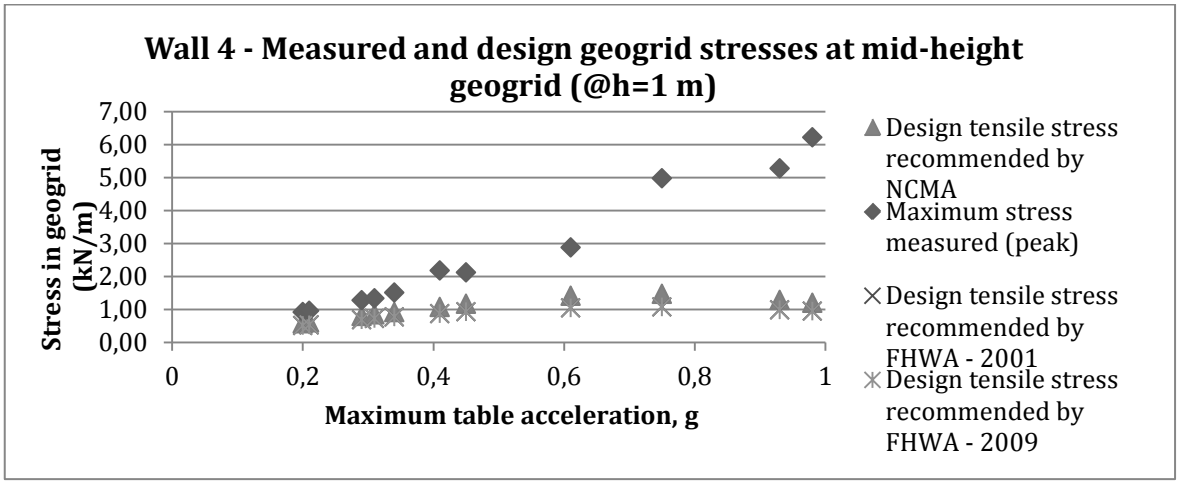


c)

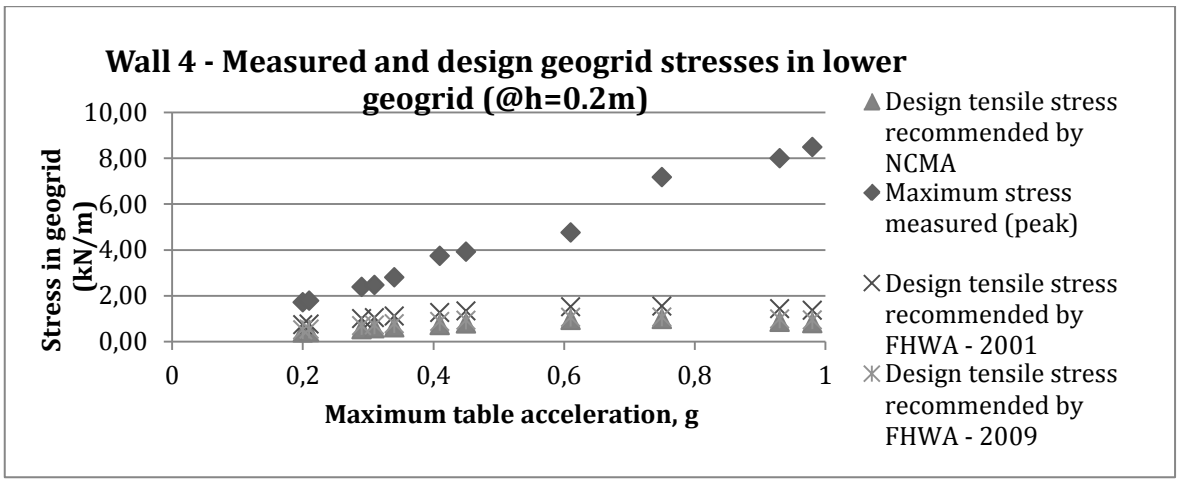
Figure 6.12.Comparison Of Measured And Design Tensile Loads On a) top, b)midheight, c)lower Geogrid Reinforcement for Wall 3



a)



b)



c)

Figure 6.13.Comparison Of Measured And Design Tensile Loads On a) top, b)midheight, c)lower Geogrid Reinforcement for Wall 4

For Wall 3; the measured and calculated seismic induced stresses on lower and midheightgeogrids show good agreement (although a the measured stresses are observed to be a bit higher than the recommended values) up to El Centro 150% earthquake baseexcitation that corresponds to a base acceleration amplitude of 0.6 g. Past that acceleration amplitude, the measured stresses are observed to be much higher than the design stresses.

For Wall 4 (sand backfill), the measured seismic induced stresses stresses on lower and midheightgeogrids are higher than the recommended design stresses. The measured seismic induced tensile stresses show a linearly increasing behavior with the increasing base acceleration amplitude. The stresses measured on reinforcements are slightly higher than the wall 3 reinforcement stresses due to differences in backfill material.

When a threshold limit of base acceleration amplitude (i.e. 0.5 g) is exceeded on the structure, the seismic induced stresses on geogrids tend to increase significantly and the current methodologies are inadequate to predict the bottom and midheight reinforcement stresses under extreme seismic activity.

At top geogrid layer, the measured values are observed to be lower than the NCMA approach for all base excitation amplitudes. The measured stresses on top geogrid layer are observed to be between the FHWA 2001 and FHWA 2009 design stresses. According to the measurements, NCMA Design methodology for top reinforcement seems to over-estimate the tensile stresses;however even at extreme seismic motion the methodologies show good prediction of the measured stresses.

7. GENERAL CONCLUSIONS

This study investigates the seismic performance of geogrid reinforced segmental block walls. The general conclusions drawn from shaking table tests on four ½ reduced scale instrumented walls can be summarized as:

- The maximum acceleration amplification factors on the wall face tend to increase with the increase in height of wall as stated in the literature. Almost all acceleration amplification factors were relatively small (between 1.0 and 1.5) but tend to increase significantly after an input base acceleration of 0.56 g (corresponding to El Centro 150% base excitation) is applied on the models. This acceleration value may be referred to as critical acceleration value sincethe in each acceleration vs. wall height curve at this point corresponds to a sharp decrease in the slope of the plots. There was little influence of wall inclination on the measured acceleration amplification factors for the entire range of base excitations. The magnitude of acceleration amplification factors decreased with increasing length and tensile strength of reinforcement. Among the wall configurations that have thesame reinforcement type and wall facing type with different backfill type (Wall 3 and Wall 4), the gravel backfilled (Wall 3) model has higher maximum acceleration amplification factor values than sand backfilled model. This may be due to stiff soils being strong and tend to amplify the accelerations, loose soils being ideal dampers and they decrease the acceleration amplification.

- The walls in fact behave almost elastically and the residual displacements observed on the front of the wall were very small under the design earthquake accelerations. In terms of maximum and residual facing deformations the wall inclination had no significant effect. At low lateral accelerations (below 0.70 g base acceleration amplitudes), the backfill material has no significant effect on the maximum face deformations. However, when more than 0,7 g is applied on the Wall 3 and Wall 4, the Wall 3 (gravel backfill) showed slightly lower face deformation values than Wall 4. This may be due to the better interlocking of gravel material and geogrid. Increasing the reinforcement length and to wall height ratio,L/H from 0.47 to 0.7 and

tensile strength, reduced the maximum wall deformations, especially at the top layers.

- At the end of construction strain gage readings obtained from the model walls are below 1% strain value. Post construction potential internal failure surface is obtained by joining the locus points of maximum stresses. Measured and Rankine potential failure surface show good agreement.

- Strain gages on geogrids performed well under earthquake loading conditions. The top reinforcement layer experienced the lowest strains among the instrumented layers. The strains tensile stresses generated on the top reinforcement had no peaks as the other layers meaning that the earthquake loads were distributed almost equally at the top reinforcement. For Wall 1 and Wall 2; the peak strains and tensile stresses are generated very close (20 cm. away from the front facing) to the facing at the bottom geogrid layer. Where for Wall 3 and Wall 4 the peak strains and tensile stresses generated at the second strain gage location (40 cm. away from the front facing). This may be due to usage of different geogrid types (PolypropleneGeogrid 20/20 for Wall 1 and Wall 2 and PET Geogrid 45/15-20 for Wall 3 and Wall 4). For the weaker reinforcement the peak strains at the bottom geogrid layer occurred at very close distance to the facing. It can be stated that the high tensile load near the wall base is a result of both high overburden stress and restraining effect due to the geogrid reinforcements. Sand backfilled model experienced higher strains and tensile stresses on reinforcements than gravel backfilled model at each instrumented reinforcement layer confirming that the gravel backfill showed good performance against the dynamic increment pressure distribution during the earthquake loading proposed by the pseudo static approach of FHWA. The tensile loads generated in stronger reinforced (in terms of ultimate tensile strength and reinforcement length) Wall 3 are lower compared to the weaker reinforced wall (Wall 2). This is due to the difference in the stiffness of the geogrids. Wall 3 has less stiff geogrid reinforcement arrangement and as a result of this the tensile loads in the geogrids are lower compared to the Wall 2. A 20% reduction in the reinforcement stiffness resulted in an approximately 25% reduction in the measured values of tensile loads generated in the reinforcement.

- For critical acceleration ratios below 1 ((k_c/k_m)<1), the calculated displacement values and measured values show no residual displacements. When the base acceleration values exceed 0.58 g (corresponding to El Centro 150% earthquake motion) the residual displacements are observed on walls. As can be seen from the comparison of measured and calculated theoretical Newmark and Bathurst and Cai analysis of permanent displacements, the theoretical calculations are in good agreement with the measurements at El Centro 150% earthquake motions for each wall type. However, past 0.73 g base acceleration amplitudes, the calculated values over-estimate the permanent displacement values especially on the top portion of the wall. This may be due to the over estimation of critical acceleration values in the empirical formulas (proposed by Newmark, Bathurst and Cai) for the high lateral acceleration amplitudes.

- The measured and calculated seismic induced stresses on lower and midheightgeogrids show good correlation up to El Centro 150% earthquake base excitation that corresponds to base acceleration amplitude of 0.59 g. Past that acceleration amplitude, the measured stresses are observed to be much higher than the design stresses. This may be due to the fact that, when a threshold limit of base acceleration amplitude (i.e. 0.5 g) is exceeded on the structure, the seismic induced stresses on geogrids tend to increase significantly and the current methodologies are inadequate to predict the bottom and midheight reinforcement stresses under extreme seismic activity. When selecting reinforcement, this condition should be kept in mind. At top geogrid layer, the measured values are observed to be lower than the NCMA approach for all base excitation amplitudes. The measured stresses on top geogrid layer are observed to fall in between the FHWA 2001 and FHWA 2009 design stresses. According to the measurements, NCMA Design methodology for top reinforcement seems to over-estimate the tensile stresses; however even at extreme seismic motion the methodologies show good prediction of the measured stresses.

- The fundamental frequency of the geogrid reinforced model walls were calculated using an empirical equation proposed by Wu (1994). Even when the peak amplitudes of the applied earthquake records (El-Centro, Izmit and Sakarya) are doubled and almost tripled, the predominant frequencies of the scaled records of the earthquakes

cannot attain the calculated empirical fundamental frequency of the models. As a result, a resonant behavior was not expected and observed during the experiments.

- One of the most important conclusions that may be drawn from this study is that even at extreme seismic loading conditions, no facing stability problems occurred on the geogrid reinforced walls although the connection between the geogrid reinforcement and facing blocks were purely frictional.

Finally, it can be stated that the geogrid reinforced segmental block walls designed according to current specifications showed a very good resistance to earthquake loading conditions. They remained stable even under extreme lateral accelerations (peak lateral acceleration values up to 0.97 g). All four wall configurations designed in this study showed very successful behavior. No stability problem occurred even under extreme lateral accelerations. The Geogrid Reinforced Segmental Block Walls showed minimal residual deformations and acceptable maximum deformations under extreme lateral earthquake accelerations.

APPENDIX A: ACCELERATION-TIME HISTORY GRAPHS OBTAINED FROM THE TESTS

This appendix contains acceleration-time history graphs for each wall configuration together with Fourier Amplitude Spectra. The locations and abbreviations used for the accelerometers are given in Section 4.

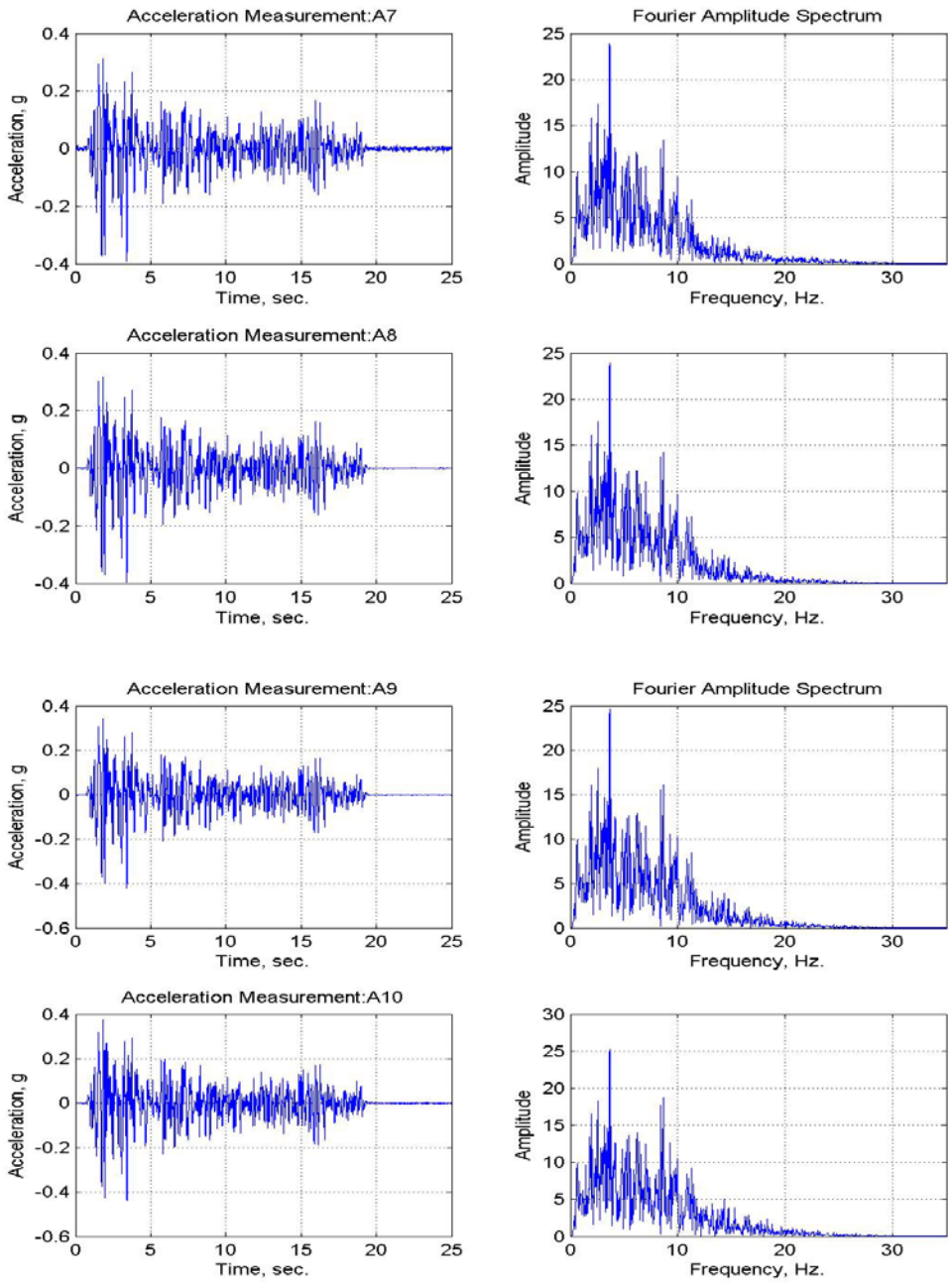


Figure A.1. Accelerations Measured for Wall Configuration 1- El Centro 100%

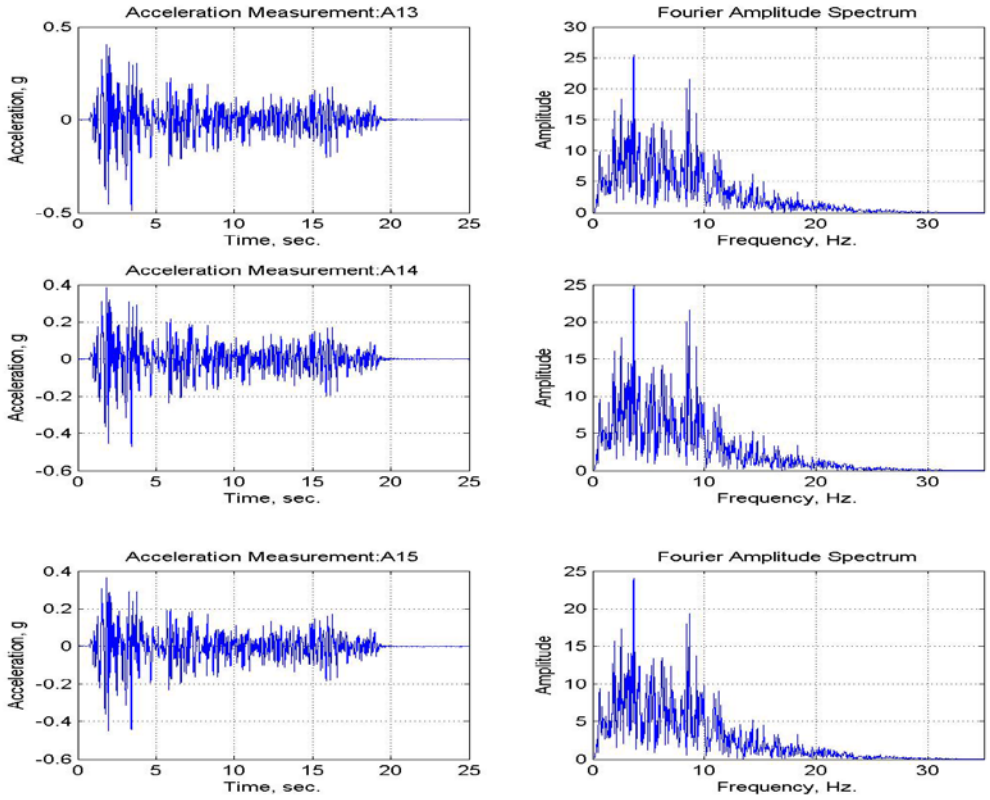


Figure A.1. Accelerations Measured for Wall Configuration 1- El Centro 100% (continued)

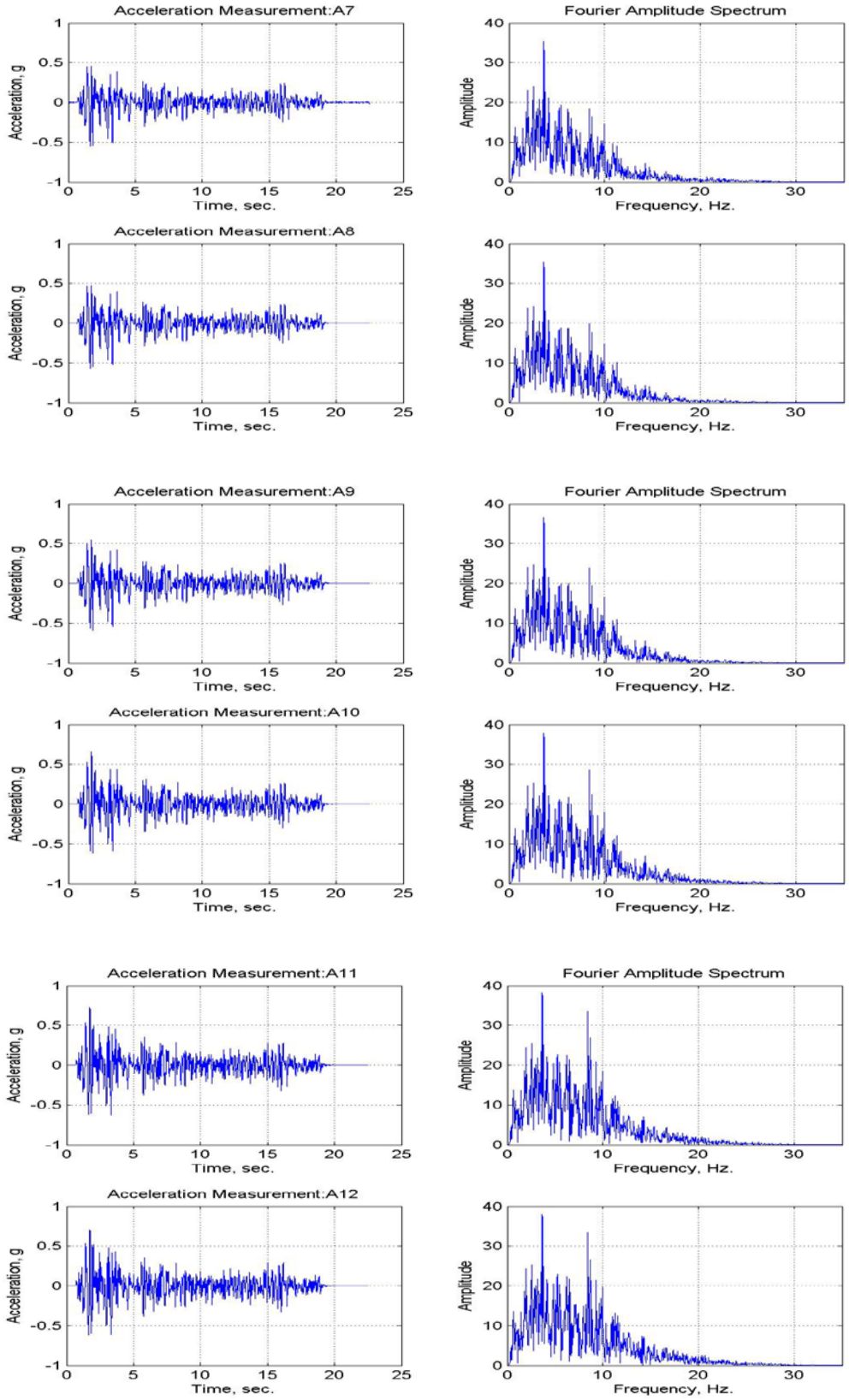


Figure A.2. Accelerations Measured for Wall Configuration 1- El Centro 150%

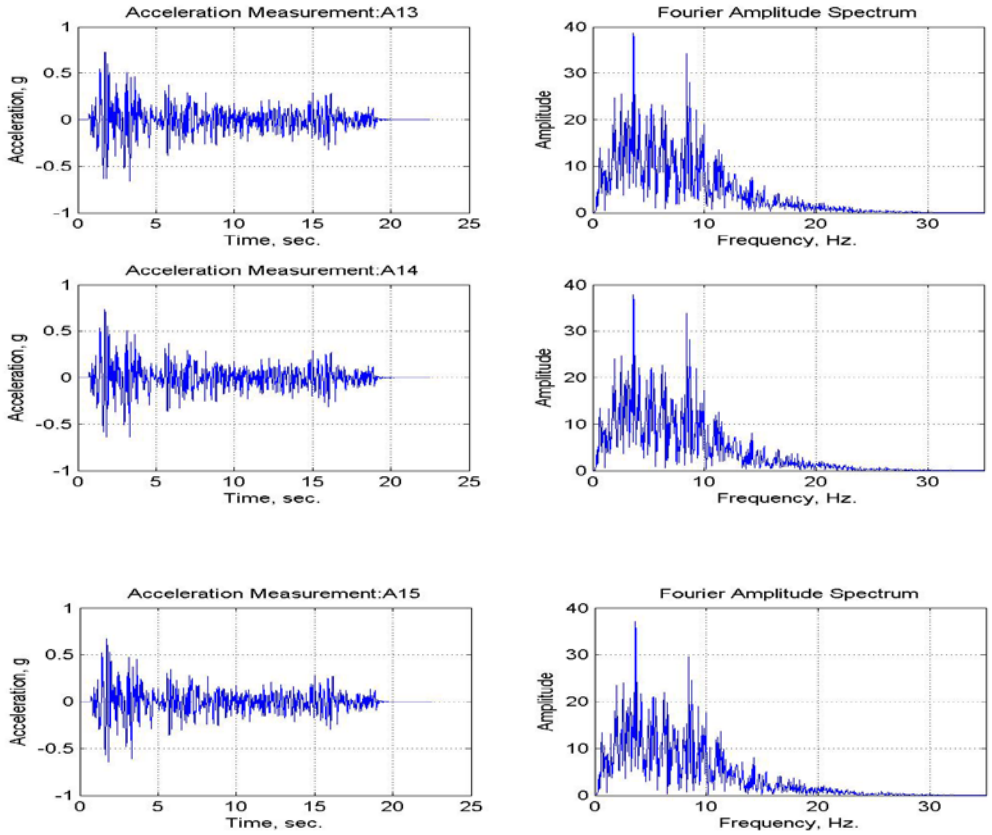


Figure A.2. Accelerations Measured for Wall Configuration 1- El Centro 150% (continued)

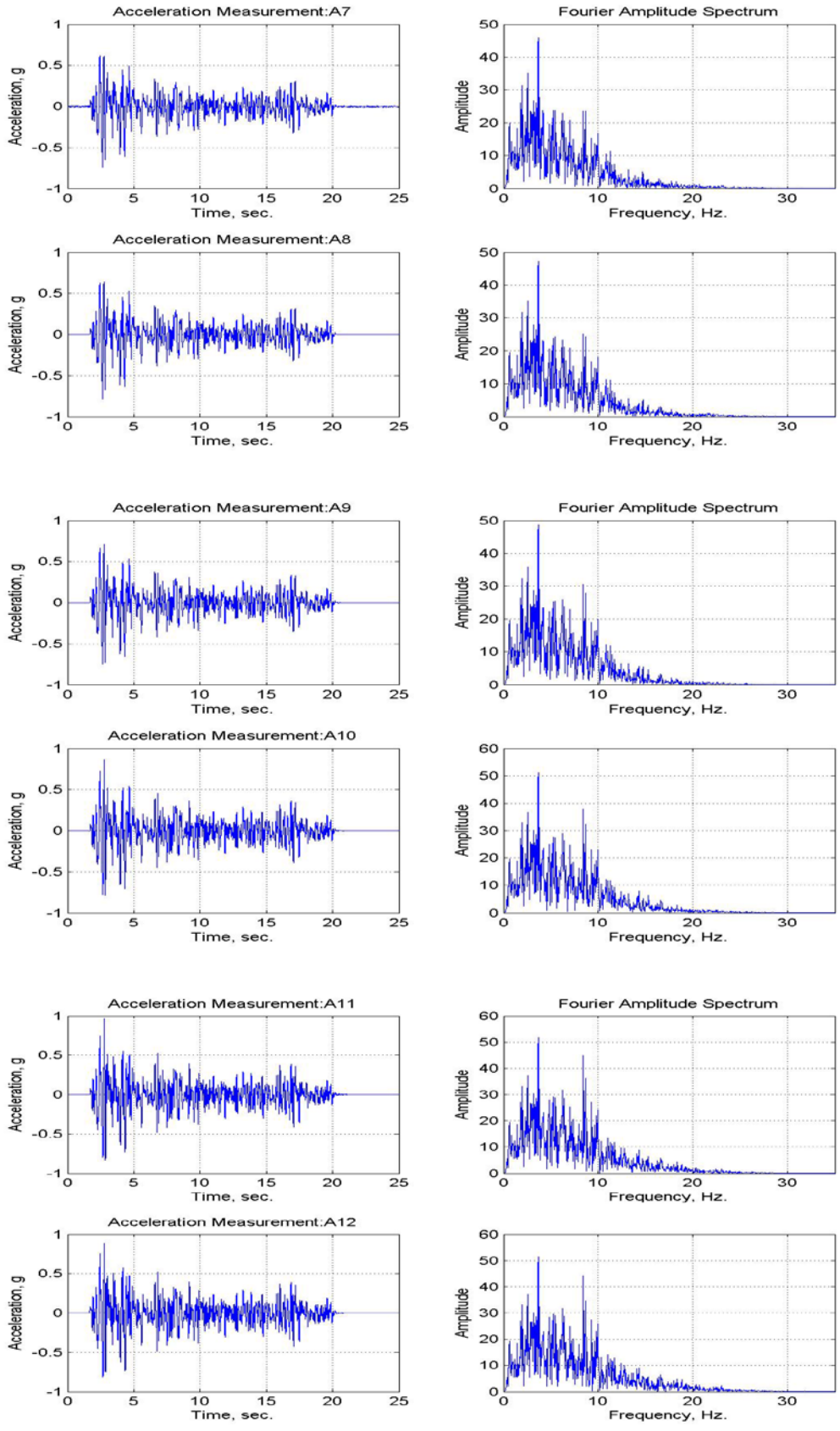


Figure A.3. Accelerations Measured for Wall Configuration 1- El Centro 200%

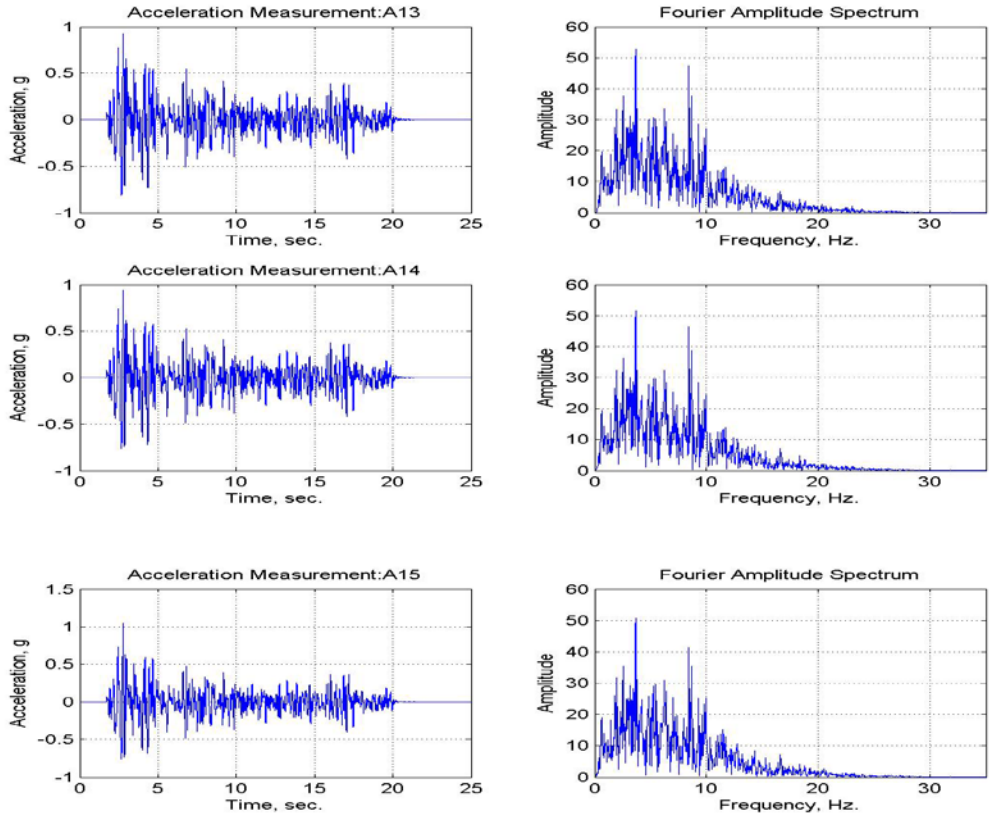


Figure A.3. Accelerations Measured for Wall Configuration 1- El Centro 200% (continued)

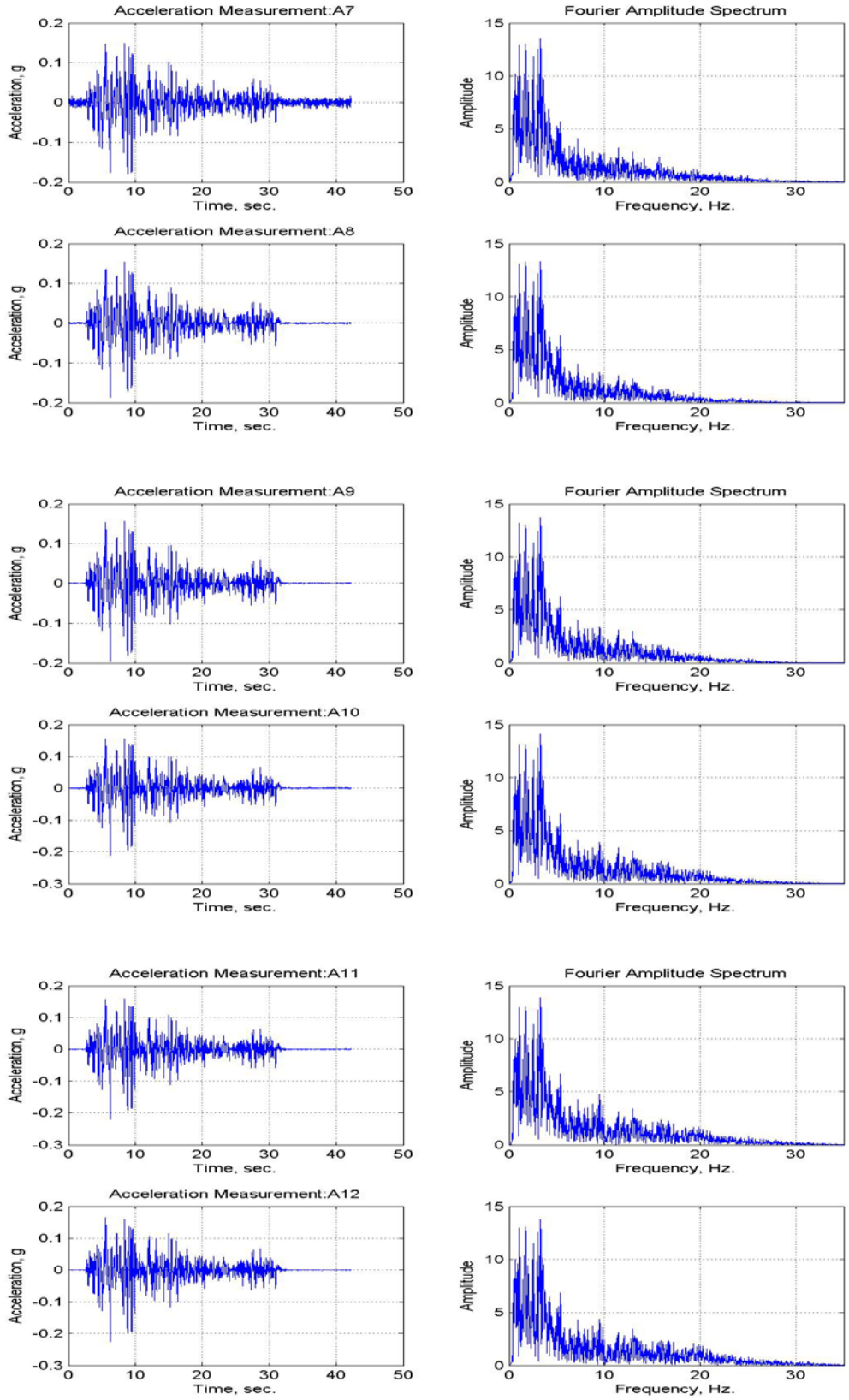


Figure A.4. Accelerations Measured for Wall Configuration 1- Izmit 100%

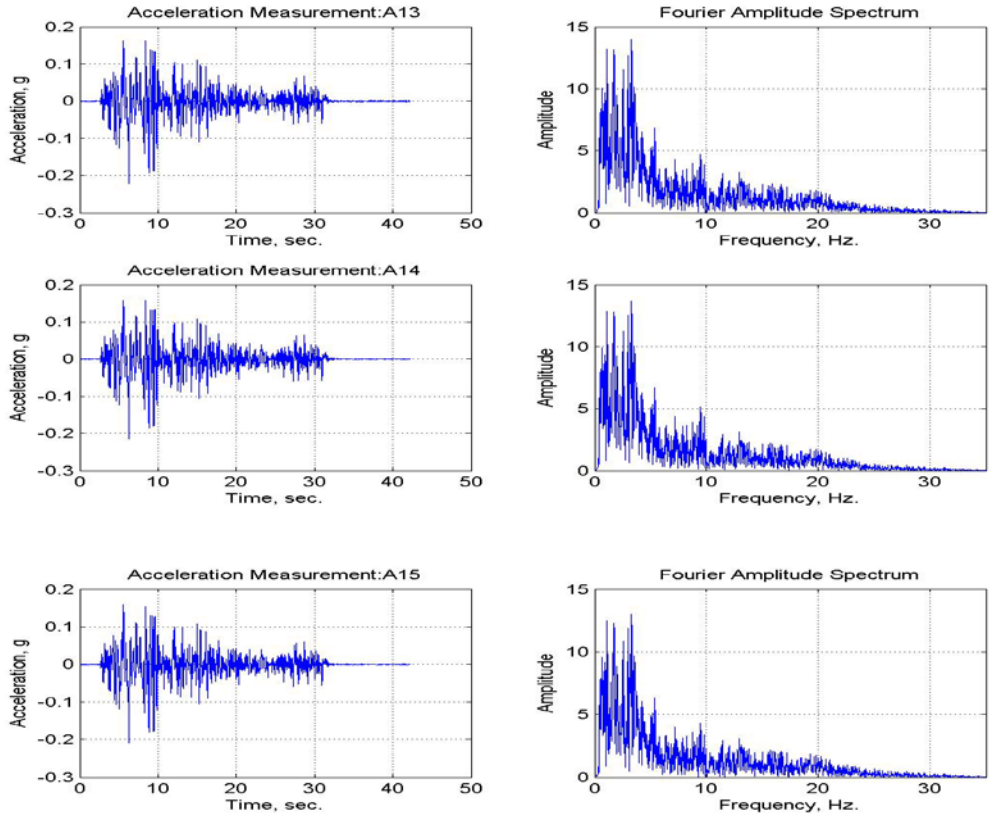


Figure A.4. Accelerations Measured for Wall Configuration 1- Izmit 100% (continued)

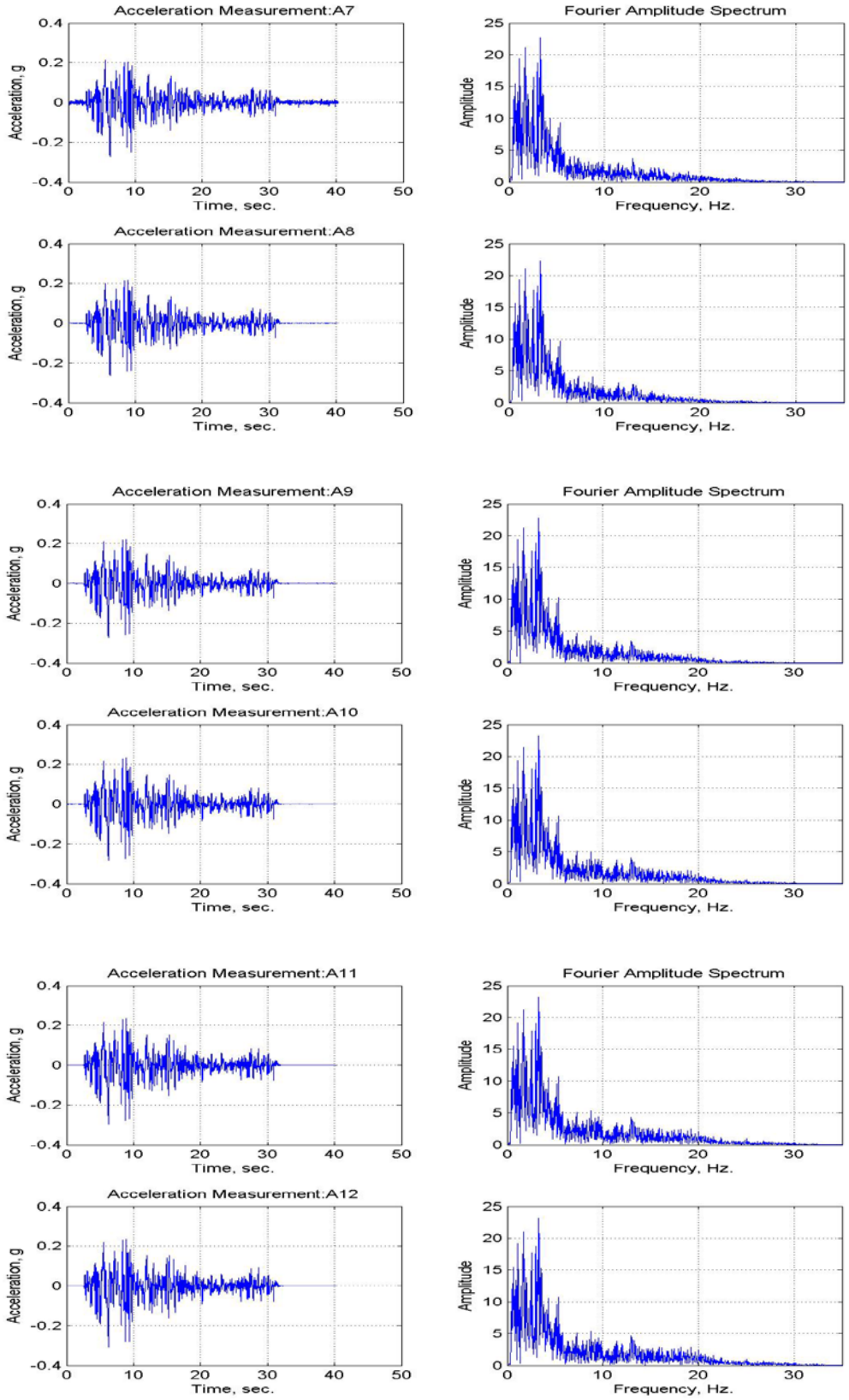
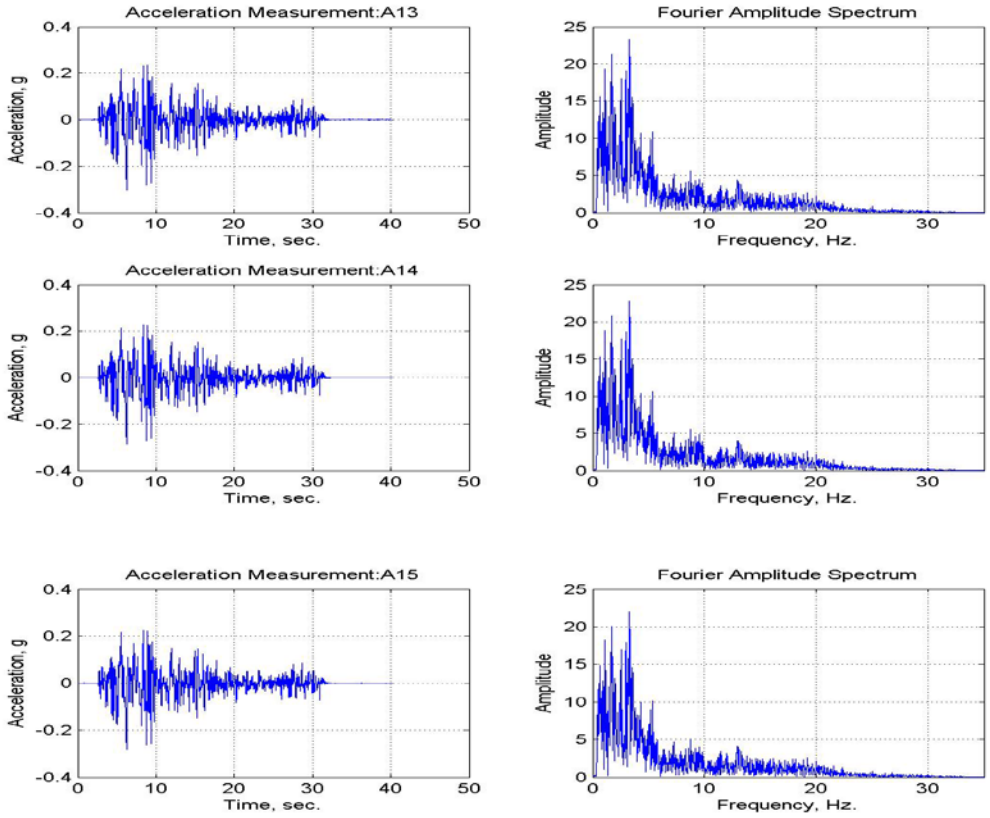


Figure A.5. Accelerations Measured for Wall Configuration 1- Izmit 150%



re A.5. Accelerations Measured for Wall Configuration 1- Izmit 150% (continued)

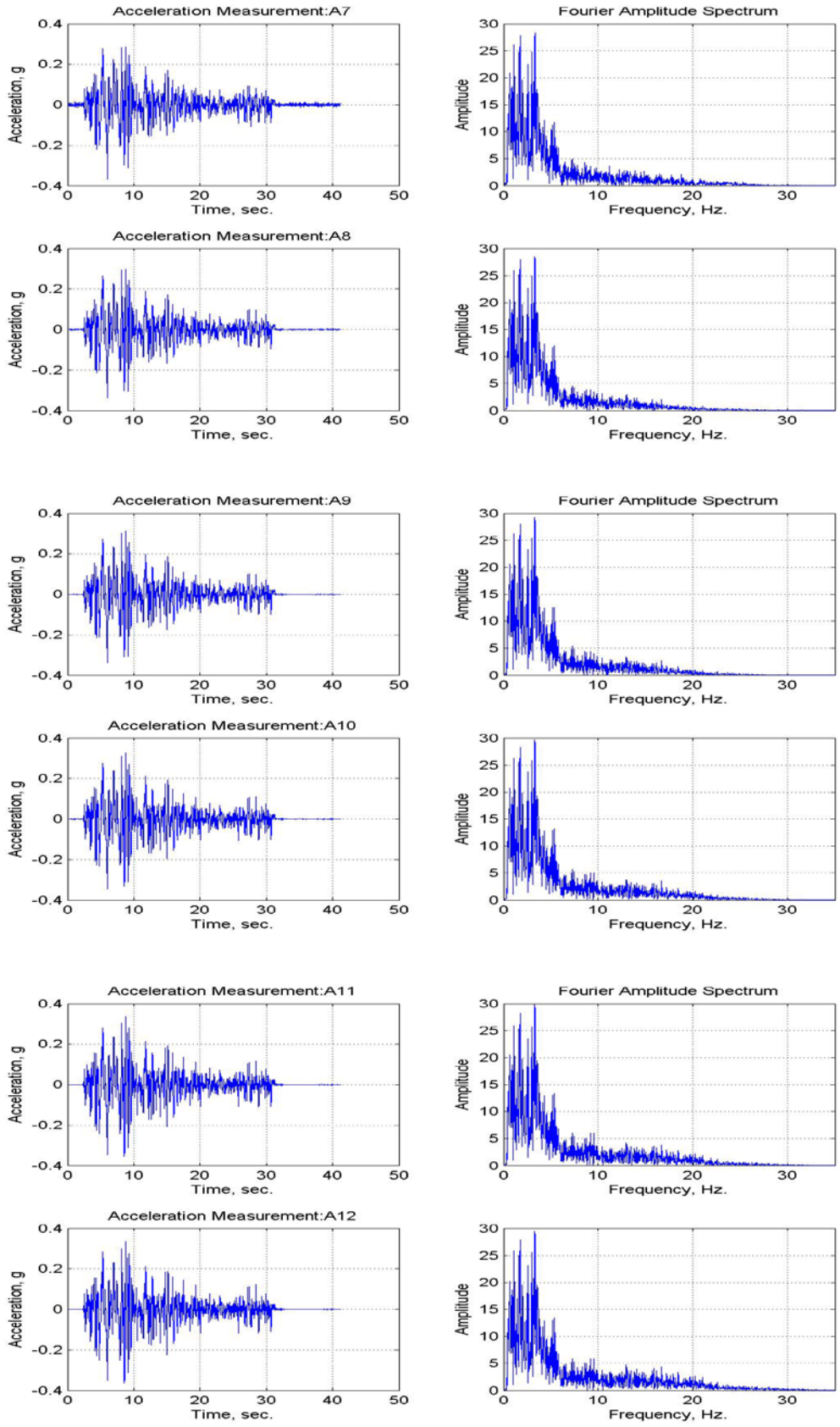


Figure A.6. Accelerations Measured for Wall Configuration 1- Izmit 200%

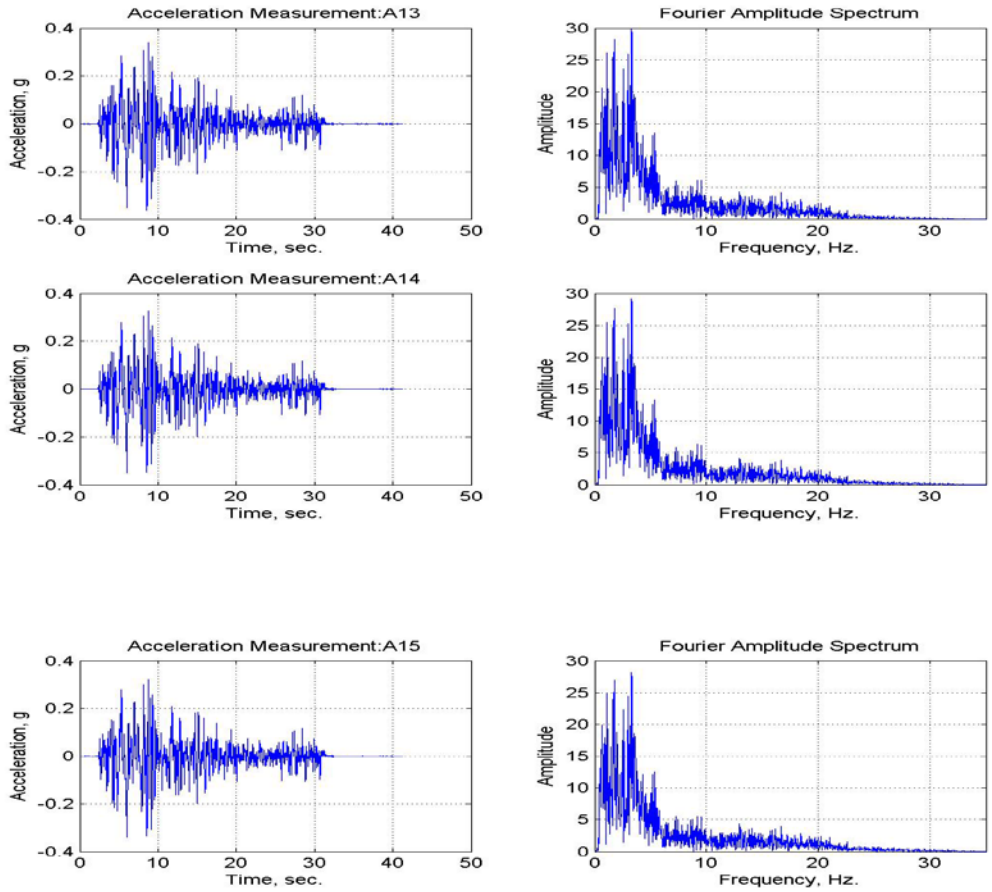


Figure A.6. Accelerations Measured for Wall Configuration 1- Izmit 200% (continued)

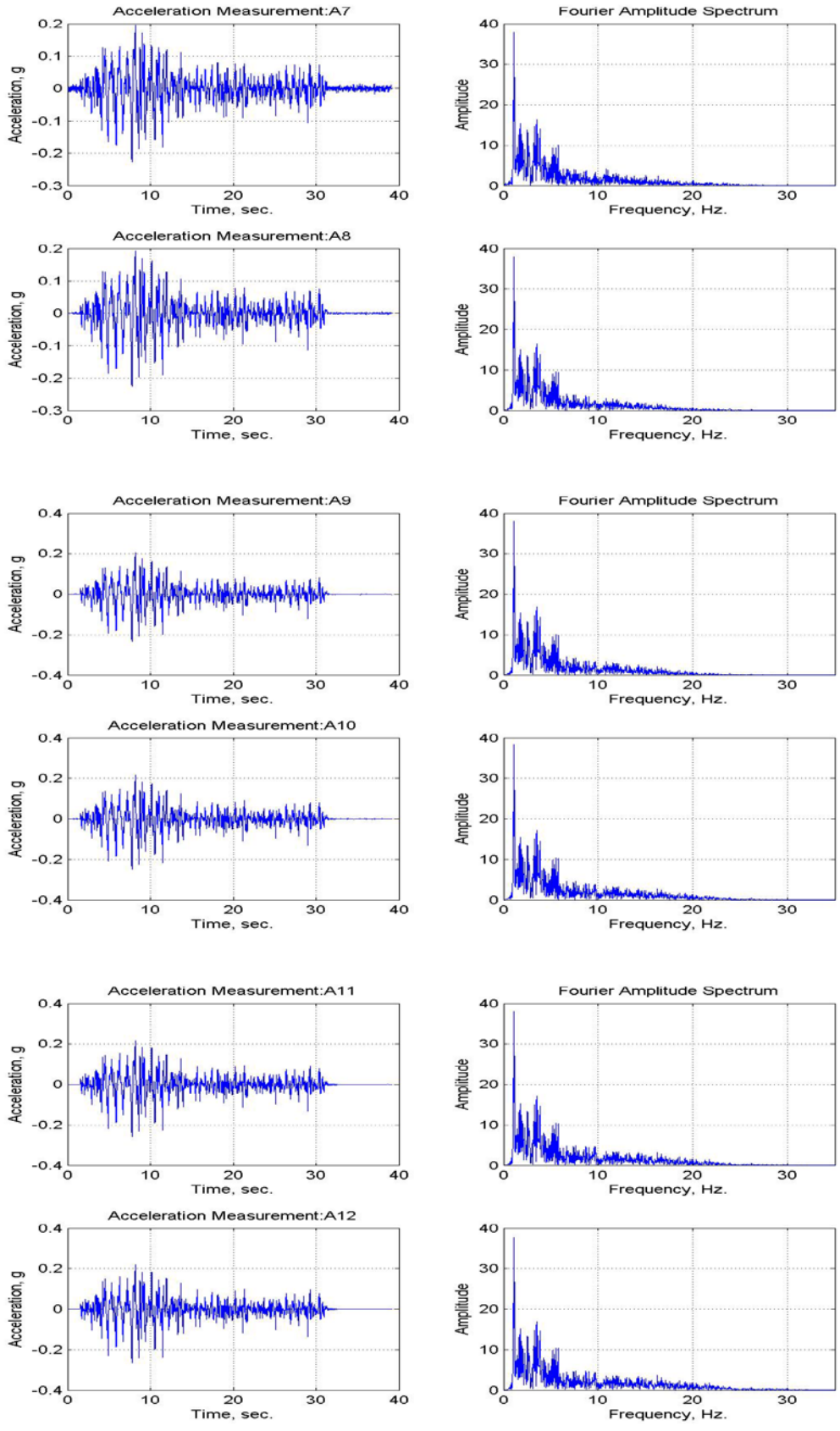


Figure A.7. Accelerations Measured for Wall Configuration 1- Sakarya 100%

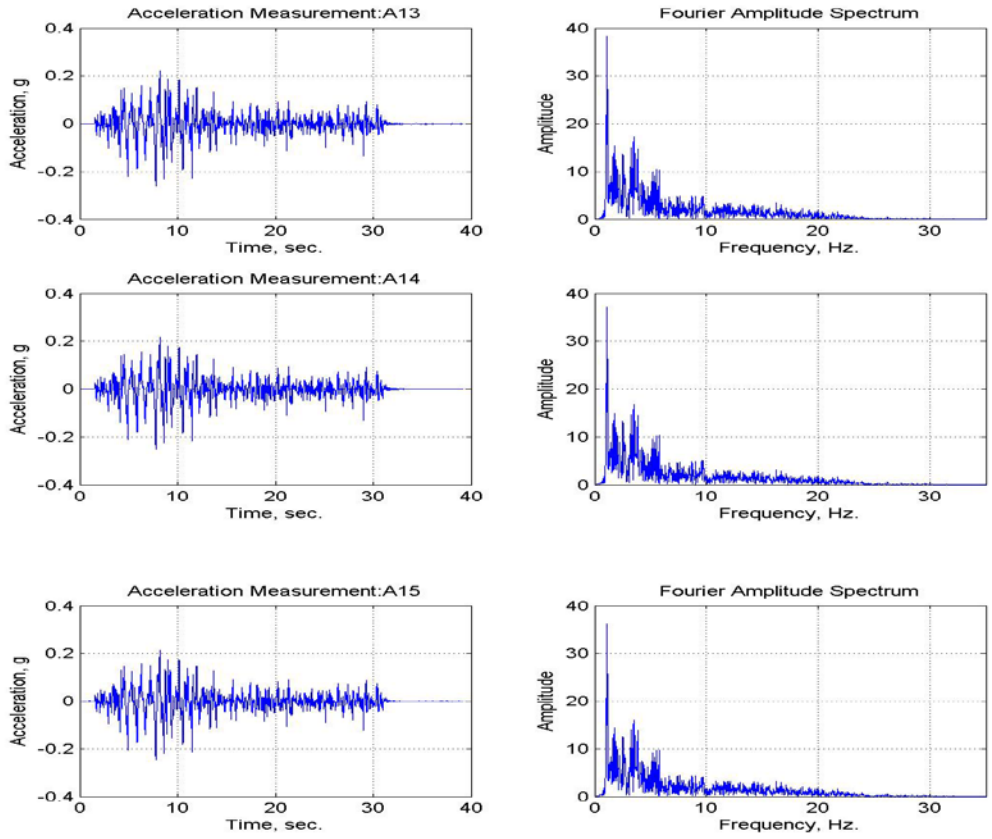


Figure A.7. Accelerations Measured for Wall Configuration 1- Sakarya 100% (continued)

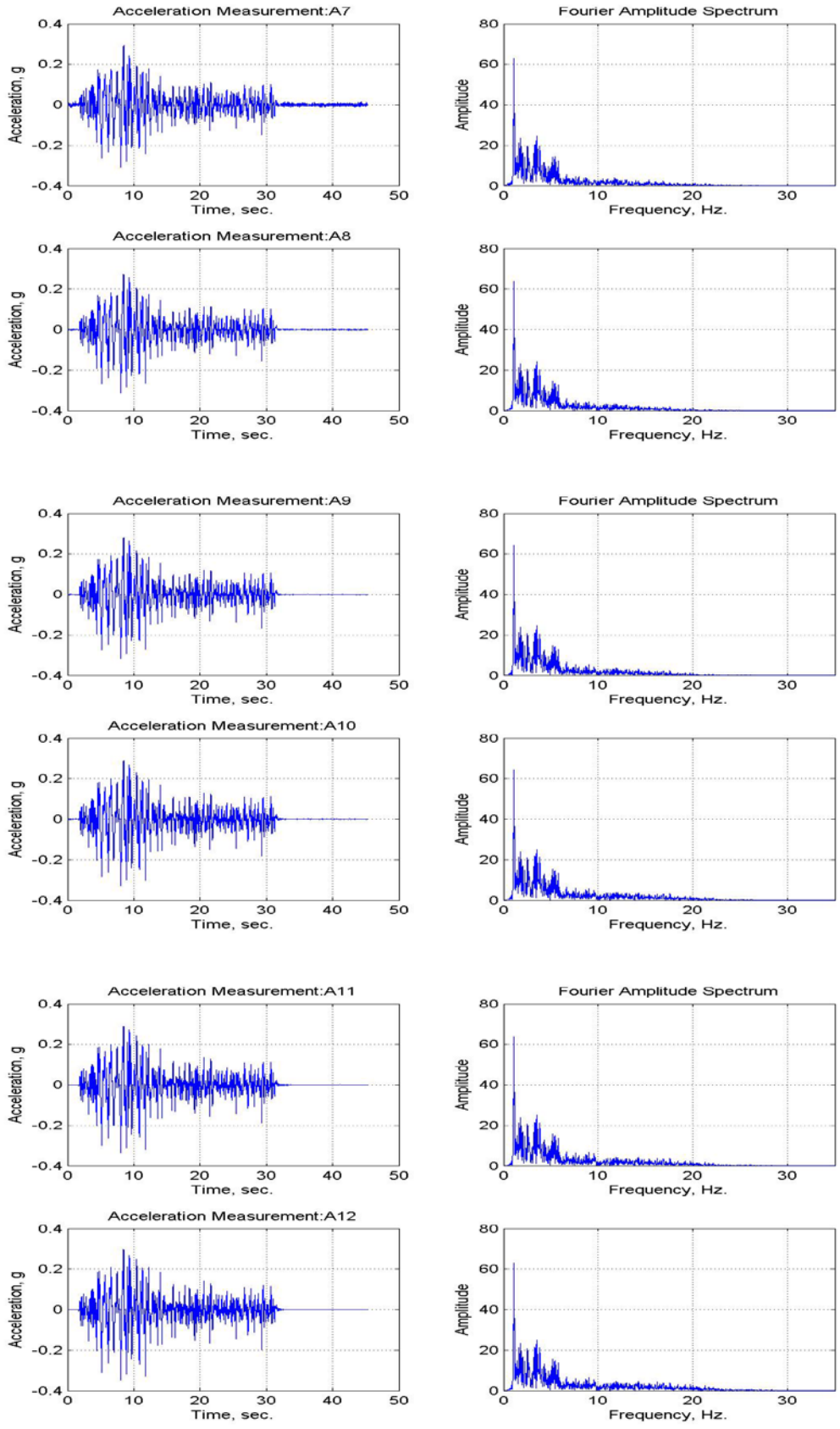


Figure A.8. Accelerations Measured for Wall Configuration 1- Sakarya 150%

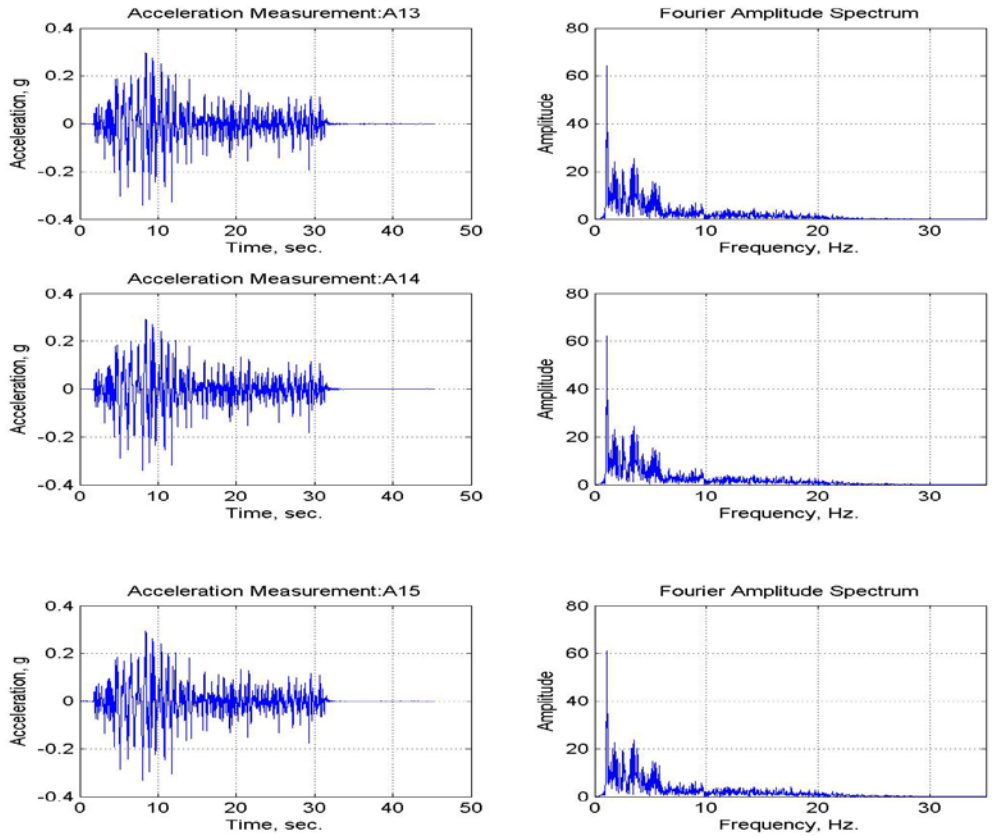


Figure A.8. Accelerations Measured for Wall Configuration 1- Sakarya 150% (continued)

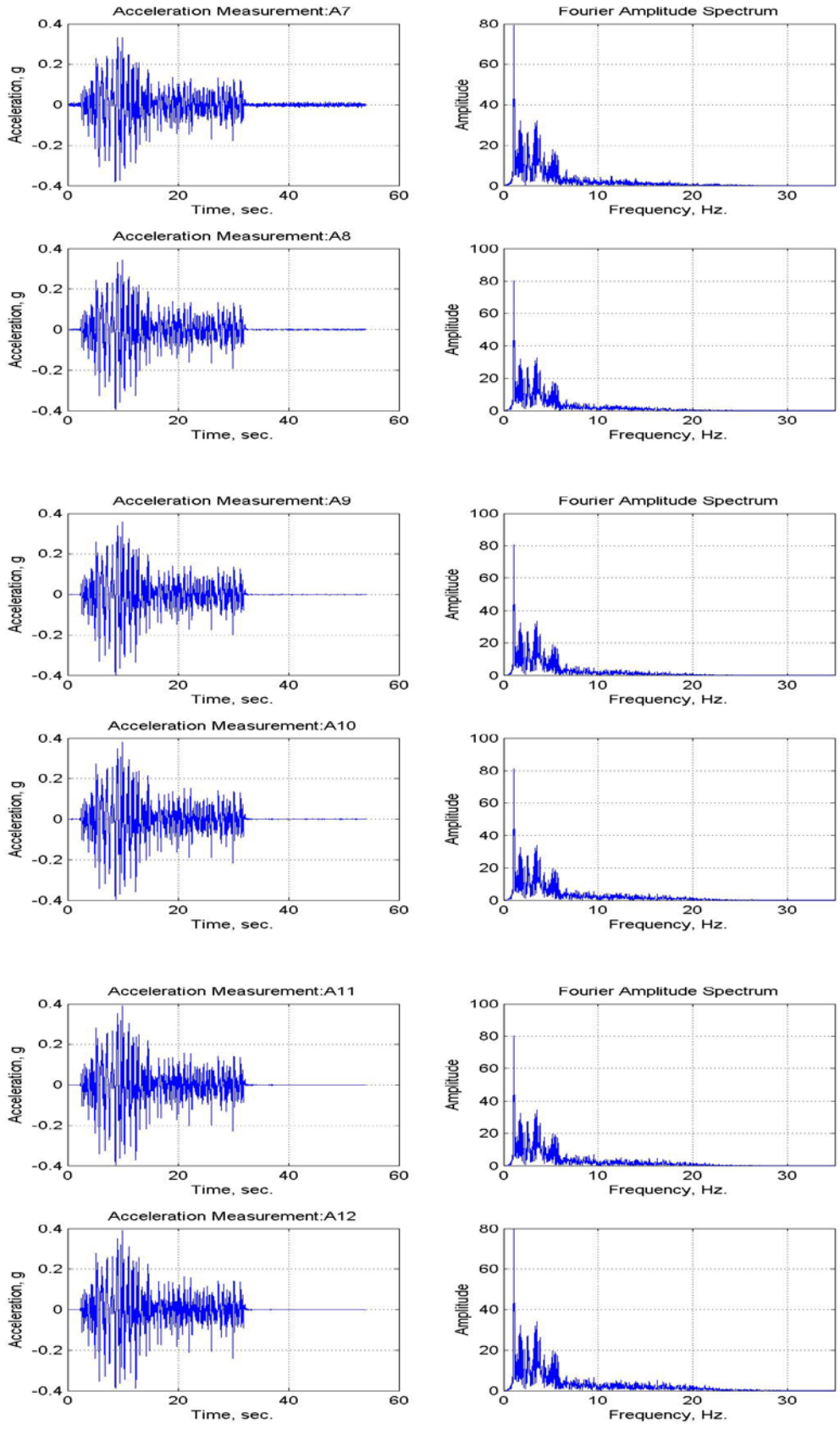


Figure A.9. Accelerations Measured for Wall Configuration 1- Sakarya 200%

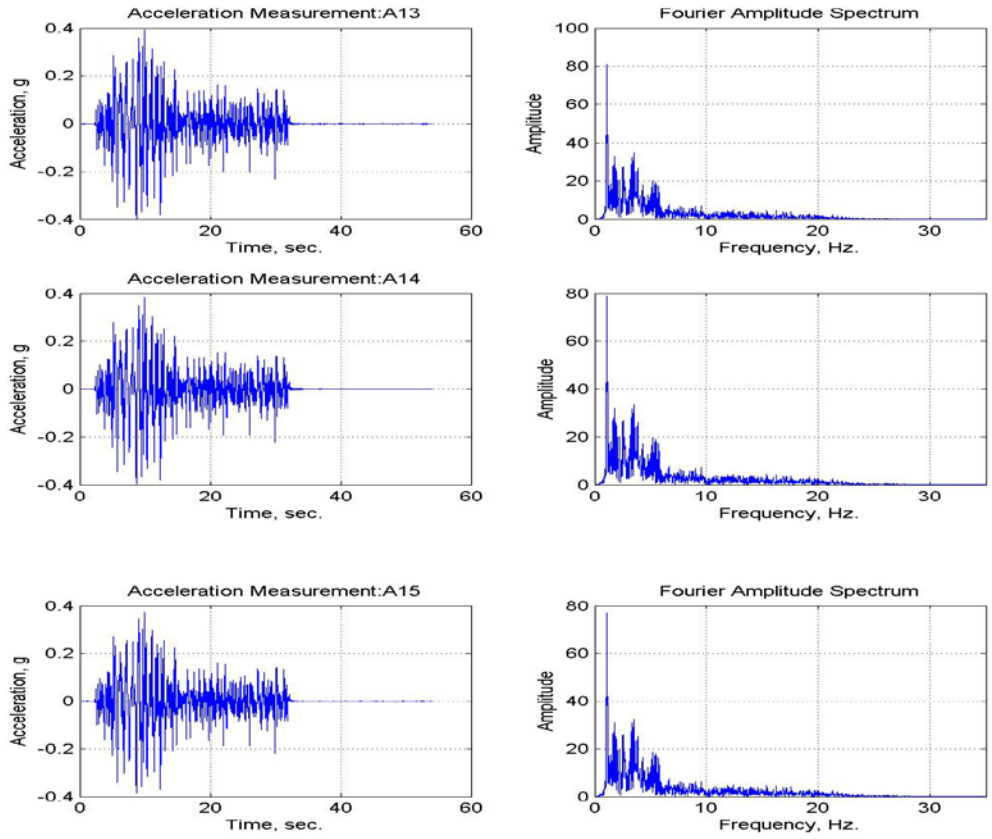


Figure A.9. Accelerations Measured for Wall Configuration 1- Sakarya 200% (continued)

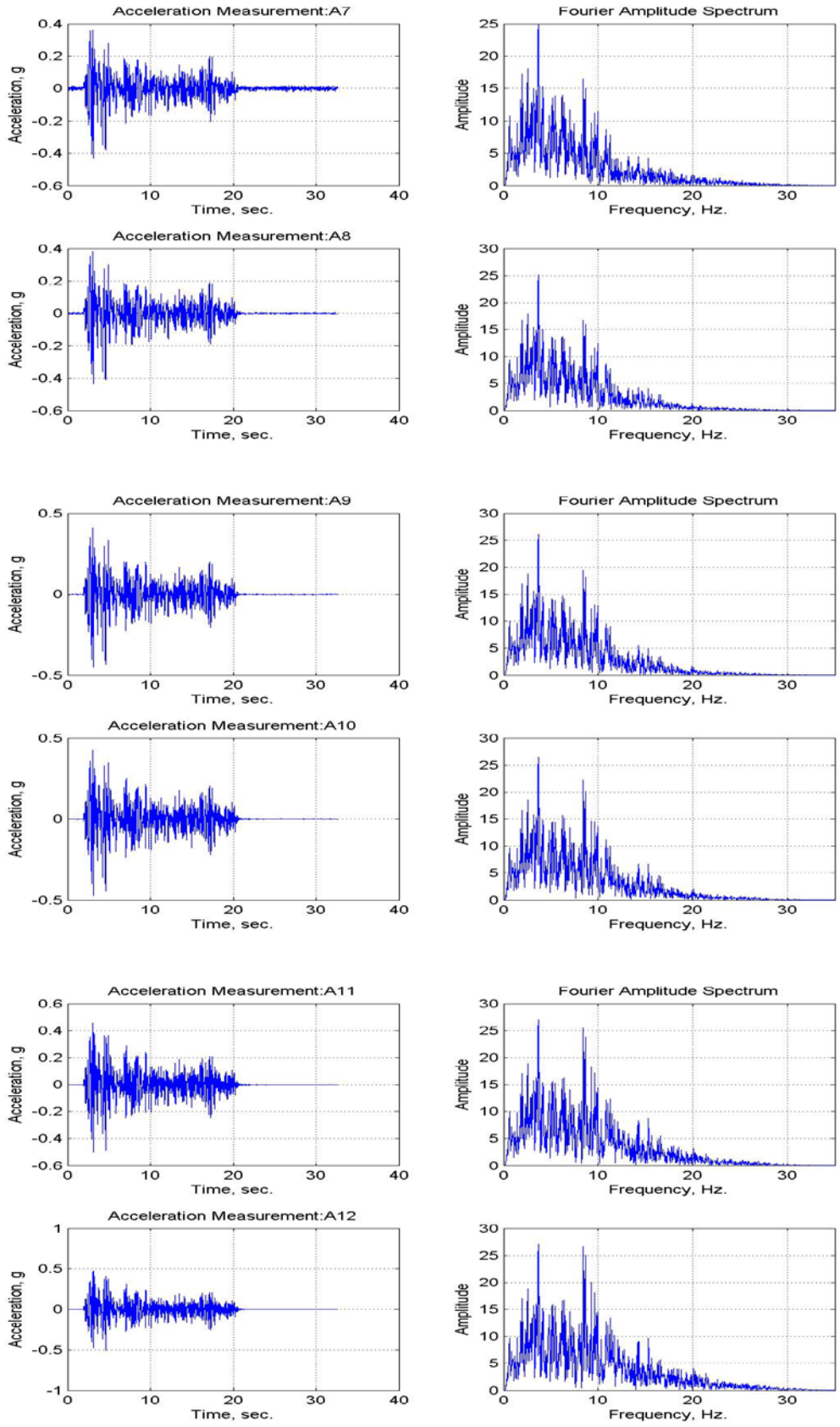


Figure A.10. Accelerations Measured for Wall Configuration 2- El Centro 100%

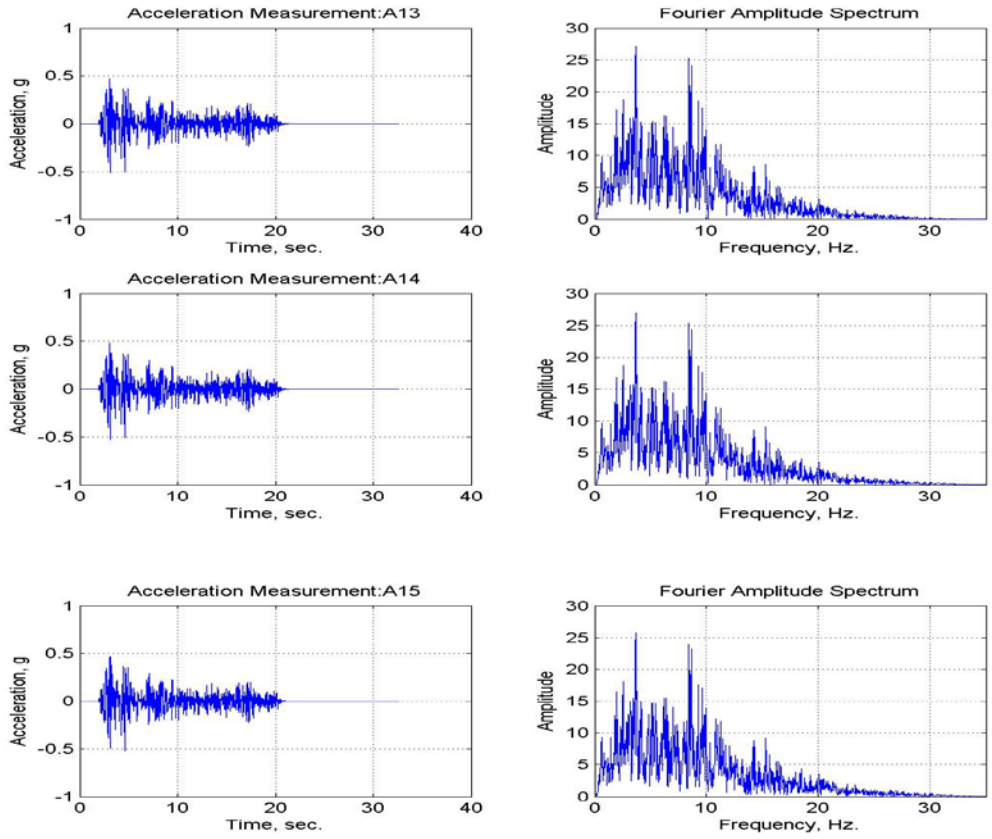


Figure A.10. Accelerations Measured for Wall Configuration 2- El Centro 100% (continued)

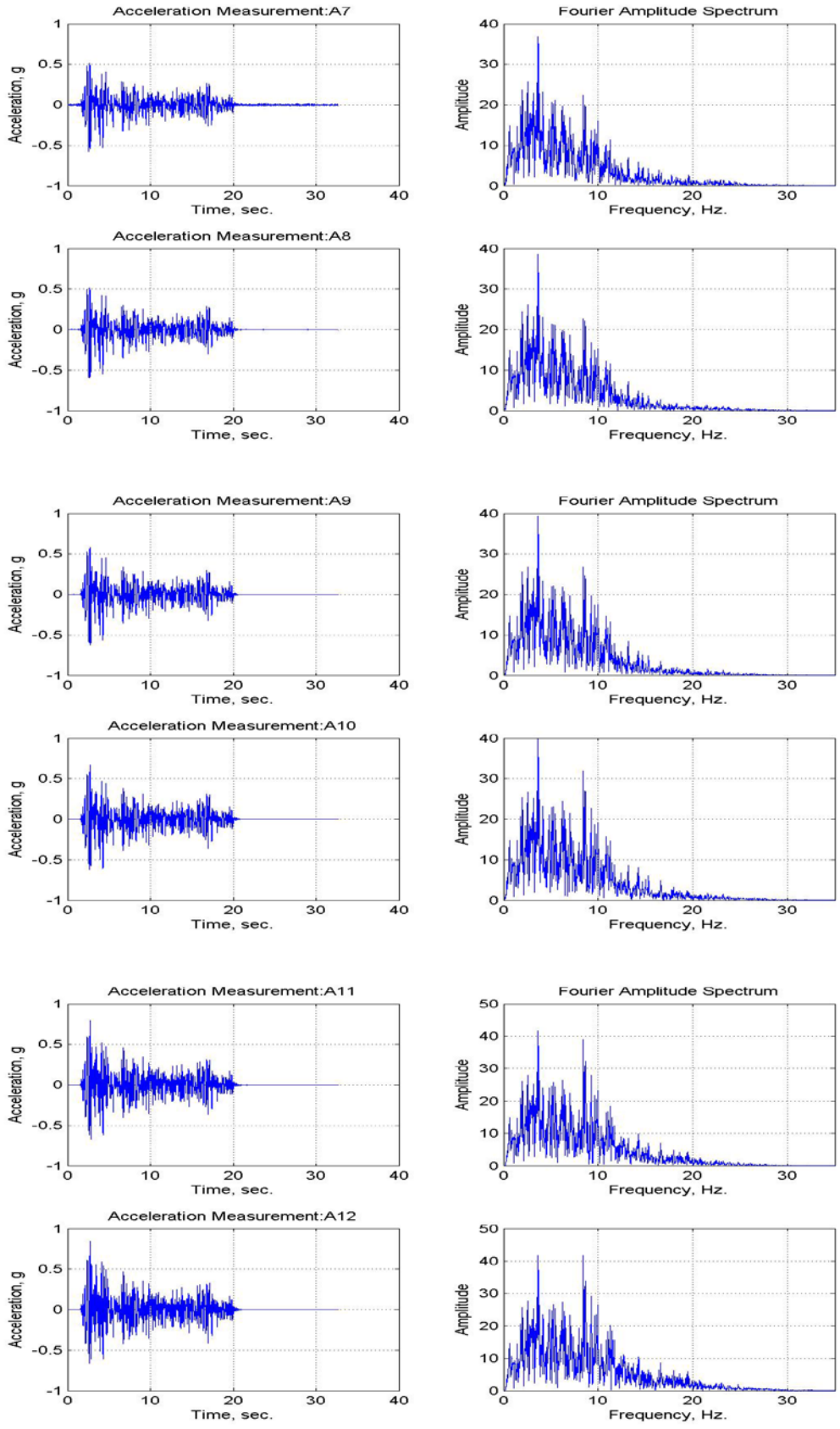


Figure A.11. Accelerations Measured for Wall Configuration 2- El Centro 150%

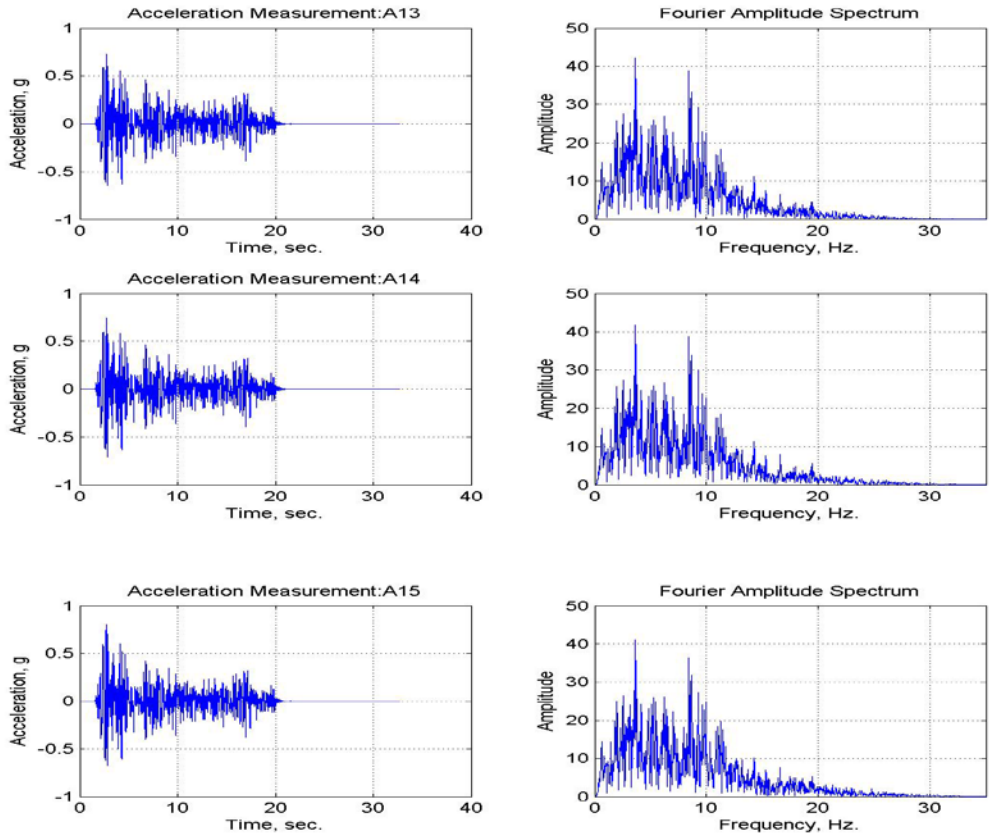


Figure A.11. Accelerations Measured for Wall Configuration 2- El Centro 150% (continued)

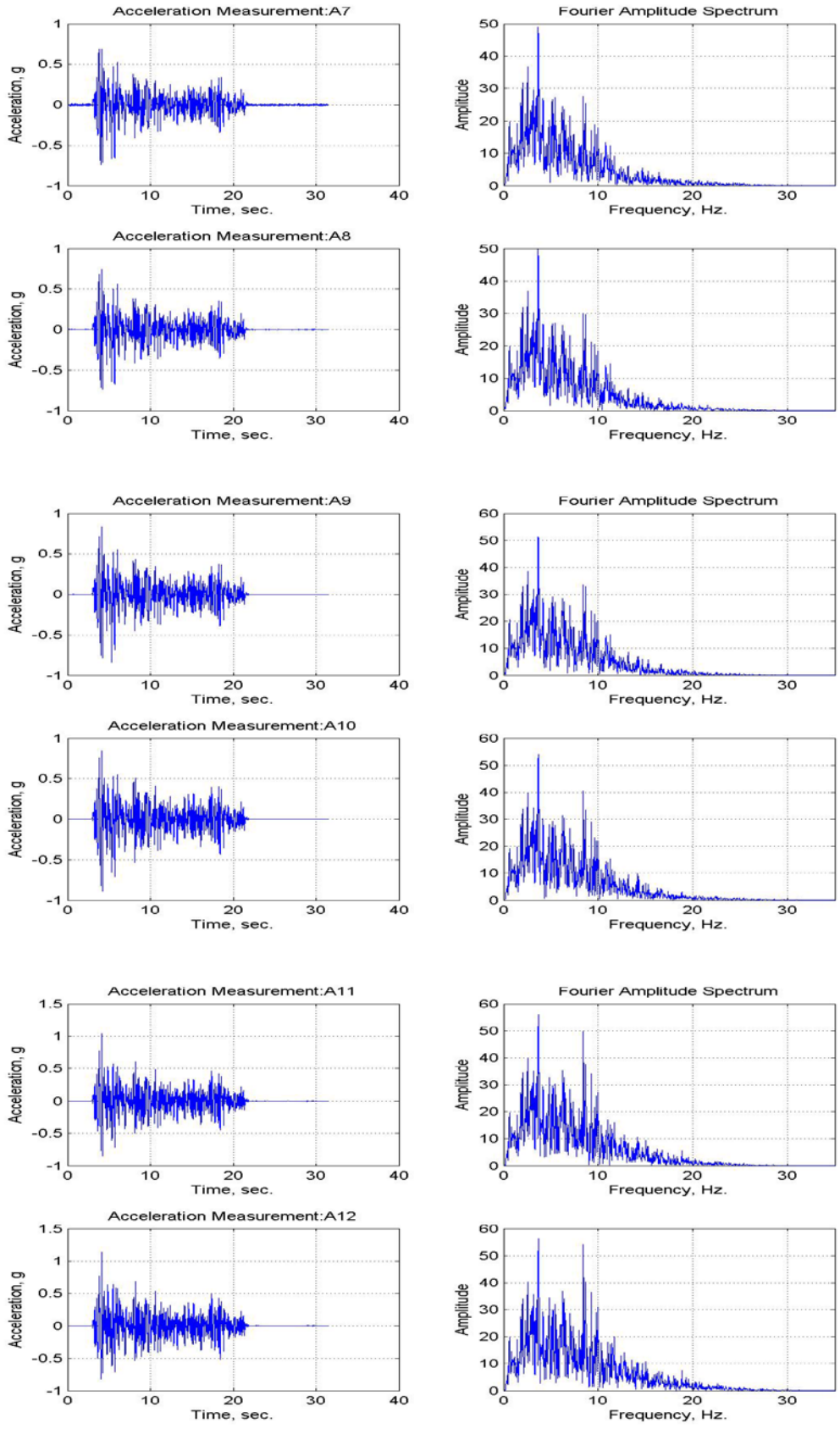


Figure A.12. Accelerations Measured for Wall Configuration 2- El Centro 200%

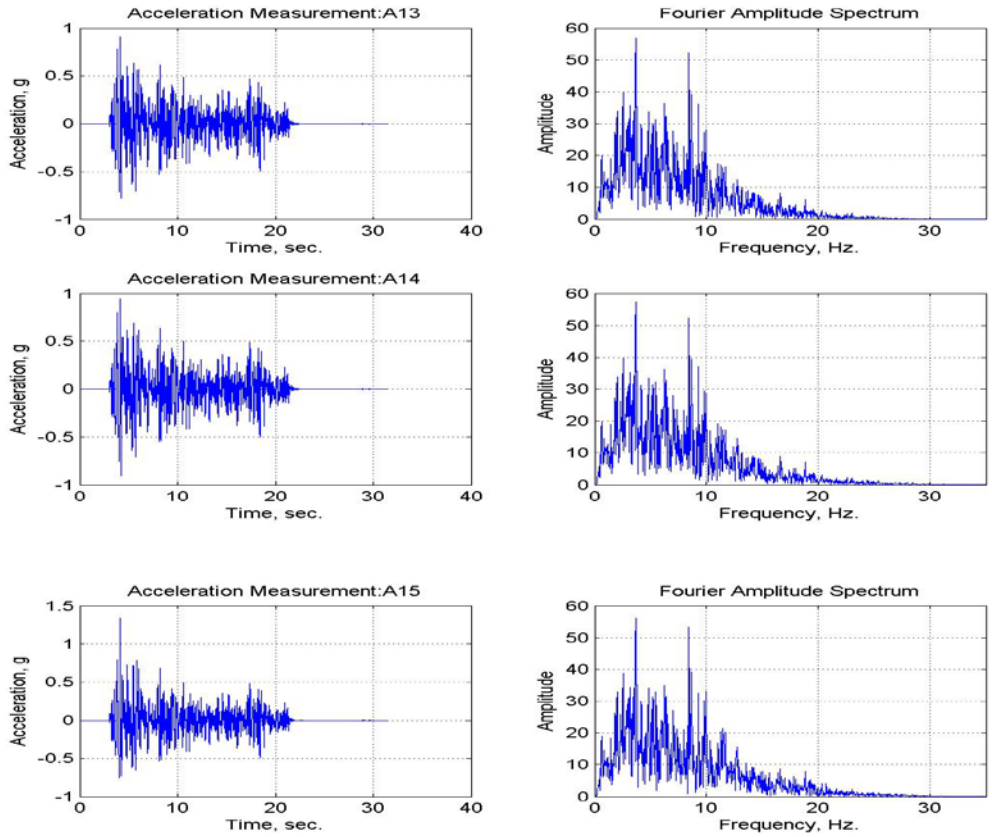


Figure A.12. Accelerations Measured for Wall Configuration 2- El Centro 200% (continued)

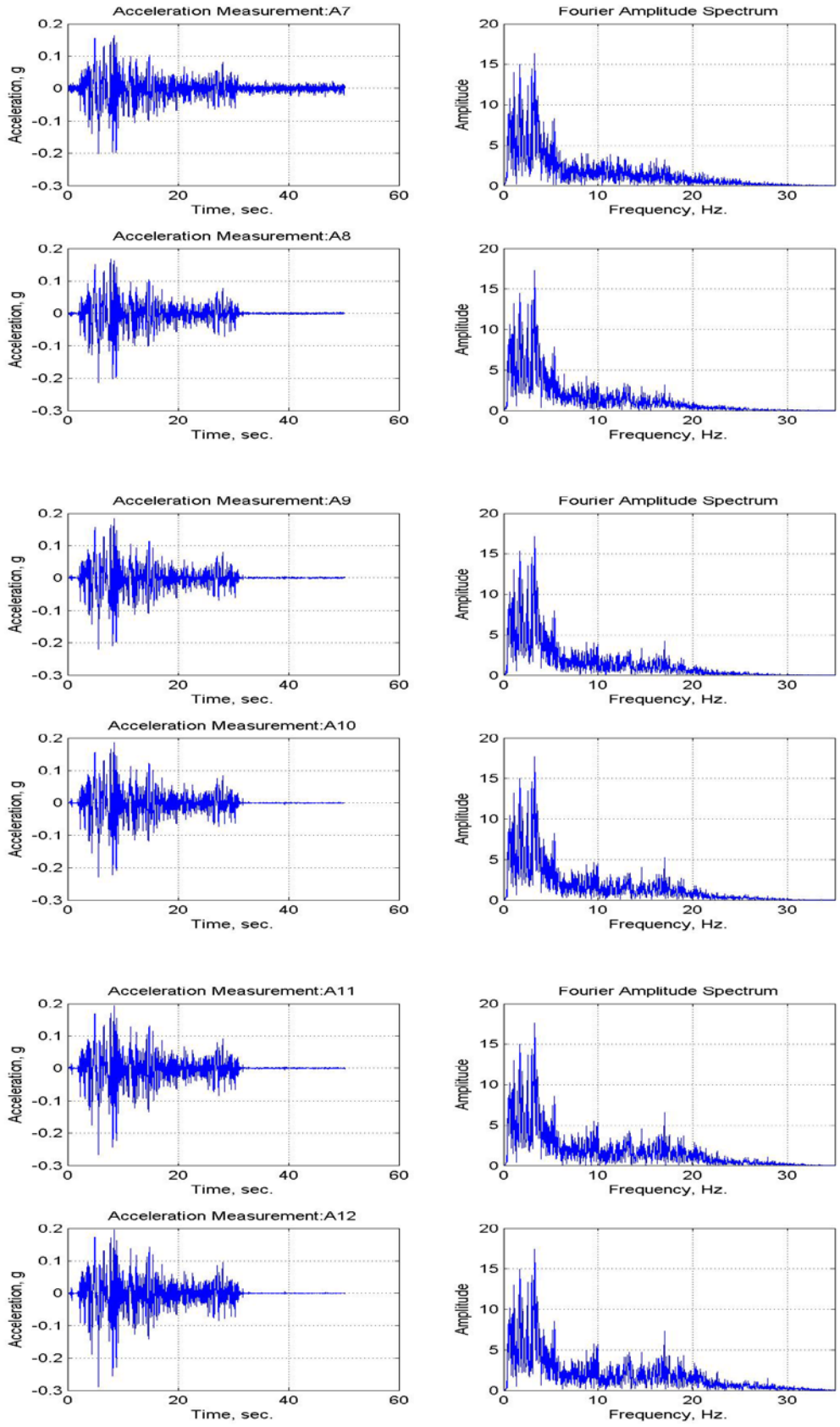


Figure A.13. Accelerations Measured for Wall Configuration 2- Izmit 100%

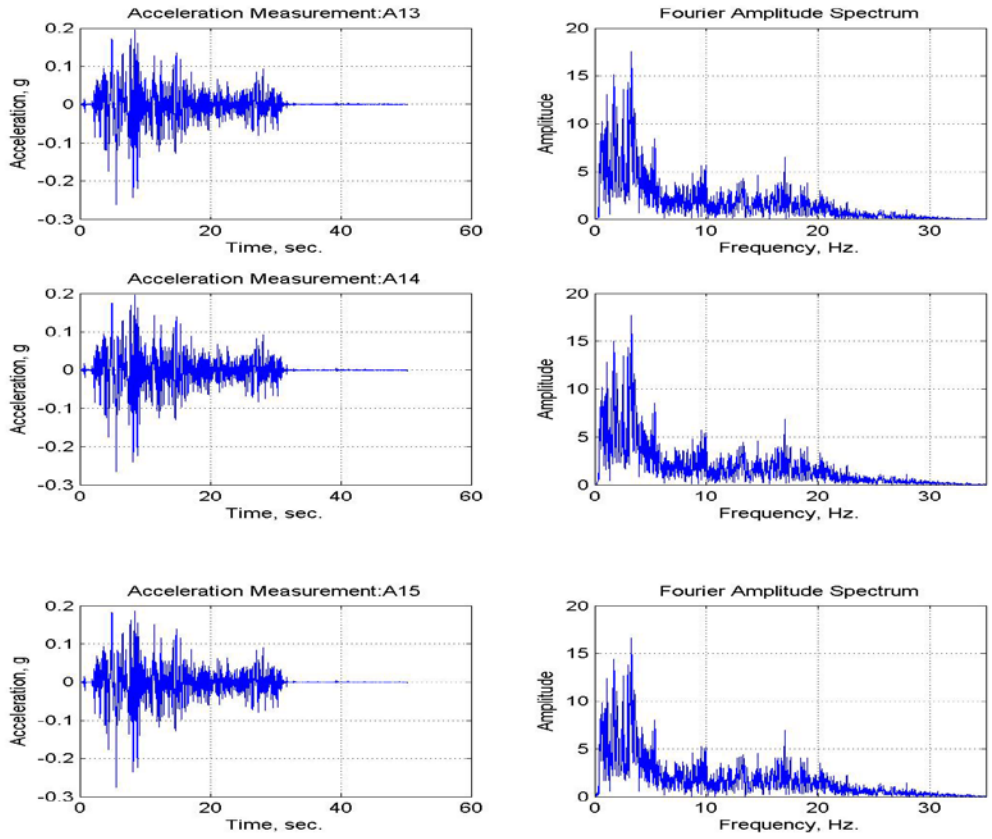


Figure A.13. Accelerations Measured for Wall Configuration 2- Izmit 100% (continued)

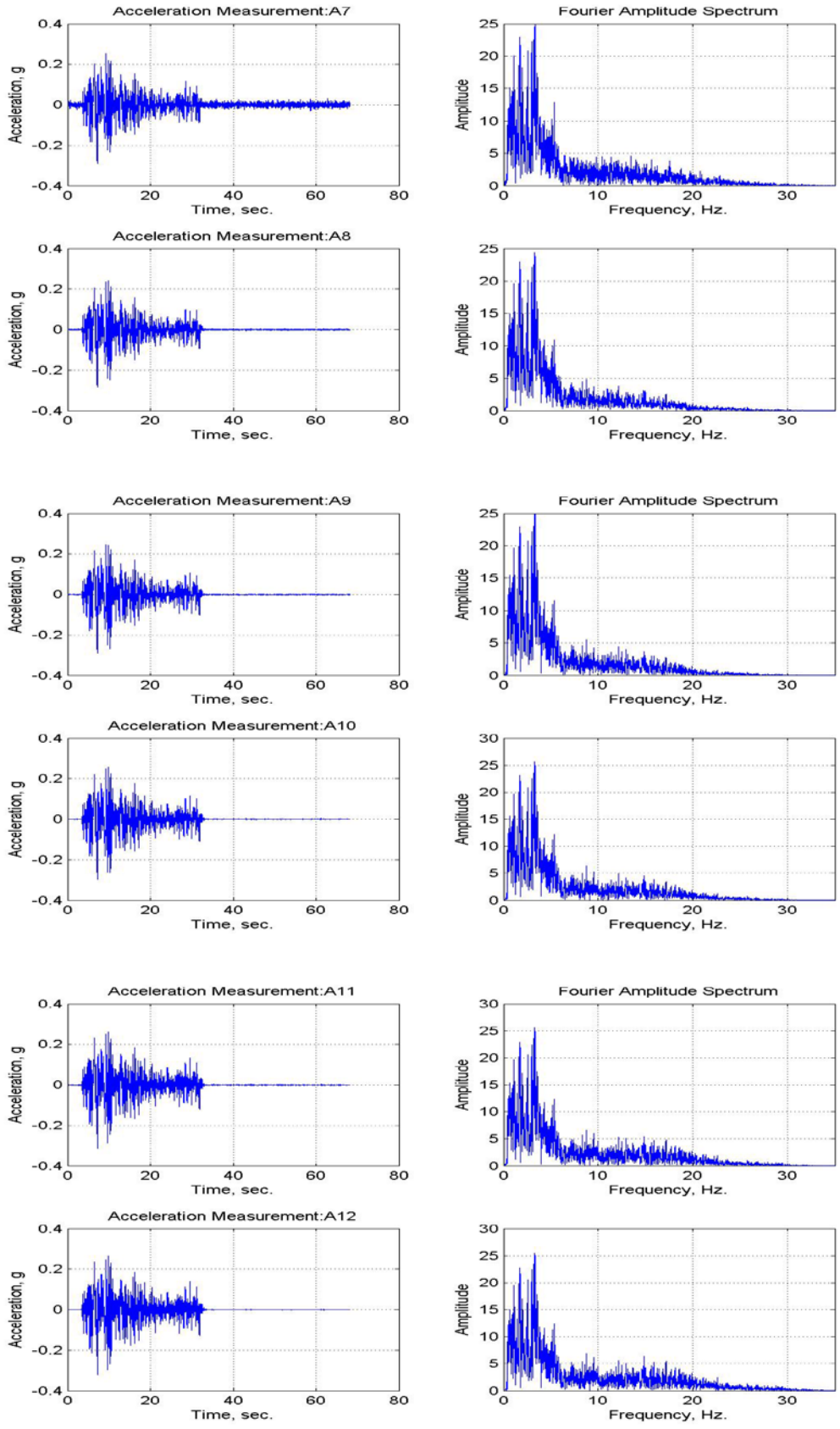


Figure A.14. Accelerations Measured for Wall Configuration 2- Izmit 150%

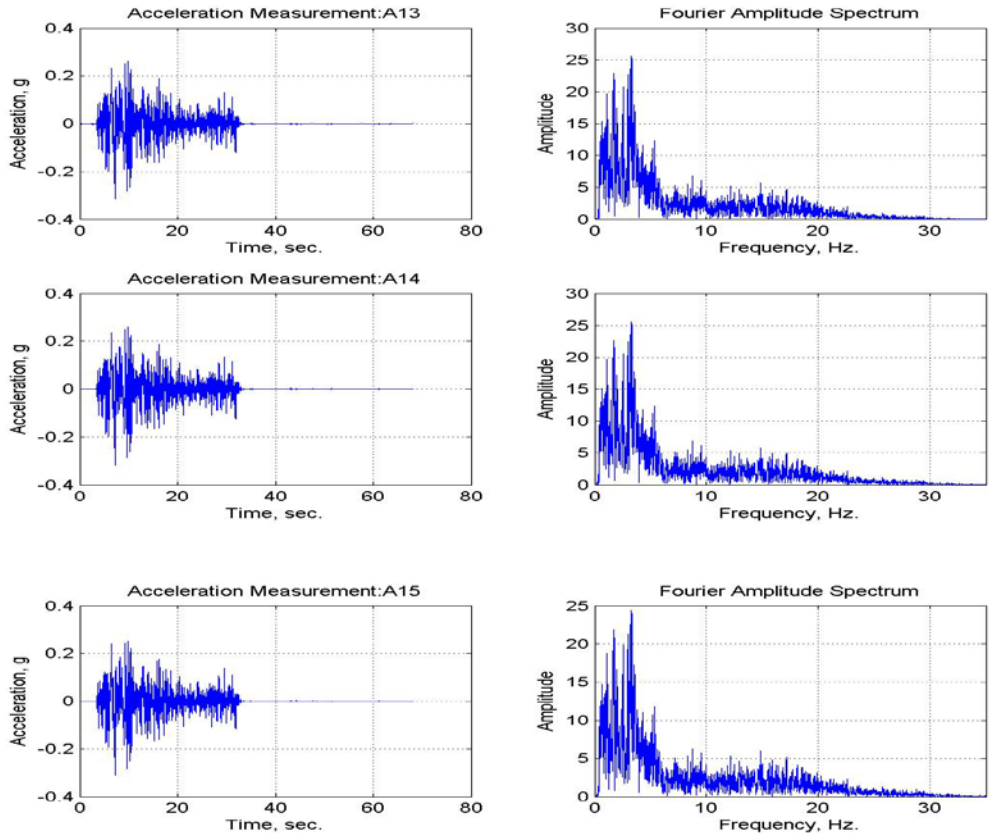


Figure A.14. Accelerations Measured for Wall Configuration 2- Izmit 150% (continued)

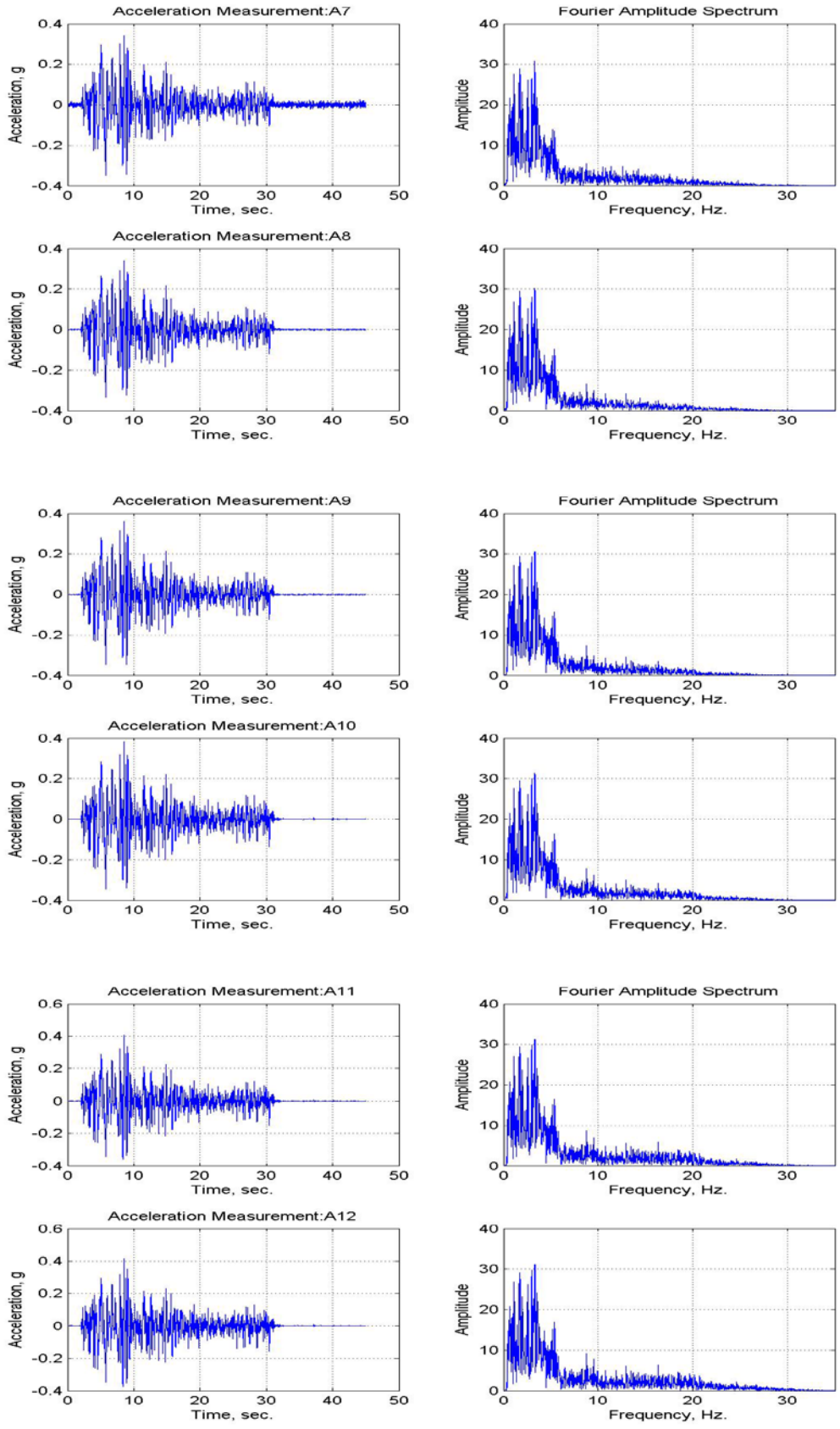


Figure A.15. Accelerations Measured for Wall Configuration 2- Izmit 200%

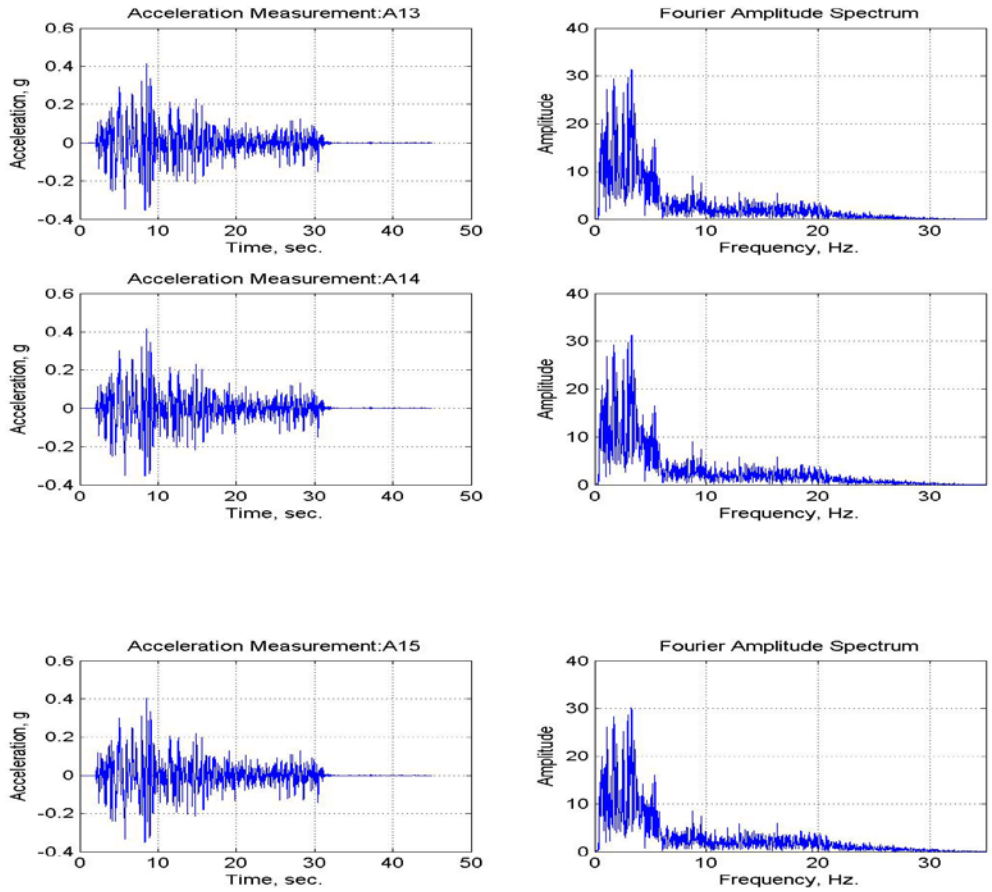


Figure A.15. Accelerations Measured for Wall Configuration 2- Izmit 200% (continued)

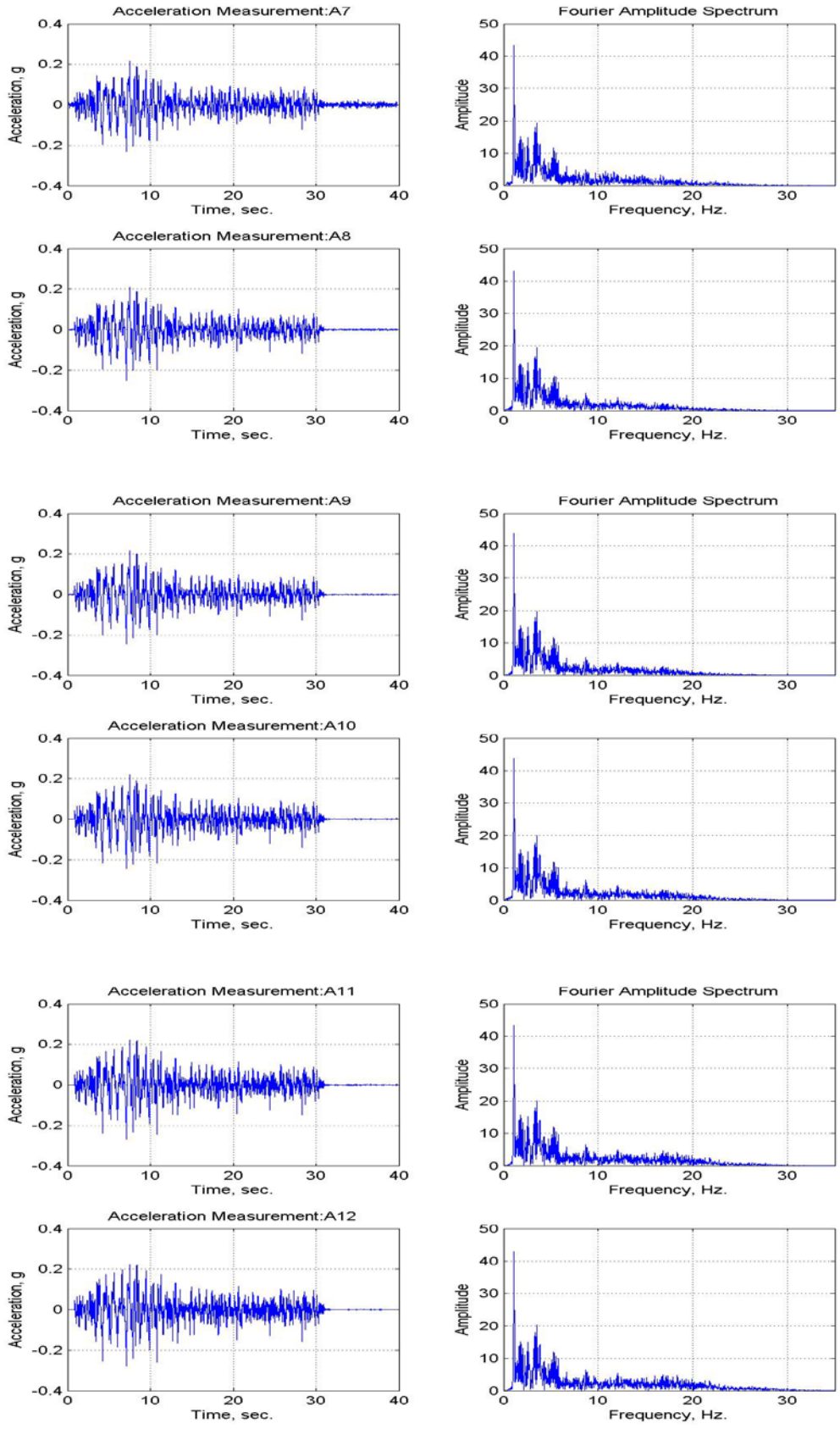


Figure A.16. Accelerations Measured for Wall Configuration 2- Sakarya 100%

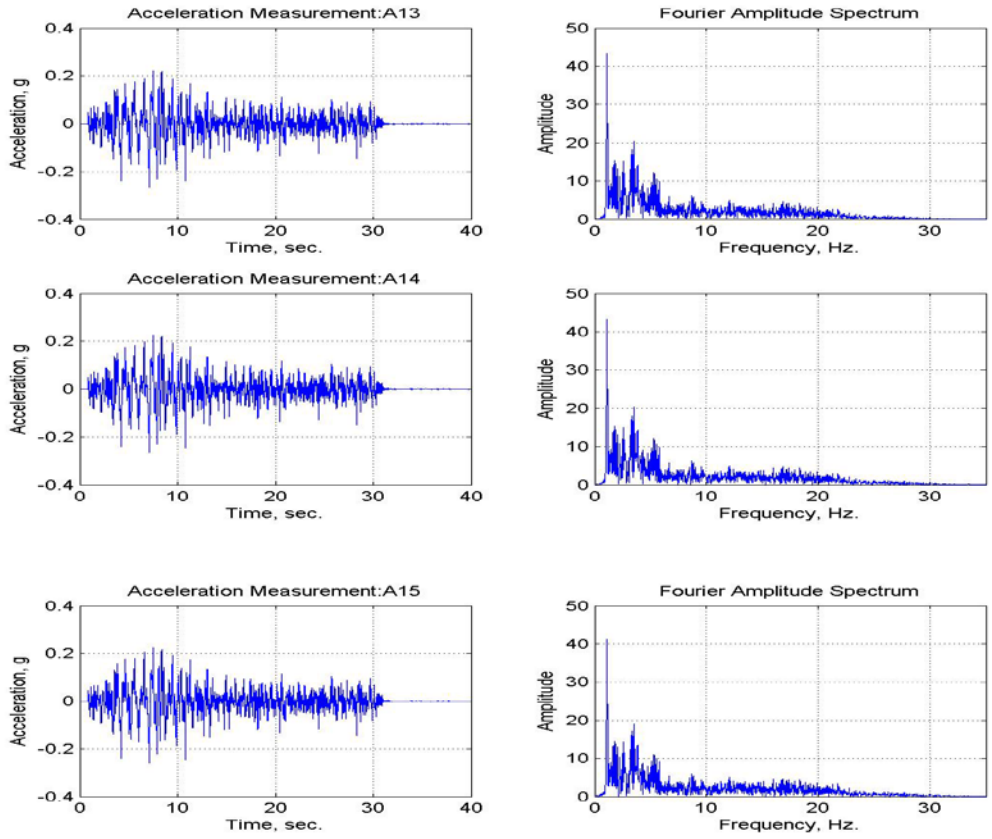


Figure A.16. Accelerations Measured for Wall Configuration 2- Sakarya 100% (continued)

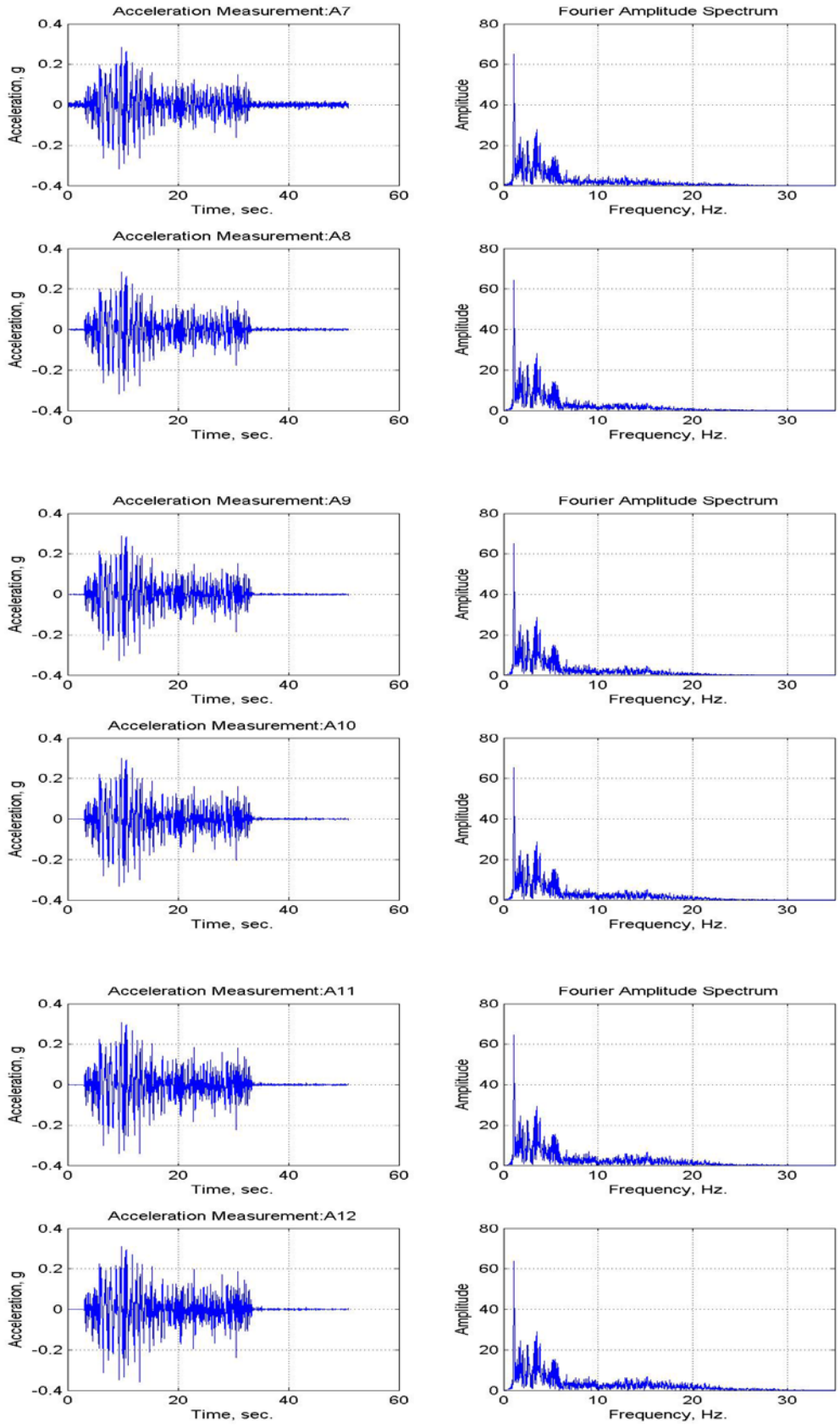


Figure A.17. Accelerations Measured for Wall Configuration 2- Sakarya 150%

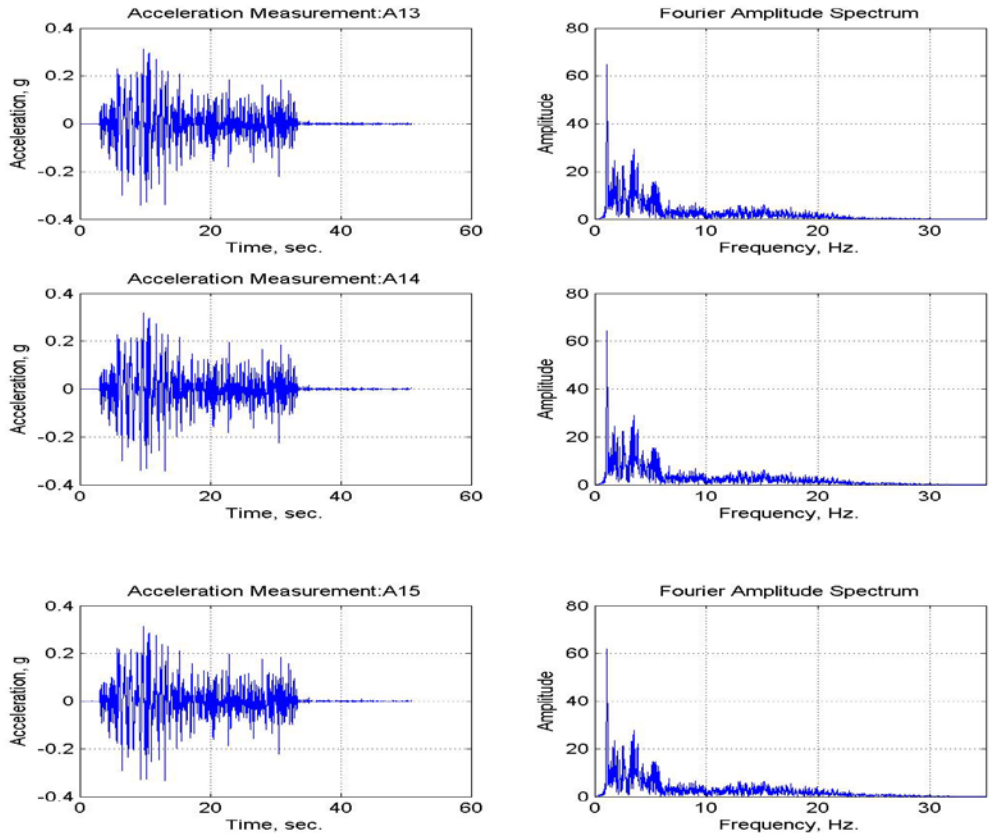


Figure A.17. Accelerations Measured for Wall Configuration 2- Sakarya 150% (continued)

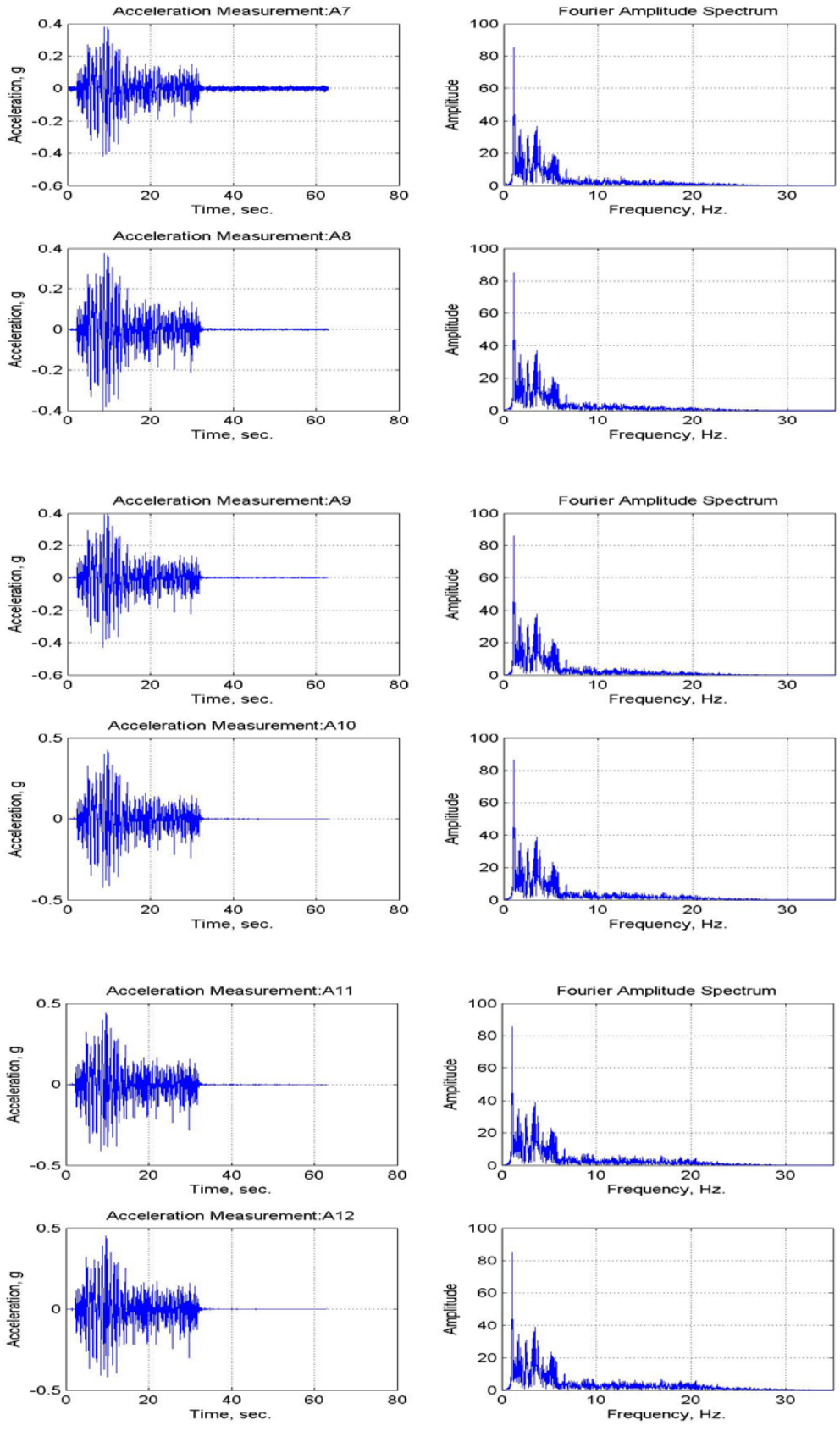


Figure A.18. Accelerations Measured for Wall Configuration 2- Sakarya 200%

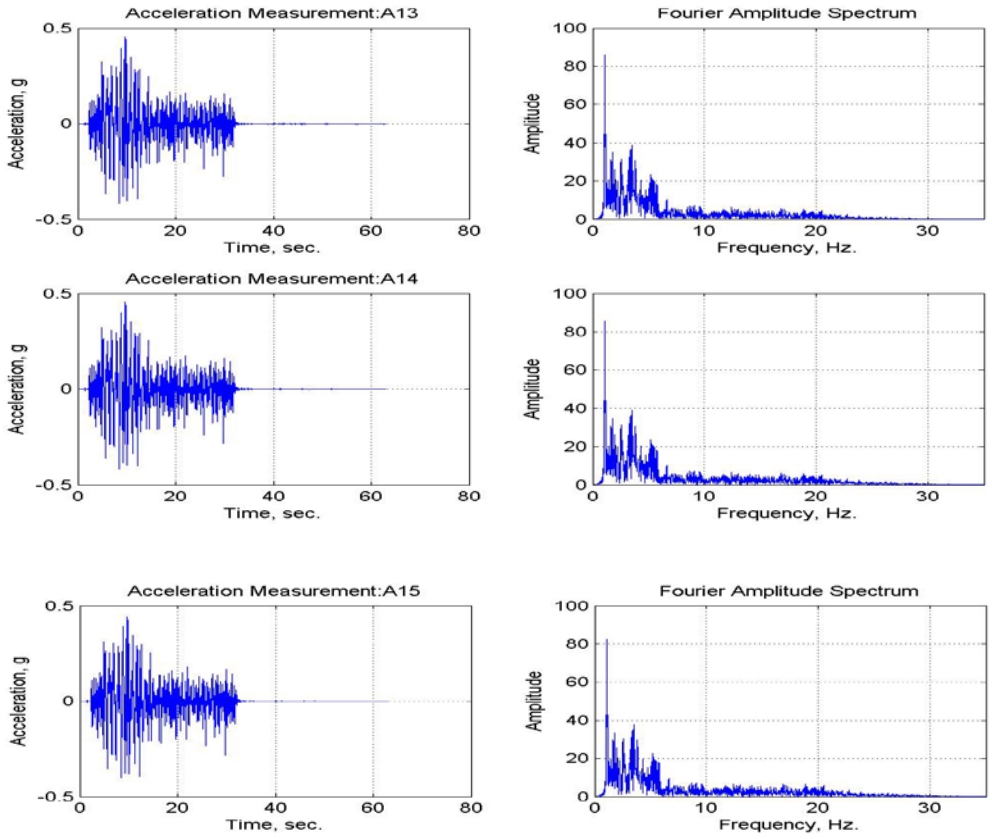


Figure A.18. Accelerations Measured for Wall Configuration 2- Sakarya 200% (continued)

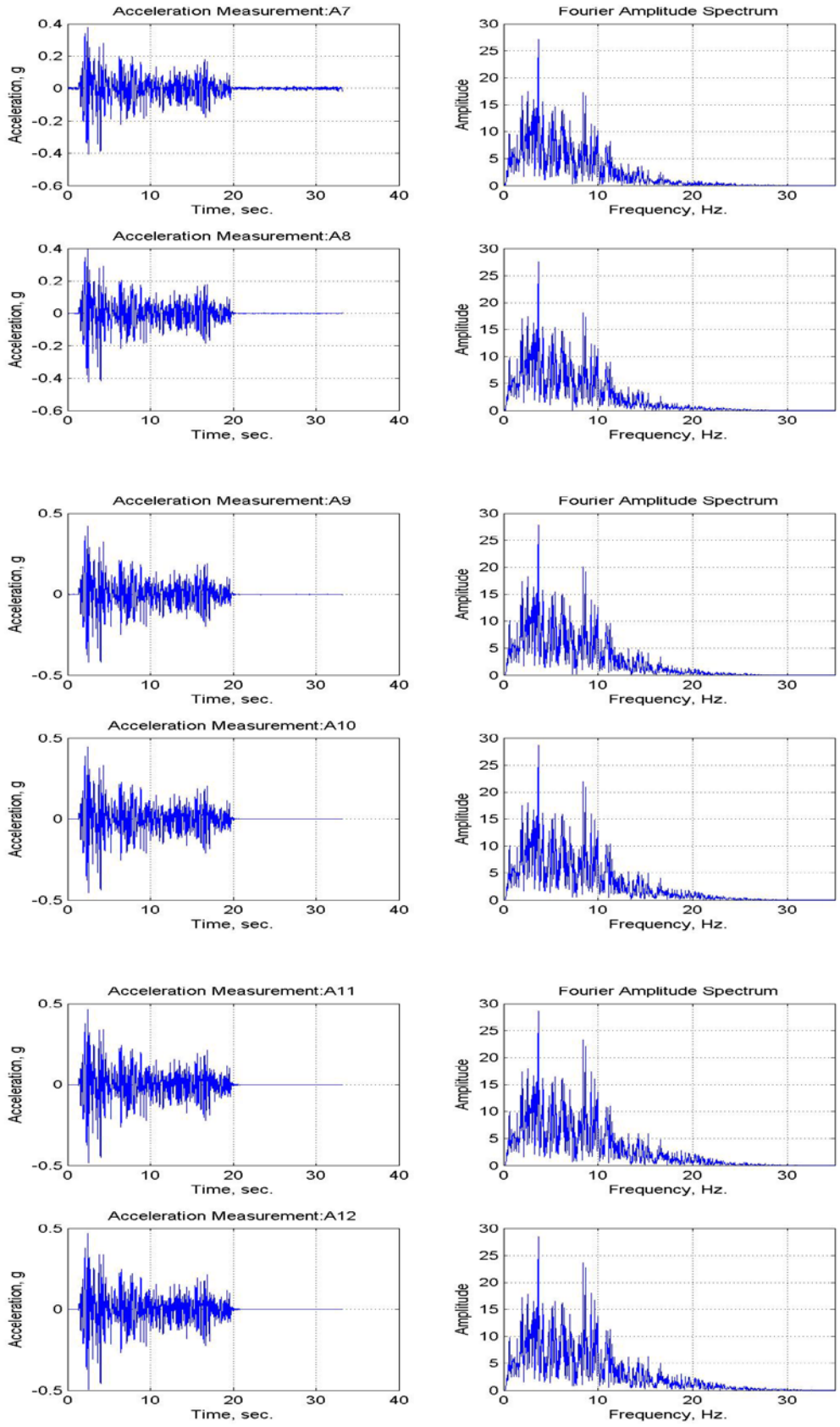


Figure A.19. Accelerations Measured for Wall Configuration 3- El Centro 100%

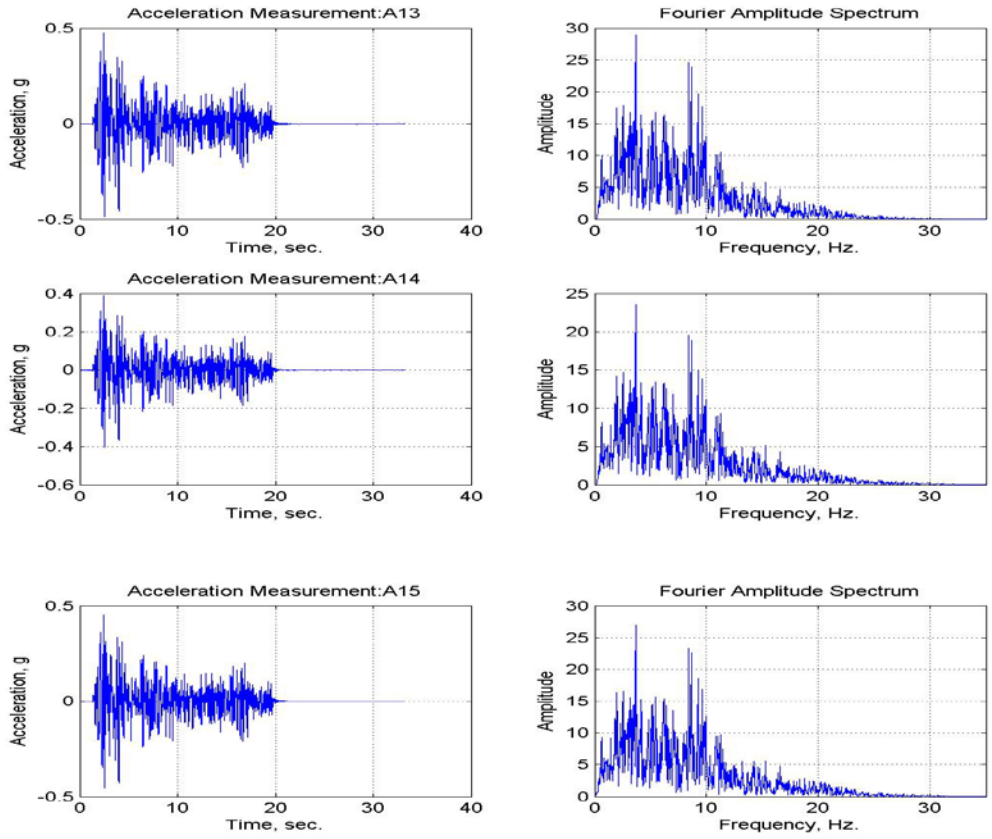


Figure A.19. Accelerations Measured for Wall Configuration 3- El Centro 100% (continued)

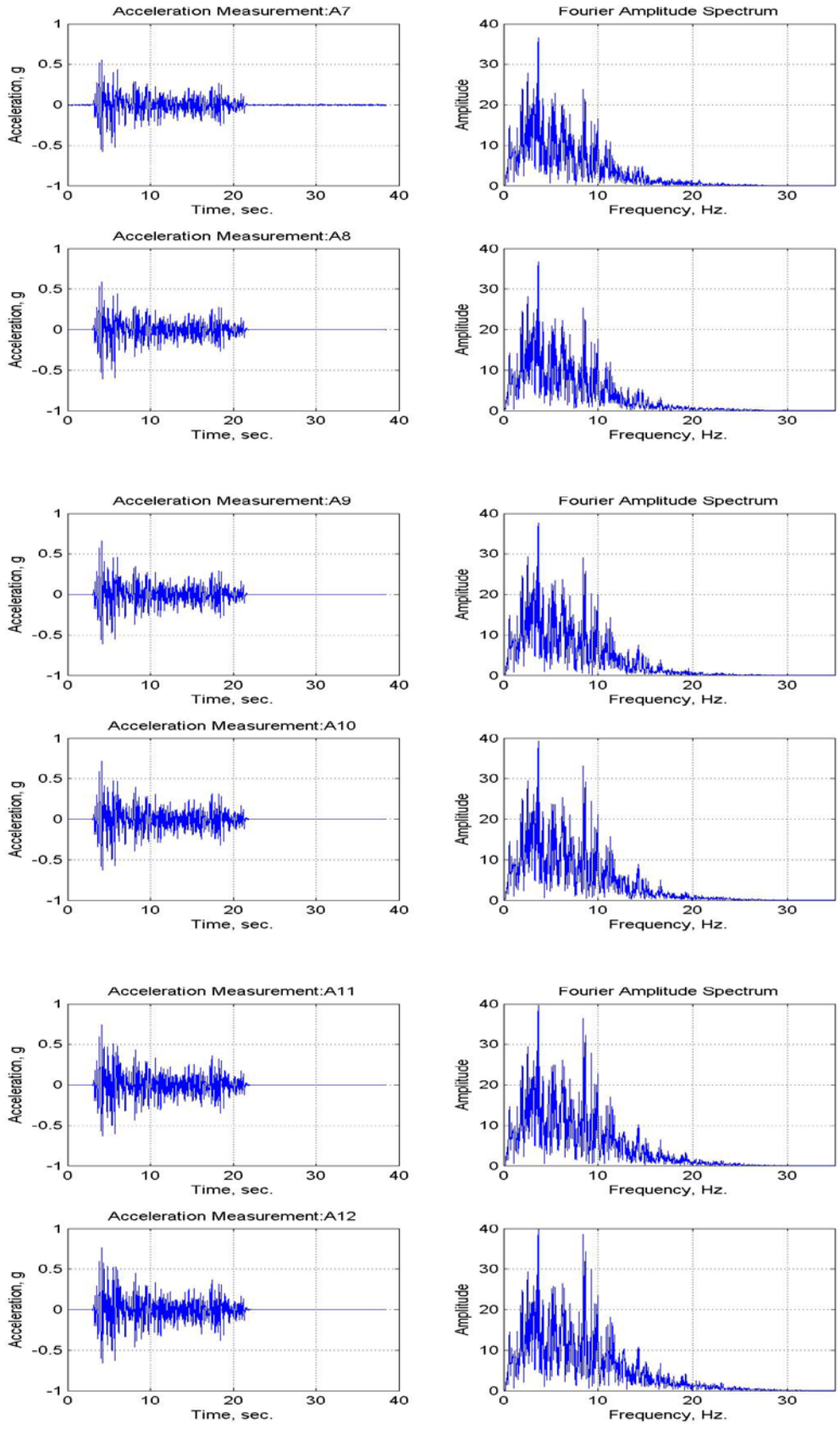


Figure A.20. Accelerations Measured for Wall Configuration 3- El Centro 150%

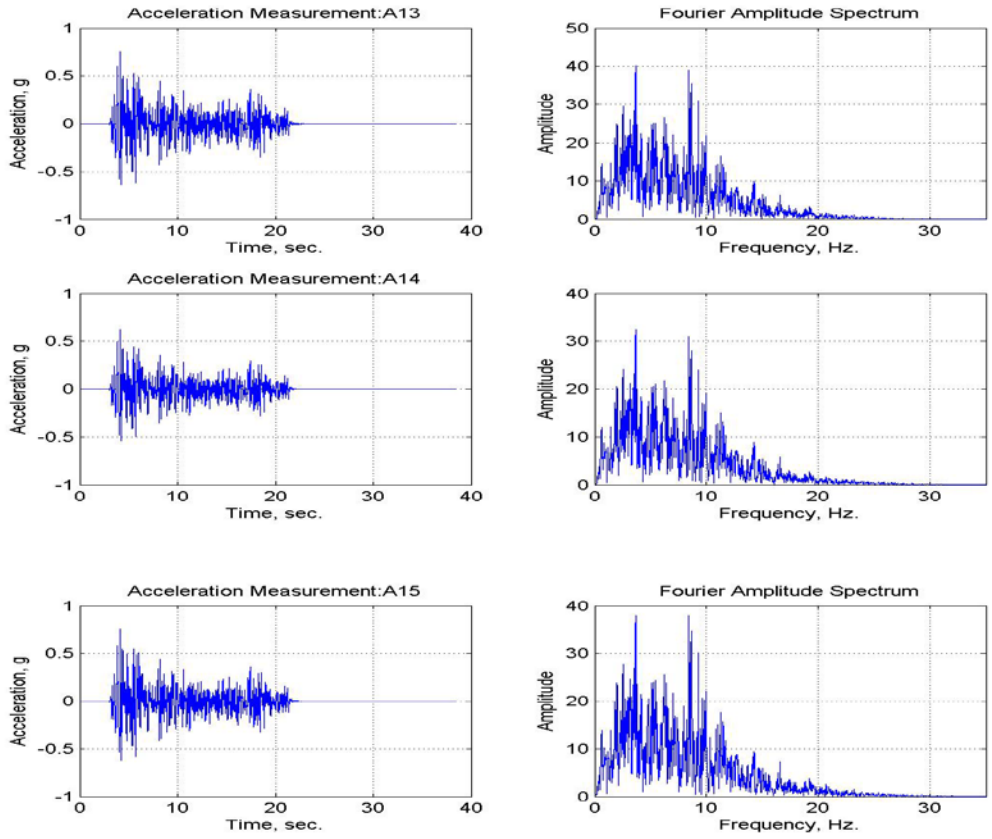


Figure A.20. Accelerations Measured for Wall Configuration 3- El Centro 150% (continued)

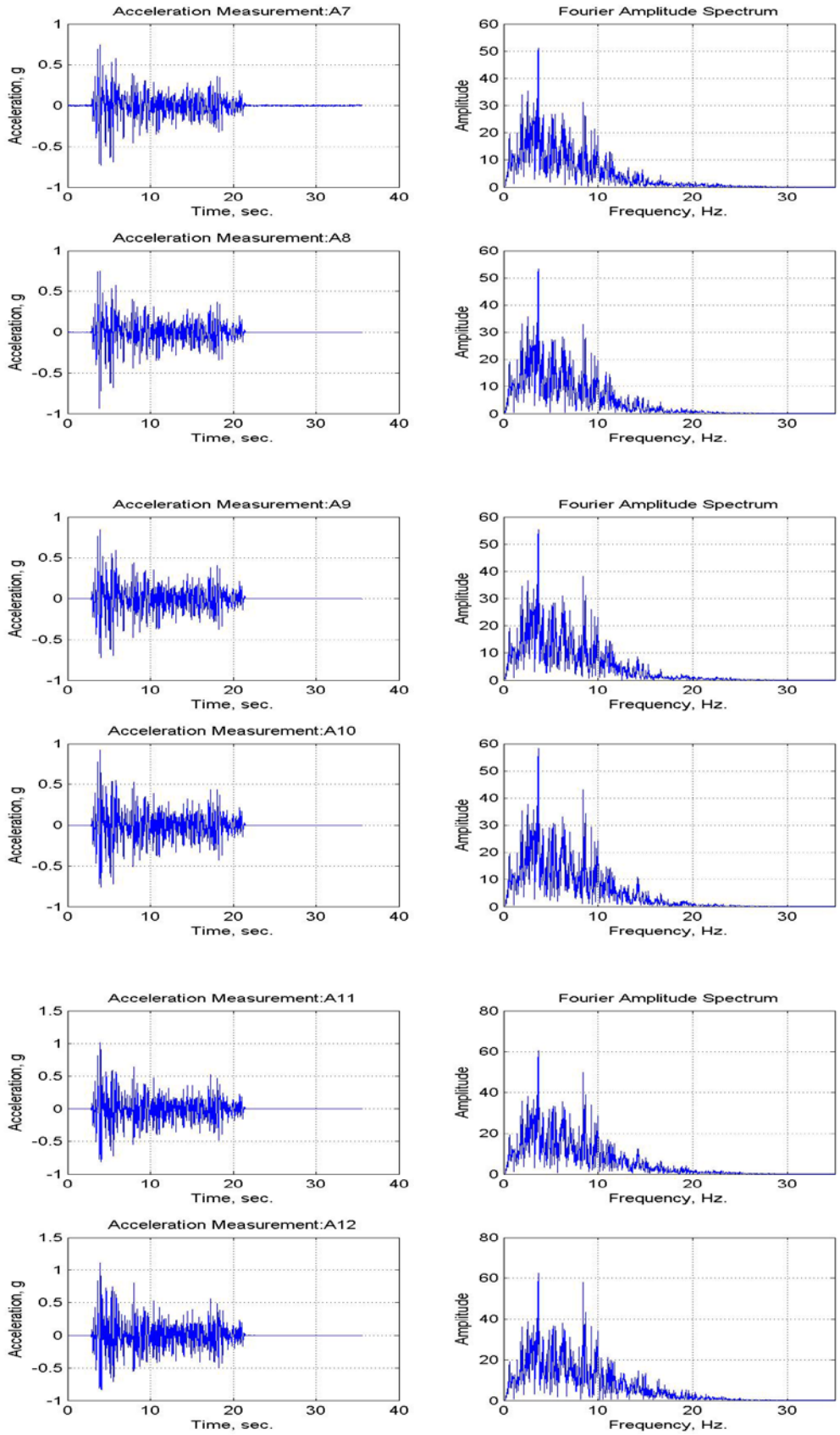


Figure A.21. Accelerations Measured for Wall Configuration 3- El Centro 200%

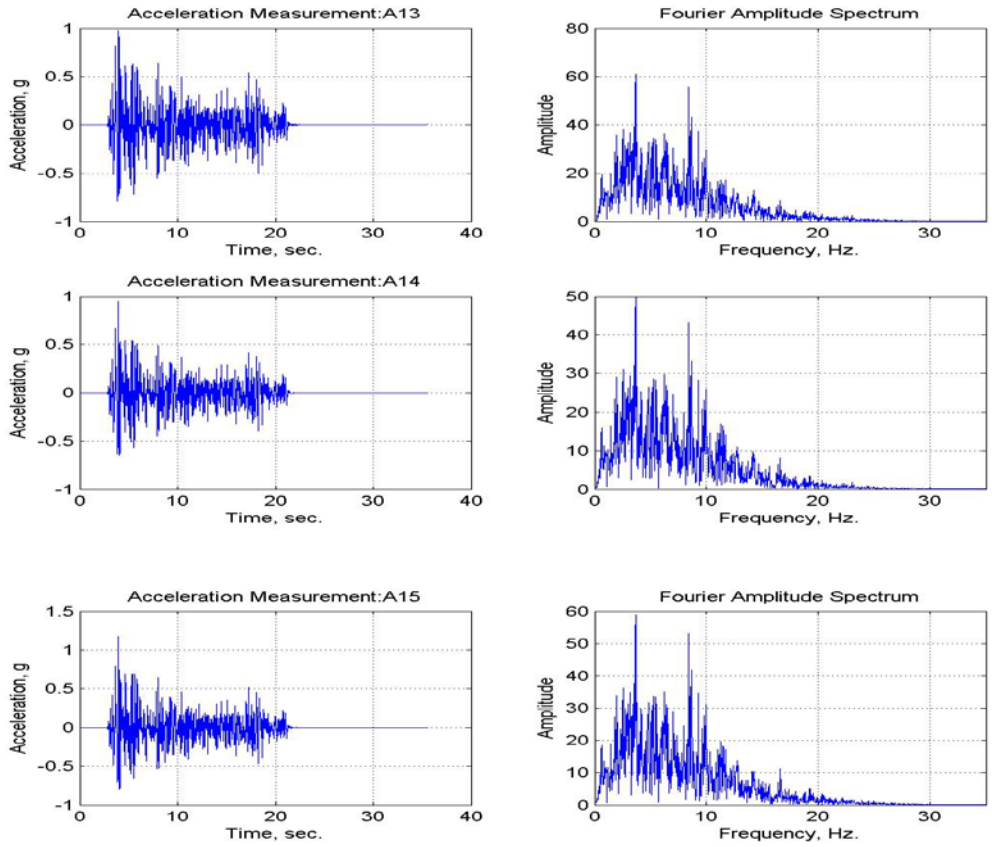


Figure A.21. Accelerations Measured for Wall Configuration 3- El Centro 200% (continued)

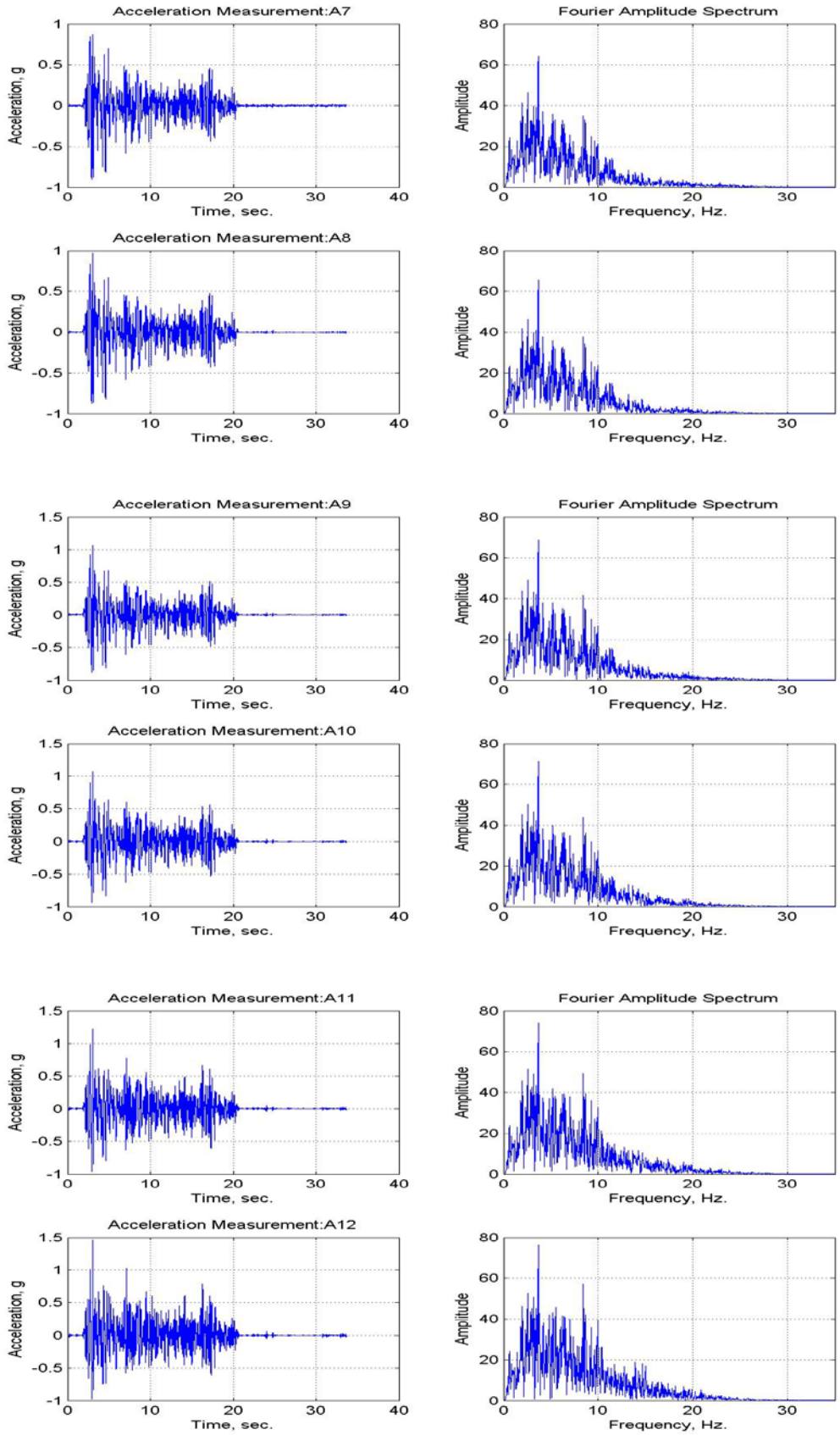


Figure A.22. Accelerations Measured for Wall Configuration 3- El Centro 250%

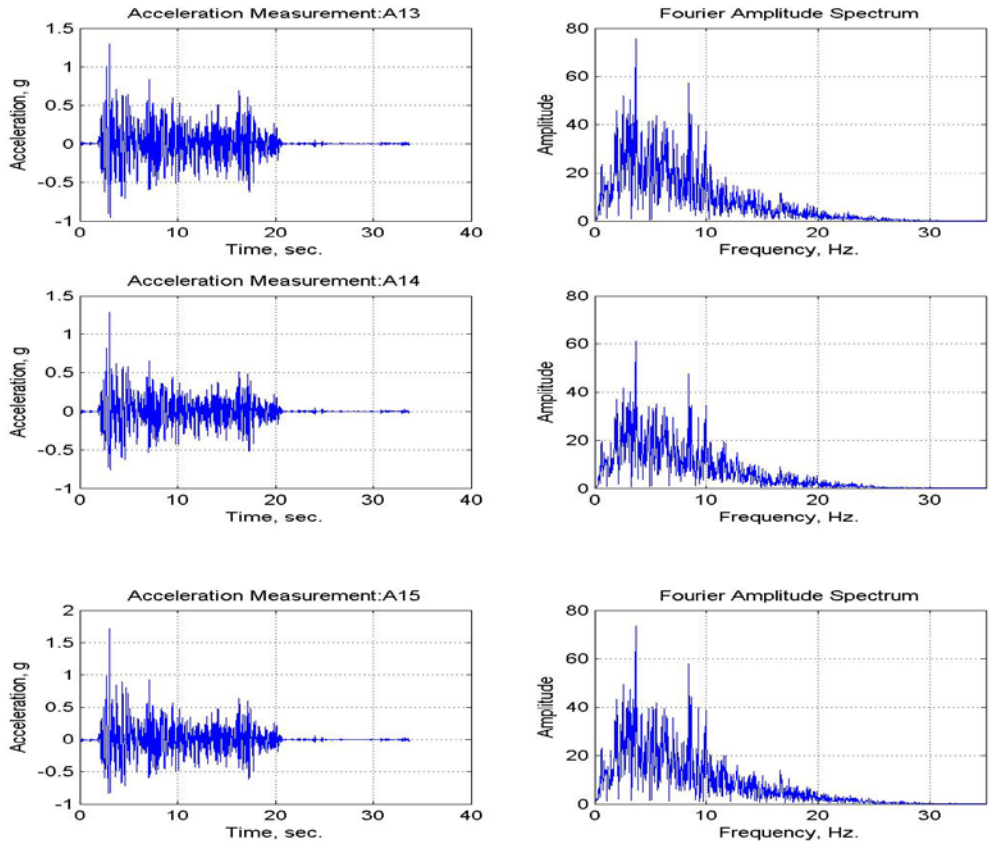


Figure A.22. Accelerations Measured for Wall Configuration 3- El Centro 250% (continued)

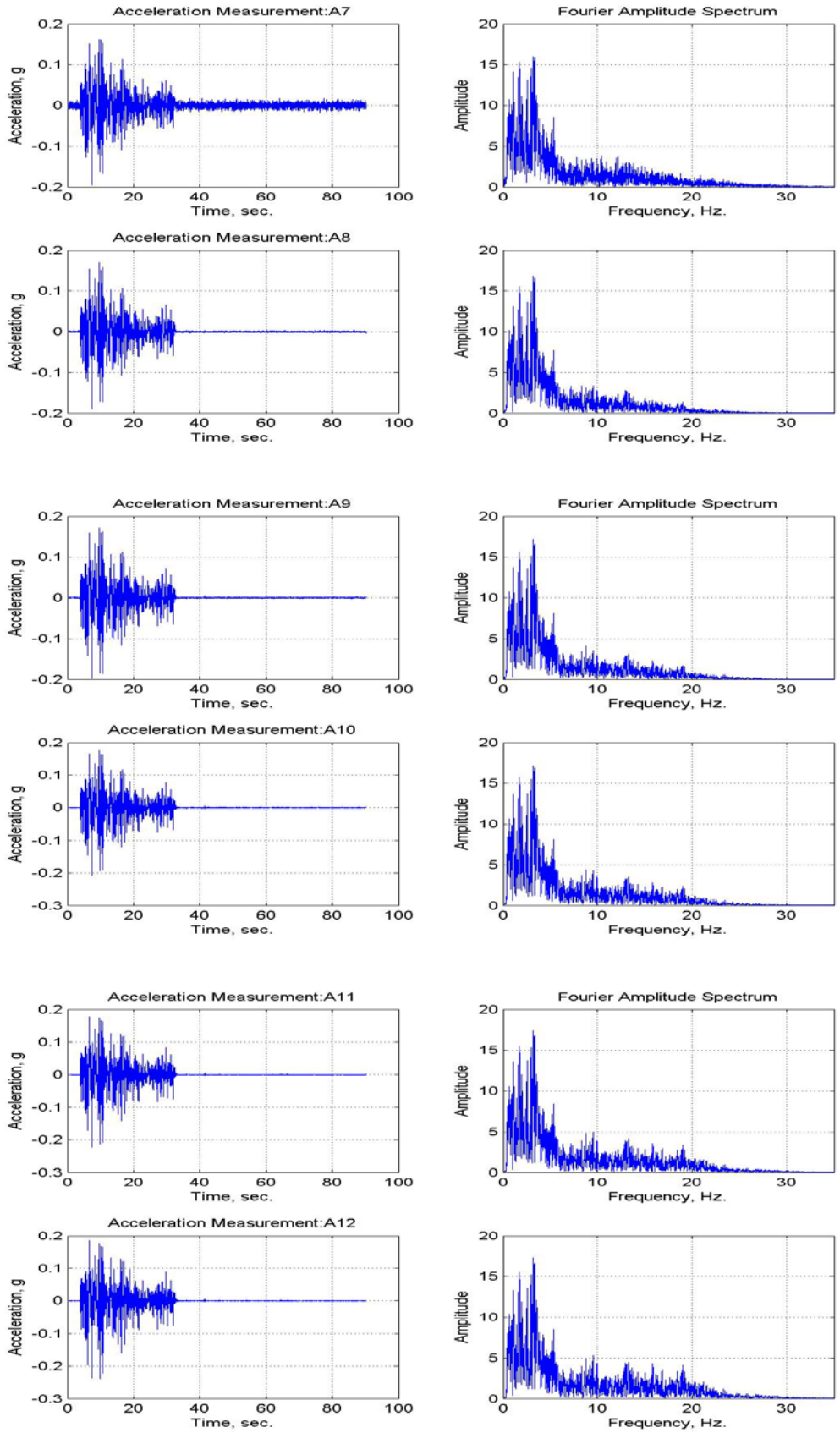


Figure A.23. Accelerations Measured for Wall Configuration 3- Izmit 100%

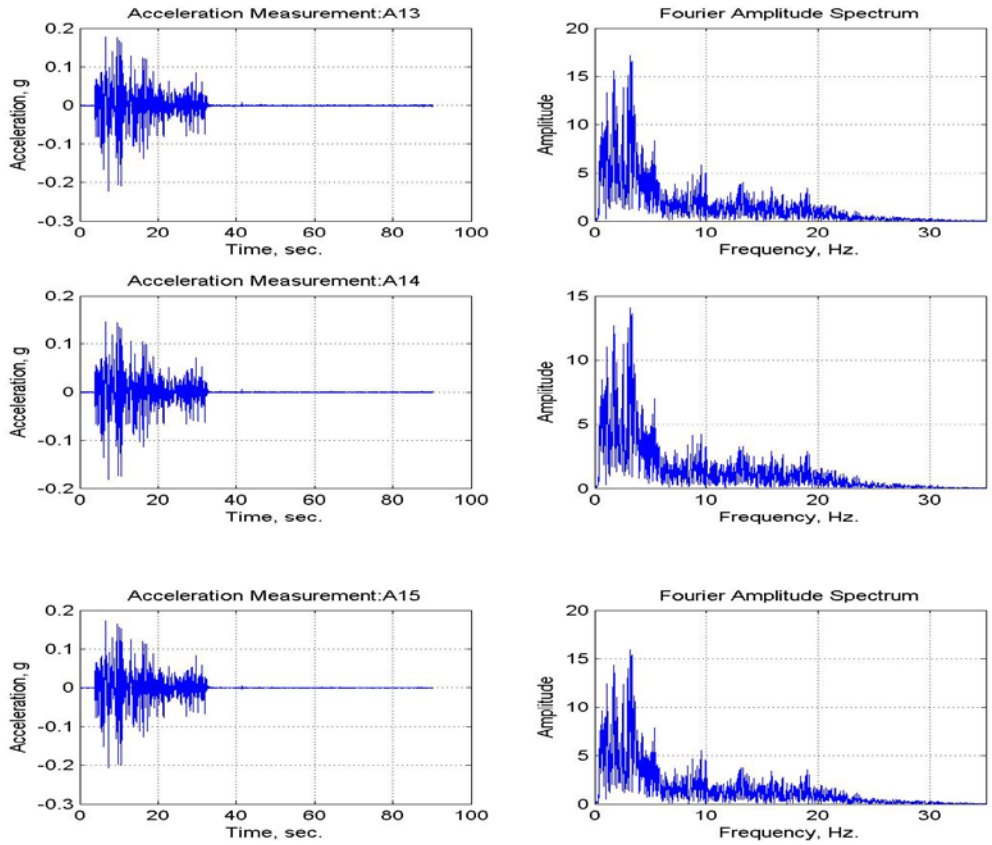


Figure A.23. Accelerations Measured for Wall Configuration 3- Izmit 100% (continued)

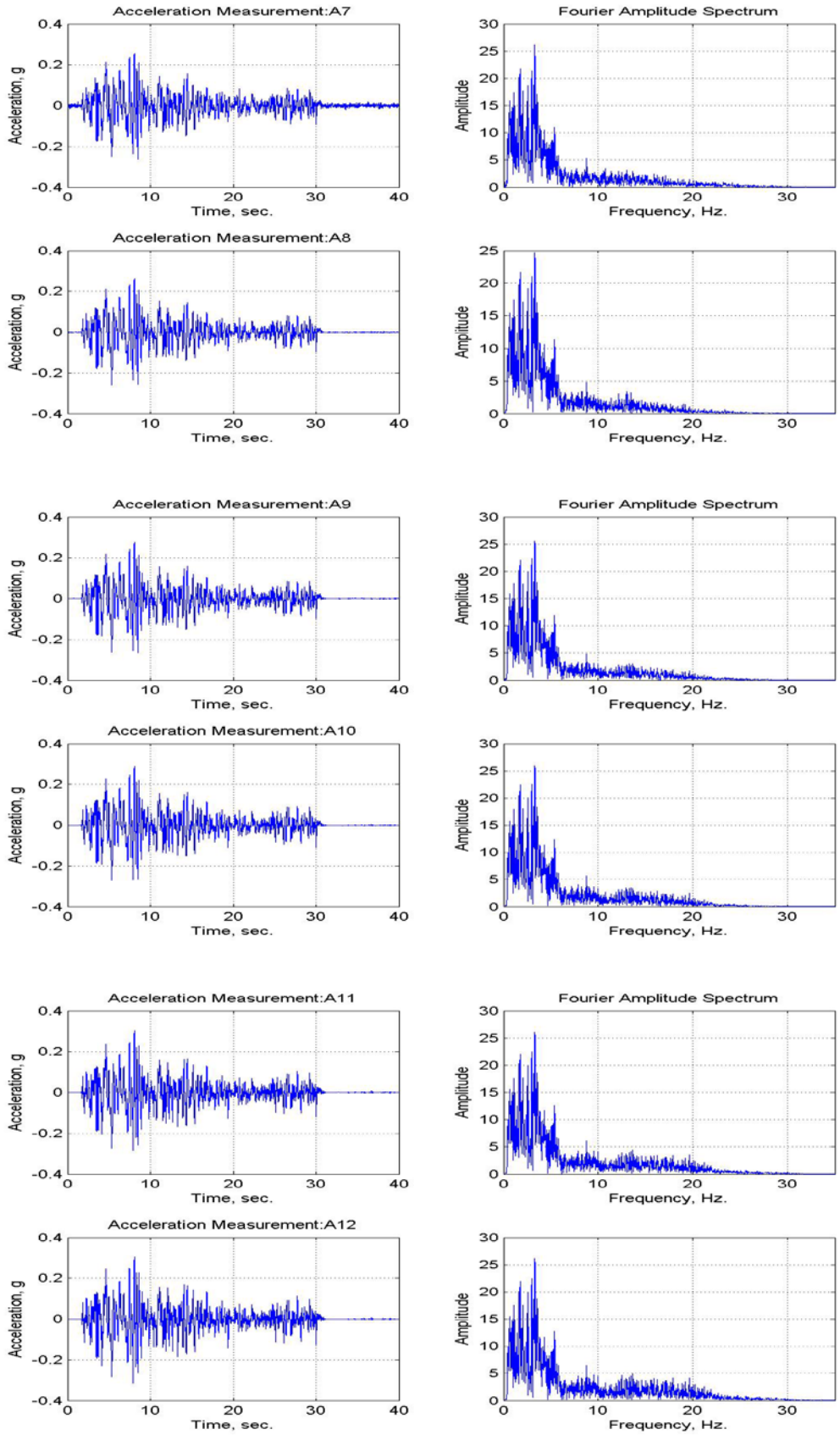


Figure A.24. Accelerations Measured for Wall Configuration 3- Izmit 150%

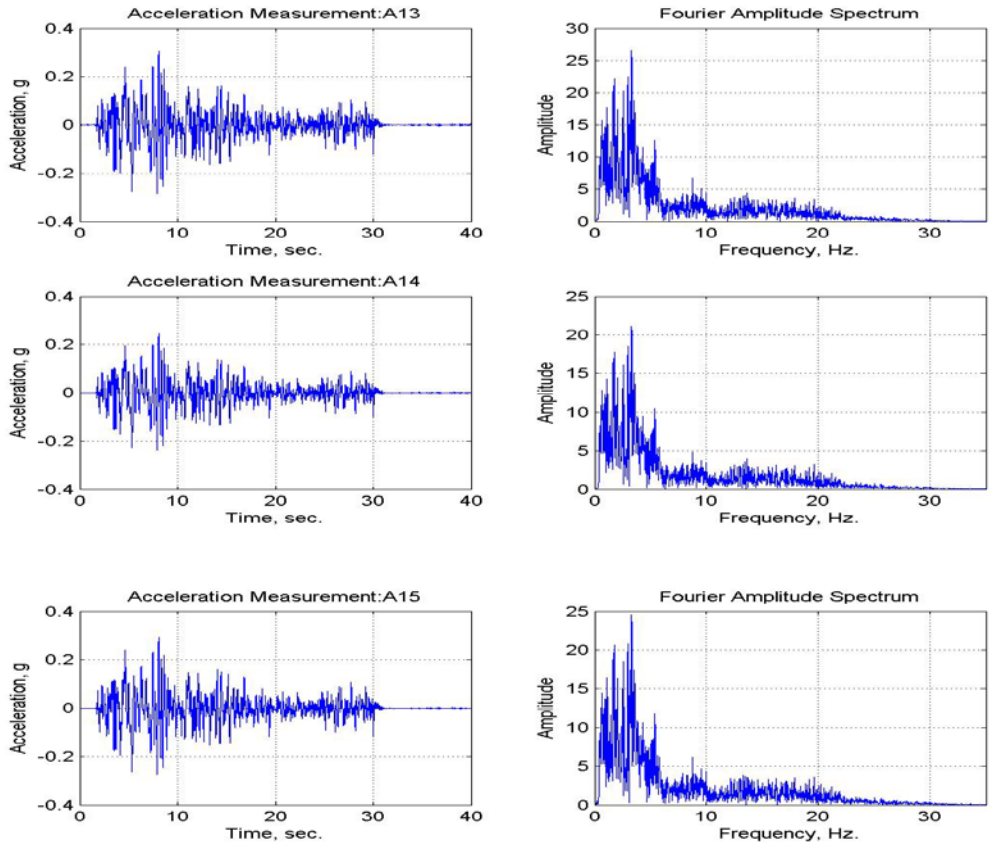


Figure A.24. Accelerations Measured for Wall Configuration 3- Izmit 150%

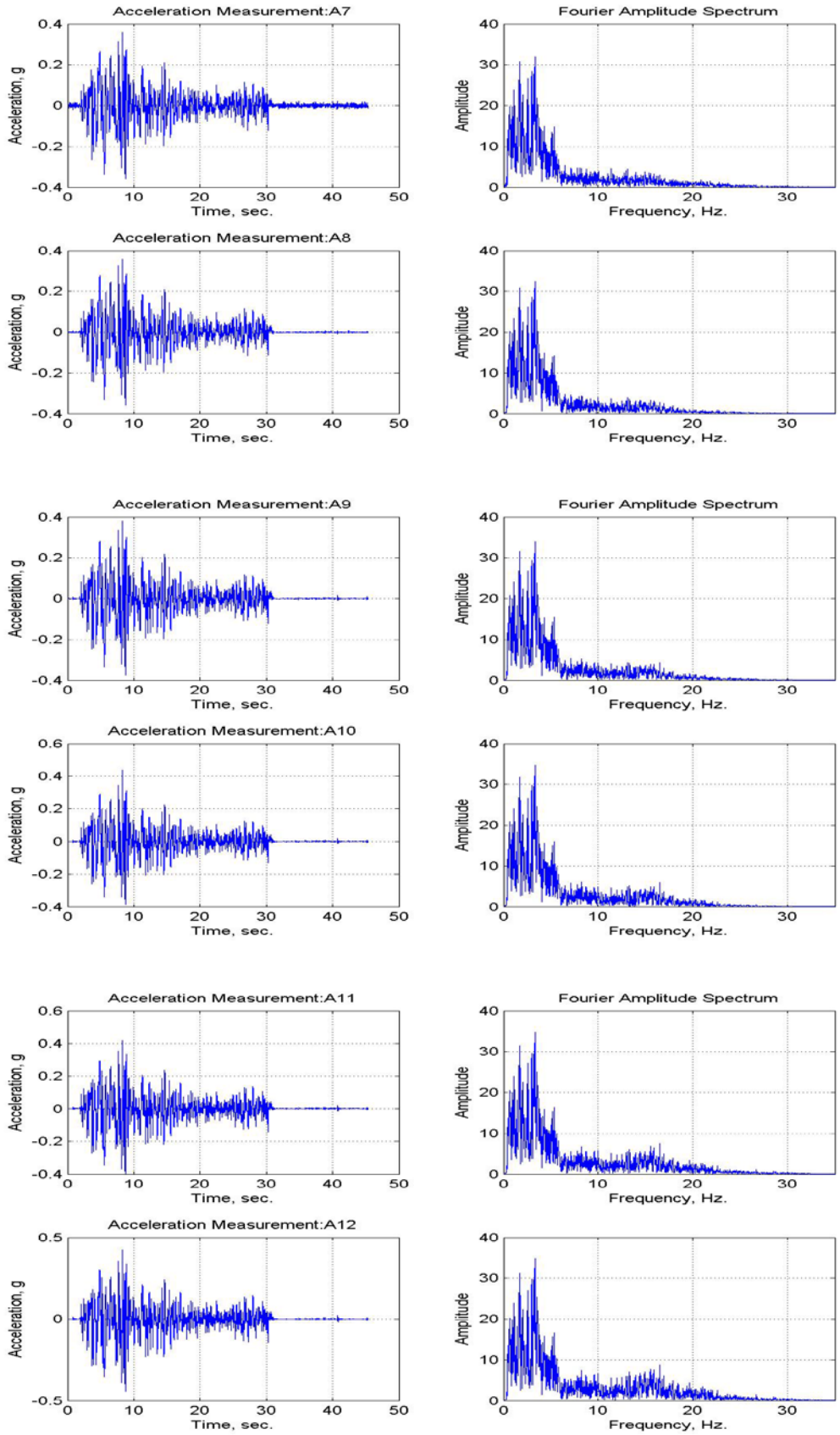


Figure A.25. Accelerations Measured for Wall Configuration 3- Izmit 200%

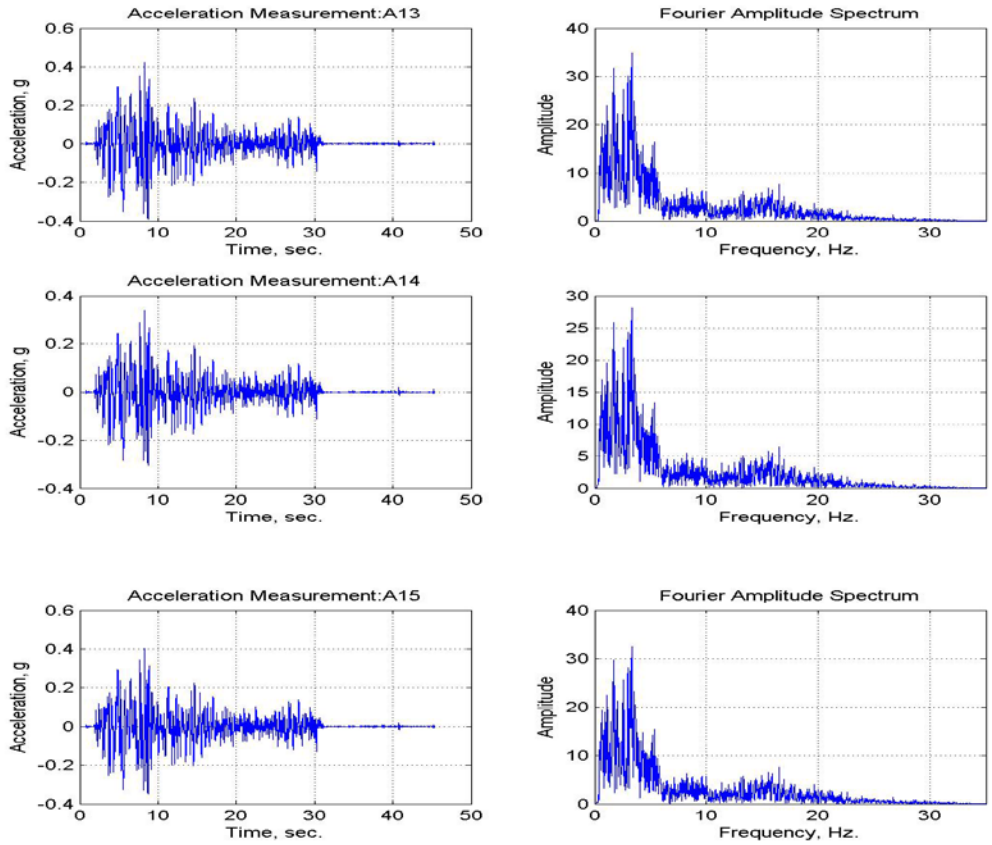


Figure A.25. Accelerations Measured for Wall Configuration 3- Izmit 200% (continued)

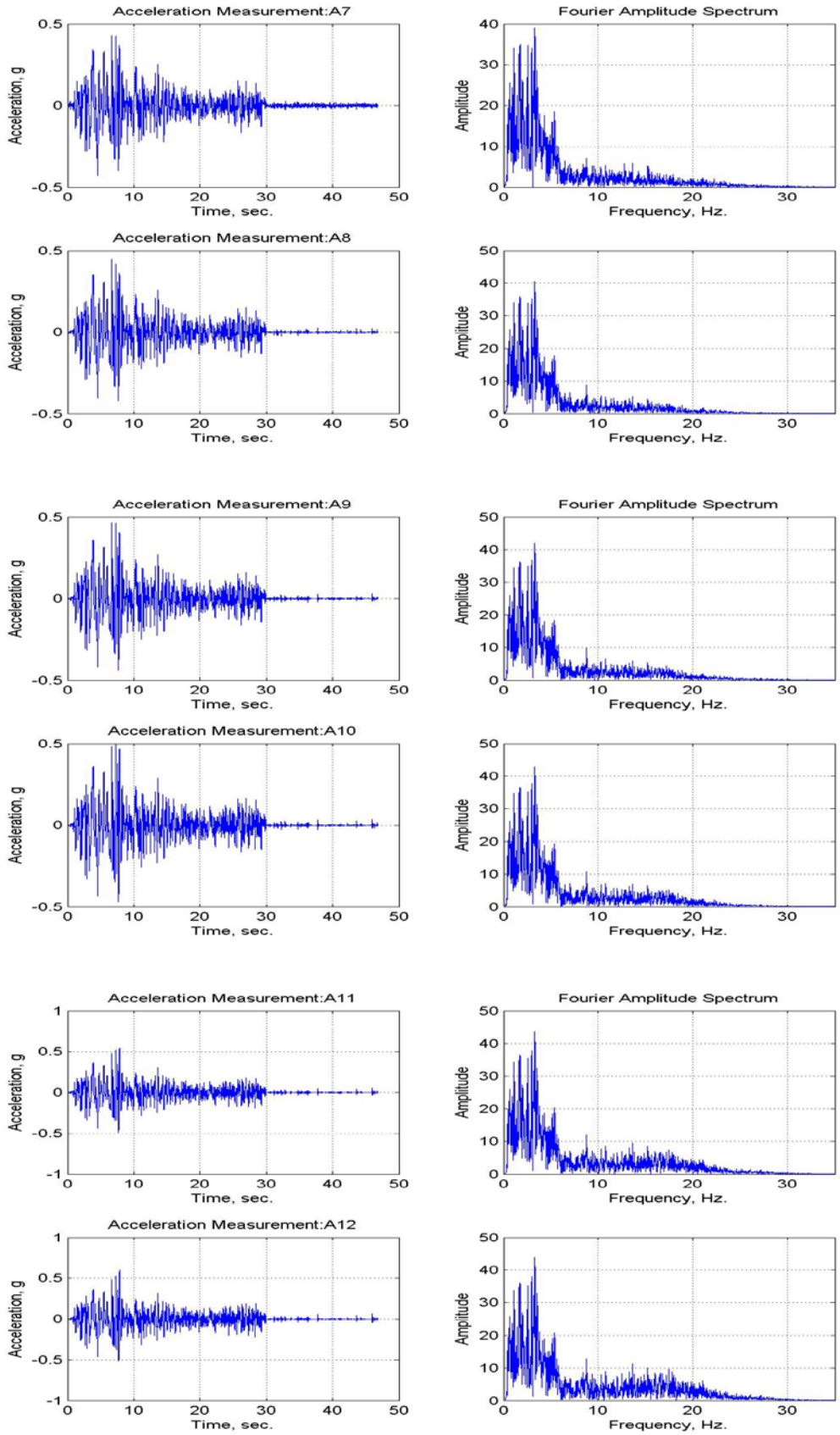


Figure A.26. Accelerations Measured for Wall Configuration 3- Izmit 250%

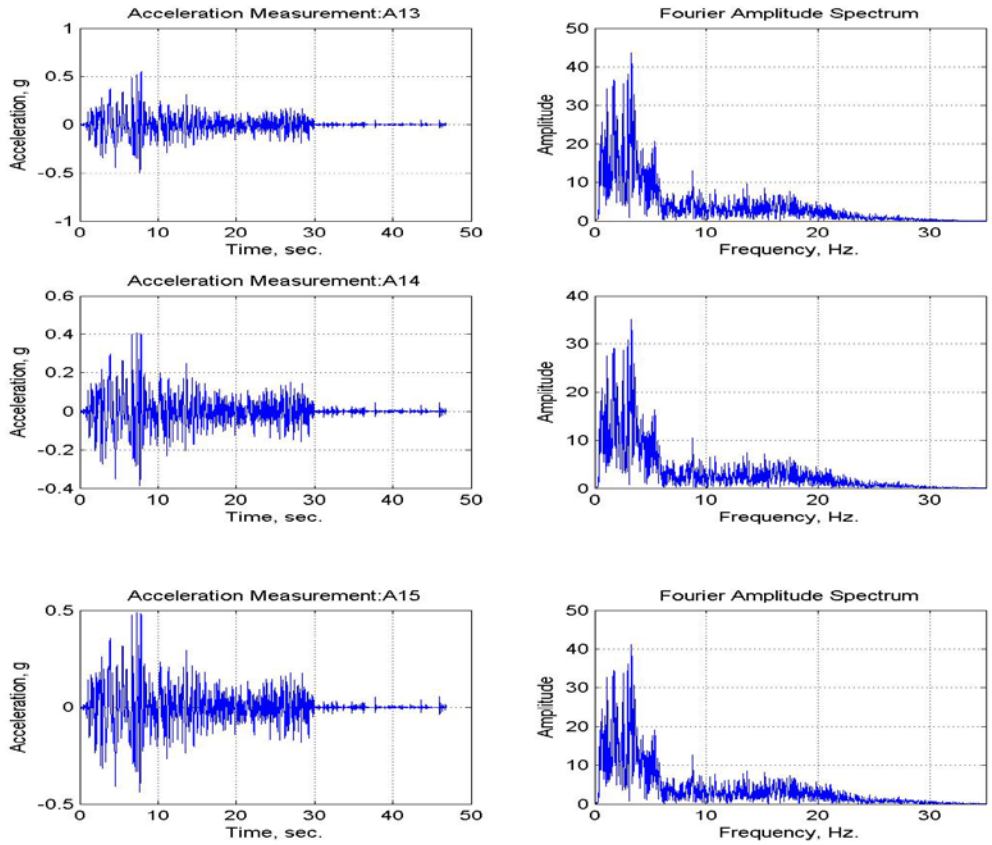


Figure A.26. Accelerations Measured for Wall Configuration 3- Izmit 250% (continued)

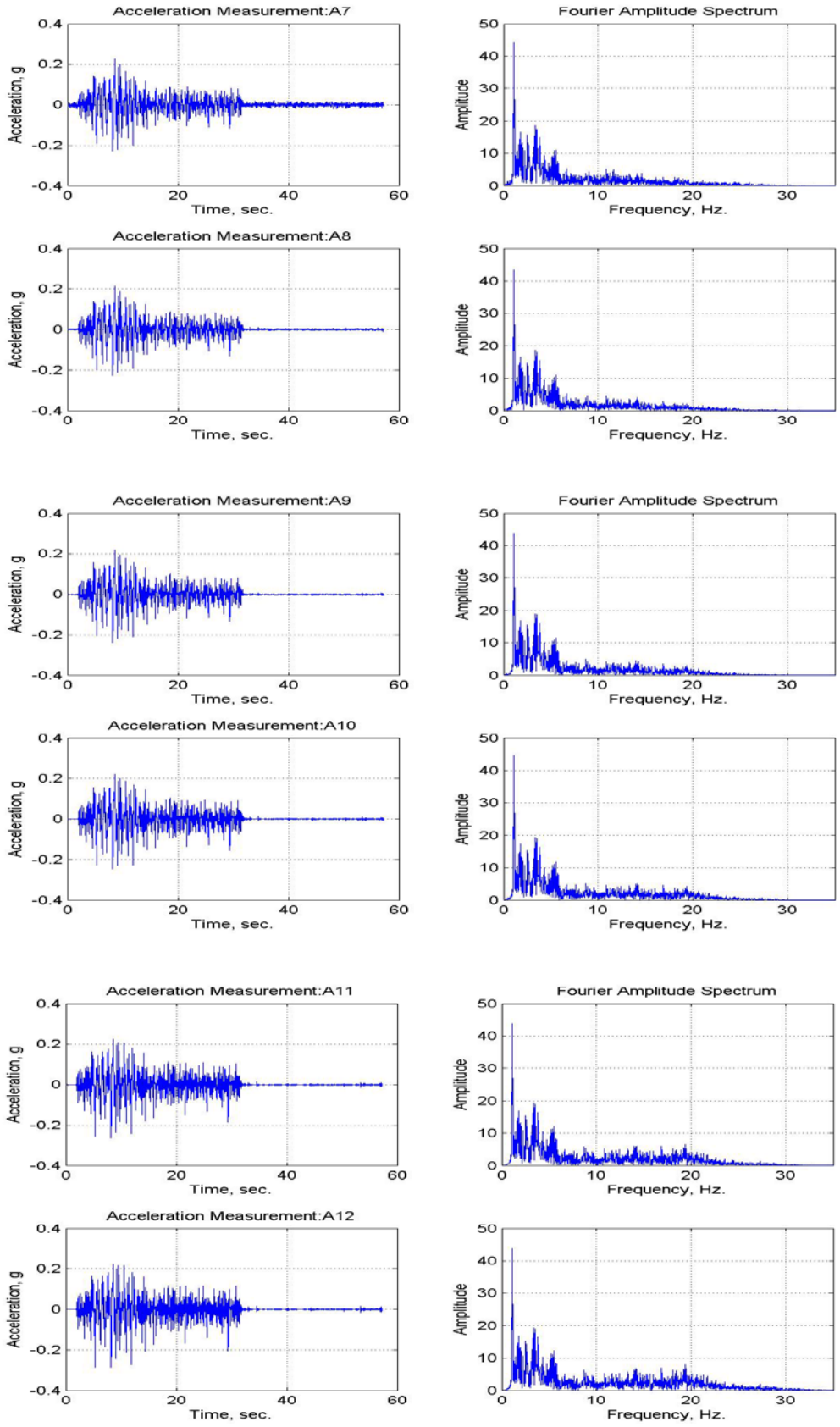


Figure A.27. Accelerations Measured for Wall Configuration 3- Sakarya 100%

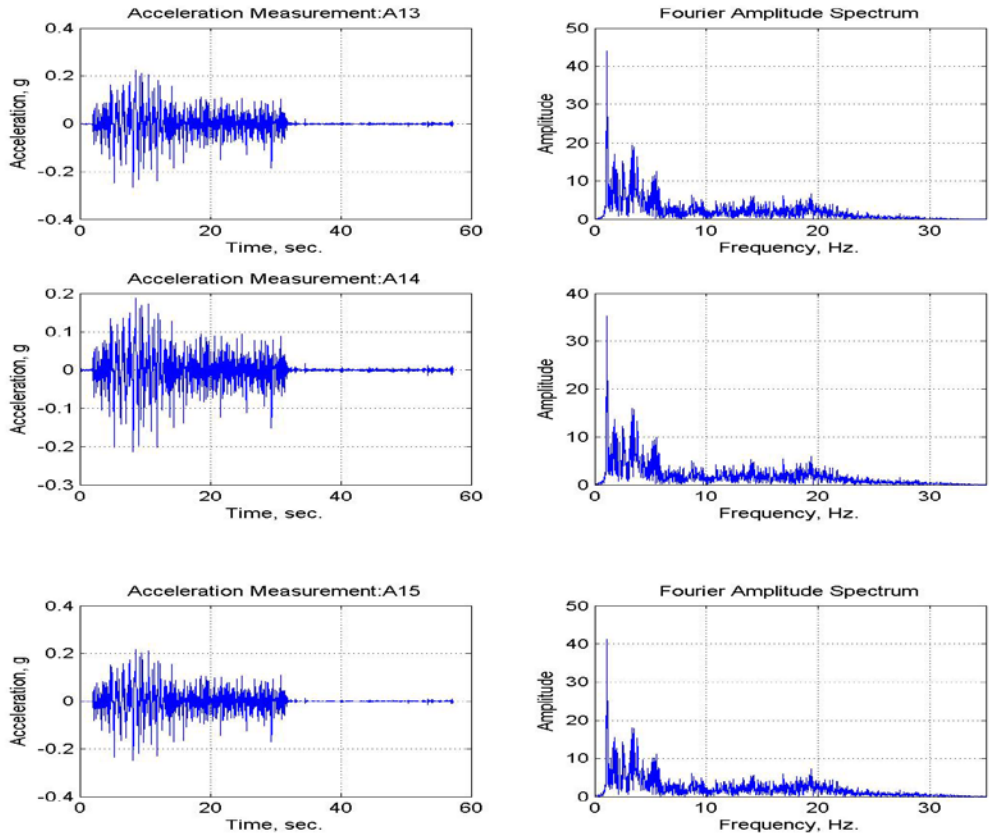


Figure A.27. Accelerations Measured for Wall Configuration 3- Sakarya 100% (continued)

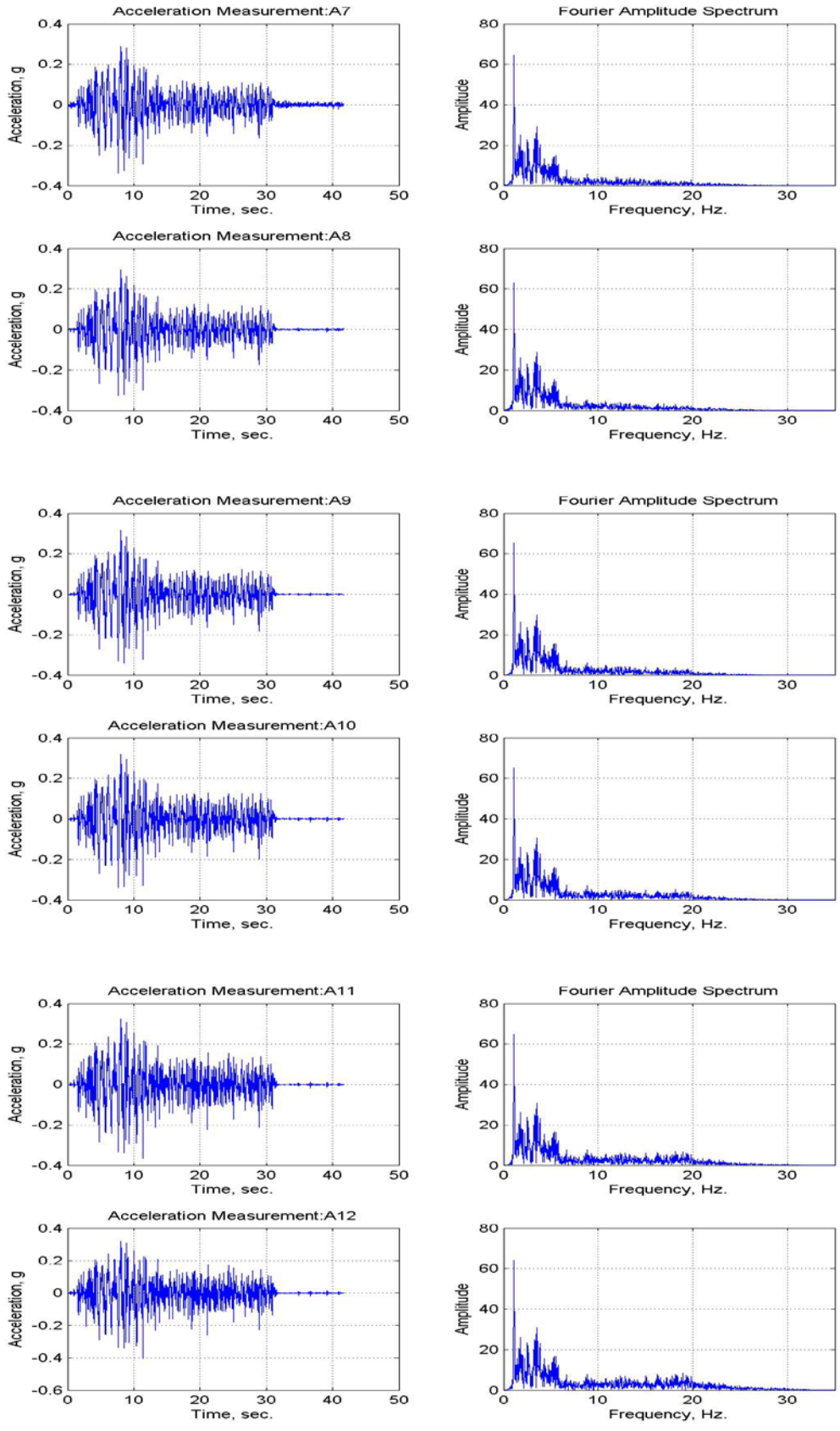


Figure A.28. Accelerations Measured for Wall Configuration 3- Sakarya 150%

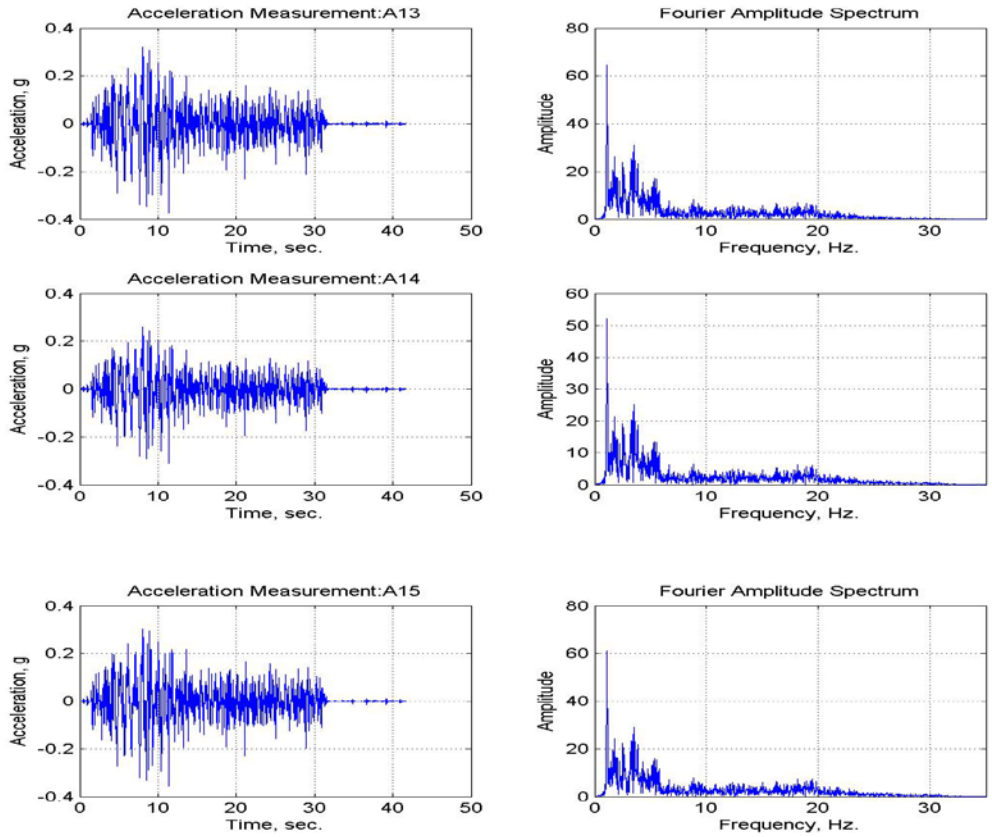


Figure A.28. Accelerations Measured for Wall Configuration 3- Sakarya 150% (continued)

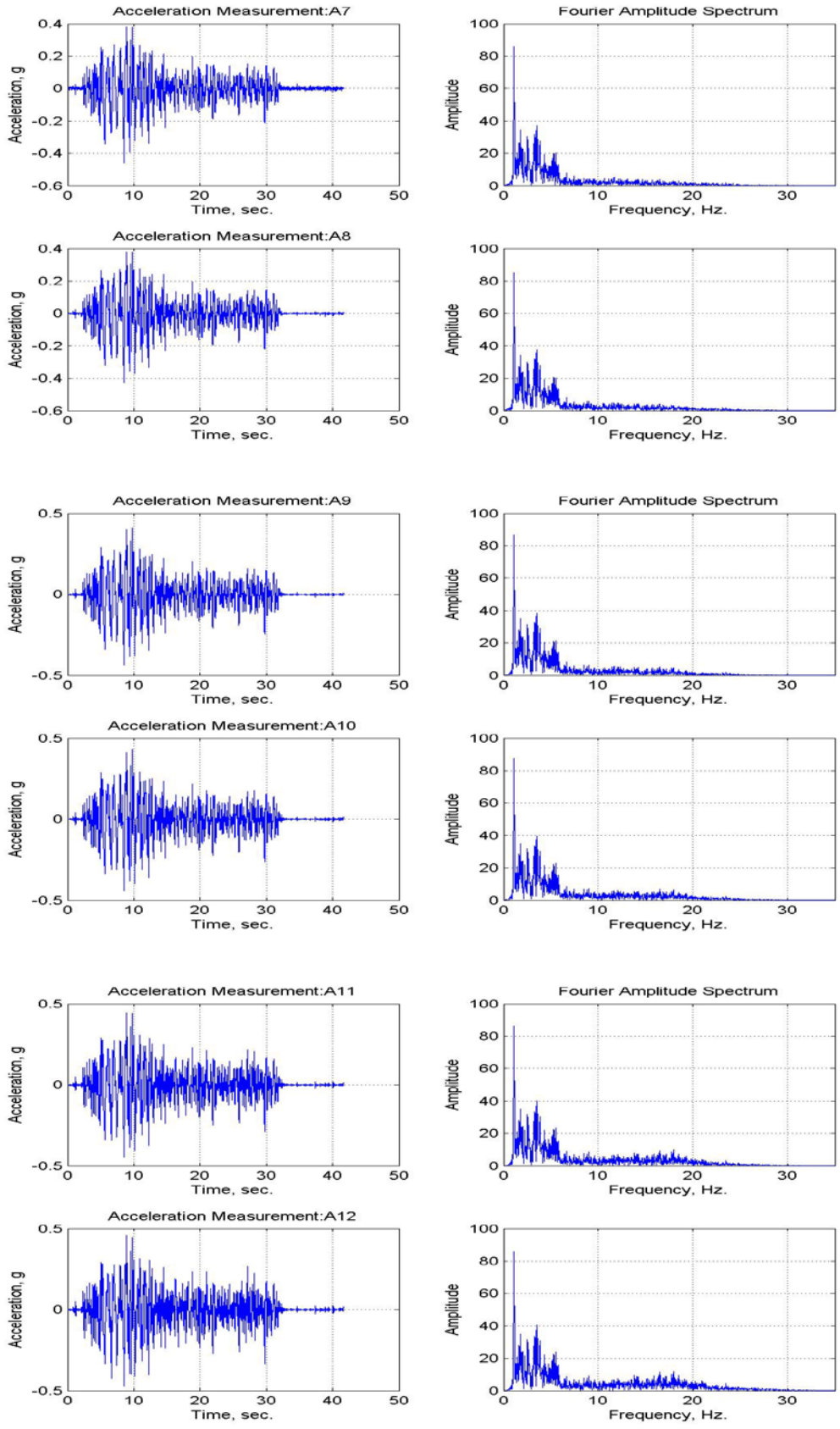


Figure A.29. Accelerations Measured for Wall Configuration 3- Sakarya 200%

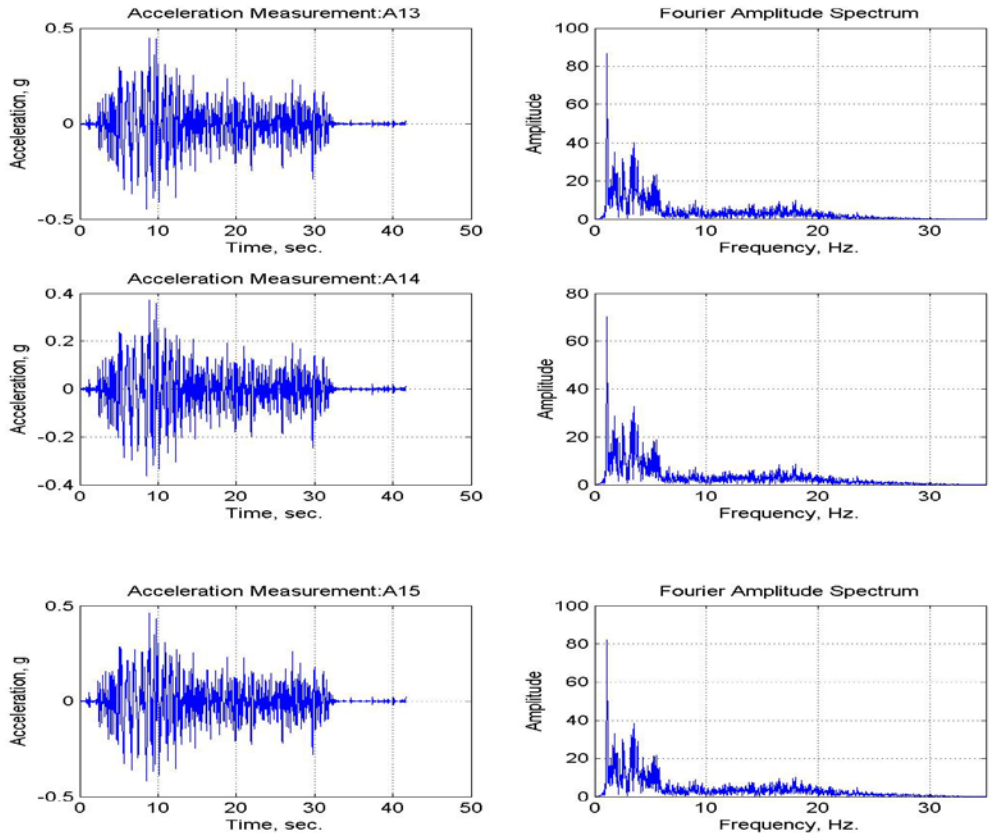


Figure A.29. Accelerations Measured for Wall Configuration 3- Sakarya 200% (continued)

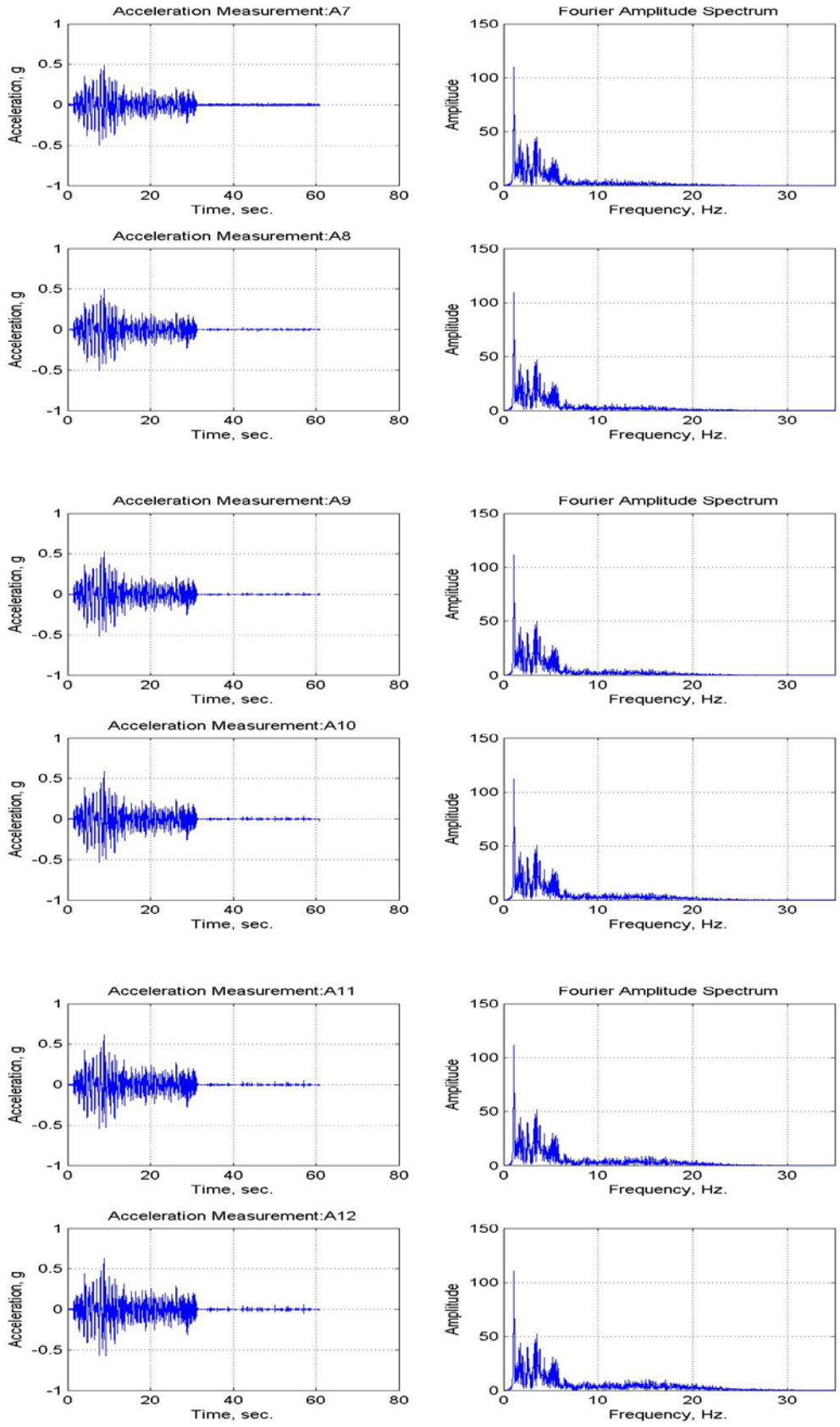


Figure A.30. Accelerations Measured for Wall Configuration 3- Sakarya 250%

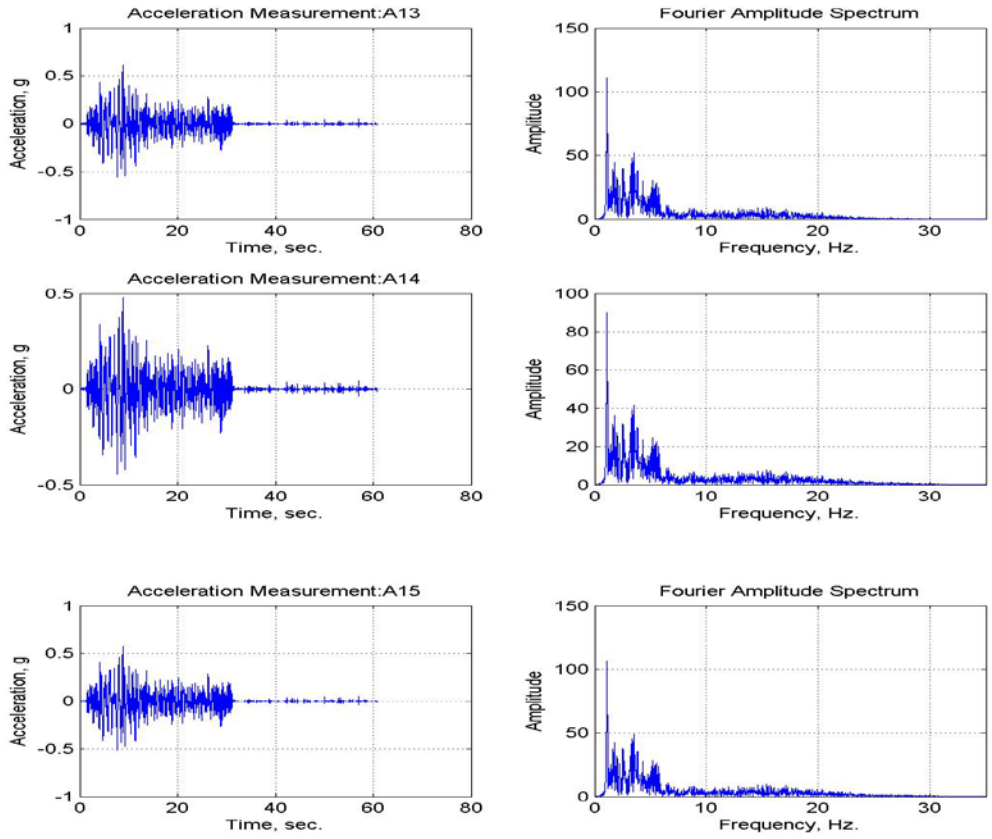


Figure A.30. Accelerations Measured for Wall Configuration 3- Sakarya 250% (continued)

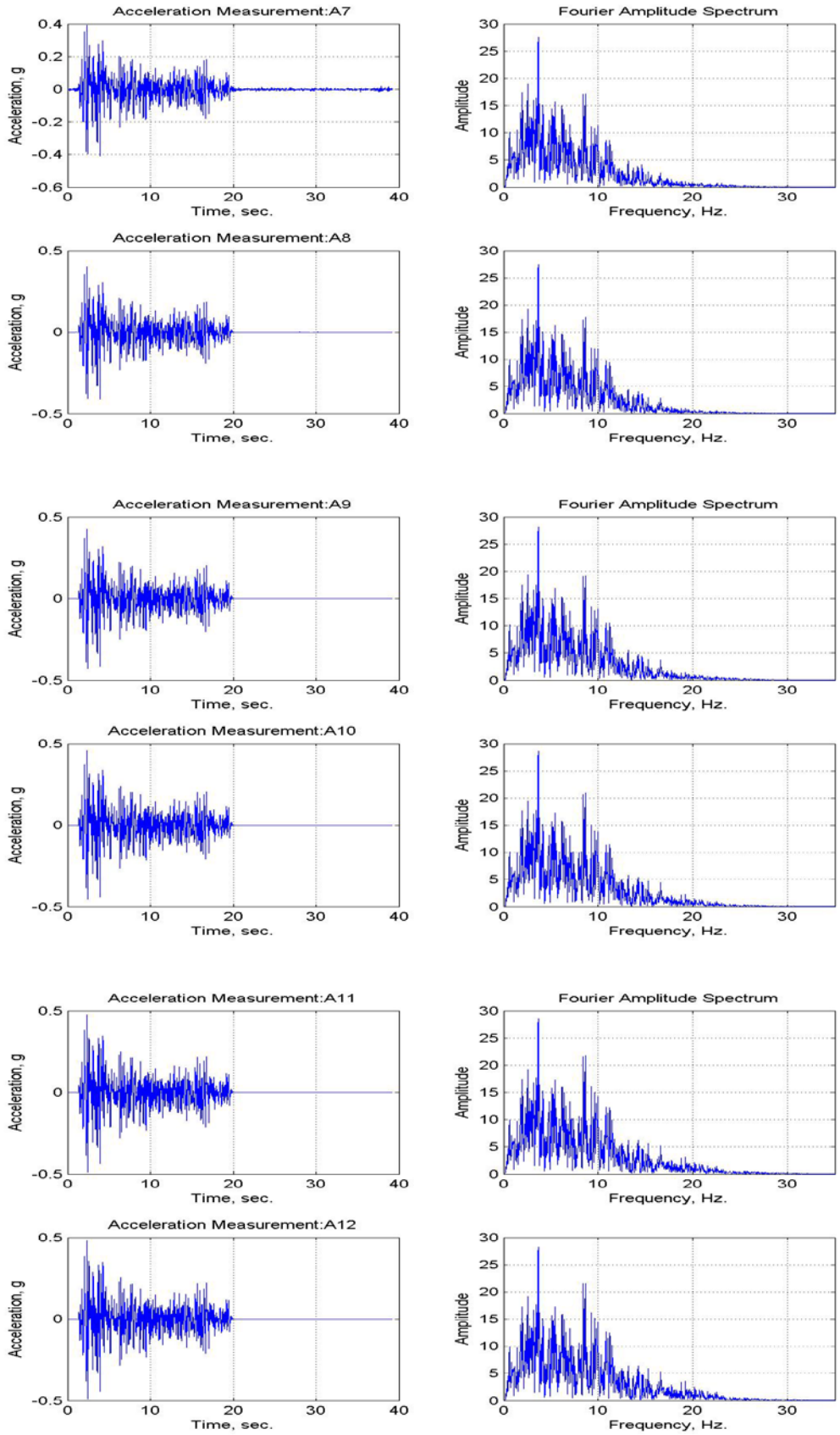


Figure A.31. Accelerations Measured for Wall Configuration 4- El Centro 100%

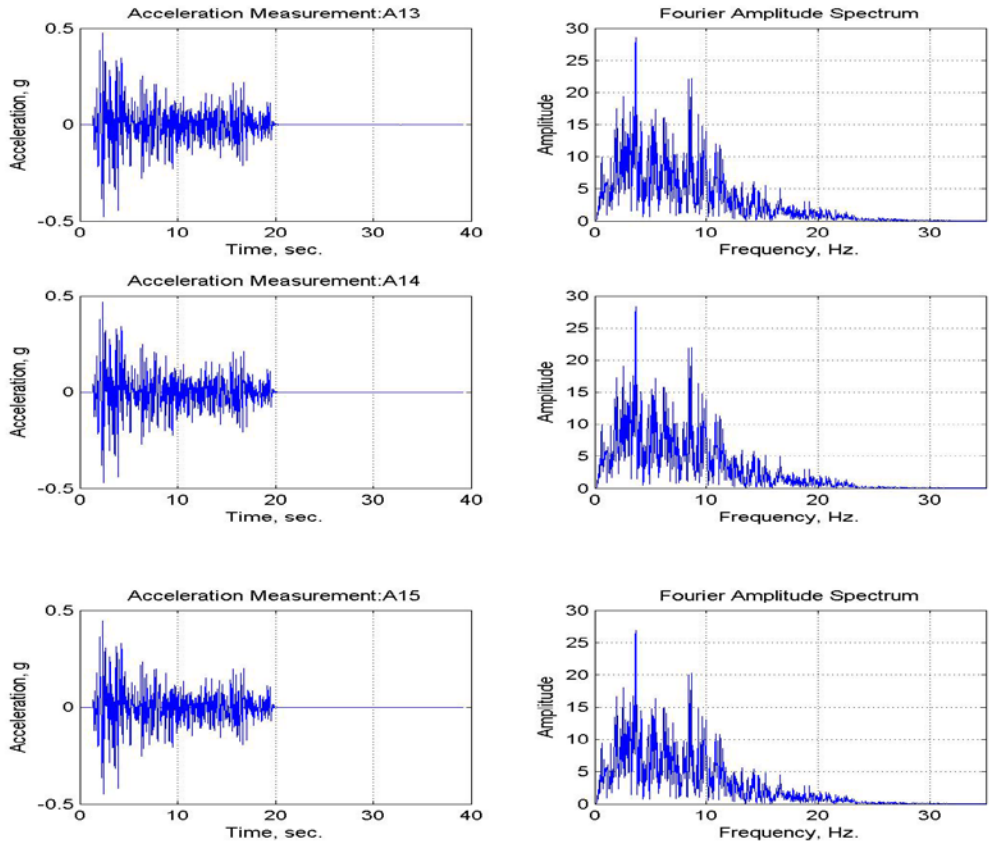


Figure A.31. Accelerations Measured for Wall Configuration 4- El Centro 100% (continued)

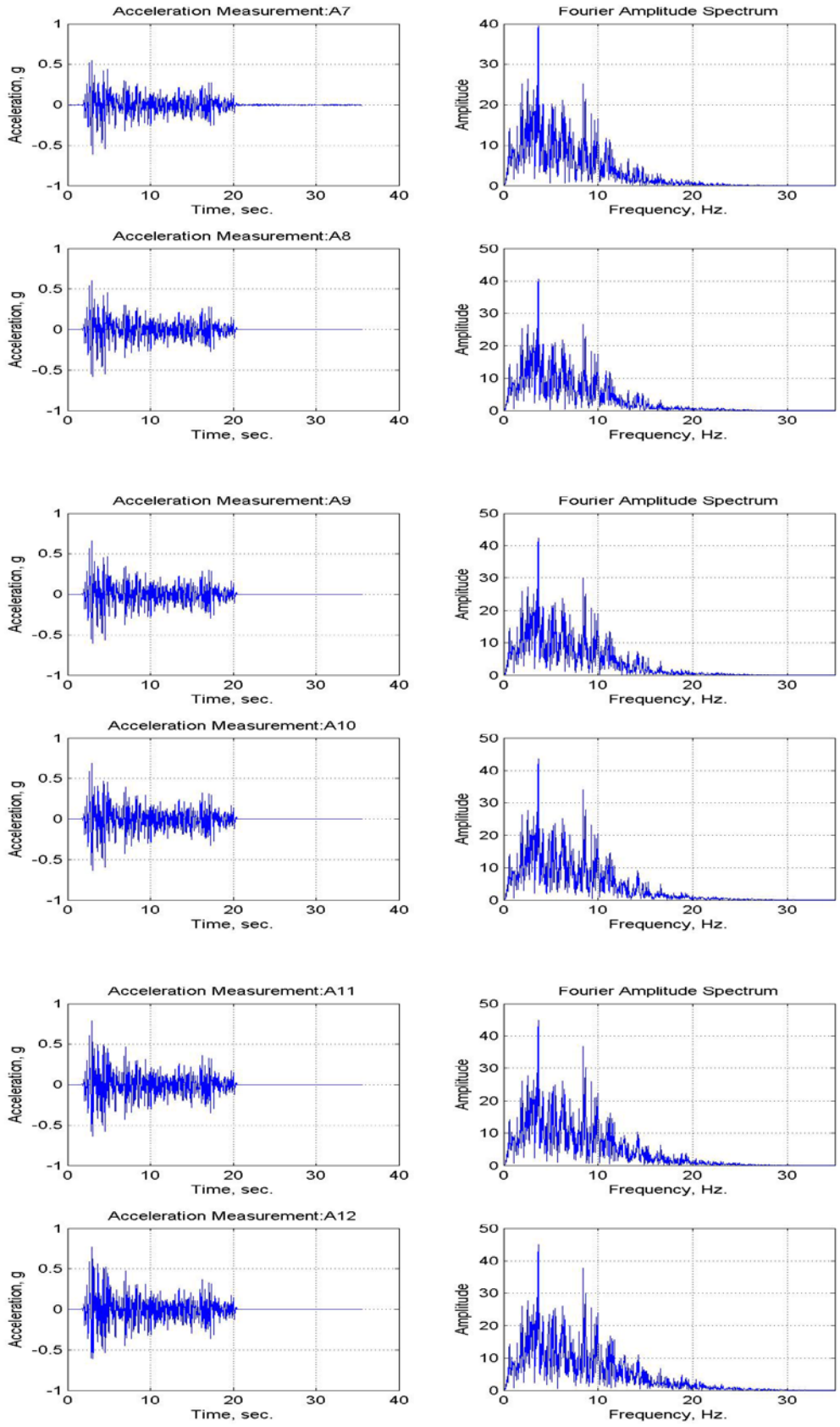


Figure A.32. Accelerations Measured for Wall Configuration 4- El Centro 150%

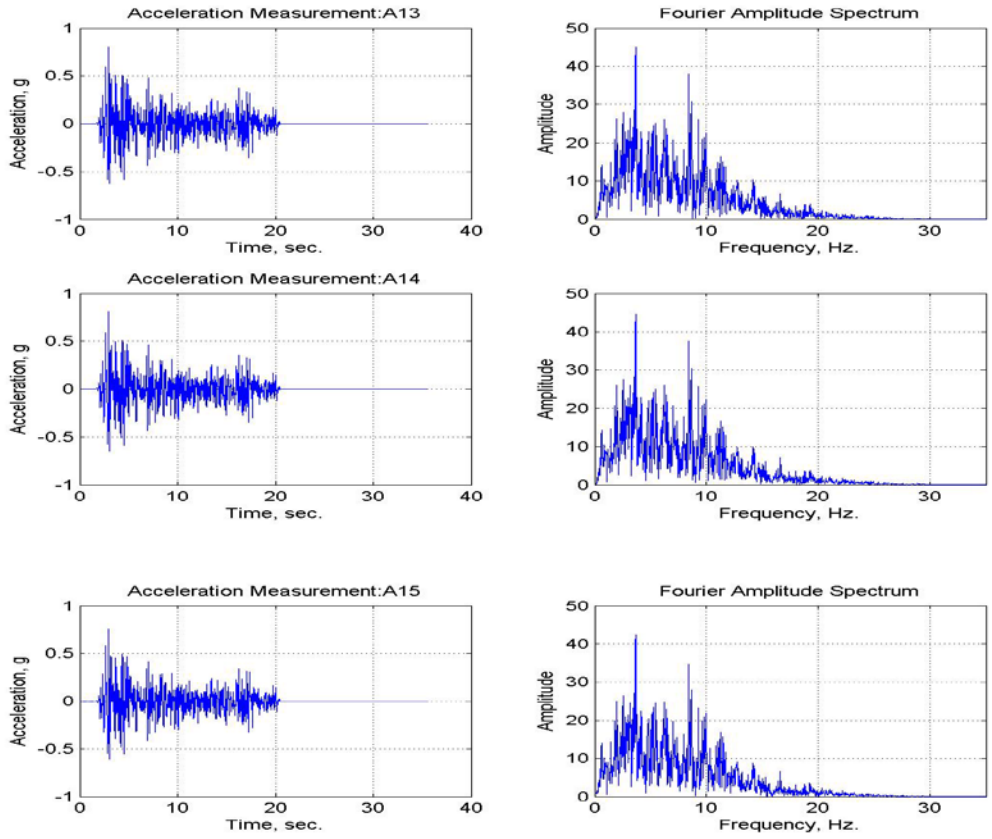


Figure A.32. Accelerations Measured for Wall Configuration 4- El Centro 150% (continued)

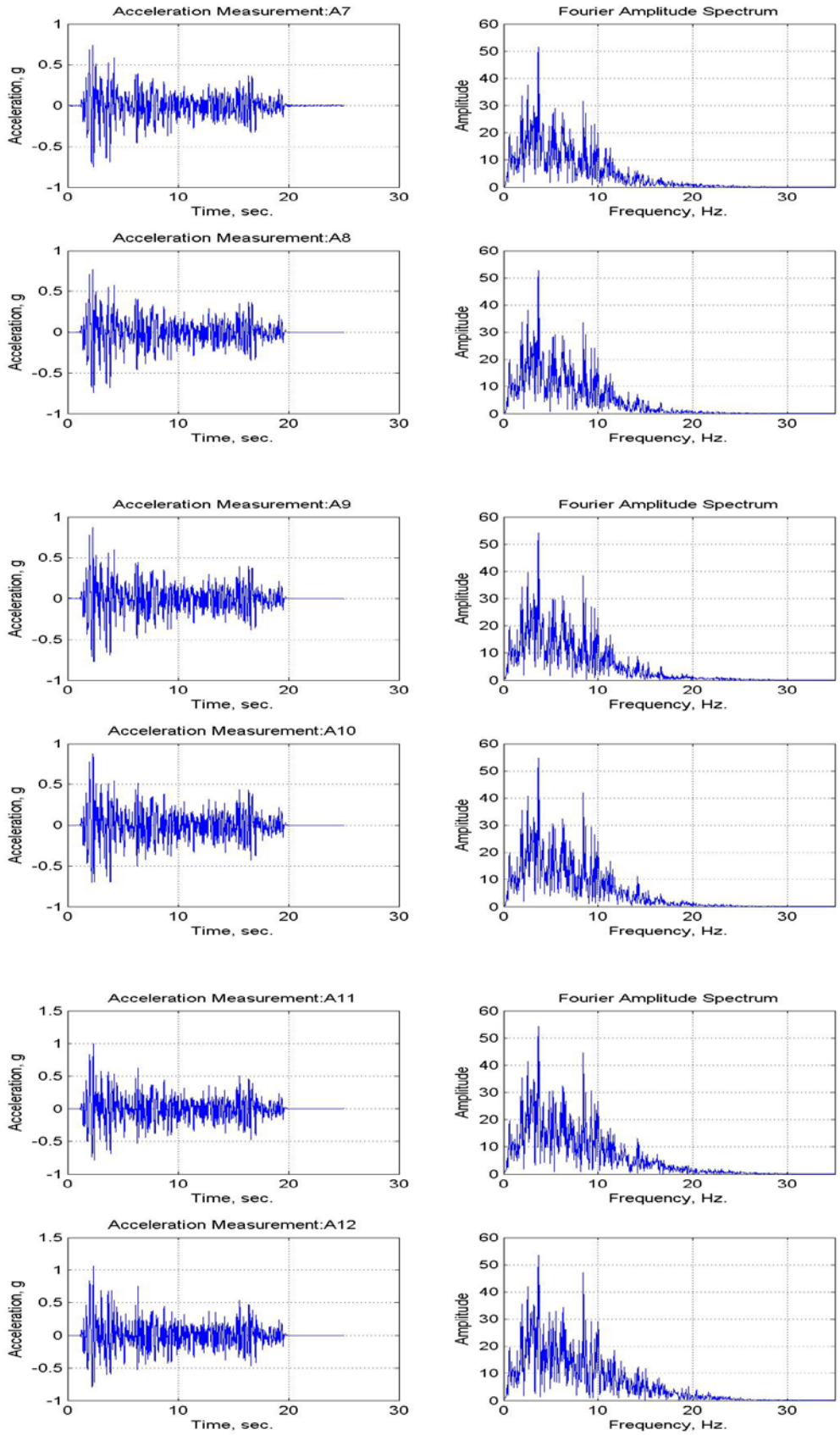


Figure A.33. Accelerations Measured for Wall Configuration 4- El Centro 200%

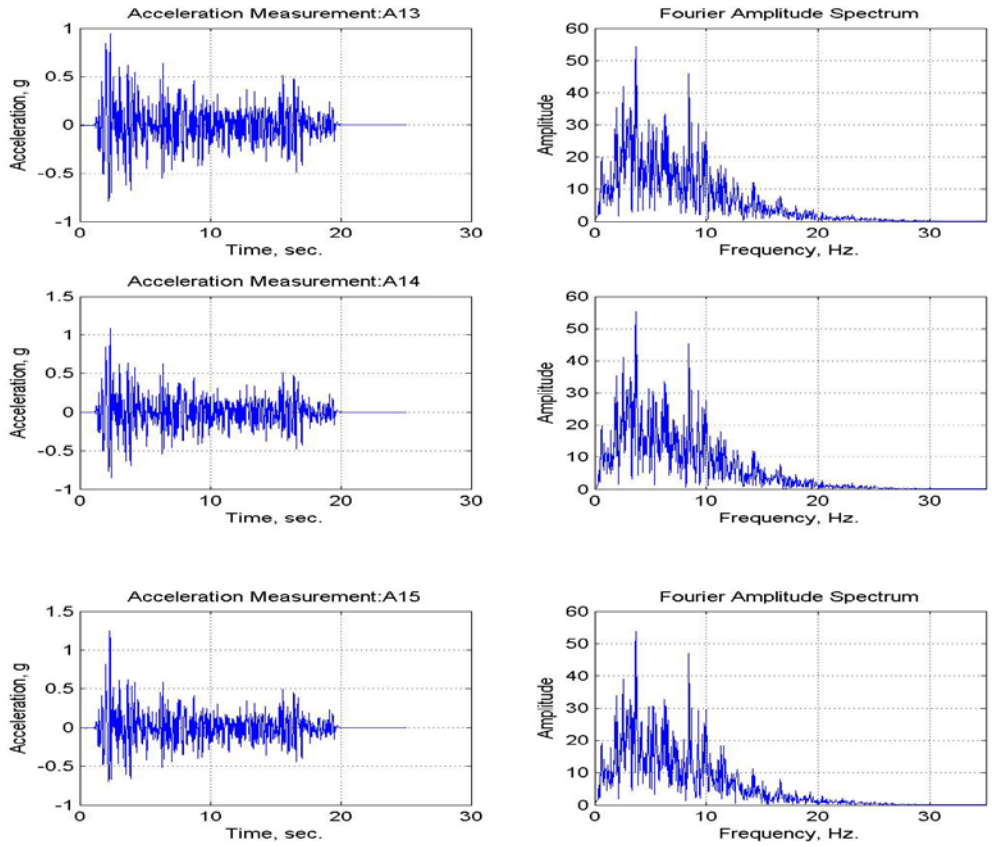


Figure A.33. Accelerations Measured for Wall Configuration 4- El Centro 200% (continued)

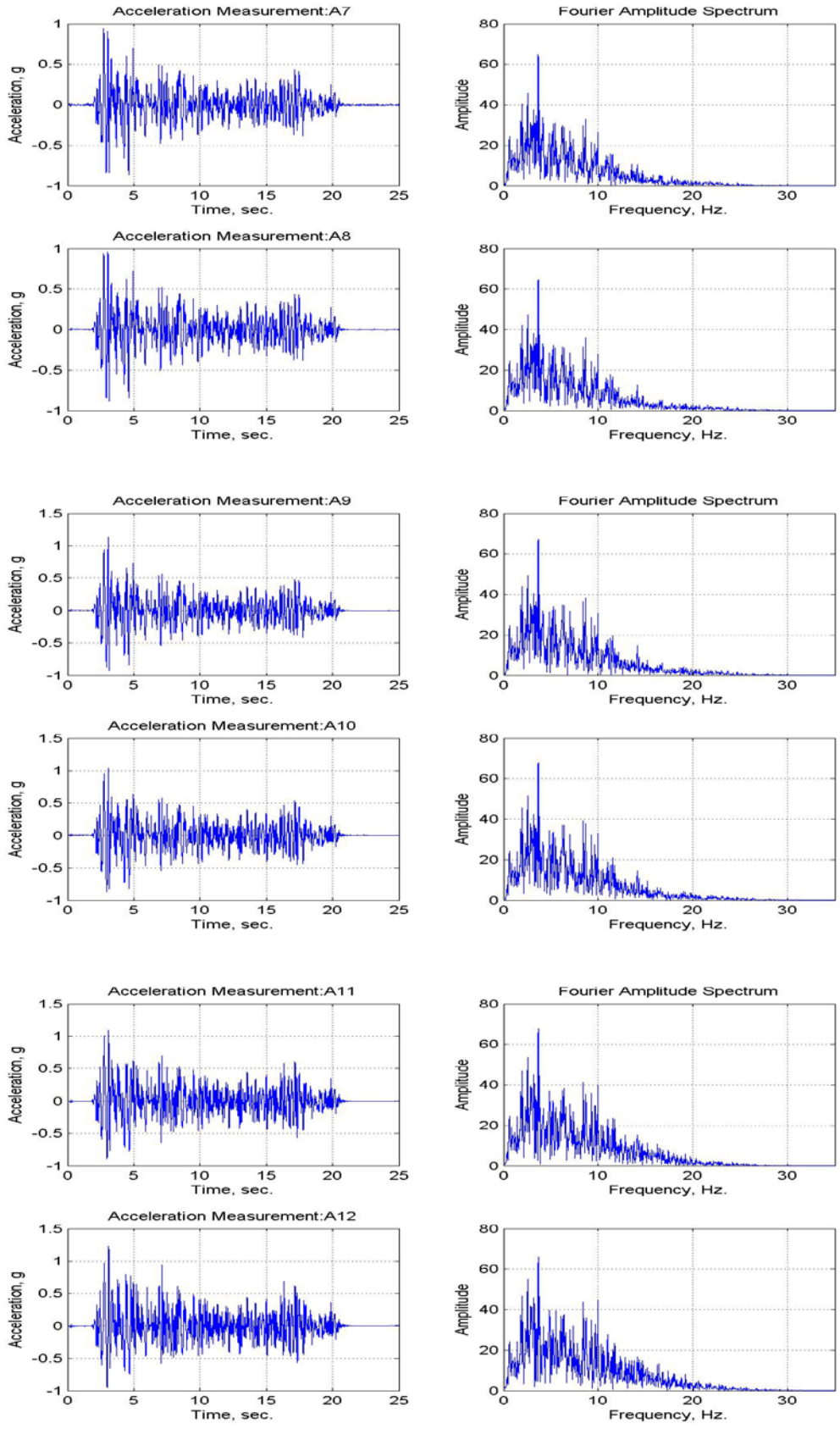


Figure A.34. Accelerations Measured for Wall Configuration 4- El Centro 250%

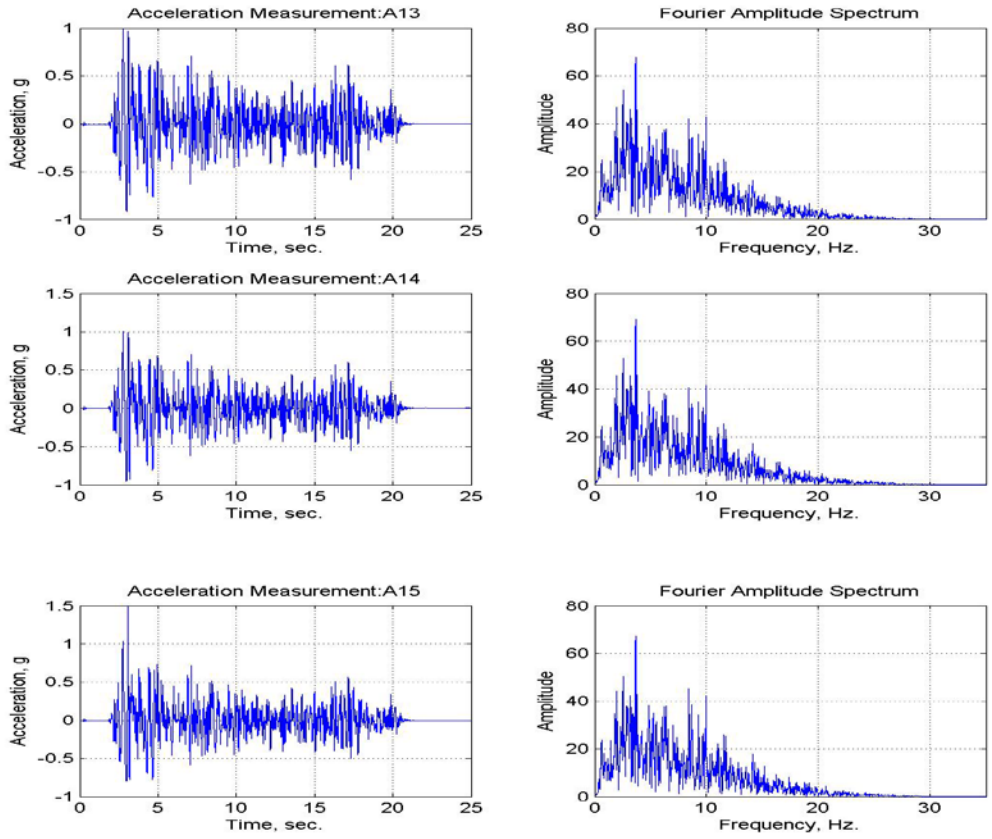


Figure A.34. Accelerations Measured for Wall Configuration 4- El Centro 250% (continued)

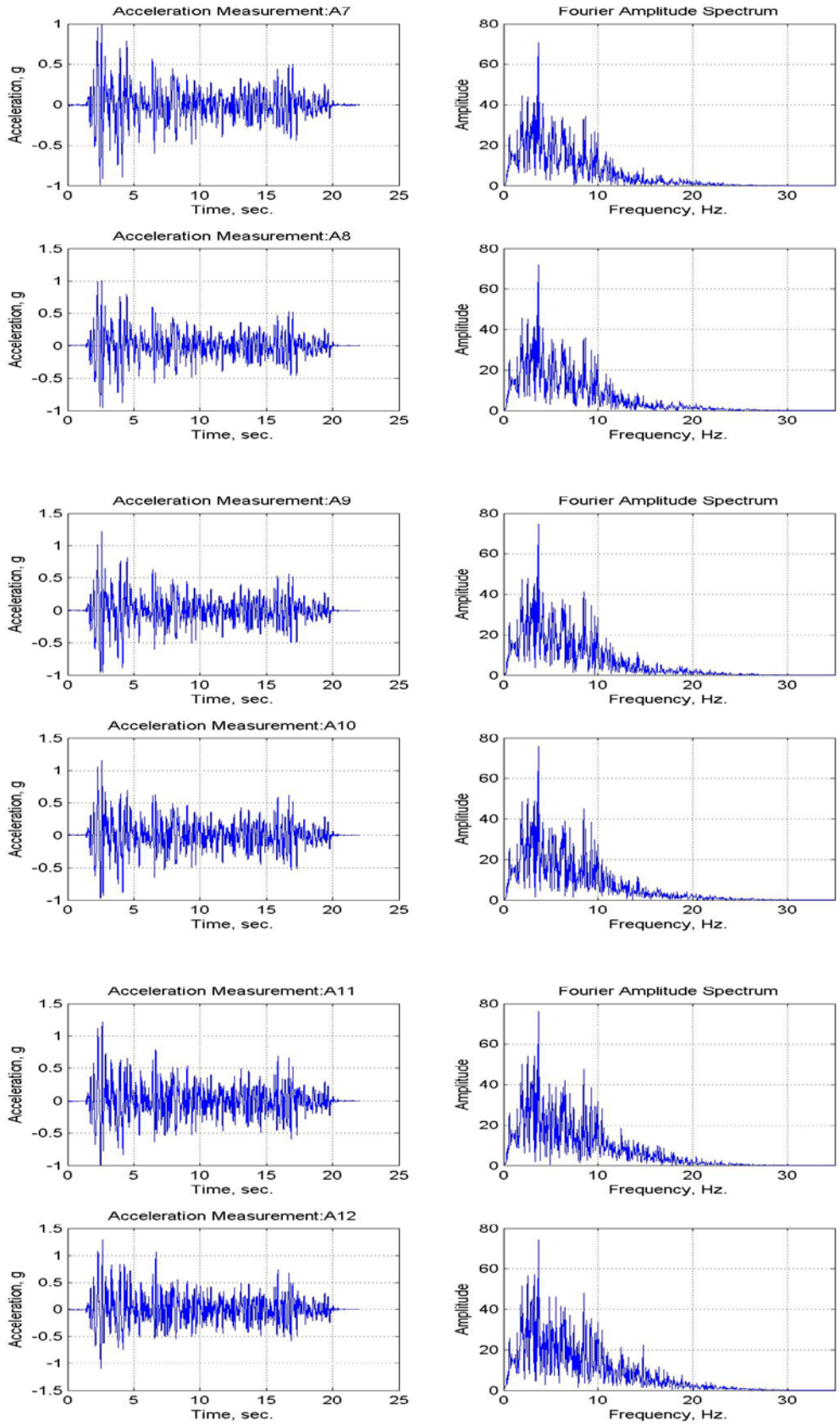


Figure A.35. Accelerations Measured for Wall Configuration 4- El Centro 275%

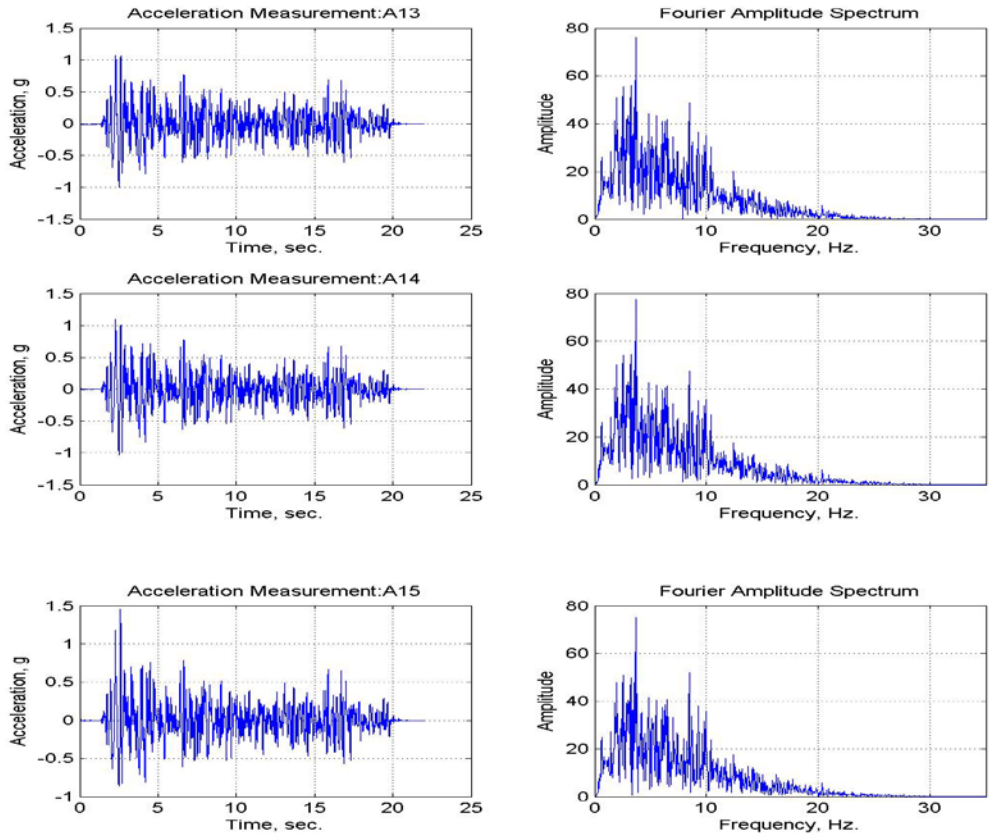


Figure A.35. Accelerations Measured for Wall Configuration 4- El Centro 275% (continued)

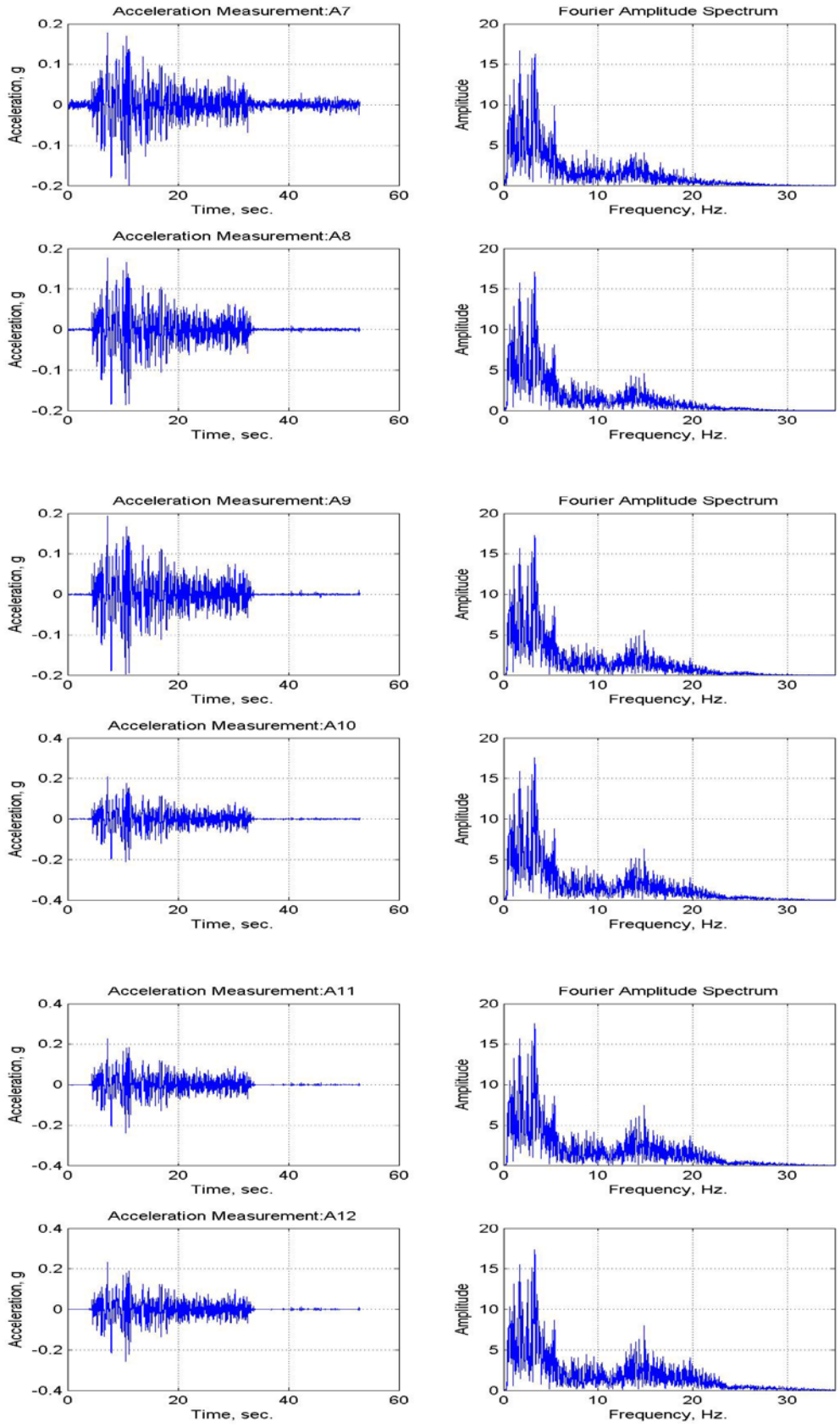


Figure A.36. Accelerations Measured for Wall Configuration 4- Izmit 100%

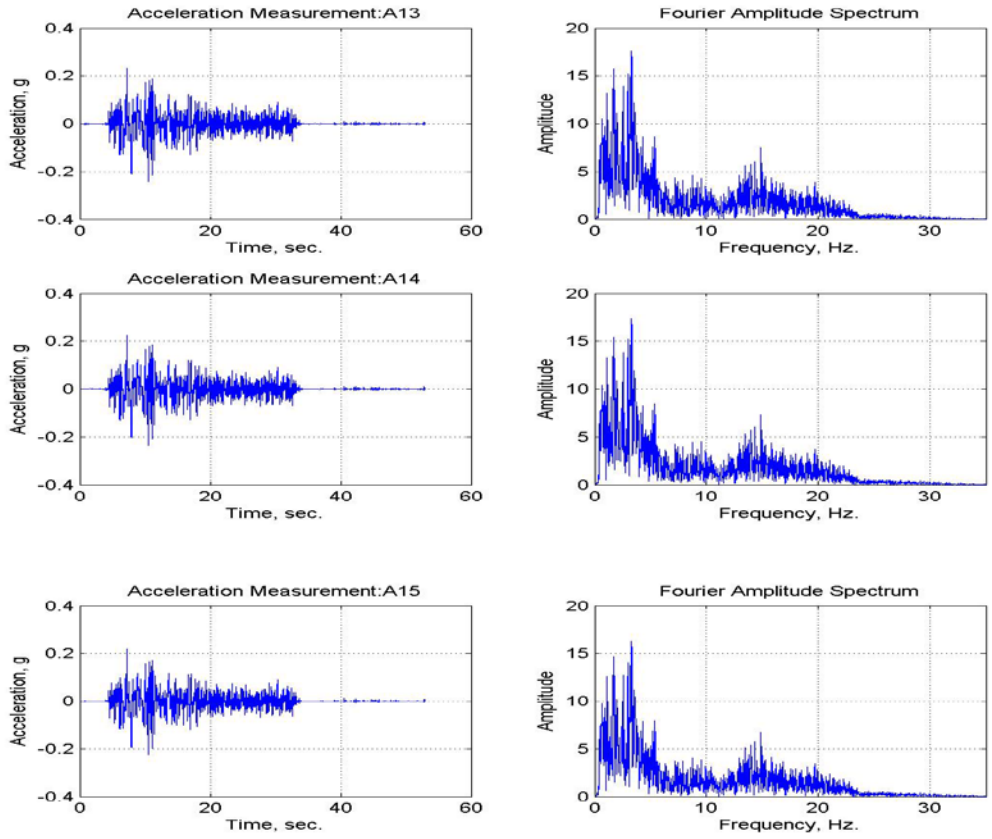


Figure A.36. Accelerations Measured for Wall Configuration 4- Izmit 100% (continued)

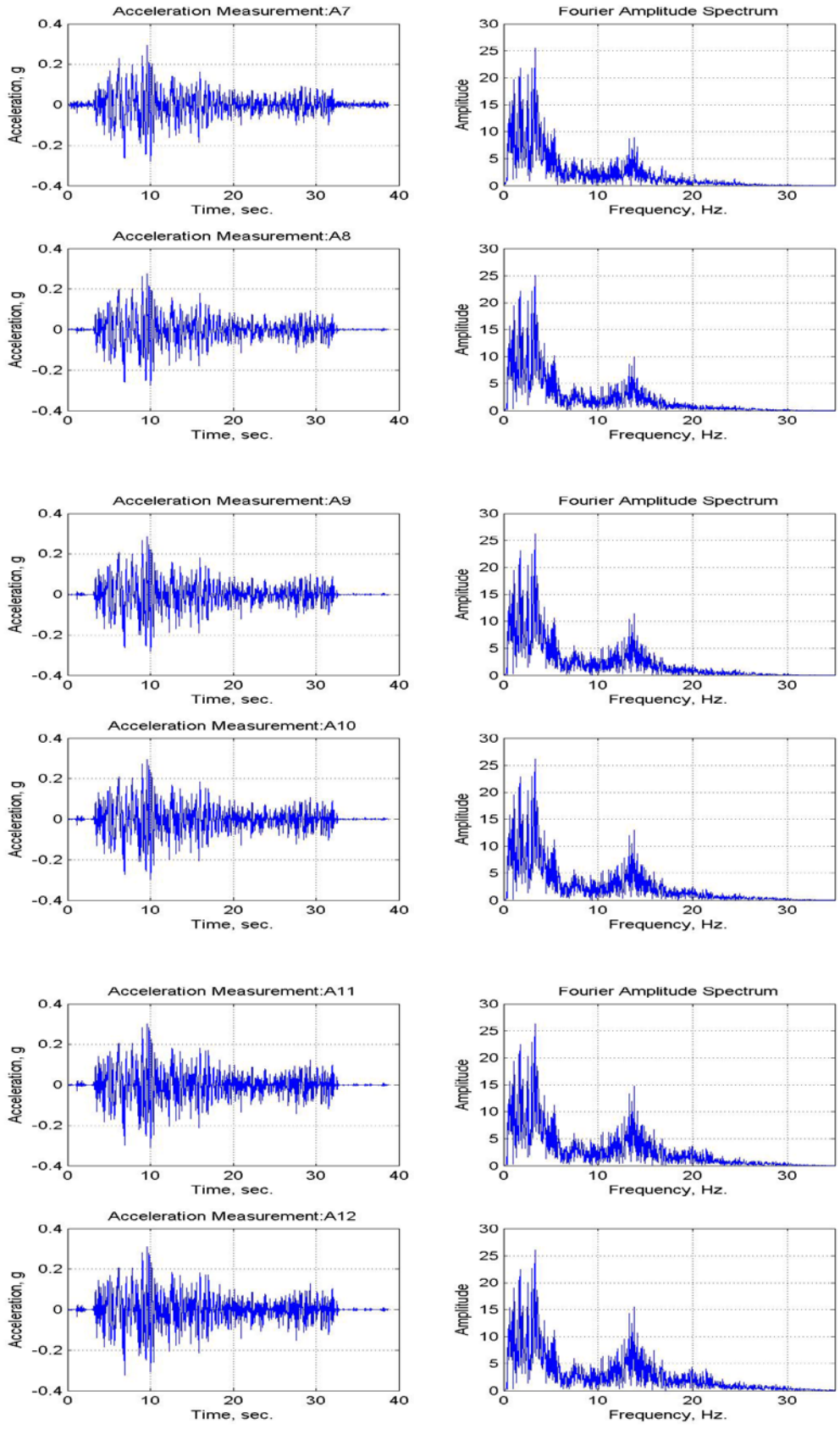


Figure A.37. Accelerations Measured for Wall Configuration 4- Izmit 150%

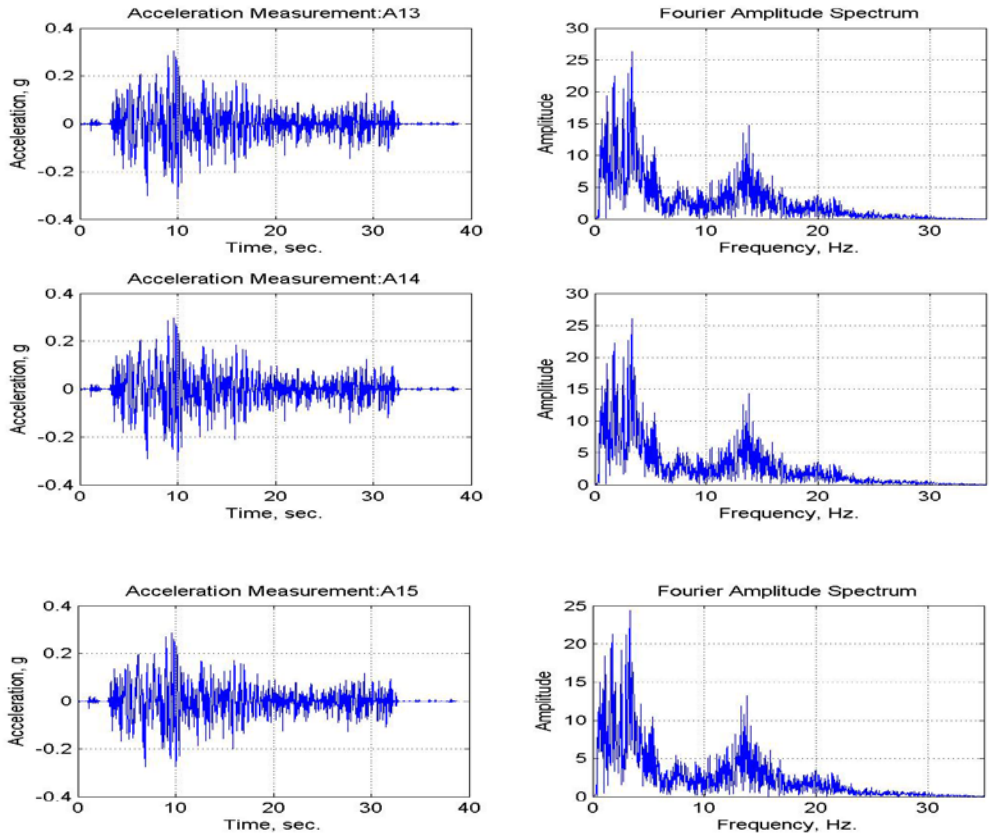


Figure A.37. Accelerations Measured for Wall Configuration 4- Izmit 150% (continued)

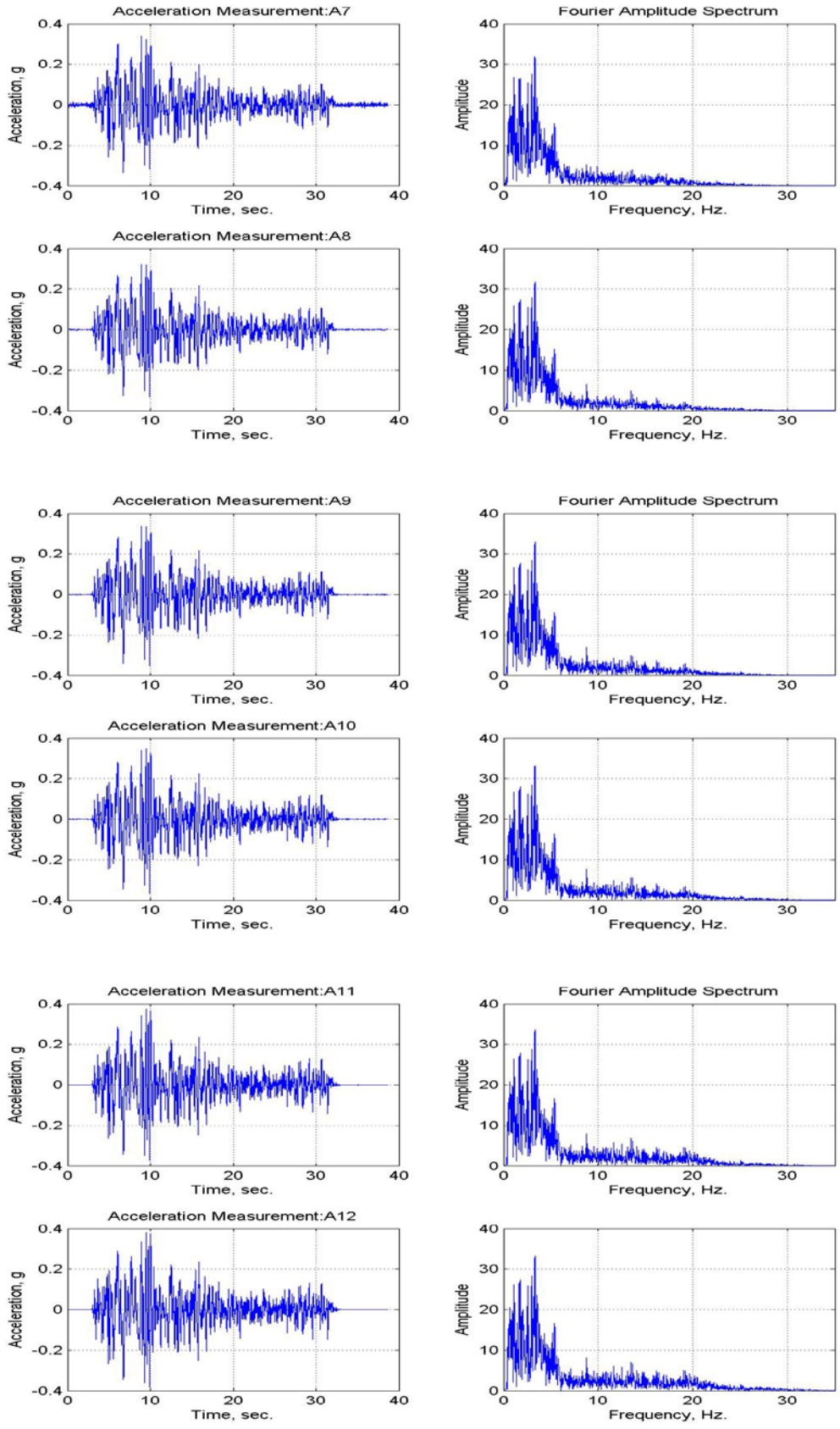


Figure A.38. Accelerations Measured for Wall Configuration 4- Izmit 200%

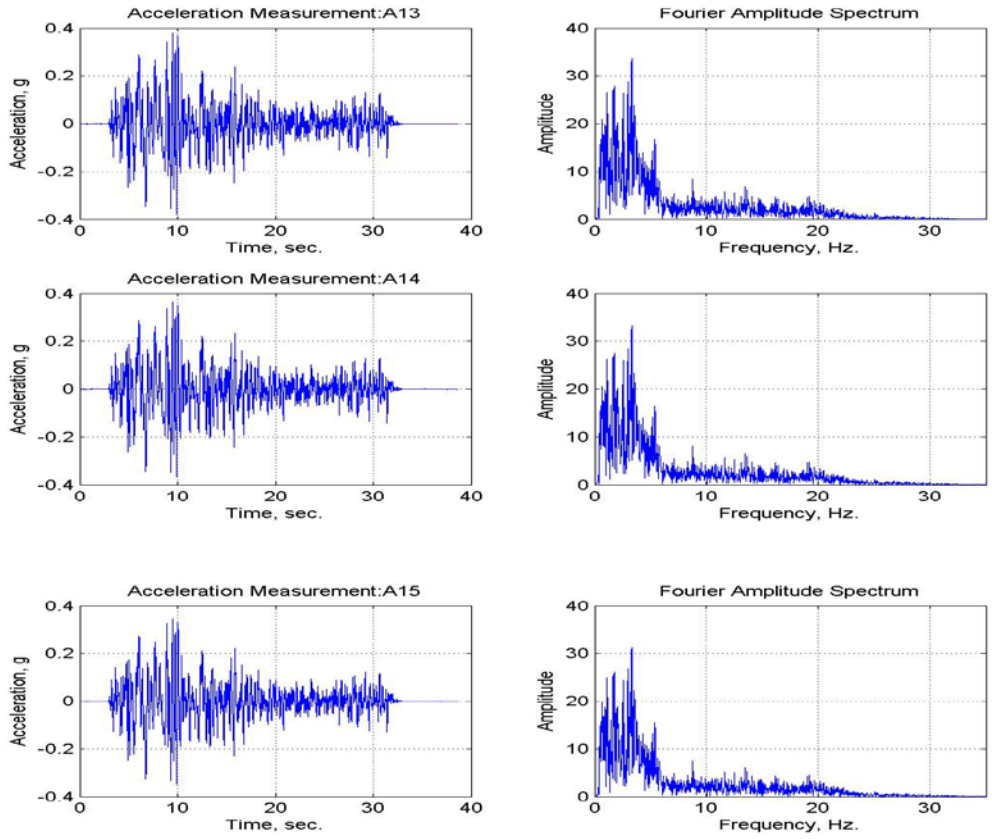


Figure A.38. Accelerations Measured for Wall Configuration 4- Izmit 200% (continued)

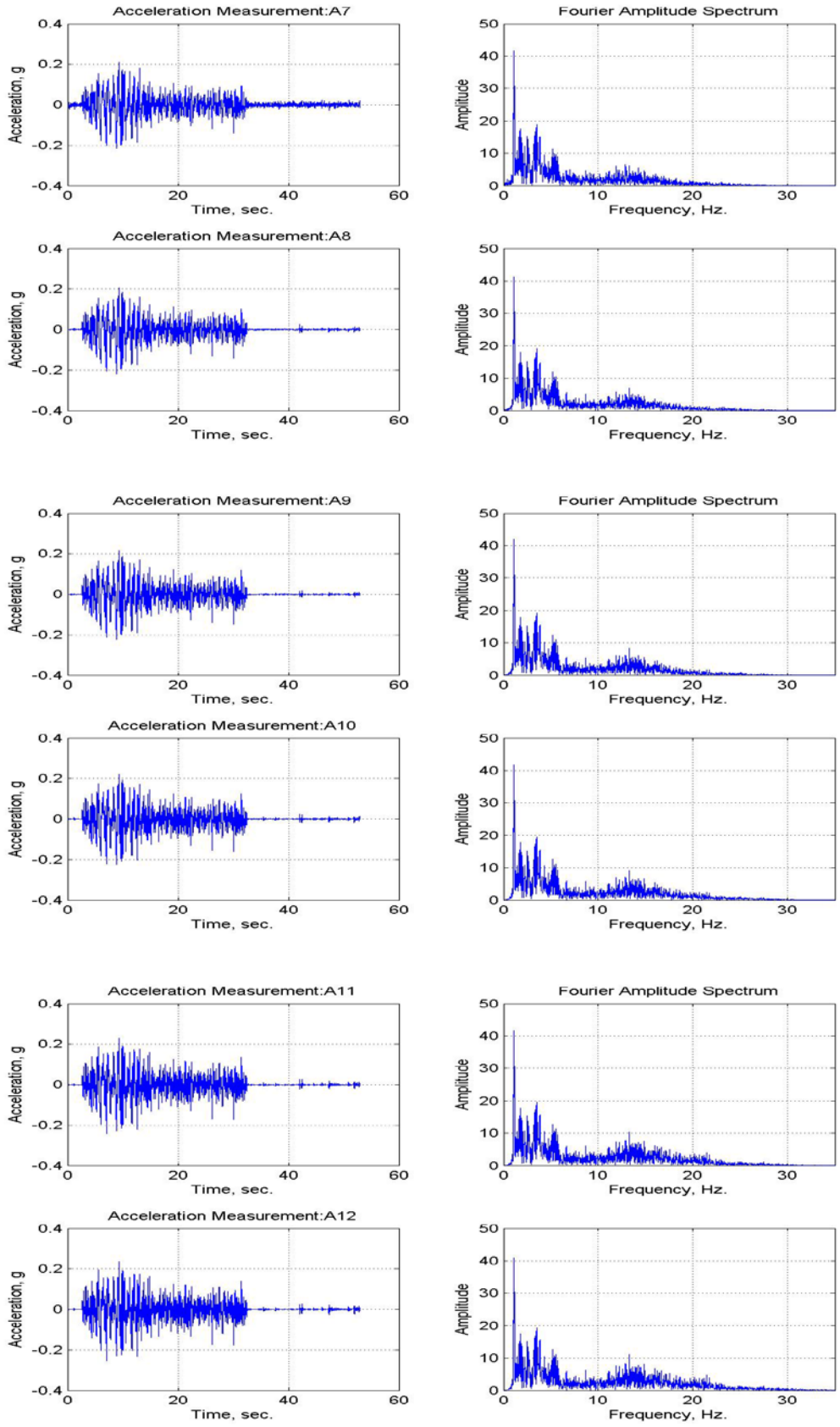


Figure A.39. Accelerations Measured for Wall Configuration 4- Sakarya 100%

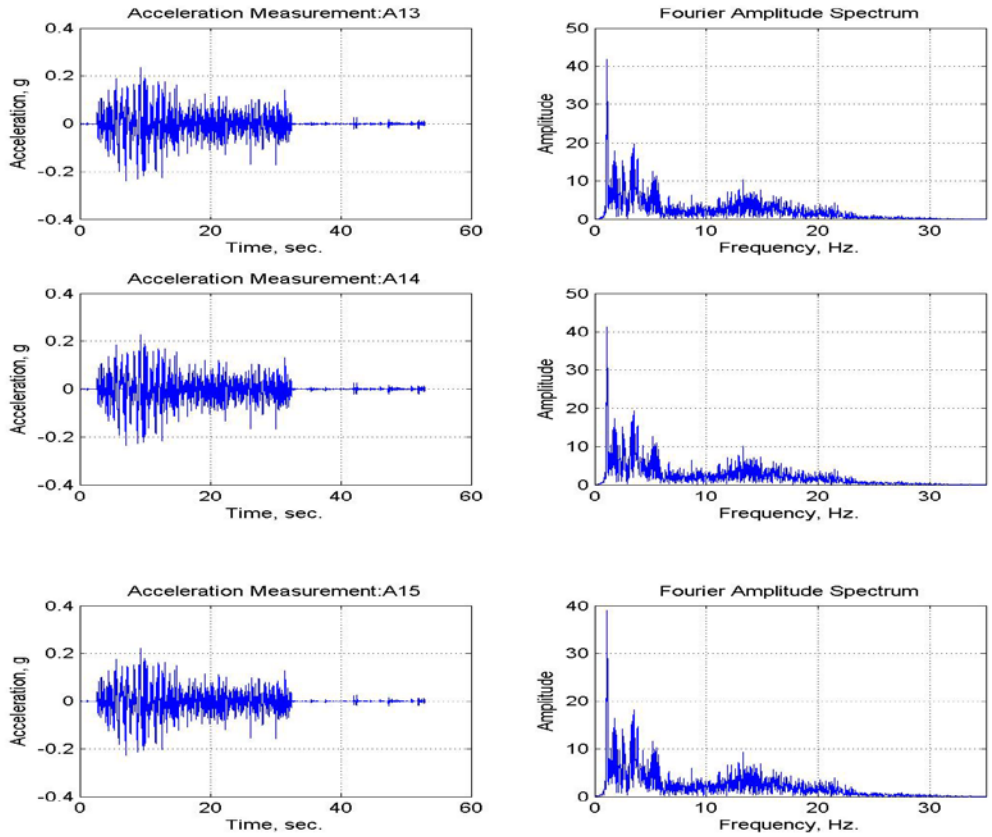


Figure A.39. Accelerations Measured for Wall Configuration 4- Sakarya 100% (continued)

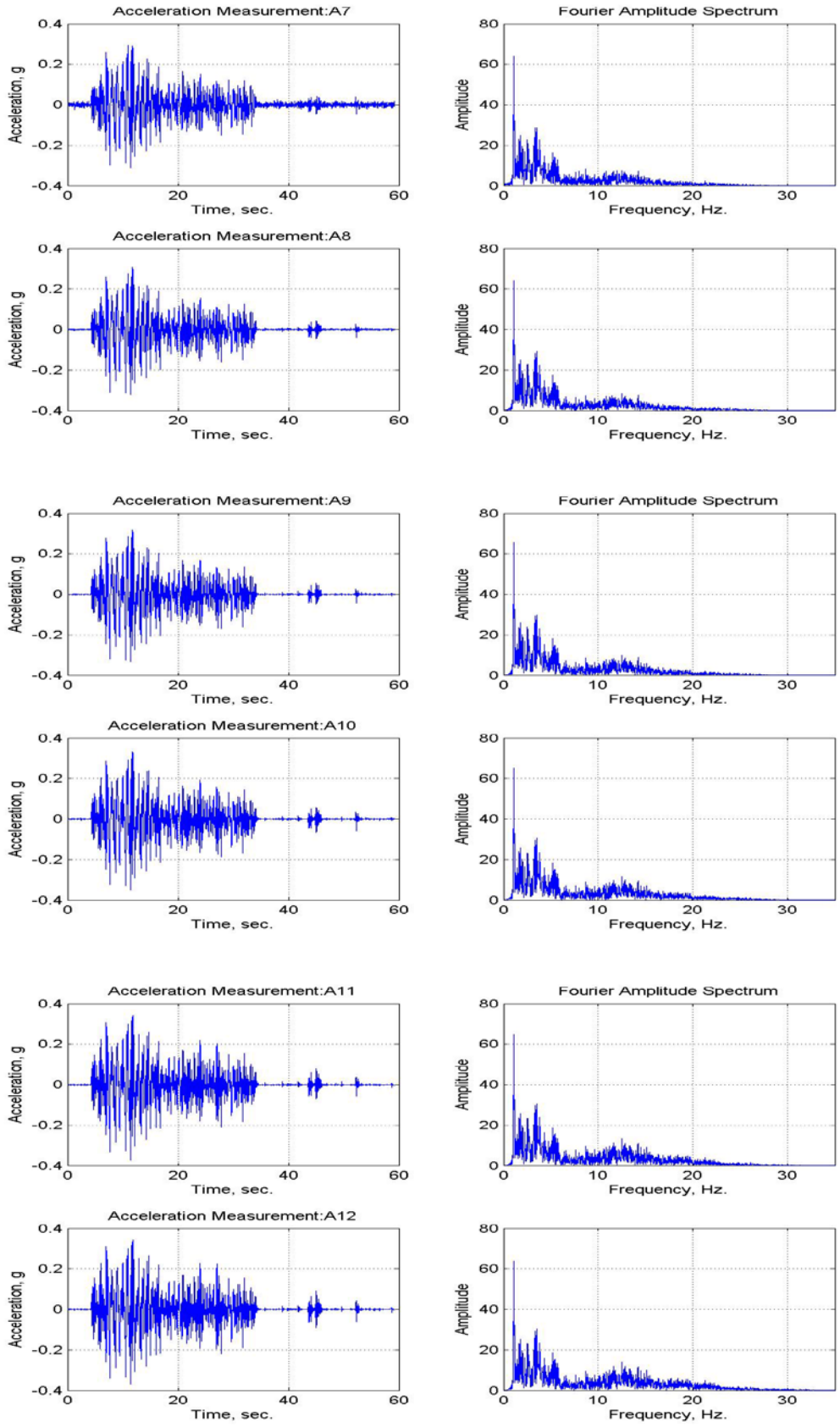


Figure A.40. Accelerations Measured for Wall Configuration 4- Sakarya 150%

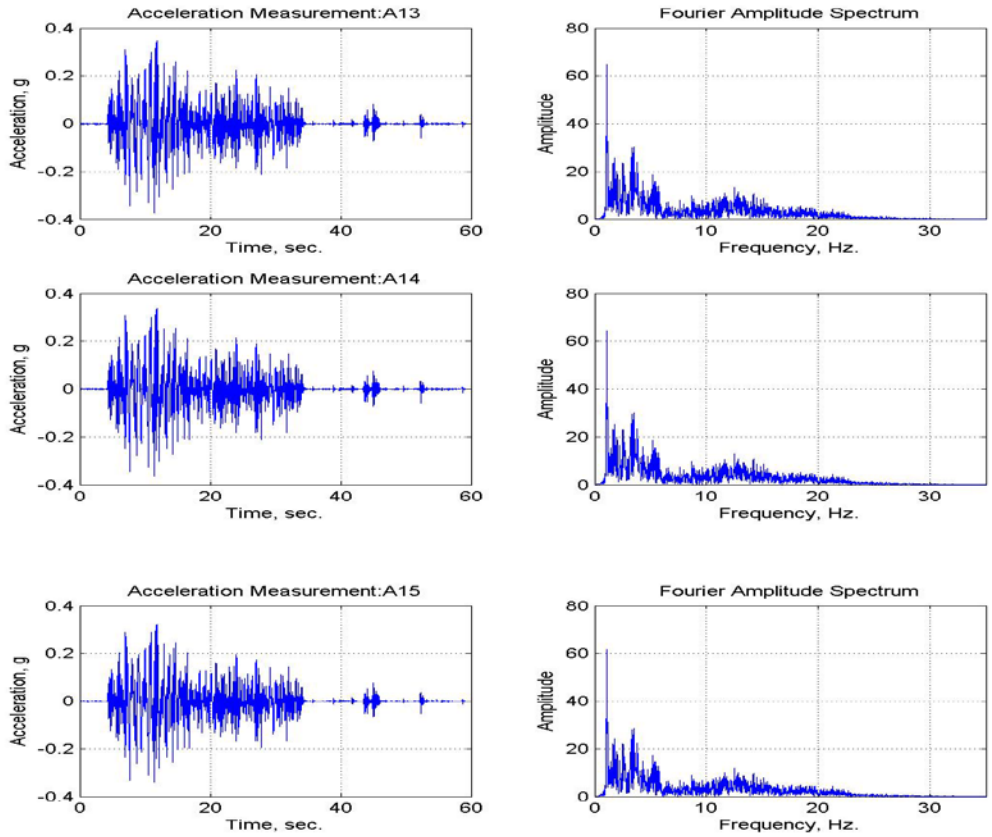


Figure A.40. Accelerations Measured for Wall Configuration 4- Sakarya 150% (continued)

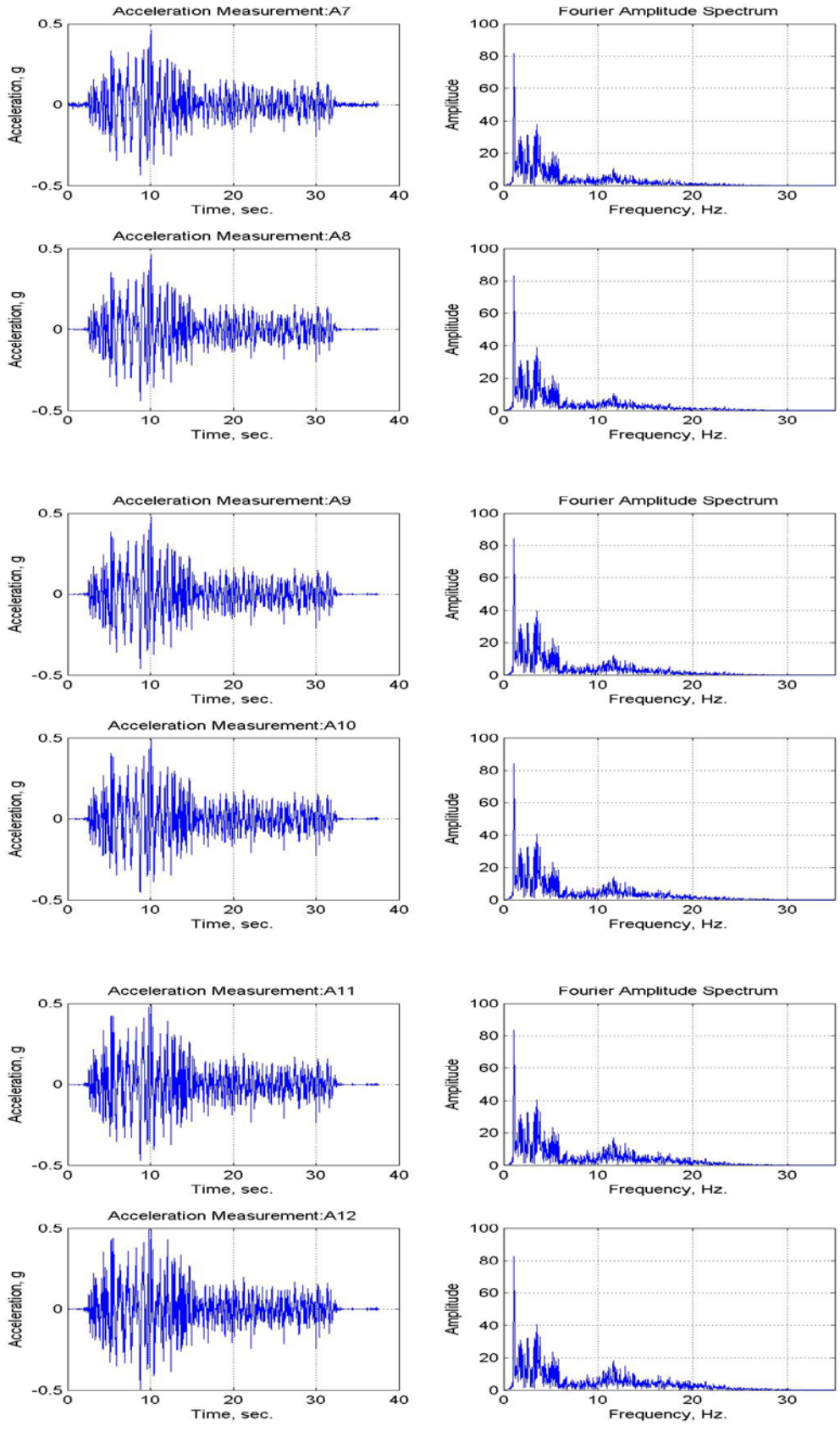


Figure A.41. Accelerations Measured for Wall Configuration 4- Sakarya 200%

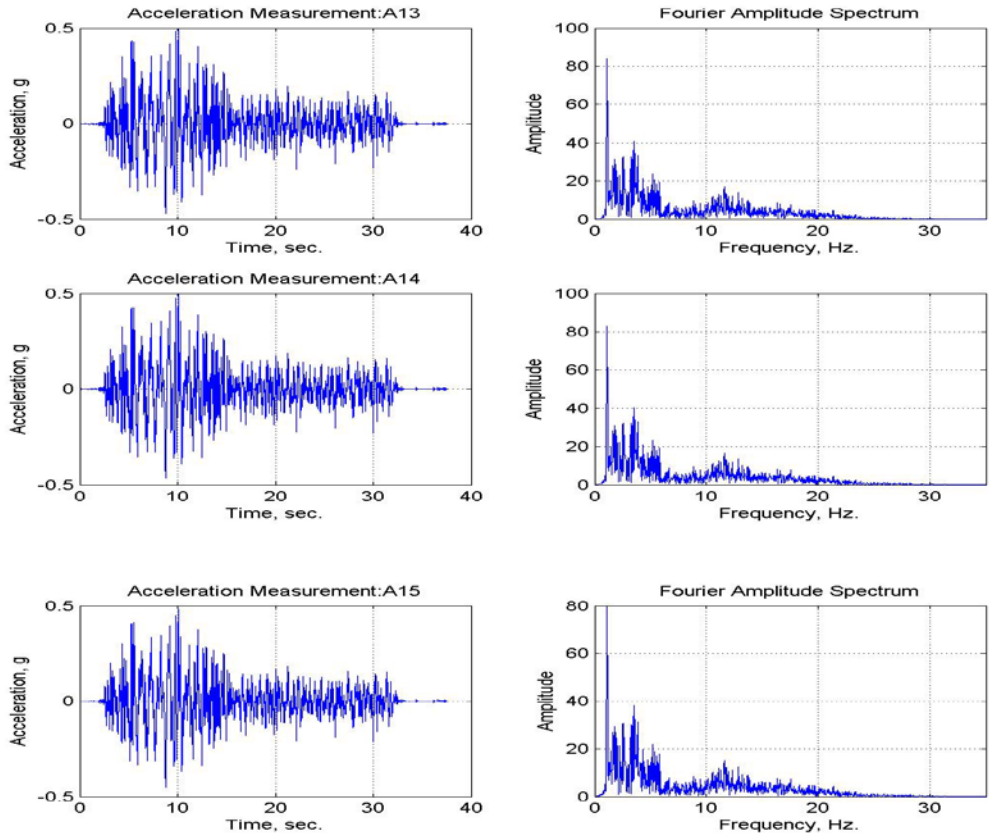


Figure A.41. Accelerations Measured for Wall Configuration 4- Sakarya 200% (continued)

APPENDIX B: FACE DISPLACEMENT-TIME HISTORY GRAPHS OBTAINED FROM THE TESTS

This appendix contains face displacement-time history graphs for each wall configuration and applied excitations. The locations and abbreviations used for the laser displacement transducers are given in Section 4.

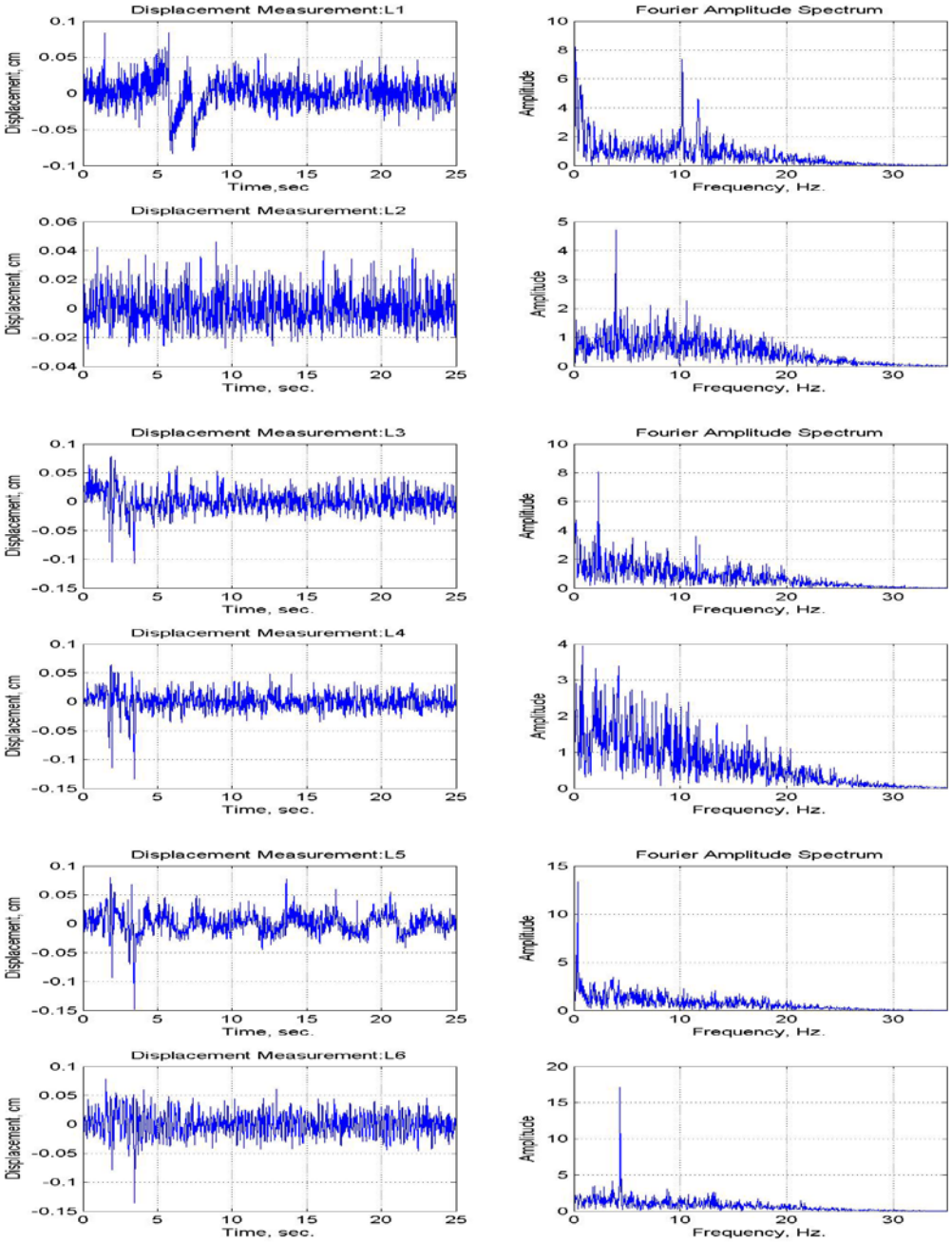


Figure B.1. Facing Displacements Measured for Wall Configuration 1- El Centro 100%

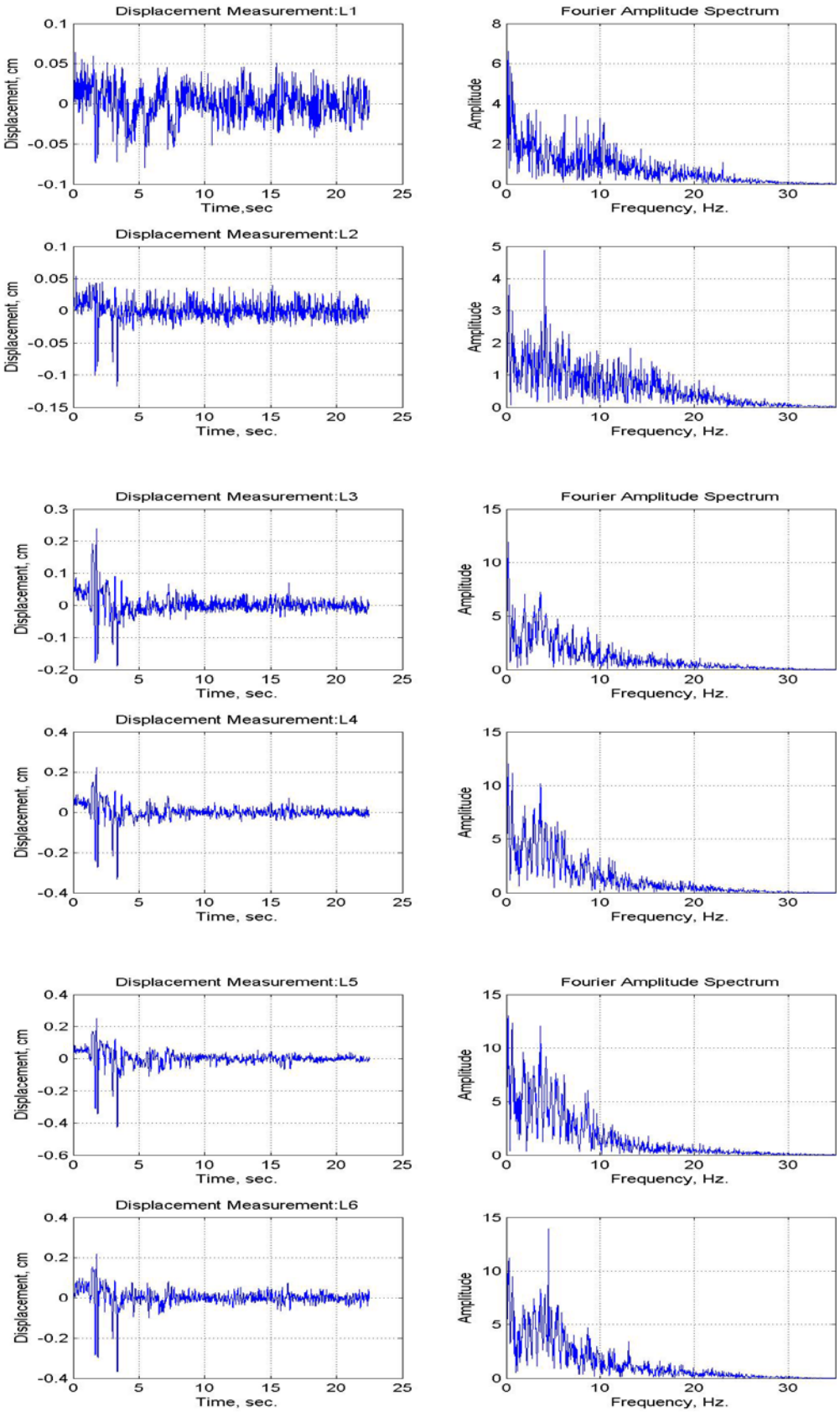


Figure B.2. Facing Displacements Measured for Wall Configuration 1- El Centro 150%

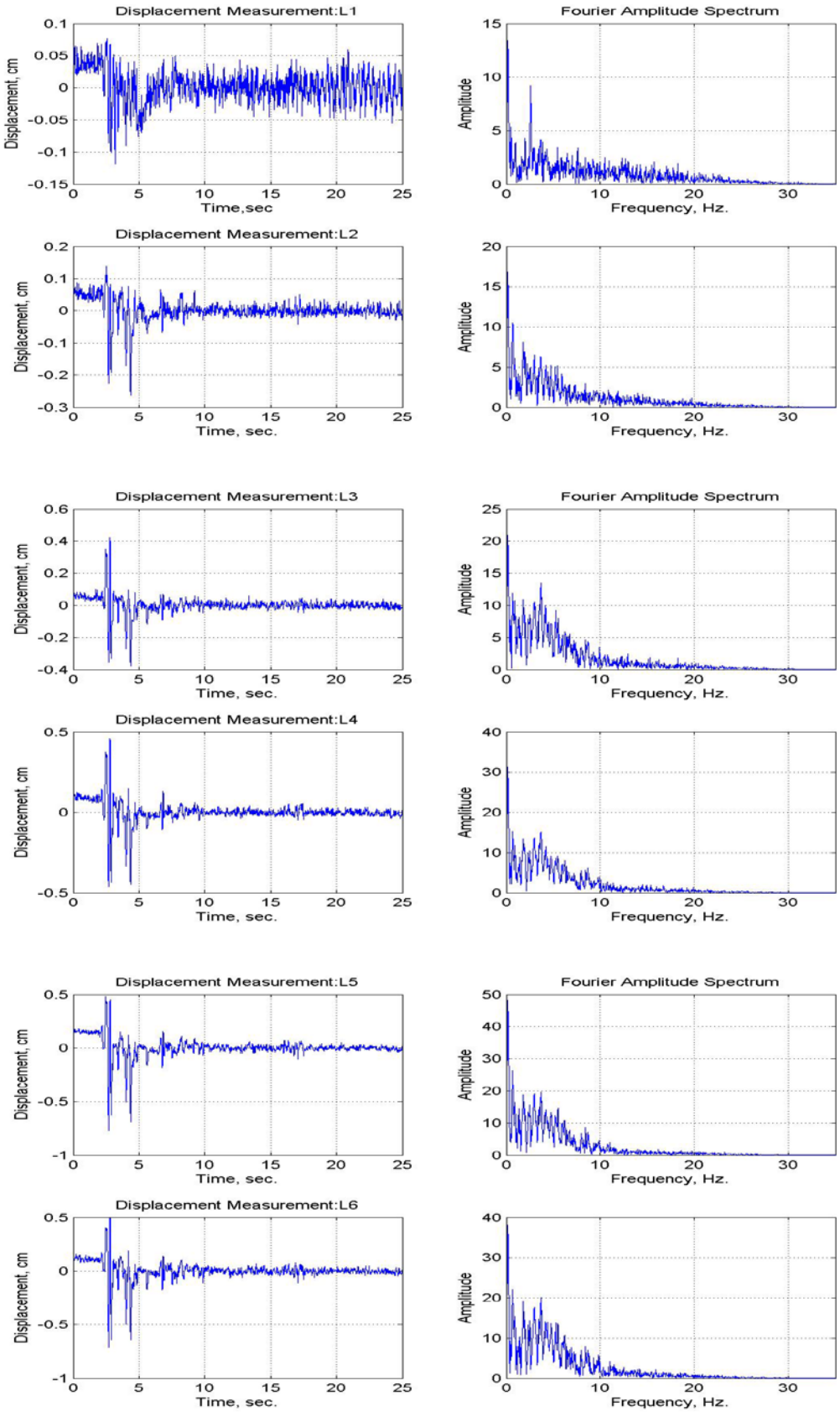


Figure B.3. Facing Displacements Measured for Wall Configuration 1- El Centro 200%

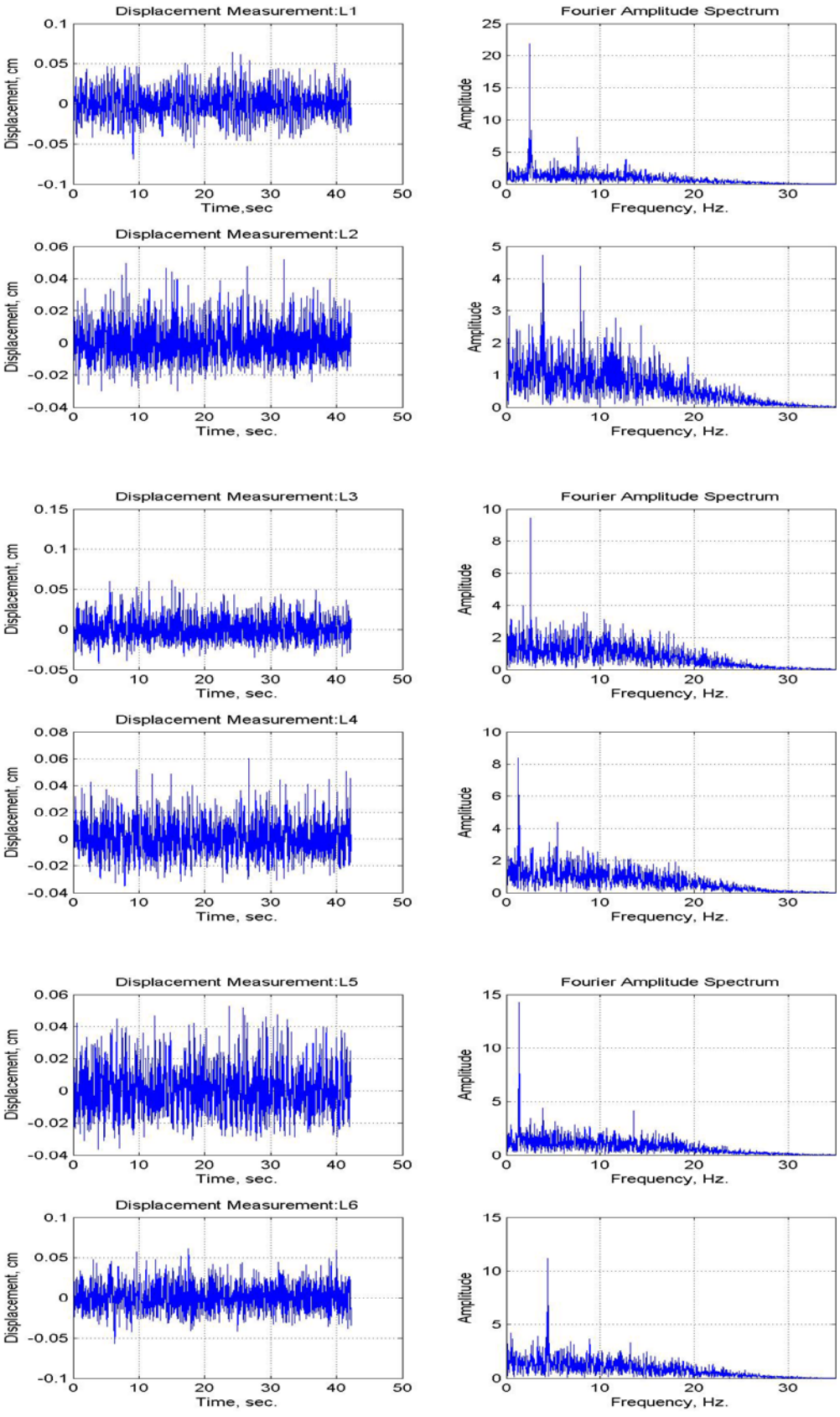


Figure B.4. Facing Displacements Measured for Wall Configuration 1- Izmit 100%

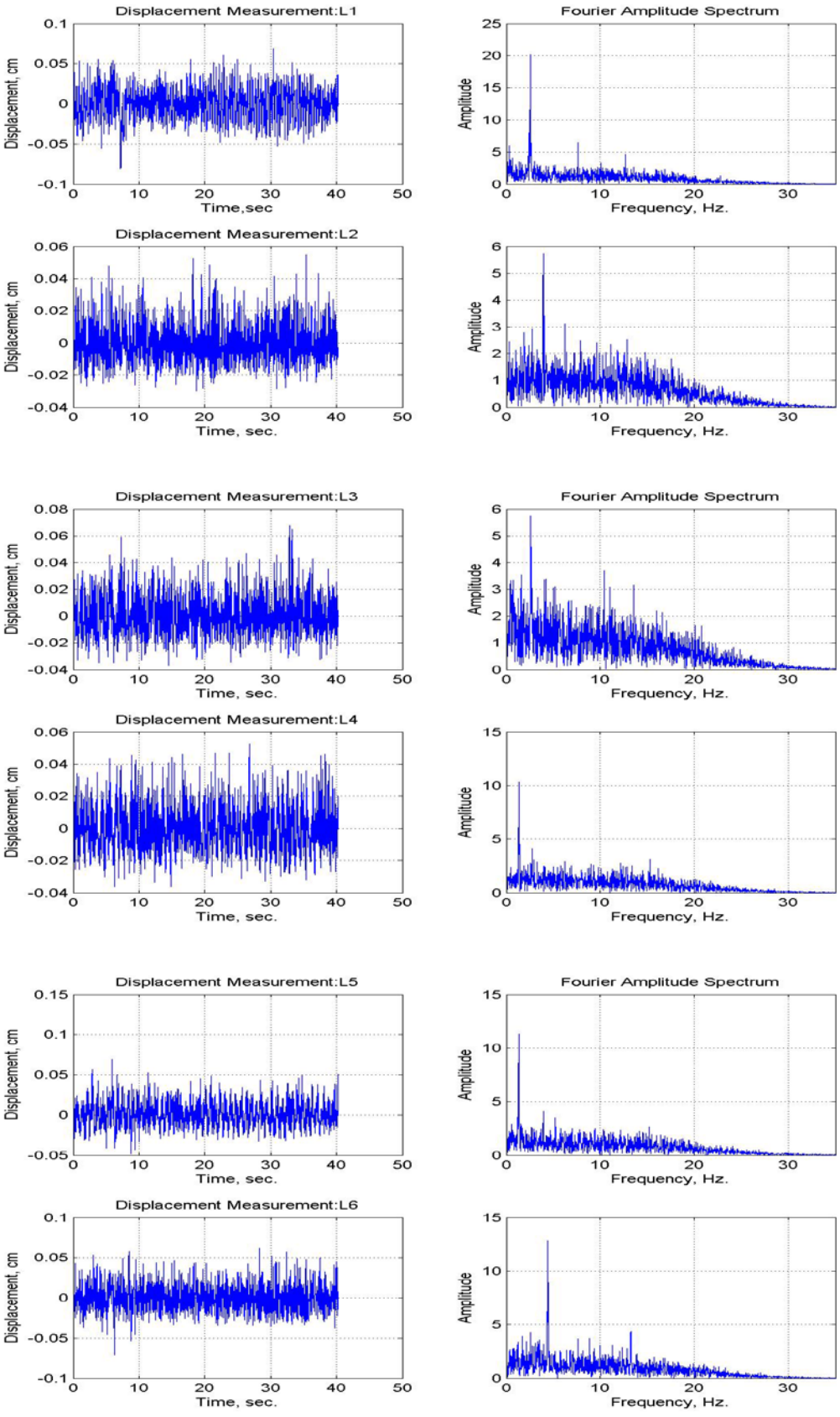


Figure B.5. Facing Displacements Measured for Wall Configuration 1- Izmit 150%

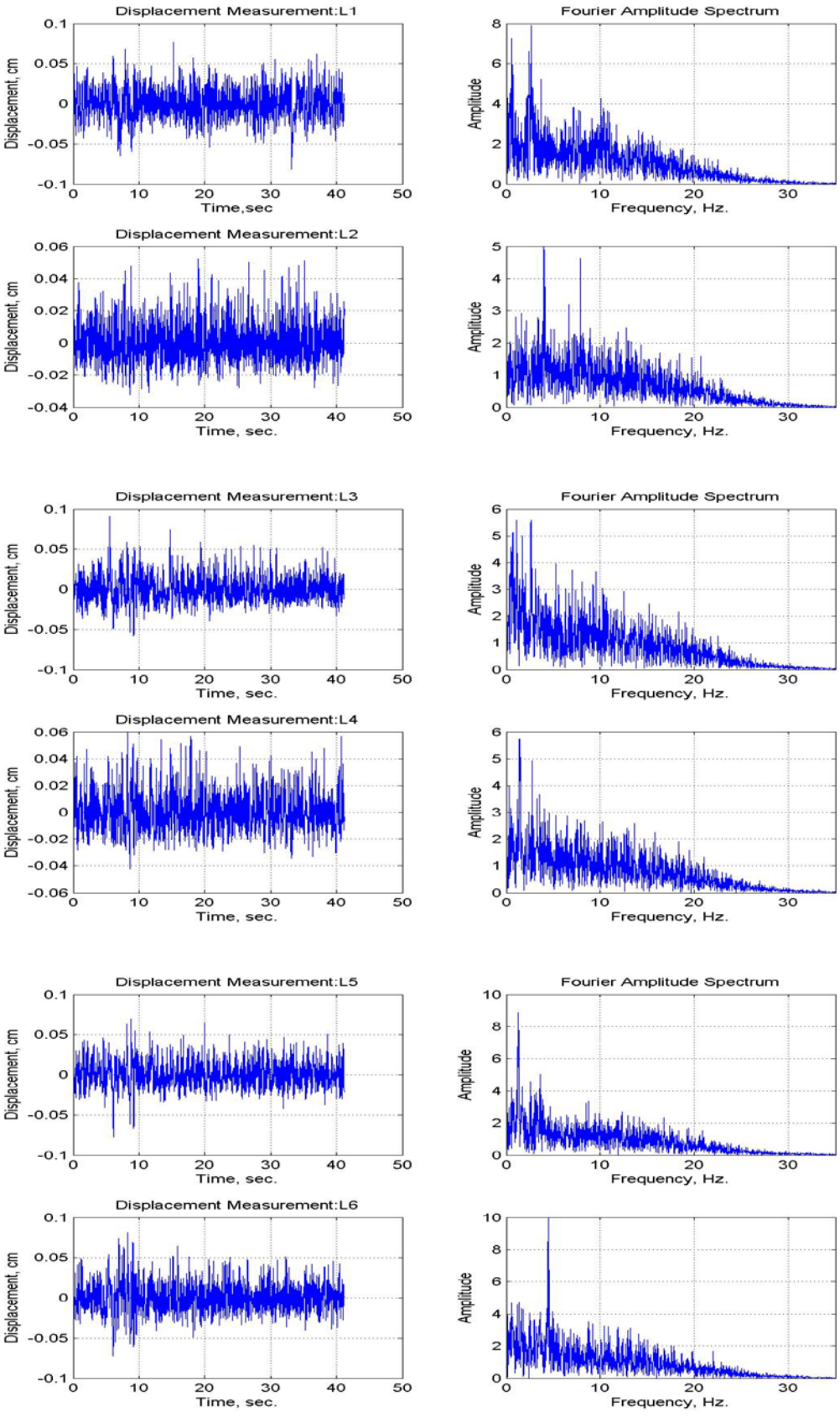


Figure B.6. Facing Displacements Measured for Wall Configuration 1- Izmit 200%

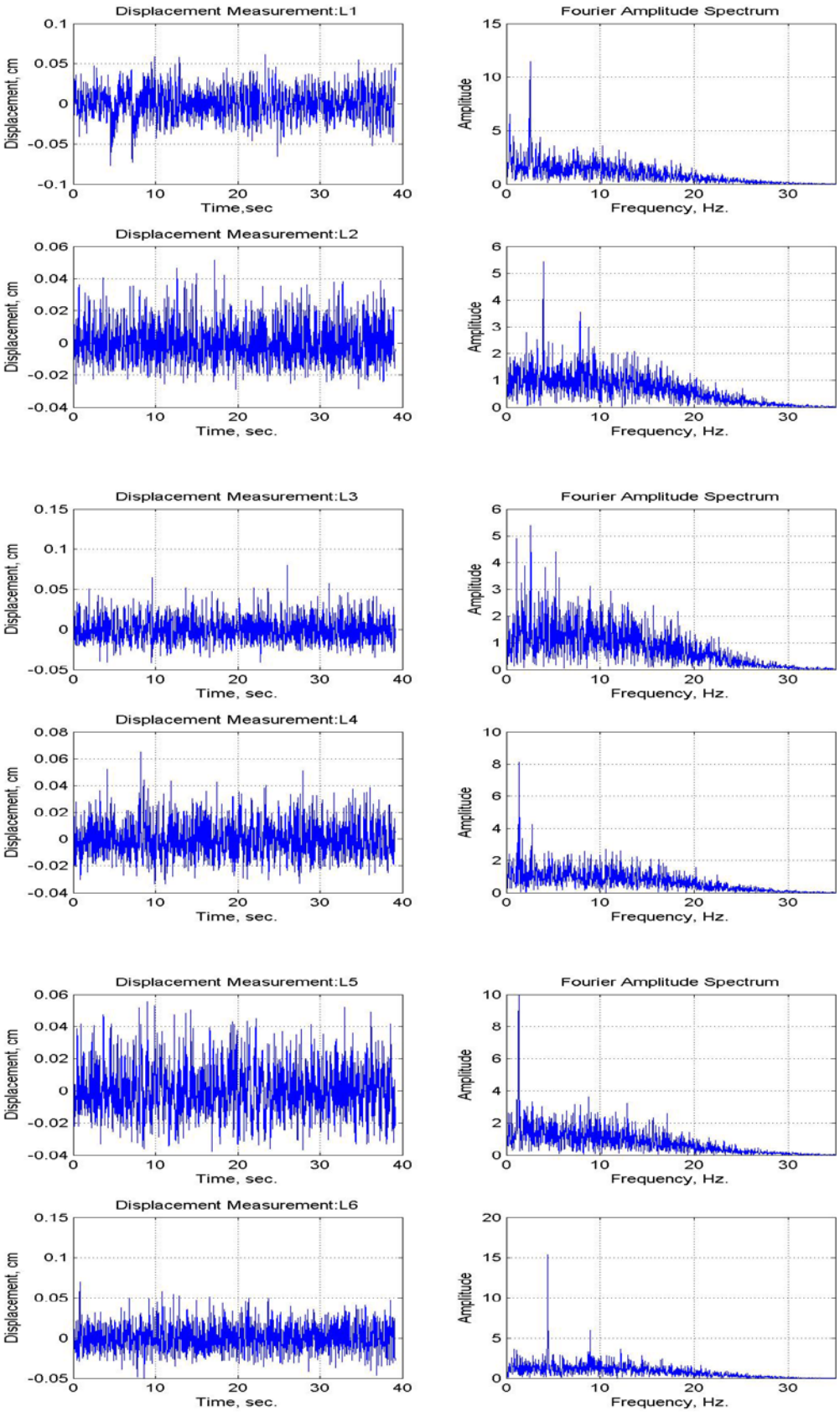


Figure B.7. Facing Displacements Measured for Wall Configuration 1- Sakarya 100%

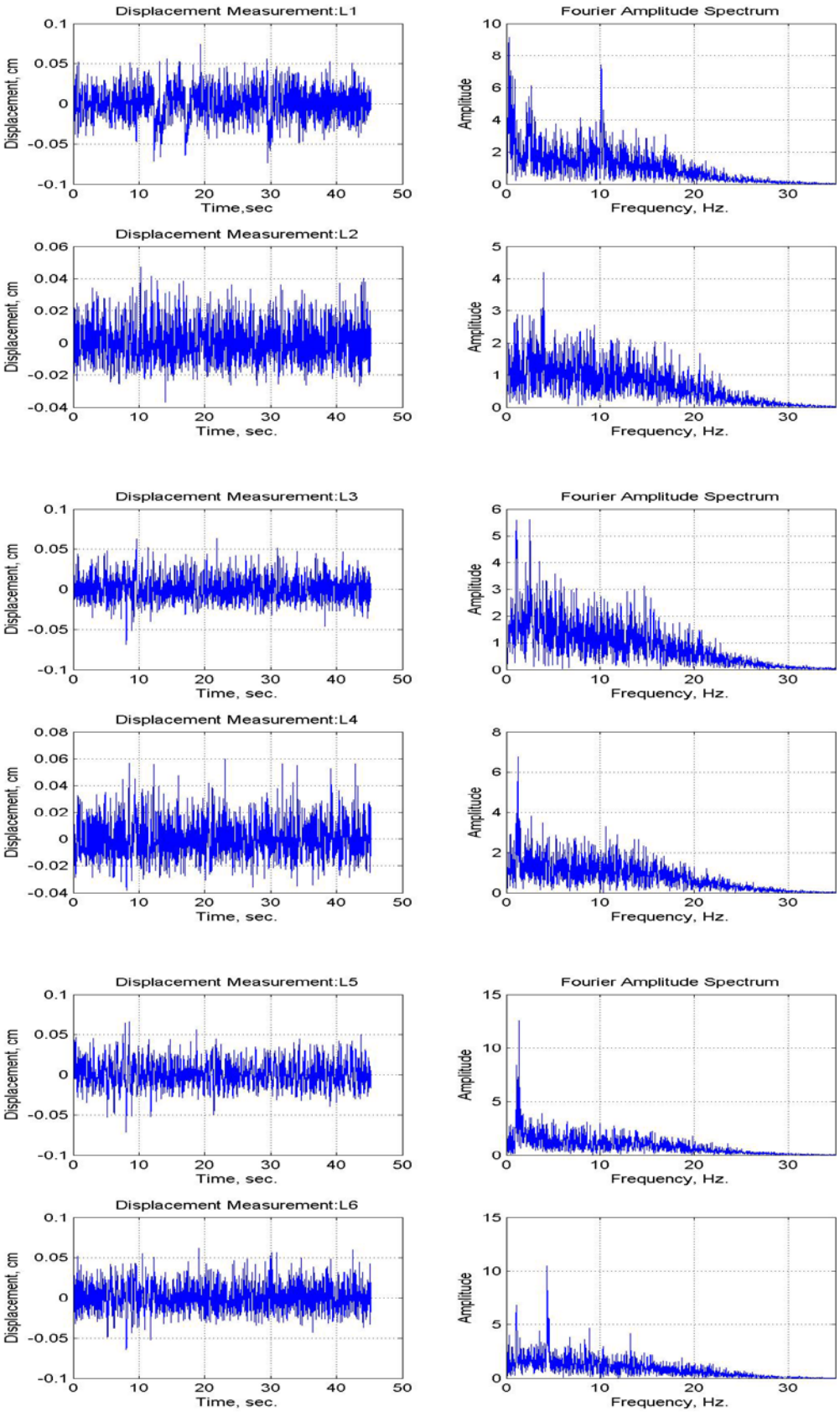


Figure B.8. Facing Displacements Measured for Wall Configuration 1- Sakarya 150%

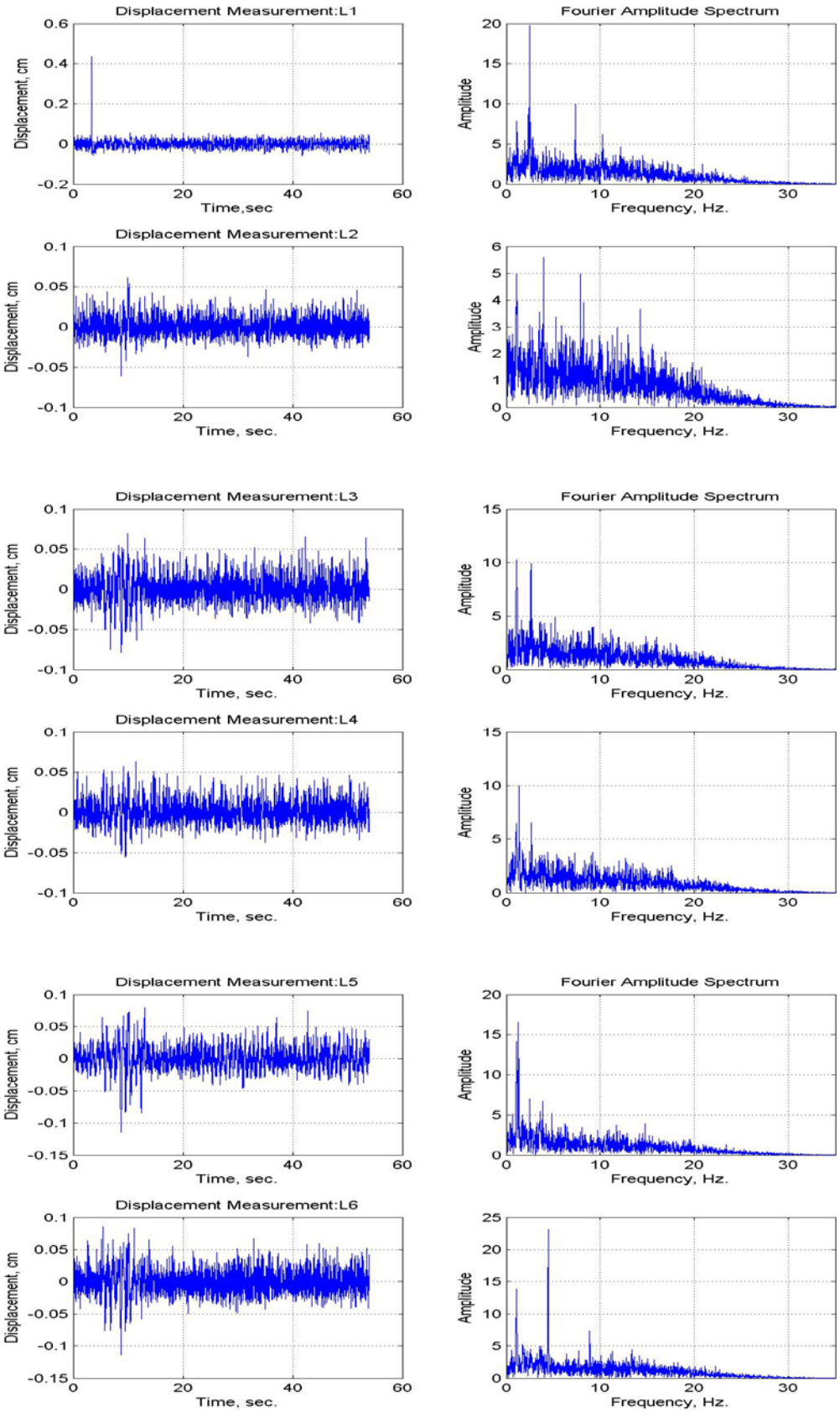


Figure B.9. Facing Displacements Measured for Wall Configuration 1- Sakarya 200%

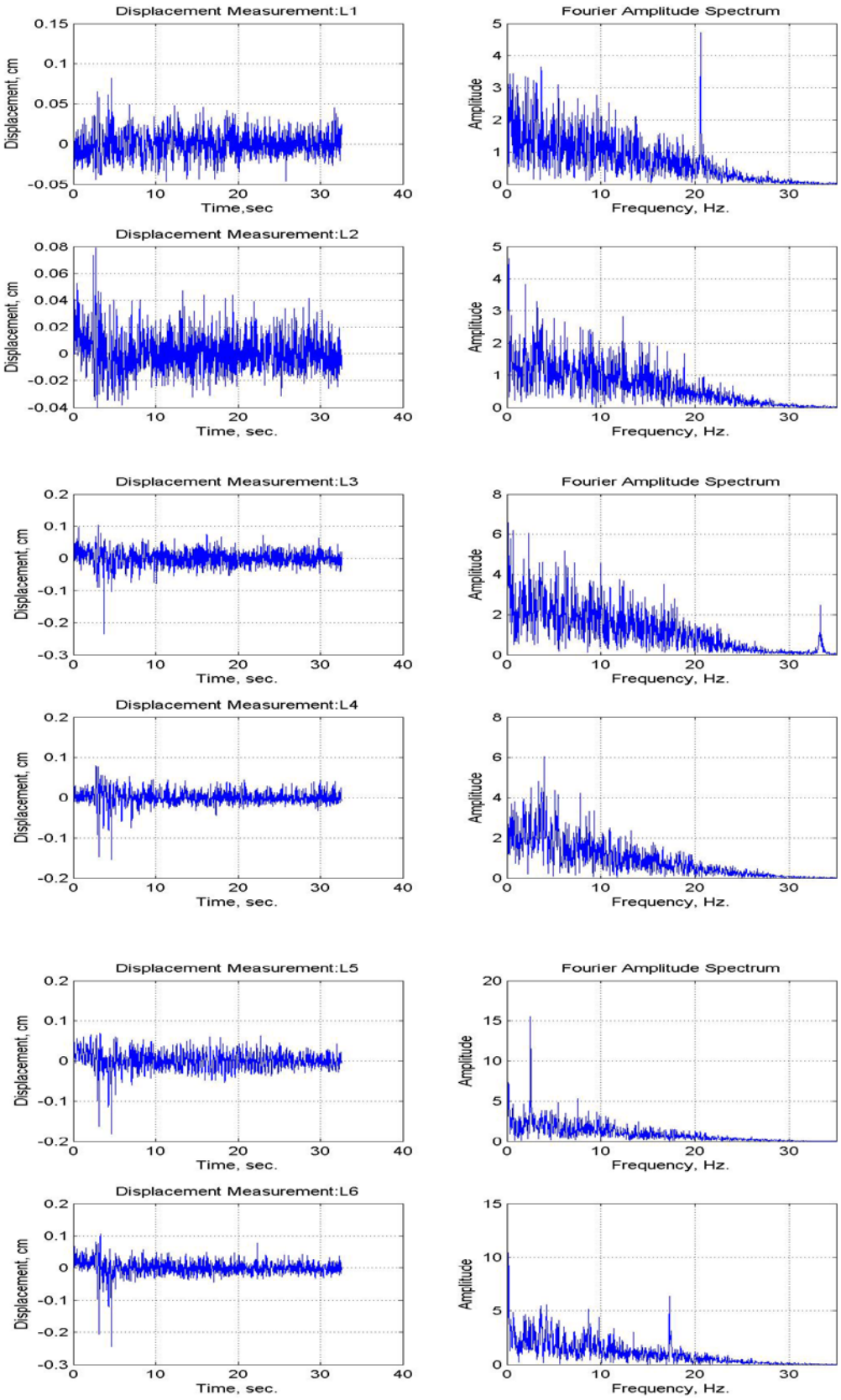


Figure B.10. Facing Displacements Measured for Wall Configuration 2- El Centro 100%

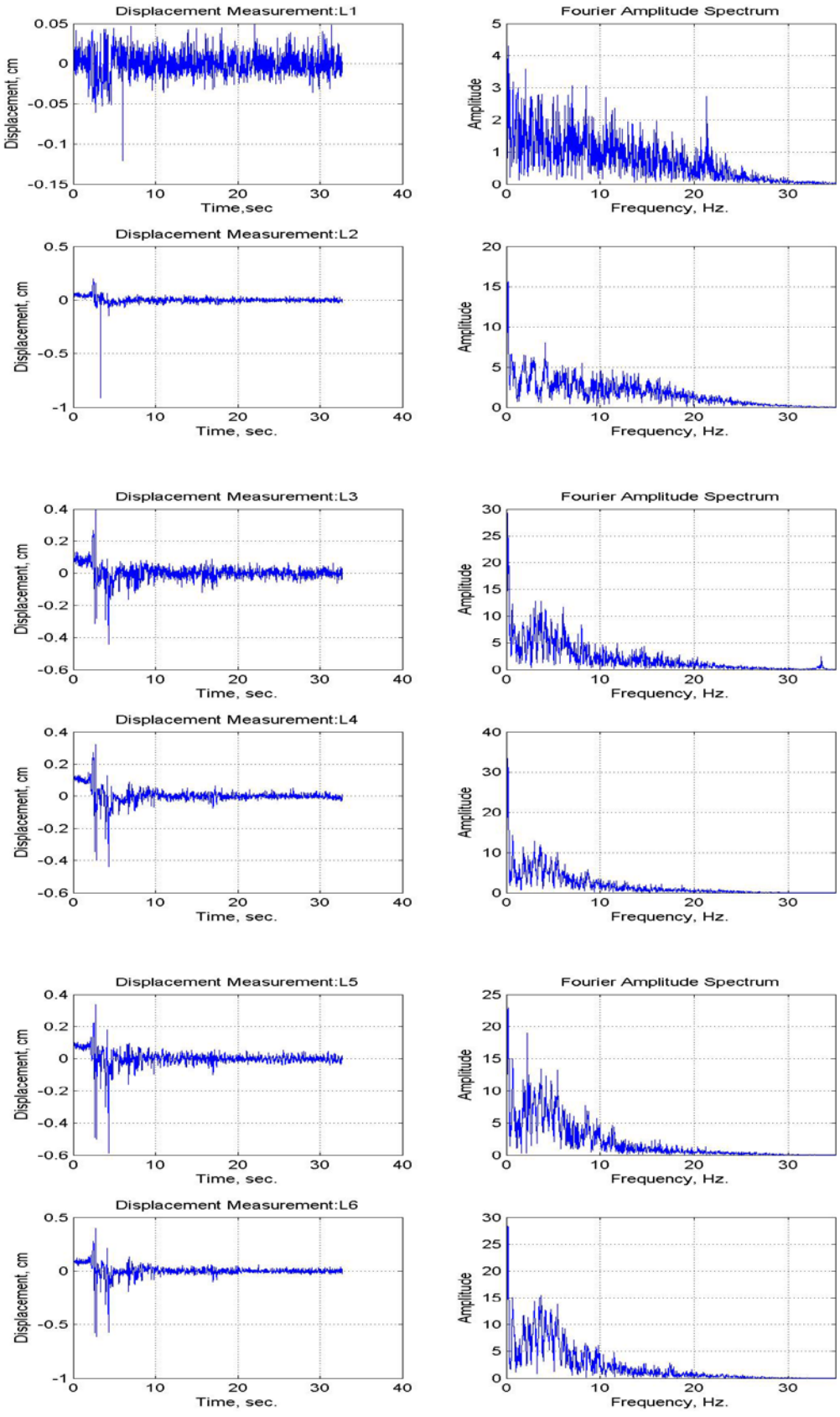


Figure B.11. Facing Displacements Measured for Wall Configuration 2- El Centro 150%

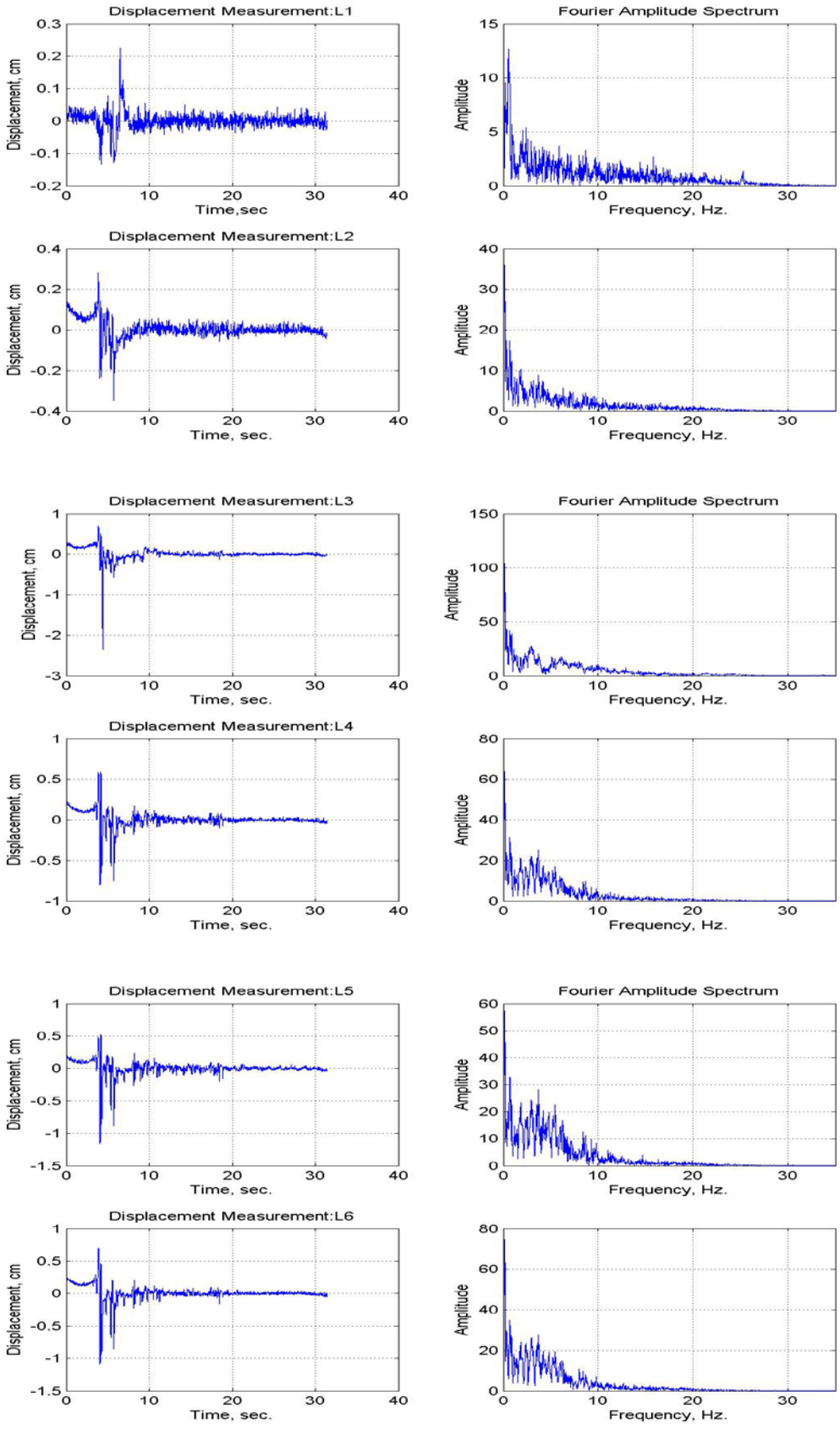


Figure B.12. Facing Displacements Measured for Wall Configuration 2- El Centro 200%

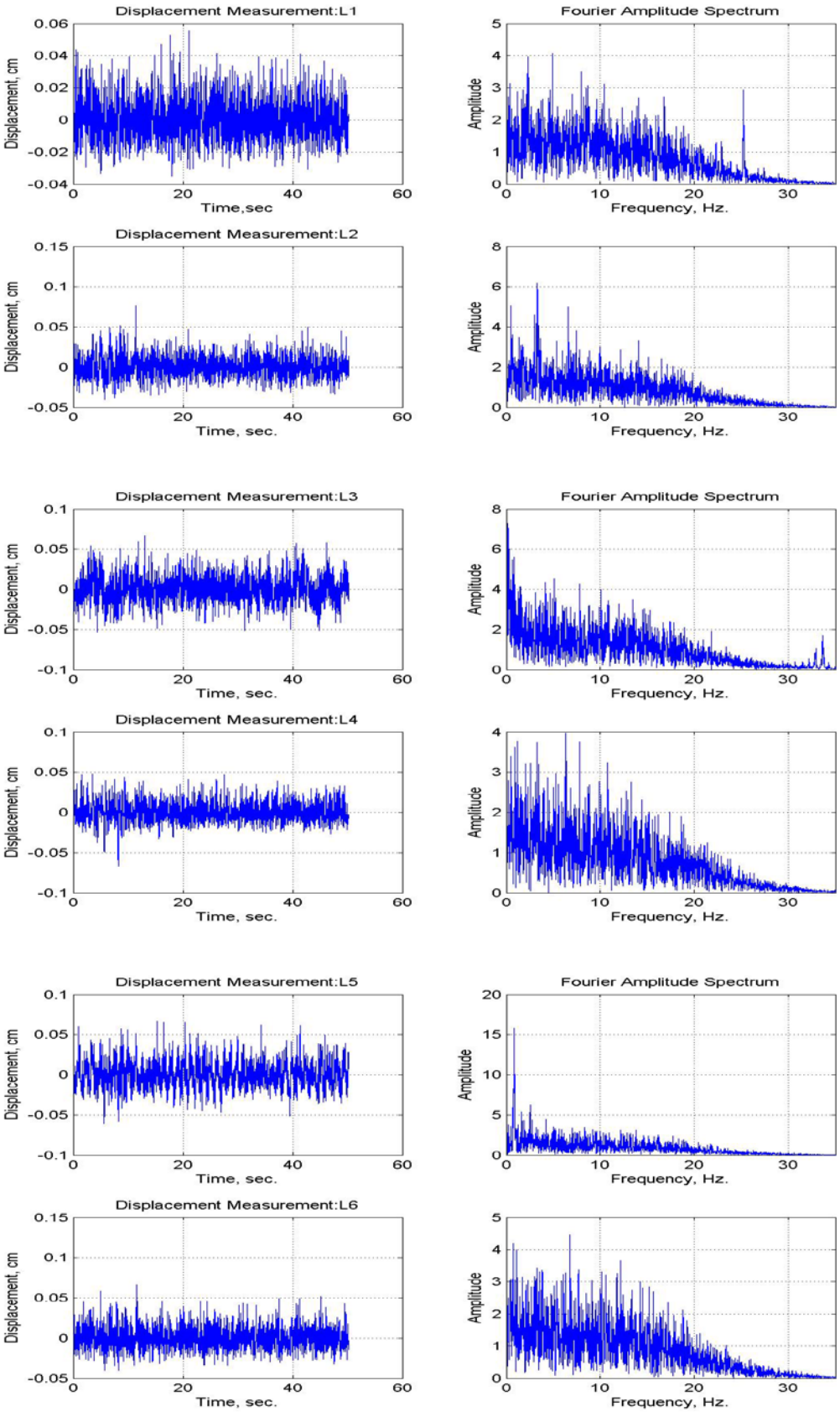


Figure B.13. Facing Displacements Measured for Wall Configuration 2- Izmit 100%

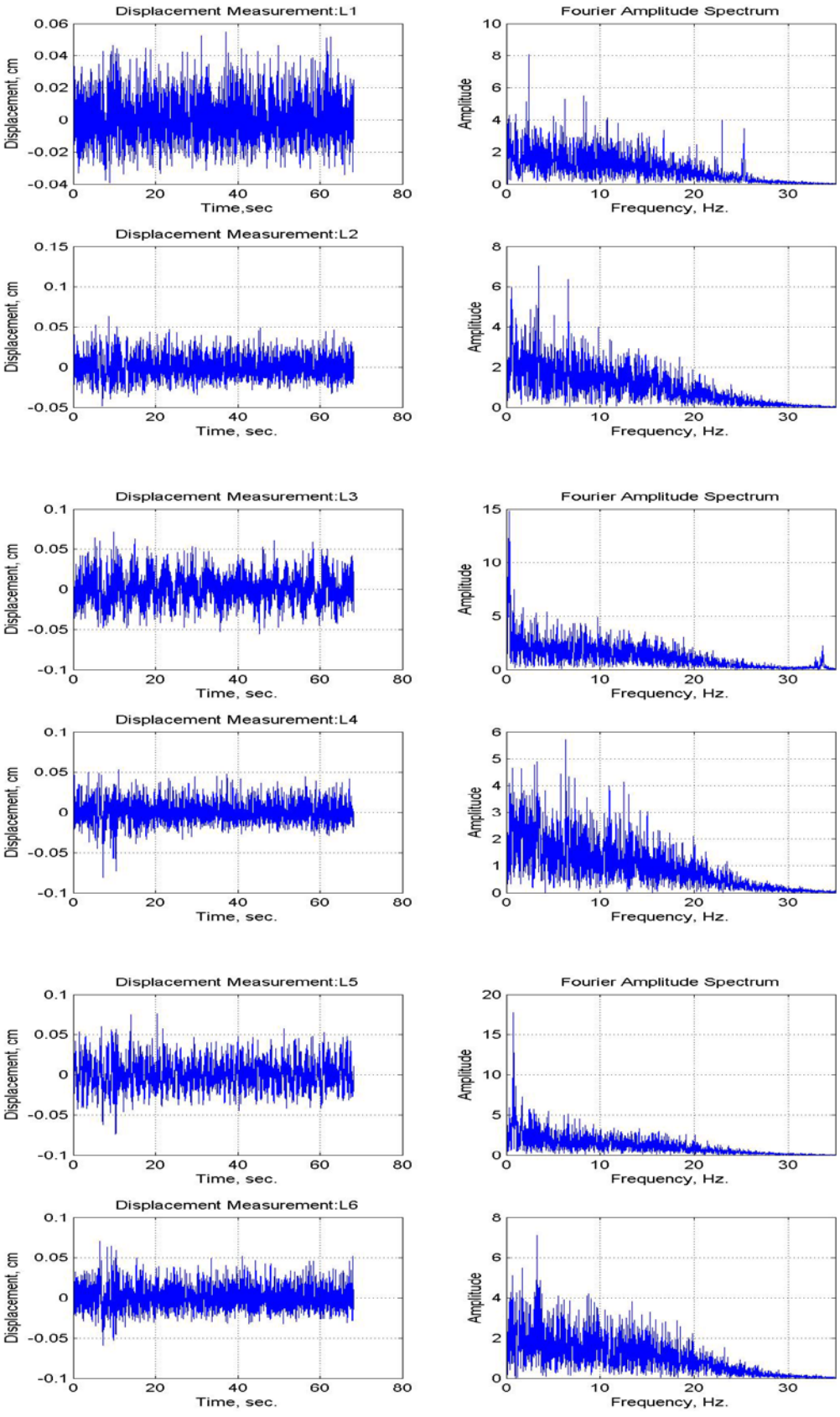


Figure B.14. Facing Displacements Measured for Wall Configuration 2- Izmit 150%

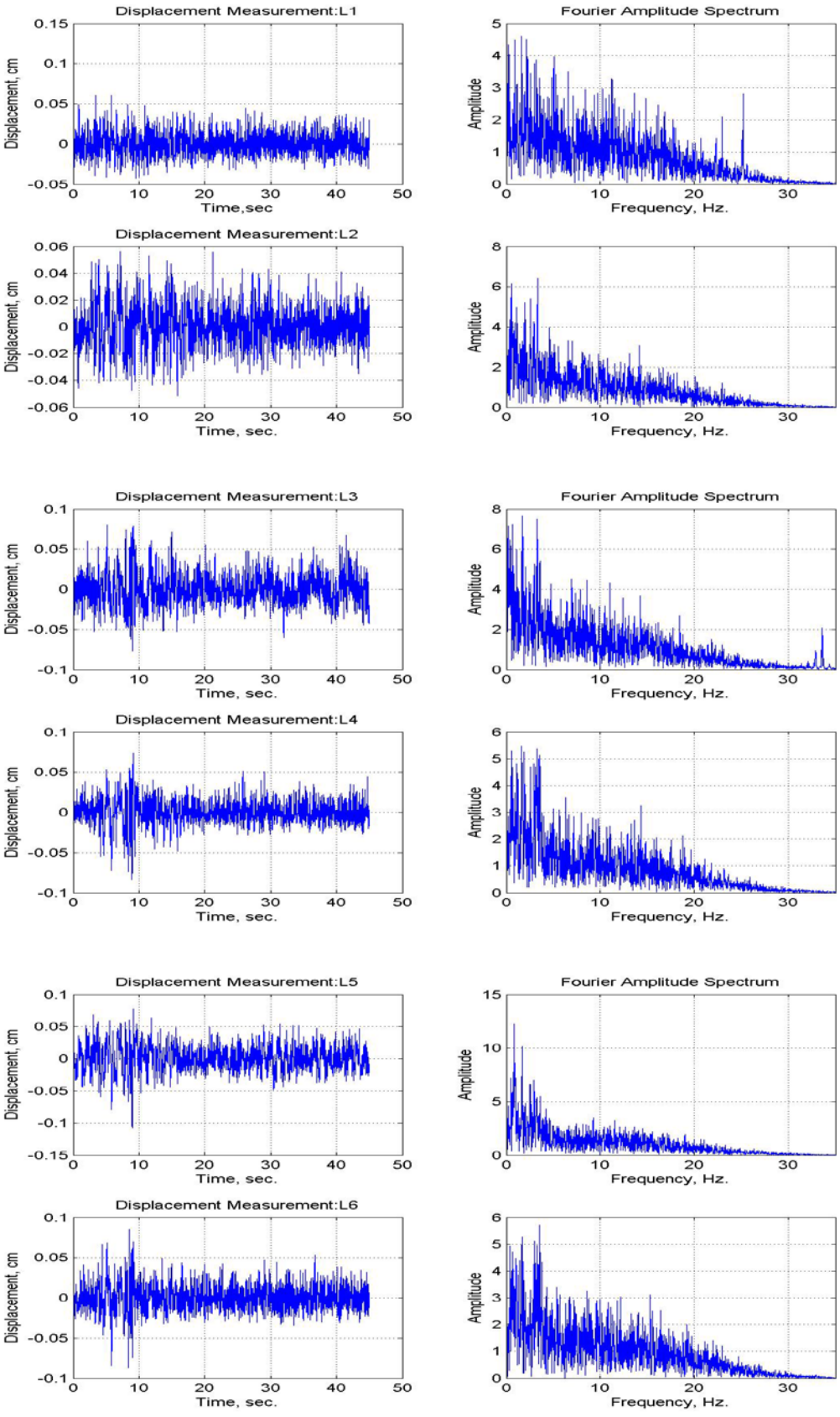


Figure B.15. Facing Displacements Measured for Wall Configuration 2- Izmit 200%

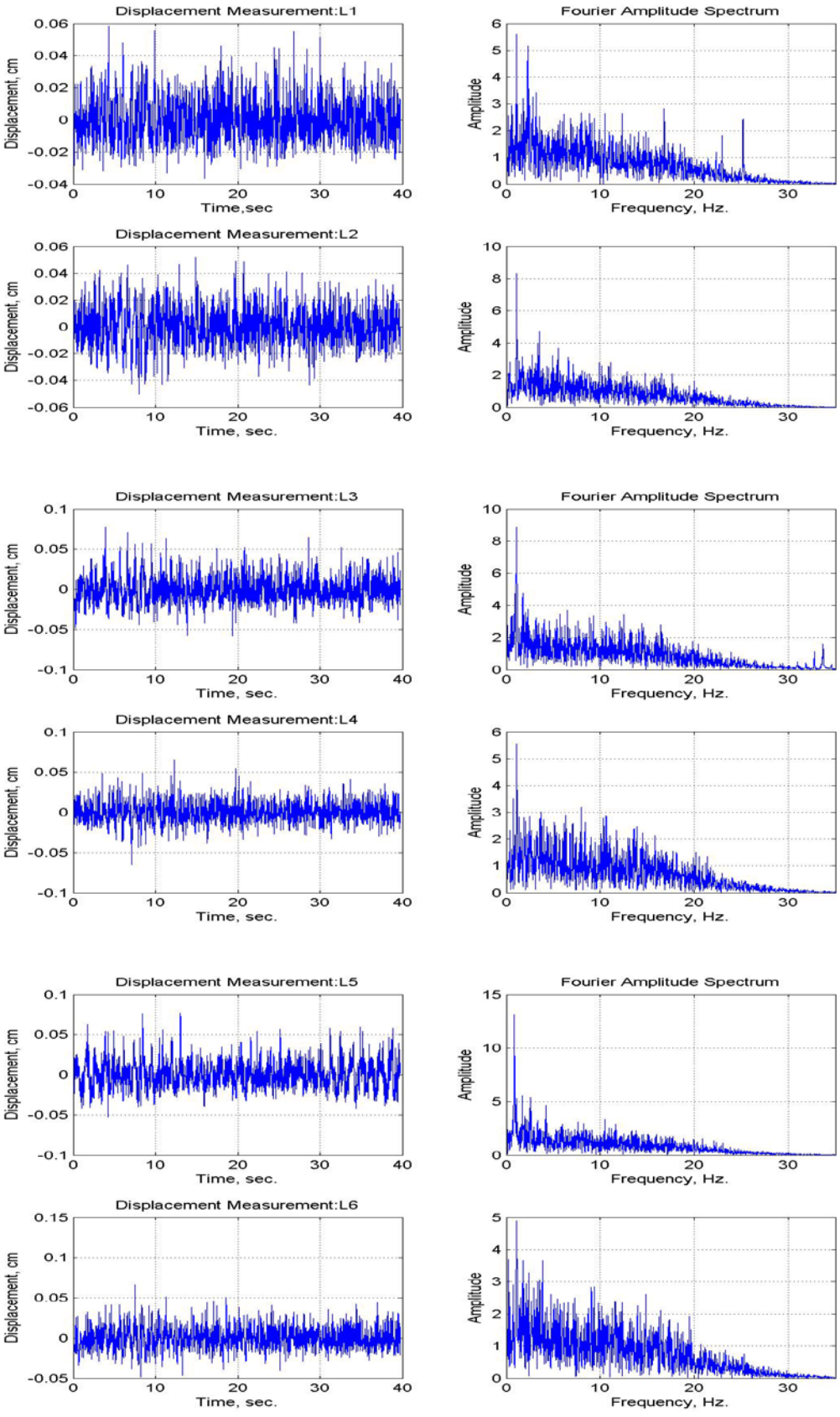


Figure B.16. Facing Displacements Measured for Wall Configuration 2- Sakarya 100%

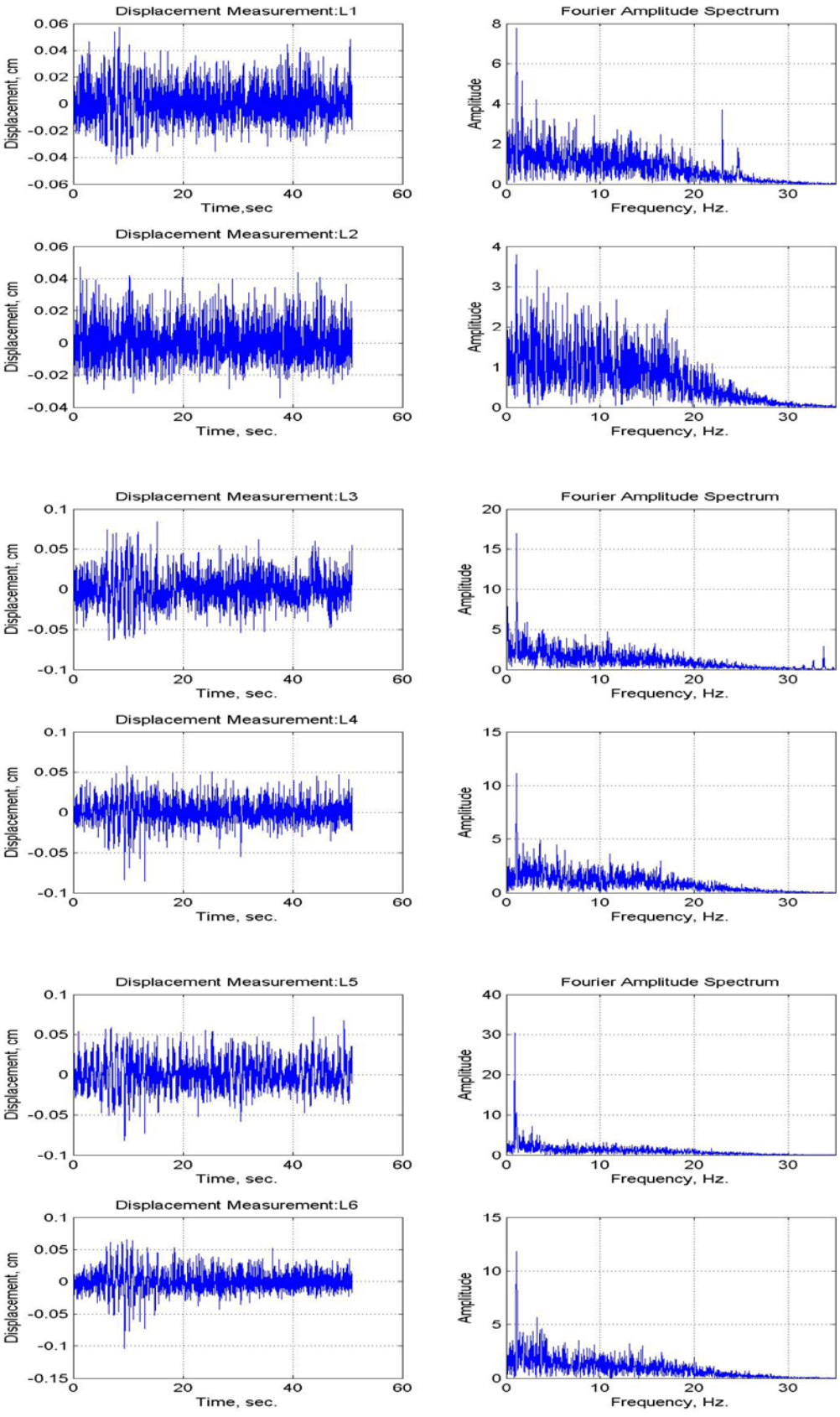


Figure B.17. Facing Displacements Measured for Wall Configuration 2- Sakarya 150%

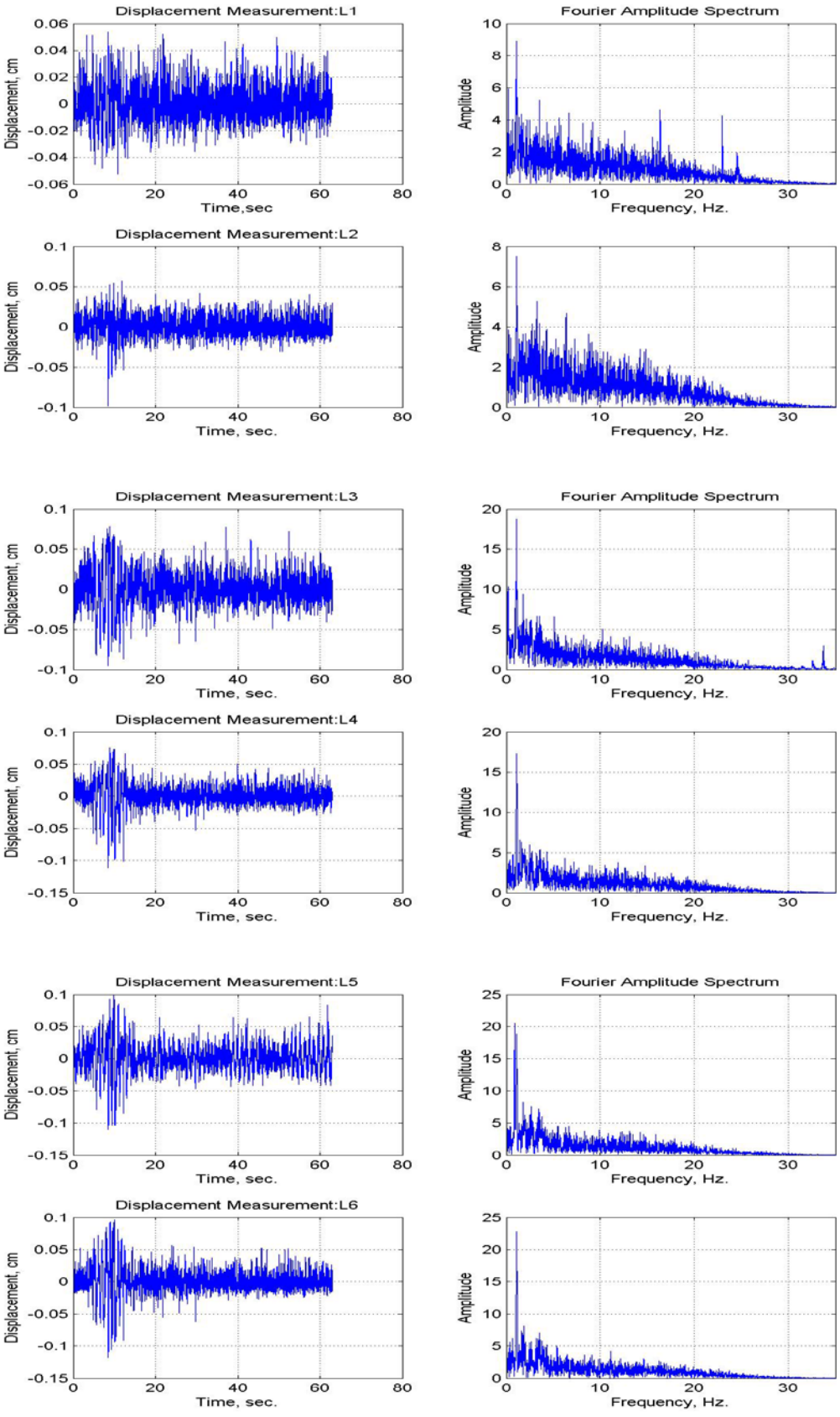


Figure B.18. Facing Displacements Measured for Wall Configuration 2- Sakarya 200%

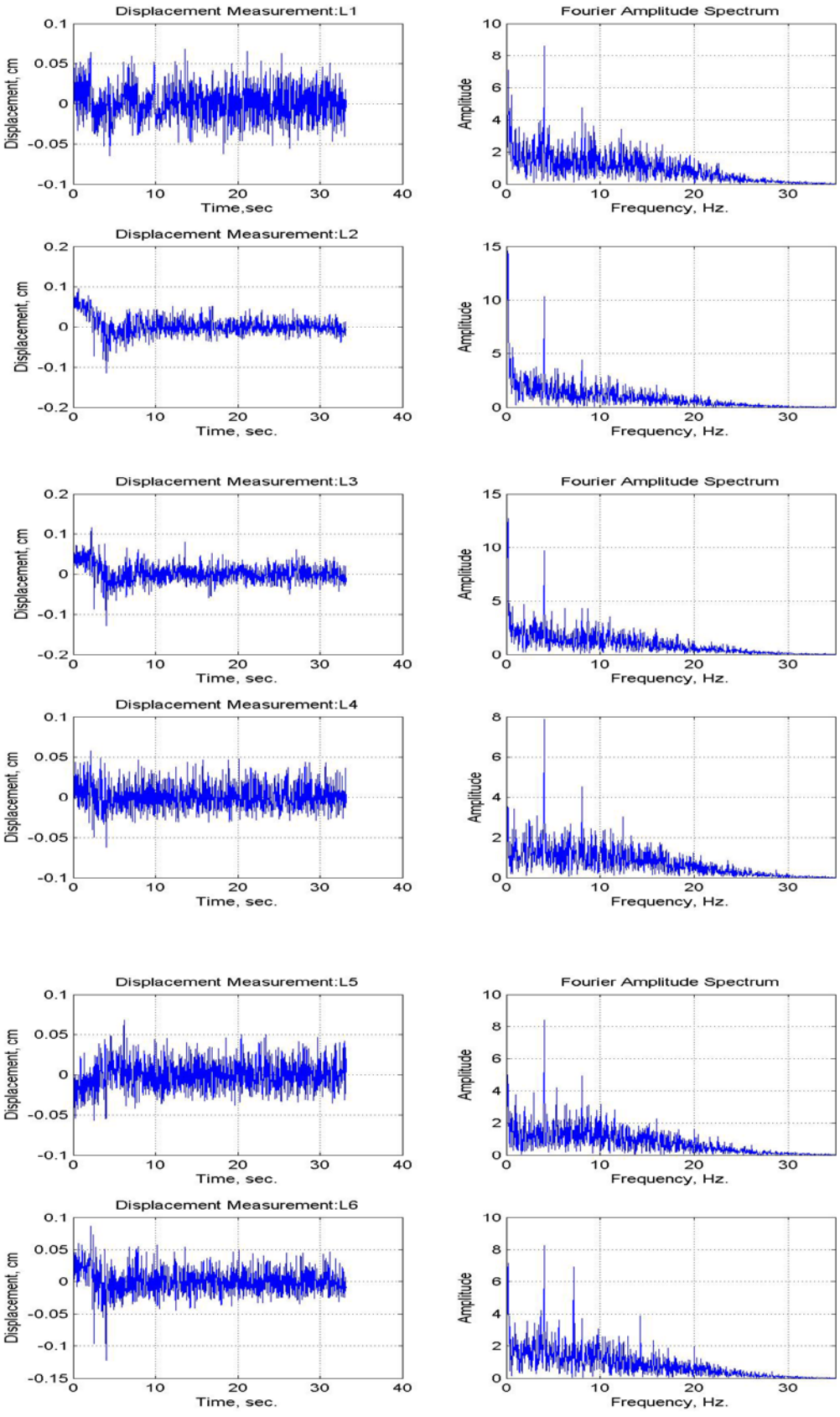


Figure B.19. Facing Displacements Measured for Wall Configuration 3- El Centro 100%

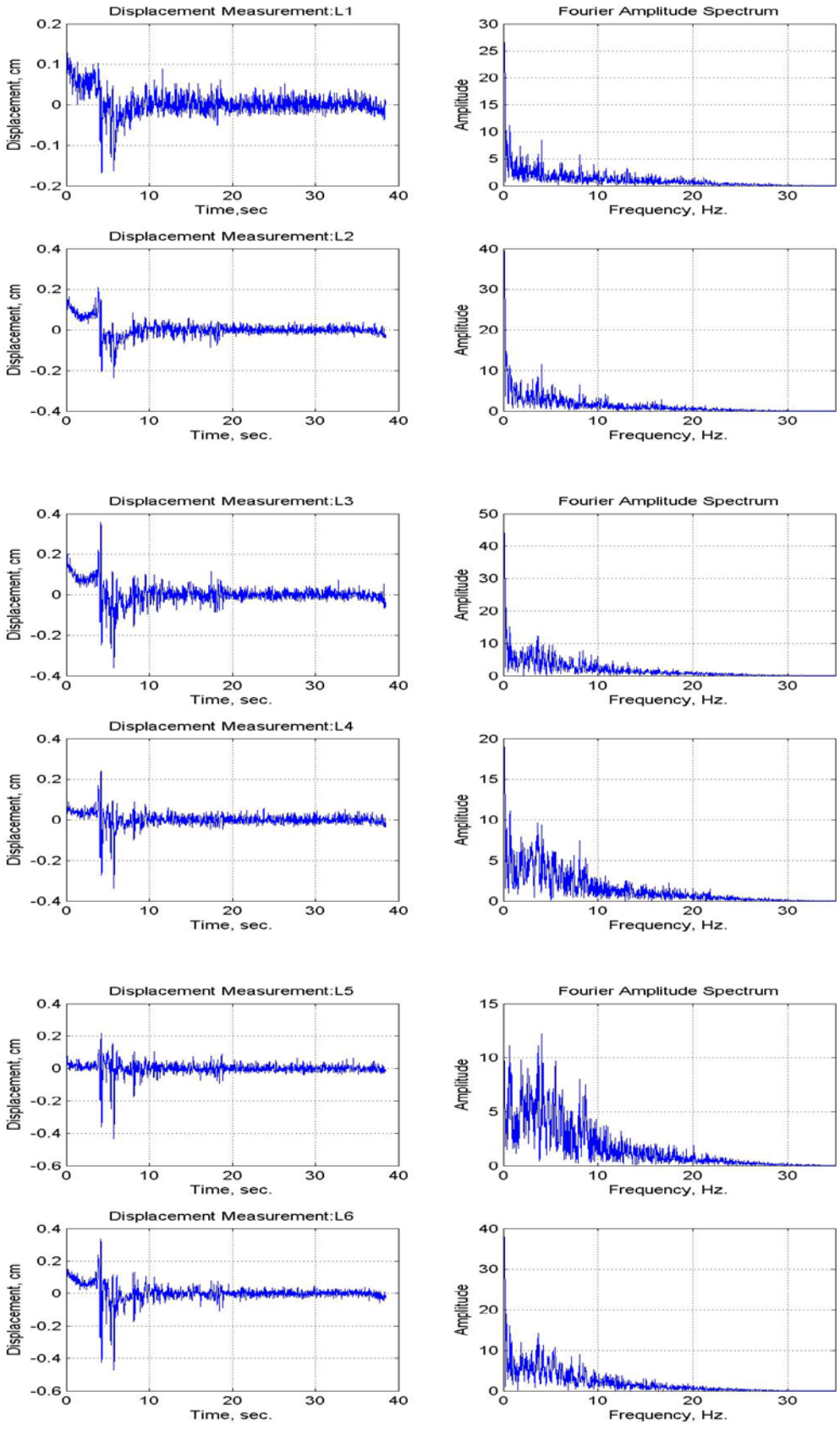


Figure B.20. Facing Displacements Measured for Wall Configuration 3- El Centro 150%

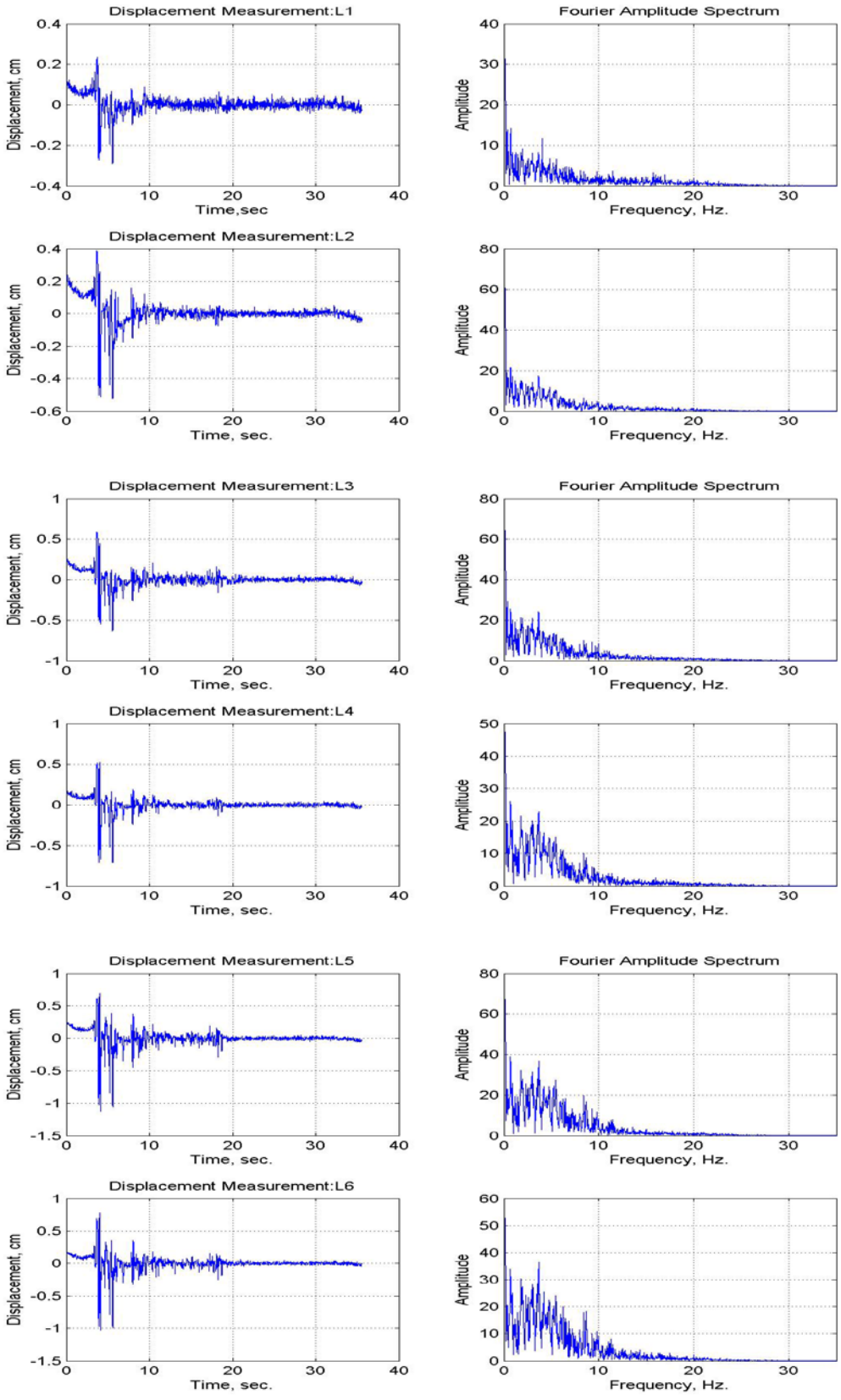


Figure B.21. Facing Displacements Measured for Wall Configuration 3- El Centro 200%

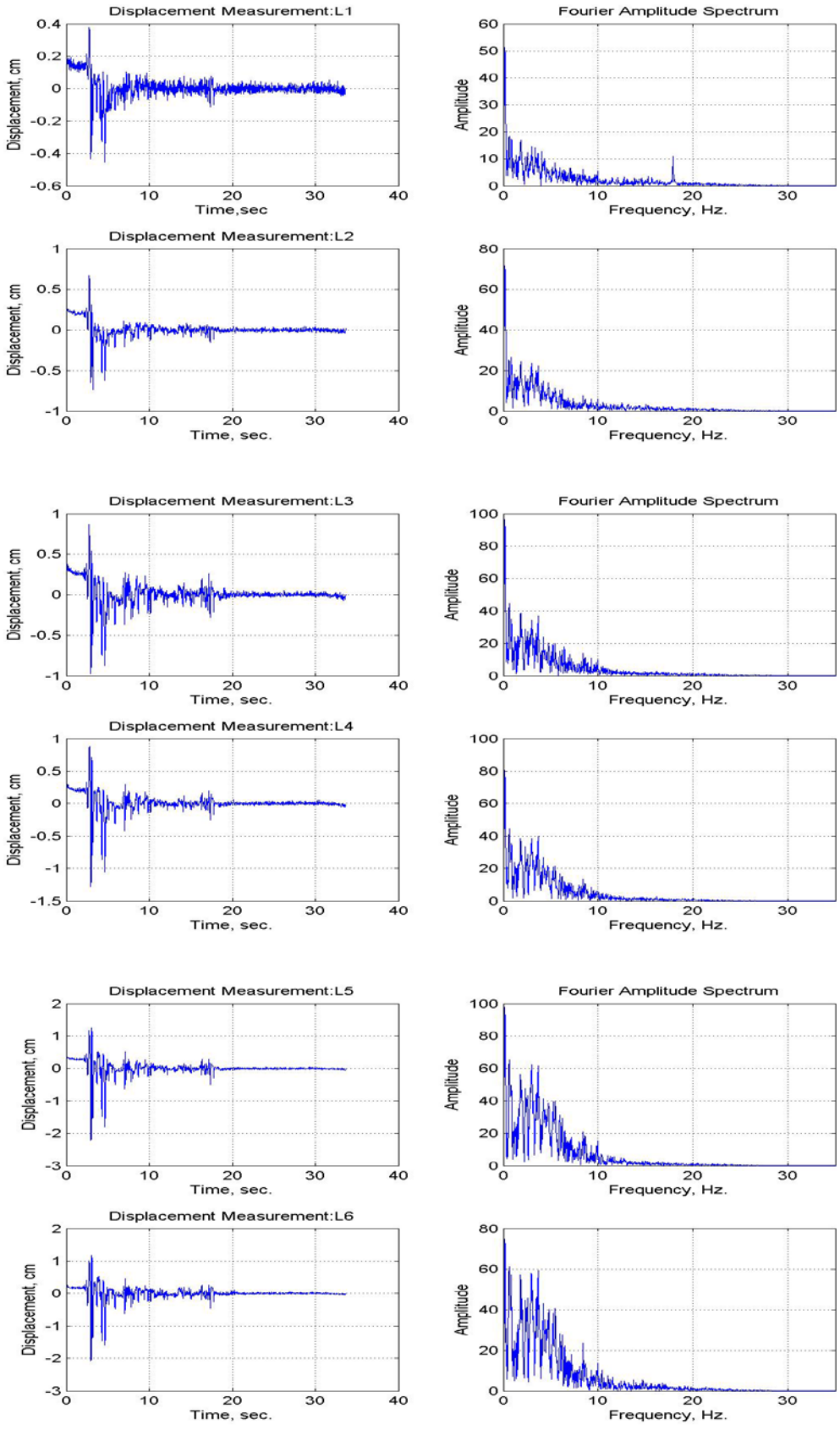


Figure B.22. Facing Displacements Measured for Wall Configuration 3- El Centro 250%

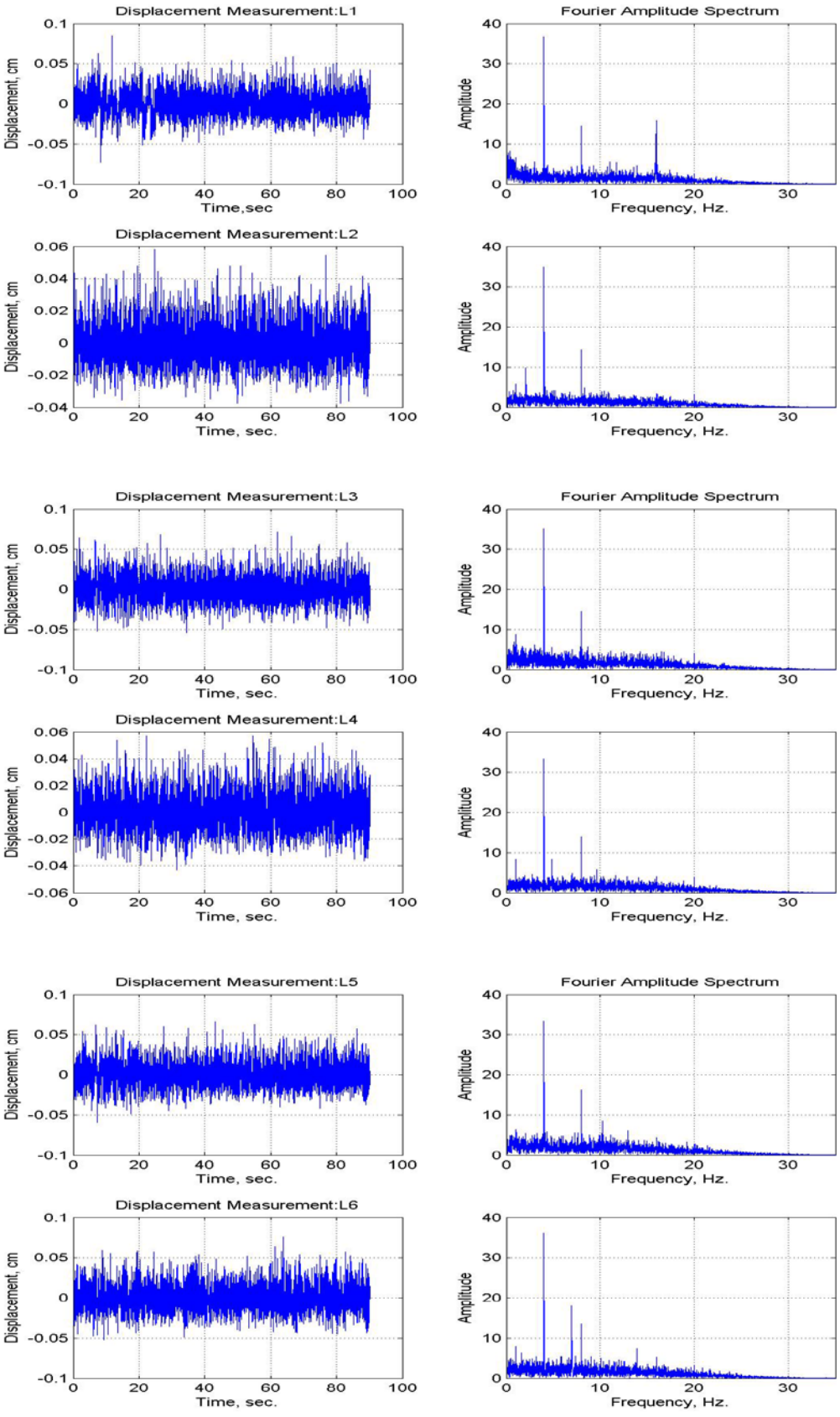


Figure B.23. Facing Displacements Measured for Wall Configuration 3- Izmit 100%

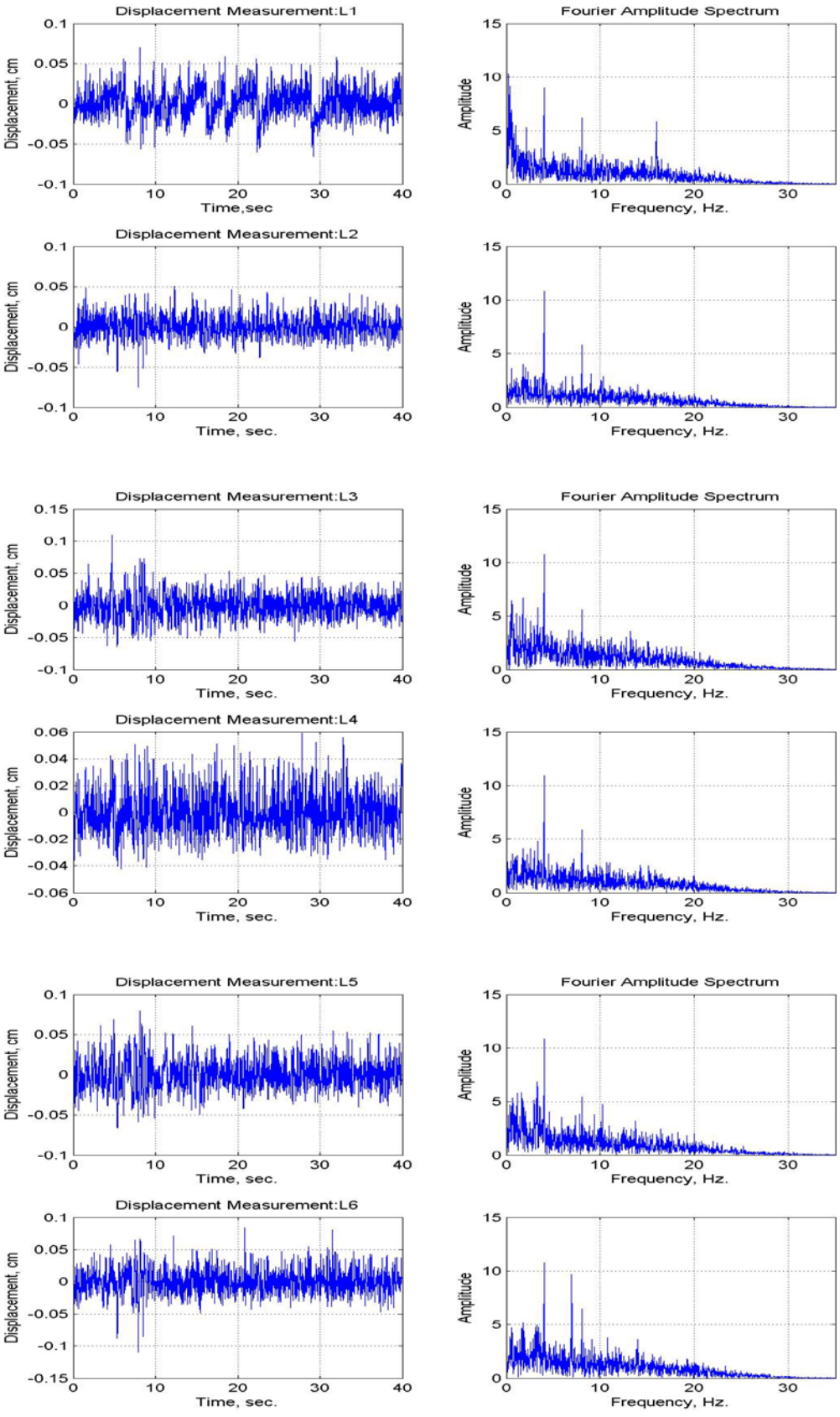


Figure B.24. Facing Displacements Measured for Wall Configuration 3- Izmit 150%

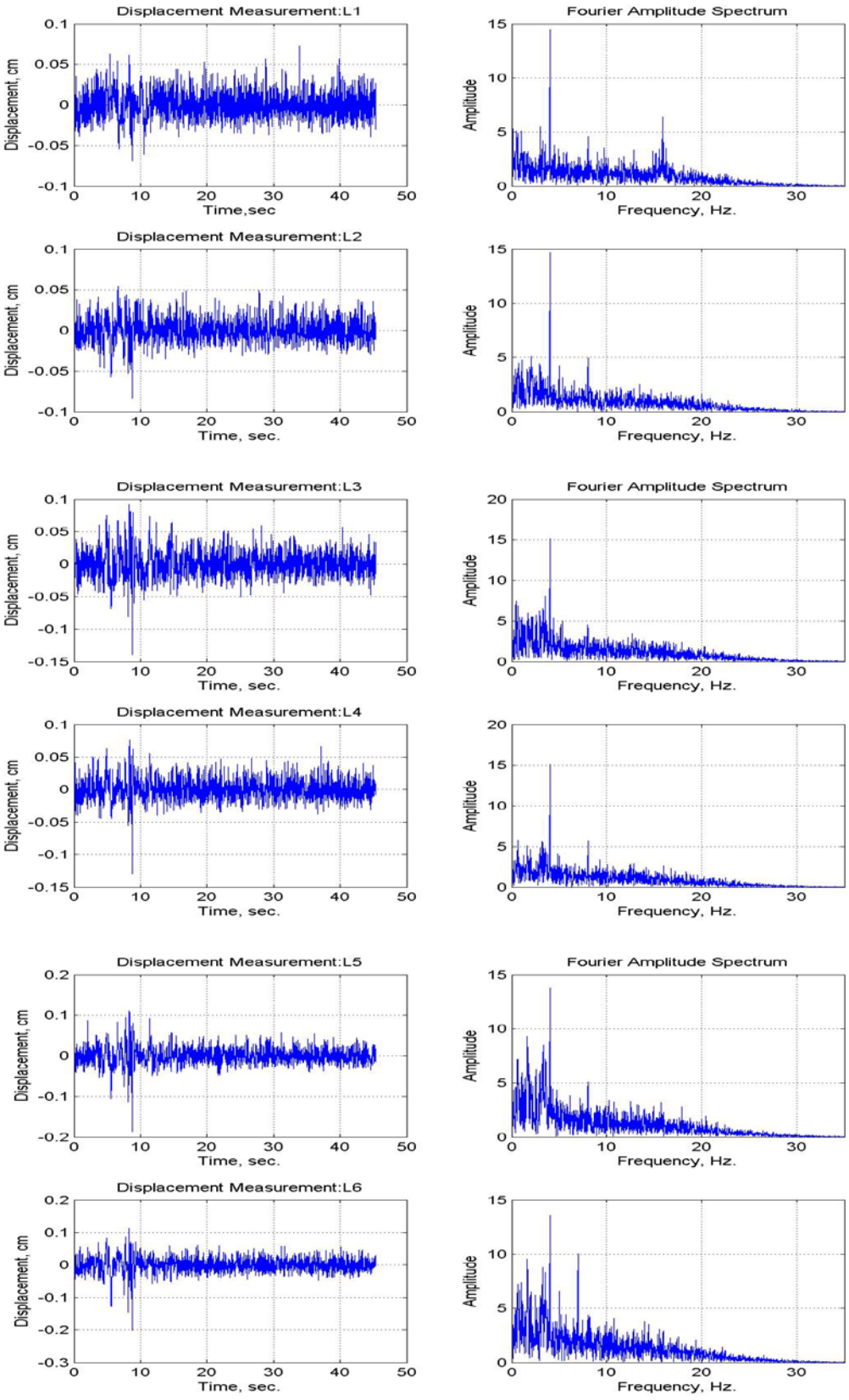


Figure B.25. Facing Displacements Measured for Wall Configuration 3- Izmit 200%

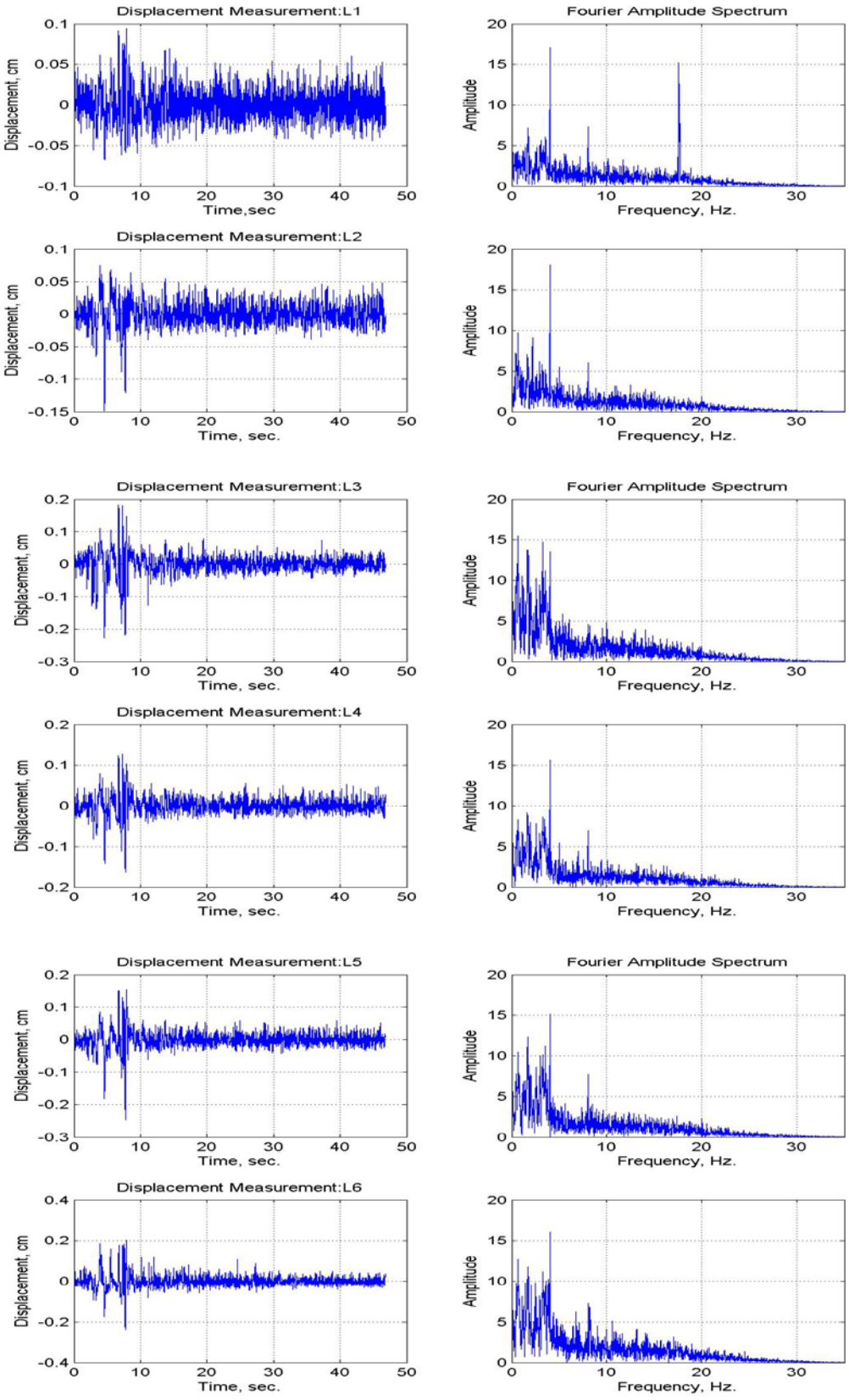


Figure B.26. Facing Displacements Measured for Wall Configuration 3- Izmit 250%

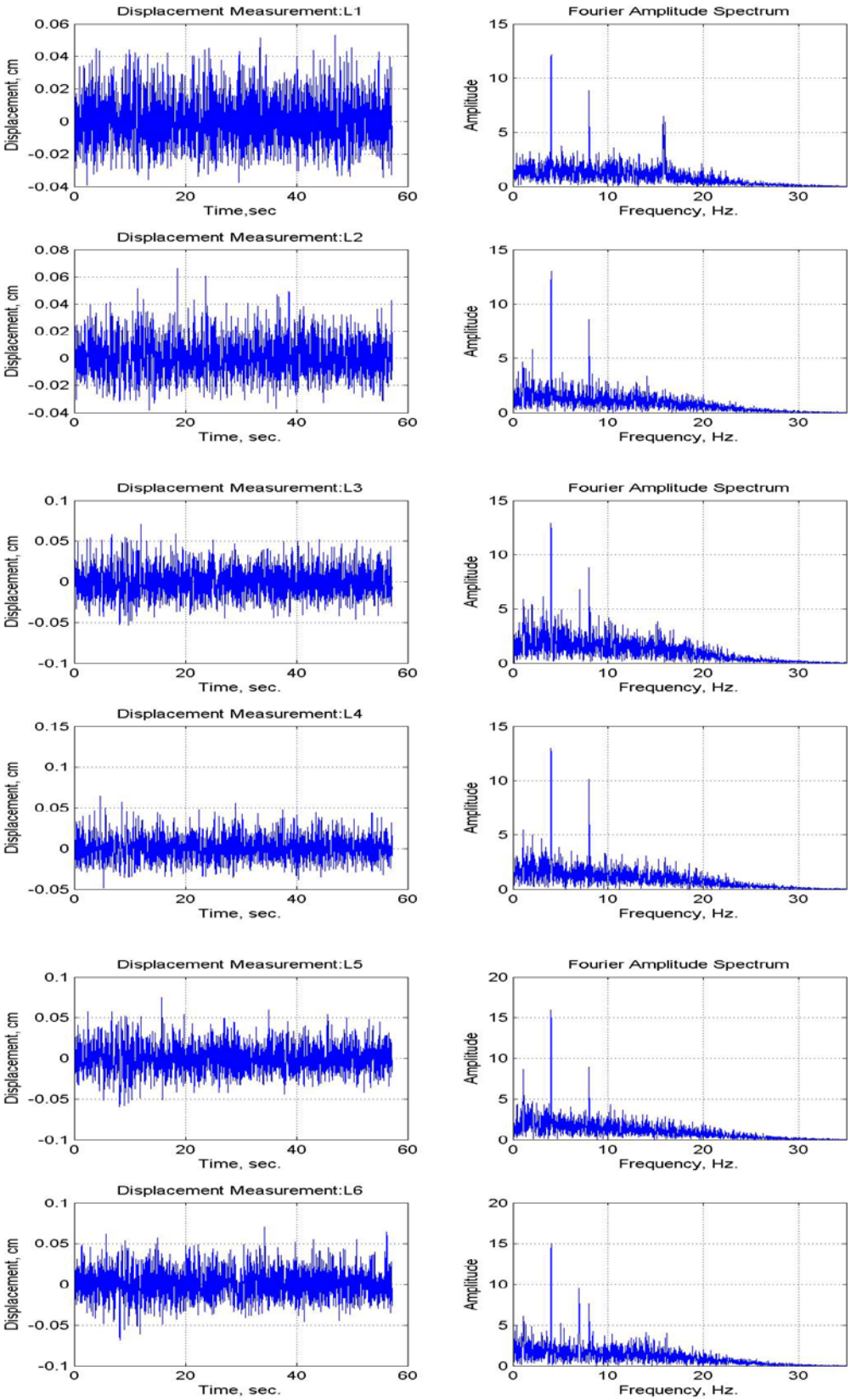


Figure B.27. Facing Displacements Measured for Wall Configuration 3- Sakarya 100%

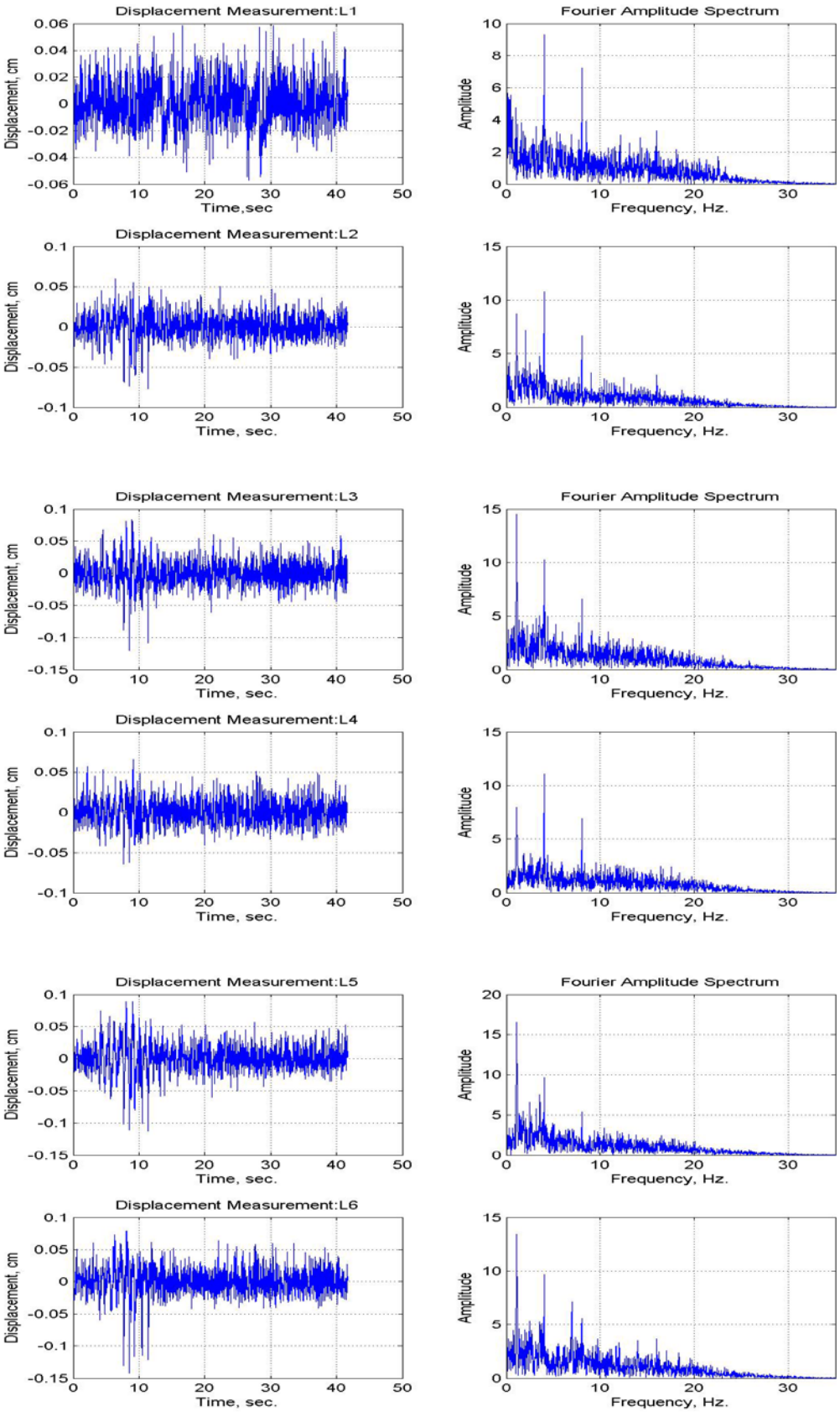


Figure B.28. Facing Displacements Measured for Wall Configuration 3- Sakarya 150%

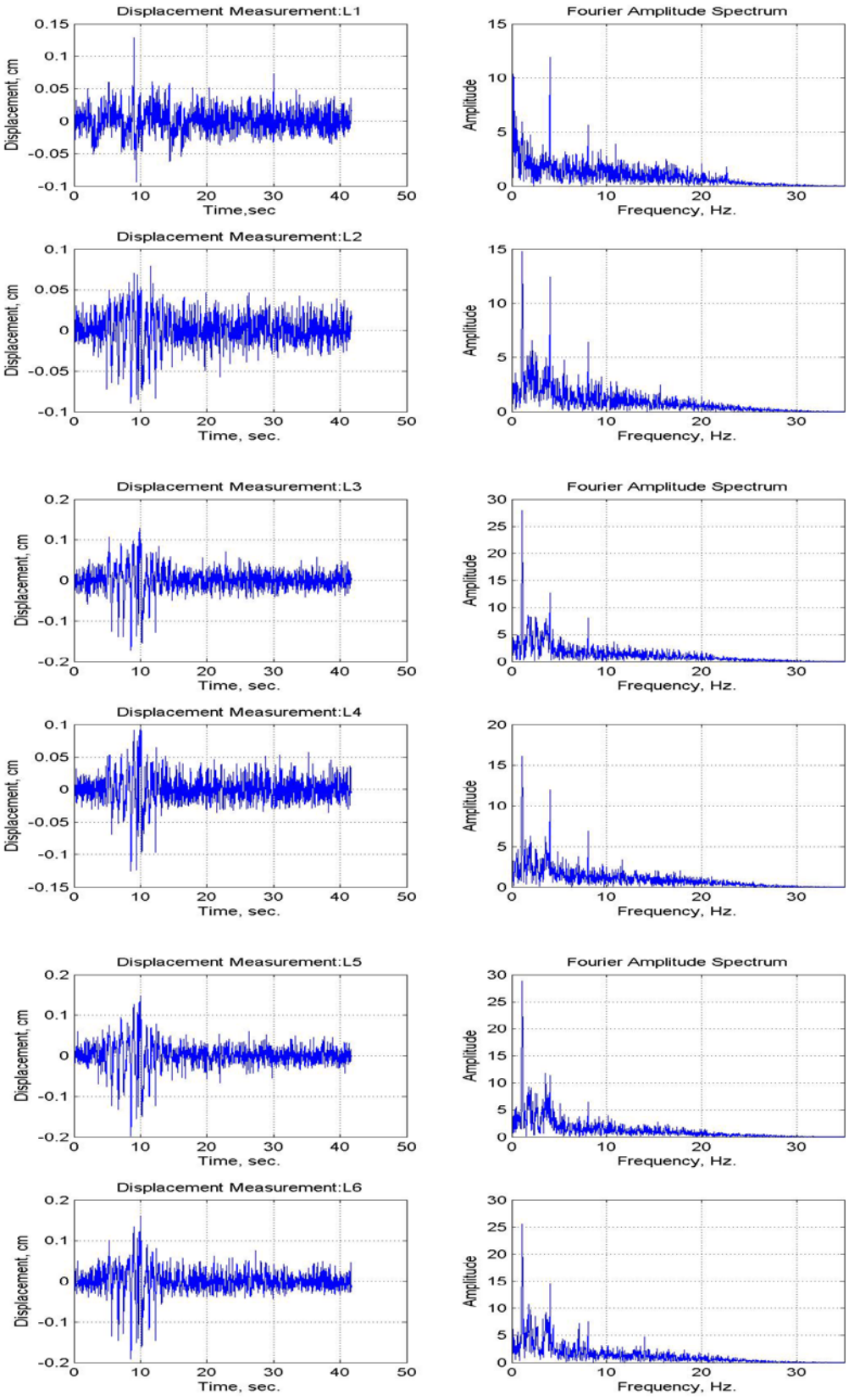


Figure B.29. Facing Displacements Measured for Wall Configuration 3- Sakarya 200%

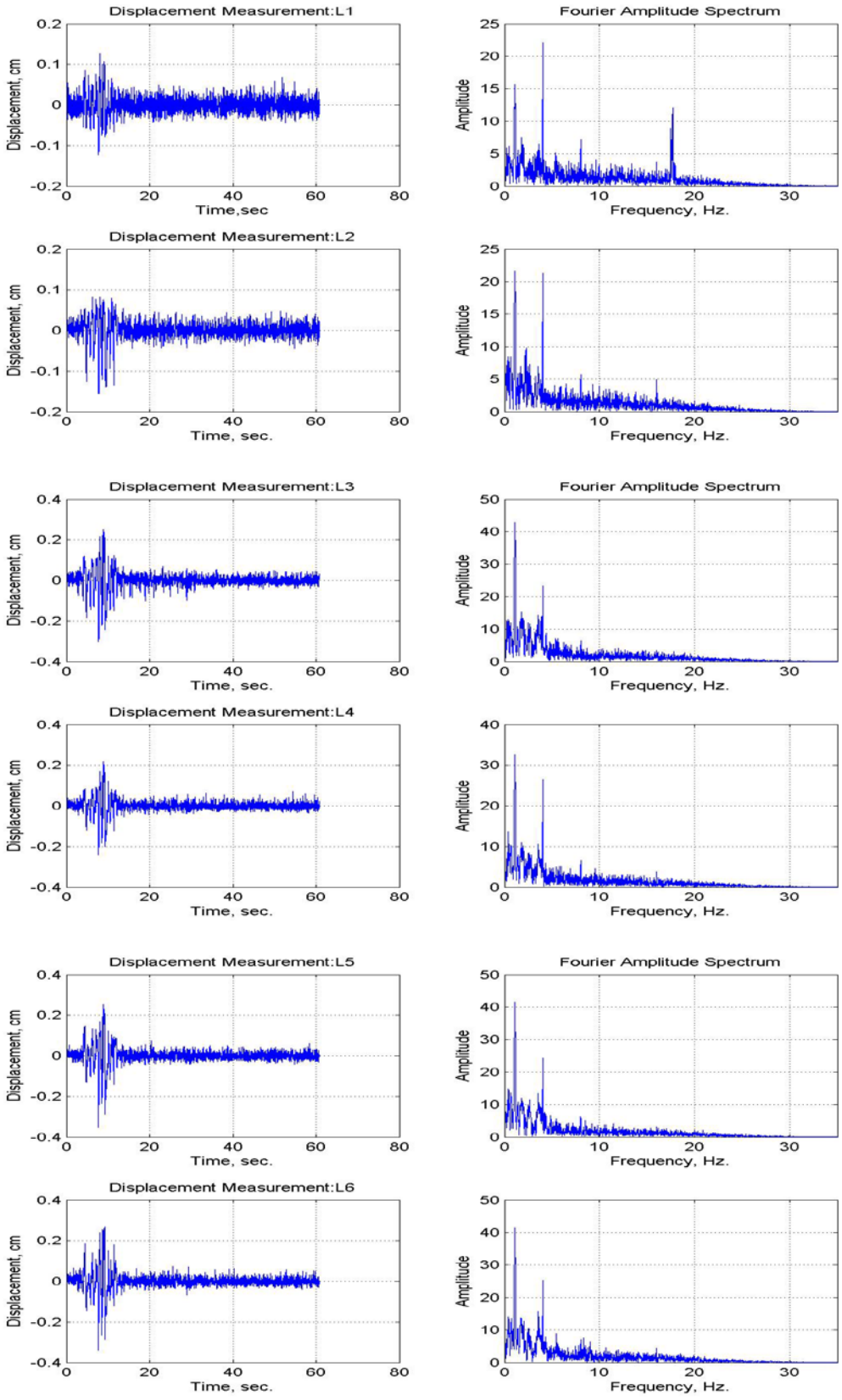


Figure B.30. Facing Displacements Measured for Wall Configuration 3- Sakarya 250%

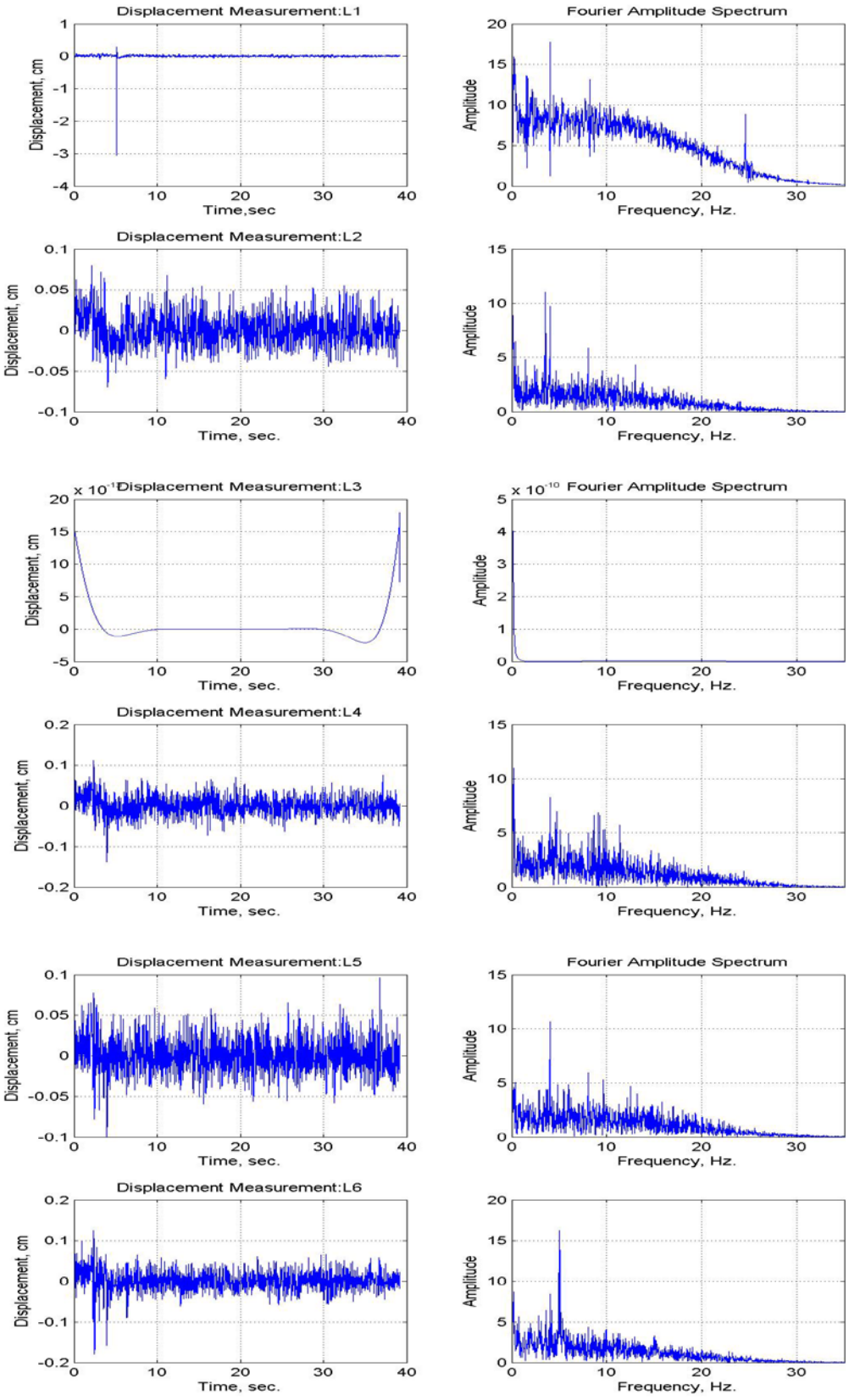


Figure B.31. Facing Displacements Measured for Wall Configuration 4- El Centro 100%

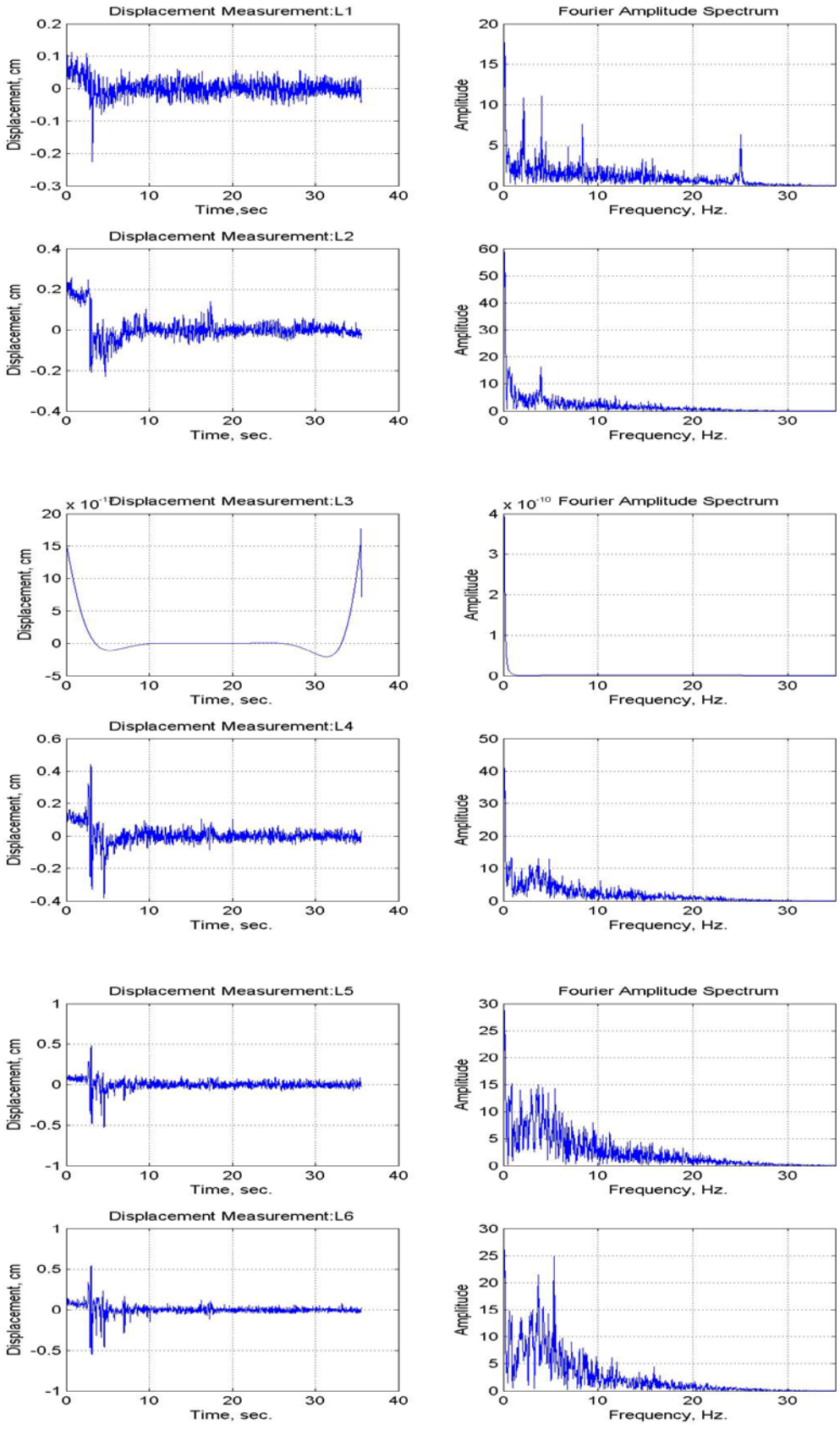


Figure B.32. Facing Displacements Measured for Wall Configuration 4- El Centro 150%

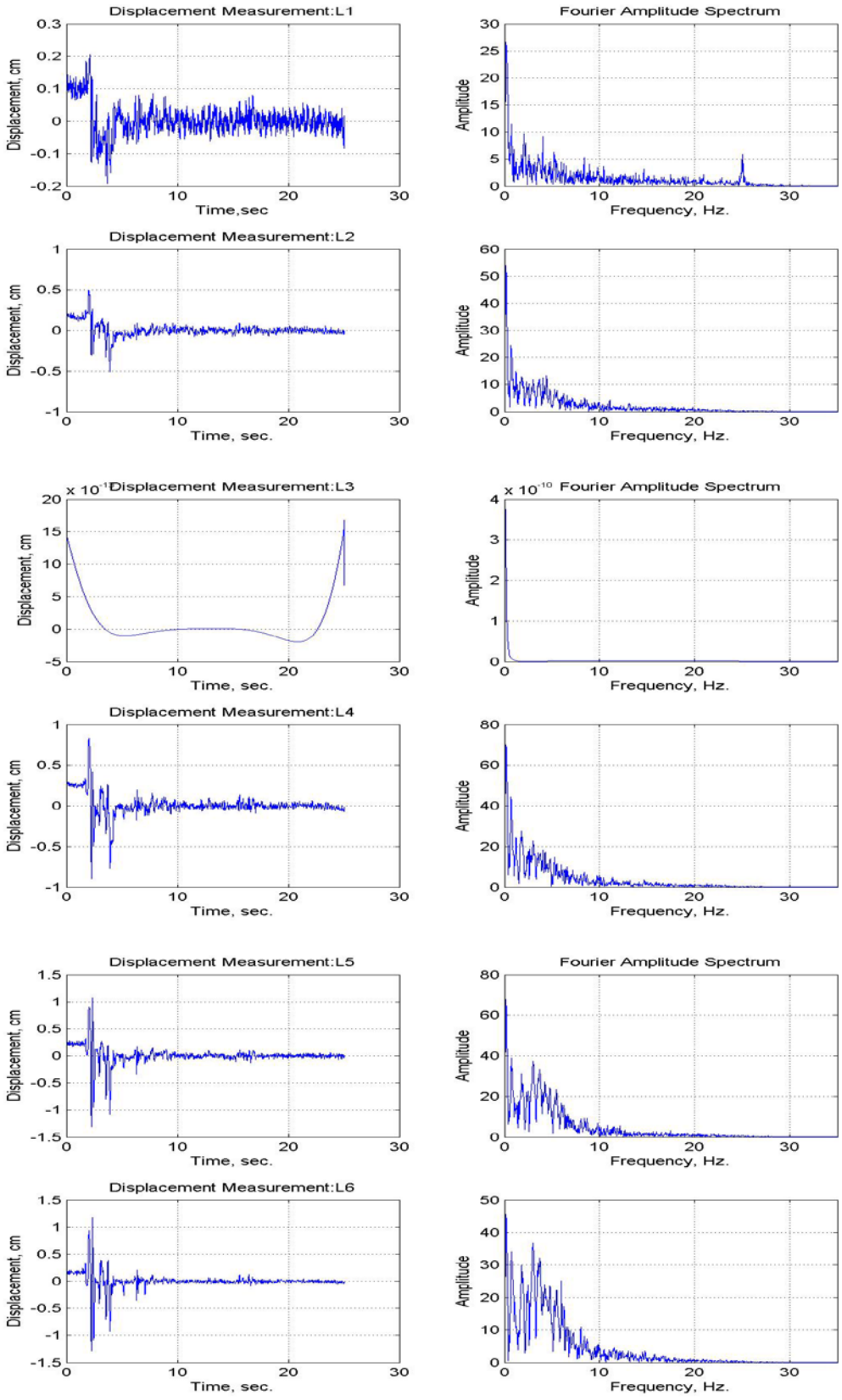


Figure B.33. Facing Displacements Measured for Wall Configuration 4- El Centro 200%

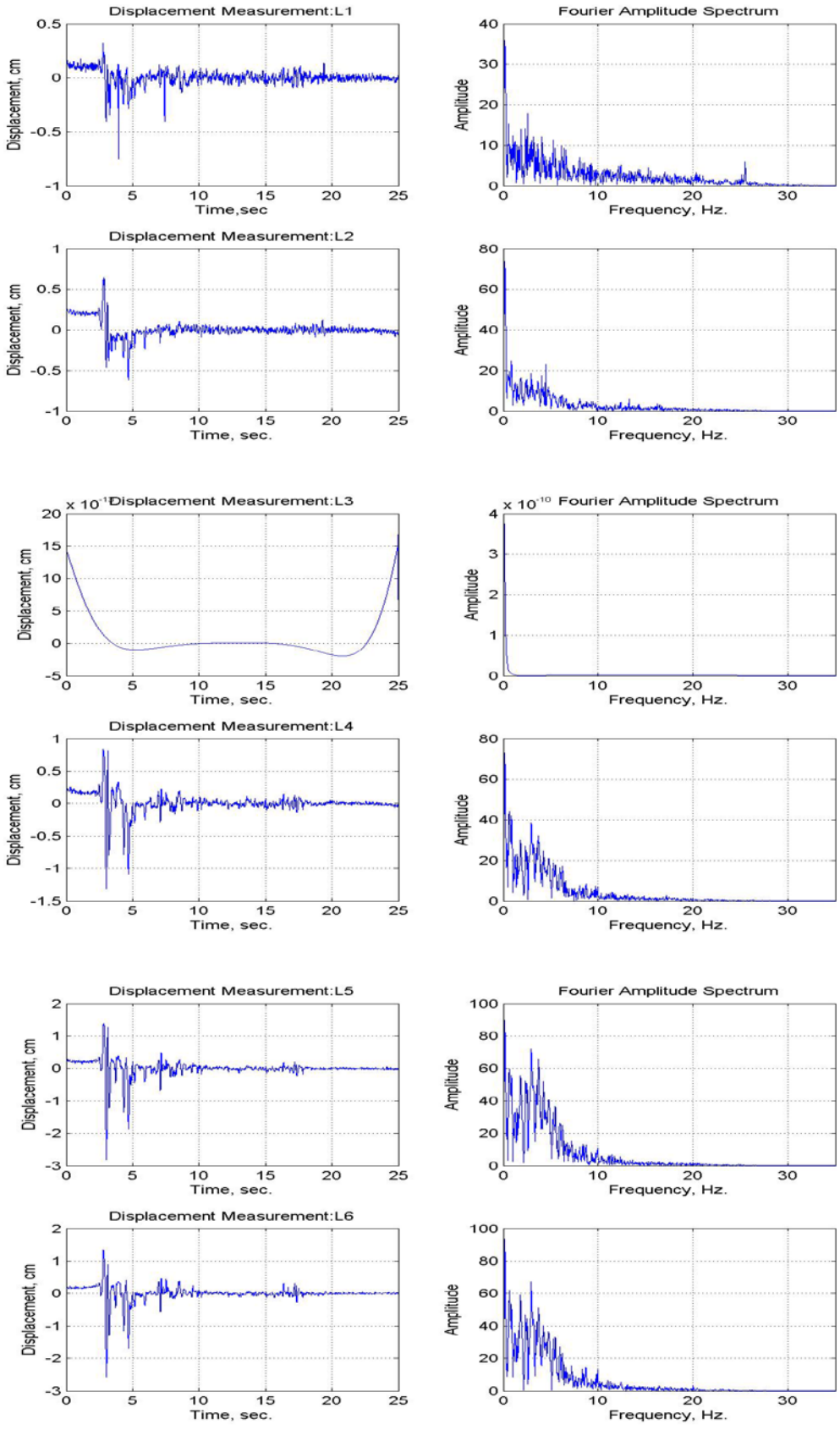


Figure B.34. Facing Displacements Measured for Wall Configuration 4- El Centro 250%

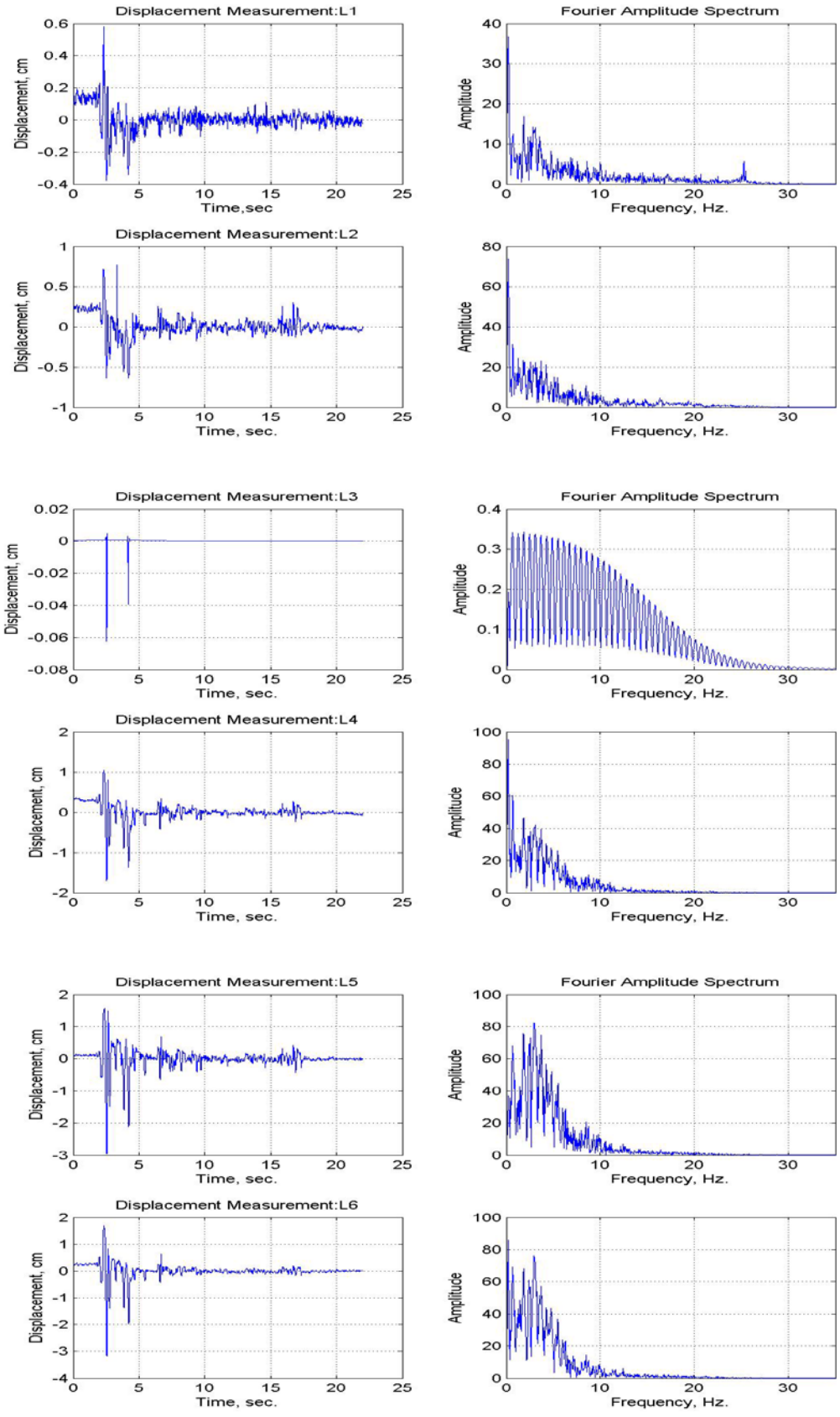


Figure B.35. Facing Displacements Measured for Wall Configuration 4- El Centro 275%

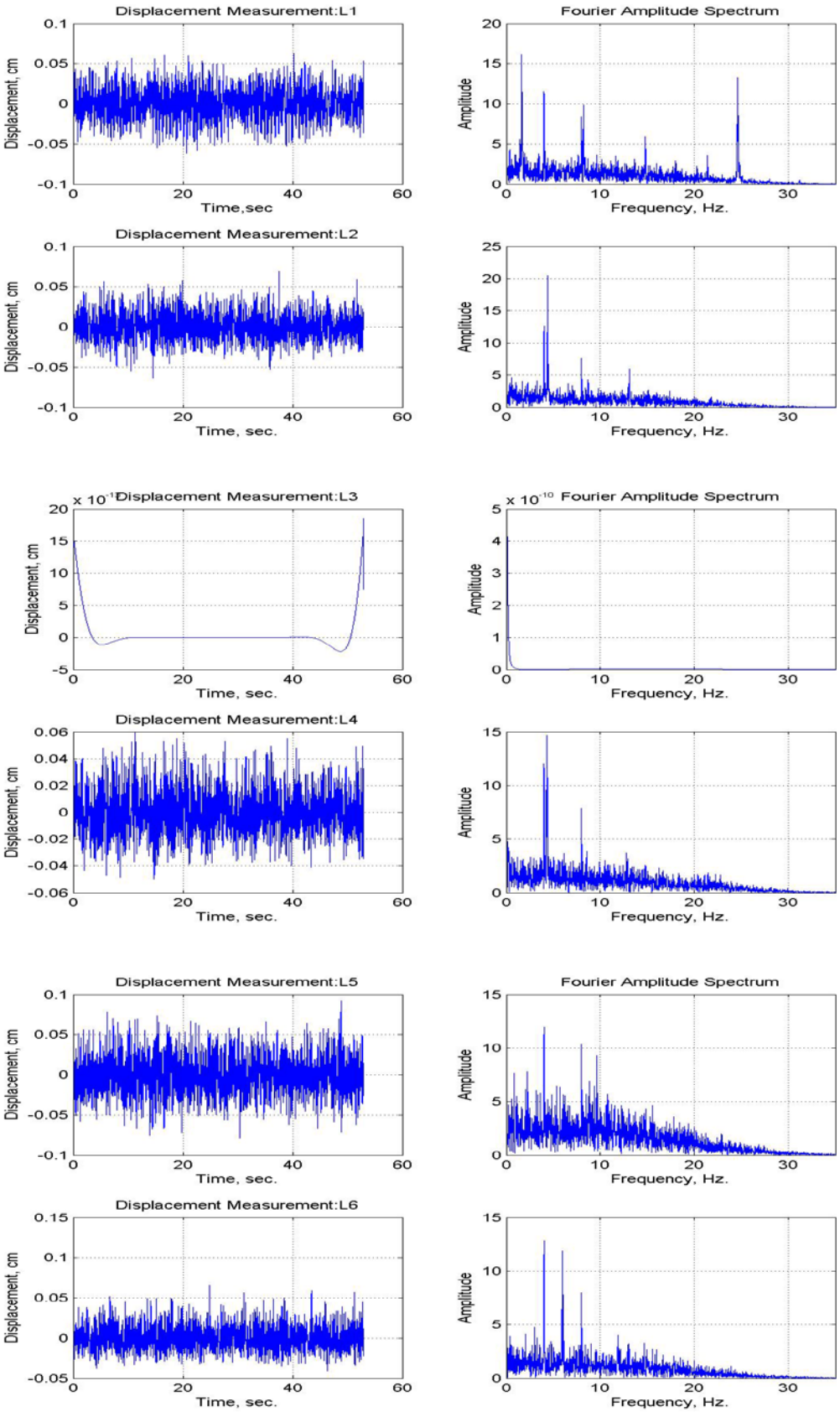


Figure B.36. Facing Displacements Measured for Wall Configuration 4- Izmit 100%

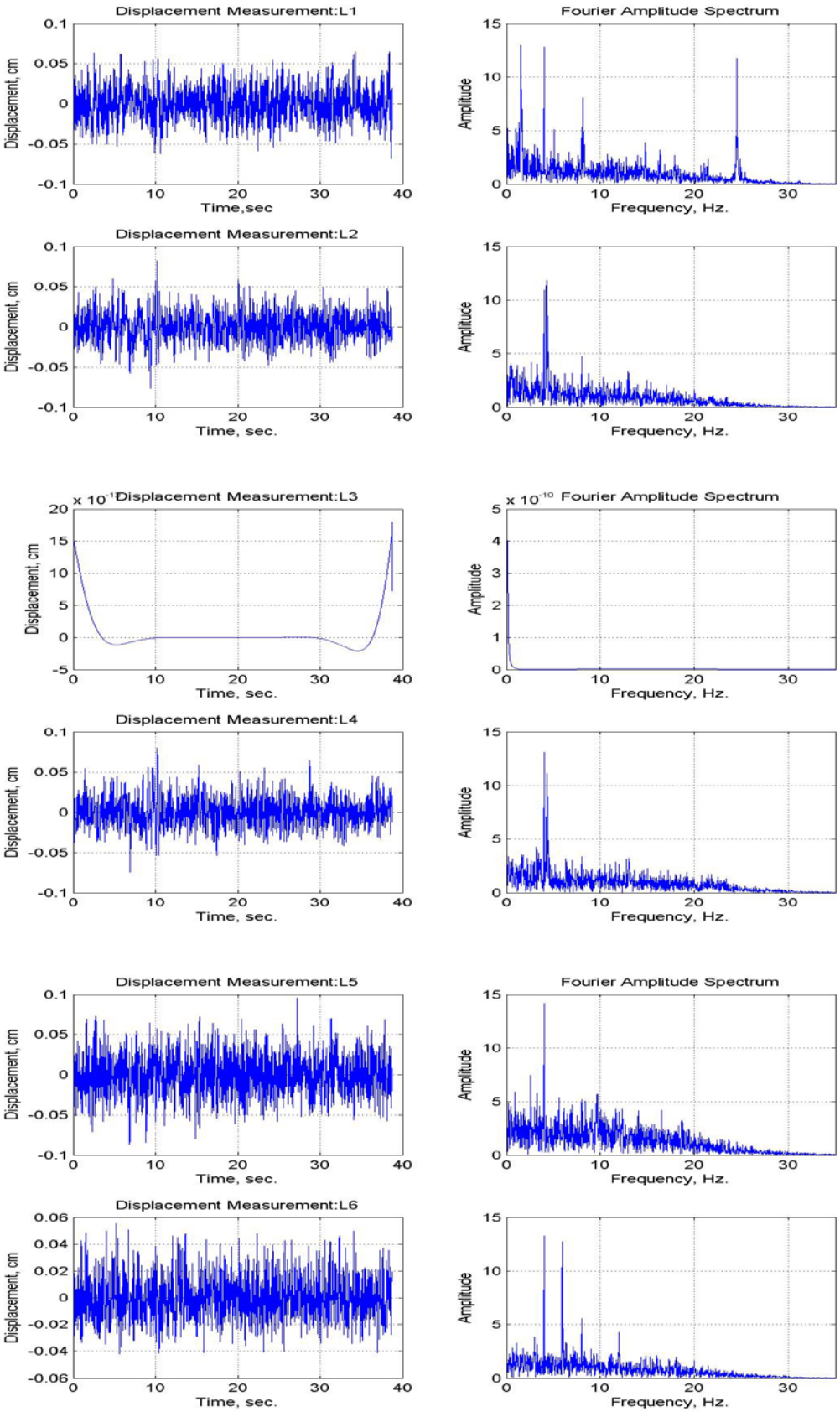


Figure B.37. Facing Displacements Measured for Wall Configuration 4- Izmit 150%

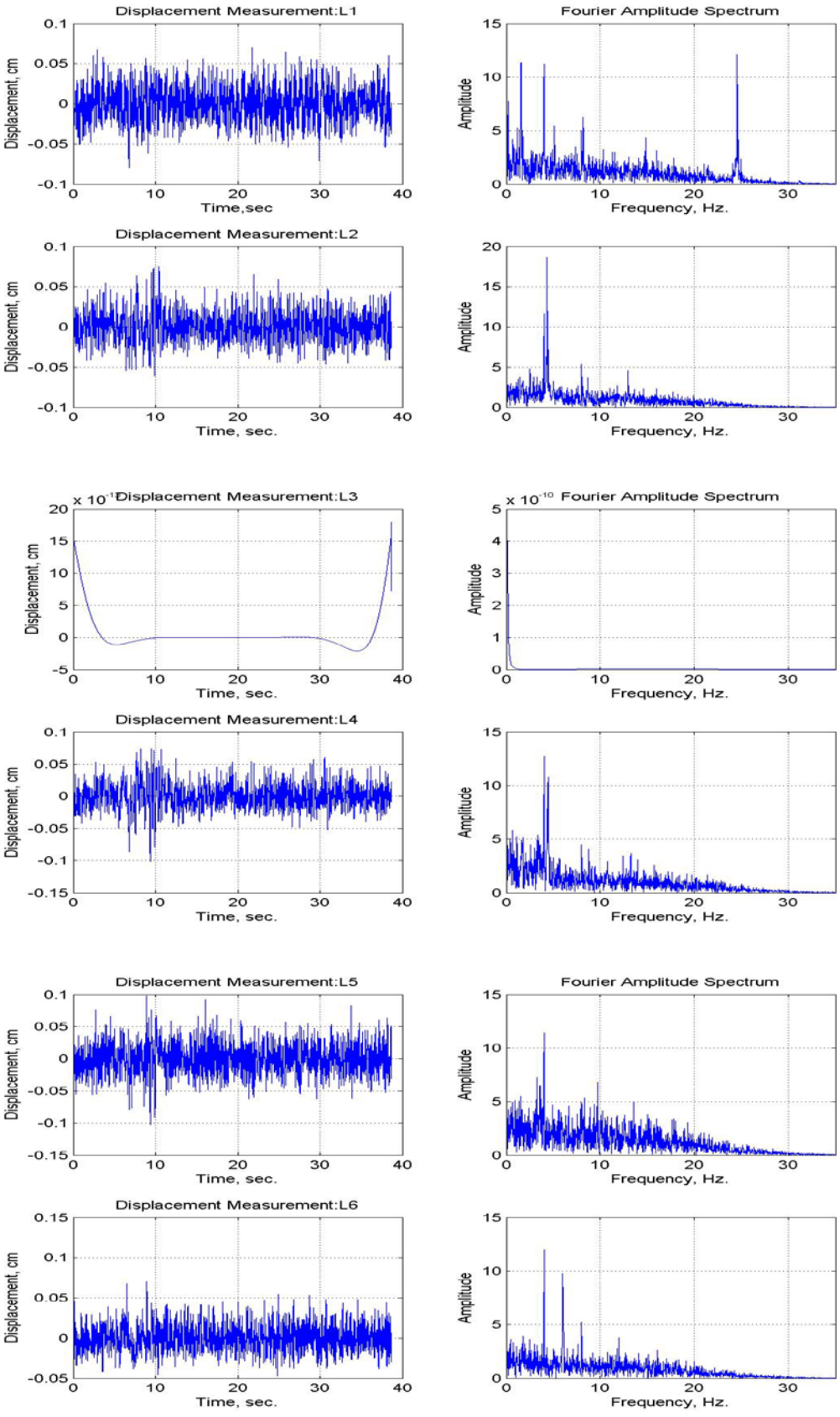


Figure B.38. Facing Displacements Measured for Wall Configuration 4- Izmit 200%

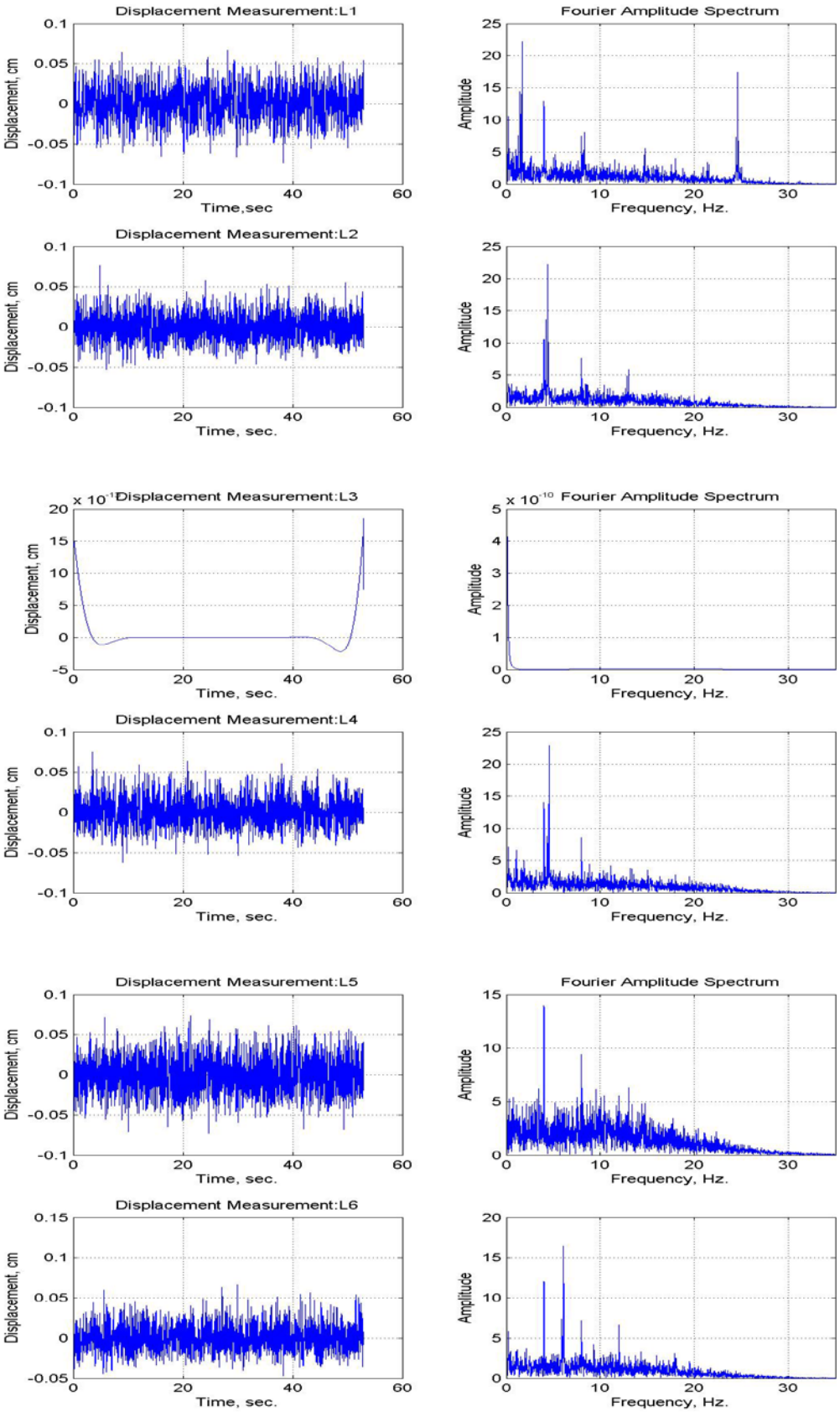


Figure B.39. Facing Displacements Measured for Wall Configuration 4- Sakarya 100%

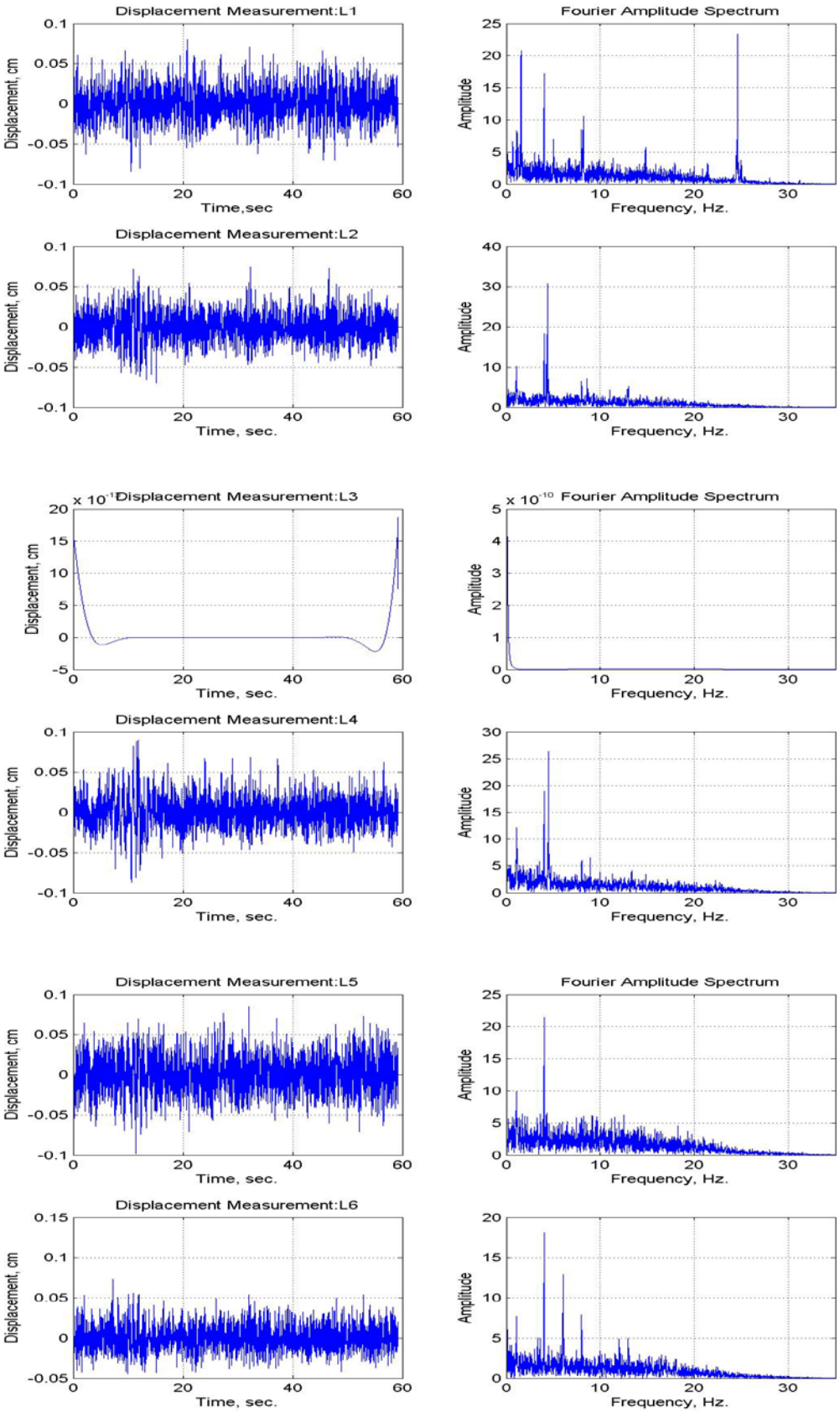


Figure B.40. Facing Displacements Measured for Wall Configuration 4- Sakarya 150%

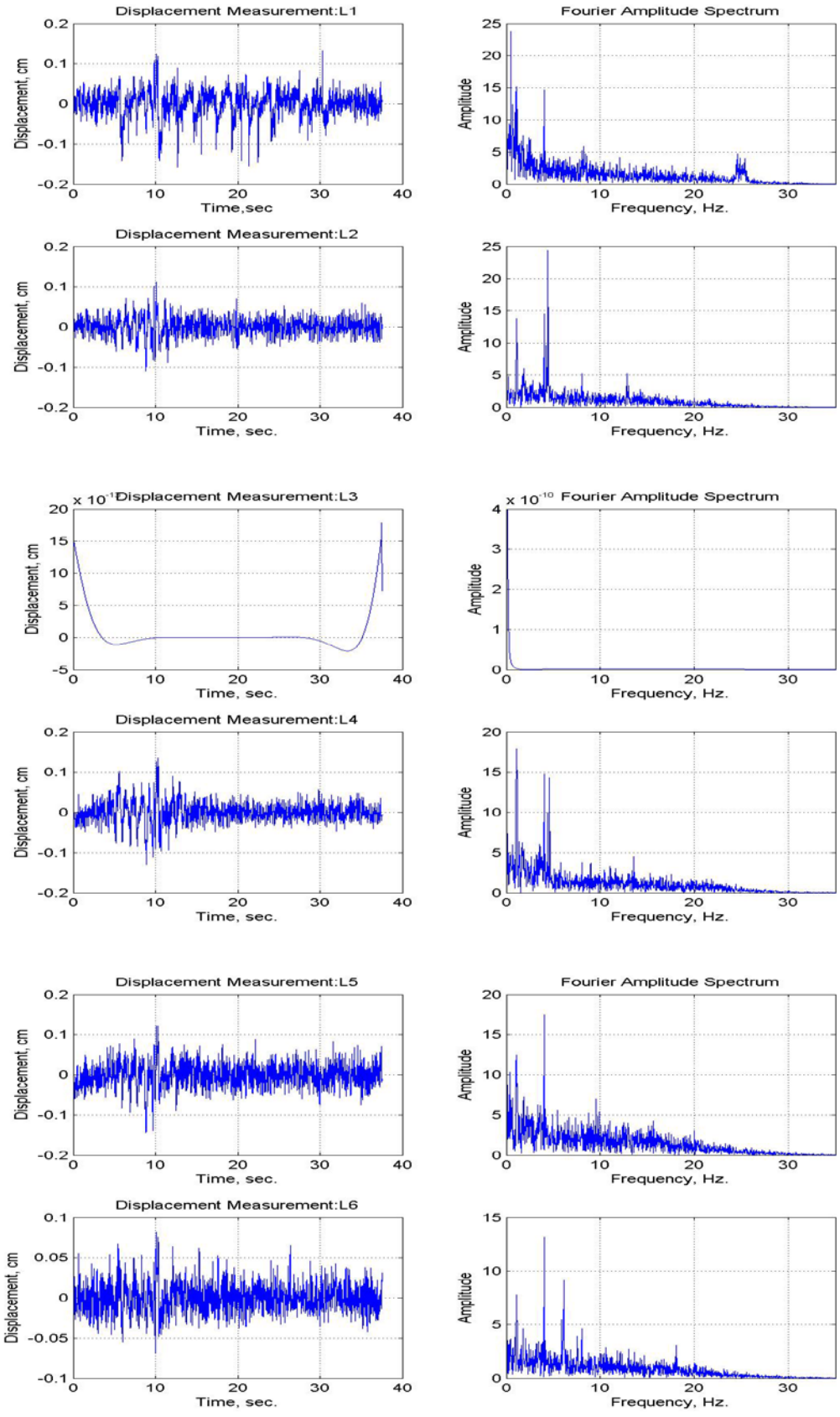


Figure B.41. Facing Displacements Measured for Wall Configuration 4- Sakarya 200%

APPENDIX C:STRAIN-TIME HISTORY GRAPHS OBTAINED FROM THE TESTS

This appendix contains strain-time history graphs for each wall configuration and base acceleration. The locations and abbreviations used for the strain gages are given in Section 4.

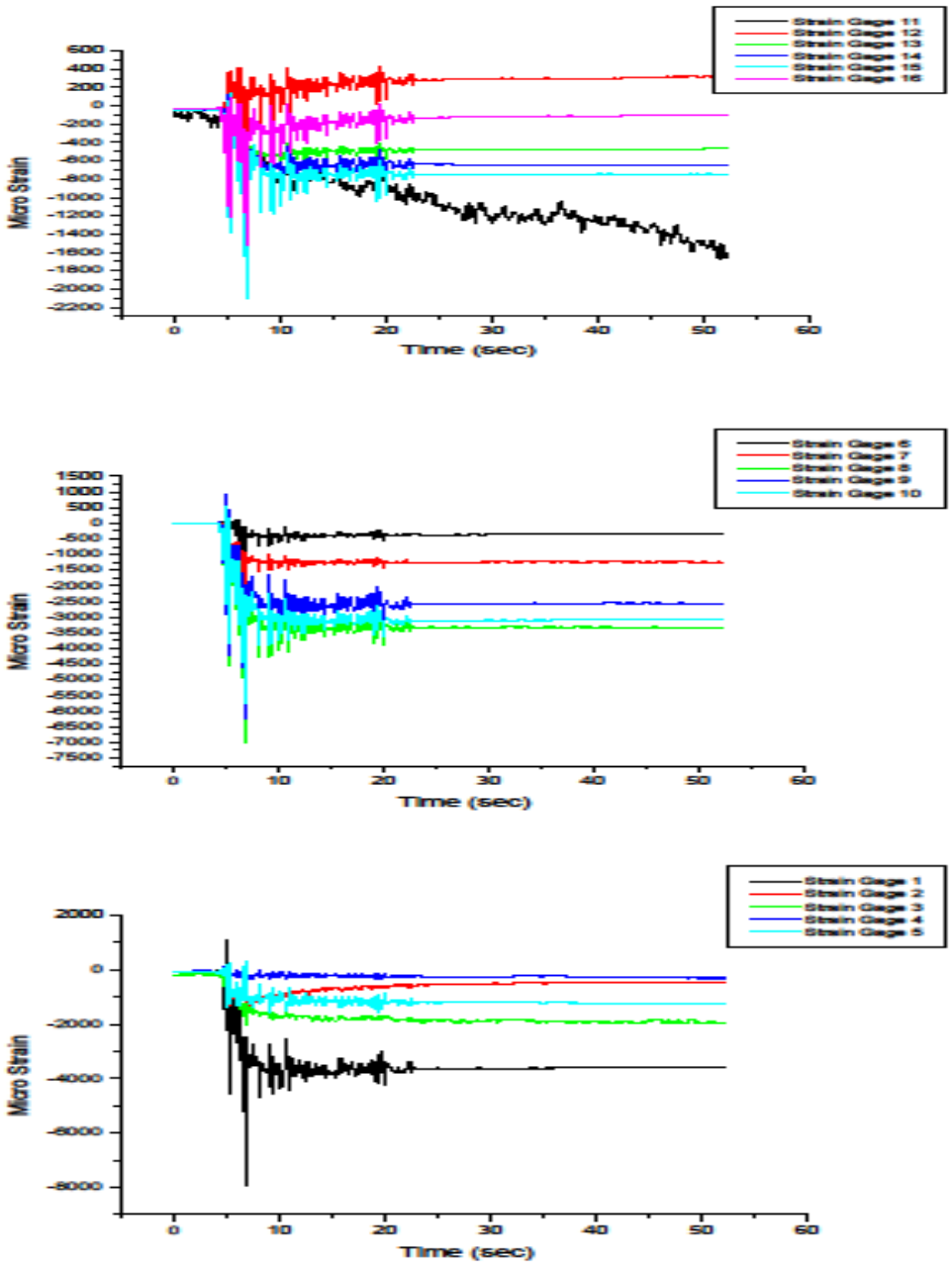


Figure C.1. Strains Measured at Top, Midheight and Bottom Geogrids for Wall 1- El Centro 100%

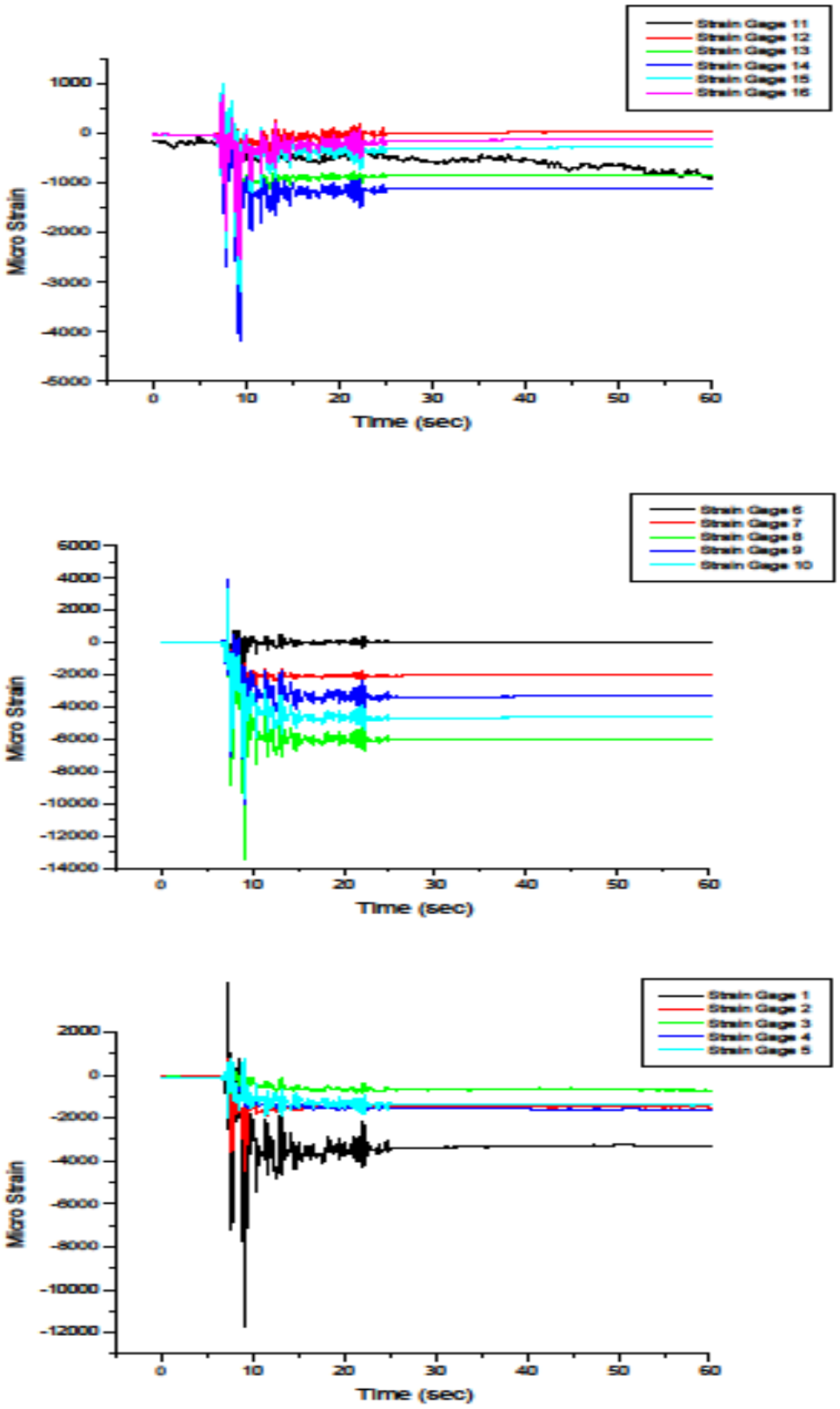


Figure C.2. Strains Measured at Top, Midheight and Bottom Geogrids for Wall 1- El Centro 150%

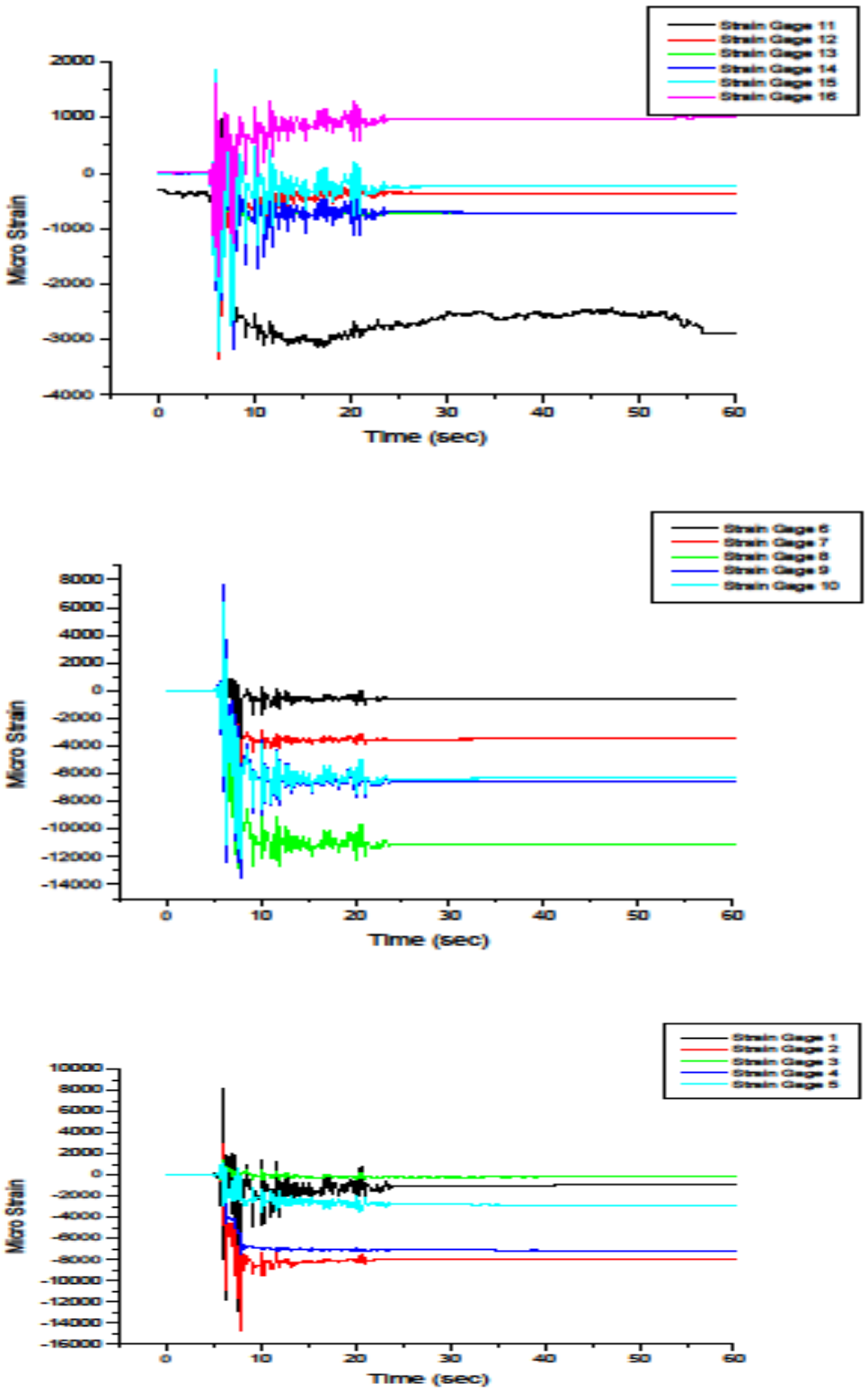


Figure C.3. Strains Measured at Top, Midheight and Bottom Geogrids for Wall 1- El Centro 200%

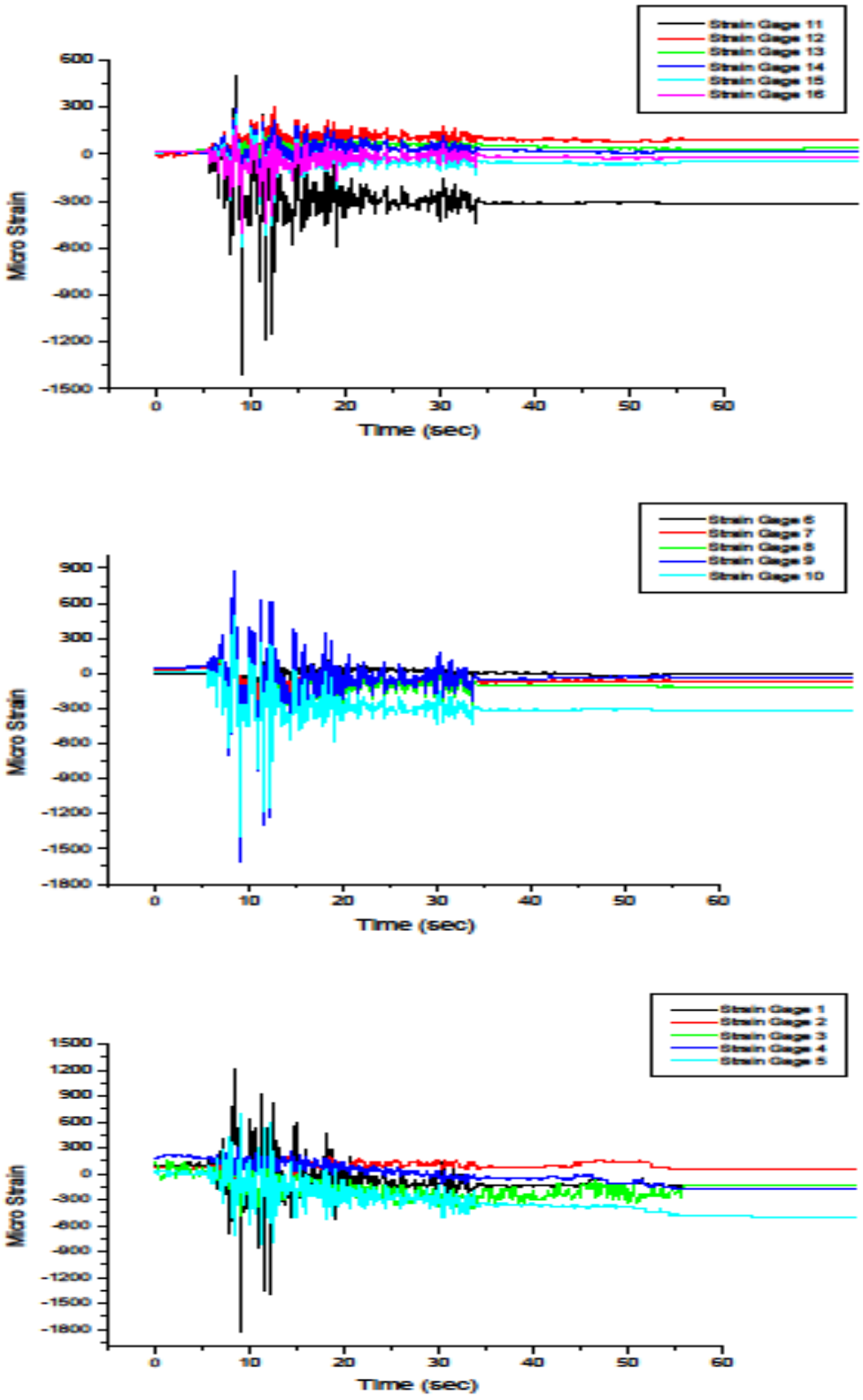


Figure C.4. Strains Measured at Top, Midheight and Bottom Geogrids for Wall 1- Izmit 100%

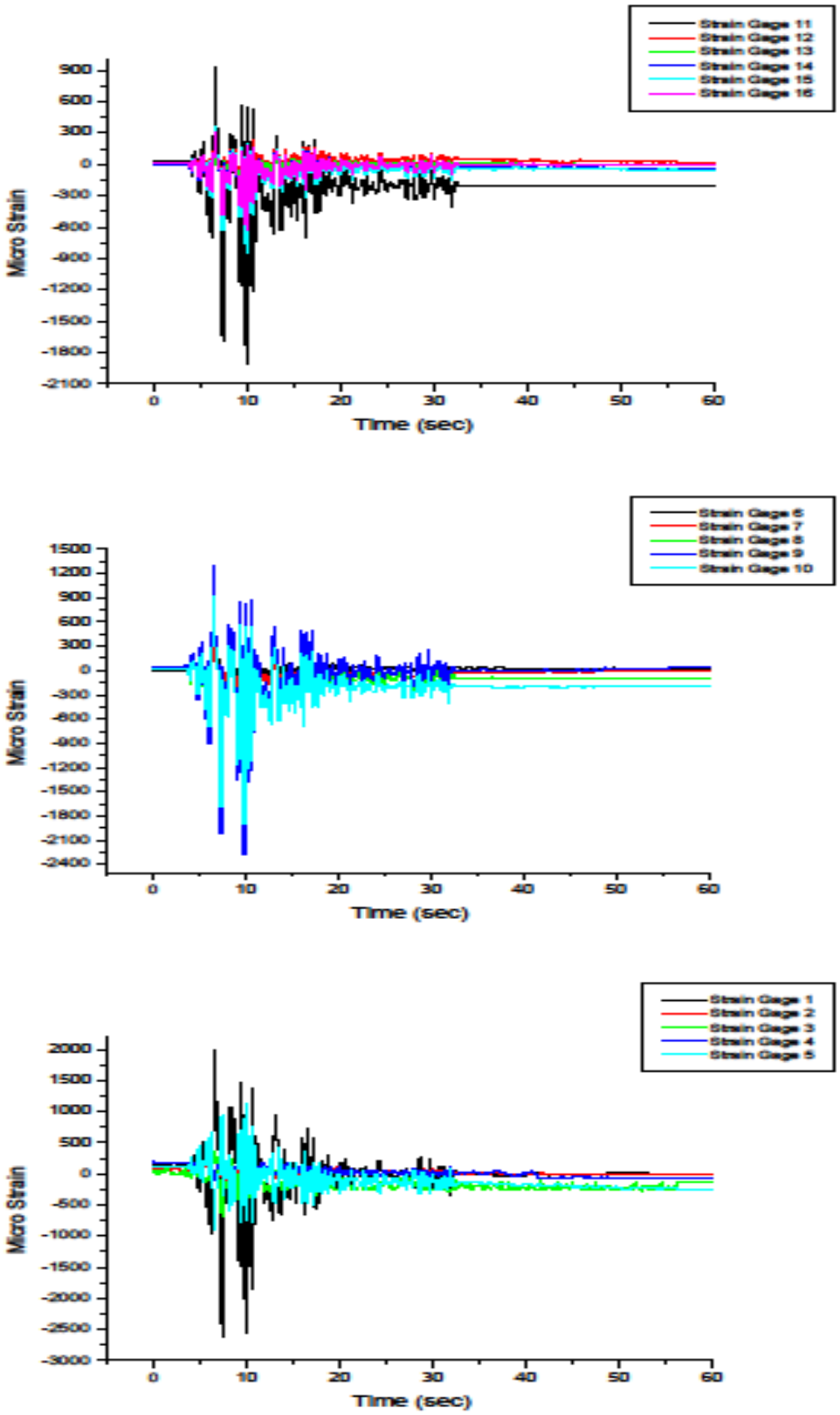


Figure C.5. Strains Measured at Top, Midheight and Bottom Geogrids for Wall 1- Izmit 150%

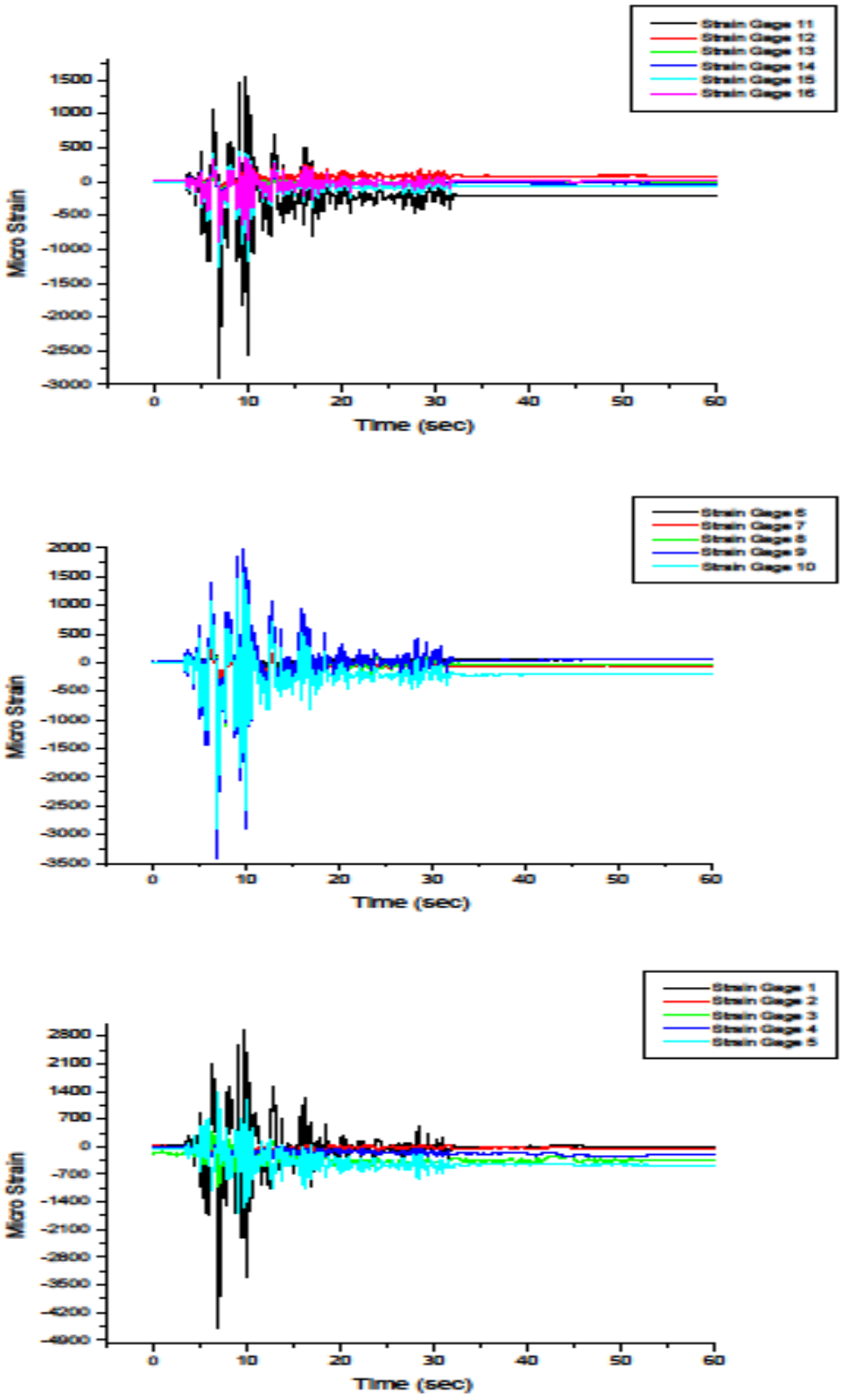


Figure C.6. Strains Measured at Top, Midheight and Bottom Geogrids for Wall 1- Izmit 200%

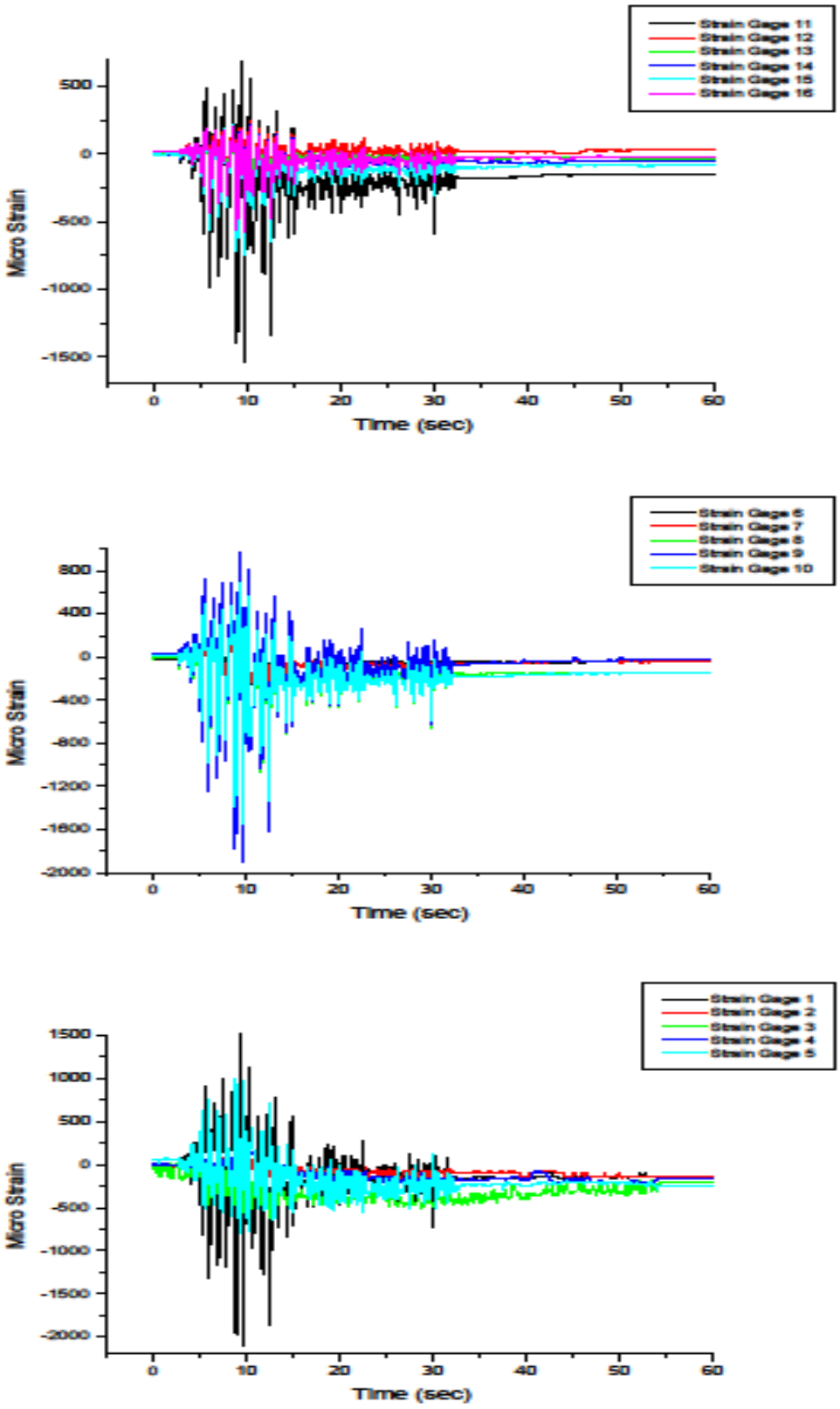


Figure C.7. Strains Measured at Top, Midheight and Bottom Geogrids for Wall 1-Sakarya 100%

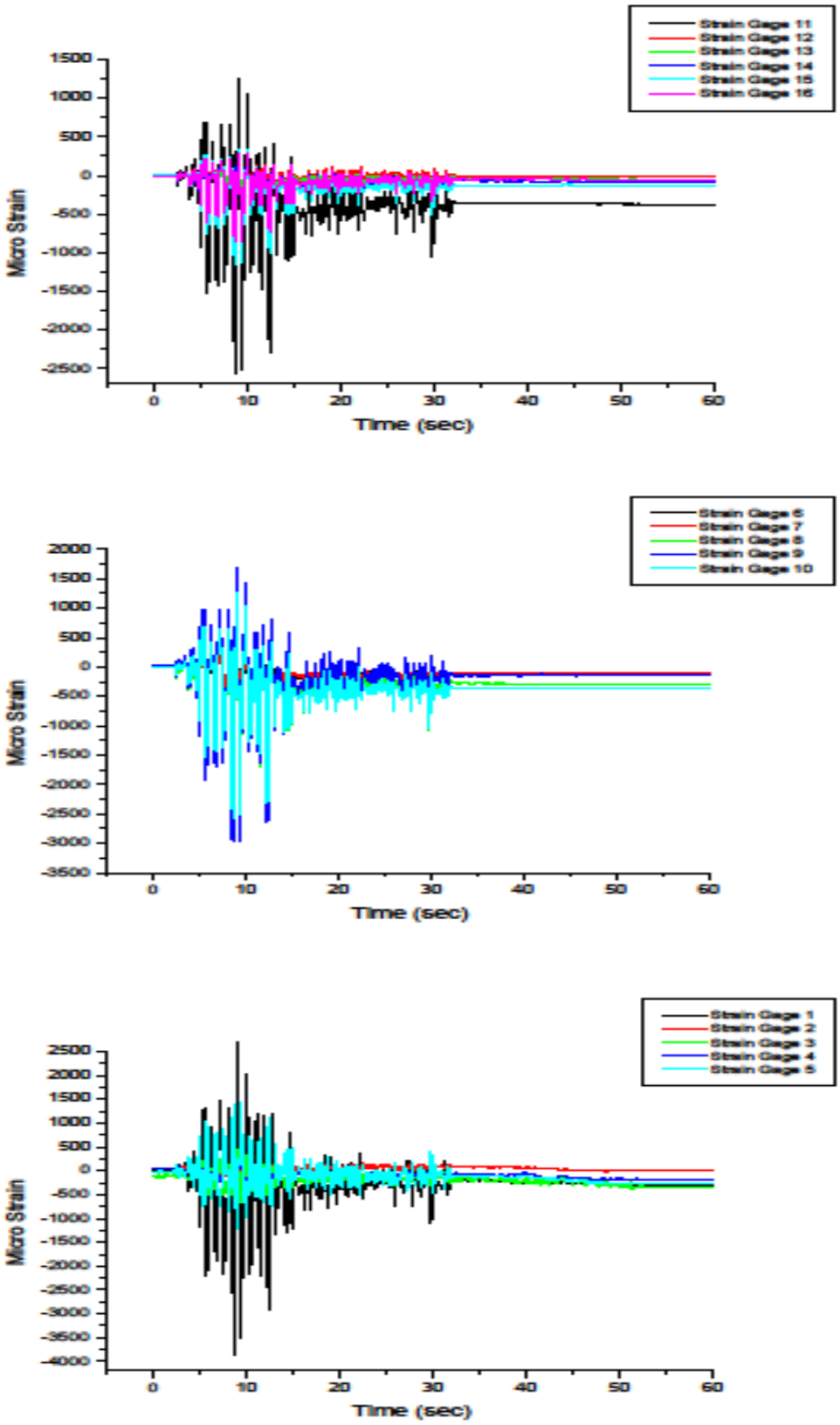


Figure C.8. Strains Measured at Top, Midheight and Bottom Geogrids for Wall 1-Sakarya 150%

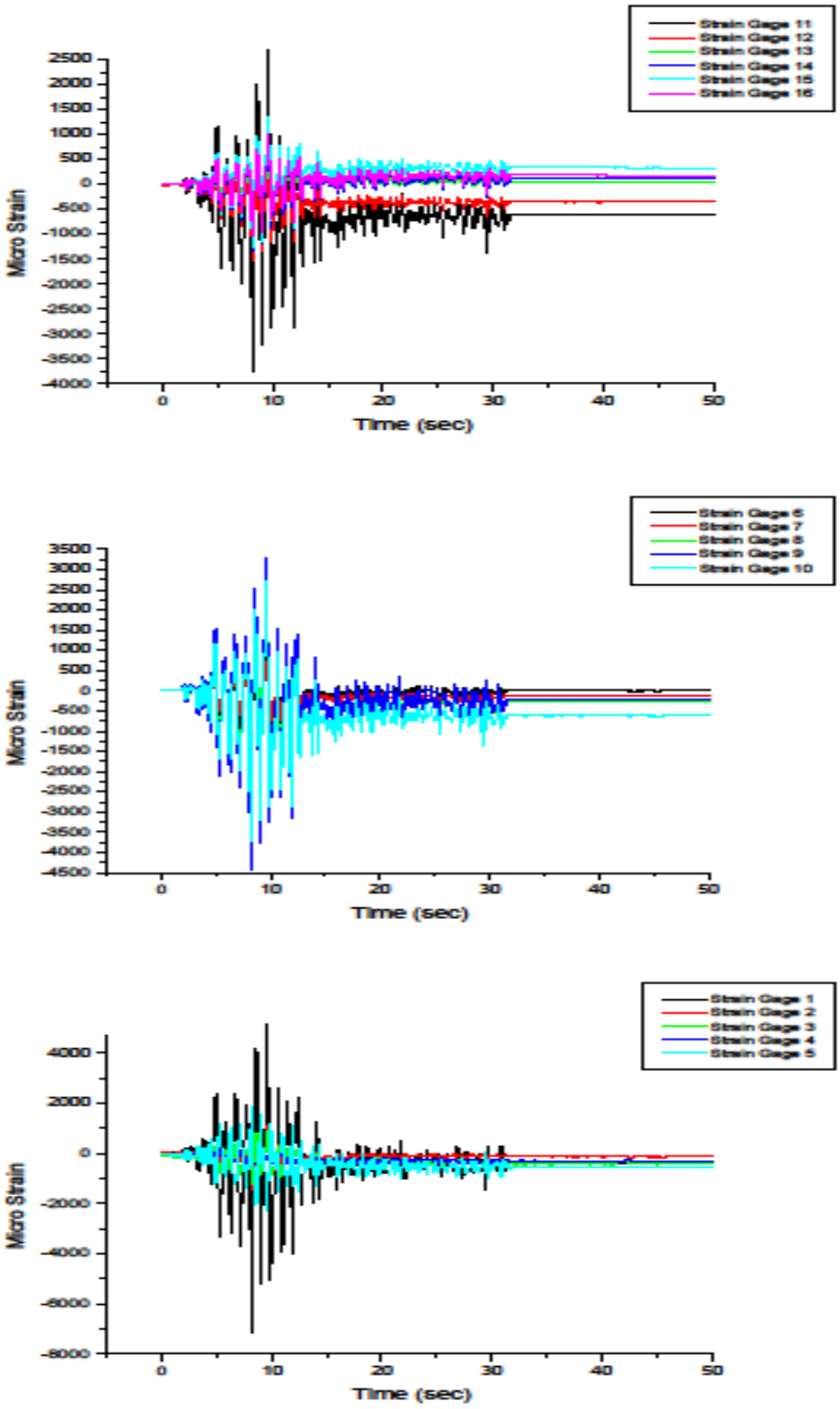
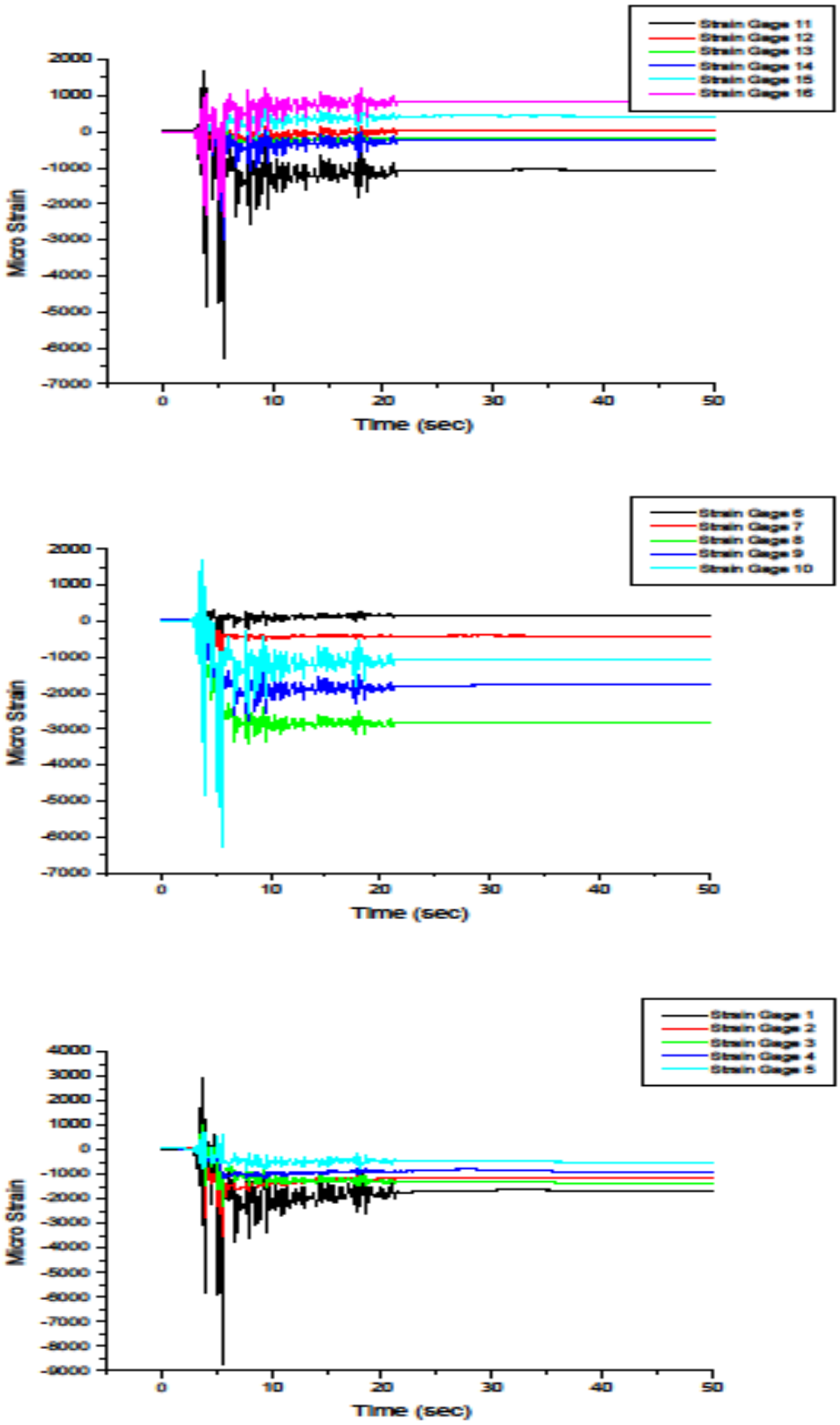


Figure C.9. Strains Measured at Top, Midheight and Bottom Geogrids for Wall 1-Sakarya 200%



igure C.10. Strains Measured at Top, Midheight and Bottom Geogrids for Wall 2- El Centro 100%

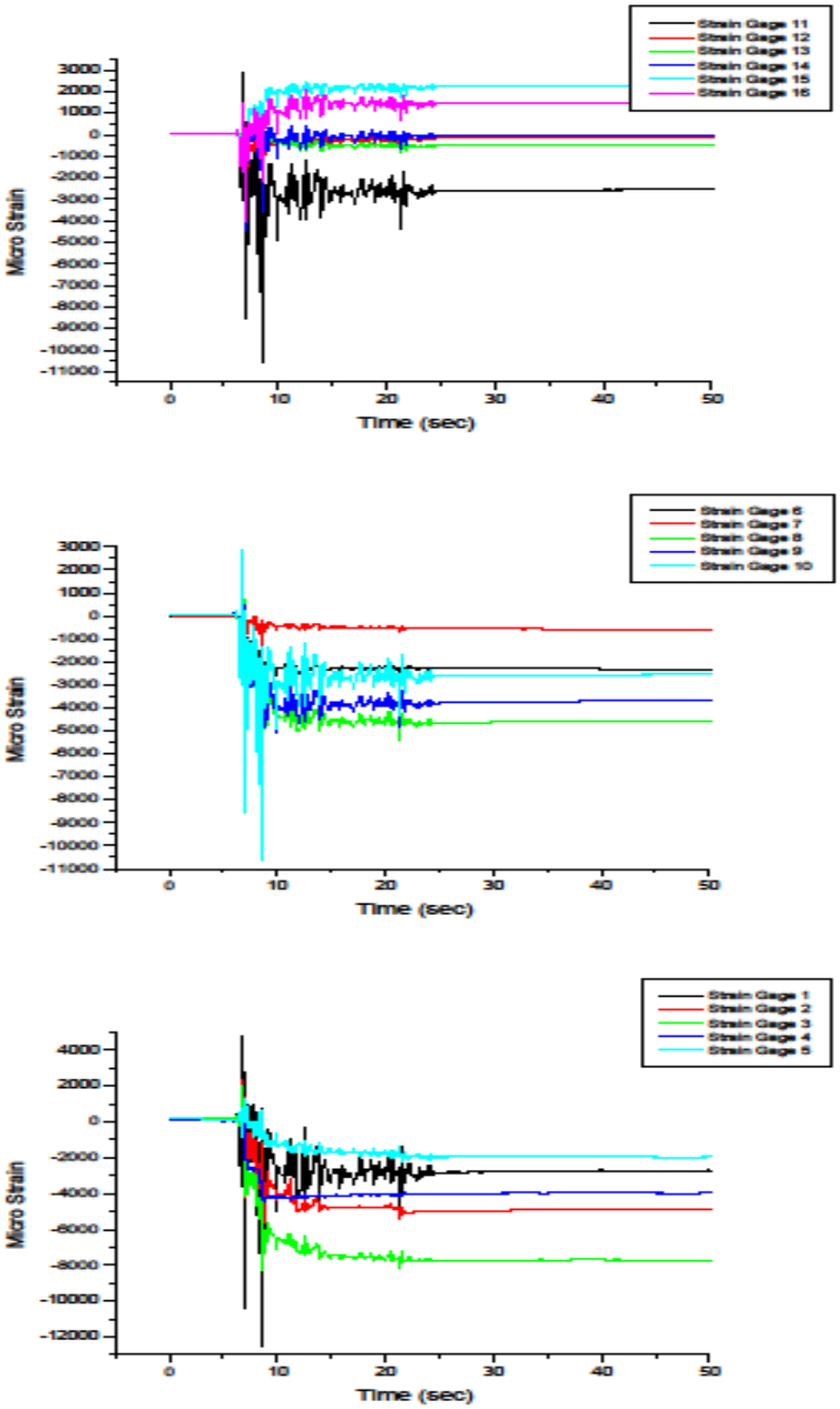


Figure C.11. Strains Measured at Top, Midheight and Bottom Geogrids for Wall 2- El Centro 150%

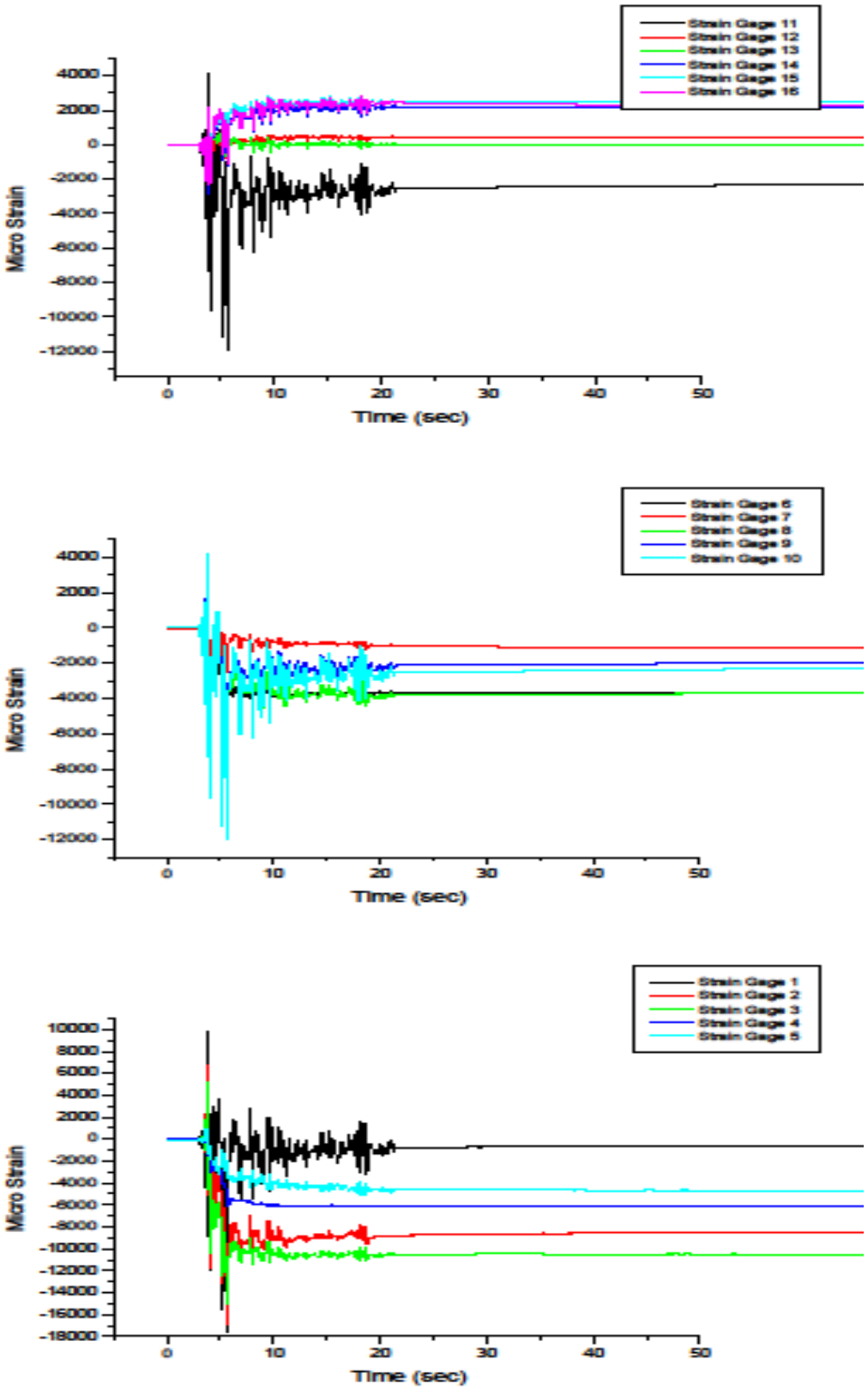


Figure C.12. Strains Measured at Top, Midheight and Bottom Geogrids for Wall 2- El Centro 200%

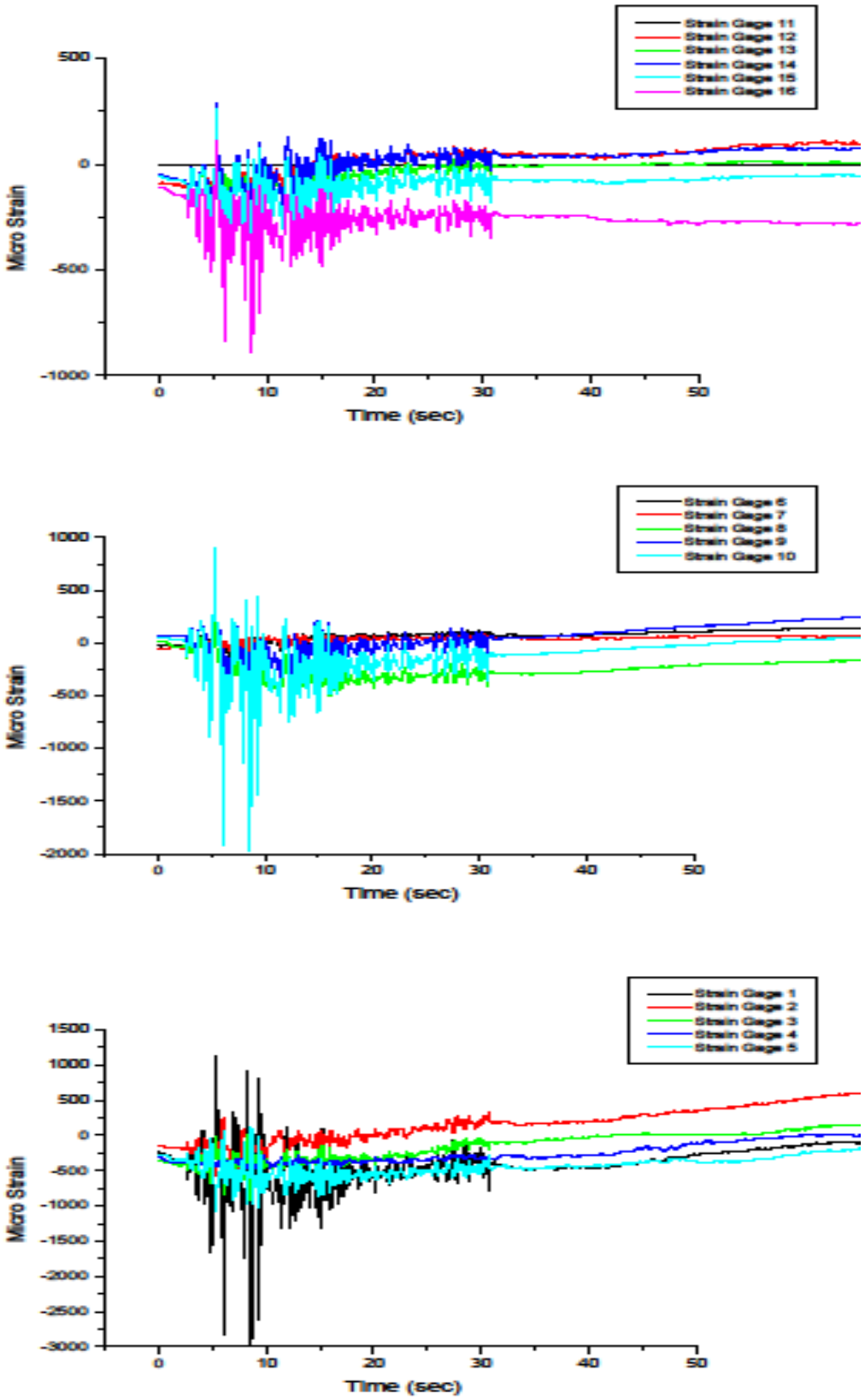


Figure C.13. Strains Measured at Top, Midheight and Bottom Geogrids for Wall 2- Izmit 100%

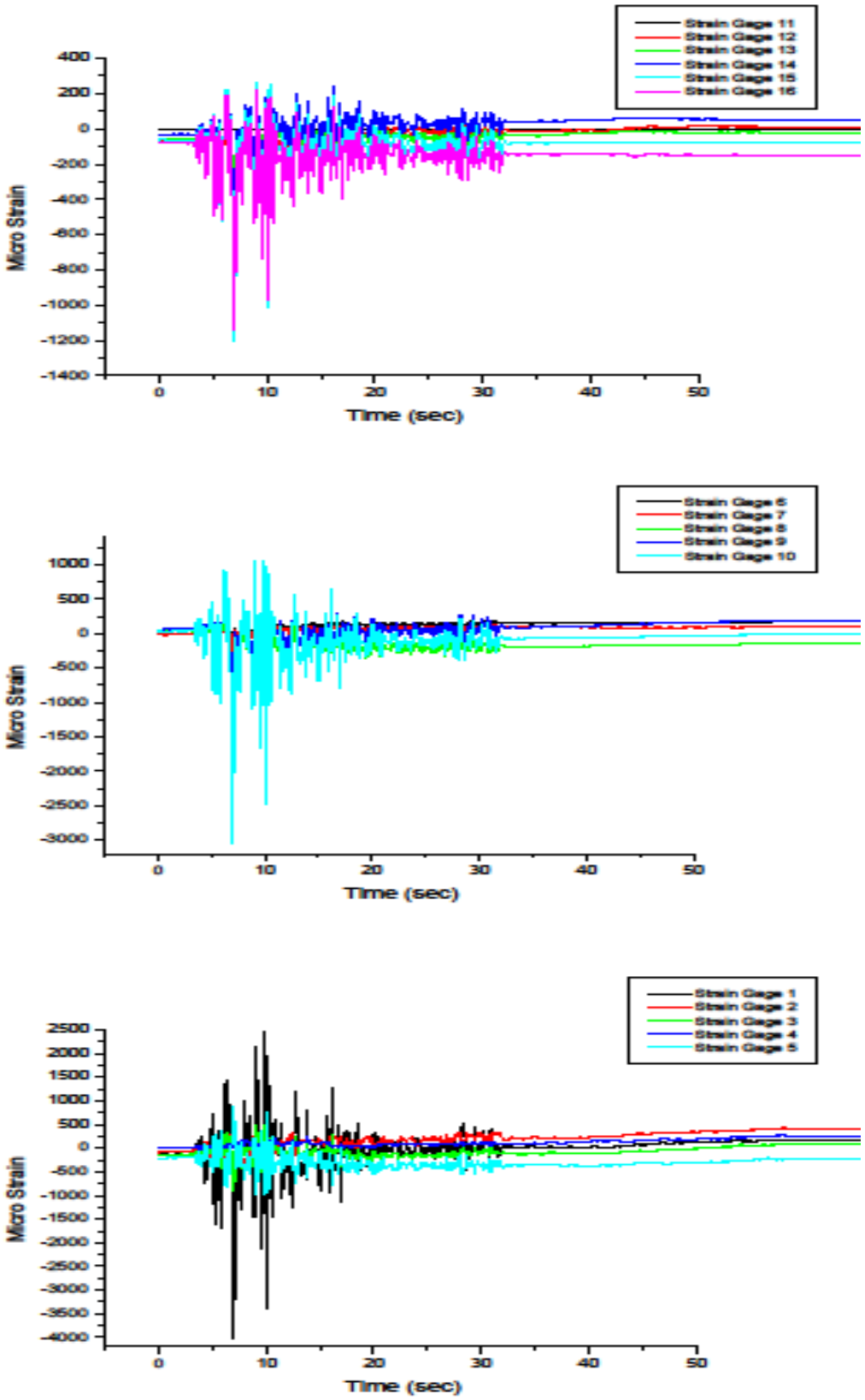


Figure C.14. Strains Measured at Top, Midheight and Bottom Geogrids for Wall 2- Izmit 150%

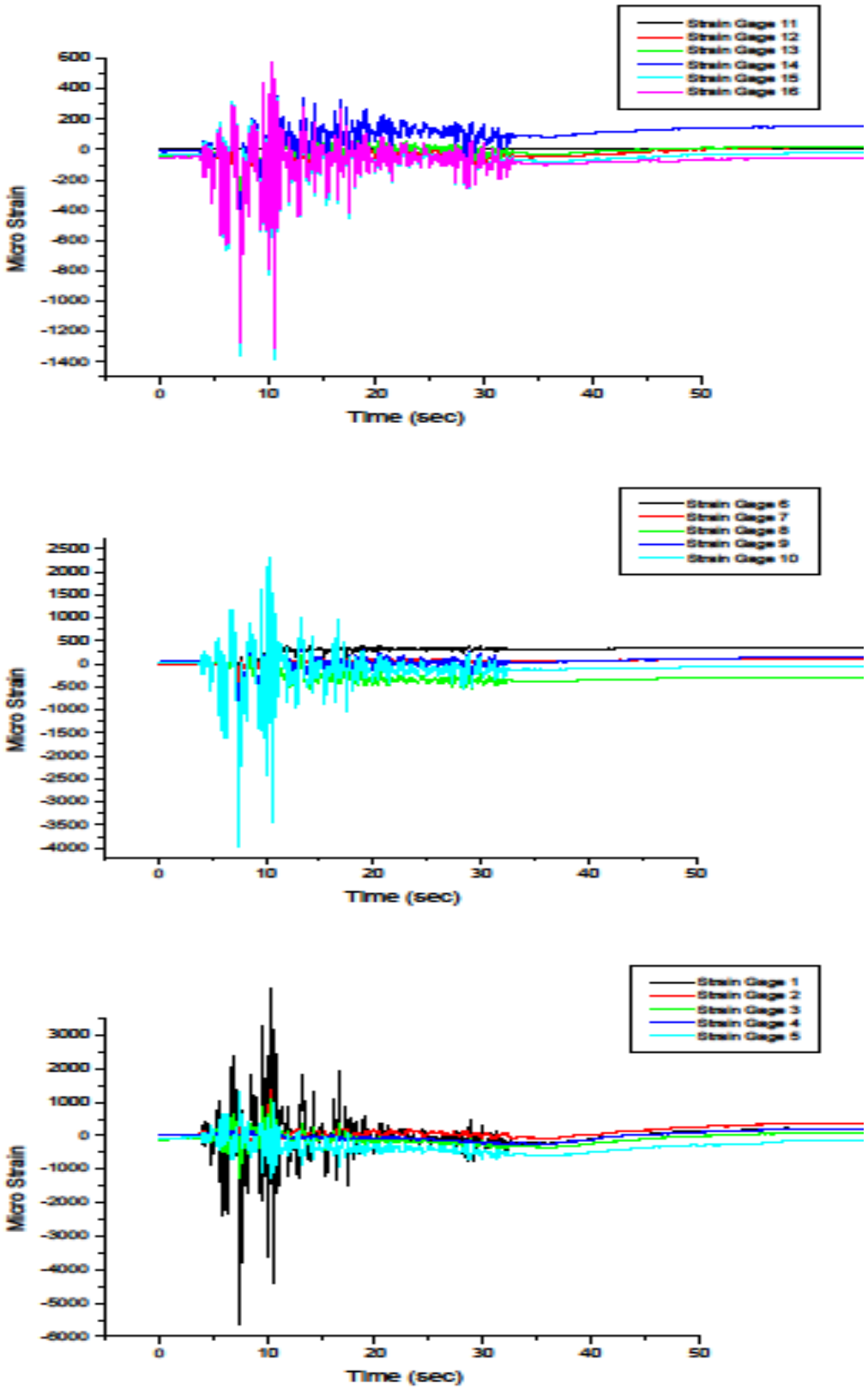


Figure C.15. Strains Measured at Top, Midheight and Bottom Geogrids for Wall 2- Izmit 200%

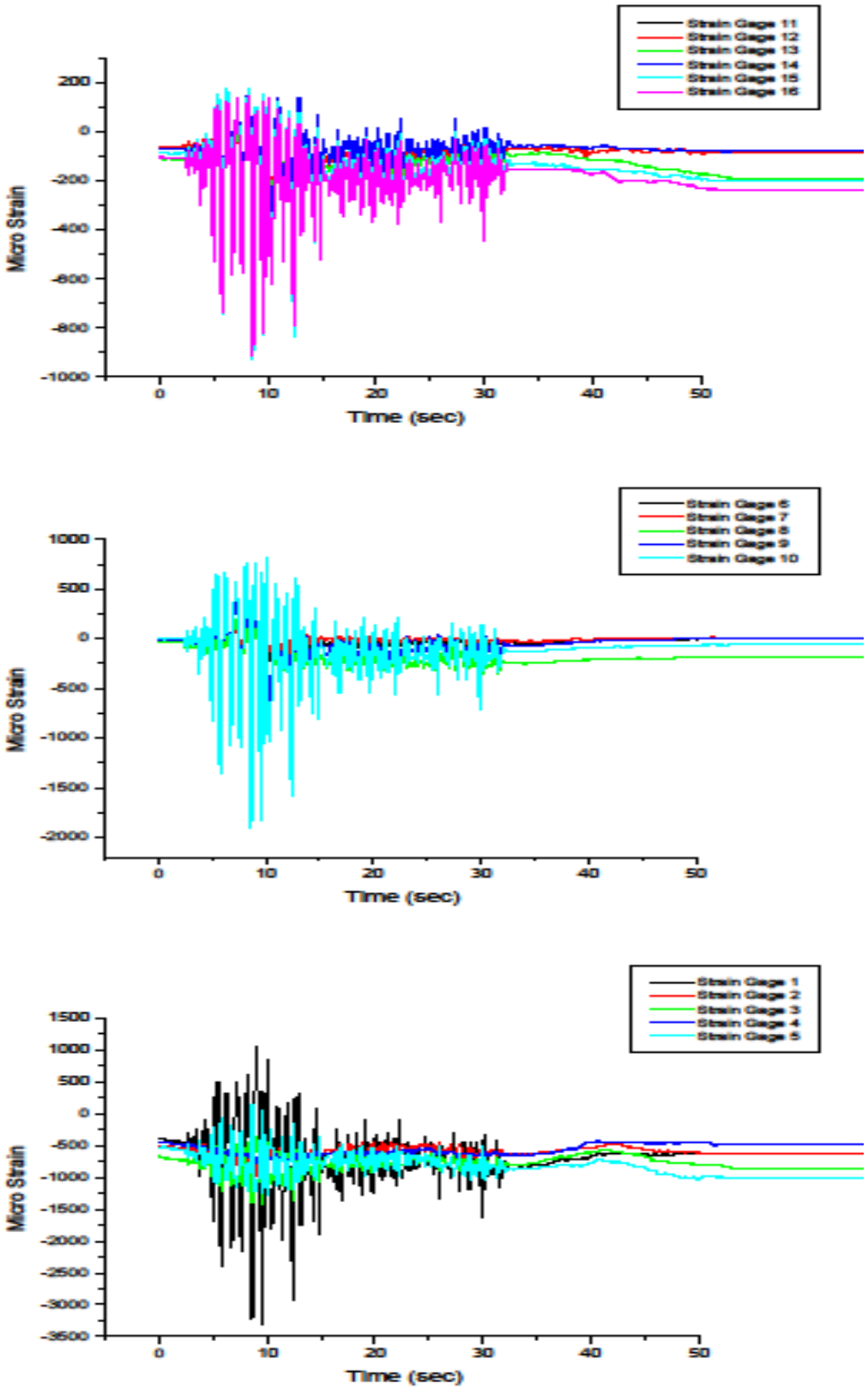


Figure C.16. Strains Measured at Top, Midheight and Bottom Geogrids for Wall 2-Sakarya 100%

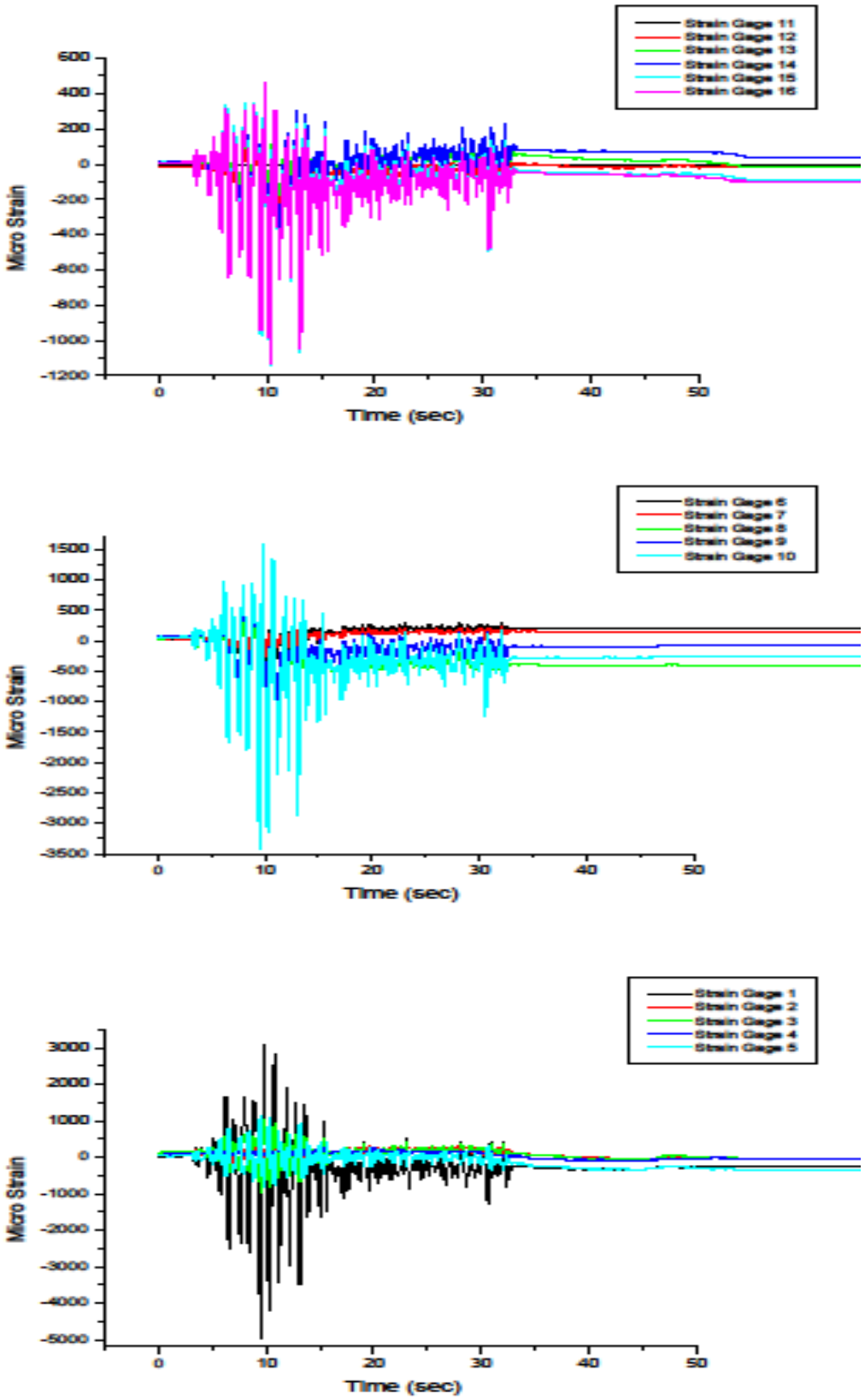


Figure C.17. Strains Measured at Top, Midheight and Bottom Geogrids for Wall 2-Sakarya 150%

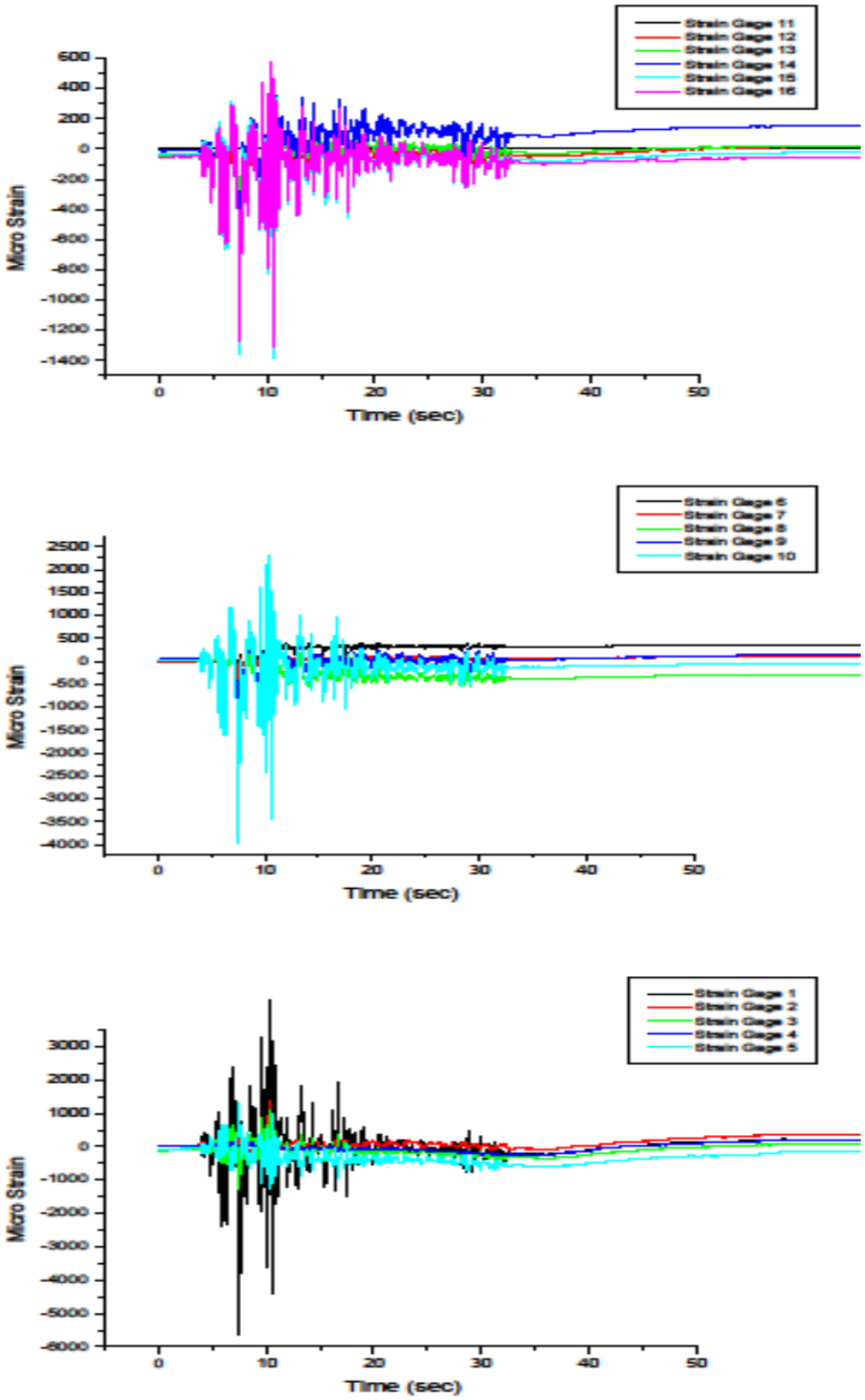


Figure C.18. Strains Measured at Top, Midheight and Bottom Geogrids for Wall 2-Sakarya 200%

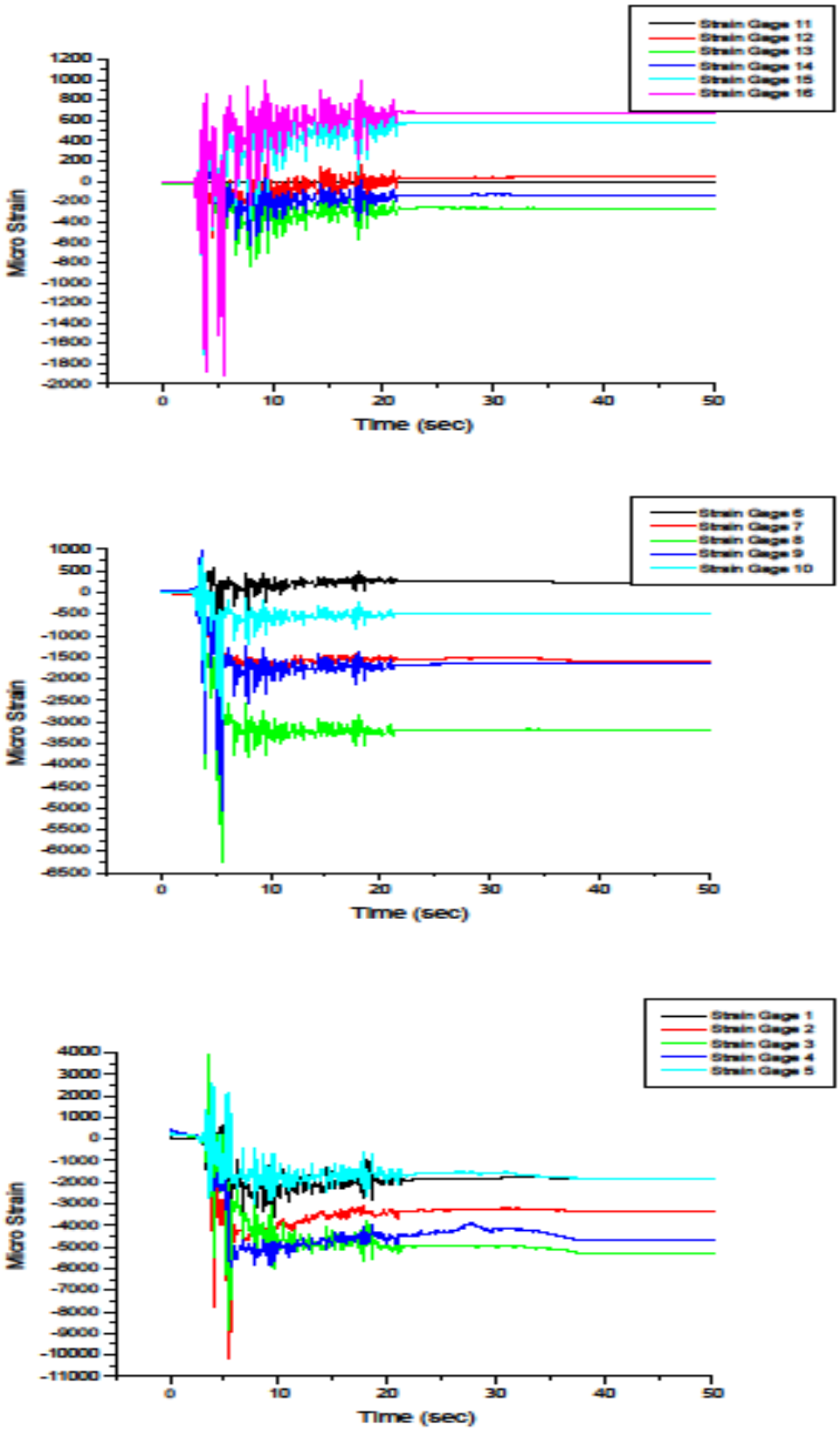


Figure C.19. Strains Measured at Top, Midheight and Bottom Geogrids for Wall 3- El Centro 100%

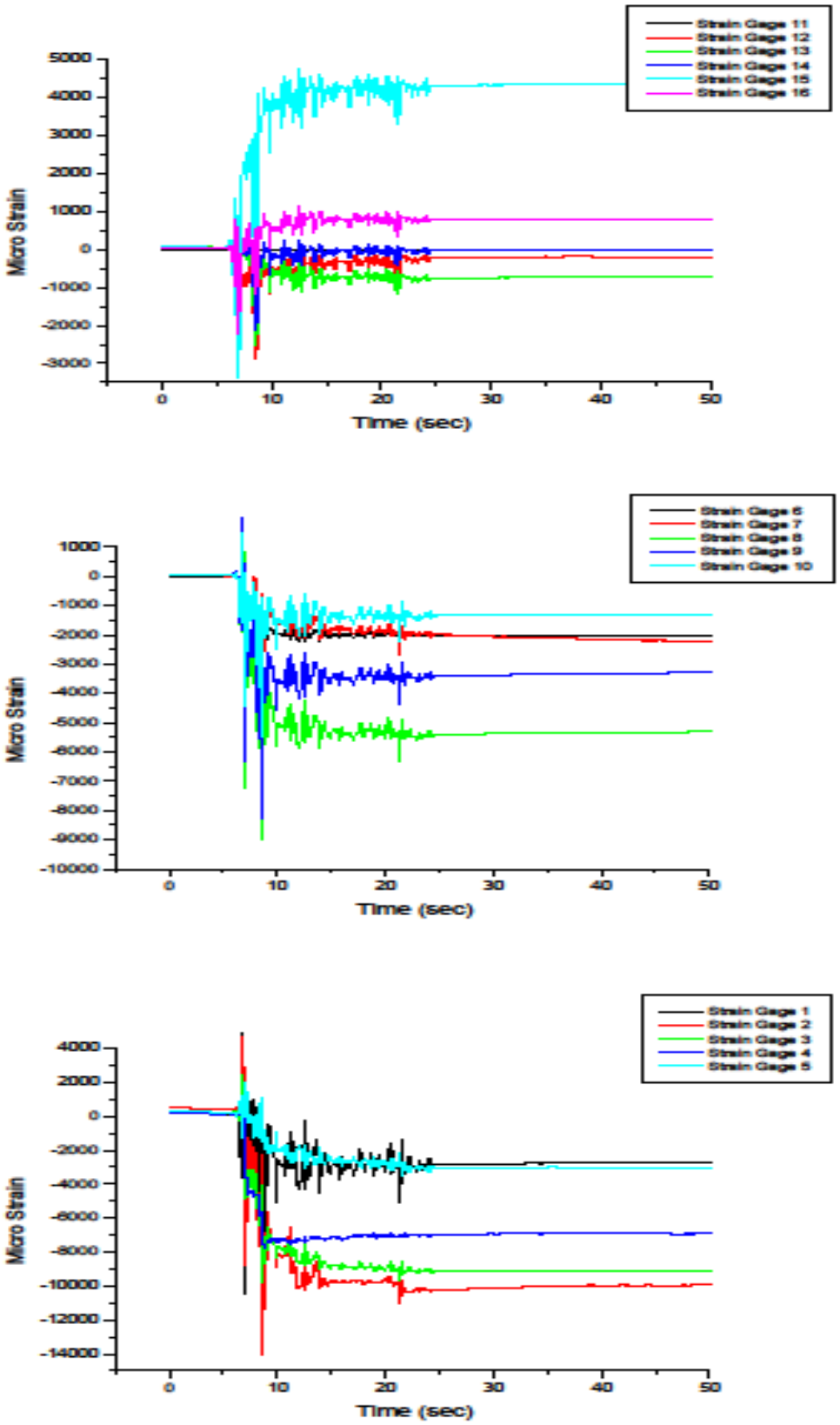


Figure C.20. Strains Measured at Top, Midheight and Bottom Geogrids for Wall 3- El Centro 150%

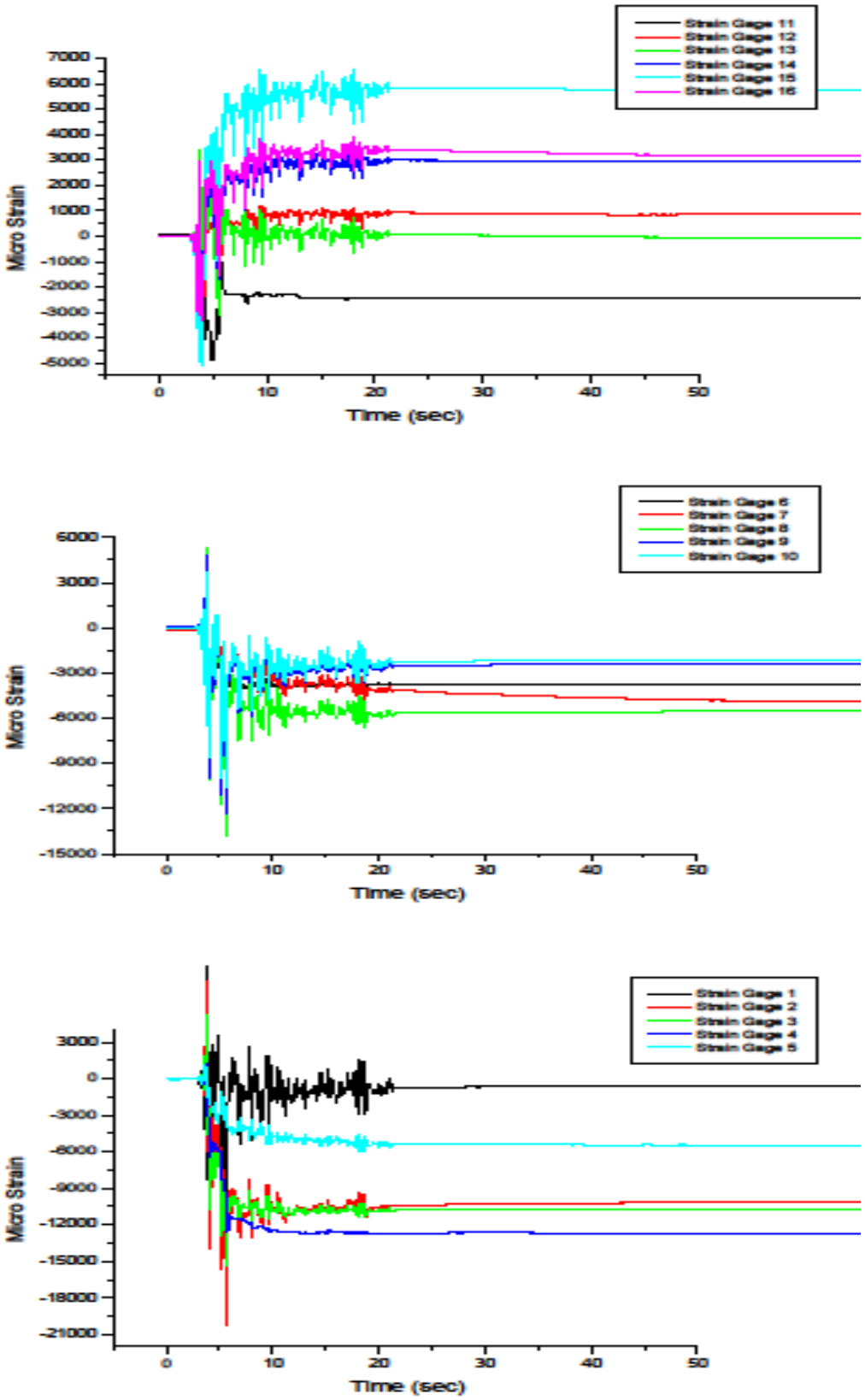


Figure C.21. Strains Measured at Top, Midheight and Bottom Geogrids for Wall 3- El Centro 200%

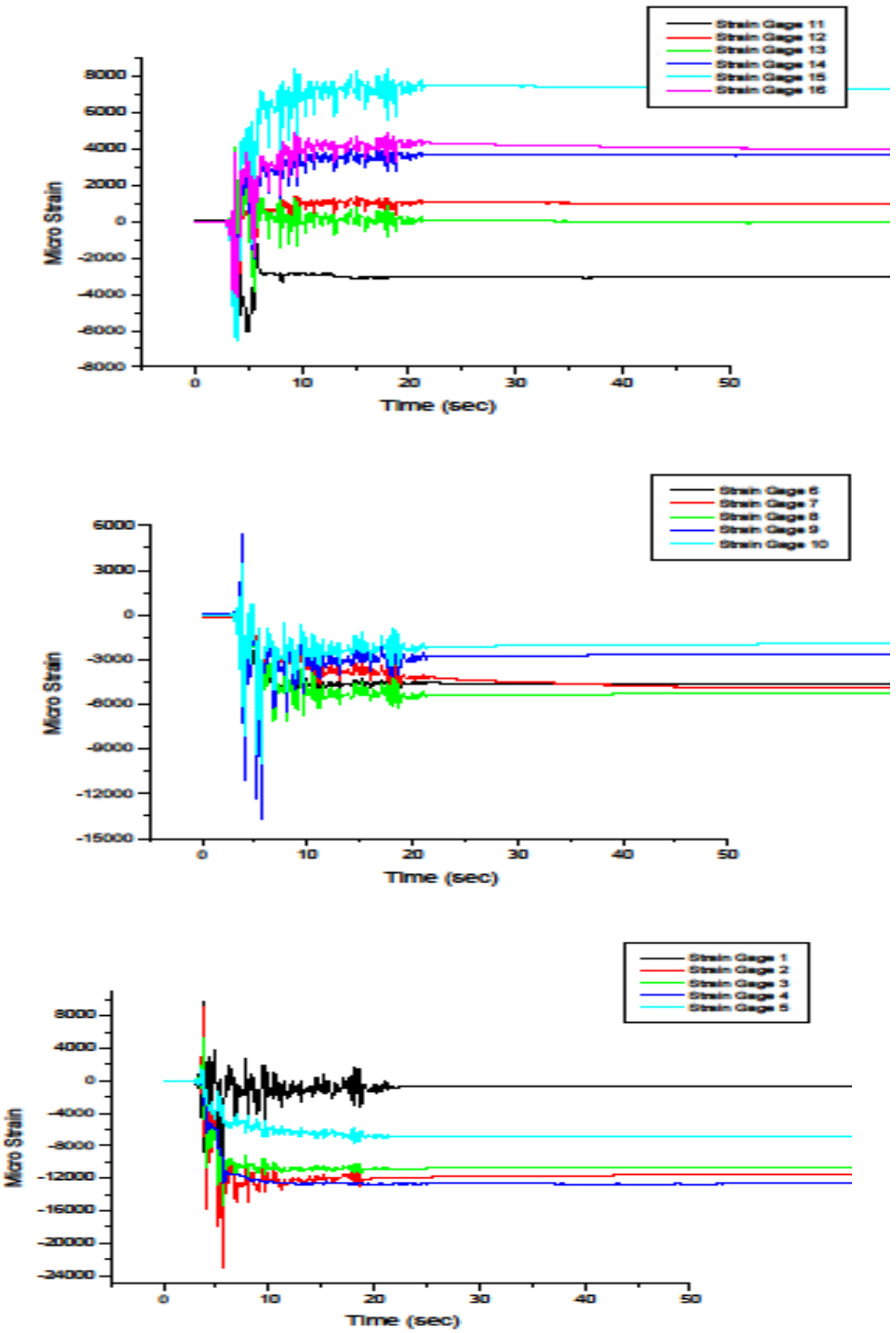


Figure C.22. Strains Measured at Top, Midheight and Bottom Geogrids for Wall 3- El Centro 250%

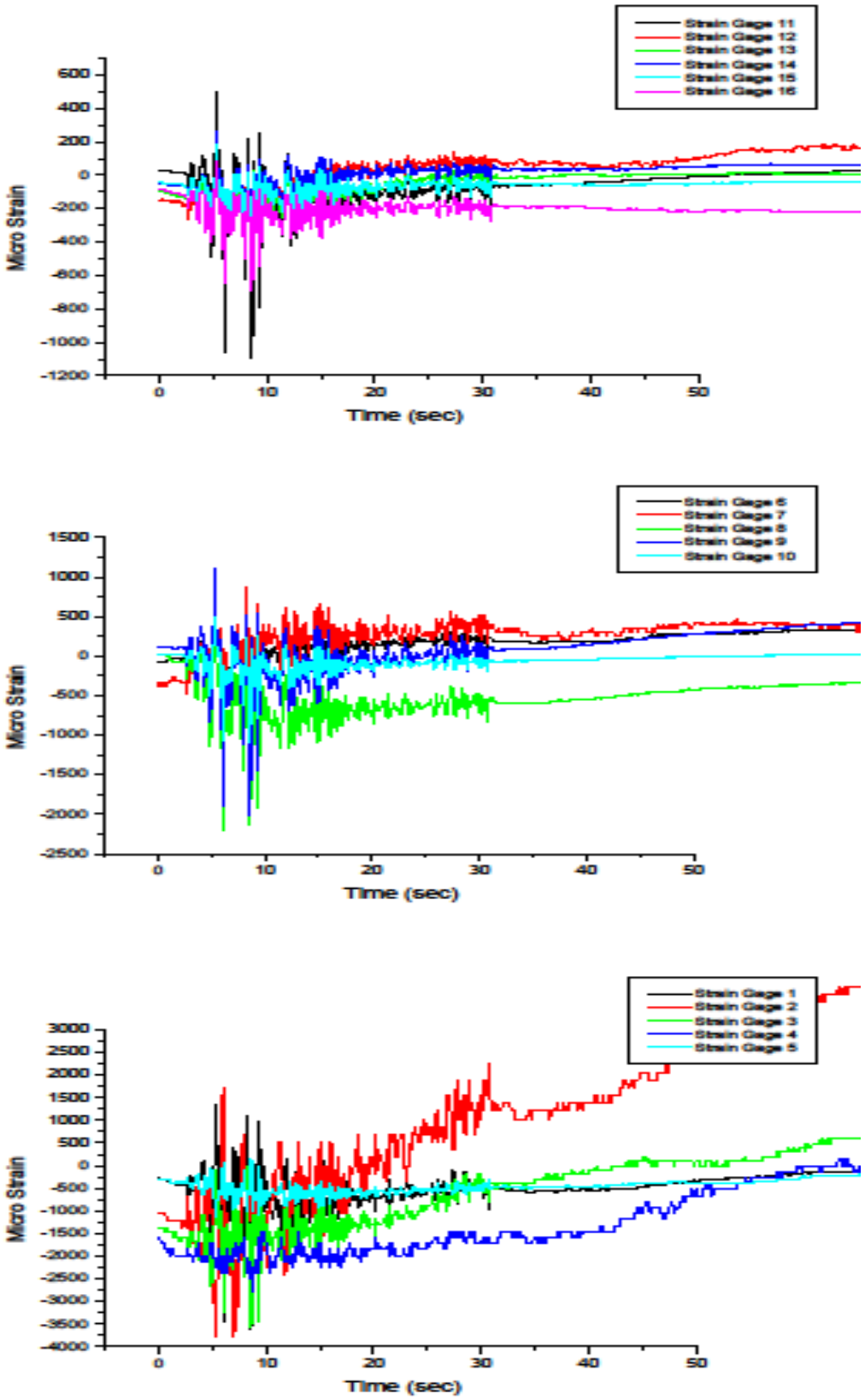


Figure C.23. Strains Measured at Top, Midheight and Bottom Geogrids for Wall 3- Izmit 100%

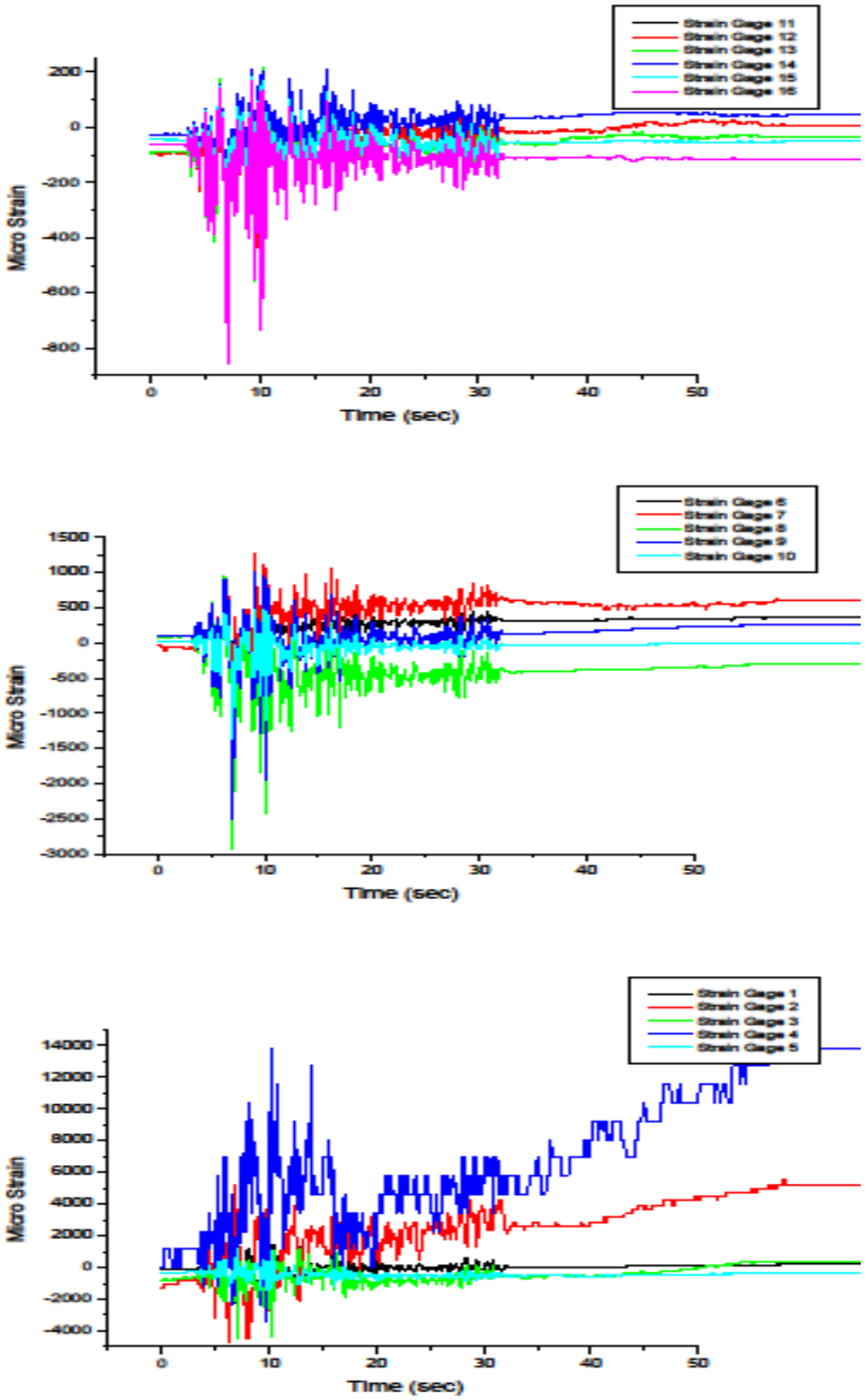


Figure C.24. Strains Measured at Top, Midheight and Bottom Geogrids for Wall 3- Izmit 150%

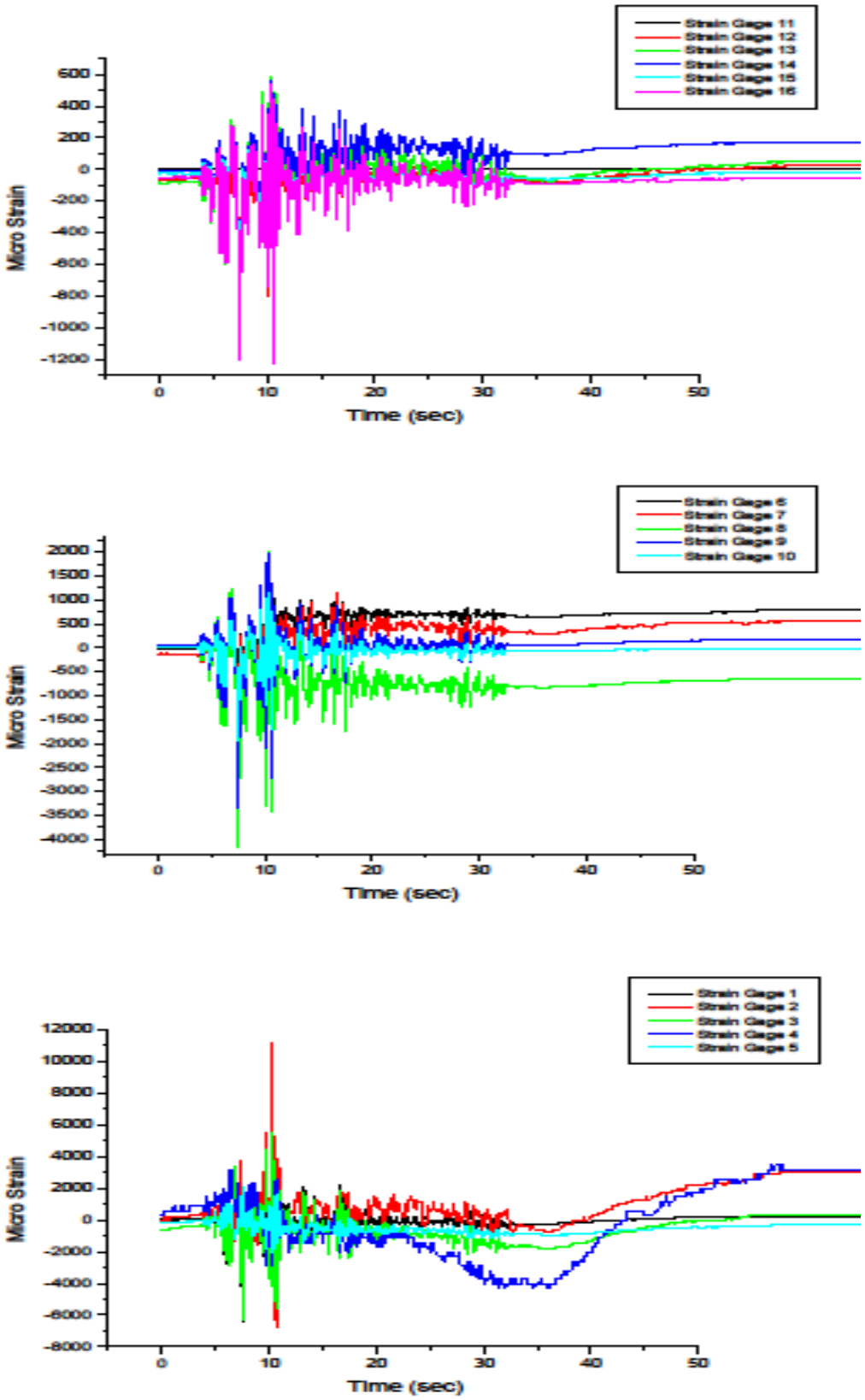


Figure C.25. Strains Measured at Top, Midheight and Bottom Geogrids for Wall 3- Izmit 200%

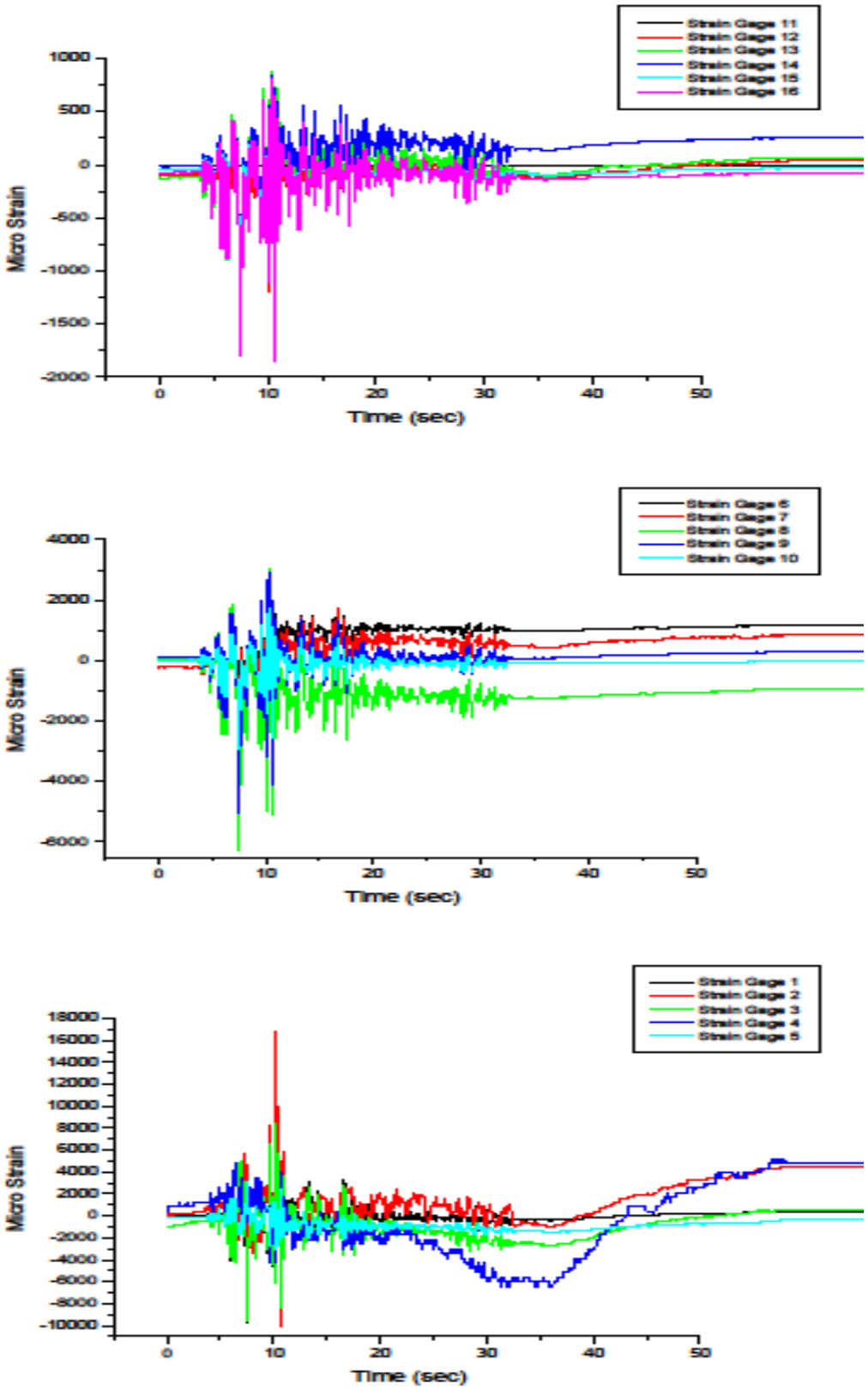


Figure C.26. Strains Measured at Top, Midheight and Bottom Geogrids for Wall 3- Izmit 250%

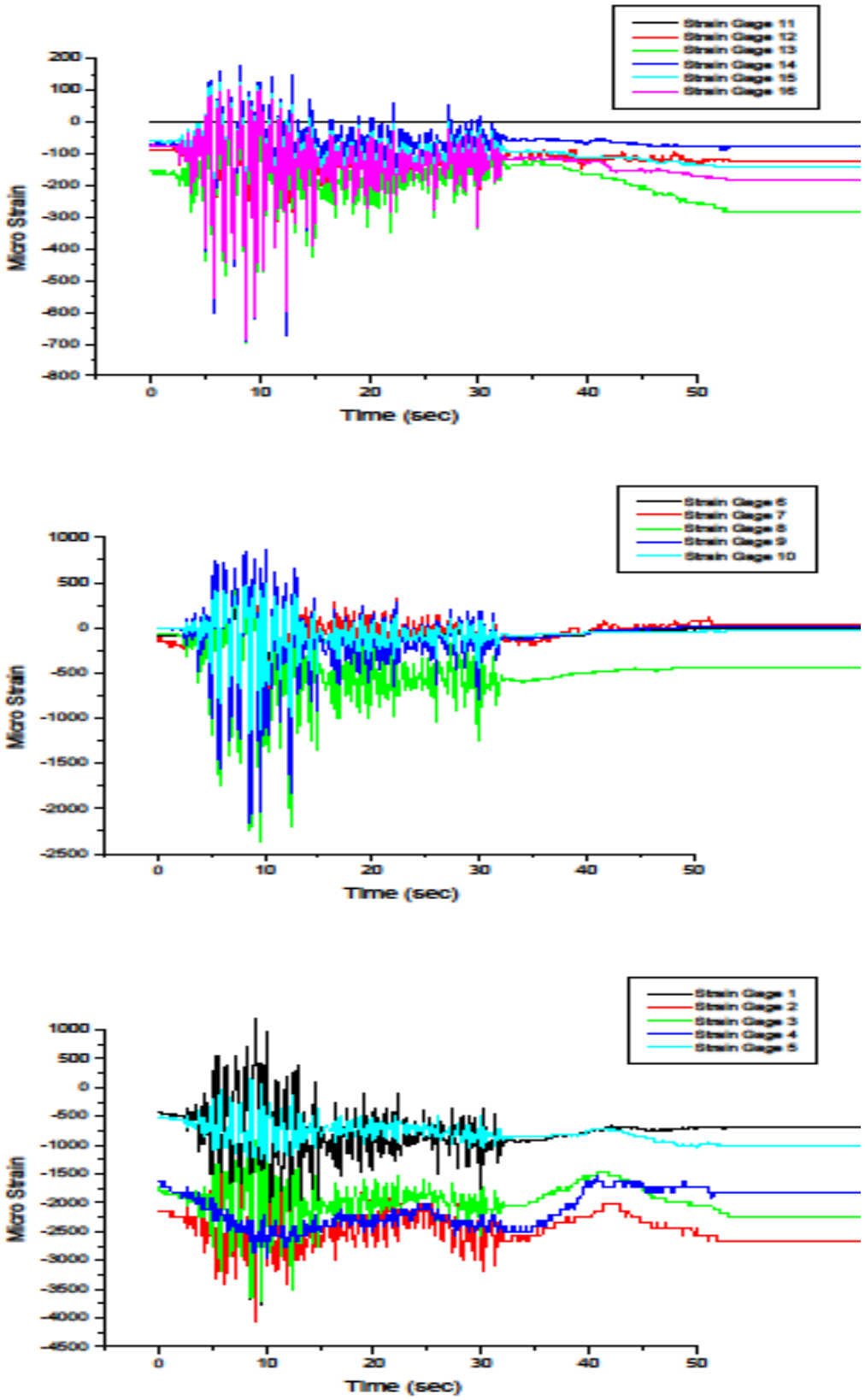


Figure C.27. Strains Measured at Top, Midheight and Bottom Geogrids for Wall 3-Sakarya 100%

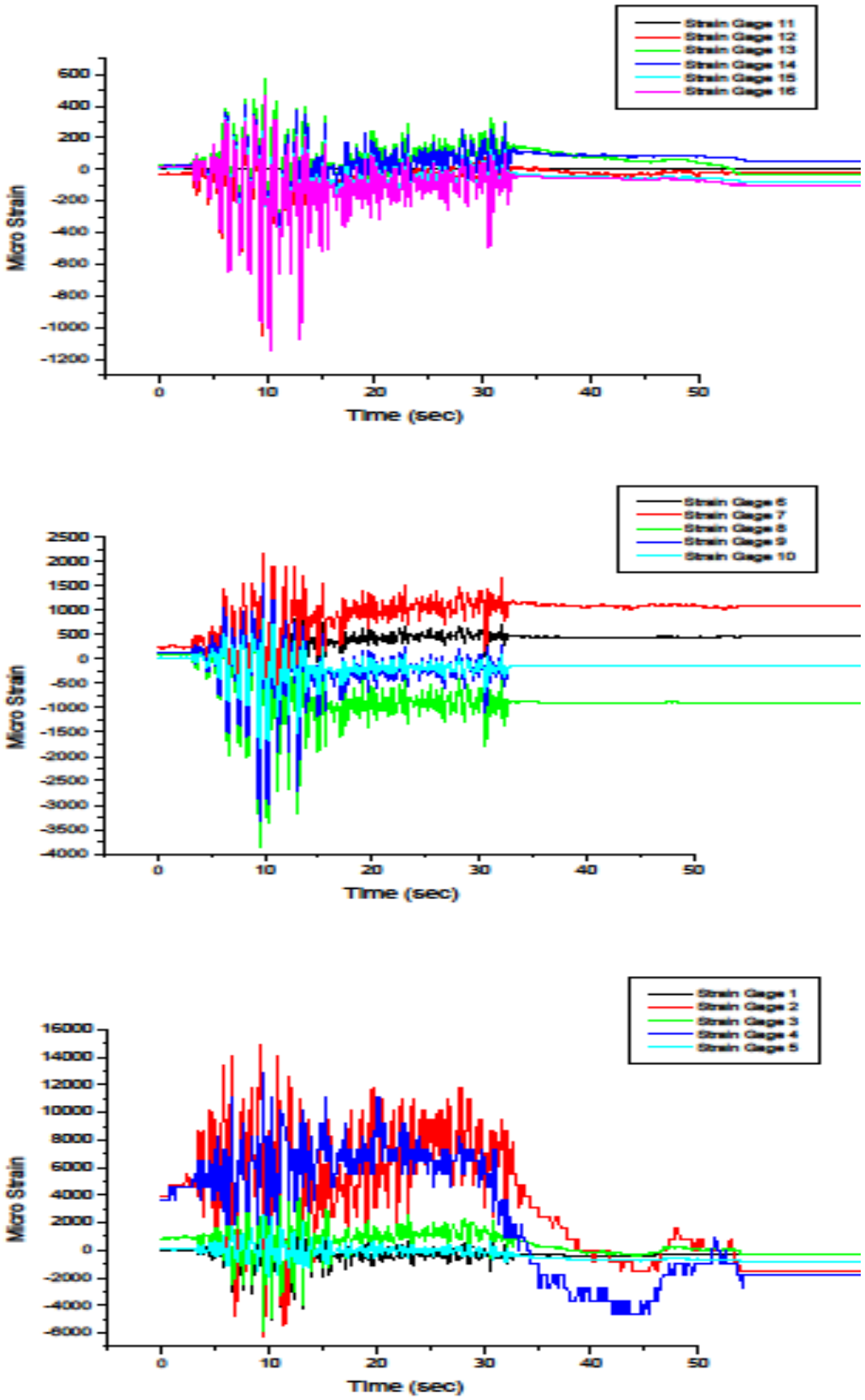


Figure C.28. Strains Measured at Top, Midheight and Bottom Geogrids for Wall 3-Sakarya 150%

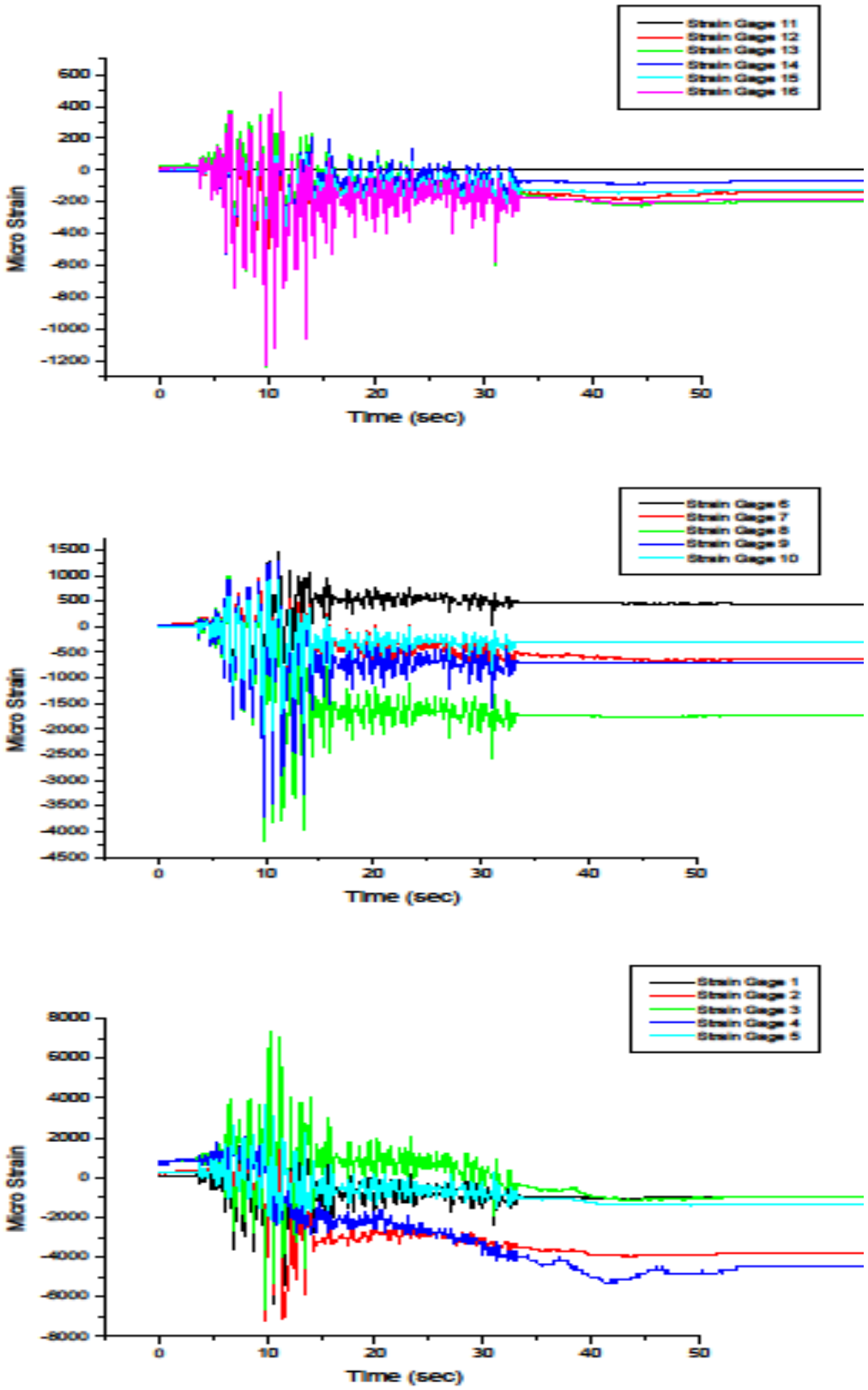


Figure C.29. Strains Measured at Top, Midheight and Bottom Geogrids for Wall 3-Sakarya 200%

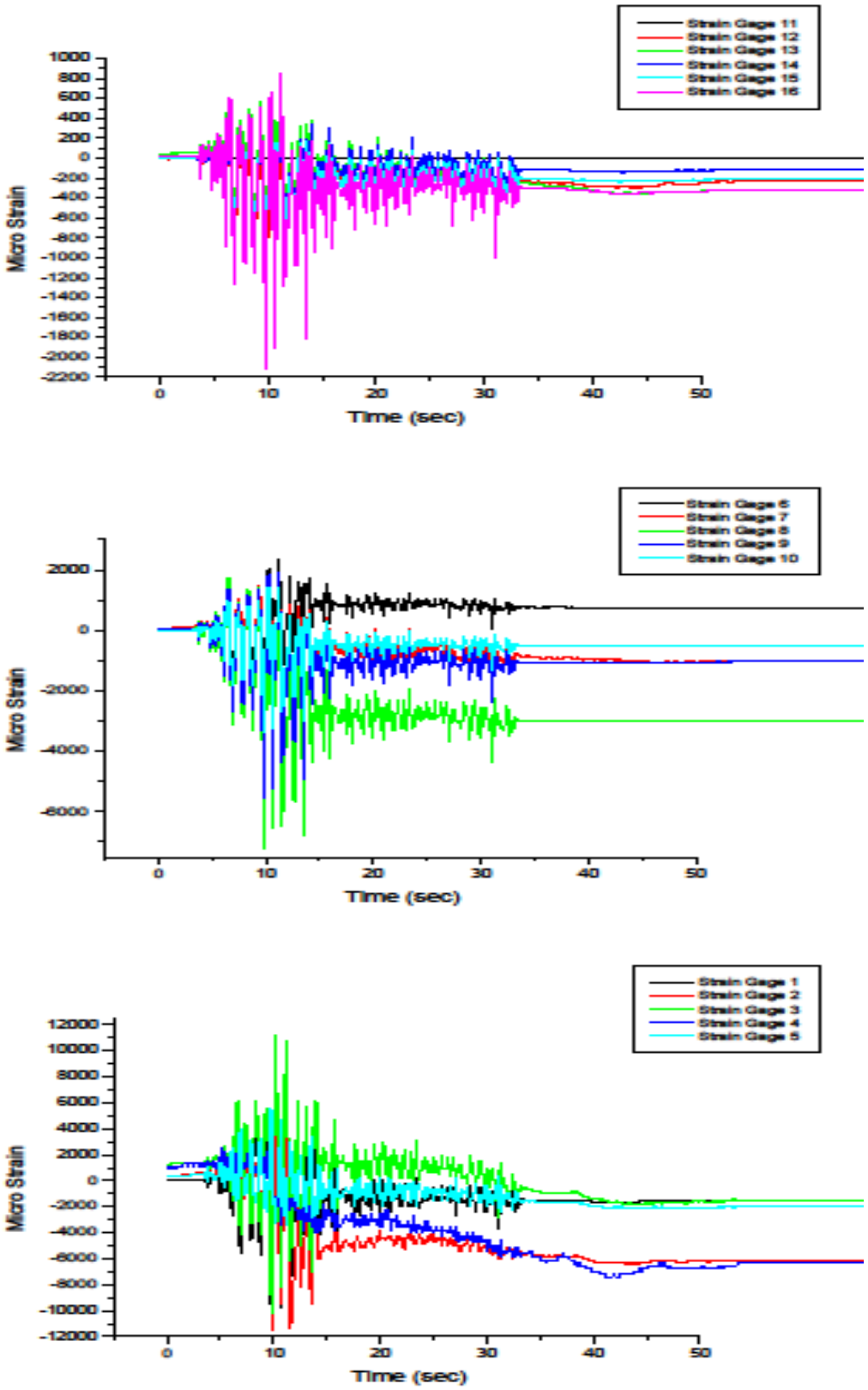


Figure C.30. Strains Measured at Top, Midheight and Bottom Geogrids for Wall 3-Sakarya 250%

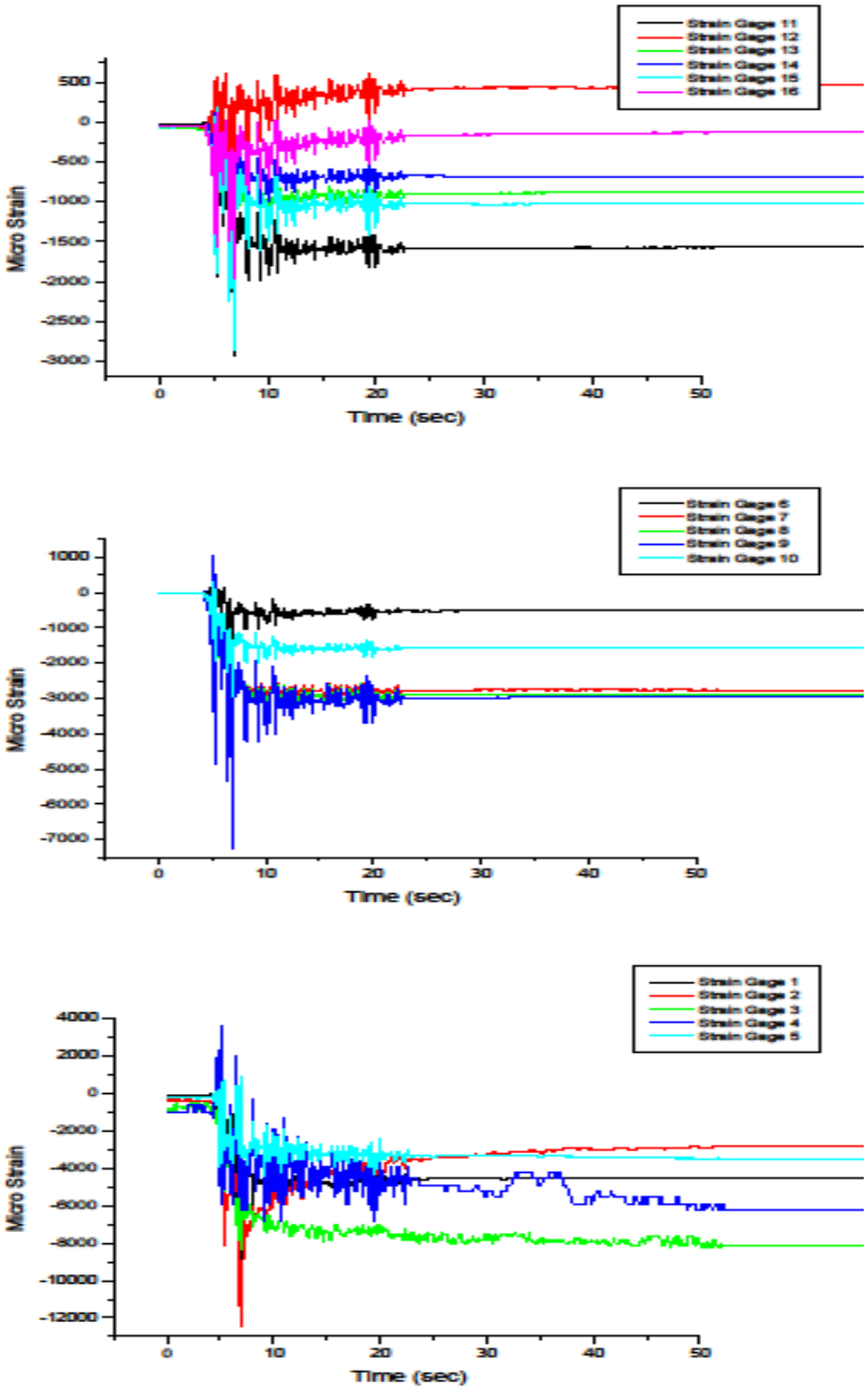


Figure C.31. Strains Measured at Top, Midheight and Bottom Geogrids for Wall 4- El Centro 100%

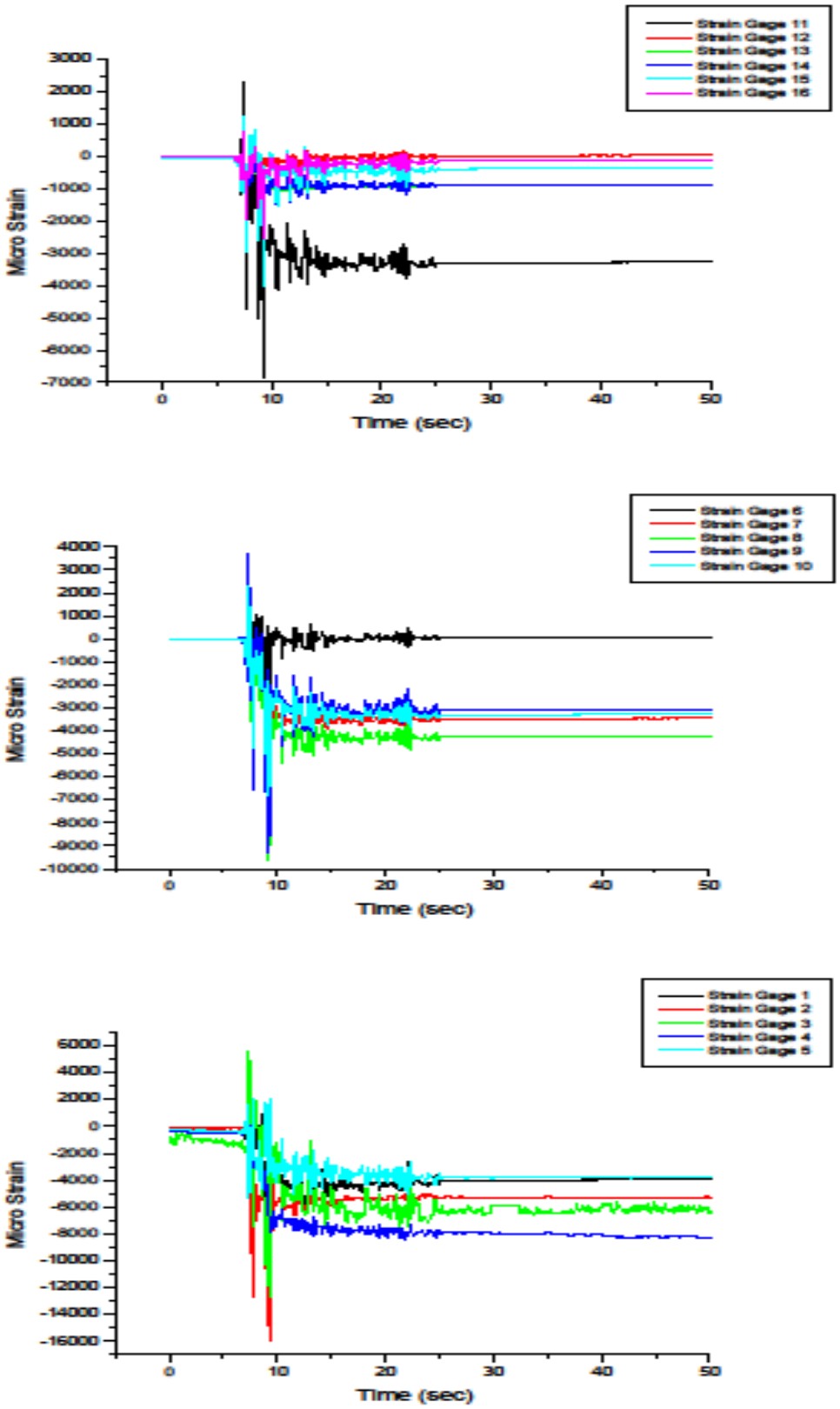


Figure C.32. Strains Measured at Top, Midheight and Bottom Geogrids for Wall 4- El Centro 150%

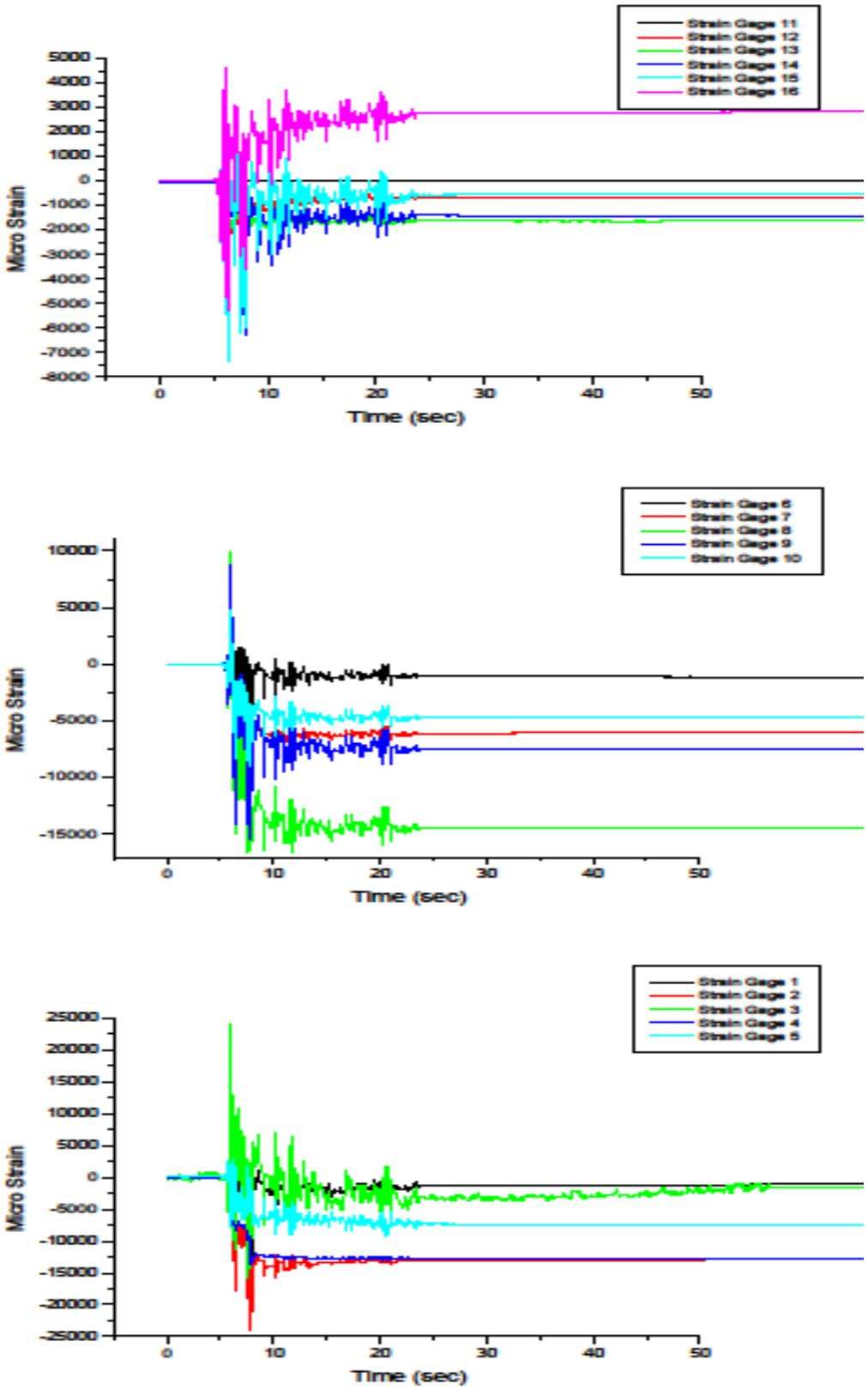


Figure C.33. Strains Measured at Top, Midheight and Bottom Geogrids for Wall 4- El Centro 200%

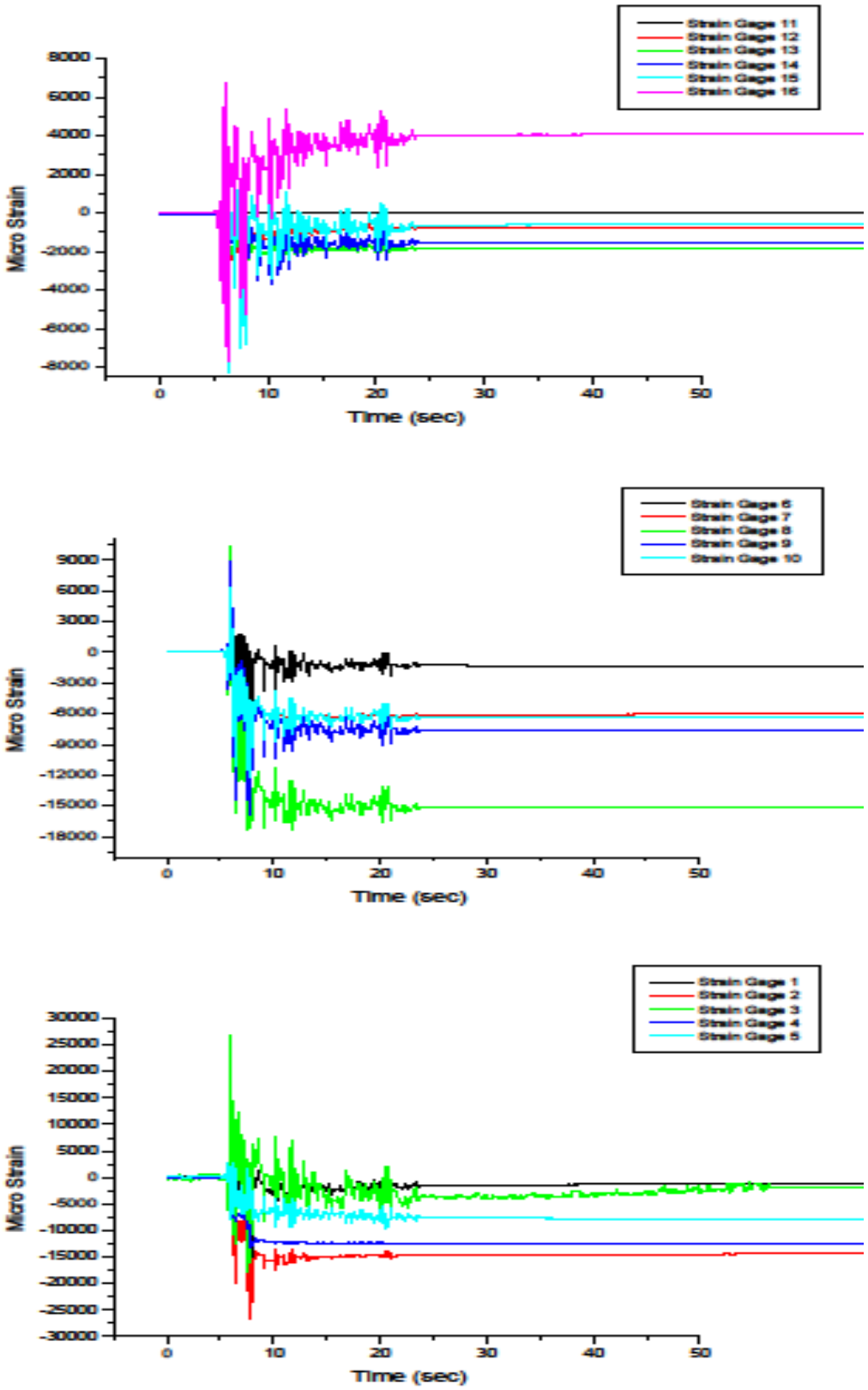


Figure C.34. Strains Measured at Top, Midheight and Bottom Geogrids for Wall 4- El Centro 250%

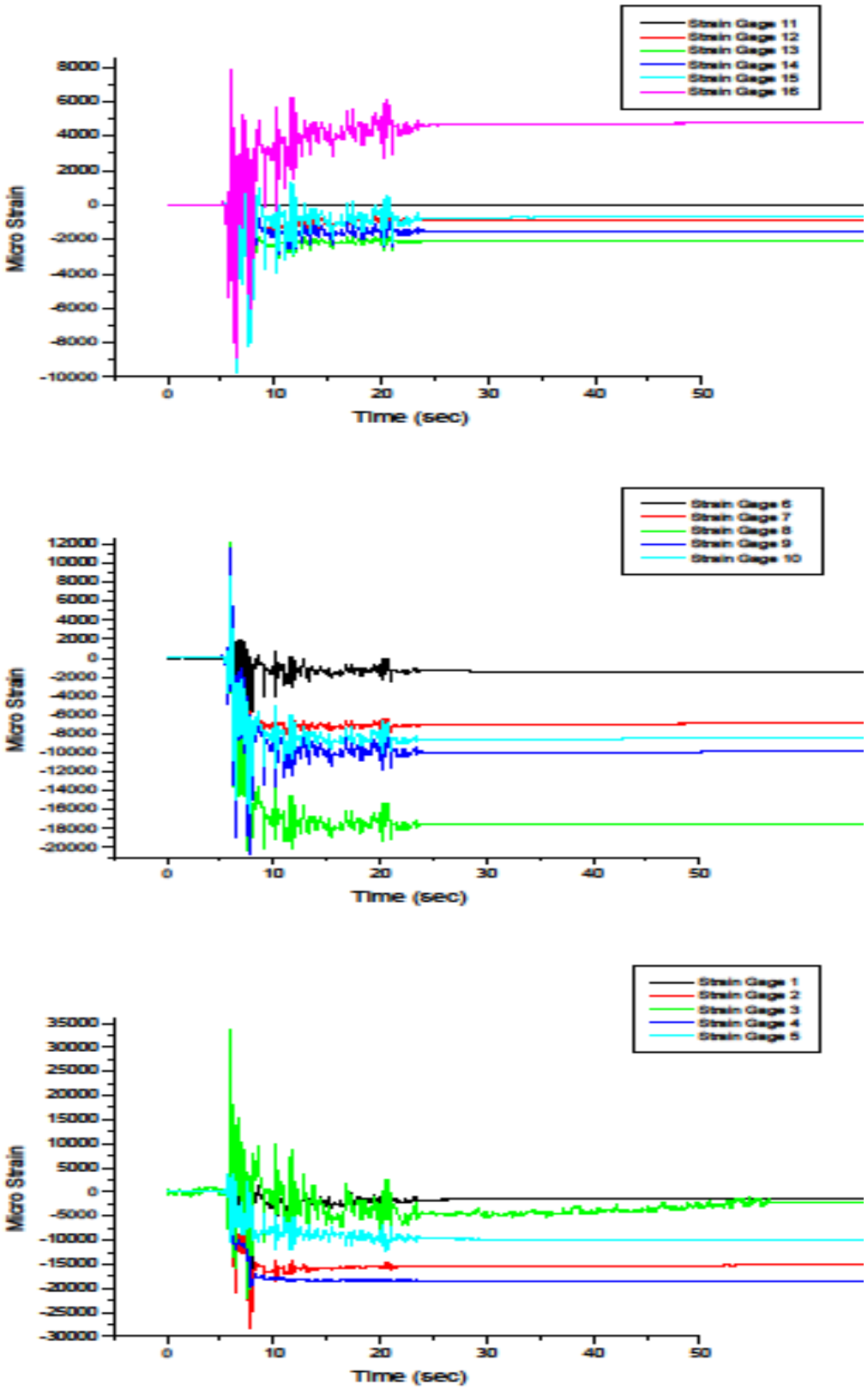


Figure C.35. Strains Measured at Top, Midheight and Bottom Geogrids for Wall 4- El Centro 275%

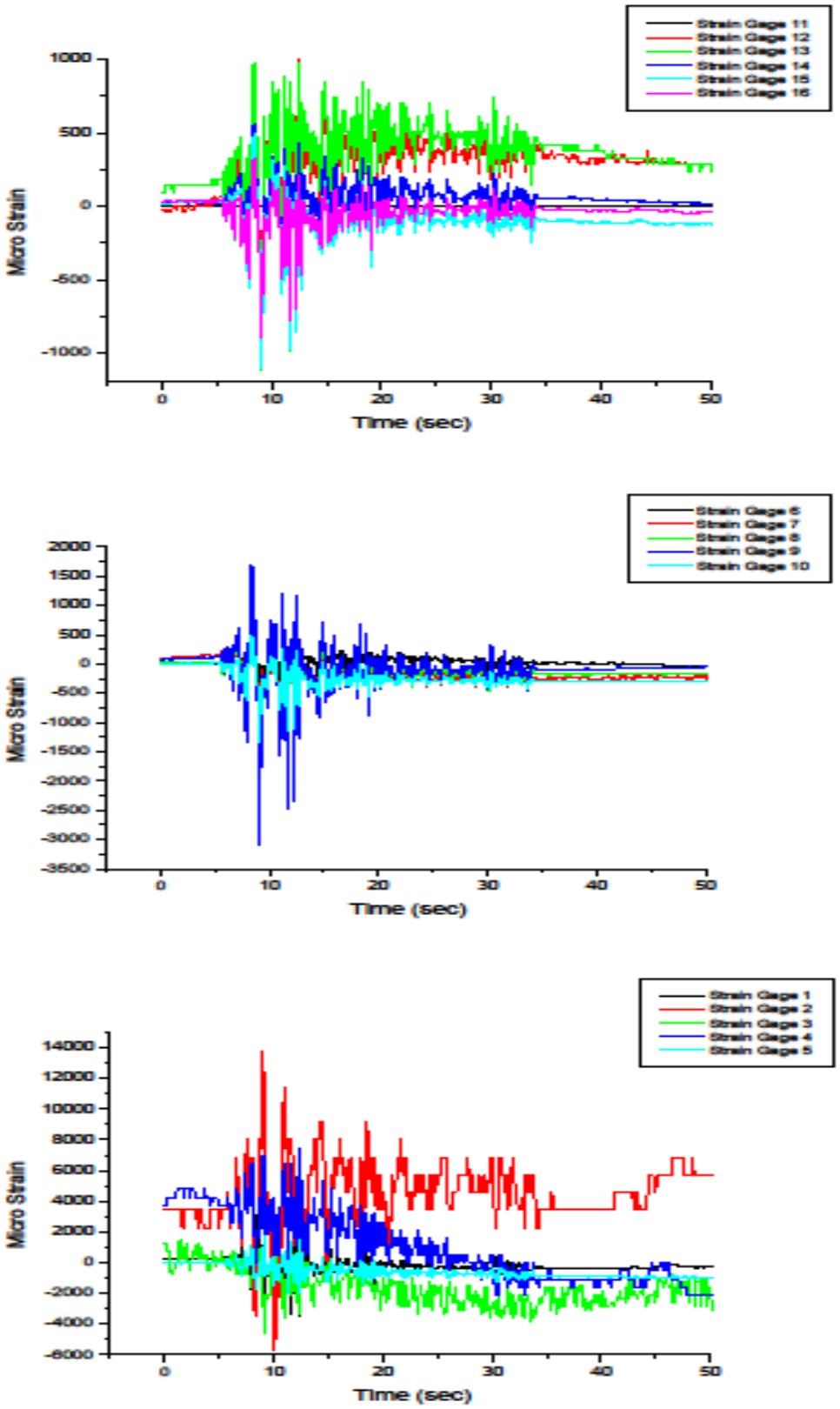


Figure C.36. Strains Measured at Top, Midheight and Bottom Geogrids for Wall 4- Izmit 100%

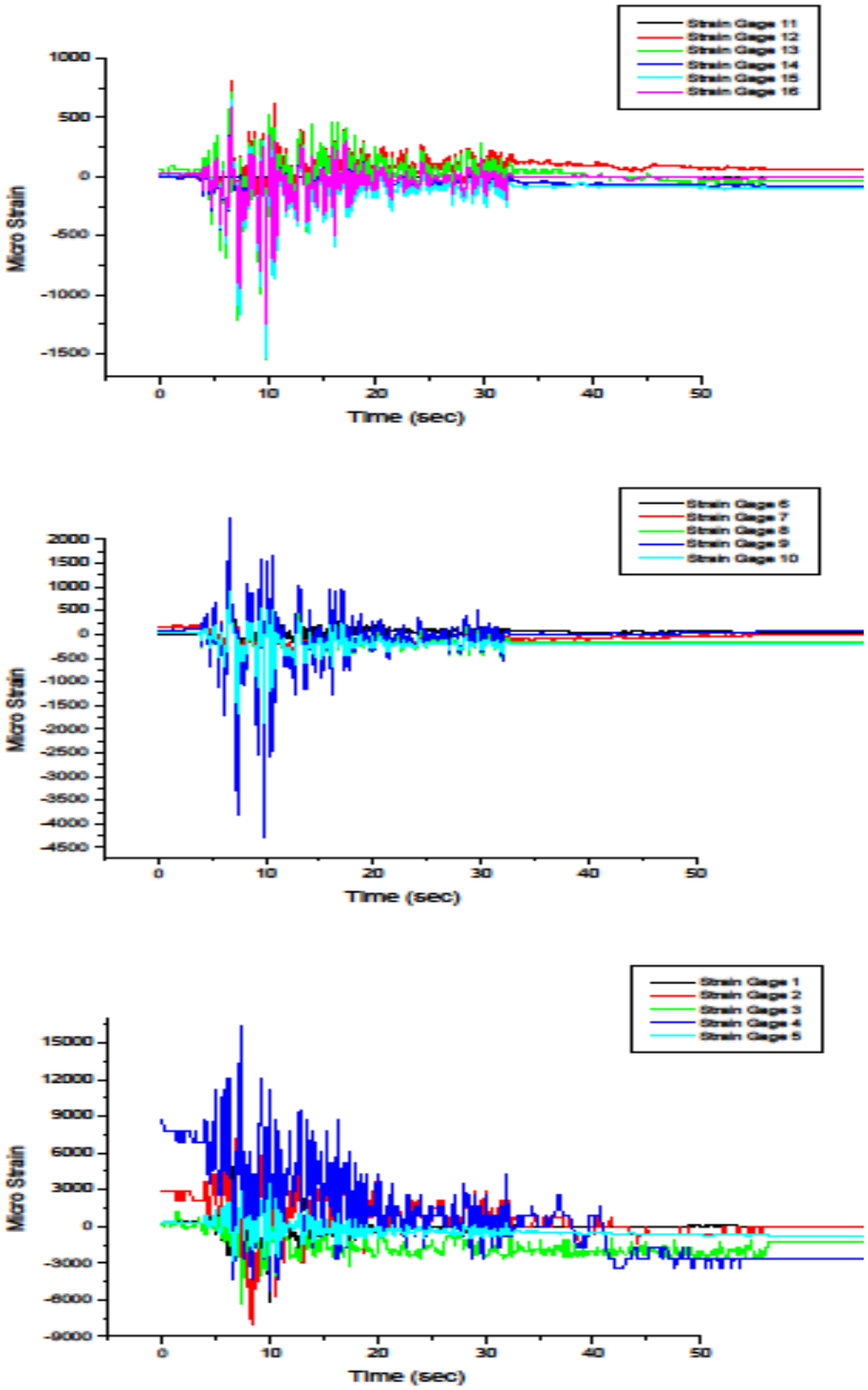


Figure C.37. Strains Measured at Top, Midheight and Bottom Geogrids for Wall 4- Izmit 150%

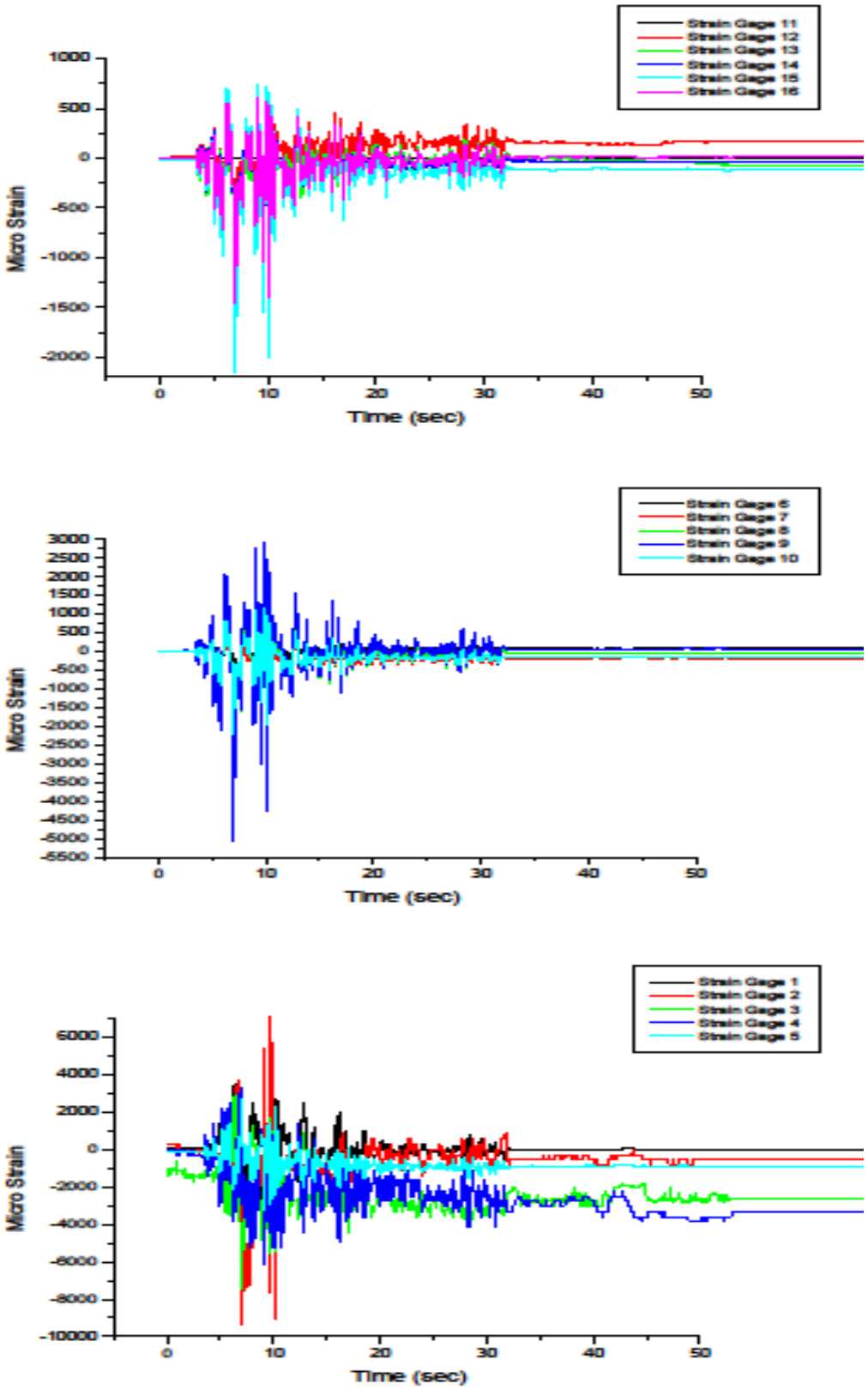


Figure C.38. Strains Measured at Top, Midheight and Bottom Geogrids for Wall 4- Izmit 200%

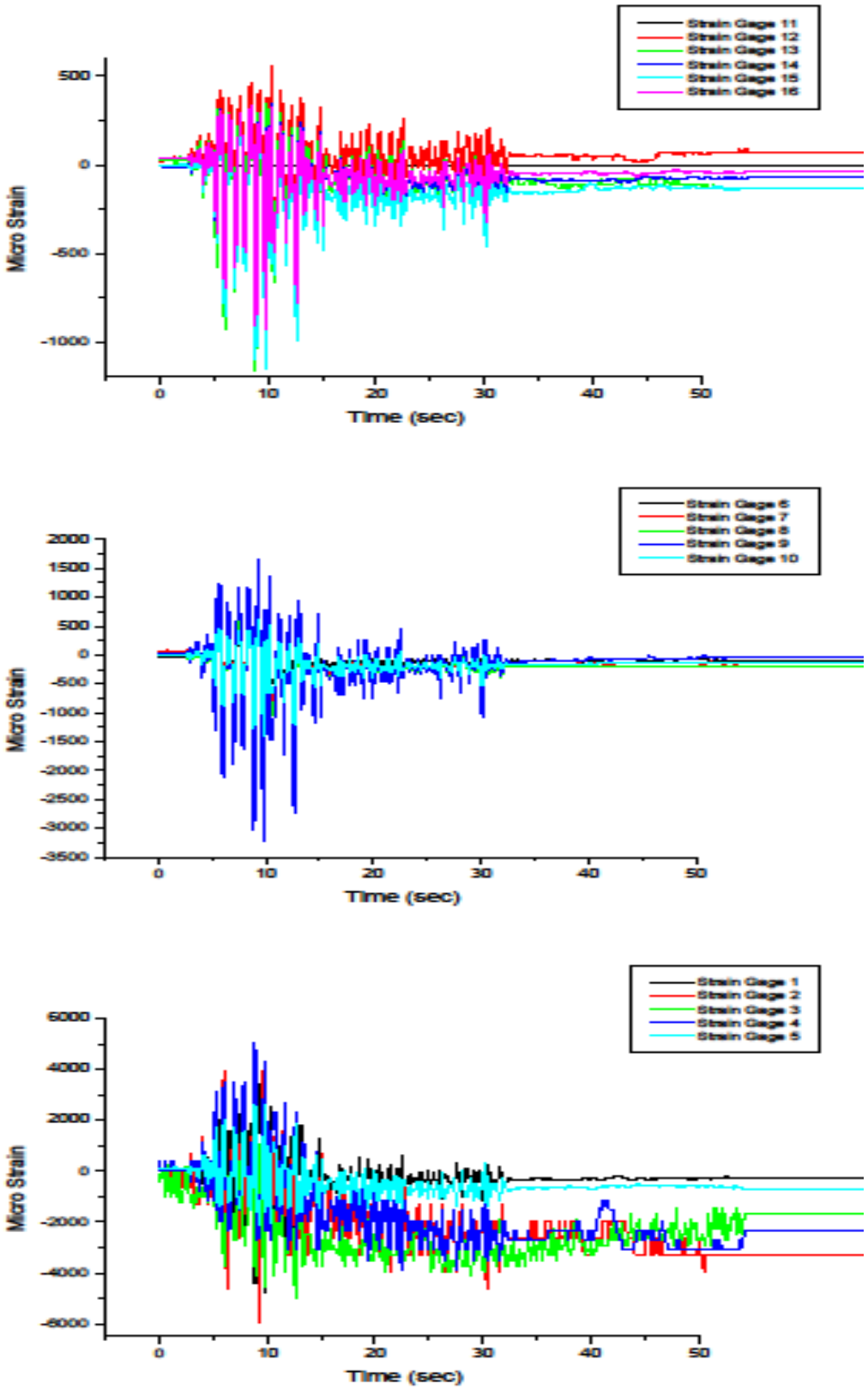


Figure C.39. Strains Measured at Top, Midheight and Bottom Geogrids for Wall 4-Sakarya 100%

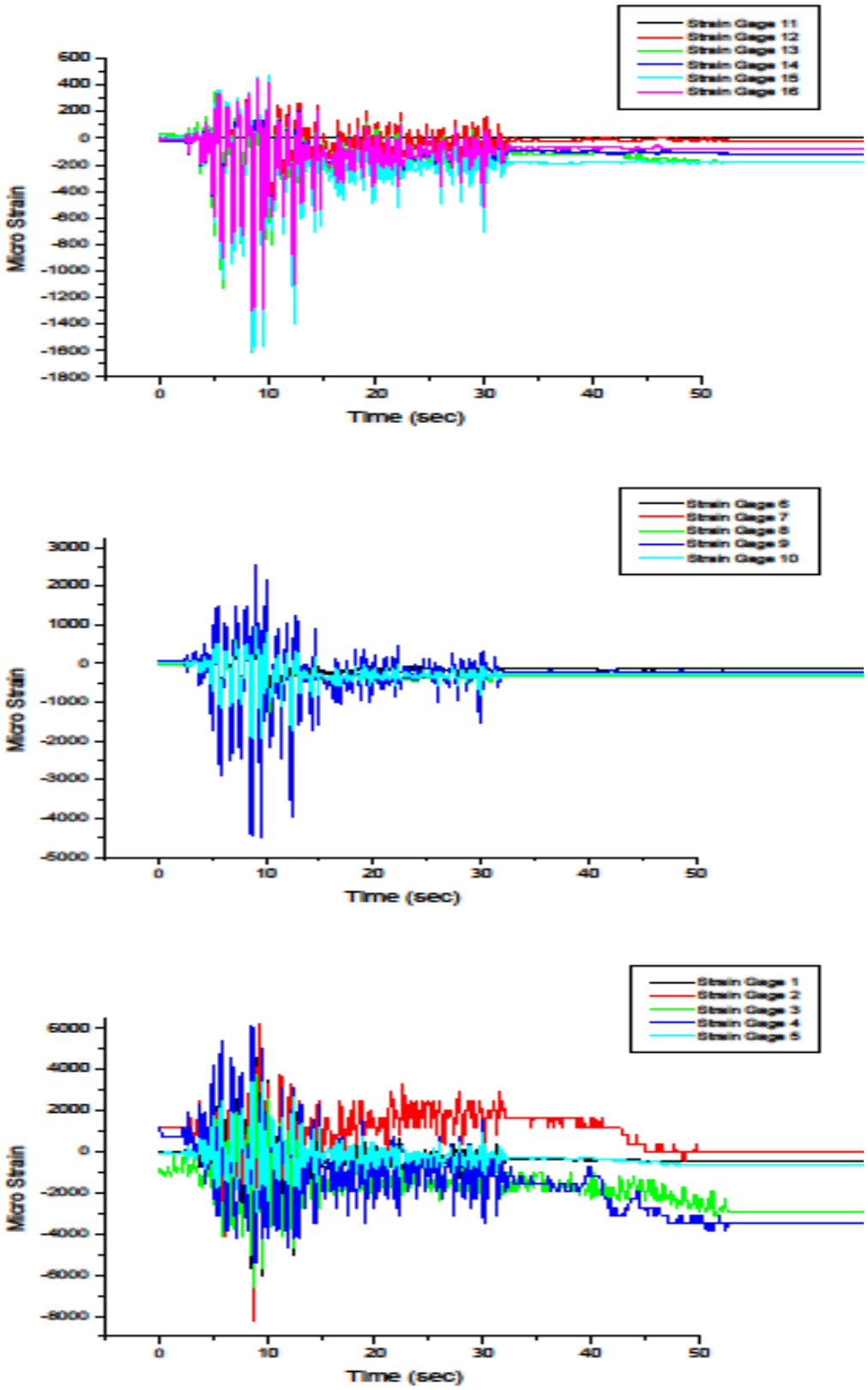


Figure C.40. Strains Measured at Top, Midheight and Bottom Geogrids for Wall 4-Sakarya 150%

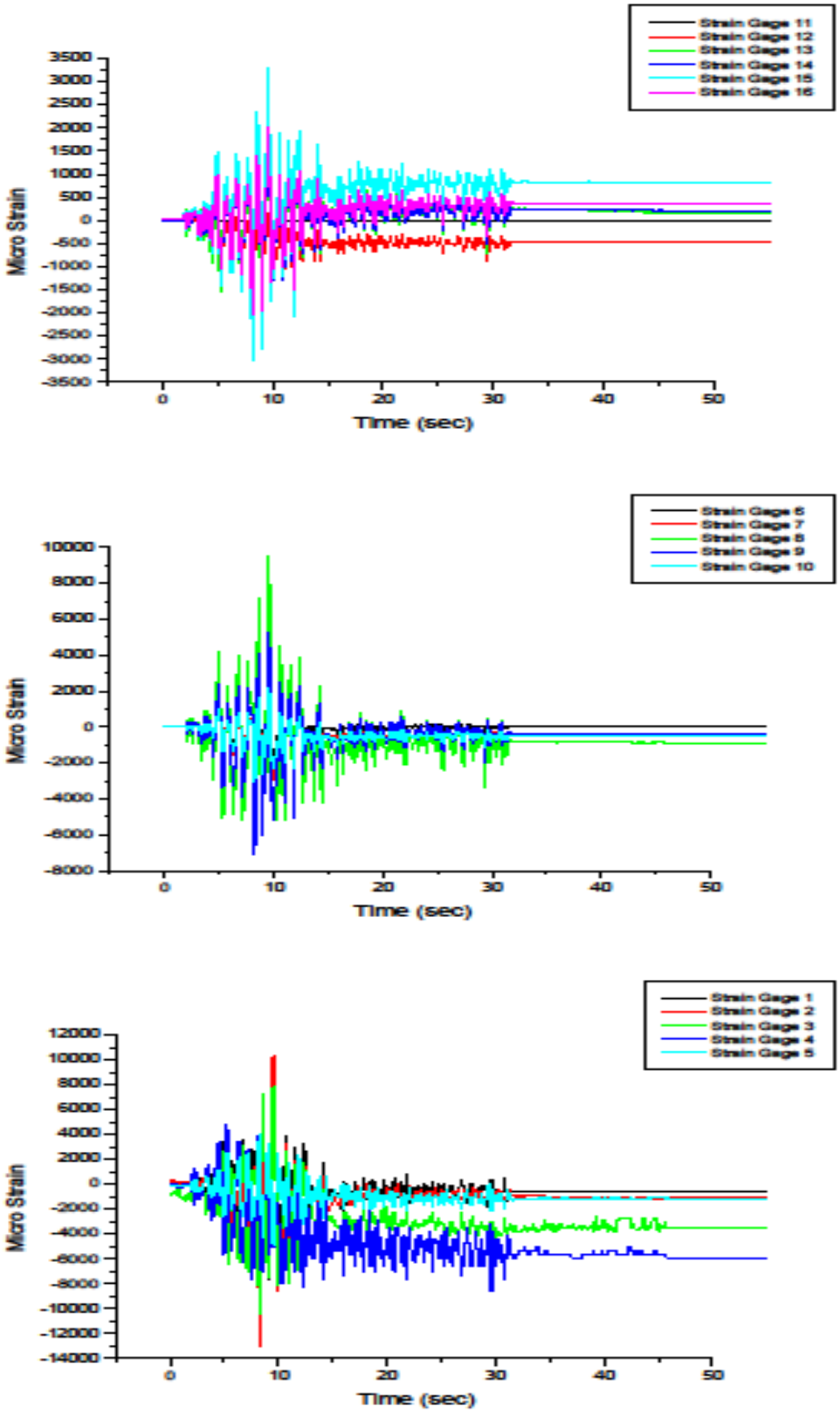


Figure C.41. Strains Measured at Top, Midheight and Bottom Geogrids for Wall 4-Sakarya 200%

APPENDIX D: EXCEL CALCULATION SHEETS FOR DETERMINING THE CRITICAL ACCELERATIONS AND WALL DISPLACEMENTS

This appendix contains Excel calculation sheets for determining the critical accelerations (k_c) and wall displacements.

Table D.1. Calculation of k_c for the external base sliding for Wall 1

1-External Base Sliding

k_c	0.484
Ψ	25.84
K_A	0.22
K_{AE}	0.82
ΔK_{dyn}	0.60

W_w	3.99
W_f	26.60
W_r	30.59

R_S	28.526
P_{IR}	15.62
P_{AEH}	12.55
FS_{sl}	1.00

H	1.90
L	0.90
K_{AH}	0.17
K_{AEH}	0.63
ΔK_{dynH}	0.46

W_f'	28.26

Table D.2. Calculation of k_c for the internal base sliding for Wall 1

2-Internal Sliding

Layer Number	Elevation	Depth	S_{vi}	Z_{vi}	L_i	H
1	0.20	1.70	0.30	1.75	0.90	1.90
2	0.40	1.50	0.20	1.50	0.90	1.90
3	0.60	1.30	0.20	1.30	0.90	1.90
4	0.80	1.10	0.20	1.10	0.90	1.90
5	1.00	0.90	0.20	0.90	0.90	1.90
6	1.20	0.70	0.20	0.70	0.90	1.90
7	1.40	0.50	0.20	0.50	0.90	1.90
8	1.60	0.30	0.20	0.30	0.90	1.90
9	1.80	0.10	0.20	0.10	0.90	1.90

Layer Number	Elevation	Depth	ΔW_w	$\Delta W_f'$	$\Delta P_{IR}(z)$	h_{zi}	$P_{AEH}(z)$	$V_s(z)$	ΔWi	$R_s(z)$	FS_{sl}
1	0.20	1.70	3.57	25.29	15.01	1.70	10.89	8.07	24	26.01	1.00
2	0.40	1.50	3.15	22.31	13.72	1.50	9.91	7.83	21	23.65	1.00
3	0.60	1.30	2.73	19.34	12.31	1.30	8.93	7.58	18	21.30	1.00
4	0.80	1.10	2.31	16.36	10.87	1.10	8.07	7.34	15	18.94	1.00
5	1.00	0.90	1.89	13.39	9.34	0.90	7.26	7.10	13	16.59	1.00
6	1.20	0.70	1.47	10.41	7.70	0.70	6.53	6.85	10	14.24	1.00
7	1.40	0.50	1.05	7.44	5.94	0.50	5.95	6.61	7	11.88	1.00
8	1.60	0.30	0.63	4.46	3.89	0.30	5.64	6.37	4	9.53	1.00
9	1.80	0.10	0.21	1.49	1.32	0.10	2.44	6.12	1	7.18	1.91

Layer Number	k_c	Ψ	K_A	K_{AE}	ΔK_{dyn}	K_{AH}	K_{AEH}	ΔK_{dynH}
1	0.520	27.47	0.25	0.78	0.53	0.19	0.59	0.40
2	0.539	28.32	0.25	0.82	0.57	0.19	0.63	0.44
3	0.558	29.16	0.25	0.87	0.62	0.19	0.67	0.47
4	0.582	30.21	0.25	0.94	0.69	0.19	0.72	0.53
5	0.611	31.43	0.25	1.03	0.78	0.19	0.79	0.60
6	0.648	32.96	0.25	1.18	0.93	0.19	0.90	0.71
7	0.699	34.97	0.25	1.45	1.20	0.19	1.11	0.92
8	0.764	37.39	0.25	2.16	1.91	0.19	1.65	1.46
9	0.780	37.94	0.25	2.68	2.43	0.19	2.05	1.86

Table D.3. Calculation of k_c for the interface shear for Wall 1

3-Interface Shear

Layer Number	Elevation	Depth	ΔW_w	$P_{AEH}(z)$	F_i	Sum of F_i	$S_i(z)$	$V_s(z)$	FS_{st}
1	0.20	1.70	3.57	47.11	5.95	42.14	7.75	8.07	1.0
2	0.40	1.50	3.15	42.93	4.48	37.66	7.71	7.83	1.0
3	0.60	1.30	2.73	38.36	4.87	32.78	7.69	7.58	1.0
4	0.80	1.10	2.31	33.06	5.22	27.56	7.28	7.34	1.0
5	1.00	0.90	1.89	27.52	5.55	22.02	6.95	7.10	1.0
6	1.20	0.70	1.47	21.74	5.86	16.16	6.71	6.85	1.0
7	1.40	0.50	1.05	15.76	6.15	10.01	6.55	6.61	1.0
8	1.60	0.30	0.63	9.39	6.31	3.71	6.16	6.37	1.0
9	1.80	0.10	0.21	1.75	3.71	0.00	1.88	6.12	2.0

Layer Number	k_c	Ψ	K_A	K_{AE}	ΔK_{dyn}	K_{AH}	K_{AEH}	ΔK_{dynH}
1	0.776	37.81	0.25	1.79	1.54	0.22	1.60	1.38
2	0.775	37.78	0.25	1.78	1.53	0.22	1.60	1.37
3	0.774	37.74	0.25	1.77	1.52	0.22	1.59	1.36
4	0.771	37.63	0.25	1.75	1.50	0.22	1.56	1.34
5	0.768	37.52	0.25	1.72	1.47	0.22	1.54	1.32
6	0.765	37.42	0.25	1.70	1.45	0.22	1.52	1.30
7	0.762	37.31	0.25	1.67	1.42	0.22	1.50	1.27
8	0.755	37.05	0.25	1.62	1.37	0.22	1.45	1.23
9	0.620	31.80	0.25	0.99	0.74	0.22	0.89	0.66

Layer Number	Elevation	Depth	S_{vi}	Z_{vi}	ΔW_{wi}	F_{stai}	F_{dyni}
1	0.20	1.70	0.30	1.75	0.63	2.06	3.40
2	0.40	1.50	0.20	1.50	0.42	1.18	2.98
3	0.60	1.30	0.20	1.30	0.42	1.02	3.53
4	0.80	1.10	0.20	1.10	0.42	0.86	4.03
5	1.00	0.90	0.20	0.90	0.42	0.71	4.52
6	1.20	0.70	0.20	0.70	0.42	0.55	4.99
7	1.40	0.50	0.20	0.50	0.42	0.39	5.44
8	1.60	0.30	0.20	0.30	0.42	0.24	5.75
9	1.80	0.10	0.20	0.15	0.42	0.12	3.33

Table D.4. Calculation of Displacements for Wall 1-El Centro 100%

External Base Sliding

	k_c	k_m	k_c/k_m	v_m (cm/sn)	d (Newmark) (cm)	d (Bathurst and Cai) (cm)
	0.484	0.39	1.24	24.54	0.00	0.01

Internal Sliding

Layer	k_c	k_m	k_c/k_m	v_m (cm/sn)	d (Newmark) (cm)	d (Bathurst and Cai) (cm)
1	0.520	0.40	1.30	25.17	0.00	0.00
2	0.539	0.41	1.31	25.80	0.00	0.00
3	0.558	0.41	1.36	25.80	0.00	0.00
4	0.582	0.41	1.42	25.80	0.00	0.00
5	0.611	0.43	1.42	27.06	0.00	0.00
6	0.648	0.43	1.51	27.06	0.00	0.00
7	0.699	0.43	1.63	27.06	0.00	0.00
8	0.764	0.47	1.63	29.57	0.00	0.00
9	0.780	0.47	1.66	29.57	0.00	0.00

Interface Shear

Layer	k_c	k_m	k_c/k_m	v_m (cm/sn)	d (Newmark) (cm)	d (Bathurst and Cai) (cm)
1	0.776	0.40	1.94	25.17	0.00	0.00
2	0.775	0.41	1.89	25.80	0.00	0.00
3	0.774	0.41	1.89	25.80	0.00	0.00
4	0.771	0.41	1.88	25.80	0.00	0.00
5	0.768	0.43	1.79	27.06	0.00	0.00
6	0.765	0.43	1.78	27.06	0.00	0.00
7	0.762	0.43	1.77	27.06	0.00	0.00
8	0.755	0.47	1.61	29.57	0.00	0.00
9	0.620	0.47	1.32	29.57	0.00	0.00

Table D.5. Calculation of Displacements for Wall 1-El Centro 150%

External Base Sliding

	k_c	k_m	k_c/k_m	v_m (cm/sn)	d (Newmark) (cm)	d (Bathurst and Cai) (cm)
	0.484	0.55	0.88	37.54	0.20	0.22

Internal Sliding

Layer	k_c	k_m	k_c/k_m	v_m (cm/sn)	d (Newmark) (cm)	d (Bathurst and Cai) (cm)
1	0.520	0.56	0.93	38.22	0.11	0.16
2	0.539	0.59	0.91	40.27	0.15	0.18
3	0.558	0.59	0.95	40.27	0.08	0.15
4	0.582	0.59	0.99	40.27	0.02	0.11
5	0.611	0.65	0.94	44.37	0.10	0.17
6	0.648	0.66	0.98	45.05	0.03	0.12
7	0.699	0.72	0.97	49.14	0.05	0.15
8	0.764	0.72	1.06	49.14	0.00	0.00
9	0.780	0.67	1.16	45.73	0.00	0.00

Interface Shear

Layer	k_c	k_m	k_c/k_m	v_m (cm/sn)	d (Newmark) (cm)	d (Bathurst and Cai) (cm)
1	0.776	0.56	1.39	38.22	0.00	0.00
2	0.775	0.59	1.31	40.27	0.00	0.00
3	0.774	0.59	1.31	40.27	0.00	0.00
4	0.771	0.59	1.31	40.27	0.00	0.00
5	0.768	0.65	1.18	44.37	0.00	0.00
6	0.765	0.66	1.16	45.05	0.00	0.00
7	0.762	0.67	1.14	45.73	0.00	0.00
8	0.755	0.72	1.05	49.14	0.00	0.00
9	0.620	0.67	0.93	45.73	0.14	0.19

Table D.6. Calculation of Displacements for Wall 1-El Centro 200%

External Base Sliding

	k_c	k_m	k_c/k_m	v_m (cm/sn)	d (Newmark) (cm)	d (Bathurst and Cai) (cm)
	0.484	0.74	0.65	46.97	1.23	1.36

Internal Sliding

Layer	k_c	k_m	k_c/k_m	v_m (cm/sn)	d (Newmark) (cm)	d (Bathurst and Cai) (cm)
1	0.520	0.78	0.67	49.51	1.20	1.31
2	0.539	0.75	0.72	47.60	0.84	0.85
3	0.558	0.76	0.73	48.24	0.77	0.77
4	0.582	0.77	0.76	48.87	0.67	0.66
5	0.611	0.86	0.71	54.59	1.01	1.04
6	0.648	0.87	0.75	55.22	0.82	0.81
7	0.699	0.88	0.79	55.86	0.59	0.57
8	0.764	0.96	0.80	60.93	0.63	0.61
9	0.780	0.88	0.89	55.86	0.26	0.29

Interface Shear

Layer	k_c	k_m	k_c/k_m	v_m (cm/sn)	d (Newmark) (cm)	d (Bathurst and Cai) (cm)
1	0.776	0.78	0.99	49.51	0.01	0.12
2	0.775	0.75	1.03	47.60	0.00	0.00
3	0.774	0.76	1.02	48.24	0.00	0.00
4	0.771	0.77	1.00	48.87	0.00	0.00
5	0.768	0.86	0.89	54.59	0.24	0.27
6	0.765	0.87	0.88	55.22	0.28	0.30
7	0.762	0.88	0.87	55.86	0.32	0.34
8	0.755	0.96	0.79	60.93	0.68	0.66
9	0.620	0.88	0.70	55.86	1.08	1.11

Table D.7. Calculation of k_c for the external base sliding for Wall 2

1-External Base Sliding

k_c	0.452
Ψ	24.32
K_A	0.20
K_{AE}	0.62
ΔK_{dyn}	0.42

H	1.90
L	0.90
K_{AH}	0.17
K_{AEH}	0.51
ΔK_{dynH}	0.35

W_w	3.99
W_i	26.60
W_r	30.59

W_i'	28.26

R_S	25.668
P_{IR}	14.57
P_{AEH}	10.70
FS_{sl}	1.00

Table D.8. Calculation of k_c for the internal base sliding for Wall 2

2-Internal Sliding

Layer Number	Elevation	Depth	S_v	Z_{ai}	L_i	H
1	0.20	1.70	0.30	1.75	0.90	1.90
2	0.40	1.50	0.20	1.50	0.90	1.90
3	0.60	1.30	0.20	1.30	0.90	1.90
4	0.80	1.10	0.20	1.10	0.90	1.90
5	1.00	0.90	0.20	0.90	0.90	1.90
6	1.20	0.70	0.20	0.70	0.90	1.90
7	1.40	0.50	0.20	0.50	0.90	1.90
8	1.60	0.30	0.20	0.30	0.90	1.90
9	1.80	0.10	0.20	0.10	0.90	1.90

Layer Number	Elevation	Depth	ΔW_w	$\Delta W_i'$	$\Delta P_{IR}(z)$	h_{ai}	$P_{AEH}(z)$	$V_a(z)$	ΔWi	$R_S(z)$	FS_{sli}
1	0.20	1.70	3.57	25.29	15.24	1.70	10.76	8.07	24	26.01	1.00
2	0.40	1.50	3.15	22.31	13.90	1.50	9.75	7.83	21	23.65	1.00
3	0.60	1.30	2.73	19.34	12.49	1.30	8.81	7.58	18	21.30	1.00
4	0.80	1.10	2.31	16.36	11.02	1.10	7.93	7.34	15	18.94	1.00
5	1.00	0.90	1.89	13.39	9.47	0.90	7.12	7.10	13	16.59	1.00
6	1.20	0.70	1.47	10.41	7.83	0.70	6.40	6.85	10	14.24	1.00
7	1.40	0.50	1.05	7.44	6.07	0.50	5.82	6.61	7	11.88	1.00
8	1.60	0.30	0.63	4.46	4.05	0.30	5.48	6.37	4	9.53	1.00
9	1.80	0.10	0.21	1.49	1.42	0.10	3.26	6.12	1	7.18	1.53

Layer Number	k_c	Ψ	K_A	K_{AE}	ΔK_{dyn}	K_{AH}	K_{AEH}	ΔK_{dynH}
1	0.528	27.84	0.23	0.71	0.48	0.19	0.59	0.40
2	0.546	28.63	0.23	0.75	0.52	0.19	0.62	0.43
3	0.566	29.51	0.23	0.79	0.56	0.19	0.66	0.47
4	0.590	30.54	0.23	0.85	0.62	0.19	0.71	0.52
5	0.620	31.79	0.23	0.94	0.71	0.19	0.78	0.59
6	0.659	33.39	0.23	1.07	0.84	0.19	0.89	0.70
7	0.715	35.56	0.23	1.32	1.09	0.19	1.09	0.90
8	0.796	38.51	0.23	1.94	1.71	0.19	1.61	1.42
9	0.839	40.00	0.23	3.23	3.00	0.19	2.68	2.49

Table D.9. Calculation of k_c for the interface shear for Wall 2

3-Interface Shear

Layer Number	Elevation	Depth	ΔW_w	$P_{AEH}(z)$	F_i	Sum of F_i	$S_i(z)$	$V_w(z)$	FS_w
1	0.20	1.70	3.57	55.63	6.50	51.06	7.22	8.07	1
2	0.40	1.50	3.15	51.19	5.03	46.03	7.50	7.83	1
3	0.60	1.30	2.73	46.18	5.60	40.43	7.78	7.58	1
4	0.80	1.10	2.31	39.11	5.96	34.47	6.37	7.34	1
5	1.00	0.90	1.89	33.20	6.49	27.98	6.64	7.10	1
6	1.20	0.70	1.47	26.50	6.97	21.01	6.60	6.85	1
7	1.40	0.50	1.05	19.40	7.43	13.58	6.61	6.61	1
8	1.60	0.30	0.63	11.72	7.75	5.83	6.37	6.37	1
9	1.80	0.10	0.21	2.85	5.83	0.00	2.99	6.12	2

Layer Number	k_c	Ψ	K_A	K_{AE}	ΔK_{dyn}	K_{AH}	K_{AEH}	ΔK_{dynH}
1	0.743	36.61	0.23	2.10	1.87	0.21	1.88	1.68
2	0.743	36.61	0.23	2.10	1.87	0.21	1.88	1.68
3	0.743	36.61	0.23	2.10	1.87	0.21	1.88	1.68
4	0.750	36.87	0.23	2.03	1.80	0.21	1.82	1.61
5	0.750	36.87	0.23	2.03	1.80	0.21	1.82	1.61
6	0.752	36.94	0.23	2.01	1.78	0.21	1.80	1.60
7	0.754	37.02	0.23	1.99	1.76	0.21	1.79	1.58
8	0.761	37.26	0.23	1.95	1.72	0.21	1.75	1.54
9	0.660	33.42	0.23	1.44	1.21	0.21	1.29	1.09

Layer Number	Elevation	Depth	S_{vi}	Z_{vi}	ΔWwi	F_{stat}	F_{dyni}
1	0.20	1.70	0.30	1.75	0.63	1.89	4.14
2	0.40	1.50	0.20	1.50	0.42	1.08	3.64
3	0.60	1.30	0.20	1.30	0.42	0.94	4.35
4	0.80	1.10	0.20	1.10	0.42	0.79	4.85
5	1.00	0.90	0.20	0.90	0.42	0.65	5.53
6	1.20	0.70	0.20	0.70	0.42	0.50	6.15
7	1.40	0.50	0.20	0.50	0.42	0.36	6.75
8	1.60	0.30	0.20	0.30	0.42	0.22	7.22
9	1.80	0.10	0.20	0.15	0.42	0.11	5.44

Table D.10. Calculation of Displacements for Wall 2-El Centro 100%

External Base Sliding

	k_c	k_m	k_c/k_m	v_m (cm/sn)	d (Newmark) (cm)	d (Bathurst and Cai) (cm)
	0.452	0.42	1.08	24.98	0.00	0.00

Internal Sliding

Layer	k_c	k_m	k_c/k_m	v_m (cm/sn)	d (Newmark) (cm)	d (Bathurst and Cai) (cm)
1	0.528	0.42	1.26	24.98	0.00	0.00
2	0.546	0.42	1.30	24.98	0.00	0.00
3	0.566	0.42	1.35	24.98	0.00	0.00
4	0.590	0.43	1.37	25.57	0.00	0.00
5	0.620	0.43	1.44	25.57	0.00	0.00
6	0.659	0.43	1.53	25.57	0.00	0.00
7	0.715	0.43	1.66	25.57	0.00	0.00
8	0.796	0.47	1.69	27.95	0.00	0.00
9	0.839	0.47	1.79	27.95	0.00	0.00

Interface Shear

Layer	k_c	k_m	k_c/k_m	v_m (cm/sn)	d (Newmark) (cm)	d (Bathurst and Cai) (cm)
1	0.743	0.42	1.77	24.98	0.00	0.00
2	0.743	0.42	1.77	24.98	0.00	0.00
3	0.743	0.42	1.77	24.98	0.00	0.00
4	0.750	0.43	1.74	25.57	0.00	0.00
5	0.750	0.43	1.74	25.57	0.00	0.00
6	0.752	0.43	1.75	25.57	0.00	0.00
7	0.754	0.43	1.75	25.57	0.00	0.00
8	0.761	0.47	1.62	27.95	0.00	0.00
9	0.660	0.47	1.40	27.95	0.00	0.00

Table D.11. Calculation of Displacements for Wall 2-El Centro 150%

External Base Sliding

	k_c	k_m	k_c/k_m	v_m (cm/sn)	d (Newmark) (cm)	d (Bathurst and Cai) (cm)
	0.452	0.57	0.79	37.70	0.42	0.41

Internal Sliding

Layer	k_c	k_m	k_c/k_m	v_m (cm/sn)	d (Newmark) (cm)	d (Bathurst and Cai) (cm)
1	0.528	0.59	0.90	39.02	0.17	0.20
2	0.546	0.62	0.88	41.01	0.21	0.23
3	0.566	0.62	0.91	41.01	0.14	0.18
4	0.590	0.62	0.95	41.01	0.07	0.14
5	0.620	0.68	0.91	44.98	0.16	0.20
6	0.659	0.68	0.97	44.98	0.05	0.13
7	0.715	0.68	1.05	44.98	0.00	0.00
8	0.796	0.78	1.02	51.59	0.00	0.00
9	0.839	0.83	1.01	54.90	0.00	0.00

Interface Shear

Layer	k_c	k_m	k_c/k_m	v_m (cm/sn)	d (Newmark) (cm)	d (Bathurst and Cai) (cm)
1	0.743	0.59	1.26	39.02	0.00	0.00
2	0.743	0.62	1.20	41.01	0.00	0.00
3	0.743	0.62	1.20	41.01	0.00	0.00
4	0.750	0.62	1.21	41.01	0.00	0.00
5	0.750	0.68	1.10	44.98	0.00	0.00
6	0.752	0.68	1.11	44.98	0.00	0.00
7	0.754	0.68	1.11	44.98	0.00	0.00
8	0.761	0.78	0.98	51.59	0.05	0.15
9	0.660	0.83	0.80	54.90	0.60	0.58

Table D.12. Calculation of Displacements for Wall 2-El Centro 200%

External Base Sliding

	k_c	k_m	k_c/k_m	v_m (cm/sn)	d (Newmark) (cm)	d (Bathurst and Cai) (cm)
	0.452	0.73	0.62	46.95	1.53	1.79

Internal Sliding

Layer	k_c	k_m	k_c/k_m	v_m (cm/sn)	d (Newmark) (cm)	d (Bathurst and Cai) (cm)
1	0.528	0.74	0.71	47.59	0.88	0.89
2	0.546	0.84	0.65	54.02	1.47	1.64
3	0.566	0.84	0.67	54.02	1.27	1.37
4	0.590	0.84	0.70	54.02	1.07	1.11
5	0.620	0.88	0.70	56.60	1.11	1.14
6	0.659	0.88	0.75	56.60	0.83	0.82
7	0.715	0.88	0.81	56.60	0.53	0.51
8	0.796	1.04	0.77	66.89	0.88	0.86
9	0.839	1.14	0.74	73.32	1.17	1.17

Interface Shear

Layer	k_c	k_m	k_c/k_m	v_m (cm/sn)	d (Newmark) (cm)	d (Bathurst and Cai) (cm)
1	0.743	0.74	1.00	47.59	0.01	0.11
2	0.743	0.84	0.88	54.02	0.26	0.29
3	0.743	0.84	0.88	54.02	0.26	0.29
4	0.750	0.84	0.89	54.02	0.24	0.27
5	0.750	0.88	0.85	56.60	0.38	0.38
6	0.752	0.88	0.85	56.60	0.37	0.38
7	0.754	0.88	0.86	56.60	0.36	0.37
8	0.761	1.04	0.73	66.89	1.10	1.10
9	0.660	1.14	0.58	73.32	3.02	3.79

Table D.13. Calculation of k_c for the external base sliding for Wall 3

1-External Base Sliding

k_c	0.633
Ψ	32.34
K_A	0.20
K_{AE}	1.13
ΔK_{dyn}	0.93

H	1.90
L	1.35
K_{AH}	0.17
K_{AEH}	0.94
ΔK_{dynH}	0.77

W_w	3.99
W_i	41.56
W_r	45.55

W_i'	28.26

R_S	38.223
P_{IR}	20.42
P_{AEH}	17.41
FS_{sl}	1.00

Table D.14. Calculation of k_c for the internal base sliding for Wall 3

2-Internal Sliding

Layer Number	Elevation	Depth	S_{vi}	Z_{vi}	L_i	H
1	0.20	1.70	0.30	1.75	1.35	1.90
2	0.40	1.50	0.20	1.50	1.35	1.90
3	0.60	1.30	0.20	1.30	1.35	1.90
4	0.80	1.10	0.20	1.10	1.35	1.90
5	1.00	0.90	0.20	0.90	1.35	1.90
6	1.20	0.70	0.20	0.70	1.35	1.90
7	1.40	0.50	0.20	0.50	1.35	1.90
8	1.60	0.30	0.20	0.30	1.35	1.90
9	1.80	0.10	0.20	0.10	1.35	1.90

Layer Number	Elevation	Depth	AW_w	AW_i'	$\Delta P_{IR}(z)$	h_{ii}	$P_{AEH}(z)$	$V_w(z)$	AWi	$R_s(z)$	FS_{sli}
1	0.20	1.70	3.57	25.29	20.20	1.70	17.42	9.57	37	37.59	1.0
2	0.40	1.50	3.15	22.31	17.95	1.50	15.81	9.39	33	34.11	1.0
3	0.60	1.30	2.73	19.34	15.82	1.30	14.51	9.20	28	30.63	1.0
4	0.80	1.10	2.31	16.36	13.59	1.10	13.02	9.02	24	27.15	1.0
5	1.00	0.90	1.89	13.39	11.31	0.90	11.40	8.83	20	23.67	1.0
6	1.20	0.70	1.47	10.41	9.15	0.70	10.48	8.65	15	20.19	1.0
7	1.40	0.50	1.05	7.44	6.87	0.50	9.90	8.46	11	16.70	1.0
8	1.60	0.30	0.63	4.46	4.27	0.30	8.75	8.28	7	13.22	1.0
9	1.80	0.10	0.21	1.49	1.42	0.10	3.26	8.09	2	9.74	2.1

Layer Number	k_c	Ψ	K_A	K_{AE}	ΔK_{dyn}	K_{AH}	K_{AEH}	ΔK_{dynH}
1	0.700	34.99	0.23	1.24	1.01	0.19	1.03	0.84
2	0.705	35.18	0.23	1.27	1.04	0.19	1.05	0.86
3	0.717	35.64	0.23	1.33	1.10	0.19	1.10	0.91
4	0.728	36.05	0.23	1.39	1.16	0.19	1.15	0.96
5	0.740	36.50	0.23	1.46	1.23	0.19	1.21	1.02
6	0.770	37.60	0.23	1.68	1.45	0.19	1.39	1.20
7	0.810	39.01	0.23	2.14	1.91	0.19	1.77	1.58
8	0.838	39.96	0.23	2.99	2.76	0.19	2.48	2.29
9	0.839	40.00	0.23	3.23	3.00	0.19	2.68	2.49

Table D.15. Calculation of k_c for the interface shear for Wall 3

3-Interface Shear

Layer Number	Elevation	Depth	ΔW_w	$P_{AEH}(z)$	F_i	Sum of F_i	$S_i(z)$	$V_w(z)$	FS_w
1	0.20	1.70	3.57	58.75	6.74	58.75	2.57	9.57	1.00
2	0.40	1.50	3.15	54.10	5.25	53.50	2.87	9.39	1.00
3	0.60	1.30	2.73	48.85	5.85	47.64	3.17	9.20	1.00
4	0.80	1.10	2.31	43.00	6.46	41.18	3.48	9.02	1.00
5	1.00	0.90	1.89	37.77	7.28	33.91	5.23	8.83	1.00
6	1.20	0.70	1.47	31.78	8.22	25.68	7.16	8.65	1.00
7	1.40	0.50	1.05	25.13	9.46	16.23	9.67	8.46	1.00
8	1.60	0.30	0.63	15.97	10.40	5.83	10.60	8.28	1.00
9	1.80	0.10	0.21	2.85	5.83	0.00	2.99	8.09	2.00

Layer Number	k_c	Ψ	K_A	K_{AE}	ΔK_{dyn}	K_{AH}	K_{AEH}	ΔK_{dynH}
1	0.720	35.75	0.23	2.22	1.99	0.21	1.99	1.78
2	0.720	35.75	0.23	2.22	1.99	0.21	1.99	1.78
3	0.720	35.75	0.23	2.22	1.99	0.21	1.99	1.78
4	0.720	35.75	0.23	2.22	1.99	0.21	1.99	1.78
5	0.722	35.83	0.23	2.29	2.06	0.21	2.05	1.84
6	0.724	35.90	0.23	2.38	2.15	0.21	2.13	1.93
7	0.726	35.98	0.23	2.53	2.30	0.21	2.27	2.06
8	0.726	35.99	0.23	2.58	2.35	0.21	2.31	2.11
9	0.660	33.42	0.23	1.44	1.21	0.21	1.29	1.09

Layer Number	Elevation	Depth	S_{vi}	Z_{vi}	ΔW_{wi}	F_{stat}	F_{dyni}
1	0.20	1.70	0.30	1.75	0.63	1.89	4.40
2	0.40	1.50	0.20	1.50	0.42	1.08	3.87
3	0.60	1.30	0.20	1.30	0.42	0.94	4.61
4	0.80	1.10	0.20	1.10	0.42	0.79	5.36
5	1.00	0.90	0.20	0.90	0.42	0.65	6.33
6	1.20	0.70	0.20	0.70	0.42	0.50	7.41
7	1.40	0.50	0.20	0.50	0.42	0.36	8.79
8	1.60	0.30	0.20	0.30	0.42	0.22	9.88
9	1.80	0.10	0.20	0.15	0.42	0.11	5.44

Table D.16. Calculation of Displacements for Wall 3-El Centro 100%

External Base Sliding

	k_c	k_m	k_c/k_m	v_m (cm/sn)	d (Newmark) (cm)	d (Bathurst and Cai) (cm)
	0.633	0.42	1.51	24.98	0.00	0.00

Internal Sliding

Layer	k_c	k_m	k_c/k_m	v_m (cm/sn)	d (Newmark) (cm)	d (Bathurst and Cai) (cm)
1	0.700	0.42	1.67	24.98	0.00	0.00
2	0.705	0.42	1.68	24.98	0.00	0.00
3	0.717	0.42	1.71	24.98	0.00	0.00
4	0.728	0.43	1.69	25.57	0.00	0.00
5	0.740	0.43	1.72	25.57	0.00	0.00
6	0.770	0.43	1.79	25.57	0.00	0.00
7	0.810	0.43	1.88	25.57	0.00	0.00
8	0.838	0.47	1.78	27.95	0.00	0.00
9	0.839	0.47	1.79	27.95	0.00	0.00

Interface Shear

Layer	k_c	k_m	k_c/k_m	v_m (cm/sn)	d (Newmark) (cm)	d (Bathurst and Cai) (cm)
1	0.720	0.42	1.71	24.98	0.00	0.00
2	0.720	0.42	1.71	24.98	0.00	0.00
3	0.720	0.42	1.71	24.98	0.00	0.00
4	0.720	0.43	1.67	25.57	0.00	0.00
5	0.722	0.43	1.68	25.57	0.00	0.00
6	0.724	0.43	1.68	25.57	0.00	0.00
7	0.726	0.43	1.69	25.57	0.00	0.00
8	0.726	0.47	1.55	27.95	0.00	0.00
9	0.660	0.47	1.40	27.95	0.00	0.00

Table D.17. Calculation of Displacements for Wall 3-El Centro 150%

External Base Sliding

	k_c	k_m	k_c/k_m	v_m (cm/sn)	d (Newmark) (cm)	d (Bathurst and Cai) (cm)
	0.633	0.58	1.09	37.70	0.00	0.00

Internal Sliding

Layer	k_c	k_m	k_c/k_m	v_m (cm/sn)	d (Newmark) (cm)	d (Bathurst and Cai) (cm)
1	0.700	0.60	1.17	39.00	0.00	0.00
2	0.705	0.66	1.07	42.90	0.00	0.00
3	0.717	0.66	1.09	42.90	0.00	0.00
4	0.728	0.68	1.07	44.20	0.00	0.00
5	0.740	0.71	1.04	46.15	0.00	0.00
6	0.770	0.71	1.08	46.15	0.00	0.00
7	0.810	0.71	1.14	46.15	0.00	0.00
8	0.838	0.74	1.13	48.10	0.00	0.00
9	0.839	0.76	1.10	49.40	0.00	0.00

Interface Shear

Layer	k_c	k_m	k_c/k_m	v_m (cm/sn)	d (Newmark) (cm)	d (Bathurst and Cai) (cm)
1	0.720	0.60	1.20	39.00	0.00	0.00
2	0.720	0.66	1.09	42.90	0.00	0.00
3	0.720	0.66	1.09	42.90	0.00	0.00
4	0.720	0.68	1.06	44.20	0.00	0.00
5	0.722	0.71	1.02	46.15	0.00	0.00
6	0.724	0.71	1.02	46.15	0.00	0.00
7	0.726	0.71	1.02	46.15	0.00	0.00
8	0.726	0.74	0.98	48.10	0.03	0.13
9	0.660	0.76	0.87	49.40	0.29	0.30

Table D.18. Calculation of Displacements for Wall 3-El Centro 200%

External Base Sliding

	k_c	k_m	k_c/k_m	v_m (cm/sn)	d (Newmark) (cm)	d (Bathurst and Cai) (cm)
	0.633	0.73	0.87	46.95	0.27	0.28

Internal Sliding

Layer	k_c	k_m	k_c/k_m	v_m (cm/sn)	d (Newmark) (cm)	d (Bathurst and Cai) (cm)
1	0.700	0.93	0.75	59.81	0.86	0.84
2	0.705	0.87	0.81	55.95	0.53	0.51
3	0.717	0.87	0.82	55.95	0.47	0.46
4	0.728	0.87	0.84	55.95	0.43	0.42
5	0.740	0.90	0.82	57.88	0.50	0.49
6	0.770	0.90	0.86	57.88	0.37	0.38
7	0.810	0.90	0.90	57.88	0.23	0.28
8	0.838	1.03	0.81	66.24	0.61	0.59
9	0.839	1.10	0.76	70.75	0.95	0.92

Interface Shear

Layer	k_c	k_m	k_c/k_m	v_m (cm/sn)	d (Newmark) (cm)	d (Bathurst and Cai) (cm)
1	0.720	0.93	0.77	59.81	0.74	0.72
2	0.720	0.87	0.83	55.95	0.46	0.45
3	0.720	0.87	0.83	55.95	0.46	0.45
4	0.720	0.87	0.83	55.95	0.46	0.45
5	0.722	0.90	0.80	57.88	0.58	0.57
6	0.724	0.90	0.80	57.88	0.57	0.56
7	0.726	0.90	0.81	57.88	0.56	0.55
8	0.726	1.03	0.71	66.24	1.29	1.33
9	0.660	1.10	0.60	70.75	2.58	3.12

Table D.19. Calculation of Displacements for Wall 3-El Centro 250%

External Base Sliding

	k_c	k_m	k_c/k_m	v_m (cm/sn)	d (Newmark) (cm)	d (Bathurst and Cai) (cm)
	0.633	0.90	0.70	58.79	0.34	0.36

Internal Sliding

Layer	k_c	k_m	k_c/k_m	v_m (cm/sn)	d (Newmark) (cm)	d (Bathurst and Cai) (cm)
1	0.700	0.94	0.74	61.40	1.07	1.05
2	0.705	1.07	0.66	69.89	0.66	0.64
3	0.717	1.07	0.67	69.89	0.59	0.58
4	0.728	1.07	0.68	69.89	0.53	0.53
5	0.740	1.06	0.70	69.24	0.62	0.61
6	0.770	1.06	0.73	69.24	0.47	0.48
7	0.810	1.06	0.76	69.24	0.29	0.34
8	0.838	1.20	0.70	78.39	0.76	0.74
9	0.839	1.46	0.57	95.37	1.18	1.16

Interface Shear

Layer	k_c	k_m	k_c/k_m	v_m (cm/sn)	d (Newmark) (cm)	d (Bathurst and Cai) (cm)
1	0.720	0.94	0.77	61.40	0.92	0.90
2	0.720	1.07	0.67	69.89	0.58	0.57
3	0.720	1.07	0.67	69.89	0.58	0.57
4	0.720	1.07	0.67	69.89	0.58	0.57
5	0.722	1.06	0.68	69.24	0.73	0.71
6	0.724	1.06	0.68	69.24	0.72	0.69
7	0.726	1.06	0.68	69.24	0.70	0.68
8	0.726	1.20	0.61	78.39	1.61	1.66
9	0.660	1.46	0.45	95.37	3.22	3.90

Table D.20. Calculation of k_c for the external base sliding for Wall 4

1-External Base Sliding

k_c	0.442
Ψ	23.85
K_A	0.25
K_{AE}	0.72
ΔK_{dyn}	0.47

W_w	3.99
W_i	35.63
W_r	39.62

R_S	26.721
P_{IR}	12.47
P_{AEH}	13.55
FS_{sl}	1.00

H	1.90
L	1.35
K_{AH}	0.22
K_{AEH}	0.64
ΔK_{dynH}	0.42

W_i'	24.23

Table D.21. Calculation of k_c for the internal base sliding for Wall 4

2-Internal Sliding

Layer Number	Elevation	Depth	S_{si}	Z_{si}	L_i	H
1	0.20	1.70	0.30	1.75	1.35	1.90
2	0.40	1.50	0.20	1.50	1.35	1.90
3	0.60	1.30	0.20	1.30	1.35	1.90
4	0.80	1.10	0.20	1.10	1.35	1.90
5	1.00	0.90	0.20	0.90	1.35	1.90
6	1.20	0.70	0.20	0.70	1.35	1.90
7	1.40	0.50	0.20	0.50	1.35	1.90
8	1.60	0.30	0.20	0.30	1.35	1.90
9	1.80	0.10	0.20	0.10	1.35	1.90

Layer Number	Elevation	Depth	ΔW_w	$\Delta W_i'$	$\Delta P_{IR}(z)$	h_{ir}	$P_{AEH}(z)$	$V_w(z)$	ΔWi	$R_i(z)$	FS_{si}
1	0.20	1.70	3.57	21.68	15.15	1.70	13.32	9.57	32	28.72	1.0
2	0.40	1.50	3.15	19.13	13.48	1.50	11.71	9.39	28	26.29	1.0
3	0.60	1.30	2.73	16.58	12.16	1.30	10.75	9.20	24	23.85	1.0
4	0.80	1.10	2.31	14.03	10.70	1.10	9.75	9.02	21	21.41	1.0
5	1.00	0.90	1.89	11.48	9.22	0.90	9.00	8.83	17	18.97	1.0
6	1.20	0.70	1.47	8.93	7.59	0.70	8.27	8.65	13	16.53	1.0
7	1.40	0.50	1.05	6.38	5.87	0.50	8.10	8.46	9	14.10	1.0
8	1.60	0.30	0.63	3.83	3.72	0.30	7.29	8.28	6	11.66	1.1
9	1.80	0.10	0.21	1.28	1.23	0.10	2.35	8.09	2	9.22	2.6

Layer Number	k_c	Ψ	K_A	K_{AE}	ΔK_{dyn}	K_{AH}	K_{AEH}	ΔK_{dynH}
1	0.600	30.96	0.30	0.97	0.67	0.26	0.85	0.59
2	0.605	31.17	0.30	0.98	0.68	0.26	0.87	0.60
3	0.630	32.21	0.30	1.06	0.76	0.26	0.94	0.67
4	0.655	33.22	0.30	1.15	0.85	0.26	1.01	0.75
5	0.690	34.61	0.30	1.29	0.99	0.26	1.14	0.88
6	0.730	36.13	0.30	1.50	1.20	0.26	1.33	1.06
7	0.790	38.31	0.30	1.98	1.68	0.26	1.75	1.48
8	0.834	39.83	0.30	2.80	2.50	0.26	2.48	2.21
9	0.830	39.69	0.30	2.66	2.36	0.26	2.35	2.08

Table D.22. Calculation of k_c for the interface shear for Wall 4

3-Interface Shear

Layer Number	Elevation	Depth	ΔW_w	$P_{AEH}(z)$	F_i	Sum of F_i	$S_i(z)$	$V_w(z)$	FS_{sr}
1	0.20	1.70	3.57	29.47	4.50	30.46	1.25	9.57	1.00
2	0.40	1.50	3.15	26.62	3.20	27.25	1.33	9.39	1.00
3	0.60	1.30	2.73	23.61	3.37	23.89	1.42	9.20	1.00
4	0.80	1.10	2.31	20.43	3.53	20.36	1.52	9.02	1.00
5	1.00	0.90	1.89	17.10	3.69	16.66	1.61	8.83	1.00
6	1.20	0.70	1.47	13.60	3.86	12.80	1.71	8.65	1.00
7	1.40	0.50	1.05	9.93	4.03	8.77	1.82	8.46	1.00
8	1.60	0.30	0.63	6.10	4.20	4.57	1.93	8.28	1.00
9	1.80	0.10	0.21	2.21	4.57	0.00	2.33	8.09	2.00

Layer Number	k_c	Ψ	K_A	K_{AE}	ΔK_{dyn}	K_{AH}	K_{AEH}	ΔK_{dynH}
1	0.625	31.99	0.30	1.29	0.99	0.28	1.19	0.91
2	0.624	31.98	0.30	1.29	0.99	0.28	1.19	0.91
3	0.624	31.97	0.30	1.29	0.99	0.28	1.19	0.91
4	0.624	31.95	0.30	1.29	0.99	0.28	1.19	0.91
5	0.623	31.93	0.30	1.29	0.99	0.28	1.19	0.91
6	0.622	31.89	0.30	1.29	0.99	0.28	1.19	0.91
7	0.621	31.84	0.30	1.29	0.99	0.28	1.19	0.92
8	0.619	31.76	0.30	1.30	1.00	0.28	1.20	0.92
9	0.588	30.46	0.30	1.36	1.06	0.28	1.25	0.98

Layer Number	Elevation	Depth	S_{si}	Z_{si}	ΔWwi	F_{stai}	F_{dyni}
1	0.20	1.70	0.30	1.75	0.63	2.18	1.93
2	0.40	1.50	0.20	1.50	0.42	1.25	1.70
3	0.60	1.30	0.20	1.30	0.42	1.08	2.02
4	0.80	1.10	0.20	1.10	0.42	0.91	2.35
5	1.00	0.90	0.20	0.90	0.42	0.75	2.69
6	1.20	0.70	0.20	0.70	0.42	0.58	3.02
7	1.40	0.50	0.20	0.50	0.42	0.42	3.35
8	1.60	0.30	0.20	0.30	0.42	0.25	3.69
9	1.80	0.10	0.20	0.15	0.42	0.12	4.19

Table D.23. Calculation of Displacements for Wall 4-El Centro 100%

External Base Sliding

	k_c	k_m	k_c/k_m	v_m (cm/sn)	d (Newmark) (cm)	d (Bathurst and Cai) (cm)
	0.442	0.41	1.08	24.85	0.00	0.00

Internal Sliding

Layer	k_c	k_m	k_c/k_m	v_m (cm/sn)	d (Newmark) (cm)	d (Bathurst and Cai) (cm)
1	0.600	0.42	1.43	25.46	0.00	0.00
2	0.605	0.42	1.44	25.46	0.00	0.00
3	0.630	0.42	1.50	25.46	0.00	0.00
4	0.655	0.43	1.52	26.06	0.00	0.00
5	0.690	0.43	1.60	26.06	0.00	0.00
6	0.730	0.43	1.70	26.06	0.00	0.00
7	0.790	0.43	1.84	26.06	0.00	0.00
8	0.834	0.47	1.77	28.49	0.00	0.00
9	0.830	0.47	1.77	28.49	0.00	0.00

Interface Shear

Layer	k_c	k_m	k_c/k_m	v_m (cm/sn)	d (Newmark) (cm)	d (Bathurst and Cai) (cm)
1	0.625	0.42	1.49	25.46	0.00	0.00
2	0.624	0.42	1.49	25.46	0.00	0.00
3	0.624	0.42	1.49	25.46	0.00	0.00
4	0.624	0.43	1.45	26.06	0.00	0.00
5	0.623	0.43	1.45	26.06	0.00	0.00
6	0.622	0.43	1.45	26.06	0.00	0.00
7	0.621	0.43	1.44	26.06	0.00	0.00
8	0.619	0.47	1.32	28.49	0.00	0.00
9	0.588	0.47	1.25	28.49	0.00	0.00

Table D.24. Calculation of Displacements for Wall 4-El Centro 150%

External Base Sliding						
	k_c	k_m	k_c/k_m	v_m (cm/sn)	d (Newmark) (cm)	d (Bathurst and Cai) (cm)
	0.442	0.58	0.76	37.70	0.51	0.50
Internal Sliding						
Layer	k_c	k_m	k_c/k_m	v_m (cm/sn)	d (Newmark) (cm)	d (Bathurst and Cai) (cm)
1	0.600	0.60	1.00	39.00	0.00	0.09
2	0.605	0.66	0.92	42.90	0.14	0.18
3	0.630	0.66	0.95	42.90	0.07	0.14
4	0.655	0.68	0.96	44.20	0.06	0.13
5	0.690	0.71	0.97	46.15	0.05	0.13
6	0.730	0.71	1.03	46.15	0.00	0.00
7	0.790	0.71	1.11	46.15	0.00	0.00
8	0.834	0.74	1.13	48.10	0.00	0.00
9	0.830	0.76	1.09	49.40	0.00	0.00
Interface Shear						
Layer	k_c	k_m	k_c/k_m	v_m (cm/sn)	d (Newmark) (cm)	d (Bathurst and Cai) (cm)
1	0.625	0.60	1.04	39.00	0.00	0.00
2	0.624	0.66	0.95	42.90	0.09	0.15
3	0.624	0.66	0.95	42.90	0.09	0.15
4	0.624	0.68	0.92	44.20	0.14	0.19
5	0.623	0.71	0.88	46.15	0.24	0.26
6	0.622	0.71	0.88	46.15	0.25	0.26
7	0.621	0.71	0.87	46.15	0.25	0.27
8	0.619	0.74	0.84	48.10	0.37	0.37
9	0.588	0.76	0.77	49.40	0.62	0.60

Table D.25. Calculation of Displacements for Wall 4-El Centro 200%

External Base Sliding						
	k_c	k_m	k_c/k_m	v_m (cm/sn)	d (Newmark) (cm)	d (Bathurst and Cai) (cm)
	0.442	0.73	0.61	46.95	1.66	1.99
Internal Sliding						
Layer	k_c	k_m	k_c/k_m	v_m (cm/sn)	d (Newmark) (cm)	d (Bathurst and Cai) (cm)
1	0.600	0.93	0.65	59.81	1.67	1.88
2	0.605	0.87	0.70	55.95	1.16	1.21
3	0.630	0.87	0.72	55.95	0.96	0.97
4	0.655	0.87	0.75	55.95	0.80	0.79
5	0.690	0.90	0.77	57.88	0.75	0.74
6	0.730	0.90	0.81	57.88	0.54	0.53
7	0.790	0.90	0.88	57.88	0.30	0.32
8	0.834	1.03	0.81	66.24	0.63	0.61
9	0.830	1.10	0.75	70.75	1.00	0.98
Interface Shear						
Layer	k_c	k_m	k_c/k_m	v_m (cm/sn)	d (Newmark) (cm)	d (Bathurst and Cai) (cm)
1	0.625	0.93	0.67	59.81	1.43	1.54
2	0.624	0.87	0.72	55.95	1.00	1.02
3	0.624	0.87	0.72	55.95	1.01	1.02
4	0.624	0.87	0.72	55.95	1.01	1.03
5	0.623	0.90	0.69	57.88	1.22	1.28
6	0.622	0.90	0.69	57.88	1.22	1.29
7	0.621	0.90	0.69	57.88	1.24	1.30
8	0.619	1.03	0.60	66.24	2.40	2.90
9	0.588	1.10	0.53	70.75	3.78	5.12

Table D.26. Calculation of Displacements for Wall 4-El Centro 250%

External Base Sliding						
	k_c	k_m	k_c/k_m	v_m (cm/sn)	d (Newmark) (cm)	d (Bathurst and Cai) (cm)
	0.442	0.90	0.49	58.79	2.07	2.48
Internal Sliding						
Layer	k_c	k_m	k_c/k_m	v_m (cm/sn)	d (Newmark) (cm)	d (Bathurst and Cai) (cm)
1	0.600	0.94	0.64	61.40	2.09	2.35
2	0.605	1.07	0.57	69.89	1.44	1.51
3	0.630	1.07	0.59	69.89	1.21	1.22
4	0.655	1.07	0.61	69.89	1.00	0.98
5	0.690	1.06	0.65	69.24	0.94	0.92
6	0.730	1.06	0.69	69.24	0.68	0.66
7	0.790	1.06	0.75	69.24	0.38	0.41
8	0.834	1.20	0.70	78.39	0.79	0.77
9	0.830	1.46	0.57	95.37	1.25	1.23
Interface Shear						
Layer	k_c	k_m	k_c/k_m	v_m (cm/sn)	d (Newmark) (cm)	d (Bathurst and Cai) (cm)
1	0.625	0.94	0.66	61.40	1.78	1.92
2	0.624	1.07	0.58	69.89	1.26	1.28
3	0.624	1.07	0.58	69.89	1.26	1.28
4	0.624	1.07	0.58	69.89	1.26	1.28
5	0.623	1.06	0.59	69.24	1.52	1.60
6	0.622	1.06	0.59	69.24	1.53	1.61
7	0.621	1.06	0.59	69.24	1.54	1.62
8	0.619	1.20	0.52	78.39	3.00	3.63
9	0.588	1.46	0.40	95.37	4.72	6.41

Table D.27. Calculation of Displacements for Wall 4-El Centro 275%

External Base Sliding

	k_c	k_m	k_c/k_m	v_m (cm/sn)	d (Newmark) (cm)	d (Bathurst and Cai) (cm)
	0.442	0.98	0.45	66.69	2.24	2.68

Internal Sliding

Layer	k_c	k_m	k_c/k_m	v_m (cm/sn)	d (Newmark) (cm)	d (Bathurst and Cai) (cm)
1	0.600	1.00	0.60	68.05	2.26	2.54
2	0.605	1.19	0.51	80.98	1.56	1.63
3	0.630	1.19	0.53	80.98	1.30	1.32
4	0.655	1.19	0.55	80.98	1.08	1.06
5	0.690	1.20	0.58	81.66	1.02	0.99
6	0.730	1.20	0.61	81.66	0.74	0.71
7	0.790	1.20	0.66	81.66	0.41	0.44
8	0.834	1.21	0.69	82.34	0.85	0.83
9	0.830	1.25	0.66	85.06	1.35	1.33

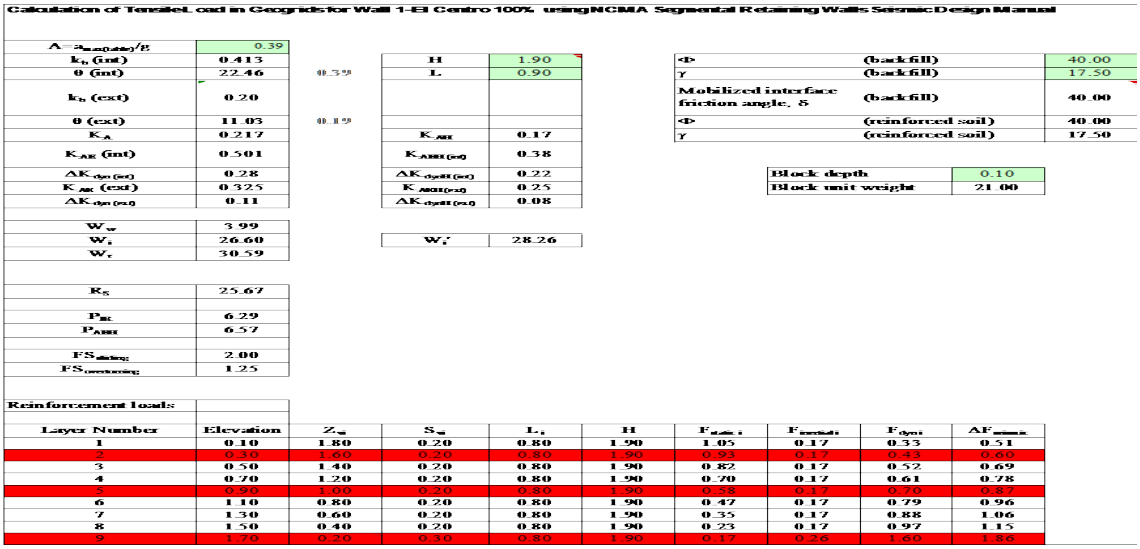
Interface Shear

Layer	k_c	k_m	k_c/k_m	v_m (cm/sn)	d (Newmark) (cm)	d (Bathurst and Cai) (cm)
1	0.625	1.00	0.62	68.05	1.93	2.08
2	0.624	1.19	0.52	80.98	1.36	1.38
3	0.624	1.19	0.52	80.98	1.36	1.38
4	0.624	1.19	0.52	80.98	1.36	1.39
5	0.623	1.20	0.52	81.66	1.64	1.72
6	0.622	1.20	0.52	81.66	1.65	1.74
7	0.621	1.20	0.52	81.66	1.67	1.75
8	0.619	1.21	0.51	82.34	3.24	3.92
9	0.588	1.25	0.47	85.06	5.10	6.92

APPENDIX E: EXCEL CALCULATION SHEETS FOR COMPARISON OF MEASURED STRESSES IN GEOGRID WITH STRESSES USED IN DESIGN METHODOLOGIES

This appendix contains Excel calculation sheets for comparison of measured stresses in geogrid with stresses used in design methodologies.

Table E.1. Calculation of Tensile Load in Geogrids for Wall 1-El Centro 100% using a)NCMA Segmental Retaining Walls Seismic Design Manual b) FHWA Recommendations



Calculation of Tensile Load in Geogrids for Wall 1-El Centro 100% using NCMA Segmental Retaining Walls Seismic Design Manual

$A = a_{max(0.4g)}/g$	0.39
k_h (int)	0.413
θ (int)	22.46
k_h (ext)	0.20
θ (ext)	11.03
K_A	0.217
K_{AE} (int)	0.501
$\Delta K_{dyn\,(int)}$	0.28
K_{AE} (ext)	0.325
$\Delta K_{dyn\,(ext)}$	0.11
W_w	3.99
W_s	26.60
W_r	30.59
K_S	25.67
P_{IE}	6.29
P_{AIH}	6.57
$FS_{sliding}$	2.00
$FS_{overturning}$	1.25

0.39 0.19

H	1.90
L	0.90
K_{AE}	0.17
$K_{AIH\,(int)}$	0.38
$\Delta K_{dyn\,(int)}$	0.22
$K_{AIH\,(ext)}$	0.25
$\Delta K_{dyn\,(ext)}$	0.08
W_s'	28.26

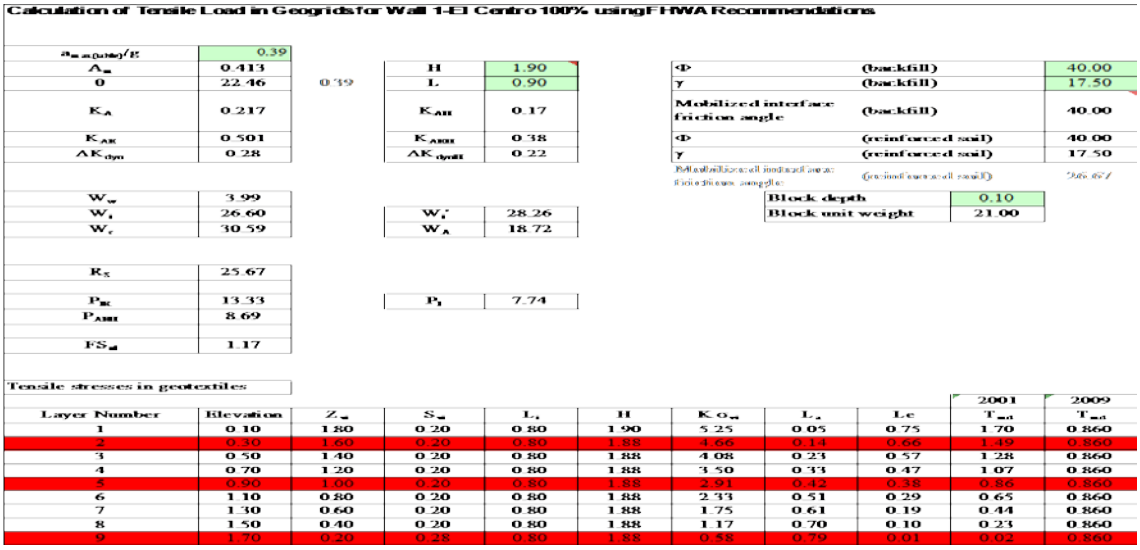
Φ	(backfill)	40.00
γ	(backfill)	17.50
Mobilized interface friction angle, δ	(backfill)	40.00
Φ	(reinforced soil)	40.00
γ	(reinforced soil)	17.50

Block depth	0.10
Block unit weight	21.00

Reinforcement loads:

Layer Number	Elevation	Z_w	S_v	L_1	H	F_{max}	$F_{pullout}$	F_{dyn}	AF_{max}
1	0.10	1.80	0.20	0.80	1.90	1.05	0.17	0.33	0.51
2	0.30	1.60	0.20	0.80	1.90	0.93	0.17	0.43	0.60
3	0.50	1.40	0.20	0.80	1.90	0.82	0.17	0.52	0.69
4	0.70	1.20	0.20	0.80	1.90	0.70	0.17	0.61	0.78
5	0.90	1.00	0.20	0.80	1.90	0.58	0.17	0.70	0.87
6	1.10	0.80	0.20	0.80	1.90	0.47	0.17	0.79	0.96
7	1.30	0.60	0.20	0.80	1.90	0.35	0.17	0.88	1.06
8	1.50	0.40	0.20	0.80	1.90	0.23	0.17	0.97	1.15
9	1.70	0.20	0.30	0.80	1.90	0.17	0.26	1.60	1.86

(a)



Calculation of Tensile Load in Geogrids for Wall 1-El Centro 100% using FHWA Recommendations

$A = a_{max(0.4g)}/g$	0.39
A_m	0.413
θ	22.46
K_A	0.217
K_{AE}	0.501
ΔK_{dyn}	0.28
W_w	3.99
W_s	26.60
W_r	30.59
K_S	25.67
P_{IE}	13.33
P_{AIH}	8.69
FS_{sl}	1.17

0.39

H	1.90
L	0.90
K_{AH}	0.17
K_{AIH}	0.38
ΔK_{dynH}	0.22
W_s'	28.26
W_A	18.72
P_I	7.74

Φ	(backfill)	40.00
γ	(backfill)	17.50
Mobilized interface friction angle	(backfill)	40.00
Φ	(reinforced soil)	40.00
γ	(reinforced soil)	17.50
Mobilized soil induced area:	(reinforced soil)	286.67
Friction cone angle:		

Block depth	0.10
Block unit weight	21.00

Tensile stresses in geotextiles:

Layer Number	Elevation	Z_w	S_v	L_1	H	$K\sigma_H$	L_2	Le	2001 T_{all}	2009 T_{all}
1	0.10	1.80	0.20	0.80	1.90	5.25	0.05	0.75	1.70	0.860
2	0.30	1.60	0.20	0.80	1.88	4.66	0.14	0.66	1.49	0.860
3	0.50	1.40	0.20	0.80	1.88	4.08	0.23	0.57	1.28	0.860
4	0.70	1.20	0.20	0.80	1.88	3.50	0.33	0.47	1.07	0.860
5	0.90	1.00	0.20	0.80	1.88	2.91	0.42	0.38	0.86	0.860
6	1.10	0.80	0.20	0.80	1.88	2.33	0.51	0.29	0.65	0.860
7	1.30	0.60	0.20	0.80	1.88	1.75	0.61	0.19	0.44	0.860
8	1.50	0.40	0.20	0.80	1.88	1.17	0.70	0.10	0.23	0.860
9	1.70	0.20	0.28	0.80	1.88	0.58	0.79	0.01	0.02	0.860

b)

Table E.2. Calculation of Tensile Load in Geogrids for Wall 1-El Centro 150% using a)NCMA Segmental Retaining Walls Seismic Design Manual b) FHWA Recommendations

Calculation of Tensile Load in Geogrids for Wall 1-El Centro 150% using NCMA Segmental Retaining Walls Seismic Design Manual

$A=a_{max(table)}/g$	0.59								
k_h (int)	0.507		H	1.90		Φ	(backfill)	40.00	
θ (int)	26.90	0.47	L	0.90		γ	(backfill)	17.50	
k_h (ext)	0.30					Mobilized interface friction angle, δ	(backfill)	40.00	
θ (ext)	16.44	0.29				Φ	(reinforced soil)	40.00	
K_A	0.217		K_{AH}	0.17		γ	(reinforced soil)	17.50	
K_{AE} (int)	0.605		$K_{AEH\ (int)}$	0.46					
$\Delta K_{dyn\ (int)}$	0.39		$\Delta K_{dynH\ (int)}$	0.30		Block depth	0.10		
K_{AE} (ext)	0.397		$K_{AEH\ (ext)}$	0.30		Block unit weight	21.00		
$\Delta K_{dyn\ (ext)}$	0.18		$\Delta K_{dynH\ (ext)}$	0.14					
W_w	3.99								
W_i	26.60		W_i'	28.26					
W_r	30.59								
R_S	25.67								
P_{IR}	9.51								
P_{AEH}	7.43								
$FS_{sliding}$	1.51								
$FS_{overturning}$	0.91								

Reinforcement loads

Layer Number	Elevation	Z_{vi}	S_{vi}	L_i	H	$F_{static\ i}$	$F_{inertial\ i}$	$F_{dyn\ i}$	$\Delta F_{seismic}$
1	0.10	1.80	0.20	0.80	1.90	1.05	0.21	0.46	0.67
2	0.30	1.60	0.20	0.80	1.90	0.93	0.21	0.58	0.80
3	0.50	1.40	0.20	0.80	1.90	0.82	0.21	0.71	0.92
4	0.70	1.20	0.20	0.80	1.90	0.70	0.21	0.83	1.04
5	0.90	1.00	0.20	0.80	1.90	0.58	0.21	0.96	1.17
6	1.10	0.80	0.20	0.80	1.90	0.47	0.21	1.08	1.29
7	1.30	0.60	0.20	0.80	1.90	0.35	0.21	1.21	1.42
8	1.50	0.40	0.20	0.80	1.90	0.23	0.21	1.33	1.54
9	1.70	0.20	0.30	0.80	1.90	0.17	0.32	2.18	2.50

a)

Calculation of Tensile Load in Geogrids for Wall 1-El Centro 150% using FHWA Recommendations

$a_{max(table)}/g$	0.59								
A_m	0.507		H	1.90		Φ	(backfill)	40.00	
θ	26.90	0.47	L	0.90		γ	(backfill)	17.50	
K_A	0.217		K_{AH}	0.17		Mobilized interface friction angle	(backfill)	40.00	
K_{AE}	0.605		K_{AEH}	0.46		Φ	(reinforced soil)	40.00	
ΔK_{dyn}	0.39		ΔK_{dynH}	0.30		γ	(reinforced soil)	17.50	
W_w	3.99					Block depth	0.10		
W_i	26.60		W_i'	28.26		Block unit weight	21.00		
W_r	30.59		W_A	18.72					
R_S	25.67								
P_{IR}	16.36		P_I	9.50					
P_{AEH}	9.95								
FS_{sl}	0.98								

Tensile stresses in geotextiles

Layer Number	Elevation	Z_{vi}	S_{vi}	L_i	H	$K\sigma_{vi}$	L_a	Le	2001 T_{md}	2009 T_{md}
1	0.10	1.80	0.20	0.80	1.90	5.25	0.05	0.75	2.09	1.055
2	0.30	1.60	0.20	0.80	1.88	4.66	0.14	0.66	1.83	1.055
3	0.50	1.40	0.20	0.80	1.88	4.08	0.23	0.57	1.57	1.055
4	0.70	1.20	0.20	0.80	1.88	3.50	0.33	0.47	1.31	1.055
5	0.90	1.00	0.20	0.80	1.88	2.91	0.42	0.38	1.06	1.055
6	1.10	0.80	0.20	0.80	1.88	2.33	0.51	0.29	0.80	1.055
7	1.30	0.60	0.20	0.80	1.88	1.75	0.61	0.19	0.54	1.055
8	1.50	0.40	0.20	0.80	1.88	1.17	0.70	0.10	0.28	1.055
9	1.70	0.20	0.28	0.80	1.88	0.58	0.79	0.01	0.02	1.055

(b)

Table E.3. Calculation of Tensile Load in Geogrids for Wall 1-El Centro 200% using a)NCMA Segmental Retaining Walls Seismic Design Manual b) FHWA Recommendations

Calculation of Tensile Load in Geogrids for Wall 1-El Centro 200% using NCMA Segmental Retaining Walls Seismic Design Manual

$A=a_{max(table)}/g$	0.74					Φ	(backfill)	40.00	
k_h (int)	0.525		H	1.90		γ	(backfill)	17.50	
θ (int)	27.72	0.48	L	0.90		Mobilized interface friction angle, δ	(backfill)	40.00	
k_h (ext)	0.37					Φ	(reinforced soil)	40.00	
θ (ext)	20.30	0.35				γ	(reinforced soil)	17.50	
K_A	0.217		K_{AH}	0.17					
K_{AE} (int)	0.628		$K_{AEH\ (int)}$	0.48		Block depth	0.10		
$\Delta K_{dyn\ (int)}$	0.41		$\Delta K_{dynH\ (int)}$	0.31		Block unit weight	21.00		
K_{AE} (ext)	0.460		$K_{AEH\ (ext)}$	0.35					
$\Delta K_{dyn\ (ext)}$	0.24		$\Delta K_{dynH\ (ext)}$	0.19					
W_w	3.99								
W_i	26.60		W_i'	28.26					
W_r	30.59								
R_S	25.67								
P_{IR}	11.93								
P_{AEH}	8.19								
$FS_{sliding}$	1.28								
$FS_{overturning}$	0.75								

Reinforcement loads

Layer Number	Elevation	Z_{vi}	S_{vi}	L_i	H	$F_{static\ i}$	$F_{inertial\ i}$	$F_{dyn\ i}$	$\Delta F_{seismic}$
1	0.10	1.80	0.20	0.80	1.90	1.05	0.22	0.48	0.70
2	0.30	1.60	0.20	0.80	1.90	0.93	0.22	0.62	0.84
3	0.50	1.40	0.20	0.80	1.90	0.82	0.22	0.75	0.97
4	0.70	1.20	0.20	0.80	1.90	0.70	0.22	0.88	1.10
5	0.90	1.00	0.20	0.80	1.90	0.58	0.22	1.01	1.23
6	1.10	0.80	0.20	0.80	1.90	0.47	0.22	1.14	1.36
7	1.30	0.60	0.20	0.80	1.90	0.35	0.22	1.28	1.50
8	1.50	0.40	0.20	0.80	1.90	0.23	0.22	1.41	1.63
9	1.70	0.20	0.30	0.80	1.90	0.17	0.33	2.31	2.64

(a)

Calculation of Tensile Load in Geogrids for Wall 1-El Centro 200% using FHWA Recommendations

$a_{max(table)}/g$	0.74					Φ	(backfill)	40.00	
A_m	0.525		H	1.90		γ	(backfill)	17.50	
θ	27.72	0.48	L	0.90		Mobilized interface friction angle	(backfill)	40.00	
K_A	0.217		K_{AH}	0.17		Φ	(reinforced soil)	40.00	
K_{AE}	0.628		K_{AEH}	0.48		γ	(reinforced soil)	17.50	
ΔK_{dyn}	0.41		ΔK_{dynH}	0.31					
W_w	3.99					Block depth	0.10		
W_i	26.60		W_i'	28.26		Block unit weight	21.00		
W_r	30.59		W_A	18.72					
R_S	25.67								
P_{IR}	16.95		P_I	9.84					
P_{AEH}	10.23								
FS_{sl}	0.94								

Tensile stresses in geotextiles

Layer Number	Elevation	Z_{vi}	S_{vi}	L_i	H	$K\sigma_{vi}$	L_a	Le	2001 T_{md}	2009 T_{md}
1	0.10	1.80	0.20	0.80	1.90	5.25	0.05	0.75	2.16	1.093
2	0.30	1.60	0.20	0.80	1.88	4.66	0.14	0.66	1.90	1.093
3	0.50	1.40	0.20	0.80	1.88	4.08	0.23	0.57	1.63	1.093
4	0.70	1.20	0.20	0.80	1.88	3.50	0.33	0.47	1.36	1.093
5	0.90	1.00	0.20	0.80	1.88	2.91	0.42	0.38	1.09	1.093
6	1.10	0.80	0.20	0.80	1.88	2.33	0.51	0.29	0.82	1.093
7	1.30	0.60	0.20	0.80	1.88	1.75	0.61	0.19	0.56	1.093
8	1.50	0.40	0.20	0.80	1.88	1.17	0.70	0.10	0.29	1.093
9	1.70	0.20	0.28	0.80	1.88	0.58	0.79	0.01	0.02	1.093

(b)

Table E.4. Calculation of Tensile Load in Geogrids for Wall 1-Izmit 100% using a)NCMA Segmental Retaining Walls Seismic Design Manual b) FHWA Recommendations

Calculation of Tensile Load in Geogrids for Wall 1-Izmit 100% using NCMA Segmental Retaining Walls Seismic Design Manual

$A=a_{max(table)}/g$	0.18								
k_h (int)	0.229		H	1.90					
θ (int)	12.88	0.22	L	0.90					
k_h (ext)	0.09								
θ (ext)	5.14	0.09							
K_A	0.217		K_{AH}	0.17					
K_{AE} (int)	0.348		$K_{AEH\ (int)}$	0.27					
$\Delta K_{dyn\ (int)}$	0.13		$\Delta K_{dynH\ (int)}$	0.10					
K_{AE} (ext)	0.263		$K_{AEH\ (ext)}$	0.20					
$\Delta K_{dyn\ (ext)}$	0.05		$\Delta K_{dynH\ (ext)}$	0.03					
W_w	3.99								
W_i	26.60		W_i'	28.26					
W_r	30.59								
R_S	25.67								
P_{IR}	2.90								
P_{AEH}	5.81								
$FS_{sliding}$	2.95								
$FS_{overturning}$	2.01								

Φ	(backfill)	40.00	
γ	(backfill)	17.50	
Mobilized interface friction angle, δ	(backfill)	40.00	
Φ	(reinforced soil)	40.00	
γ	(reinforced soil)	17.50	

Block depth	0.10
Block unit weight	21.00

Reinforcement loads

Layer Number	Elevation	Z_{vi}	S_{vi}	L_i	H	$F_{static\ i}$	$F_{inertial\ i}$	$F_{dyn\ i}$	$\Delta F_{seismic}$
1	0.10	1.80	0.20	0.80	1.90	1.05	0.10	0.15	0.25
2	0.30	1.60	0.20	0.80	1.90	0.93	0.10	0.20	0.29
3	0.50	1.40	0.20	0.80	1.90	0.82	0.10	0.24	0.33
4	0.70	1.20	0.20	0.80	1.90	0.70	0.10	0.28	0.38
5	0.90	1.00	0.20	0.80	1.90	0.58	0.10	0.32	0.42
6	1.10	0.80	0.20	0.80	1.90	0.47	0.10	0.36	0.46
7	1.30	0.60	0.20	0.80	1.90	0.35	0.10	0.41	0.50
8	1.50	0.40	0.20	0.80	1.90	0.23	0.10	0.45	0.54
9	1.70	0.20	0.30	0.80	1.90	0.17	0.14	0.73	0.88

(a)

Calculation of Tensile Load in Geogrids for Wall 1-Izmit 100% using FHWA Recommendations

$a_{max(table)}/g$	0.18								
A_m	0.229		H	1.90					
θ	12.88	0.22	L	0.90					
K_A	0.217		K_{AH}	0.17					
K_{AE}	0.348		K_{AEH}	0.27					
ΔK_{dyn}	0.13		ΔK_{dynH}	0.10					
W_w	3.99								
W_i	26.60		W_i'	28.26					
W_r	30.59		W_A	18.72					
R_S	25.67								
P_{IR}	7.37		P_I	4.28					
P_{AEH}	6.84								
FS_{sl}	1.81								

Φ	(backfill)	40.00	
γ	(backfill)	17.50	
Mobilized interface friction angle	(backfill)	40.00	
Φ	(reinforced soil)	40.00	
γ	(reinforced soil)	17.50	

Block depth	0.10
Block unit weight	21.00

Tensile stresses in geotextiles

									2001	2009
Layer Number	Elevation	Z_{vi}	S_{vi}	L_i	H	$K\sigma_{vi}$	L_a	Le	T_{md}	T_{md}
1	0.10	1.80	0.20	0.80	1.90	5.25	0.05	0.75	0.94	0.475
2	0.30	1.60	0.20	0.80	1.88	4.66	0.14	0.66	0.83	0.475
3	0.50	1.40	0.20	0.80	1.88	4.08	0.23	0.57	0.71	0.475
4	0.70	1.20	0.20	0.80	1.88	3.50	0.33	0.47	0.59	0.475
5	0.90	1.00	0.20	0.80	1.88	2.91	0.42	0.38	0.48	0.475
6	1.10	0.80	0.20	0.80	1.88	2.33	0.51	0.29	0.36	0.475
7	1.30	0.60	0.20	0.80	1.88	1.75	0.61	0.19	0.24	0.475
8	1.50	0.40	0.20	0.80	1.88	1.17	0.70	0.10	0.13	0.475
9	1.70	0.20	0.28	0.80	1.88	0.58	0.79	0.01	0.01	0.475

(b)

Table E.5. Calculation of Tensile Load in Geogrids for Wall 1-Izmit 150% using a) NCMA Segmental Retaining Walls Seismic Design Manual b) FHWA Recommendations

Calculation of Tensile Load in Geogrids for Wall 1-Izmit 150% using NCMA Segmental Retaining Walls Seismic Design Manual

$A=a_{max(table)}/g$	0.27
k_h (int)	0.319
θ (int)	17.67
k_h (ext)	0.14
θ (ext)	7.69
K_A	0.217
K_{AE} (int)	0.415
$\Delta K_{dyn\ (int)}$	0.20
K_{AE} (ext)	0.288
$\Delta K_{dyn\ (ext)}$	0.07
W_w	3.99
W_i	26.60
W_r	30.59
R_S	25.67
P_{IR}	4.35
P_{AEH}	6.12
$FS_{sliding}$	2.45
$FS_{overturning}$	1.60

0.31

0.13

H	1.90
L	0.90
K_{AH}	0.17
$K_{AEH\ (int)}$	0.32
$\Delta K_{dynH\ (int)}$	0.15
$K_{AEH\ (ext)}$	0.22
$\Delta K_{dynH\ (ext)}$	0.05
W_i'	28.26

Φ	(backfill)	40.00
γ	(backfill)	17.50
Mobilized interface friction angle, δ	(backfill)	40.00
Φ	(reinforced soil)	40.00
γ	(reinforced soil)	17.50

Block depth	0.10
Block unit weight	21.00

Reinforcement loads

Layer Number	Elevation	Z_{vi}	S_{vi}	L_i	H	$F_{static\ i}$	$F_{inertial\ i}$	$F_{dyn\ i}$	$\Delta F_{seismic}$
1	0.10	1.80	0.20	0.80	1.90	1.05	0.13	0.23	0.37
2	0.30	1.60	0.20	0.80	1.90	0.93	0.13	0.30	0.43
3	0.50	1.40	0.20	0.80	1.90	0.82	0.13	0.36	0.49
4	0.70	1.20	0.20	0.80	1.90	0.70	0.13	0.42	0.56
5	0.90	1.00	0.20	0.80	1.90	0.58	0.13	0.49	0.62
6	1.10	0.80	0.20	0.80	1.90	0.47	0.13	0.55	0.69
7	1.30	0.60	0.20	0.80	1.90	0.35	0.13	0.62	0.75
8	1.50	0.40	0.20	0.80	1.90	0.23	0.13	0.68	0.81
9	1.70	0.20	0.30	0.80	1.90	0.17	0.20	1.11	1.32

(a)

Calculation of Tensile Load in Geogrids for Wall 1-Izmit 150% using FHWA Recommendations

$a_{max(table)}/g$	0.27
A_m	0.319
θ	17.67
K_A	0.217
K_{AE}	0.415
ΔK_{dyn}	0.20
W_w	3.99
W_i	26.60
W_r	30.59
R_S	25.67
P_{IR}	10.28
P_{AEH}	7.66
FS_{sl}	1.43

0.31

H	1.90
L	0.90
K_{AH}	0.17
K_{AEH}	0.32
ΔK_{dynH}	0.15
W_i'	28.26
W_A	18.72
P_I	5.96

Φ	(backfill)	40.00
γ	(backfill)	17.50
Mobilized interface friction angle	(backfill)	40.00
Φ	(reinforced soil)	40.00
γ	(reinforced soil)	17.50

Block depth	0.10
Block unit weight	21.00

Tensile stresses in geotextiles

Layer Number	Elevation	Z_{vi}	S_{vi}	L_i	H	$K\sigma_{vi}$	L_a	Le	2001 T_{md}	2009 T_{md}
1	0.10	1.80	0.20	0.80	1.90	5.25	0.05	0.75	1.31	0.663
2	0.30	1.60	0.20	0.80	1.88	4.66	0.14	0.66	1.15	0.663
3	0.50	1.40	0.20	0.80	1.88	4.08	0.23	0.57	0.99	0.663
4	0.70	1.20	0.20	0.80	1.88	3.50	0.33	0.47	0.83	0.663
5	0.90	1.00	0.20	0.80	1.88	2.91	0.42	0.38	0.66	0.663
6	1.10	0.80	0.20	0.80	1.88	2.33	0.51	0.29	0.50	0.663
7	1.30	0.60	0.20	0.80	1.88	1.75	0.61	0.19	0.34	0.663
8	1.50	0.40	0.20	0.80	1.88	1.17	0.70	0.10	0.18	0.663
9	1.70	0.20	0.28	0.80	1.88	0.58	0.79	0.01	0.01	0.663

(b)

Table E.6. Calculation of Tensile Load in Geogrids for Wall 1-Izmit 200% using a)NCMA Segmental Retaining Walls Seismic Design Manual b) FHWA Recommendations

Calculation of Tensile Load in Geogrids for Wall 1-Izmit 200% using NCMA Segmental Retaining Walls Seismic Design Manual

$A=a_{max(table)}/g$	0.36		H	1.90		Φ	(backfill)	40.00	
k_h (int)	0.392		L	0.90		γ	(backfill)	17.50	
θ (int)	21.43	0.37				Mobilized interface friction angle, δ	(backfill)	40.00	
k_h (ext)	0.18					Φ	(reinforced soil)	40.00	
θ (ext)	10.20	0.18				γ	(reinforced soil)	17.50	
K_A	0.217		K_{AH}	0.17					
K_{AE} (int)	0.480		$K_{AEH\ (int)}$	0.37					
$\Delta K_{dyn\ (int)}$	0.26		$\Delta K_{dynH\ (int)}$	0.20		Block depth		0.10	
K_{AE} (ext)	0.316		$K_{AEH\ (ext)}$	0.24		Block unit weight		21.00	
$\Delta K_{dyn\ (ext)}$	0.10		$\Delta K_{dynH\ (ext)}$	0.08					
W_w	3.99								
W_i	26.60		W_i'	28.26					
W_r	30.59								
R_S	25.67								
P_{IR}	5.81								
P_{AEH}	6.45								
$FS_{sliding}$	2.09								
$FS_{overturning}$	1.32								

Reinforcement loads

Layer Number	Elevation	Z_{vi}	S_{vi}	L_i	H	$F_{static\ i}$	$F_{inertial\ i}$	$F_{dyn\ i}$	$\Delta F_{seismic}$
1	0.10	1.80	0.20	0.80	1.90	1.05	0.16	0.31	0.48
2	0.30	1.60	0.20	0.80	1.90	0.93	0.16	0.39	0.56
3	0.50	1.40	0.20	0.80	1.90	0.82	0.16	0.48	0.64
4	0.70	1.20	0.20	0.80	1.90	0.70	0.16	0.56	0.73
5	0.90	1.00	0.20	0.80	1.90	0.58	0.16	0.65	0.81
6	1.10	0.80	0.20	0.80	1.90	0.47	0.16	0.73	0.90
7	1.30	0.60	0.20	0.80	1.90	0.35	0.16	0.82	0.98
8	1.50	0.40	0.20	0.80	1.90	0.23	0.16	0.90	1.07
9	1.70	0.20	0.30	0.80	1.90	0.17	0.25	1.48	1.73

(a)

Calculation of Tensile Load in Geogrids for Wall 1-Izmit 200% using FHWA Recommendations

$a_{max(table)}/g$	0.36		H	1.90		Φ	(backfill)	40.00	
A_m	0.392		L	0.90		γ	(backfill)	17.50	
θ	21.43	0.37				Mobilized interface friction angle	(backfill)	40.00	
K_A	0.217		K_{AH}	0.17		Φ	(reinforced soil)	40.00	
K_{AE}	0.480		K_{AEH}	0.37		γ	(reinforced soil)	17.50	
ΔK_{dyn}	0.26		ΔK_{dynH}	0.20					
W_w	3.99					Block depth		0.10	
W_i	26.60		W_i'	28.26		Block unit weight		21.00	
W_r	30.59		W_A	18.72					
R_S	25.67								
P_{IR}	12.66		P_I	7.35					
P_{AEH}	8.44								
FS_{sl}	1.22								

Tensile stresses in geotextiles

Layer Number	Elevation	Z_{vi}	S_{vi}	L_i	H	$K\sigma_{vi}$	L_a	Le	2001 T_{md}	2009 T_{md}
1	0.10	1.80	0.20	0.80	1.90	5.25	0.05	0.75	1.62	0.816
2	0.30	1.60	0.20	0.80	1.88	4.66	0.14	0.66	1.42	0.816
3	0.50	1.40	0.20	0.80	1.88	4.08	0.23	0.57	1.22	0.816
4	0.70	1.20	0.20	0.80	1.88	3.50	0.33	0.47	1.02	0.816
5	0.90	1.00	0.20	0.80	1.88	2.91	0.42	0.38	0.82	0.816
6	1.10	0.80	0.20	0.80	1.88	2.33	0.51	0.29	0.62	0.816
7	1.30	0.60	0.20	0.80	1.88	1.75	0.61	0.19	0.42	0.816
8	1.50	0.40	0.20	0.80	1.88	1.17	0.70	0.10	0.22	0.816
9	1.70	0.20	0.28	0.80	1.88	0.58	0.79	0.01	0.02	0.816

(b)

Table E.7. Calculation of Tensile Load in Geogrids for Wall 1-Sakarya 100% using a)NCMA Segmental Retaining Walls Seismic Design Manual b) FHWA Recommendations

Calculation of Tensile Load in Geogrids for Wall 1-Sakarya 100% using NCMA Segmental Retaining Walls Seismic Design Manual

$A=a_{max(table)}/g$	0.22
k_h (int)	0.271
θ (int)	15.14
k_h (ext)	0.11
θ (ext)	6.28
K_A	0.217
K_{AE} (int)	0.378
$\Delta K_{dyn\ (int)}$	0.16
K_{AE} (ext)	0.274
$\Delta K_{dyn\ (ext)}$	0.06
W_w	3.99
W_i	26.60
W_r	30.59
R_S	25.67
P_{IR}	3.55
P_{AEH}	5.94
$FS_{sliding}$	2.70
$FS_{overturning}$	1.80

0.26

0.11

H	1.90
L	0.90
K_{AH}	0.17
$K_{AEH\ (int)}$	0.29
$\Delta K_{dynH\ (int)}$	0.12
$K_{AEH\ (ext)}$	0.21
$\Delta K_{dynH\ (ext)}$	0.04
W_i'	28.26

Φ	(backfill)	40.00
γ	(backfill)	17.50
Mobilized interface friction angle, δ	(backfill)	40.00
Φ	(reinforced soil)	40.00
γ	(reinforced soil)	17.50

Block depth	0.10
Block unit weight	21.00

Reinforcement loads

Layer Number	Elevation	Z_{vi}	S_{vi}	L_i	H	$F_{static\ i}$	$F_{inertial\ i}$	$F_{dyn\ i}$	$\Delta F_{seismic}$
1	0.10	1.80	0.20	0.80	1.90	1.05	0.11	0.19	0.30
2	0.30	1.60	0.20	0.80	1.90	0.93	0.11	0.24	0.35
3	0.50	1.40	0.20	0.80	1.90	0.82	0.11	0.29	0.41
4	0.70	1.20	0.20	0.80	1.90	0.70	0.11	0.34	0.46
5	0.90	1.00	0.20	0.80	1.90	0.58	0.11	0.40	0.51
6	1.10	0.80	0.20	0.80	1.90	0.47	0.11	0.45	0.56
7	1.30	0.60	0.20	0.80	1.90	0.35	0.11	0.50	0.61
8	1.50	0.40	0.20	0.80	1.90	0.23	0.11	0.55	0.66
9	1.70	0.20	0.30	0.80	1.90	0.17	0.17	0.90	1.07

(a)

Calculation of Tensile Load in Geogrids for Wall 1-Sakarya 100% using FHWA Recommendations

$a_{max(table)}/g$	0.22
A_m	0.271
θ	15.14
K_A	0.217
K_{AE}	0.378
ΔK_{dyn}	0.16
W_w	3.99
W_i	26.60
W_r	30.59
R_S	25.67
P_{IR}	8.73
P_{AEH}	7.20
FS_{sl}	1.61

0.26

H	1.90
L	0.90
K_{AH}	0.17
K_{AEH}	0.29
ΔK_{dynH}	0.12
W_i'	28.26
W_A	18.72
P_I	5.07

Φ	(backfill)	40.00
γ	(backfill)	17.50
Mobilized interface friction angle	(backfill)	40.00
Φ	(reinforced soil)	40.00
γ	(reinforced soil)	17.50

Block depth	0.10
Block unit weight	21.00

Tensile stresses in geotextiles

Layer Number	Elevation	Z_{vi}	S_{vi}	L_i	H	$K\sigma_{vi}$	L_a	Le	2001 T_{md}	2009 T_{md}
1	0.10	1.80	0.20	0.80	1.90	5.25	0.05	0.75	1.11	0.563
2	0.30	1.60	0.20	0.80	1.88	4.66	0.14	0.66	0.98	0.563
3	0.50	1.40	0.20	0.80	1.88	4.08	0.23	0.57	0.84	0.563
4	0.70	1.20	0.20	0.80	1.88	3.50	0.33	0.47	0.70	0.563
5	0.90	1.00	0.20	0.80	1.88	2.91	0.42	0.38	0.56	0.563
6	1.10	0.80	0.20	0.80	1.88	2.33	0.51	0.29	0.42	0.563
7	1.30	0.60	0.20	0.80	1.88	1.75	0.61	0.19	0.29	0.563
8	1.50	0.40	0.20	0.80	1.88	1.17	0.70	0.10	0.15	0.563
9	1.70	0.20	0.28	0.80	1.88	0.58	0.79	0.01	0.01	0.563

(b)

Table E.8. Calculation of Tensile Load in Geogrids for Wall 1-Sakarya 150% using a)NCMA Segmental Retaining Walls Seismic Design Manual b) FHWA Recommendations

Calculation of Tensile Load in Geogrids for Wall 1-Sakarya 150% using NCMA Segmental Retaining Walls Seismic Design Manual

$A=a_{max(table)}/g$	0.31								
k_h (int)	0.353		H	1.90		Φ	(backfill)	40.00	
θ (int)	19.46	0.34	L	0.90		γ	(backfill)	17.50	
k_h (ext)	0.16					Mobilized interface friction angle, δ	(backfill)	40.00	
θ (ext)	8.81	0.15				Φ	(reinforced soil)	40.00	
K_A	0.217		K_{AH}	0.17		γ	(reinforced soil)	17.50	
K_{AE} (int)	0.445		$K_{AEH\ (int)}$	0.34					
$\Delta K_{dyn\ (int)}$	0.23		$\Delta K_{dynH\ (int)}$	0.17		Block depth	0.10		
K_{AE} (ext)	0.300		$K_{AEH\ (ext)}$	0.23		Block unit weight	21.00		
$\Delta K_{dyn\ (ext)}$	0.08		$\Delta K_{dynH\ (ext)}$	0.06					
W_w	3.99								
W_i	26.60		W_i'	28.26					
W_r	30.59								
R_S	25.67								
P_{IR}	5.00								
P_{AEH}	6.26								
$FS_{sliding}$	2.28								
$FS_{overturning}$	1.46								

Reinforcement loads

Layer Number	Elevation	Z_{vi}	S_{vi}	L_i	H	$F_{static\ i}$	$F_{inertial\ i}$	$F_{dyn\ i}$	$\Delta F_{seismic}$
1	0.10	1.80	0.20	0.80	1.90	1.05	0.15	0.27	0.42
2	0.30	1.60	0.20	0.80	1.90	0.93	0.15	0.34	0.49
3	0.50	1.40	0.20	0.80	1.90	0.82	0.15	0.41	0.56
4	0.70	1.20	0.20	0.80	1.90	0.70	0.15	0.49	0.64
5	0.90	1.00	0.20	0.80	1.90	0.58	0.15	0.56	0.71
6	1.10	0.80	0.20	0.80	1.90	0.47	0.15	0.63	0.78
7	1.30	0.60	0.20	0.80	1.90	0.35	0.15	0.71	0.86
8	1.50	0.40	0.20	0.80	1.90	0.23	0.15	0.78	0.93
9	1.70	0.20	0.30	0.80	1.90	0.17	0.22	1.28	1.50

(a)

Calculation of Tensile Load in Geogrids for Wall 1-Sakarya 150% using FHWA Recommendations

$a_{max(table)}/g$	0.31						
A_m	0.353		H	1.90	Φ	(backfill)	40.00
θ	19.46	0.34	L	0.90	γ	(backfill)	17.50
K_A	0.217		K_{AH}	0.17	Mobilized interface friction angle	(backfill)	40.00
K_{AE}	0.445		K_{AEH}	0.34	Φ	(reinforced soil)	40.00
ΔK_{dyn}	0.23		ΔK_{dynH}	0.17	γ	(reinforced soil)	17.50
W_w	3.99				Block depth	0.10	
W_i	26.60		W_i'	28.26	Block unit weight	21.00	
W_r	30.59		W_A	18.72			
R_S	25.67						
P_{IR}	11.40		P_I	6.62			
P_{AEH}	8.01						
FS_{sl}	1.32						

Tensile stresses in geotextiles

Layer Number	Elevation	Z_{vi}	S_{vi}	L_i	H	$K\sigma_{vi}$	L_a	Le	2001 T_{md}	2009 T_{md}
1	0.10	1.80	0.20	0.80	1.90	5.25	0.05	0.75	1.46	0.735
2	0.30	1.60	0.20	0.80	1.88	4.66	0.14	0.66	1.28	0.735
3	0.50	1.40	0.20	0.80	1.88	4.08	0.23	0.57	1.10	0.735
4	0.70	1.20	0.20	0.80	1.88	3.50	0.33	0.47	0.92	0.735
5	0.90	1.00	0.20	0.80	1.88	2.91	0.42	0.38	0.74	0.735
6	1.10	0.80	0.20	0.80	1.88	2.33	0.51	0.29	0.55	0.735
7	1.30	0.60	0.20	0.80	1.88	1.75	0.61	0.19	0.37	0.735
8	1.50	0.40	0.20	0.80	1.88	1.17	0.70	0.10	0.19	0.735
9	1.70	0.20	0.28	0.80	1.88	0.58	0.79	0.01	0.01	0.735

(b)

Table E.9. Calculation of Tensile Load in Geogrids for Wall 1-Sakarya 200% using a)NCMA Segmental Retaining Walls Seismic Design Manual b) FHWA Recommendations

Calculation of Tensile Load in Geogrids for Wall 1-Sakarya 200% using NCMA Segmental Retaining Walls Seismic Design Manual

$A=a_{max(table)}/g$	0.38					Φ	(backfill)	40.00	
k_h (int)	0.407		H	1.90		γ	(backfill)	17.50	
θ (int)	22.13	0.39	L	0.90		Mobilized interface friction angle, δ	(backfill)	40.00	
k_h (ext)	0.19					Φ	(reinforced soil)	40.00	
θ (ext)	10.76	0.19				γ	(reinforced soil)	17.50	
K_A	0.217		K_{AH}	0.17					
K_{AE} (int)	0.494		$K_{AEH\ (int)}$	0.38					
$\Delta K_{dyn\ (int)}$	0.28		$\Delta K_{dynH\ (int)}$	0.21		Block depth	0.10		
K_{AE} (ext)	0.322		$K_{AEH\ (ext)}$	0.25		Block unit weight	21.00		
$\Delta K_{dyn\ (ext)}$	0.10		$\Delta K_{dynH\ (ext)}$	0.08					
W_w	3.99								
W_i	26.60		W_i'	28.26					
W_r	30.59								
R_S	25.67								
P_{IR}	6.13								
P_{AEH}	6.53								
$FS_{sliding}$	2.03								
$FS_{overturning}$	1.27								

Reinforcement loads

Layer Number	Elevation	Z_{vi}	S_{vi}	L_i	H	$F_{static\ i}$	$F_{inertial\ i}$	$F_{dyn\ i}$	$\Delta F_{seismic}$
1	0.10	1.80	0.20	0.80	1.90	1.05	0.17	0.33	0.50
2	0.30	1.60	0.20	0.80	1.90	0.93	0.17	0.42	0.59
3	0.50	1.40	0.20	0.80	1.90	0.82	0.17	0.50	0.68
4	0.70	1.20	0.20	0.80	1.90	0.70	0.17	0.59	0.76
5	0.90	1.00	0.20	0.80	1.90	0.58	0.17	0.68	0.85
6	1.10	0.80	0.20	0.80	1.90	0.47	0.17	0.77	0.94
7	1.30	0.60	0.20	0.80	1.90	0.35	0.17	0.86	1.03
8	1.50	0.40	0.20	0.80	1.90	0.23	0.17	0.95	1.12
9	1.70	0.20	0.30	0.80	1.90	0.17	0.26	1.56	1.81

(a)

Calculation of Tensile Load in Geogrids for Wall 1-Sakarya 200% using FHWA Recommendations

$a_{max(table)}/g$	0.38					Φ	(backfill)	40.00	
A_m	0.407		H	1.90		γ	(backfill)	17.50	
θ	22.13	0.39	L	0.90		Mobilized interface friction angle	(backfill)	40.00	
K_A	0.217		K_{AH}	0.17		Φ	(reinforced soil)	40.00	
K_{AE}	0.494		K_{AEH}	0.38		γ	(reinforced soil)	17.50	
ΔK_{dyn}	0.28		ΔK_{dynH}	0.21					
W_w	3.99					Block depth	0.10		
W_i	26.60		W_i'	28.26		Block unit weight	21.00		
W_r	30.59		W_A	18.72					
R_S	25.67								
P_{IR}	13.11		P_I	7.61					
P_{AEH}	8.61								
FS_{sl}	1.18								

Tensile stresses in geotextiles

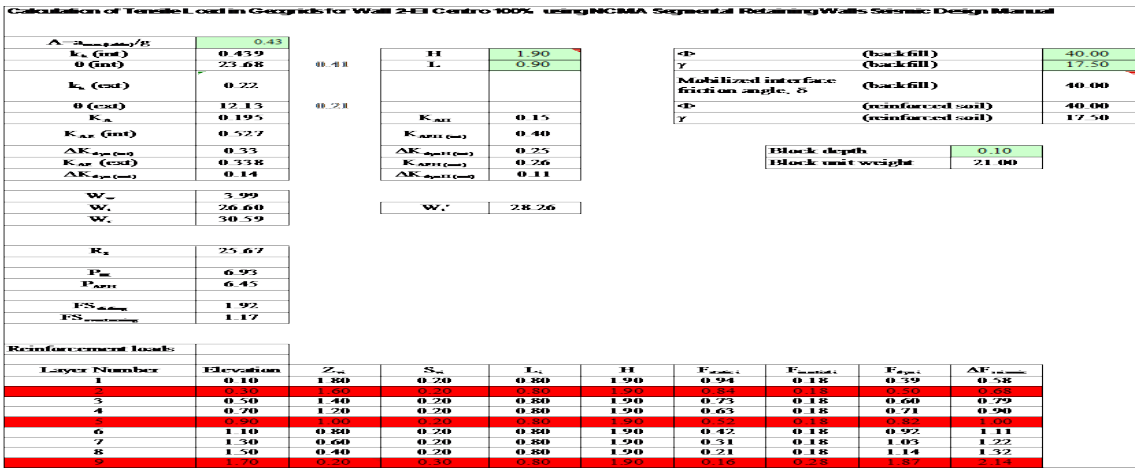
Layer Number	Elevation	Z_{vi}	S_{vi}	L_i	H	$K\sigma_{vi}$	L_a	Le	2001 T_{md}	2009 T_{md}
1	0.10	1.80	0.20	0.80	1.90	5.25	0.05	0.75	1.68	0.846
2	0.30	1.60	0.20	0.80	1.88	4.66	0.14	0.66	1.47	0.846
3	0.50	1.40	0.20	0.80	1.88	4.08	0.23	0.57	1.26	0.846
4	0.70	1.20	0.20	0.80	1.88	3.50	0.33	0.47	1.05	0.846
5	0.90	1.00	0.20	0.80	1.88	2.91	0.42	0.38	0.85	0.846
6	1.10	0.80	0.20	0.80	1.88	2.33	0.51	0.29	0.64	0.846
7	1.30	0.60	0.20	0.80	1.88	1.75	0.61	0.19	0.43	0.846
8	1.50	0.40	0.20	0.80	1.88	1.17	0.70	0.10	0.22	0.846

(b)

Table E.10. Comparison of Calculatedand Measured Seismic Induced Tensile Loads in Geogrids for Wall 1

Wall / Base Excitation	Maximum Table Acceleration-Base Input (g)	Design (NCMA) ΔTmax in lower geogrid (@h=0.2 m) (kN/m)	Design (FHWA2001) ΔTmax in lower geogrid (@h=0.2 m) (kN/m)	Design (FHWA2009) ΔTmax in lower geogrid (@h=0.2 m) (kN/m)	Measured Geogrid Stress Max Stresses (peak values) (kN/m)	Design (NCMA) ΔTmax at midheight geogrid (@h=1 m) (kN/m)	Design (FHWA2001) ΔTmax at midheight geogrid (@h=1 m) (kN/m)	Design (FHWA2009) ΔTmax at midheight geogrid (@h=1 m) (kN/m)	Measured Geogrid Stress Max Stresses (peak values) (kN/m)	Design (NCMA) ΔTmax in upper geogrid (@h=1.8 m) (kN/m)	Design (FHWA2001) ΔTmax in upper geogrid (@h=1.8 m) (kN/m)	Design (FHWA2009) ΔTmax in upper geogrid (@h=1.8 m) (kN/m)	Measured Geogrid Stress Max Stresses (peak values) (kN/m)
Wall 1 / El Centro 100%	0.39	0.60	1.49	0.86	3.24	0.87	0.86	0.86	2.88	1.86	0.02	0.86	0.83
Wall 1 / El Centro 150%	0.59	0.80	1.83	1.06	4.8	1.17	1.06	1.06	5.54	2.50	0.02	1.06	1.71
Wall 1 / El Centro 200%	0.74	0.94	1.90	1.09	6	1.23	1.09	1.09	5.22	2.64	0.02	1.09	1.3
Wall 1 / Izmit 100%	0.18	0.29	0.83	0.48	0.75	0.42	0.48	0.48	0.66	0.88	0.01	0.48	0.23
Wall 1 / Izmit 150%	0.27	0.43	1.15	0.66	1.07	0.62	0.66	0.66	0.93	1.32	0.01	0.66	0.34
Wall 1 / Izmit 200%	0.36	0.56	1.42	0.82	1.87	0.81	0.82	0.82	1.4	1.73	0.02	0.82	0.51
Wall 1 / Sakarya 100%	0.22	0.35	0.98	0.56	0.86	0.51	0.56	0.56	0.77	1.07	0.01	0.56	0.3
Wall 1 / Sakarya 150%	0.31	0.49	1.28	0.74	1.57	0.71	0.74	0.74	1.22	1.50	0.01	0.74	0.46
Wall 1 / Sakarya 200%	0.38	0.59	1.47	0.85	2.94	0.85	0.85	0.85	1.8	1.81	0.02	0.85	0.62

Table E.11. Calculation of Tensile Load in Geogrids for Wall 2-El Centro 100% using a)NCMA Segmental Retaining Walls Seismic Design Manual b) FHWA Recommendations



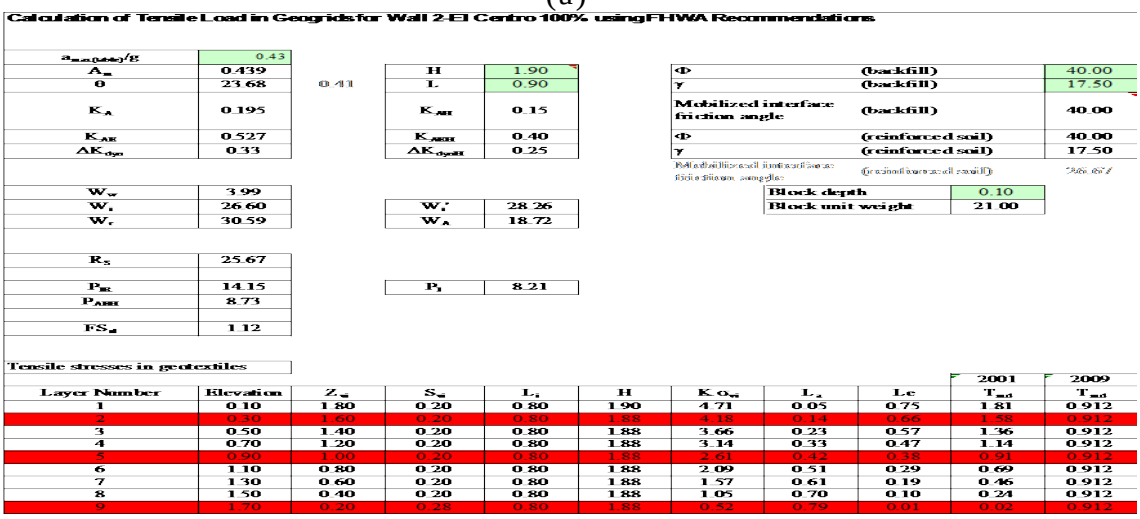
Calculation of Tensile Load in Geogrids for Wall 2-El Centro 100% using NCMA Segmental Retaining Walls Seismic Design Manual

$A=a_{max(des)}/g$	0.43		H	1.90	Φ	(backfill)	40.00		
k_s (int)	0.439		L	0.90	γ	(backfill)	17.50		
θ (int)	23.68	0.41			Mobilized interface friction angle, δ	(backfill)	40.00		
k_s (ext)	0.22				Φ	(reinforced soil)	40.00		
θ (ext)	12.13	0.21	K_{AH}	0.15	γ	(reinforced soil)	17.50		
K_A	0.195		$K_{AH(int)}$	0.40					
K_{AE} (int)	0.527		$AK_{dyn(int)}$	0.25	Block depth		0.10		
$AK_{dyn(int)}$	0.33		$K_{AH(ext)}$	0.26	Block unit weight		21.00		
K_{AE} (ext)	0.338		$AK_{dyn(ext)}$	0.11					
$AK_{dyn(ext)}$	0.14								
W_w	3.99								
W_s	26.60		W_s'	28.26					
W_r	30.59								
R_s	25.67								
P_{IE}	6.93								
P_{AEH}	6.45								
$FS_{sliding}$	1.92								
$FS_{overturning}$	1.17								

Reinforcement loads

Layer Number	Elevation	Z_w	S_v	L_i	H	F_{max}	$F_{connect}$	$F_{pullout}$	$\Delta F_{reinforc}$
1	0.10	1.80	0.20	0.80	1.90	0.94	0.18	0.59	0.58
2	0.30	1.60	0.20	0.80	1.90	0.84	0.18	0.50	0.68
3	0.50	1.40	0.20	0.80	1.90	0.73	0.18	0.60	0.79
4	0.70	1.20	0.20	0.80	1.90	0.63	0.18	0.71	0.90
5	0.90	1.00	0.20	0.80	1.90	0.52	0.18	0.82	1.00
6	1.10	0.80	0.20	0.80	1.90	0.42	0.18	0.92	1.11
7	1.30	0.60	0.20	0.80	1.90	0.31	0.18	1.03	1.22
8	1.50	0.40	0.20	0.80	1.90	0.21	0.18	1.14	1.32
9	1.70	0.20	0.30	0.80	1.90	0.16	0.28	1.87	2.14

(a)



Calculation of Tensile Load in Geogrids for Wall 2-El Centro 100% using FHWA Recommendations

$a_{max(des)}/g$	0.43		H	1.90	Φ	(backfill)	40.00		
A_E	0.439		L	0.90	γ	(backfill)	17.50		
θ	23.68	0.41			Mobilized interface friction angle	(backfill)	40.00		
K_A	0.195		K_{AH}	0.15	Φ	(reinforced soil)	40.00		
K_{AE}	0.527		K_{AEH}	0.40	γ	(reinforced soil)	17.50		
ΔK_{dyn}	0.33		ΔK_{dynH}	0.25	Mobilized soil-reinforcement interface friction angle	(reinforced soil)	26.67		
W_w	3.99				Block depth		0.10		
W_s	26.60		W_s'	28.26	Block unit weight		21.00		
W_r	30.59		W_A	18.72					
R_s	25.67								
P_{IE}	14.15		P_I	8.21					
P_{AEH}	8.73								
FS_{sl}	1.12								

Tensile stresses in geotextiles

Layer Number	Elevation	Z_w	S_v	L_i	H	$K\sigma_H$	L_e	Le	2001 T_{ad}	2009 T_{ad}
1	0.10	1.80	0.20	0.80	1.90	4.71	0.05	0.75	1.81	0.912
2	0.30	1.60	0.20	0.80	1.88	4.18	0.14	0.66	1.58	0.912
3	0.50	1.40	0.20	0.80	1.88	3.66	0.23	0.57	1.36	0.912
4	0.70	1.20	0.20	0.80	1.88	3.14	0.33	0.47	1.14	0.912
5	0.90	1.00	0.20	0.80	1.88	2.61	0.42	0.38	0.91	0.912
6	1.10	0.80	0.20	0.80	1.88	2.09	0.51	0.29	0.69	0.912
7	1.30	0.60	0.20	0.80	1.88	1.57	0.61	0.19	0.46	0.912
8	1.50	0.40	0.20	0.80	1.88	1.05	0.70	0.10	0.24	0.912
9	1.70	0.20	0.28	0.80	1.88	0.52	0.79	0.01	0.02	0.912

(b)

Table E.12. Calculation of Tensile Load in Geogrids for Wall 2-El Centro 150% using a)NCMA Segmental Retaining Walls Seismic Design Manual b) FHWA Recommendations

Calculation of Tensile Load in Geogrids for Wall 2-El Centro 150% using NCMA Segmental Retaining Walls Seismic Design Manu

$A=a_{max(rock)}/g$	0.57						
k_h (int)	0.502		H	1.90	Φ	(backfill)	40.00
θ (int)	26.64	0.46	L	0.90	γ	(backfill)	17.50
k_h (ext)	0.29				Mobilized interface friction angle, δ	(backfill)	40.00
θ (ext)	15.91	0.28			Φ	(reinforced soil)	40.00
K_A	0.195		K_{AH}	0.15	γ	(reinforced soil)	17.50
K_{AE} (int)	0.598		$K_{AEH\ (int)}$	0.46			
$\Delta K_{dyn\ (int)}$	0.40		$\Delta K_{dynH\ (int)}$	0.31	Block depth		0.10
K_{AE} (ext)	0.389		$K_{AEH\ (ext)}$	0.30	Block unit weight		21.00
$\Delta K_{dyn\ (ext)}$	0.19		$\Delta K_{dynH\ (ext)}$	0.15			
W_w	3.99						
W_s	26.60		W_s'	28.26			
W_r	30.59						
R_s	25.67						
P_{IE}	9.19						
P_{AEH}	7.06						
$FS_{sliding}$	1.58						
$FS_{overturning}$	0.94						

Reinforcement loads

Layer Number	Elevation	Z_{vi}	S_{vi}	L_i	H	$F_{static\ i}$	$F_{inertial\ i}$	$F_{dyn\ i}$	$\Delta F_{seismic}$
1	0.10	1.80	0.20	0.80	1.90	0.94	0.21	0.48	0.69
2	0.30	1.60	0.20	0.80	1.90	0.84	0.21	0.60	0.82
3	0.50	1.40	0.20	0.80	1.90	0.73	0.21	0.73	0.95
4	0.70	1.20	0.20	0.80	1.90	0.63	0.21	0.86	1.07
5	0.90	1.00	0.20	0.80	1.90	0.52	0.21	0.99	1.20
6	1.10	0.80	0.20	0.80	1.90	0.42	0.21	1.12	1.33
7	1.30	0.60	0.20	0.80	1.90	0.31	0.21	1.25	1.46
8	1.50	0.40	0.20	0.80	1.90	0.21	0.21	1.38	1.59
9	1.70	0.20	0.30	0.80	1.90	0.16	0.32	2.27	2.58

(a)

Calculation of Tensile Load in Geogrids for Wall 2-El Centro 150% using FHWA Recommendations

$a_{max(table)}/g$	0.57						
A_m	0.502		H	1.90	Φ	(backfill)	40.00
θ	26.64	0.46	L	0.90	γ	(backfill)	17.50
K_A	0.195		K_{AH}	0.15	Mobilized interface friction angle	(backfill)	40.00
K_{AE}	0.598		K_{AEH}	0.46	Φ	(reinforced soil)	40.00
ΔK_{dyn}	0.40		ΔK_{dynH}	0.31	γ	(reinforced soil)	17.50
					Mobilized interface friction angle:	(reinforced soil)	26.67
W_w	3.99				Block depth		0.10
W_s	26.60		W_s'	28.26	Block unit weight		21.00
W_r	30.59		W_A	18.72			
R_s	25.67						
P_{IE}	16.18		P_i	9.39			
P_{AEH}	9.59						
FS_{sl}	1.00						

Tensile stresses in geotextiles

Layer Number	Elevation	Z_{vi}	S_{vi}	L_i	H	$K\sigma_{vi}$	L_a	Lc	2001 T_{ml}	2009 T_{ml}
1	0.10	1.80	0.20	0.80	1.90	4.71	0.05	0.75	2.07	1.043
2	0.30	1.60	0.20	0.80	1.88	4.18	0.14	0.66	1.81	1.043
3	0.50	1.40	0.20	0.80	1.88	3.66	0.23	0.57	1.55	1.043
4	0.70	1.20	0.20	0.80	1.88	3.14	0.33	0.47	1.30	1.043
5	0.90	1.00	0.20	0.80	1.88	2.61	0.42	0.38	1.04	1.043
6	1.10	0.80	0.20	0.80	1.88	2.09	0.51	0.29	0.79	1.043
7	1.30	0.60	0.20	0.80	1.88	1.57	0.61	0.19	0.53	1.043
8	1.50	0.40	0.20	0.80	1.88	1.05	0.70	0.10	0.28	1.043
9	1.70	0.20	0.28	0.80	1.88	0.52	0.79	0.01	0.02	1.043

(b)

Table E.13. Calculation of Tensile Load in Geogrids for Wall 2-El Centro 200% using a)NCMA Segmental Retaining Walls Seismic Design Manual b) FHWA Recommendations

Calculation of Tensile Load in Geogrids for Wall 2-El Centro 200% using NCMA Segmental Retaining Walls Seismic Design Manu

A=a_max(rock)/g	0.74		H	1.90	Φ	(backfill)	40.00	
k_h (int)	0.525		L	0.90	γ	(backfill)	17.50	
θ (int)	27.72	0.48			Mobilized interface friction angle, δ	(backfill)	40.00	
k_h (ext)	0.37				Φ	(reinforced soil)	40.00	
θ (ext)	20.30	0.35			γ	(reinforced soil)	17.50	
K_A	0.195		K_AH	0.15				
K_AE (int)	0.628		K_AEH (int)	0.48				
ΔK_dyn (int)	0.43		ΔK_dynH (int)	0.33	Block depth		0.10	
K_AE (ext)	0.460		K_AEH (ext)	0.35	Block unit weight		21.00	
ΔK_dyn (ext)	0.26		ΔK_dynH (ext)	0.20				
W_w	3.99							
W_s	26.60		W_s'	28.26				
W_r	30.59							
R_c	25.67							
P_IR	11.93							
P_AEH	7.92							
FS_sliding	1.29							
FS_overturning	0.75							

Reinforcement loads

Layer Number	Elevation	Z_ci	S_ci	L_i	H	F_static i	F_inertial i	F_dyn i	ΔF_seismic
1	0.10	1.80	0.20	0.80	1.90	0.94	0.22	0.51	0.73
2	0.30	1.60	0.20	0.80	1.90	0.84	0.22	0.65	0.87
3	0.50	1.40	0.20	0.80	1.90	0.73	0.22	0.79	1.01
4	0.70	1.20	0.20	0.80	1.90	0.63	0.22	0.93	1.15
5	0.90	1.00	0.20	0.80	1.90	0.52	0.22	1.07	1.29
6	1.10	0.80	0.20	0.80	1.90	0.42	0.22	1.21	1.43
7	1.30	0.60	0.20	0.80	1.90	0.31	0.22	1.35	1.57
8	1.50	0.40	0.20	0.80	1.90	0.21	0.22	1.49	1.71
9	1.70	0.20	0.30	0.80	1.90	0.16	0.33	2.44	2.77

(a)

Calculation of Tensile Load in Geogrids for Wall 2-El Centro 200% using FHWA Recommendations

a_max(rock)/g	0.74		H	1.90	Φ	(backfill)	40.00	
A_m	0.525		L	0.90	γ	(backfill)	17.50	
θ	27.72	0.48			Mobilized interface friction angle	(backfill)	40.00	
K_A	0.195		K_AH	0.15	Φ	(reinforced soil)	40.00	
K_AE	0.628		K_AEH	0.48	γ	(reinforced soil)	17.50	
ΔK_dyn	0.43		ΔK_dynH	0.33	Mobilized interface friction angle	(reinforced soil)	26.67	
W_w	3.99				Block depth		0.10	
W_s	26.60		W_s'	28.26	Block unit weight		21.00	
W_r	30.59		W_A	18.72				
R_c	25.67							
P_IR	16.95		P_I	9.84				
P_AEH	9.96							
FS_sl	0.95							

Tensile stresses in geotextiles

Layer Number	Elevation	Z_ci	S_ci	L_i	H	K σ_ci	L_ai	Le	2001 T_mi	2009 T_mi
1	0.10	1.80	0.20	0.80	1.90	4.71	0.05	0.75	2.16	1.093
2	0.30	1.60	0.20	0.80	1.88	4.18	0.14	0.66	1.90	1.093
3	0.50	1.40	0.20	0.80	1.88	3.66	0.23	0.57	1.63	1.093
4	0.70	1.20	0.20	0.80	1.88	3.14	0.33	0.47	1.36	1.093
5	0.90	1.00	0.20	0.80	1.88	2.61	0.42	0.38	1.09	1.093
6	1.10	0.80	0.20	0.80	1.88	2.09	0.51	0.29	0.82	1.093
7	1.30	0.60	0.20	0.80	1.88	1.57	0.61	0.19	0.56	1.093
8	1.50	0.40	0.20	0.80	1.88	1.05	0.70	0.10	0.29	1.093
9	1.70	0.20	0.28	0.80	1.88	0.52	0.79	0.01	0.02	1.093

(b)

Table E.14. Calculation of Tensile Load in Geogrids for Wall 2-Izmit 100% using a)NCMA Segmental Retaining Walls Seismic Design Manual b) FHWA Recommendations

Calculation of Tensile Load in Geogrids for Wall 2-Izmit 100% using NCMA Segmental Retaining Walls Seismic Design Manual

A $a_{max(static)}/g$	0.2					Φ	(backfill)	40.00
k_h (int)	0.250		H	1.90		γ	(backfill)	17.50
θ (int)	14.04	0.24	L	0.90		Mobilized interface friction angle, δ	(backfill)	40.00
k_h (ext)	0.10					Φ	(reinforced soil)	40.00
θ (ext)	5.71	0.10				γ	(reinforced soil)	17.50
K_A	0.195		K_{AH}	0.15				
K_{AE} (int)	0.363		K_{AEH} (int)	0.28				
ΔK_{dyn} (int)	0.17		ΔK_{dynH} (int)	0.13		Block depth	0.10	
K_{AE} (ext)	0.268		K_{AEH} (ext)	0.21		Block unit weight	21.00	
ΔK_{dyn} (ext)	0.07		ΔK_{dynH} (ext)	0.06				
W_w	3.99							
W_s	26.60		W_s'	28.26				
W_r	30.59							
R_S	25.67							
P_{IE}	3.23							
P_{AEH}	5.60							
$FS_{sliding}$	2.91							
$FS_{overturning}$	1.91							

Reinforcement loads

Layer Number	Elevation	Z_{wi}	S_{vi}	L_i	H	F_{static}	$F_{inertial}$	F_{dyn}	$\Delta F_{seismic}$
1	0.10	1.80	0.20	0.80	1.90	0.94	0.11	0.20	0.30
2	0.30	1.60	0.20	0.80	1.90	0.84	0.11	0.25	0.36
3	0.50	1.40	0.20	0.80	1.90	0.73	0.11	0.31	0.41
4	0.70	1.20	0.20	0.80	1.90	0.63	0.11	0.36	0.46
5	0.90	1.00	0.20	0.80	1.90	0.52	0.11	0.41	0.52
6	1.10	0.80	0.20	0.80	1.90	0.42	0.11	0.47	0.57
7	1.30	0.60	0.20	0.80	1.90	0.31	0.11	0.52	0.63
8	1.50	0.40	0.20	0.80	1.90	0.21	0.11	0.58	0.68
9	1.70	0.20	0.30	0.80	1.90	0.16	0.16	0.94	1.10

(a)

Calculation of Tensile Load in Geogrids for Wall 2-Izmit 100% using FHWA Recommendations

$a_{max(static)}/g$	0.2					Φ	(backfill)	40.00
A_m	0.250		H	1.90		γ	(backfill)	17.50
θ	14.04	0.24	L	0.90		Mobilized interface friction angle	(backfill)	40.00
K_A	0.195		K_{AH}	0.15		Φ	(reinforced soil)	40.00
K_{AE}	0.363		K_{AEH}	0.28		γ	(reinforced soil)	17.50
ΔK_{dyn}	0.17		ΔK_{dynH}	0.13		Mobilized interface friction angle	(reinforced soil)	26.67
W_w	3.99					Block depth	0.10	
W_s	26.60		W_s'	28.26		Block unit weight	21.00	
W_r	30.59		W_A	18.72				
R_S	25.67							
P_{IE}	8.06		P_I	4.68				
P_{AEH}	6.75							
FS_{sl}	1.73							

Tensile stresses in geotextiles

Layer Number	Elevation	Z_{wi}	S_{vi}	L_i	H	$K\sigma_{vi}$	L_a	Le	2001 T_{ad}	2009 T_{ad}
1	0.10	1.80	0.20	0.80	1.90	4.71	0.05	0.75	1.03	0.520
2	0.30	1.60	0.20	0.80	1.88	4.18	0.14	0.66	0.90	0.520
3	0.50	1.40	0.20	0.80	1.88	3.66	0.23	0.57	0.78	0.520
4	0.70	1.20	0.20	0.80	1.88	3.14	0.33	0.47	0.65	0.520
5	0.90	1.00	0.20	0.80	1.88	2.61	0.42	0.38	0.52	0.520
6	1.10	0.80	0.20	0.80	1.88	2.09	0.51	0.29	0.39	0.520
7	1.30	0.60	0.20	0.80	1.88	1.57	0.61	0.19	0.26	0.520
8	1.50	0.40	0.20	0.80	1.88	1.05	0.70	0.10	0.14	0.520
9	1.70	0.20	0.28	0.80	1.88	0.52	0.79	0.01	0.01	0.520

(b)

Table E.15. Calculation of Tensile Load in Geogrids for Wall 2-Izmit 150% using a)NCMA Segmental Retaining Walls Seismic Design Manual b) FHWA Recommendations

Calculation of Tensile Load in Geogrids for Wall 2-Izmit 150% using NCMA Segmental Retaining Walls Seismic Design Manual

$A=a_{max(table)}/g$	0.29								
k_h (int)	0.336		H	1.90		Φ	(backfill)	40.00	
θ (int)	18.59	0.32	L	0.90		γ	(backfill)	17.50	
k_h (ext)	0.15					Mobilized interface friction angle, δ	(backfill)	40.00	
θ (ext)	8.25	0.14				Φ	(reinforced soil)	40.00	
K_A	0.195		K_{AH}	0.15		γ	(reinforced soil)	17.50	
K_{AE} (int)	0.430		$K_{AEH(int)}$	0.33					
$\Delta K_{dyn(int)}$	0.24		$\Delta K_{dynH(int)}$	0.18		Block depth		0.10	
K_{AE} (ext)	0.294		$K_{AEH(ext)}$	0.23		Block unit weight		21.00	
$\Delta K_{dyn(ext)}$	0.10		$\Delta K_{dynH(ext)}$	0.08					
W_w	3.99								
W_s	26.60		W_s'	28.26					
W_r	30.59								
R_R	25.67								
P_{IR}	4.68								
P_{AEH}	5.92								
$FS_{sliding}$	2.42								
$FS_{overturning}$	1.53								

Reinforcement loads

Layer Number	Elevation	Z_{wi}	S_{vi}	L_{ri}	H	$F_{static\,i}$	$F_{inertial\,i}$	$F_{dyn\,i}$	$AF_{seismic}$
1	0.10	1.80	0.20	0.80	1.90	0.94	0.14	0.28	0.42
2	0.30	1.60	0.20	0.80	1.90	0.84	0.14	0.35	0.49
3	0.50	1.40	0.20	0.80	1.90	0.73	0.14	0.43	0.57
4	0.70	1.20	0.20	0.80	1.90	0.63	0.14	0.50	0.65
5	0.90	1.00	0.20	0.80	1.90	0.52	0.14	0.58	0.72
6	1.10	0.80	0.20	0.80	1.90	0.42	0.14	0.66	0.80
7	1.30	0.60	0.20	0.80	1.90	0.31	0.14	0.73	0.87
8	1.50	0.40	0.20	0.80	1.90	0.21	0.14	0.81	0.95
9	1.70	0.20	0.30	0.80	1.90	0.16	0.21	1.32	1.54

(a)

Calculation of Tensile Load in Geogrids for Wall 2-Izmit 150% using FHWA Recommendations

$a_{max(table)}/g$	0.29								
A_m	0.336		H	1.90		Φ	(backfill)	40.00	
θ	18.59	0.32	L	0.90		γ	(backfill)	17.50	
K_A	0.195		K_{AH}	0.15		Mobilized interface friction angle	(backfill)	40.00	
K_{AE}	0.430		K_{AEH}	0.33		Φ	(reinforced soil)	40.00	
ΔK_{dyn}	0.24		ΔK_{dynH}	0.18		γ	(reinforced soil)	17.50	
						Mobilized interface friction angle	(reinforced soil)	26.67	
W_w	3.99					Block depth		0.10	
W_s	26.60		W_s'	28.26		Block unit weight		21.00	
W_r	30.59		W_A	18.72					
R_R	25.67								
P_{IR}	10.85		P_I	6.30					
P_{AEH}	7.56								
FS_{sl}	1.39								

Tensile stresses in geotextiles

									2001	2009
Layer Number	Elevation	Z_{wi}	S_{vi}	L_{ri}	H	$K\sigma_{vi}$	L_a	Le	T_{mal}	T_{mal}
1	0.10	1.80	0.20	0.80	1.90	4.71	0.05	0.75	1.39	0.700
2	0.30	1.60	0.20	0.80	1.88	4.18	0.14	0.66	1.21	0.700
3	0.50	1.40	0.20	0.80	1.88	3.66	0.23	0.57	1.04	0.700
4	0.70	1.20	0.20	0.80	1.88	3.14	0.33	0.47	0.87	0.700
5	0.90	1.00	0.20	0.80	1.88	2.61	0.42	0.38	0.70	0.700
6	1.10	0.80	0.20	0.80	1.88	2.09	0.51	0.29	0.53	0.700
7	1.30	0.60	0.20	0.80	1.88	1.57	0.61	0.19	0.36	0.700
8	1.50	0.40	0.20	0.80	1.88	1.05	0.70	0.10	0.18	0.700
9	1.70	0.20	0.28	0.80	1.88	0.52	0.79	0.01	0.01	0.700

(b)

Table E.16. Calculation of Tensile Load in Geogrids for Wall 2-Izmit 200% using a)NCMA Segmental Retaining Walls Seismic Design Manual b) FHWA Recommendations

Calculation of Tensile Load in Geogrids for Wall 2-Izmit 200% using NCMA Segmental Retaining Walls Seismic Design Manual

$A=a_{max(table)}/g$	0.34				
k_h (int)	0.377		H	1.90	
θ (int)	20.68	0.36	L	0.90	
k_h (ext)	0.17				
θ (ext)	9.65	0.17			
K_A	0.195		K_{AH}	0.15	
K_{AE} (int)	0.466		$K_{AEH(int)}$	0.36	
$\Delta K_{dyn(int)}$	0.27		$\Delta K_{dynH(int)}$	0.21	
K_{AE} (ext)	0.309		$K_{AEH(ext)}$	0.24	
$\Delta K_{dyn(ext)}$	0.11		$\Delta K_{dynH(ext)}$	0.09	

Φ	(backfill)	40.00	
γ	(backfill)	17.50	
Mobilized interface friction angle, δ	(backfill)	40.00	
Φ	(reinforced soil)	40.00	
γ	(reinforced soil)	17.50	

Block depth	0.10
Block unit weight	21.00

W_w	3.99		
W_i	26.60	W_i'	28.26
W_r	30.59		

R_S	25.67
P_{IE}	5.48
P_{AEH}	6.10
$FS_{sliding}$	2.22
$FS_{(overturning)}$	1.38

Reinforcement loads

Layer Number	Elevation	Z_{wi}	S_{wi}	L_i	H	$F_{static\,i}$	$F_{inertial\,i}$	$F_{dyn\,i}$	$\Delta F_{seismic}$
1	0.10	1.80	0.20	0.80	1.90	0.94	0.16	0.32	0.48
2	0.30	1.60	0.20	0.80	1.90	0.84	0.16	0.41	0.57
3	0.50	1.40	0.20	0.80	1.90	0.73	0.16	0.49	0.65
4	0.70	1.20	0.20	0.80	1.90	0.63	0.16	0.58	0.74
5	0.90	1.00	0.20	0.80	1.90	0.52	0.16	0.67	0.83
6	1.10	0.80	0.20	0.80	1.90	0.42	0.16	0.76	0.92
7	1.30	0.60	0.20	0.80	1.90	0.31	0.16	0.84	1.00
8	1.50	0.40	0.20	0.80	1.90	0.21	0.16	0.93	1.09
9	1.70	0.20	0.30	0.80	1.90	0.16	0.24	1.53	1.77

(a)

Calculation of Tensile Load in Geogrids for Wall 2-Izmit 200% using FHWA Recommendations

$a_{max(table)}/g$	0.34				
A_m	0.377		H	1.90	
θ	20.68	0.36	L	0.90	
K_A	0.195		K_{AH}	0.15	
K_{AE}	0.466		K_{AEH}	0.36	
ΔK_{dyn}	0.27		ΔK_{dynH}	0.21	

Φ	(backfill)	40.00	
γ	(backfill)	17.50	
Mobilized interface friction angle	(backfill)	40.00	
Φ	(reinforced soil)	40.00	
γ	(reinforced soil)	17.50	
Mobilized interface friction angle	(reinforced soil)	26.07	

Block depth	0.10
Block unit weight	21.00

W_w	3.99			
W_i	26.60	W_i'	28.26	
W_r	30.59	W_A	18.72	

R_S	25.67
P_{IE}	12.17
P_{AEH}	8.00
FS_{sl}	1.27

P_I	7.06		

Tensile stresses in geotextiles

Layer Number	Elevation	Z_{wi}	S_{wi}	L_i	H	$K\sigma_{wi}$	L_a	Le	2001 T_{md}	2009 T_{md}
1	0.10	1.80	0.20	0.80	1.90	4.71	0.05	0.75	1.55	0.785
2	0.30	1.60	0.20	0.80	1.88	4.18	0.14	0.66	1.36	0.785
3	0.50	1.40	0.20	0.80	1.88	3.66	0.23	0.57	1.17	0.785
4	0.70	1.20	0.20	0.80	1.88	3.14	0.33	0.47	0.98	0.785
5	0.90	1.00	0.20	0.80	1.88	2.61	0.42	0.38	0.78	0.785
6	1.10	0.80	0.20	0.80	1.88	2.09	0.51	0.29	0.59	0.785
7	1.30	0.60	0.20	0.80	1.88	1.57	0.61	0.19	0.40	0.785
8	1.50	0.40	0.20	0.80	1.88	1.05	0.70	0.10	0.21	0.785
9	1.70	0.20	0.28	0.80	1.88	0.52	0.79	0.01	0.02	0.785

(b)

Table E.17. Calculation of Tensile Load in Geogrids for Wall 2-Sakarya 100% using a)NCMA Segmental Retaining Walls Seismic Design Manual b) FHWA Recommendations

Calculation of Tensile Load in Geogrids for Wall 2-Sakarya 100% using NCMA Segmental Retaining Walls Seismic Design Manual

$A=a_{max(table)}/g$	0.23							
k_h (int)	0.281		H	1.90	Φ	(backfill)	40.00	
θ (int)	15.67	0.27	L	0.90	γ	(backfill)	17.50	
k_h (ext)	0.12				Mobilized interface friction angle, δ	(backfill)	40.00	
θ (ext)	6.56	0.11			Φ	(reinforced soil)	40.00	
K_A	0.195		K_{AH}	0.15	γ	(reinforced soil)	17.50	
K_{AE} (int)	0.385		$K_{AEH(int)}$	0.30				
$\Delta K_{dyn(int)}$	0.19		$\Delta K_{dynH(int)}$	0.15		Block depth	0.10	
K_{AE} (ext)	0.277		$K_{AEH(ext)}$	0.21		Block unit weight	21.00	
$\Delta K_{dyn(ext)}$	0.08		$\Delta K_{dynH(ext)}$	0.06				
W_w	3.99							
W_s	26.60		W_s'	28.26				
W_r	30.59							
R_S	25.67							
P_{IR}	3.71							
P_{AEH}	5.71							
$FS_{sliding}$	2.73							
$FS_{overturning}$	1.77							

Reinforcement loads

Layer Number	Elevation	Z_{vi}	S_{vi}	L_i	H	$F_{static\,i}$	$F_{inertial\,i}$	$F_{dyn\,i}$	$\Delta F_{seismic}$
1	0.10	1.80	0.20	0.80	1.90	0.94	0.12	0.22	0.34
2	0.30	1.60	0.20	0.80	1.90	0.84	0.12	0.29	0.40
3	0.50	1.40	0.20	0.80	1.90	0.73	0.12	0.35	0.47
4	0.70	1.20	0.20	0.80	1.90	0.63	0.12	0.41	0.53
5	0.90	1.00	0.20	0.80	1.90	0.52	0.12	0.47	0.59
6	1.10	0.80	0.20	0.80	1.90	0.42	0.12	0.53	0.65
7	1.30	0.60	0.20	0.80	1.90	0.31	0.12	0.59	0.71
8	1.50	0.40	0.20	0.80	1.90	0.21	0.12	0.65	0.77
9	1.70	0.20	0.30	0.80	1.90	0.16	0.18	1.07	1.25

(a)

Calculation of Tensile Load in Geogrids for Wall 2-Sakarya 100% using FHWA Recommendations

$a_{max(table)}/g$	0.23							
A_m	0.281		H	1.90	Φ	(backfill)	40.00	
θ	15.67	0.27	L	0.90	γ	(backfill)	17.50	
K_A	0.195		K_{AH}	0.15	Mobilized interface friction angle	(backfill)	40.00	
K_{AE}	0.385		K_{AEH}	0.30	Φ	(reinforced soil)	40.00	
ΔK_{dyn}	0.19		ΔK_{dynH}	0.15	γ	(reinforced soil)	17.50	
					Mobilized interface friction angle	(reinforced soil)	26.67	
W_w	3.99				Block depth		0.10	
W_s	26.60		W_s'	28.26	Block unit weight		21.00	
W_r	30.59		W_A	18.72				
R_S	25.67							
P_{IR}	9.05		P_I	5.25				
P_{AEH}	7.02							
FS_{sl}	1.60							

Tensile stresses in geotextiles

Layer Number	Elevation	Z_{vi}	S_{vi}	L_i	H	$K\sigma_{vi}$	L_a	Le	2001 T_{ad}	2009 T_{ad}
1	0.10	1.80	0.20	0.80	1.90	4.71	0.05	0.75	1.16	0.584
2	0.30	1.60	0.20	0.80	1.88	4.18	0.14	0.66	1.01	0.584
3	0.50	1.40	0.20	0.80	1.88	3.66	0.23	0.57	0.87	0.584
4	0.70	1.20	0.20	0.80	1.88	3.14	0.33	0.47	0.73	0.584
5	0.90	1.00	0.20	0.80	1.88	2.61	0.42	0.38	0.58	0.584
6	1.10	0.80	0.20	0.80	1.88	2.09	0.51	0.29	0.44	0.584
7	1.30	0.60	0.20	0.80	1.88	1.57	0.61	0.19	0.30	0.584
8	1.50	0.40	0.20	0.80	1.88	1.05	0.70	0.10	0.15	0.584
9	1.70	0.20	0.28	0.80	1.88	0.52	0.79	0.01	0.01	0.584

(b)

Table E.18. Calculation of Tensile Load in Geogrids for Wall 2-Sakarya 150% using a)NCMA Segmental Retaining Walls Seismic Design Manual b) FHWA Recommendations

Calculation of Tensile Load in Geogrids for Wall 2-Sakarya 150% using NCMA Segmental Retaining Walls Seismic Design Manual

A = $a_{max(table)}/g$	0.32						
k_h (int)	0.362		H	1.90	Φ	(backfill)	40.00
θ (int)	19.88	0.35	L	0.90	γ	(backfill)	17.50
k_h (ext)	0.16				Mobilized interface friction angle, δ	(backfill)	40.00
θ (ext)	9.09	0.16			Φ	(reinforced soil)	40.00
K_A	0.195		K_{AH}	0.15	γ	(reinforced soil)	17.50
K_{AE} (int)	0.452		K_{AEH} (int)	0.35			
ΔK_{dyn} (int)	0.26		ΔK_{dynH} (int)	0.20	Block depth	0.10	
K_{AE} (ext)	0.303		K_{AEH} (ext)	0.23	Block unit weight	21.00	
ΔK_{dyn} (ext)	0.11		ΔK_{dynH} (ext)	0.08			
W_w	3.99						
W_s	26.60		W_s'	28.26			
W_r	30.59						
R_R	25.67						
P_{IE}	5.16						
P_{AEH}	6.03						
$FS_{sliding}$	2.29						
$FS_{overturning}$	1.44						

Reinforcement loads

Layer Number	Elevation	Z_{wi}	S_{vi}	L_i	H	F_{static}	$F_{inertial}$	F_{dyn}	$AF_{seismic}$
1	0.10	1.80	0.20	0.80	1.90	0.94	0.15	0.30	0.46
2	0.30	1.60	0.20	0.80	1.90	0.84	0.15	0.39	0.54
3	0.50	1.40	0.20	0.80	1.90	0.73	0.15	0.47	0.62
4	0.70	1.20	0.20	0.80	1.90	0.63	0.15	0.55	0.70
5	0.90	1.00	0.20	0.80	1.90	0.52	0.15	0.63	0.79
6	1.10	0.80	0.20	0.80	1.90	0.42	0.15	0.72	0.87
7	1.30	0.60	0.20	0.80	1.90	0.31	0.15	0.80	0.95
8	1.50	0.40	0.20	0.80	1.90	0.21	0.15	0.88	1.03
9	1.70	0.20	0.30	0.80	1.90	0.16	0.23	1.45	1.68

(a)

Calculation of Tensile Load in Geogrids for Wall 2-Sakarya 150% using FHWA Recommendations

$a_{max(table)}/g$	0.32						
A_m	0.362		H	1.90	Φ	(backfill)	40.00
θ	19.88	0.35	L	0.90	γ	(backfill)	17.50
K_A	0.195		K_{AH}	0.15	Mobilized interface friction angle	(backfill)	40.00
K_{AE}	0.452		K_{AEH}	0.35	Φ	(reinforced soil)	40.00
ΔK_{dyn}	0.26		ΔK_{dynH}	0.20	γ	(reinforced soil)	17.50
					Mobilized interface friction angle	(reinforced soil)	26.67
W_w	3.99				Block depth	0.10	
W_s	26.60		W_s'	28.26	Block unit weight	21.00	
W_r	30.59		W_A	18.72			
R_R	25.67						
P_{IE}	11.66		P_I	6.77			
P_{AEH}	7.83						
FS_{sl}	1.32						

Tensile stresses in geotextiles

Layer Number	Elevation	Z_{wi}	S_{vi}	L_i	H	$K\sigma_{vi}$	L_a	Lc	2001 T_{ad}	2009 T_{ad}
1	0.10	1.80	0.20	0.80	1.90	4.71	0.05	0.75	1.49	0.752
2	0.30	1.60	0.20	0.80	1.88	4.18	0.14	0.66	1.31	0.752
3	0.50	1.40	0.20	0.80	1.88	3.66	0.23	0.57	1.12	0.752
4	0.70	1.20	0.20	0.80	1.88	3.14	0.33	0.47	0.94	0.752
5	0.90	1.00	0.20	0.80	1.88	2.61	0.42	0.38	0.75	0.752
6	1.10	0.80	0.20	0.80	1.88	2.09	0.51	0.29	0.57	0.752
7	1.30	0.60	0.20	0.80	1.88	1.57	0.61	0.19	0.38	0.752
8	1.50	0.40	0.20	0.80	1.88	1.05	0.70	0.10	0.20	0.752
9	1.70	0.20	0.28	0.80	1.88	0.52	0.79	0.01	0.01	0.752

(b)

Table E.19. Calculation of Tensile Load in Geogrids for Wall 2-Sakarya 200% using a)NCMA Segmental Retaining Walls Seismic Design Manual b) FHWA Recommendations

Calculation of Tensile Load in Geogrids for Wall 2-Sakarya 200% using NCMA Segmental Retaining Walls Seismic Design Manual

$A=a_{max(table)}/g$	0.42						
k_h (int)	0.433		H	1.90	Φ	(backfill)	40.00
θ (int)	23.39	0.41	L	0.90	γ	(backfill)	17.50
k_h (ext)	0.21				Mobilized interface friction angle, δ	(backfill)	40.00
θ (ext)	11.86	0.21			Φ	(reinforced soil)	40.00
K_A	0.195		K_{AH}	0.15	γ	(reinforced soil)	17.50
K_{AE} (int)	0.520		$K_{AEH\ (int)}$	0.40			
$\Delta K_{dyn\ (int)}$	0.33		$\Delta K_{dynH\ (int)}$	0.25	Block depth	0.10	
K_{AE} (ext)	0.335		$K_{AEH\ (ext)}$	0.26	Block unit weight	21.00	
$\Delta K_{dyn\ (ext)}$	0.14		$\Delta K_{dynH\ (ext)}$	0.11			
W_w	3.99						
W_s	26.60		W_s'	28.26			
W_r	30.59						
R_E	25.67						
P_{IE}	6.77						
P_{AEH}	6.41						
$FS_{sliding}$	1.95						
$FS_{overturning}$	1.19						

Reinforcement loads

Layer Number	Elevation	Z_w	S_w	L_e	H	$F_{max\ e}$	$F_{internal}$	F_{dyn}	$AF_{seismic}$
1	0.10	1.80	0.20	0.80	1.90	0.94	0.18	0.38	0.57
2	0.30	1.60	0.20	0.80	1.90	0.84	0.18	0.49	0.67
3	0.50	1.40	0.20	0.80	1.90	0.73	0.18	0.59	0.77
4	0.70	1.20	0.20	0.80	1.90	0.63	0.18	0.70	0.88
5	0.90	1.00	0.20	0.80	1.90	0.52	0.18	0.80	0.98
6	1.10	0.80	0.20	0.80	1.90	0.42	0.18	0.91	1.09
7	1.30	0.60	0.20	0.80	1.90	0.31	0.18	1.01	1.19
8	1.50	0.40	0.20	0.80	1.90	0.21	0.18	1.12	1.30
9	1.70	0.20	0.30	0.80	1.90	0.16	0.27	1.83	2.10

(a)

Calculation of Tensile Load in Geogrids for Wall 2-Sakarya 200% using FHWA Recommendations

$a_{max(table)}/g$	0.42						
A_m	0.433		H	1.90	Φ	(backfill)	40.00
θ	23.39	0.41	L	0.90	γ	(backfill)	17.50
K_A	0.195		K_{AH}	0.15	Mobilized interface friction angle	(backfill)	40.00
K_{AE}	0.520		K_{AEH}	0.40	Φ	(reinforced soil)	40.00
ΔK_{dyn}	0.33		ΔK_{dynH}	0.25	γ	(reinforced soil)	17.50
					Mobilized interface friction angle	(reinforced soil)	26.67
W_w	3.99				Block depth	0.10	
W_s	26.60		W_s'	28.26	Block unit weight	21.00	
W_r	30.59		W_A	18.72			
R_E	25.67						
P_{IE}	13.95		P_I	8.10			
P_{AEH}	8.66						
FS_d	1.14						

Tensile stresses in geotextiles

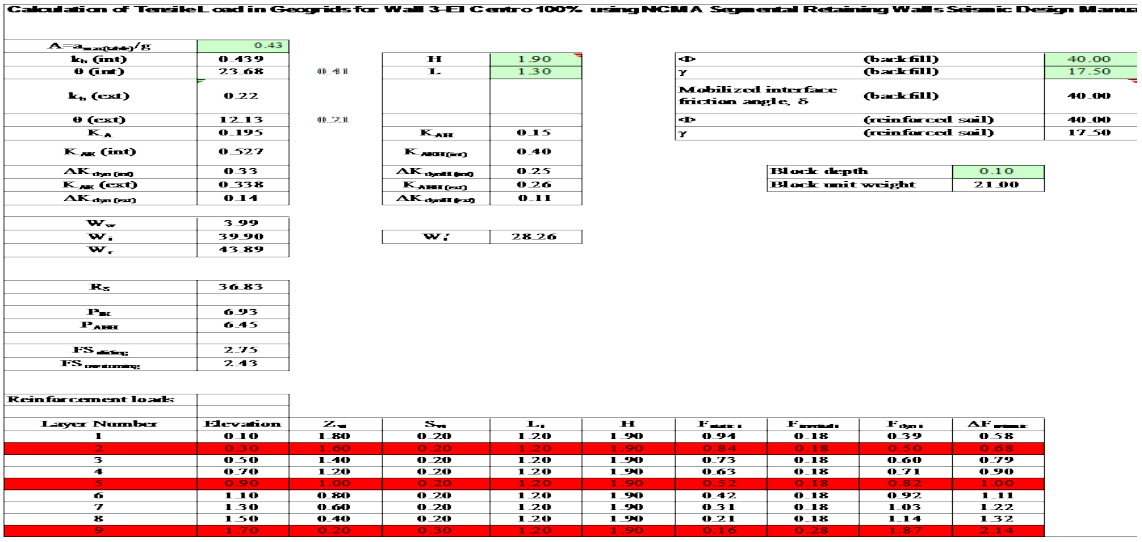
Layer Number	Elevation	Z_w	S_w	L_e	H	$K\sigma_w$	L_a	Le	2001 T_{al}	2009 T_{al}
1	0.10	1.80	0.20	0.80	1.90	4.71	0.05	0.75	1.78	0.900
2	0.30	1.60	0.20	0.80	1.88	4.18	0.14	0.66	1.56	0.900
3	0.50	1.40	0.20	0.80	1.88	3.66	0.23	0.57	1.34	0.900
4	0.70	1.20	0.20	0.80	1.88	3.14	0.33	0.47	1.12	0.900
5	0.90	1.00	0.20	0.80	1.88	2.61	0.42	0.38	0.90	0.900
6	1.10	0.80	0.20	0.80	1.88	2.09	0.51	0.29	0.68	0.900
7	1.30	0.60	0.20	0.80	1.88	1.57	0.61	0.19	0.46	0.900
8	1.50	0.40	0.20	0.80	1.88	1.05	0.70	0.10	0.24	0.900
9	1.70	0.20	0.28	0.80	1.88	0.52	0.79	0.01	0.02	0.900

(b)

Table E.20. Comparison of Calculatedand Measured Seismic Induced Tensile Loads in Geogrids for Wall 2

Wall / Base Excitation	Maximum Table Acceleration-Base Input (g)	Design (NCMA) ΔTmax in lower geogrid (@h=0.2 m) (kN/m)	Design (FHWA2001) ΔTmax in lower geogrid (@h=0.2 m) (kN/m)	Design (FHWA2009) ΔTmax in lower geogrid (@h=0.2 m) (kN/m)	Measured Geogrid Stress Max Stresses (peak values) (kN/m)	Design (NCMA) ΔTmax at midheight geogrid (@h=1 m) (kN/m)	Design (FHWA2001) ΔTmax at midheight geogrid (@h=1 m) (kN/m)	Design (FHWA2009) ΔTmax at midheight geogrid (@h=1 m) (kN/m)	Measured Geogrid Stress Max Stresses (peak values) (kN/m)	Design (NCMA) ΔTmax in upper geogrid (@h=1.8 m) (kN/m)	Design (FHWA2001) ΔTmax in upper geogrid (@h=1.8 m) (kN/m)	Design (FHWA2009) ΔTmax in upper geogrid (@h=1.8 m) (kN/m)	Measured Geogrid Stress Max Stresses (peak values) (kN/m)
Wall 2 / El Centro 100%	0.43	0.68	1.58	0.91	3.57	1.00	0.91	0.91	2.57	2.14	0.02	0.91	1.23
Wall 2 / El Centro 150%	0.57	0.82	1.81	1.04	5.15	1.20	1.04	1.04	4.35	2.58	0.02	1.04	1.84
Wall 2 / El Centro 200%	0.73	0.87	1.90	1.09	7.17	1.29	1.09	1.09	4.91	2.77	0.02	1.09	1.19
Wall 2 / Izmit 100%	0.2	0.36	0.90	0.52	1.21	0.52	0.52	0.52	0.81	1.10	0.01	0.52	0.36
Wall 2 / Izmit 150%	0.28	0.49	1.21	0.70	1.65	0.72	0.70	0.70	1.24	1.54	0.01	0.70	0.49
Wall 2 / Izmit 200%	0.34	0.57	1.36	0.78	2.3	0.83	0.78	0.78	1.63	1.77	0.02	0.78	0.56
Wall 2 / Sakarya 100%	0.23	0.40	1.01	0.58	1.35	0.59	0.58	0.58	0.78	1.25	0.01	0.58	0.38
Wall 2 / Sakarya 150%	0.32	0.54	1.31	0.75	2.04	0.79	0.75	0.75	1.4	1.68	0.01	0.75	0.46
Wall 2 / Sakarya 200%	0.42	0.67	1.56	0.90	3.23	0.98	0.90	0.90	2.04	2.10	0.02	0.90	0.7

Table E.21. Calculation of Tensile Load in Geogrids for Wall 3-El Centro 100% using a)NCMA Segmental Retaining Walls Seismic Design Manual b) FHWA Recommendations



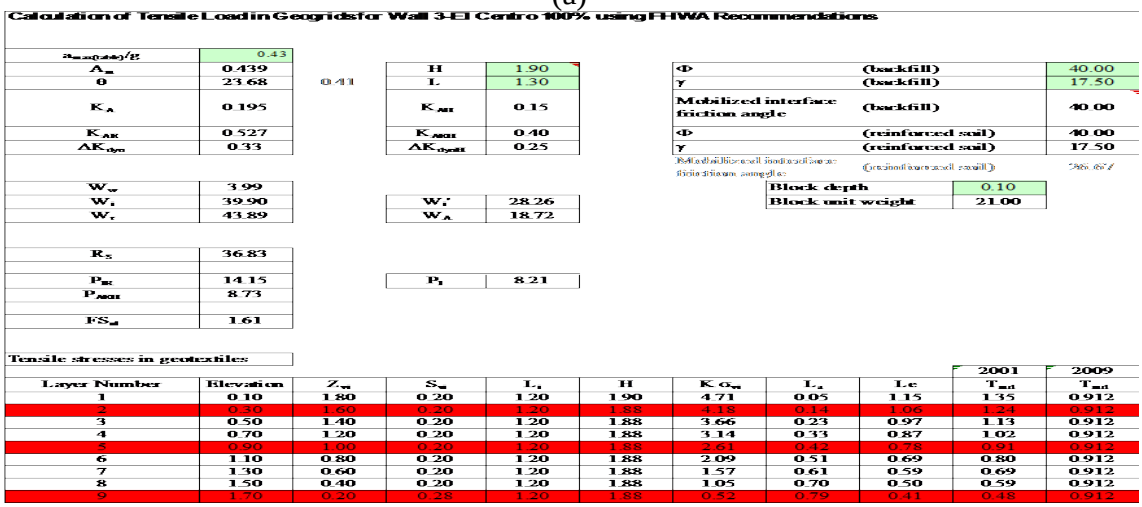
Calculation of Tensile Load in Geogrids for Wall 3-El Centro 100% using NCMA Segmental Retaining Walls Seismic Design Manu

$A=a_{max(0.43g)}/g$	0.43		H	1.90	Φ	(backfill)	40.00		
k_h (int)	0.439		L	1.30	γ	(backfill)	17.50		
θ (int)	23.68	0.41			Mobilized interface friction angle, δ	(backfill)	40.00		
k_h (ext)	0.22				Φ	(reinforced soil)	40.00		
θ (ext)	12.13	0.21			γ	(reinforced soil)	17.50		
K_A	0.195		K_{AH}	0.15					
K_{AE} (int)	0.527		$K_{AEH(int)}$	0.40					
$\Delta K_{dyn\,(int)}$	0.33		$\Delta K_{dynH\,(int)}$	0.25	Block depth	0.10			
K_{AE} (ext)	0.338		$K_{AEH\,(ext)}$	0.26	Block unit weight	21.00			
$\Delta K_{dyn\,(ext)}$	0.14		$\Delta K_{dynH\,(ext)}$	0.11					
W_w	3.99								
W_s	39.90		W_s'	28.26					
W_r	43.89								
R_x	36.83								
P_{IE}	6.93								
P_{AEH}	6.45								
$FS_{sliding}$	2.75								
$FS_{overturning}$	2.43								

Reinforcement loads:

Layer Number	Elevation	Z_w	S_v	L_1	H	F_{max1}	F_{max2}	F_{dyn}	ΔF_{max}
1	0.10	1.80	0.20	1.20	1.90	0.94	0.18	0.39	0.58
2	0.30	1.60	0.20	1.20	1.90	0.84	0.18	0.50	0.68
3	0.50	1.40	0.20	1.20	1.90	0.73	0.18	0.60	0.79
4	0.70	1.20	0.20	1.20	1.90	0.63	0.18	0.71	0.90
5	0.90	1.00	0.20	1.20	1.90	0.52	0.18	0.82	1.00
6	1.10	0.80	0.20	1.20	1.90	0.42	0.18	0.92	1.11
7	1.30	0.60	0.20	1.20	1.90	0.31	0.18	1.03	1.22
8	1.50	0.40	0.20	1.20	1.90	0.21	0.18	1.14	1.32
9	1.70	0.20	0.30	1.20	1.90	0.16	0.28	1.87	2.14

(a)



Calculation of Tensile Load in Geogrids for Wall 3-El Centro 100% using FHWA Recommendations

$a_{max(0.43g)}/g$	0.43		H	1.90	Φ	(backfill)	40.00		
A_m	0.439		L	1.30	γ	(backfill)	17.50		
θ	23.68	0.41			Mobilized interface friction angle	(backfill)	40.00		
K_A	0.195		K_{AH}	0.15	Φ	(reinforced soil)	40.00		
K_{AE}	0.527		K_{AEH}	0.40	γ	(reinforced soil)	17.50		
ΔK_{dyn}	0.33		ΔK_{dynH}	0.25	Reinforced soil inclination	(retained soil)	26.57		
					Backface angle				
W_w	3.99				Block depth	0.10			
W_s	39.90		W_s'	28.26	Block unit weight	21.00			
W_r	43.89		W_A	18.72					
R_x	36.83								
P_{IE}	14.15		P_I	8.21					
P_{AEH}	8.73								
FS_{sl}	1.61								

Tensile stresses in geotextiles:

Layer Number	Elevation	Z_w	S_v	L_1	H	$K\sigma_H$	L_2	Le	2001 T_{all}	2009 T_{all}
1	0.10	1.80	0.20	1.20	1.90	4.71	0.05	1.15	1.35	0.912
2	0.30	1.60	0.20	1.20	1.88	4.18	0.14	1.06	1.24	0.912
3	0.50	1.40	0.20	1.20	1.88	3.66	0.23	0.97	1.13	0.912
4	0.70	1.20	0.20	1.20	1.88	3.14	0.33	0.87	1.02	0.912
5	0.90	1.00	0.20	1.20	1.88	2.61	0.42	0.78	0.91	0.912
6	1.10	0.80	0.20	1.20	1.88	2.09	0.51	0.69	0.80	0.912
7	1.30	0.60	0.20	1.20	1.88	1.57	0.61	0.59	0.69	0.912
8	1.50	0.40	0.20	1.20	1.88	1.05	0.70	0.50	0.59	0.912
9	1.70	0.20	0.28	1.20	1.88	0.52	0.79	0.41	0.48	0.912

(b)

Table E.22. Calculation of Tensile Load in Geogrids for Wall 3-El Centro 150% using a)NCMA Segmental Retaining Walls Seismic Design Manual b) FHWA Recommendations

Calculation of Tensile Load in Geogrids for Wall 3-El Centro 150% using NCMA Segmental Retaining Walls Seismic Design Manual

$A=a_{max(table)}/g$	0.57					Φ	(backfill)	40.00
k_h (int)	0.502		H	1.90		γ	(backfill)	17.50
θ (int)	26.64	0.46	L	1.30		Mobilized interface friction angle, δ	(backfill)	40.00
k_h (ext)	0.29					Φ	(reinforced soil)	40.00
θ (ext)	15.91	0.28				γ	(reinforced soil)	17.50
K_A	0.195		K_{AH}	0.15				
K_{AE} (int)	0.598		$K_{AEH\ (int)}$	0.46				
$\Delta K_{dyn\ (int)}$	0.40		$\Delta K_{dynH\ (int)}$	0.31		Block depth	0.10	
K_{AE} (ext)	0.389		$K_{AEH\ (ext)}$	0.30		Block unit weight	21.00	
$\Delta K_{dyn\ (ext)}$	0.19		$\Delta K_{dynH\ (ext)}$	0.15				
W_w	3.99							
W_s	39.90		W_s'	28.26				
W_r	43.89							
R_S	36.83							
P_{IE}	9.19							
P_{AEH}	7.06							
$FS_{sliding}$	2.27							
$FS_{overturning}$	1.95							

Reinforcement loads

Layer Number	Elevation	Z_{wi}	S_{vi}	L_i	H	$F_{static\ i}$	$F_{inertial\ i}$	$F_{dyn\ i}$	$\Delta F_{seismic}$
1	0.10	1.80	0.20	1.20	1.90	0.94	0.21	0.48	0.69
2	0.30	1.60	0.20	1.20	1.90	0.84	0.21	0.60	0.82
3	0.50	1.40	0.20	1.20	1.90	0.73	0.21	0.73	0.95
4	0.70	1.20	0.20	1.20	1.90	0.63	0.21	0.86	1.07
5	0.90	1.00	0.20	1.20	1.90	0.52	0.21	0.99	1.20
6	1.10	0.80	0.20	1.20	1.90	0.42	0.21	1.12	1.33
7	1.30	0.60	0.20	1.20	1.90	0.31	0.21	1.25	1.46
8	1.50	0.40	0.20	1.20	1.90	0.21	0.21	1.38	1.59
9	1.70	0.20	0.30	1.20	1.90	0.16	0.32	2.27	2.58

(a)

Calculation of Tensile Load in Geogrids for Wall 3-El Centro 150% using FHWA Recommendations

$a_{max(table)}/g$	0.57					Φ	(backfill)	40.00
A_m	0.502		H	1.90		γ	(backfill)	17.50
θ	26.64	0.46	L	1.30		Mobilized interface friction angle	(backfill)	40.00
K_A	0.195		K_{AH}	0.15		Φ	(reinforced soil)	40.00
K_{AE}	0.598		K_{AEH}	0.46		γ	(reinforced soil)	17.50
ΔK_{dyn}	0.40		ΔK_{dynH}	0.31		Mobilized interface friction angle:	(reinforced soil)	26.67
W_w	3.99					Block depth	0.10	
W_s	39.90		W_s'	28.26		Block unit weight	21.00	
W_r	43.89		W_A	18.72				
R_S	36.83							
P_{IE}	16.18		P_I	9.39				
P_{AEH}	9.59							
FS_d	1.43							

Tensile stresses in geotextiles

Layer Number	Elevation	Z_{wi}	S_{vi}	L_i	H	$K\sigma_{vi}$	L_a	Lc	2001 T_{mxi}	2009 T_{mxi}
1	0.10	1.80	0.20	1.20	1.90	4.71	0.05	1.15	1.54	1.043
2	0.30	1.60	0.20	1.20	1.88	4.18	0.14	1.06	1.42	1.043
3	0.50	1.40	0.20	1.20	1.88	3.66	0.23	0.97	1.29	1.043
4	0.70	1.20	0.20	1.20	1.88	3.14	0.33	0.87	1.17	1.043
5	0.90	1.00	0.20	1.20	1.88	2.61	0.42	0.78	1.04	1.043
6	1.10	0.80	0.20	1.20	1.88	2.09	0.51	0.69	0.92	1.043
7	1.30	0.60	0.20	1.20	1.88	1.57	0.61	0.59	0.79	1.043
8	1.50	0.40	0.20	1.20	1.88	1.05	0.70	0.50	0.67	1.043
9	1.70	0.20	0.28	1.20	1.88	0.52	0.79	0.41	0.54	1.043

(b)

Table E.23. Calculation of Tensile Load in Geogrids for Wall 3-El Centro 200% using a)NCMA Segmental Retaining Walls Seismic Design Manual b) FHWA Recommendations

Calculation of Tensile Load in Geogrids for Wall 3-El Centro 200% using NCMA Segmental Retaining Walls Seismic Design Manual

$A=a_{max(kh/g)}/g$	0.74							
k_h (int)	0.525			H	1.90	Φ	(backfill)	40.00
θ (int)	27.72	0.48		L	1.30	γ	(backfill)	17.50
k_h (ext)	0.37					Mobilized interface friction angle, δ	(backfill)	40.00
θ (ext)	20.30	0.35				Φ	(reinforced soil)	40.00
K_A	0.195			K_{AH}	0.15	γ	(reinforced soil)	17.50
K_{AE} (int)	0.628			$K_{AEH\,(int)}$	0.48			
$\Delta K_{dyn\,(int)}$	0.43			$\Delta K_{dynH\,(int)}$	0.33	Block depth		0.10
K_{AE} (ext)	0.460			$K_{AEH\,(ext)}$	0.35	Block unit weight		21.00
$\Delta K_{dyn\,(ext)}$	0.26			$\Delta K_{dynH\,(ext)}$	0.20			
W_w	3.99							
W_t	39.90			W_t'	28.26			
W_r	43.89							
R_R	36.83							
P_{IE}	11.93							
P_{AEH}	7.92							
$FS_{sliding}$	1.85							
$FS_{overturning}$	1.56							

Reinforcement loads

Layer Number	Elevation	Z_{wi}	S_{vi}	L_i	H	$F_{static\,i}$	$F_{inertial\,i}$	$F_{dyn\,i}$	$\Delta F_{seismic}$
1	0.10	1.80	0.20	1.20	1.90	0.94	0.22	0.51	0.73
2	0.30	1.60	0.20	1.20	1.90	0.84	0.22	0.65	0.87
3	0.50	1.40	0.20	1.20	1.90	0.73	0.22	0.79	1.01
4	0.70	1.20	0.20	1.20	1.90	0.63	0.22	0.93	1.15
5	0.90	1.00	0.20	1.20	1.90	0.52	0.22	1.07	1.29
6	1.10	0.80	0.20	1.20	1.90	0.42	0.22	1.21	1.43
7	1.30	0.60	0.20	1.20	1.90	0.31	0.22	1.35	1.57
8	1.50	0.40	0.20	1.20	1.90	0.21	0.22	1.49	1.71
9	1.70	0.20	0.30	1.20	1.90	0.16	0.33	2.44	2.77

(a)

Calculation of Tensile Load in Geogrids for Wall 3-El Centro 200% using FHWA Recommendations

$a_{max(kh/g)}/g$	0.74							
A_m	0.525			H	1.90	Φ	(backfill)	40.00
θ	27.72	0.48		L	1.30	γ	(backfill)	17.50
K_A	0.195			K_{AH}	0.15	Mobilized interface friction angle	(backfill)	40.00
K_{AE}	0.628			K_{AEH}	0.48	Φ	(reinforced soil)	40.00
ΔK_{dyn}	0.43			ΔK_{dynH}	0.33	γ	(reinforced soil)	17.50
						Mobilized interface friction angle	(reinforced soil)	26.67
W_w	3.99					Block depth		0.10
W_t	39.90			W_t'	28.26	Block unit weight		21.00
W_r	43.89			W_A	18.72			
R_R	36.83							
P_{IE}	16.95			P_I	9.84			
P_{AEH}	9.96							
FS_{sl}	1.37							

Tensile stresses in geotextiles

Layer Number	Elevation	Z_{wi}	S_{vi}	L_i	H	$K\sigma_{vi}$	L_a	Le	2001 T_{ml}	2009 T_{ml}
1	0.10	1.80	0.20	1.20	1.90	4.71	0.05	1.15	1.62	1.093
2	0.30	1.60	0.20	1.20	1.88	4.18	0.14	1.06	1.48	1.093
3	0.50	1.40	0.20	1.20	1.88	3.66	0.23	0.97	1.35	1.093
4	0.70	1.20	0.20	1.20	1.88	3.14	0.33	0.87	1.22	1.093
5	0.90	1.00	0.20	1.20	1.88	2.61	0.42	0.78	1.09	1.093
6	1.10	0.80	0.20	1.20	1.88	2.09	0.51	0.69	0.96	1.093
7	1.30	0.60	0.20	1.20	1.88	1.57	0.61	0.59	0.83	1.093
8	1.50	0.40	0.20	1.20	1.88	1.05	0.70	0.50	0.70	1.093
9	1.70	0.20	0.28	1.20	1.88	0.52	0.79	0.41	0.57	1.093

(b)

Table E.24. Calculation of Tensile Load in Geogrids for Wall 3-El Centro 250% using a)NCMA Segmental Retaining Walls Seismic Design Manual b) FHWA Recommendations

Calculation of Tensile Load in Geogrids for Wall 3-El Centro 250% using NCMA Segmental Retaining Walls Seismic Design Manual

A = $a_{max(table)}/g$	0.9					Φ	(backfill)	40.00
k_h (int)	0.495		H	1.90		γ	(backfill)	17.50
θ (int)	26.34	0.46	L	1.30		Mobilized interface friction angle, δ	(backfill)	40.00
k_h (ext)	0.45					Φ	(reinforced soil)	40.00
θ (ext)	24.23	0.42				γ	(reinforced soil)	17.50
K_A	0.195		K_{AH}	0.15				
K_{AE} (int)	0.590		K_{AEH} (int)	0.45		Block depth	0.10	
ΔK_{dyn} (int)	0.39		ΔK_{dynH} (int)	0.30		Block unit weight	21.00	
K_{AE} (ext)	0.539		K_{AEH} (ext)	0.41				
ΔK_{dyn} (ext)	0.34		ΔK_{dynH} (ext)	0.26				
W_w	3.99							
W_s	39.90		W_s'	28.26				
W_r	43.89							
R_S	36.83							
P_{IE}	14.51							
P_{AEH}	8.88							
$FS_{sliding}$	1.57							
$FS_{overturning}$	1.31							

Reinforcement loads

Layer Number	Elevation	Z_{wi}	S_{vi}	L_i	H	F_{static}	$F_{inertial}$	F_{dyn}	$AF_{seismic}$
1	0.10	1.80	0.20	1.20	1.90	0.94	0.21	0.47	0.67
2	0.30	1.60	0.20	1.20	1.90	0.84	0.21	0.59	0.80
3	0.50	1.40	0.20	1.20	1.90	0.73	0.21	0.72	0.93
4	0.70	1.20	0.20	1.20	1.90	0.63	0.21	0.85	1.05
5	0.90	1.00	0.20	1.20	1.90	0.52	0.21	0.97	1.18
6	1.10	0.80	0.20	1.20	1.90	0.42	0.21	1.10	1.31
7	1.30	0.60	0.20	1.20	1.90	0.31	0.21	1.23	1.44
8	1.50	0.40	0.20	1.20	1.90	0.21	0.21	1.36	1.56
9	1.70	0.20	0.30	1.20	1.90	0.16	0.31	2.22	2.54

(a)

Calculation of Tensile Load in Geogrids for Wall 3-El Centro 250% using FHWA Recommendations

$a_{max(table)}/g$	0.9					Φ	(backfill)	40.00
A_m	0.495		H	1.90		γ	(backfill)	17.50
θ	26.34	0.46	L	1.30		Mobilized interface friction angle	(backfill)	40.00
K_A	0.195		K_{AH}	0.15		Φ	(reinforced soil)	40.00
K_{AE}	0.590		K_{AEH}	0.45		γ	(reinforced soil)	17.50
ΔK_{dyn}	0.39		ΔK_{dynH}	0.30		Mobilized interface friction angle	(reinforced soil)	26.07
W_w	3.99					Block depth	0.10	
W_s	39.90		W_s'	28.26		Block unit weight	21.00	
W_r	43.89		W_A	18.72				
R_S	36.83							
P_{IE}	15.96		P_I	9.27				
P_{AEH}	9.50							
FS_{sl}	1.45							

Tensile stresses in geotextiles

Layer Number	Elevation	Z_{wi}	S_{vi}	L_i	H	$K\sigma_{hi}$	L_a	Lc	2001 T_{ml}	2009 T_{ml}
1	0.10	1.80	0.20	1.20	1.90	4.71	0.05	1.15	1.52	1.030
2	0.30	1.60	0.20	1.20	1.88	4.18	0.14	1.06	1.40	1.030
3	0.50	1.40	0.20	1.20	1.88	3.66	0.23	0.97	1.28	1.030
4	0.70	1.20	0.20	1.20	1.88	3.14	0.33	0.87	1.15	1.030
5	0.90	1.00	0.20	1.20	1.88	2.61	0.42	0.78	1.03	1.030
6	1.10	0.80	0.20	1.20	1.88	2.09	0.51	0.69	0.91	1.030
7	1.30	0.60	0.20	1.20	1.88	1.57	0.61	0.59	0.78	1.030
8	1.50	0.40	0.20	1.20	1.88	1.05	0.70	0.50	0.66	1.030
9	1.70	0.20	0.28	1.20	1.88	0.52	0.79	0.41	0.54	1.030

(b)

Table E.25. Calculation of Tensile Load in Geogrids for Wall 3-Izmit 100% using a)NCMA Segmental Retaining Walls Seismic Design Manual b) FHWA Recommendations

Calculation of Tensile Load in Geogrids for Wall 3-Izmit 100% using NCMA Segmental Retaining Walls Seismic Design Manual

A = $a_{max(table)}/g$	0.2					Φ	(backfill)	40.00
k_h (int)	0.250		H	1.90		γ	(backfill)	17.50
θ (int)	14.04	0.24	L	1.30		Mobilized interface friction angle, δ	(backfill)	40.00
k_h (ext)	0.10					Φ	(reinforced soil)	40.00
θ (ext)	5.71	0.10				γ	(reinforced soil)	17.50
K_A	0.195		K_{AH}	0.15				
K_{AE} (int)	0.363		K_{AEH} (int)	0.28				
$\Delta K_{dyn\ (int)}$	0.17		$\Delta K_{dynH\ (int)}$	0.13		Block depth	0.10	
K_{AE} (ext)	0.268		$K_{AEH\ (ext)}$	0.21		Block unit weight	21.00	
$\Delta K_{dyn\ (ext)}$	0.07		$\Delta K_{dynH\ (ext)}$	0.06				
W_w	3.99							
W_s	39.90		W_s'	28.26				
W_r	43.89							
R_R	36.83							
P_{IE}	3.23							
P_{AEH}	5.60							
$FS_{sliding}$	4.17							
$FS_{overturning}$	3.98							

Reinforcement loads

Layer Number	Elevation	Z_{wi}	S_{vi}	L_i	H	F_{static}	$F_{inertial}$	F_{dyn}	$AF_{seismic}$
1	0.10	1.80	0.20	1.20	1.90	0.94	0.11	0.20	0.30
2	0.30	1.60	0.20	1.20	1.90	0.84	0.11	0.25	0.36
3	0.50	1.40	0.20	1.20	1.90	0.73	0.11	0.31	0.41
4	0.70	1.20	0.20	1.20	1.90	0.63	0.11	0.36	0.46
5	0.90	1.00	0.20	1.20	1.90	0.52	0.11	0.41	0.52
6	1.10	0.80	0.20	1.20	1.90	0.42	0.11	0.47	0.57
7	1.30	0.60	0.20	1.20	1.90	0.31	0.11	0.52	0.63
8	1.50	0.40	0.20	1.20	1.90	0.21	0.11	0.58	0.68
9	1.70	0.20	0.30	1.20	1.90	0.16	0.16	0.94	1.10

(a)

Calculation of Tensile Load in Geogrids for Wall 3-Izmit 100% using FHWA Recommendations

$a_{max(table)}/g$	0.2					Φ	(backfill)	40.00
A_m	0.250		H	1.90		γ	(backfill)	17.50
θ	14.04	0.24	L	1.30		Mobilized interface friction angle	(backfill)	40.00
K_A	0.195		K_{AH}	0.15		Φ	(reinforced soil)	40.00
K_{AE}	0.363		K_{AEH}	0.28		γ	(reinforced soil)	17.50
ΔK_{dyn}	0.17		ΔK_{dynH}	0.13		Mobilized interface friction angle	(reinforced soil)	26.67
W_w	3.99					Block depth	0.10	
W_s	39.90		W_s'	28.26		Block unit weight	21.00	
W_r	43.89		W_A	18.72				
R_R	36.83							
P_{IE}	8.06		P_I	4.68				
P_{AEH}	6.75							
FS_{sl}	2.49							

Tensile stresses in geotextiles

Layer Number	Elevation	Z_{wi}	S_{vi}	L_i	H	$K\sigma_{hi}$	L_a	Lc	2001 T_{ml}	2009 T_{ml}
1	0.10	1.80	0.20	1.20	1.90	4.71	0.05	1.15	0.77	0.520
2	0.30	1.60	0.20	1.20	1.88	4.18	0.14	1.06	0.71	0.520
3	0.50	1.40	0.20	1.20	1.88	3.66	0.23	0.97	0.64	0.520
4	0.70	1.20	0.20	1.20	1.88	3.14	0.33	0.87	0.58	0.520
5	0.90	1.00	0.20	1.20	1.88	2.61	0.42	0.78	0.52	0.520
6	1.10	0.80	0.20	1.20	1.88	2.09	0.51	0.69	0.46	0.520
7	1.30	0.60	0.20	1.20	1.88	1.57	0.61	0.59	0.40	0.520
8	1.50	0.40	0.20	1.20	1.88	1.05	0.70	0.50	0.33	0.520
9	1.70	0.20	0.28	1.20	1.88	0.52	0.79	0.41	0.27	0.520

(b)

Table E.26. Calculation of Tensile Load in Geogrids for Wall 3-Izmit 150% using a)NCMA Segmental Retaining Walls Seismic Design Manual b) FHWA Recommendations

Calculation of Tensile Load in Geogrids for Wall 3-Izmit 150% using NCMA Segmental Retaining Walls Seismic Design Manual

$A = a_{max(table)}/g$	0.29						
k_h (int)	0.336		H	1.90	Φ	(backfill)	40.00
θ (int)	18.59	0.32	L	1.30	γ	(backfill)	17.50
k_h (ext)	0.15				Mobilized interface friction angle, δ	(backfill)	40.00
θ (ext)	8.25	0.14			Φ	(reinforced soil)	40.00
K_A	0.195		K_{AH}	0.15	γ	(reinforced soil)	17.50
K_{AE} (int)	0.430		$K_{AEH(int)}$	0.33			
$\Delta K_{dyn(int)}$	0.24		$\Delta K_{dynH(int)}$	0.18	Block depth	0.10	
K_{AE} (ext)	0.294		$K_{AEH(ext)}$	0.23	Block unit weight	21.00	
$\Delta K_{dyn(ext)}$	0.10		$\Delta K_{dynH(ext)}$	0.08			
W_w	3.99						
W_i	39.90		W_i'	28.26			
W_r	43.89						
R_S	36.83						
P_{IR}	4.68						
P_{AEH}	5.92						
$FS_{sliding}$	3.48						
$FS_{overturning}$	3.20						

Reinforcement loads

Layer Number	Elevation	Z_{wi}	S_{vi}	L_i	H	$F_{max\,i}$	$F_{overlat\,i}$	$F_{dyn\,i}$	$\Delta F_{dynamic}$
1	0.10	1.80	0.20	1.20	1.90	0.94	0.14	0.28	0.42
2	0.30	1.60	0.20	1.20	1.90	0.84	0.14	0.35	0.49
3	0.50	1.40	0.20	1.20	1.90	0.73	0.14	0.43	0.57
4	0.70	1.20	0.20	1.20	1.90	0.63	0.14	0.50	0.65
5	0.90	1.00	0.20	1.20	1.90	0.52	0.14	0.58	0.72
6	1.10	0.80	0.20	1.20	1.90	0.42	0.14	0.66	0.80
7	1.30	0.60	0.20	1.20	1.90	0.31	0.14	0.73	0.87
8	1.50	0.40	0.20	1.20	1.90	0.21	0.14	0.81	0.95
9	1.70	0.20	0.30	1.20	1.90	0.16	0.21	1.32	1.54

(a)

Calculation of Tensile Load in Geogrids for Wall 3-Izmit 150% using FHWA Recommendations

$a_{max(table)}/g$	0.29						
A_m	0.336		H	1.90	Φ	(backfill)	40.00
θ	18.59	0.32	L	1.30	γ	(backfill)	17.50
K_A	0.195		K_{AH}	0.15	Mobilized interface friction angle	(backfill)	40.00
K_{AE}	0.430		K_{AEH}	0.33	Φ	(reinforced soil)	40.00
ΔK_{dyn}	0.24		ΔK_{dynH}	0.18	γ	(reinforced soil)	17.50
					Mobilized interface friction angle	(reinforced soil)	26.67
W_w	3.99				Block depth	0.10	
W_i	39.90		W_i'	28.26	Block unit weight	21.00	
W_r	43.89		W_A	18.72			
R_S	36.83						
P_{IR}	10.85		P_I	6.30			
P_{AEH}	7.56						
FS_{sl}	2.00						

Tensile stresses in geotextiles

Layer Number	Elevation	Z_{wi}	S_{vi}	L_i	H	$K\,\sigma_{vi}$	L_a	Le	2001 T_{ad}	2009 T_{ad}
1	0.10	1.80	0.20	1.20	1.90	4.71	0.05	1.15	1.03	0.700
2	0.30	1.60	0.20	1.20	1.88	4.18	0.14	1.06	0.95	0.700
3	0.50	1.40	0.20	1.20	1.88	3.66	0.23	0.97	0.87	0.700
4	0.70	1.20	0.20	1.20	1.88	3.14	0.33	0.87	0.78	0.700
5	0.90	1.00	0.20	1.20	1.88	2.61	0.42	0.78	0.70	0.700
6	1.10	0.80	0.20	1.20	1.88	2.09	0.51	0.69	0.62	0.700
7	1.30	0.60	0.20	1.20	1.88	1.57	0.61	0.59	0.53	0.700
8	1.50	0.40	0.20	1.20	1.88	1.05	0.70	0.50	0.45	0.700
9	1.70	0.20	0.28	1.20	1.88	0.52	0.79	0.41	0.37	0.700

(b)

Table E.27. Calculation of Tensile Load in Geogrids for Wall 3-Izmit 200% using a)NCMA Segmental Retaining Walls Seismic Design Manual b) FHWA Recommendations

Calculation of Tensile Load in Geogrids for Wall 3-Izmit 200% using NCMA Segmental Retaining Walls Seismic Design Manual

$A=a_{max(rock)}/g$	0.34					Φ	(backfill)	40.00
k_h (int)	0.377		H	1.90		γ	(backfill)	17.50
θ (int)	20.68	0.36	L	1.30		Mobilized interface friction angle, δ	(backfill)	40.00
k_h (ext)	0.17					Φ	(reinforced soil)	40.00
θ (ext)	9.65	0.17				γ	(reinforced soil)	17.50
K_A	0.195		K_{AH}	0.15				
K_{AE} (int)	0.466		$K_{AEH\ (int)}$	0.36				
$\Delta K_{dyn\ (int)}$	0.27		$\Delta K_{dynH\ (int)}$	0.21		Block depth	0.10	
K_{AE} (ext)	0.309		$K_{AEH\ (ext)}$	0.24		Block unit weight	21.00	
$\Delta K_{dyn\ (ext)}$	0.11		$\Delta K_{dynH\ (ext)}$	0.09				
W_w	3.99							
W_s	39.90		W_s'	28.26				
W_r	43.89							
R_R	36.83							
P_{IE}	5.48							
P_{AEH}	6.10							
$FS_{sliding}$	3.18							
$FS_{overturning}$	2.88							

Reinforcement loads

Layer Number	Elevation	Z_{wi}	S_{vi}	L_i	H	$F_{static\ i}$	$F_{inertial\ i}$	$F_{dyn\ i}$	$AF_{seismic}$
1	0.10	1.80	0.20	1.20	1.90	0.94	0.16	0.32	0.48
2	0.30	1.60	0.20	1.20	1.90	0.84	0.16	0.41	0.57
3	0.50	1.40	0.20	1.20	1.90	0.73	0.16	0.49	0.65
4	0.70	1.20	0.20	1.20	1.90	0.63	0.16	0.58	0.74
5	0.90	1.00	0.20	1.20	1.90	0.52	0.16	0.67	0.83
6	1.10	0.80	0.20	1.20	1.90	0.42	0.16	0.76	0.92
7	1.30	0.60	0.20	1.20	1.90	0.31	0.16	0.84	1.00
8	1.50	0.40	0.20	1.20	1.90	0.21	0.16	0.93	1.09
9	1.70	0.20	0.30	1.20	1.90	0.16	0.24	1.53	1.77

(a)

Calculation of Tensile Load in Geogrids for Wall 3-Izmit 200% using FHWA Recommendations

$a_{max(rock)}/g$	0.34					Φ	(backfill)	40.00
A_m	0.377		H	1.90		γ	(backfill)	17.50
θ	20.68	0.36	L	1.30		Mobilized interface friction angle	(backfill)	40.00
K_A	0.195		K_{AH}	0.15		Φ	(reinforced soil)	40.00
K_{AE}	0.466		K_{AEH}	0.36		γ	(reinforced soil)	17.50
ΔK_{dyn}	0.27		ΔK_{dynH}	0.21		Mobilized interface friction angle:	(reinforced soil)	26.67
W_w	3.99					Block depth	0.10	
W_s	39.90		W_s'	28.26		Block unit weight	21.00	
W_r	43.89		W_A	18.72				
R_R	36.83							
P_{IE}	12.17		P_I	7.06				
P_{AEH}	8.00							
FS_{sl}	1.83							

Tensile stresses in geotextiles

Layer Number	Elevation	Z_{wi}	S_{vi}	L_i	H	$K\sigma_{vi}$	L_a	Le	2001 T_{md}	2009 T_{md}
1	0.10	1.80	0.20	1.20	1.90	4.71	0.05	1.15	1.16	0.785
2	0.30	1.60	0.20	1.20	1.88	4.18	0.14	1.06	1.07	0.785
3	0.50	1.40	0.20	1.20	1.88	3.66	0.23	0.97	0.97	0.785
4	0.70	1.20	0.20	1.20	1.88	3.14	0.33	0.87	0.88	0.785
5	0.90	1.00	0.20	1.20	1.88	2.61	0.42	0.78	0.78	0.785
6	1.10	0.80	0.20	1.20	1.88	2.09	0.51	0.69	0.69	0.785
7	1.30	0.60	0.20	1.20	1.88	1.57	0.61	0.59	0.60	0.785
8	1.50	0.40	0.20	1.20	1.88	1.05	0.70	0.50	0.50	0.785
9	1.70	0.20	0.28	1.20	1.88	0.52	0.79	0.41	0.41	0.785

(b)

Table E.28. Calculation of Tensile Load in Geogrids for Wall 3-Izmit 250% using a)NCMA Segmental Retaining Walls Seismic Design Manual b) FHWA Recommendations

Calculation of Tensile Load in Geogrids for Wall 3-Izmit 250% using NCMA Segmental Retaining Walls Seismic Design Manual

$A=a_{max(table)}/g$	0.43
k_h (int)	0.439
θ (int)	23.68
k_h (ext)	0.22
θ (ext)	12.13
K_A	0.195
K_{AE} (int)	0.527
$\Delta K_{dyn\ (int)}$	0.33
K_{AE} (ext)	0.338
$\Delta K_{dyn\ (ext)}$	0.14

0.41

0.21

H	1.90
L	1.30
K_{AH}	0.15
$K_{AEH\ (int)}$	0.40
$\Delta K_{dynH\ (int)}$	0.25
$K_{AEH\ (ext)}$	0.26
$\Delta K_{dynH\ (ext)}$	0.11

Φ	(backfill)	40.00
γ	(backfill)	17.50
Mobilized interface friction angle, δ	(backfill)	40.00
Φ	(reinforced soil)	40.00
γ	(reinforced soil)	17.50

Block depth	0.10
Block unit weight	21.00

W_w	3.99
W_s	39.90
W_r	43.89

W_s'	28.26

R_c	36.83
P_{IE}	6.93
P_{AEH}	6.45
$FS_{sliding}$	2.75
$FS_{overturning}$	2.43

Reinforcement loads

Layer Number	Elevation	Z_{wi}	S_{vi}	L_i	H	$F_{static\ i}$	$F_{inertial\ i}$	$F_{dyn\ i}$	$\Delta F_{seismic}$
1	0.10	1.80	0.20	1.20	1.90	0.94	0.18	0.39	0.58
2	0.30	1.60	0.20	1.20	1.90	0.84	0.18	0.50	0.68
3	0.50	1.40	0.20	1.20	1.90	0.73	0.18	0.60	0.79
4	0.70	1.20	0.20	1.20	1.90	0.63	0.18	0.71	0.90
5	0.90	1.00	0.20	1.20	1.90	0.52	0.18	0.82	1.00
6	1.10	0.80	0.20	1.20	1.90	0.42	0.18	0.92	1.11
7	1.30	0.60	0.20	1.20	1.90	0.31	0.18	1.03	1.22
8	1.50	0.40	0.20	1.20	1.90	0.21	0.18	1.14	1.32
9	1.70	0.20	0.30	1.20	1.90	0.16	0.28	1.87	2.14

(a)

Calculation of Tensile Load in Geogrids for Wall 3-Izmit 250% using FHWA Recommendations

$a_{max(table)}/g$	0.43
A_m	0.439
θ	23.68
K_A	0.195
K_{AE}	0.527
ΔK_{dyn}	0.33

0.41

H	1.90
L	1.30
K_{AH}	0.15
K_{AEH}	0.40
ΔK_{dynH}	0.25

Φ	(backfill)	40.00
γ	(backfill)	17.50
Mobilized interface friction angle	(backfill)	40.00
Φ	(reinforced soil)	40.00
γ	(reinforced soil)	17.50
Mobilized interface friction angle:	(reinforced soil)	26.67

Block depth	0.10
Block unit weight	21.00

W_w	3.99
W_s	39.90
W_r	43.89

W_s'	28.26
W_A	18.72

R_c	36.83
P_{IE}	14.15
P_{AEH}	8.73
FS_{sl}	1.61

P_i	8.21

Tensile stresses in geotextiles

Layer Number	Elevation	Z_{wi}	S_{vi}	L_i	H	$K\sigma_{vi}$	L_a	Le	2001 T_{mi}	2009 T_{mi}
1	0.10	1.80	0.20	1.20	1.90	4.71	0.05	1.15	1.35	0.912
2	0.30	1.60	0.20	1.20	1.88	4.18	0.14	1.06	1.24	0.912
3	0.50	1.40	0.20	1.20	1.88	3.66	0.23	0.97	1.13	0.912
4	0.70	1.20	0.20	1.20	1.88	3.14	0.33	0.87	1.02	0.912
5	0.90	1.00	0.20	1.20	1.88	2.61	0.42	0.78	0.91	0.912
6	1.10	0.80	0.20	1.20	1.88	2.09	0.51	0.69	0.80	0.912
7	1.30	0.60	0.20	1.20	1.88	1.57	0.61	0.59	0.69	0.912
8	1.50	0.40	0.20	1.20	1.88	1.05	0.70	0.50	0.59	0.912
9	1.70	0.20	0.28	1.20	1.88	0.52	0.79	0.41	0.48	0.912

(b)

Table E.29. Calculation of Tensile Load in Geogrids for Wall 3-Sakarya 100% using a)NCMA Segmental Retaining Walls Seismic Design Manual b) FHWA Recommendations

Calculation of Tensile Load in Geogrids for Wall 3-Sakarya 100% using NCMA Segmental Retaining Walls Seismic Design Manual

$A = a_{max(table)}/g$	0.23		H	1.90	Φ	(backfill)	40.00	
k_h (int)	0.281		L	1.30	γ	(backfill)	17.50	
θ (int)	15.67	0.27			Mobilized interface friction angle, δ	(backfill)	40.00	
k_h (ext)	0.12				Φ	(reinforced soil)	40.00	
θ (ext)	6.56	0.11			γ	(reinforced soil)	17.50	
K_A	0.195		K_{AH}	0.15				
K_{AE} (int)	0.385		$K_{AEH\ (int)}$	0.30				
$\Delta K_{dyn\ (int)}$	0.19		$\Delta K_{dynH\ (int)}$	0.15	Block depth		0.10	
K_{AE} (ext)	0.277		$K_{AEH\ (ext)}$	0.21	Block unit weight		21.00	
$\Delta K_{dyn\ (ext)}$	0.08		$\Delta K_{dynH\ (ext)}$	0.06				
W_w	3.99							
W_s	39.90		W_s'	28.26				
W_r	43.89							
R_S	36.83							
P_{IE}	3.71							
P_{AEH}	5.71							
$FS_{sliding}$	3.91							
$FS_{overturning}$	3.68							

Reinforcement loads

Layer Number	Elevation	Z_{wi}	S_{vi}	L_i	H	$F_{max\ i}$	$F_{overlay\ i}$	$F_{dyn\ i}$	$\Delta F_{seismic}$
1	0.10	1.80	0.20	1.20	1.90	0.94	0.12	0.22	0.34
2	0.30	1.60	0.20	1.20	1.90	0.84	0.12	0.29	0.40
3	0.50	1.40	0.20	1.20	1.90	0.73	0.12	0.35	0.47
4	0.70	1.20	0.20	1.20	1.90	0.63	0.12	0.41	0.53
5	0.90	1.00	0.20	1.20	1.90	0.52	0.12	0.47	0.59
6	1.10	0.80	0.20	1.20	1.90	0.42	0.12	0.53	0.65
7	1.30	0.60	0.20	1.20	1.90	0.31	0.12	0.59	0.71
8	1.50	0.40	0.20	1.20	1.90	0.21	0.12	0.65	0.77
9	1.70	0.20	0.30	1.20	1.90	0.16	0.18	1.07	1.25

(a)

Calculation of Tensile Load in Geogrids for Wall 3-Sakarya 100% using FHWA Recommendations

$a_{max(table)}/g$	0.23		H	1.90	Φ	(backfill)	40.00	
A_{ss}	0.281		L	1.30	γ	(backfill)	17.50	
θ	15.67	0.27			Mobilized interface friction angle	(backfill)	40.00	
K_A	0.195		K_{AH}	0.15	Φ	(reinforced soil)	40.00	
K_{AE}	0.385		K_{AEH}	0.30	γ	(reinforced soil)	17.50	
ΔK_{dyn}	0.19		ΔK_{dynH}	0.15	Mobilized interface friction angle	(reinforced soil)	26.67	
W_w	3.99							
W_s	39.90		W_s'	28.26	Block depth		0.10	
W_r	43.89		W_A	18.72	Block unit weight		21.00	
R_S	36.83							
P_{IE}	9.05		P_I	5.25				
P_{AEH}	7.02							
FS_{sl}	2.29							

Tensile stresses in geotextiles

Layer Number	Elevation	Z_{wi}	S_{vi}	L_i	H	$K\sigma_{hi}$	L_a	Le	2001 T_{all}	2009 T_{all}
1	0.10	1.80	0.20	1.20	1.90	4.71	0.05	1.15	0.86	0.584
2	0.30	1.60	0.20	1.20	1.88	4.18	0.14	1.06	0.79	0.584
3	0.50	1.40	0.20	1.20	1.88	3.66	0.23	0.97	0.72	0.584
4	0.70	1.20	0.20	1.20	1.88	3.14	0.33	0.87	0.65	0.584
5	0.90	1.00	0.20	1.20	1.88	2.61	0.42	0.78	0.58	0.584
6	1.10	0.80	0.20	1.20	1.88	2.09	0.51	0.69	0.51	0.584
7	1.30	0.60	0.20	1.20	1.88	1.57	0.61	0.59	0.44	0.584
8	1.50	0.40	0.20	1.20	1.88	1.05	0.70	0.50	0.37	0.584
9	1.70	0.20	0.28	1.20	1.88	0.52	0.79	0.41	0.30	0.584

(b)

Table E.30. Calculation of Tensile Load in Geogrids for Wall 3-Sakarya 150% using a)NCMA Segmental Retaining Walls Seismic Design Manual b) FHWA Recommendations

Calculation of Tensile Load in Geogrids for Wall 3-Sakarya 150% using NCMA Segmental Retaining Walls Seismic Design Manual

A = $a_{max(site)}/g$	0.32						
k_h (int)	0.362		H	1.90	Φ	(backfill)	40.00
θ (int)	19.88	0.35	L	1.30	γ	(backfill)	17.50
k_h (ext)	0.16				Mobilized interface friction angle, δ	(backfill)	40.00
θ (ext)	9.09	0.16			Φ	(reinforced soil)	40.00
K_A	0.195		K_{AH}	0.15	γ	(reinforced soil)	17.50
K_{AE} (int)	0.452		$K_{AEH\,(int)}$	0.35			
$\Delta K_{dyn\,(int)}$	0.26		$\Delta K_{dynH\,(int)}$	0.20	Block depth	0.10	
K_{AE} (ext)	0.303		$K_{AEH\,(ext)}$	0.23	Block unit weight	21.00	
$\Delta K_{dyn\,(ext)}$	0.11		$\Delta K_{dynH\,(ext)}$	0.08			
W_w	3.99						
W_s	39.90		W_s'	28.26			
W_r	43.89						
R_R	36.83						
P_{IE}	5.16						
P_{AEH}	6.03						
$FS_{sliding}$	3.29						
$FS_{overturning}$	3.00						

Reinforcement loads

Layer Number	Elevation	Z_w	S_v	L_r	H	F_{static}	$F_{inertial}$	F_{dyn}	$\Delta F_{seismic}$
1	0.10	1.80	0.20	1.20	1.90	0.94	0.15	0.30	0.46
2	0.30	1.60	0.20	1.20	1.90	0.84	0.15	0.39	0.54
3	0.50	1.40	0.20	1.20	1.90	0.73	0.15	0.47	0.62
4	0.70	1.20	0.20	1.20	1.90	0.63	0.15	0.55	0.70
5	0.90	1.00	0.20	1.20	1.90	0.52	0.15	0.63	0.79
6	1.10	0.80	0.20	1.20	1.90	0.42	0.15	0.72	0.87
7	1.30	0.60	0.20	1.20	1.90	0.31	0.15	0.80	0.95
8	1.50	0.40	0.20	1.20	1.90	0.21	0.15	0.88	1.03
9	1.70	0.20	0.30	1.20	1.90	0.16	0.23	1.45	1.68

(a)

Calculation of Tensile Load in Geogrids for Wall 3-Sakarya 150% using FHWA Recommendations

$a_{max(site)}/g$	0.32						
A_m	0.362		H	1.90	Φ	(backfill)	40.00
θ	19.88	0.35	L	1.30	γ	(backfill)	17.50
K_A	0.195		K_{AH}	0.15	Mobilized interface friction angle	(backfill)	40.00
K_{AE}	0.452		K_{AEH}	0.35	Φ	(reinforced soil)	40.00
ΔK_{dyn}	0.26		ΔK_{dynH}	0.20	γ	(reinforced soil)	17.50
					Mobilized interface friction angle:	(reinforced soil)	26.67
W_w	3.99				Block depth	0.10	
W_s	39.90		W_s'	28.26	Block unit weight	21.00	
W_r	43.89		W_A	18.72			
R_R	36.83						
P_{IE}	11.66		P_I	6.77			
P_{AEH}	7.83						
FS_{sl}	1.89						

Tensile stresses in geotextiles

Layer Number	Elevation	Z_w	S_v	L_r	H	$K\sigma_v$	L_a	Le	2001 T_{ad}	2009 T_{ad}
1	0.10	1.80	0.20	1.20	1.90	4.71	0.05	1.15	1.11	0.752
2	0.30	1.60	0.20	1.20	1.88	4.18	0.14	1.06	1.02	0.752
3	0.50	1.40	0.20	1.20	1.88	3.66	0.23	0.97	0.93	0.752
4	0.70	1.20	0.20	1.20	1.88	3.14	0.33	0.87	0.84	0.752
5	0.90	1.00	0.20	1.20	1.88	2.61	0.42	0.78	0.75	0.752
6	1.10	0.80	0.20	1.20	1.88	2.09	0.51	0.69	0.66	0.752
7	1.30	0.60	0.20	1.20	1.88	1.57	0.61	0.59	0.57	0.752
8	1.50	0.40	0.20	1.20	1.88	1.05	0.70	0.50	0.48	0.752
9	1.70	0.20	0.28	1.20	1.88	0.52	0.79	0.41	0.39	0.752

(b)

Table E.31. Calculation of Tensile Load in Geogrids for Wall 3-Sakarya 200% using a)NCMA Segmental Retaining Walls Seismic Design Manual b) FHWA Recommendations

Calculation of Tensile Load in Geogrids for Wall 3-Sakarya 200% using NCMA Segmental Retaining Walls Seismic Design Manual

A = $a_{max(rock)}/g$	0.42					Φ	(backfill)	40.00
k_h (int)	0.433		H	1.90		γ	(backfill)	17.50
θ (int)	23.39	0.41	L	1.30		Mobilized interface friction angle, δ	(backfill)	40.00
k_h (ext)	0.21					Φ	(reinforced soil)	40.00
θ (ext)	11.86	0.21				γ	(reinforced soil)	17.50
K_A	0.195		K_{AH}	0.15				
K_{AE} (int)	0.520		$K_{AEH\ (int)}$	0.40				
$\Delta K_{dyn\ (int)}$	0.33		$\Delta K_{dynH\ (int)}$	0.25		Block depth	0.10	
K_{AE} (ext)	0.335		$K_{AEH\ (ext)}$	0.26		Block unit weight	21.00	
$\Delta K_{dyn\ (ext)}$	0.14		$\Delta K_{dynH\ (ext)}$	0.11				
W_w	3.99							
W_s	39.90		W_s'	28.26				
W_r	43.89							
R_R	36.83							
P_{IR}	6.77							
P_{AEH}	6.41							
$FS_{sliding}$	2.79							
$FS_{overturning}$	2.48							

Reinforcement loads

Layer Number	Elevation	Z_{wi}	S_{vi}	L_i	H	$F_{static\ i}$	$F_{inertial\ i}$	$F_{dyn\ i}$	$\Delta F_{seismic}$
1	0.10	1.80	0.20	1.20	1.90	0.94	0.18	0.38	0.57
2	0.30	1.60	0.20	1.20	1.90	0.84	0.18	0.49	0.67
3	0.50	1.40	0.20	1.20	1.90	0.73	0.18	0.59	0.77
4	0.70	1.20	0.20	1.20	1.90	0.63	0.18	0.70	0.88
5	0.90	1.00	0.20	1.20	1.90	0.52	0.18	0.80	0.98
6	1.10	0.80	0.20	1.20	1.90	0.42	0.18	0.91	1.09
7	1.30	0.60	0.20	1.20	1.90	0.31	0.18	1.01	1.19
8	1.50	0.40	0.20	1.20	1.90	0.21	0.18	1.12	1.30
9	1.70	0.20	0.30	1.20	1.90	0.16	0.27	1.83	2.10

(a)

Calculation of Tensile Load in Geogrids for Wall 3-Sakarya 200% using FHWA Recommendations

$a_{max(rock)}/g$	0.42					Φ	(backfill)	40.00
A_m	0.433		H	1.90		γ	(backfill)	17.50
θ	23.39	0.41	L	1.30		Mobilized interface friction angle	(backfill)	40.00
K_A	0.195		K_{AH}	0.15		Φ	(reinforced soil)	40.00
K_{AE}	0.520		K_{AEH}	0.40		γ	(reinforced soil)	17.50
ΔK_{dyn}	0.33		ΔK_{dynH}	0.25		Mobilized interface friction angle	(reinforced soil)	26.67
W_w	3.99					Block depth	0.10	
W_s	39.90		W_s'	28.26		Block unit weight	21.00	
W_r	43.89		W_A	18.72				
R_R	36.83							
P_{IR}	13.95		P_I	8.10				
P_{AEH}	8.66							
FS_d	1.63							

Tensile stresses in geotextiles

								2001	2009
Layer Number	Elevation	Z_{wi}	S_{vi}	L_i	H	$K\sigma_{vi}$	L_{ai}	Le	T_{ai}	T_{ai}
1	0.10	1.80	0.20	1.20	1.90	4.71	0.05	1.15	1.33	0.900
2	0.30	1.60	0.20	1.20	1.88	4.18	0.14	1.06	1.22	0.900
3	0.50	1.40	0.20	1.20	1.88	3.66	0.23	0.97	1.11	0.900
4	0.70	1.20	0.20	1.20	1.88	3.14	0.33	0.87	1.01	0.900
5	0.90	1.00	0.20	1.20	1.88	2.61	0.42	0.78	0.90	0.900
6	1.10	0.80	0.20	1.20	1.88	2.09	0.51	0.69	0.79	0.900
7	1.30	0.60	0.20	1.20	1.88	1.57	0.61	0.59	0.68	0.900
8	1.50	0.40	0.20	1.20	1.88	1.05	0.70	0.50	0.58	0.900
9	1.70	0.20	0.28	1.20	1.88	0.52	0.79	0.41	0.47	0.900

(b)

Table E.32. Calculation of Tensile Load in Geogrids for Wall 3-Sakarya 250% using a)NCMA Segmental Retaining Walls Seismic Design Manual b) FHWA Recommendations

Calculation of Tensile Load in Geogrids for Wall 3-Sakarya 250% using NCMA Segmental Retaining Walls Seismic Design Manual

A = $a_{max(table)}/g$	0.49
k_h (int)	0.470
θ (int)	25.19
k_h (ext)	0.25
θ (ext)	13.77
K_A	0.195
K_{AE} (int)	0.561
$\Delta K_{dyn\,(int)}$	0.37
K_{AE} (ext)	0.359
$\Delta K_{dyn\,(ext)}$	0.16
W_w	3.99
W_s	39.90
W_r	43.89
R_R	36.83
P_{IR}	7.90
P_{AEH}	6.71
$FS_{sliding}$	2.52
$FS_{overturning}$	2.20

0.44

0.24

H	1.90
L	1.30
K_{AH}	0.15
$K_{AEH\,(int)}$	0.43
$\Delta K_{dynH\,(int)}$	0.28
$K_{AEH\,(ext)}$	0.28
$\Delta K_{dynH\,(ext)}$	0.13
W_s'	28.26

Φ	(backfill)	40.00
γ	(backfill)	17.50
Mobilized interface friction angle, δ	(backfill)	40.00
Φ	(reinforced soil)	40.00
γ	(reinforced soil)	17.50

Block depth	0.10
Block unit weight	21.00

Reinforcement loads

Layer Number	Elevation	Z_{wi}	S_{vi}	L_i	H	$F_{static\,i}$	$F_{inertial\,i}$	$F_{dyn\,i}$	$\Delta F_{seismic}$
1	0.10	1.80	0.20	1.20	1.90	0.94	0.20	0.43	0.63
2	0.30	1.60	0.20	1.20	1.90	0.84	0.20	0.55	0.75
3	0.50	1.40	0.20	1.20	1.90	0.73	0.20	0.67	0.87
4	0.70	1.20	0.20	1.20	1.90	0.63	0.20	0.79	0.98
5	0.90	1.00	0.20	1.20	1.90	0.52	0.20	0.90	1.10
6	1.10	0.80	0.20	1.20	1.90	0.42	0.20	1.02	1.22
7	1.30	0.60	0.20	1.20	1.90	0.31	0.20	1.14	1.34
8	1.50	0.40	0.20	1.20	1.90	0.21	0.20	1.26	1.45
9	1.70	0.20	0.30	1.20	1.90	0.16	0.30	2.06	2.36

(a)

Calculation of Tensile Load in Geogrids for Wall 3-Sakarya 250% using FHWA Recommendations

$a_{max(table)}/g$	0.49
A_m	0.470
θ	25.19
K_A	0.195
K_{AE}	0.561
ΔK_{dyn}	0.37
W_w	3.99
W_s	39.90
W_r	43.89
R_R	36.83
P_{IR}	15.17
P_{AEH}	9.15
FS_{sl}	1.51

0.44

H	1.90
L	1.30
K_{AH}	0.15
K_{AEH}	0.43
ΔK_{dynH}	0.28
W_s'	28.26
W_A	18.72
P_I	8.81

Φ	(backfill)	40.00
γ	(backfill)	17.50
Mobilized interface friction angle	(backfill)	40.00
Φ	(reinforced soil)	40.00
γ	(reinforced soil)	17.50
Mobilized interface friction angle	(reinforced soil)	26.67

Block depth	0.10
Block unit weight	21.00

Tensile stresses in geotextiles

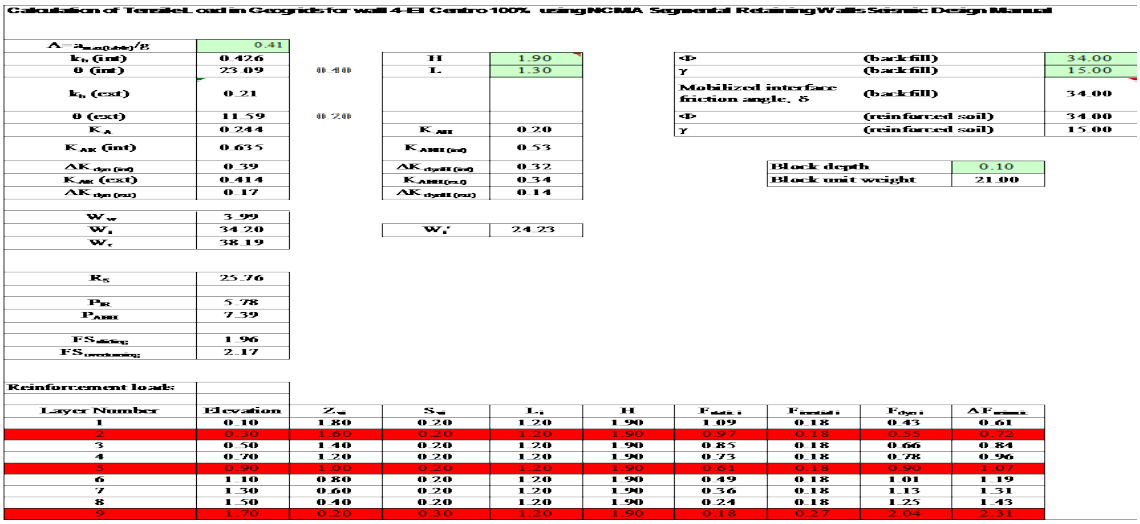
Layer Number	Elevation	Z_{wi}	S_{vi}	L_i	H	$K\sigma_{vi}$	L_a	Le	2001 T_{mt}	2009 T_{mt}
1	0.10	1.80	0.20	1.20	1.90	4.71	0.05	1.15	1.45	0.978
2	0.30	1.60	0.20	1.20	1.88	4.18	0.14	1.06	1.33	0.978
3	0.50	1.40	0.20	1.20	1.88	3.66	0.23	0.97	1.21	0.978
4	0.70	1.20	0.20	1.20	1.88	3.14	0.33	0.87	1.10	0.978
5	0.90	1.00	0.20	1.20	1.88	2.61	0.42	0.78	0.98	0.978
6	1.10	0.80	0.20	1.20	1.88	2.09	0.51	0.69	0.86	0.978
7	1.30	0.60	0.20	1.20	1.88	1.57	0.61	0.59	0.74	0.978
8	1.50	0.40	0.20	1.20	1.88	1.05	0.70	0.50	0.63	0.978
9	1.70	0.20	0.28	1.20	1.88	0.52	0.79	0.41	0.51	0.978

(b)

Table E.33. Comparison of Calculated and Measured Seismic Induced Tensile Loads in Geogrids for Wall 3

Wall / Base Excitation	Maximum Table Acceleration-Base Input (g)	Design (NCMA) ΔTmax in lower geogrid (@h=0.2 m) (kN/m)	Design (FHWA2001) ΔTmax in lower geogrid (@h=0.2 m) (kN/m)	Design (FHWA2009) ΔTmax in lower geogrid (@h=0.2 m) (kN/m)	Measured Geogrid Stress	Design (NCMA)	Design (FHWA2001)	Design (FHWA2009)	Measured Geogrid Stress	Design (NCMA)	Design (FHWA2001)	Design (FHWA2009)	Measured Geogrid Stress
					Max. Stresses (peak values) (kN/m)	ΔTmax at midheight geogrid (@h=1 m) (kN/m)	ΔTmax at midheight geogrid (@h=1 m) (kN/m)	ΔTmax at midheight geogrid (@h=1 m) (kN/m)	Max. Stresses (peak values) (kN/m)	ΔTmax in upper geogrid (@h=1.8 m) (kN/m)	ΔTmax in upper geogrid (@h=1.8 m) (kN/m)	ΔTmax in upper geogrid (@h=1.8 m) (kN/m)	Max. Stresses (peak values) (kN/m)
Wall 3 / El Centro 100%	0.4	0.68	1.24	0.91	3.04	1.00	0.91	0.91	1.87	2.14	0.48	0.91	0.73
Wall 3 / El Centro 150%	0.51	0.82	1.42	1.04	4.21	1.20	1.04	1.04	2.69	2.58	0.54	1.04	1.37
Wall 3 / El Centro 200%	0.73	0.87	1.48	1.09	6.05	1.29	1.09	1.09	4.13	2.77	0.57	1.09	2.11
Wall 3 / Izmit 100%	0.2	0.36	0.71	0.52	1.13	0.52	0.52	0.52	0.65	1.10	0.27	0.52	0.28
Wall 3 / Izmit 150%	0.26	0.49	0.95	0.70	1.42	0.72	0.70	0.70	0.87	1.54	0.37	0.70	0.36
Wall 3 / Izmit 200%	0.36	0.57	1.07	0.78	2.02	0.83	0.78	0.78	1.25	1.77	0.41	0.78	0.5
Wall 3 / Sakarya 100%	0.23	0.40	0.79	0.58	1.21	0.59	0.58	0.58	0.7	1.25	0.30	0.58	0.28
Wall 3 / Sakarya 150%	0.33	0.54	1.02	0.75	1.88	0.79	0.75	0.75	1.16	1.68	0.39	0.75	0.46
Wall 3 / Sakarya 200%	0.36	0.67	1.22	0.90	2.17	0.98	0.90	0.90	1.26	2.10	0.47	0.90	0.5
Wall 3 / El Centro 250%	0.9	0.80	1.40	1.03	6.95	1.18	1.03	1.03	4.14	2.54	0.54	1.03	2.7
Wall 3 / Izmit 250%	0.43	0.68	1.24	0.91	3.04	1.00	0.91	0.91	1.87	2.14	0.48	0.91	0.75
Wall 3 / Sakarya 200%	0.49	0.75	1.21	0.98	3.49	1.10	0.98	0.98	2.15	2.36	0.51	0.98	0.86

Table E.34. Calculation of Tensile Load in Geogrids for Wall 4-El Centro 100% using a)NCMA Segmental Retaining Walls Seismic Design Manual b) FHWA Recommendations



Calculation of Tensile Load in Geogrids for wall 4-El Centro 100% using NCMA Segmental Retaining Walls Seismic Design Manual

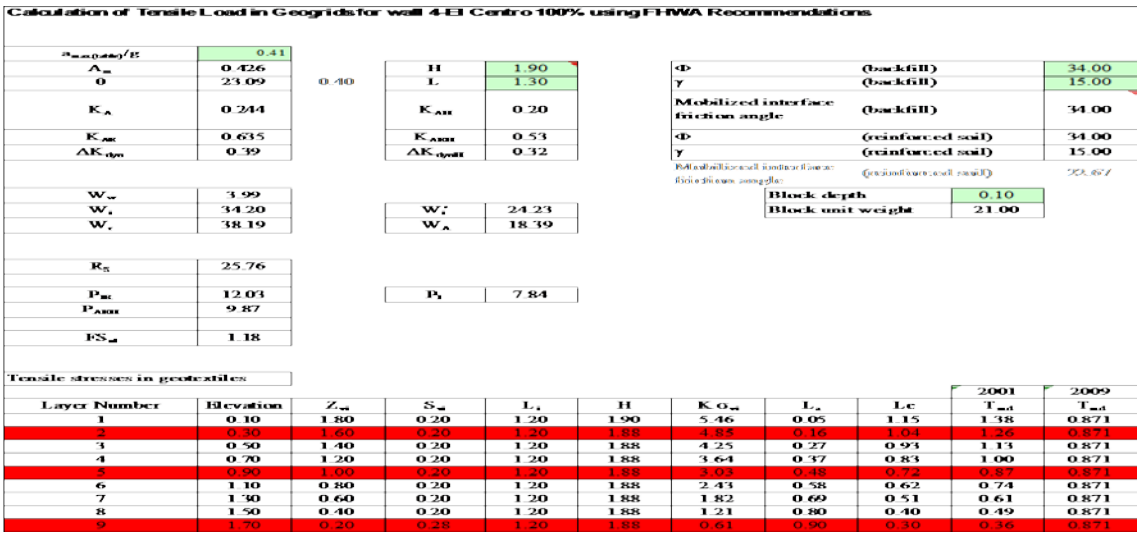
$A = a_{max(site)}/g$	0.41				
k_h (int)	0.426		H	1.90	
θ (int)	23.09	0.40	L	1.30	
k_h (ext)	0.21				
θ (ext)	11.59	0.20			
K_A	0.244		K_{AH}	0.20	
K_{AE} (int)	0.635		$K_{AEH(int)}$	0.53	
$AK_{dyn(int)}$	0.39		$AK_{dyn H(int)}$	0.32	
K_{AE} (ext)	0.414		$K_{AEH(ext)}$	0.34	
$AK_{dyn(ext)}$	0.17		$AK_{dyn H(ext)}$	0.14	
W_w	3.99				
W_s	34.20		W_s'	24.23	
W_r	38.19				
R_R	25.76				
P_{AE}	5.78				
P_{AEH}	7.39				
$FS_{sliding}$	1.96				
$FS_{overturning}$	2.17				

<φ>	(backfill)	34.00
γ	(backfill)	15.00
Mobilized interface friction angle, δ	(backfill)	34.00
<φ>	(reinforced soil)	34.00
γ	(reinforced soil)	15.00
Block depth		0.10
Block unit weight		21.00

Reinforcement loads:

Layer Number	Elevation	Z_w	S_v	L_i	H	F_{static}	$F_{seismic}$	F_{dyn}	$\Delta F_{seismic}$
1	0.10	1.80	0.20	1.20	1.90	1.09	0.18	0.43	0.61
2	0.30	1.60	0.20	1.20	1.90	0.97	0.18	0.38	0.52
3	0.50	1.40	0.20	1.20	1.90	0.85	0.18	0.66	0.84
4	0.70	1.20	0.20	1.20	1.90	0.73	0.18	0.78	0.96
5	0.90	1.00	0.20	1.20	1.90	0.61	0.18	0.90	1.07
6	1.10	0.80	0.20	1.20	1.90	0.49	0.18	1.01	1.19
7	1.30	0.60	0.20	1.20	1.90	0.36	0.18	1.13	1.31
8	1.50	0.40	0.20	1.20	1.90	0.24	0.18	1.25	1.43
9	1.70	0.20	0.30	1.20	1.90	0.18	0.27	2.04	2.31

(a)



Calculation of Tensile Load in Geogrids for wall 4-El Centro 100% using FHWA Recommendations

$A = a_{max(site)}/g$	0.41				
A_m	0.426		H	1.90	
θ	23.09	0.40	L	1.30	
K_A	0.244		K_{AH}	0.20	
K_{AE}	0.635		K_{AEH}	0.53	
AK_{dyn}	0.39		$AK_{dyn H}$	0.32	
W_w	3.99				
W_s	34.20		W_s'	24.23	
W_r	38.19		W_A	18.39	
R_R	25.76				
P_{AE}	12.03		P_i	7.84	
P_{AEH}	9.87				
FS_{sl}	1.18				

<φ>	(backfill)	34.00
γ	(backfill)	15.00
Mobilized interface friction angle	(backfill)	34.00
<φ>	(reinforced soil)	34.00
γ	(reinforced soil)	15.00
Block depth		0.10
Block unit weight		21.00

Tensile strength in geotextiles

Layer Number	Elevation	Z_w	S_v	L_i	H	$K\sigma_H$	L_e	Lc	2001 T_{ad}	2009 T_{ad}
1	0.10	1.80	0.20	1.20	1.90	5.46	0.05	1.15	1.38	0.871
2	0.30	1.60	0.20	1.20	1.88	4.85	0.16	1.04	1.26	0.871
3	0.50	1.40	0.20	1.20	1.88	4.25	0.27	0.93	1.13	0.871
4	0.70	1.20	0.20	1.20	1.88	3.64	0.37	0.83	1.00	0.871
5	0.90	1.00	0.20	1.20	1.88	3.03	0.48	0.72	0.87	0.871
6	1.10	0.80	0.20	1.20	1.88	2.43	0.58	0.62	0.74	0.871
7	1.30	0.60	0.20	1.20	1.88	1.82	0.69	0.51	0.61	0.871
8	1.50	0.40	0.20	1.20	1.88	1.21	0.80	0.40	0.49	0.871
9	1.70	0.20	0.28	1.20	1.88	0.61	0.90	0.30	0.36	0.871

(b)

Table E.35. Calculation of Tensile Load in Geogrids for Wall 4-El Centro 150% using a)NCMA Segmental Retaining Walls Seismic Design Manual b) FHWA Recommendations

Calculation of Tensile Load in Geogrids for wall 4-El Centro 150% using NCMA Segmental Retaining Walls Seismic Design Manual

$A = a_{max(table)}/g$	0.61					Φ	(backfill)	34.00	
k_h (int)	0.512		H	1.90		γ	(backfill)	15.00	
θ (int)	27.13	0.47	L	1.30		Mobilized interface friction angle, δ	(backfill)	34.00	
k_h (ext)	0.31					Φ	(reinforced soil)	34.00	
θ (ext)	16.96	0.30				γ	(reinforced soil)	15.00	
K_A	0.244		K_{AH}	0.20					
K_{AE} (int)	0.767		$K_{AEH\,(int)}$	0.64					
$\Delta K_{dyn\,(int)}$	0.52		$\Delta K_{dynH\,(int)}$	0.43		Block depth		0.10	
K_{AE} (ext)	0.500		$K_{AEH\,(ext)}$	0.41		Block unit weight		21.00	
$\Delta K_{dyn\,(ext)}$	0.26		$\Delta K_{dynH\,(ext)}$	0.21					
W_w	3.99								
W_i	34.20		W_i'	24.23					
W_r	38.19								
R_s	25.76								
P_{IE}	8.61								
P_{AEH}	8.35								
$FS_{sliding}$	1.52								
$FS_{overturning}$	1.62								

Reinforcement loads

Layer Number	Elevation	Z_{wi}	S_{vi}	L_i	H	F_{static}	$F_{inertial}$	F_{dyn}	$\Delta F_{seismic}$
1	0.10	1.80	0.20	1.20	1.90	1.09	0.22	0.57	0.79
2	0.30	1.60	0.20	1.20	1.90	0.97	0.22	0.73	0.94
3	0.50	1.40	0.20	1.20	1.90	0.85	0.22	0.88	1.10
4	0.70	1.20	0.20	1.20	1.90	0.73	0.22	1.04	1.25
5	0.90	1.00	0.20	1.20	1.90	0.61	0.22	1.20	1.41
6	1.10	0.80	0.20	1.20	1.90	0.49	0.22	1.35	1.57
7	1.30	0.60	0.20	1.20	1.90	0.36	0.22	1.51	1.72
8	1.50	0.40	0.20	1.20	1.90	0.24	0.22	1.66	1.88
9	1.70	0.20	0.30	1.20	1.90	0.18	0.32	2.73	3.05

(a)

Calculation of Tensile Load in Geogrids for wall 4-El Centro 150% using FHWA Recommendations

$a_{max(table)}/g$	0.61					Φ	(backfill)	34.00	
A_m	0.512		H	1.90		γ	(backfill)	15.00	
θ	27.13	0.47	L	1.30		Mobilized interface friction angle	(backfill)	34.00	
K_A	0.244		K_{AH}	0.20		Φ	(reinforced soil)	34.00	
K_{AE}	0.767		K_{AEH}	0.64		γ	(reinforced soil)	15.00	
ΔK_{dyn}	0.52		ΔK_{dynH}	0.43		Mobilized interface friction angle	(reinforced soil)	22.67	
W_w	3.99					Block depth		0.10	
W_i	34.20		W_i'	24.23		Block unit weight		21.00	
W_r	38.19		W_A	18.39					
R_s	25.76								
P_{IE}	14.46		P_I	9.42					
P_{AEH}	11.34								
FS_{sl}	1.00								

Tensile stresses in geotextiles

Layer Number	Elevation	Z_{wi}	S_{vi}	L_i	H	$K\sigma_{vi}$	L_a	Le	2001 T_{ml}	2009 T_{ml}
1	0.10	1.80	0.20	1.20	1.90	5.46	0.05	1.15	1.66	1.047
2	0.30	1.60	0.20	1.20	1.88	4.85	0.16	1.04	1.51	1.047
3	0.50	1.40	0.20	1.20	1.88	4.25	0.27	0.93	1.36	1.047
4	0.70	1.20	0.20	1.20	1.88	3.64	0.37	0.83	1.20	1.047
5	0.90	1.00	0.20	1.20	1.88	3.03	0.48	0.72	1.05	1.047
6	1.10	0.80	0.20	1.20	1.88	2.43	0.58	0.62	0.89	1.047
7	1.30	0.60	0.20	1.20	1.88	1.82	0.69	0.51	0.74	1.047
8	1.50	0.40	0.20	1.20	1.88	1.21	0.80	0.40	0.58	1.047
9	1.70	0.20	0.28	1.20	1.88	0.61	0.90	0.30	0.43	1.047

(b)

Table E.36. Calculation of Tensile Load in Geogrids for Wall 4-El Centro 200% using a)NCMA Segmental Retaining Walls Seismic Design Manual b) FHWA Recommendations

Calculation of Tensile Load in Geogrids for wall 4-El Centro 200% using NCMA Segmental Retaining Walls Seismic Design Manual

$A = a_{max(table)}/g$	0.75			H	1.90	Φ	(backfill)	34.00	
k_h (int)	0.525			L	1.30	γ	(backfill)	15.00	
θ (int)	27.70	0.48				Mobilized interface friction angle, δ	(backfill)	34.00	
k_h (ext)	0.38					Φ	(reinforced soil)	34.00	
θ (ext)	20.56	0.36				γ	(reinforced soil)	15.00	
K_A	0.244			K_{AH}	0.20				
K_{AE} (int)	0.790			$K_{AEH(int)}$	0.65				
$\Delta K_{dyn(int)}$	0.55			$\Delta K_{dynH(int)}$	0.45	Block depth		0.10	
K_{AE} (ext)	0.573			$K_{AEH(ext)}$	0.47	Block unit weight		21.00	
$\Delta K_{dyn(ext)}$	0.33			$\Delta K_{dynH(ext)}$	0.27				
W_w	3.99								
W_s	34.20			W_s'	24.23				
W_r	38.19								
R_S	25.76								
P_{IR}	10.58								
P_{AEH}	9.17								
$FS_{sliding}$	1.30								
$FS_{overturning}$	1.36								

Reinforcement loads

Layer Number	Elevation	Z_w	S_w	L_i	H	$F_{max,i}$	$F_{overstr,i}$	$F_{dyn,i}$	$\Delta F_{seismic}$
1	0.10	1.80	0.20	1.20	1.90	1.09	0.22	0.60	0.82
2	0.30	1.60	0.20	1.20	1.90	0.97	0.22	0.76	0.98
3	0.50	1.40	0.20	1.20	1.90	0.85	0.22	0.92	1.14
4	0.70	1.20	0.20	1.20	1.90	0.73	0.22	1.09	1.31
5	0.90	1.00	0.20	1.20	1.90	0.61	0.22	1.25	1.47
6	1.10	0.80	0.20	1.20	1.90	0.49	0.22	1.41	1.63
7	1.30	0.60	0.20	1.20	1.90	0.36	0.22	1.57	1.79
8	1.50	0.40	0.20	1.20	1.90	0.24	0.22	1.74	1.96
9	1.70	0.20	0.30	1.20	1.90	0.18	0.33	2.85	3.18

(a)

Calculation of Tensile Load in Geogrids for wall 4-El Centro 200% using FHWA Recommendations

$a_{max(table)}/g$	0.75			H	1.90	Φ	(backfill)	34.00	
A_m	0.525			L	1.30	γ	(backfill)	15.00	
θ	27.70	0.48				Mobilized interface friction angle	(backfill)	34.00	
K_A	0.244			K_{AH}	0.20	Φ	(reinforced soil)	34.00	
K_{AE}	0.790			K_{AEH}	0.65	γ	(reinforced soil)	15.00	
ΔK_{dyn}	0.55			ΔK_{dynH}	0.45	Mobilized interface friction angle	(reinforced soil)	22.67	
W_w	3.99					Block depth		0.10	
W_s	34.20			W_s'	24.23	Block unit weight		21.00	
W_r	38.19			W_A	18.39				
R_S	25.76								
P_{IR}	14.81			P_I	9.65				
P_{AEH}	11.60								
FS_{sl}	0.98								

Tensile stresses in geotextiles

Layer Number	Elevation	Z_w	S_w	L_i	H	$K\sigma_w$	L_a	Le	2001 T_{all}	2009 T_{all}
1	0.10	1.80	0.20	1.20	1.90	5.46	0.05	1.15	1.70	1.073
2	0.30	1.60	0.20	1.20	1.88	4.85	0.16	1.04	1.55	1.073
3	0.50	1.40	0.20	1.20	1.88	4.25	0.27	0.93	1.39	1.073
4	0.70	1.20	0.20	1.20	1.88	3.64	0.37	0.83	1.23	1.073
5	0.90	1.00	0.20	1.20	1.88	3.03	0.48	0.72	1.07	1.073
6	1.10	0.80	0.20	1.20	1.88	2.43	0.58	0.62	0.91	1.073
7	1.30	0.60	0.20	1.20	1.88	1.82	0.69	0.51	0.76	1.073
8	1.50	0.40	0.20	1.20	1.88	1.21	0.80	0.40	0.60	1.073
9	1.70	0.20	0.28	1.20	1.88	0.61	0.90	0.30	0.44	1.073

(b)

Table E.37. Calculation of Tensile Load in Geogrids for Wall 4-El Centro 250% using a)NCMA Segmental Retaining Walls Seismic Design Manual b) FHWA Recommendations

Calculation of Tensile Load in Geogrids for wall 4-El Centro 250% using NCMA Segmental Retaining Walls Seismic Design Manual

A = $a_{max(table)}/g$	0.93						
k_h (int)	0.484		H	1.90	Φ	(backfill)	34.00
θ (int)	25.81	0.45	L	1.30	γ	(backfill)	15.00
k_h (ext)	0.47				Mobilized interface friction angle, δ	(backfill)	34.00
θ (ext)	24.94	0.44			Φ	(reinforced soil)	34.00
K_A	0.244		K_{AH}	0.20	γ	(reinforced soil)	15.00
K_{AE} (int)	0.718		$K_{AEH\ (int)}$	0.60			
$\Delta K_{dyn\ (int)}$	0.47		$\Delta K_{dynH\ (int)}$	0.39	Block depth	0.10	
K_{AE} (ext)	0.689		$K_{AEH\ (ext)}$	0.57	Block unit weight	21.00	
$\Delta K_{dyn\ (ext)}$	0.45		$\Delta K_{dynH\ (ext)}$	0.37			
W_w	3.99						
W_s	34.20		W_s'	24.23			
W_r	38.19						
R_S	25.76						
P_{IE}	13.12						
P_{AEH}	10.48						
$FS_{sliding}$	1.09						
$FS_{overturning}$	1.12						

Reinforcement loads

Layer Number	Elevation	Z_w	S_v	L_i	H	F_{static}	$F_{inertial}$	F_{dyn}	$AF_{seismic}$
1	0.10	1.80	0.20	1.20	1.90	1.09	0.20	0.52	0.72
2	0.30	1.60	0.20	1.20	1.90	0.97	0.20	0.66	0.86
3	0.50	1.40	0.20	1.20	1.90	0.85	0.20	0.80	1.00
4	0.70	1.20	0.20	1.20	1.90	0.73	0.20	0.94	1.15
5	0.90	1.00	0.20	1.20	1.90	0.61	0.20	1.08	1.29
6	1.10	0.80	0.20	1.20	1.90	0.49	0.20	1.23	1.43
7	1.30	0.60	0.20	1.20	1.90	0.36	0.20	1.37	1.57
8	1.50	0.40	0.20	1.20	1.90	0.24	0.20	1.51	1.71
9	1.70	0.20	0.30	1.20	1.90	0.18	0.30	2.48	2.78

(a)

Calculation of Tensile Load in Geogrids for wall 4-El Centro 250% using FHWA Recommendations

$a_{max(table)}/g$	0.93						
A_m	0.484		H	1.90	Φ	(backfill)	34.00
θ	25.81	0.45	L	1.30	γ	(backfill)	15.00
K_A	0.244		K_{AH}	0.20	Mobilized interface friction angle	(backfill)	34.00
K_{AE}	0.718		K_{AEH}	0.60	Φ	(reinforced soil)	34.00
ΔK_{dyn}	0.47		ΔK_{dynH}	0.39	γ	(reinforced soil)	15.00
					Mobilized interface friction angle	(reinforced soil)	22.67
W_w	3.99				Block depth	0.10	
W_s	34.20		W_s'	24.23	Block unit weight	21.00	
W_r	38.19		W_A	18.39			
R_S	25.76						
P_{IE}	13.64		P_I	8.89			
P_{AEH}	10.80						
FS_{sl}	1.05						

Tensile stresses in geotextiles

Layer Number	Elevation	Z_w	S_v	L_i	H	$K\sigma_{vi}$	L_a	Le	2001 T_{ael}	2009 T_{ael}
1	0.10	1.80	0.20	1.20	1.90	5.46	0.05	1.15	1.57	0.988
2	0.30	1.60	0.20	1.20	1.88	4.85	0.16	1.04	1.42	0.988
3	0.50	1.40	0.20	1.20	1.88	4.25	0.27	0.93	1.28	0.988
4	0.70	1.20	0.20	1.20	1.88	3.64	0.37	0.83	1.13	0.988
5	0.90	1.00	0.20	1.20	1.88	3.03	0.48	0.72	0.99	0.988
6	1.10	0.80	0.20	1.20	1.88	2.43	0.58	0.62	0.84	0.988
7	1.30	0.60	0.20	1.20	1.88	1.82	0.69	0.51	0.70	0.988
8	1.50	0.40	0.20	1.20	1.88	1.21	0.80	0.40	0.55	0.988
9	1.70	0.20	0.28	1.20	1.88	0.61	0.90	0.30	0.41	0.988

(b)

Table E.38. Calculation of Tensile Load in Geogrids for Wall 4-El Centro 275% using a)NCMA Segmental Retaining Walls Seismic Design Manual b) FHWA Recommendations

Calculation of Tensile Load in Geogrids for wall 4-El Centro 275% using NCMA Segmental Retaining Walls Seismic Design Manual

$A=a_{max(rock)}/g$	0.98					Φ	(backfill)	34.00	
k_h (int)	0.461		H	1.90		γ	(backfill)	15.00	
θ (int)	24.73	0.43	L	1.30		Mobilized interface friction angle, δ	(backfill)	34.00	
k_h (ext)	0.49					Φ	(reinforced soil)	34.00	
θ (ext)	26.10	0.46				γ	(reinforced soil)	15.00	
K_A	0.244		K_{AE}	0.20					
K_{AE} (int)	0.683		$K_{AE(int)}$	0.57					
$\Delta K_{dyn\ (int)}$	0.44		$\Delta K_{dyn(int)}$	0.36		Block depth		0.10	
K_{AE} (ext)	0.728		$K_{AE(ext)}$	0.60		Block unit weight		21.00	
$\Delta K_{dyn\ (ext)}$	0.48		$\Delta K_{dyn(ext)}$	0.40					
W_w	3.99								
W_s	34.20		W_s'	24.23					
W_r	38.19								
R_n	25.76								
P_{IE}	13.83								
P_{AEH}	10.91								
$FS_{sliding}$	1.04								
$FS_{overturning}$	1.06								

Reinforcement loads:

Layer Number	Elevation	Z_{wi}	S_{vi}	L_{ri}	H	F_{static}	$F_{seismic}$	F_{dyn}	$\Delta F_{seismic}$
1	0.10	1.80	0.20	1.20	1.90	1.09	0.19	0.48	0.67
2	0.30	1.60	0.20	1.20	1.90	0.97	0.19	0.61	0.80
3	0.50	1.40	0.20	1.20	1.90	0.85	0.19	0.74	0.94
4	0.70	1.20	0.20	1.20	1.90	0.73	0.19	0.87	1.07
5	0.90	1.00	0.20	1.20	1.90	0.61	0.19	1.00	1.20
6	1.10	0.80	0.20	1.20	1.90	0.49	0.19	1.14	1.33
7	1.30	0.60	0.20	1.20	1.90	0.36	0.19	1.27	1.46
8	1.50	0.40	0.20	1.20	1.90	0.24	0.19	1.40	1.59
9	1.70	0.20	0.30	1.20	1.90	0.18	0.29	2.29	2.58

(a)

Calculation of Tensile Load in Geogrids for wall 4-El Centro 275% using FHWA Recommendations

$a_{max(table)}/g$	0.98					Φ	(backfill)	34.00	
A_m	0.461		H	1.90		γ	(backfill)	15.00	
θ	24.73	0.43	L	1.30		Mobilized interface friction angle	(backfill)	34.00	
K_A	0.244		K_{AE}	0.20		Φ	(reinforced soil)	34.00	
K_{AE}	0.683		K_{AEH}	0.57		γ	(reinforced soil)	15.00	
ΔK_{dyn}	0.44		ΔK_{dynE}	0.36		Mobilized interface friction angle:	(reinforced soil)	23.67	
W_w	3.99					Block depth		0.10	
W_s	34.20		W_s'	24.23		Block unit weight		21.00	
W_r	38.19		W_A	18.39					
R_n	25.76								
P_{IE}	13.00		P_I	8.47					
P_{AEH}	10.40								
FS_{sl}	1.10								

Tensile stresses in geotextiles

Layer Number	Elevation	Z_{wi}	S_{vi}	L_{ri}	H	$K\sigma_{vi}$	L_{ai}	Lc	2001 T_{ael}	2009 T_{ael}
1	0.10	1.80	0.20	1.20	1.90	5.46	0.05	1.15	1.50	0.941
2	0.30	1.60	0.20	1.20	1.88	4.85	0.16	1.04	1.36	0.941
3	0.50	1.40	0.20	1.20	1.88	4.25	0.27	0.93	1.22	0.941
4	0.70	1.20	0.20	1.20	1.88	3.64	0.37	0.83	1.08	0.941
5	0.90	1.00	0.20	1.20	1.88	3.03	0.48	0.72	0.94	0.941
6	1.10	0.80	0.20	1.20	1.88	2.43	0.58	0.62	0.80	0.941
7	1.30	0.60	0.20	1.20	1.88	1.82	0.69	0.51	0.66	0.941
8	1.50	0.40	0.20	1.20	1.88	1.21	0.80	0.40	0.52	0.941
9	1.70	0.20	0.28	1.20	1.88	0.61	0.90	0.30	0.39	0.941

(b)

Table E.39. Calculation of Tensile Load in Geogrids for Wall 4-Izmit 100% using a)NCMA Segmental Retaining Walls Seismic Design Manual b) FHWA Recommendations

Calculation of Tensile Load in Geogrids for wall 4-Izmit 100% using NCMA Segmental Retaining Walls Seismic Design Manual

$A=a_{max(table)}/g$	0.2					Φ	(backfill)	34.00
k_h (int)	0.250		H	1.90		γ	(backfill)	15.00
θ (int)	14.04	0.24	L	1.30		Mobilized interface friction angle, δ	(backfill)	34.00
k_h (ext)	0.10					Φ	(reinforced soil)	34.00
θ (ext)	5.71	0.10				γ	(reinforced soil)	15.00
K_A	0.244		K_{AH}	0.20				
K_{AE} (int)	0.450		$K_{AEH\ (int)}$	0.37				
$\Delta K_{dyn\ (int)}$	0.21		$\Delta K_{dynH\ (int)}$	0.17		Block depth	0.10	
K_{AE} (ext)	0.341		$K_{AEH\ (ext)}$	0.28		Block unit weight	21.00	
$\Delta K_{dyn\ (ext)}$	0.10		$\Delta K_{dynH\ (ext)}$	0.08				
W_w	3.99							
W_i	34.20		W_i'	24.23				
W_r	38.19							
R_s	25.76							
P_{IE}	2.82							
P_{AEH}	6.56							
$FS_{sliding}$	2.75							
$FS_{overturning}$	3.27							

Reinforcement loads

Layer Number	Elevation	Z_w	S_w	L_r	H	F_{static}	$F_{inertial}$	F_{dyn}	$\Delta F_{seismic}$
1	0.10	1.80	0.20	1.20	1.90	1.09	0.11	0.23	0.33
2	0.30	1.60	0.20	1.20	1.90	0.97	0.11	0.29	0.39
3	0.50	1.40	0.20	1.20	1.90	0.85	0.11	0.35	0.45
4	0.70	1.20	0.20	1.20	1.90	0.73	0.11	0.41	0.52
5	0.90	1.00	0.20	1.20	1.90	0.61	0.11	0.47	0.58
6	1.10	0.80	0.20	1.20	1.90	0.49	0.11	0.53	0.64
7	1.30	0.60	0.20	1.20	1.90	0.36	0.11	0.60	0.70
8	1.50	0.40	0.20	1.20	1.90	0.24	0.11	0.66	0.76
9	1.70	0.20	0.30	1.20	1.90	0.18	0.16	1.08	1.24

(a)

Calculation of Tensile Load in Geogrids for wall 4-Izmit 100% using FHWA Recommendations

$a_{max(table)}/g$	0.2					Φ	(backfill)	34.00
A_m	0.250		H	1.90		γ	(backfill)	15.00
θ	14.04	0.24	L	1.30		Mobilized interface friction angle	(backfill)	34.00
K_A	0.244		K_{AH}	0.20		Φ	(reinforced soil)	34.00
K_{AE}	0.450		K_{AEH}	0.37		γ	(reinforced soil)	15.00
ΔK_{dyn}	0.21		ΔK_{dynH}	0.17		Mobilized interface friction angle	(reinforced soil)	22.67
W_w	3.99					Block depth	0.10	
W_i	34.20		W_i'	24.23		Block unit weight	21.00	
W_r	38.19		W_A	18.39				
R_s	25.76							
P_{IE}	7.05		P_I	4.60				
P_{AEH}	7.79							
FS_d	1.73							

Tensile stresses in geotextiles

Layer Number	Elevation	Z_w	S_w	L_r	H	$K\sigma_w$	L_a	Le	2001 T_{all}	2009 T_{all}
1	0.10	1.80	0.20	1.20	1.90	5.46	0.05	1.15	0.81	0.511
2	0.30	1.60	0.20	1.20	1.88	4.85	0.16	1.04	0.74	0.511
3	0.50	1.40	0.20	1.20	1.88	4.25	0.27	0.93	0.66	0.511
4	0.70	1.20	0.20	1.20	1.88	3.64	0.37	0.83	0.59	0.511
5	0.90	1.00	0.20	1.20	1.88	3.03	0.48	0.72	0.51	0.511
6	1.10	0.80	0.20	1.20	1.88	2.43	0.58	0.62	0.44	0.511
7	1.30	0.60	0.20	1.20	1.88	1.82	0.69	0.51	0.36	0.511
8	1.50	0.40	0.20	1.20	1.88	1.21	0.80	0.40	0.28	0.511
9	1.70	0.20	0.28	1.20	1.88	0.61	0.90	0.30	0.21	0.511

(b)

Table E.40. Calculation of Tensile Load in Geogrids for Wall 4-Izmit 150% using a)NCMA Segmental Retaining Walls Seismic Design Manual b) FHWA Recommendations

Calculation of Tensile Load in Geogrids for wall 4-Izmit 150% using NCMA Segmental Retaining Walls Seismic Design Manual

$A=a_{max(table)}/g$	0.29						
k_h (int)	0.336		H	1.90	Φ	(backfill)	34.00
θ (int)	18.59	0.32	L	1.30	γ	(backfill)	15.00
k_h (ext)	0.15				Mobilized interface friction angle, δ	(backfill)	34.00
θ (ext)	8.25	0.14			Φ	(reinforced soil)	34.00
K_A	0.244		K_{AH}	0.20	γ	(reinforced soil)	15.00
K_{AE} (int)	0.531		$K_{AEH\ (int)}$	0.44			
$\Delta K_{dyn\ (int)}$	0.29		$\Delta K_{dynH\ (int)}$	0.24	Block depth	0.10	
K_{AE} (ext)	0.370		$K_{AEH\ (ext)}$	0.31	Block unit weight	21.00	
$\Delta K_{dyn\ (ext)}$	0.13		$\Delta K_{dynH\ (ext)}$	0.10			
W_w	3.99						
W_1	34.20		W_1'	24.23			
W_r	38.19						
R_g	25.76						
P_{IE}	4.09						
P_{AEH}	6.90						
$FS_{sliding}$	2.34						
$FS_{overturning}$	2.69						

Reinforcement loads

Layer Number	Elevation	Z_{wi}	S_{wi}	L_i	H	$F_{static\ i}$	$F_{inertial\ i}$	$F_{dyn\ i}$	$\Delta F_{seismic}$
1	0.10	1.80	0.20	1.20	1.90	1.09	0.14	0.31	0.46
2	0.30	1.60	0.20	1.20	1.90	0.97	0.14	0.40	0.54
3	0.50	1.40	0.20	1.20	1.90	0.85	0.14	0.49	0.63
4	0.70	1.20	0.20	1.20	1.90	0.73	0.14	0.57	0.71
5	0.90	1.00	0.20	1.20	1.90	0.61	0.14	0.66	0.80
6	1.10	0.80	0.20	1.20	1.90	0.49	0.14	0.74	0.88
7	1.30	0.60	0.20	1.20	1.90	0.36	0.14	0.83	0.97
8	1.50	0.40	0.20	1.20	1.90	0.24	0.14	0.91	1.05
9	1.70	0.20	0.30	1.20	1.90	0.18	0.21	1.50	1.71

(a)

Calculation of Tensile Load in Geogrids for wall 4-Izmit 150% using FHWA Recommendations

$a_{max(table)}/g$	0.29						
A_m	0.336		H	1.90	Φ	(backfill)	34.00
θ	18.59	0.32	L	1.30	γ	(backfill)	15.00
K_A	0.244		K_{AH}	0.20	Mobilized interface friction angle	(backfill)	34.00
K_{AE}	0.531		K_{AEH}	0.44	Φ	(reinforced soil)	34.00
ΔK_{dyn}	0.29		ΔK_{dynH}	0.24	γ	(reinforced soil)	15.00
					Mobilized interface friction angle	(reinforced soil)	22.67
W_w	3.99				Block depth	0.10	
W_1	34.20		W_1'	24.23	Block unit weight	21.00	
W_r	38.19		W_A	18.39			
R_g	25.76						
P_{IE}	9.49		P_1	6.19			
P_{AEH}	8.70						
FS_{sl}	1.42						

Tensile stresses in geotextiles

Layer Number	Elevation	Z_{wi}	S_{wi}	L_i	H	$K\sigma_{wi}$	L_{ai}	Le	2001 T_{wi}	2009 T_{wi}
1	0.10	1.80	0.20	1.20	1.90	5.46	0.05	1.15	1.09	0.687
2	0.30	1.60	0.20	1.20	1.88	4.85	0.16	1.04	0.99	0.687
3	0.50	1.40	0.20	1.20	1.88	4.25	0.27	0.93	0.89	0.687
4	0.70	1.20	0.20	1.20	1.88	3.64	0.37	0.83	0.79	0.687
5	0.90	1.00	0.20	1.20	1.88	3.03	0.48	0.72	0.69	0.687
6	1.10	0.80	0.20	1.20	1.88	2.43	0.58	0.62	0.59	0.687
7	1.30	0.60	0.20	1.20	1.88	1.82	0.69	0.51	0.48	0.687
8	1.50	0.40	0.20	1.20	1.88	1.21	0.80	0.40	0.38	0.687
9	1.70	0.20	0.28	1.20	1.88	0.61	0.90	0.30	0.28	0.687

(b)

Table E.41. Calculation of Tensile Load in Geogrids for Wall 4-Izmit 200% using a)NCMA Segmental Retaining Walls Seismic Design Manual b) FHWA Recommendations

Calculation of Tensile Load in Geogrids for wall 4-Izmit 200% using NCMA Segmental Retaining Walls Seismic Design Manual

$A = a_{max(rock)}/g$	0.34					Φ	(backfill)	34.00
k_h (int)	0.377		H	1.90		γ	(backfill)	15.00
θ (int)	20.68	0.36	L	1.30		Mobilized interface friction angle, δ	(backfill)	34.00
k_h (ext)	0.17					Φ	(reinforced soil)	34.00
θ (ext)	9.65	0.17				γ	(reinforced soil)	15.00
K_A	0.244		K_{AH}	0.20				
K_{AE} (int)	0.575		$K_{AEH(int)}$	0.48				
$\Delta K_{dyn(int)}$	0.33		$\Delta K_{dynH(int)}$	0.27		Block depth	0.10	
K_{AE} (ext)	0.388		$K_{AEH(ext)}$	0.32		Block unit weight	21.00	
$\Delta K_{dyn(ext)}$	0.14		$\Delta K_{dynH(ext)}$	0.12				
W_w	3.99							
W_s	34.20		W_s'	24.23				
W_r	38.19							
R_S	25.76							
P_{IE}	4.80							
P_{AEH}	7.09							
$FS_{sliding}$	2.17							
$FS_{overturning}$	2.45							

Reinforcement loads

Layer Number	Elevation	Z_{wi}	S_{vi}	L_i	H	$F_{static\,i}$	$F_{inertial\,i}$	$F_{dyn\,i}$	$AF_{seismic}$
1	0.10	1.80	0.20	1.20	1.90	1.09	0.16	0.36	0.52
2	0.30	1.60	0.20	1.20	1.90	0.97	0.16	0.46	0.62
3	0.50	1.40	0.20	1.20	1.90	0.85	0.16	0.56	0.72
4	0.70	1.20	0.20	1.20	1.90	0.73	0.16	0.66	0.82
5	0.90	1.00	0.20	1.20	1.90	0.61	0.16	0.76	0.92
6	1.10	0.80	0.20	1.20	1.90	0.49	0.16	0.86	1.02
7	1.30	0.60	0.20	1.20	1.90	0.36	0.16	0.96	1.11
8	1.50	0.40	0.20	1.20	1.90	0.24	0.16	1.06	1.21
9	1.70	0.20	0.30	1.20	1.90	0.18	0.24	1.73	1.97

(a)

Calculation of Tensile Load in Geogrids for wall 4-Izmit 200% using FHWA Recommendations

$a_{max(rock)}/g$	0.34					Φ	(backfill)	34.00
A_m	0.377		H	1.90		γ	(backfill)	15.00
θ	20.68	0.36	L	1.30		Mobilized interface friction angle	(backfill)	34.00
K_A	0.244		K_{AH}	0.20		Φ	(reinforced soil)	34.00
K_{AE}	0.575		K_{AEH}	0.48		γ	(reinforced soil)	15.00
ΔK_{dyn}	0.33		ΔK_{dynH}	0.27		Mobilized interface friction angle	(reinforced soil)	22.67
W_w	3.99					Block depth	0.10	
W_s	34.20		W_s'	24.23		Block unit weight	21.00	
W_r	38.19		W_A	18.39				
R_E	25.76							
P_{IE}	10.65		P_I	6.94				
P_{AEH}	9.20							
FS_{sl}	1.30							

Tensile stresses in geotextiles

Layer Number	Elevation	Z_{wi}	S_{vi}	L_i	H	$K\sigma_{vi}$	L_a	Le	2001 T_{mi}	2009 T_{mi}
1	0.10	1.80	0.20	1.20	1.90	5.46	0.05	1.15	1.23	0.771
2	0.30	1.60	0.20	1.20	1.88	4.85	0.16	1.04	1.11	0.771
3	0.50	1.40	0.20	1.20	1.88	4.25	0.27	0.93	1.00	0.771
4	0.70	1.20	0.20	1.20	1.88	3.64	0.37	0.83	0.88	0.771
5	0.90	1.00	0.20	1.20	1.88	3.03	0.48	0.72	0.77	0.771
6	1.10	0.80	0.20	1.20	1.88	2.43	0.58	0.62	0.66	0.771
7	1.30	0.60	0.20	1.20	1.88	1.82	0.69	0.51	0.54	0.771
8	1.50	0.40	0.20	1.20	1.88	1.21	0.80	0.40	0.43	0.771
9	1.70	0.20	0.28	1.20	1.88	0.61	0.90	0.30	0.32	0.771

(b)

Table E.42. Calculation of Tensile Load in Geogrids for Wall 4-Sakarya 100% using a)NCMA Segmental Retaining Walls Seismic Design Manual b) FHWA Recommendations

Calculation of Tensile Load in Geogrids for wall 4-Sakarya 100% using NCMA Segmental Retaining Walls Seismic Design Manual

$A=a_{max(table)}/g$	0.21					Φ	(backfill)	34.00
k_h (int)	0.260		H	1.90		γ	(backfill)	15.00
θ (int)	14.60	0.25	L	1.30		Mobilized interface friction angle, δ	(backfill)	34.00
k_h (ext)	0.11					Φ	(reinforced soil)	34.00
θ (ext)	5.99	0.10				γ	(reinforced soil)	15.00
K_A	0.244		K_{AH}	0.20				
K_{AE} (int)	0.459		$K_{AEH(int)}$	0.38				
$\Delta K_{dyn(int)}$	0.22		$\Delta K_{dynH(int)}$	0.18		Block depth	0.10	
K_{AE} (ext)	0.344		$K_{AEH(ext)}$	0.29		Block unit weight	21.00	
$\Delta K_{dyn(ext)}$	0.10		$\Delta K_{dynH(ext)}$	0.08				
W_w	3.99							
W_1	34.20		W_1'	24.23				
W_r	38.19							
R_E	25.76							
P_{IE}	2.96							
P_{AEH}	6.60							
$FS_{sliding}$	2.69							
$FS_{overturning}$	3.19							

Reinforcement loads

Layer Number	Elevation	Z_w	S_w	L_i	H	$F_{static\,i}$	$F_{inertial\,i}$	$F_{dyn\,i}$	$\Delta F_{seismic}$
1	0.10	1.80	0.20	1.20	1.90	1.09	0.11	0.24	0.34
2	0.30	1.60	0.20	1.20	1.90	0.97	0.11	0.30	0.41
3	0.50	1.40	0.20	1.20	1.90	0.85	0.11	0.36	0.47
4	0.70	1.20	0.20	1.20	1.90	0.73	0.11	0.43	0.54
5	0.90	1.00	0.20	1.20	1.90	0.61	0.11	0.49	0.60
6	1.10	0.80	0.20	1.20	1.90	0.49	0.11	0.56	0.67
7	1.30	0.60	0.20	1.20	1.90	0.36	0.11	0.62	0.73
8	1.50	0.40	0.20	1.20	1.90	0.24	0.11	0.69	0.79
9	1.70	0.20	0.30	1.20	1.90	0.18	0.16	1.12	1.29

(a)

Calculation of Tensile Load in Geogrids for wall 4-Sakarya 100% using FHWA Recommendations

$a_{max(table)}/g$	0.21					Φ	(backfill)	34.00
A_m	0.260		H	1.90		γ	(backfill)	15.00
0	14.60	0.25	L	1.30		Mobilized interface friction angle	(backfill)	34.00
K_A	0.244		K_{AH}	0.20		Φ	(reinforced soil)	34.00
K_{AE}	0.459		K_{AEH}	0.38		γ	(reinforced soil)	15.00
ΔK_{dyn}	0.22		ΔK_{dynH}	0.18		Mobilized interface friction angle	(reinforced soil)	22.67
W_w	3.99					Block depth	0.10	
W_1	34.20		W_1'	24.23		Block unit weight	21.00	
W_r	38.19		W_A	18.39				
R_E	25.76							
P_{IE}	7.35		P_1	4.79				
P_{AEH}	7.89							
FS_{sl}	1.69							

Tensile stresses in geotextiles

Layer Number	Elevation	Z_w	S_w	L_i	H	$K\sigma_w$	L_a	Le	2001 T_{wt}	2009 T_{wt}
1	0.10	1.80	0.20	1.20	1.90	5.46	0.05	1.15	0.85	0.532
2	0.30	1.60	0.20	1.20	1.88	4.85	0.16	1.04	0.77	0.532
3	0.50	1.40	0.20	1.20	1.88	4.25	0.27	0.93	0.69	0.532
4	0.70	1.20	0.20	1.20	1.88	3.64	0.37	0.83	0.61	0.532
5	0.90	1.00	0.20	1.20	1.88	3.03	0.48	0.72	0.53	0.532
6	1.10	0.80	0.20	1.20	1.88	2.43	0.58	0.62	0.45	0.532
7	1.30	0.60	0.20	1.20	1.88	1.82	0.69	0.51	0.38	0.532
8	1.50	0.40	0.20	1.20	1.88	1.21	0.80	0.40	0.30	0.532
9	1.70	0.20	0.28	1.20	1.88	0.61	0.90	0.30	0.22	0.532

(b)

Table E.43. Calculation of Tensile Load in Geogrids for Wall 4-Sakarya 150% using a)NCMA Segmental Retaining Walls Seismic Design Manual b) FHWA Recommendations

Calculation of Tensile Load in Geogrids for wall 4-Sakarya 150% using NCMA Segmental Retaining Walls Seismic Design Manual

$A = a_{max(table)}/g$	0.31					Φ	(backfill)	34.00
k_h (int)	0.353		H	1.90		γ	(backfill)	15.00
θ (int)	19.46	0.34	L	1.30		Mobilized interface friction angle, δ	(backfill)	34.00
k_h (ext)	0.16					Φ	(reinforced soil)	34.00
θ (ext)	8.81	0.15				γ	(reinforced soil)	15.00
K_A	0.244		K_{AH}	0.20				
K_{AK} (int)	0.549		$K_{AKH\ (int)}$	0.45				
$\Delta K_{dyn\ (int)}$	0.30		$\Delta K_{dynH\ (int)}$	0.25		Block depth	0.10	
K_{AK} (ext)	0.377		$K_{AKH\ (ext)}$	0.31		Block unit weight	21.00	
$\Delta K_{dyn\ (ext)}$	0.13		$\Delta K_{dynH\ (ext)}$	0.11				
W_w	3.99							
W_s	34.20		W_s'	24.23				
W_r	38.19							
R_R	25.76							
P_{IR}	4.37							
P_{AKH}	6.97							
$FS_{sliding}$	2.27							
$FS_{overturning}$	2.59							

Reinforcement loads

Layer Number	Elevation	Z_{wi}	S_{vi}	L_i	H	$F_{static\ i}$	$F_{inertial\ i}$	$F_{dyn\ i}$	$\Delta F_{seismic}$
1	0.10	1.80	0.20	1.20	1.90	1.09	0.15	0.33	0.48
2	0.30	1.60	0.20	1.20	1.90	0.97	0.15	0.42	0.57
3	0.50	1.40	0.20	1.20	1.90	0.85	0.15	0.52	0.66
4	0.70	1.20	0.20	1.20	1.90	0.73	0.15	0.61	0.75
5	0.90	1.00	0.20	1.20	1.90	0.61	0.15	0.70	0.85
6	1.10	0.80	0.20	1.20	1.90	0.49	0.15	0.79	0.94
7	1.30	0.60	0.20	1.20	1.90	0.36	0.15	0.88	1.03
8	1.50	0.40	0.20	1.20	1.90	0.24	0.15	0.97	1.12
9	1.70	0.20	0.30	1.20	1.90	0.18	0.22	1.59	1.81

(a)

Calculation of Tensile Load in Geogrids for wall 4-Sakarya 150% using FHWA Recommendations

$a_{max(table)}/g$	0.31					Φ	(backfill)	34.00
A_m	0.353		H	1.90		γ	(backfill)	15.00
θ	19.46	0.34	L	1.30		Mobilized interface friction angle	(backfill)	34.00
K_A	0.244		K_{AH}	0.20		Φ	(reinforced soil)	34.00
K_{AK}	0.549		K_{AKH}	0.45		γ	(reinforced soil)	15.00
ΔK_{dyn}	0.30		ΔK_{dynH}	0.25		Mobilized interface friction angle:	(reinforced soil)	22.67
W_w	3.99					Block depth	0.10	
W_s	34.20		W_s'	24.23		Block unit weight	21.00	
W_r	38.19		W_A	18.39				
R_R	25.76							
P_{IR}	9.97		P_I	6.50				
P_{AKH}	8.90							
FS_{sl}	1.37							

Tensile stresses in geotextiles

Layer Number	Elevation	Z_{wi}	S_{vi}	L_i	H	$K\sigma_{vi}$	L_a	Le	2001 T_{md}	2009 T_{md}
1	0.10	1.80	0.20	1.20	1.90	5.46	0.05	1.15	1.15	0.722
2	0.30	1.60	0.20	1.20	1.88	4.85	0.16	1.04	1.04	0.722
3	0.50	1.40	0.20	1.20	1.88	4.25	0.27	0.93	0.93	0.722
4	0.70	1.20	0.20	1.20	1.88	3.64	0.37	0.83	0.83	0.722
5	0.90	1.00	0.20	1.20	1.88	3.03	0.48	0.72	0.72	0.722
6	1.10	0.80	0.20	1.20	1.88	2.43	0.58	0.62	0.62	0.722
7	1.30	0.60	0.20	1.20	1.88	1.82	0.69	0.51	0.51	0.722
8	1.50	0.40	0.20	1.20	1.88	1.21	0.80	0.40	0.40	0.722
9	1.70	0.20	0.28	1.20	1.88	0.61	0.90	0.30	0.30	0.722

(b)

Table E.44. Calculation of Tensile Load in Geogrids for Wall 4-Sakarya 200% using a)NCMA Segmental Retaining Walls Seismic Design Manual b) FHWA Recommendations

Calculation of Tensile Load in Geogrids for wall 4-Sakarya 200% using NCMA Segmental Retaining Walls Seismic Design Manual

$A = a_{max(table)}/g$	0.453						
k_h (int)	0.452		H	1.90	Φ	(backfill)	34.00
θ (int)	24.31	0.42	L	1.30	γ	(backfill)	15.00
k_h (ext)	0.23				Mobilized interface friction angle, δ	(backfill)	34.00
θ (ext)	12.76	0.22			Φ	(reinforced soil)	34.00
K_A	0.244		K_{AH}	0.20	γ	(reinforced soil)	15.00
K_{AE} (int)	0.670		K_{AEH} (int)	0.56			
$\Delta K_{dyn\ (int)}$	0.43		$\Delta K_{dynH\ (int)}$	0.35	Block depth	0.10	
K_{AE} (ext)	0.431		$K_{AEH\ (ext)}$	0.36	Block unit weight	21.00	
$\Delta K_{dyn\ (ext)}$	0.19		$\Delta K_{dynH\ (ext)}$	0.16			
W_w	3.99						
W_s	34.20		W_s'	24.23			
W_r	38.19						
R_S	25.76						
P_{IR}	6.39						
P_{AEH}	7.58						
$FS_{sliding}$	1.84						
$FS_{overturning}$	2.02						

Reinforcement loads

Layer Number	Elevation	Z_w	S_v	L_r	H	F_{static}	$F_{inertial}$	F_{dyn}	$\Delta F_{seismic}$
1	0.10	1.80	0.20	1.20	1.90	1.09	0.19	0.47	0.66
2	0.30	1.60	0.20	1.20	1.90	0.97	0.19	0.59	0.78
3	0.50	1.40	0.20	1.20	1.90	0.85	0.19	0.72	0.91
4	0.70	1.20	0.20	1.20	1.90	0.73	0.19	0.85	1.04
5	0.90	1.00	0.20	1.20	1.90	0.61	0.19	0.97	1.16
6	1.10	0.80	0.20	1.20	1.90	0.49	0.19	1.10	1.29
7	1.30	0.60	0.20	1.20	1.90	0.36	0.19	1.23	1.42
8	1.50	0.40	0.20	1.20	1.90	0.24	0.19	1.36	1.55
9	1.70	0.20	0.30	1.20	1.90	0.18	0.28	2.22	2.51

(a)

Calculation of Tensile Load in Geogrids for wall 4-Sakarya 200% using FHWA Recommendations

$a_{max(table)}/g$	0.453						
A_m	0.452		H	1.90	Φ	(backfill)	34.00
θ	24.31	0.42	L	1.30	γ	(backfill)	15.00
K_A	0.244		K_{AH}	0.20	Mobilized interface friction angle	(backfill)	34.00
K_{AE}	0.670		K_{AEH}	0.56	Φ	(reinforced soil)	34.00
ΔK_{dyn}	0.43		ΔK_{dynH}	0.35	γ	(reinforced soil)	15.00
					Mobilized interface friction angle	(reinforced soil)	23.67
W_w	3.99				Block depth	0.10	
W_s	34.20		W_s'	24.23	Block unit weight	21.00	
W_r	38.19		W_A	18.39			
R_S	25.76						
P_{IR}	12.74		P_I	8.30			
P_{AEH}	10.26						
FS_{sl}	1.12						

Tensile stresses in geotextiles

Layer Number	Elevation	Z_w	S_v	L_r	H	$K\sigma_w$	L_a	Le	2001 T_{al}	2009 T_{al}
1	0.10	1.80	0.20	1.20	1.90	5.46	0.05	1.15	1.47	0.923
2	0.30	1.60	0.20	1.20	1.88	4.85	0.16	1.04	1.33	0.923
3	0.50	1.40	0.20	1.20	1.88	4.25	0.27	0.93	1.19	0.923
4	0.70	1.20	0.20	1.20	1.88	3.64	0.37	0.83	1.06	0.923
5	0.90	1.00	0.20	1.20	1.88	3.03	0.48	0.72	0.92	0.923
6	1.10	0.80	0.20	1.20	1.88	2.43	0.58	0.62	0.79	0.923
7	1.30	0.60	0.20	1.20	1.88	1.82	0.69	0.51	0.65	0.923
8	1.50	0.40	0.20	1.20	1.88	1.21	0.80	0.40	0.51	0.923
9	1.70	0.20	0.28	1.20	1.88	0.61	0.90	0.30	0.38	0.923

(b)

Table E.45. Comparison of Calculatedand Measured Seismic Induced Tensile Loads inGeogrids for Wall 4

Wall / Base Excitation	Maximum Table Acceleration-Base Input (g)	Design (NCMA) ΔTmax in lower geogrid (@h=0.2 m) (kN/m)	Design (FHWA2001) ΔTmax in lower geogrid (@h=0.2 m) (kN/m)	Design (FHWA2009) ΔTmax in lower geogrid (@h=0.2 m) (kN/m)	Measured Geogrid Stress Max Stresses (peak values) (kN/m)	Design (NCMA) ΔTmax at midheight geogrid (@h=1 m) (kN/m)	Design (FHWA2001) ΔTmax at midheight geogrid (@h=1 m) (kN/m)	Design (FHWA2009) ΔTmax at midheight geogrid (@h=1 m) (kN/m)	Measured Geogrid Stress Max Stresses (peak values) (kN/m)	Design (NCMA) ΔTmax in upper geogrid (@h=1.8 m) (kN/m)	Design (FHWA2001) ΔTmax in upper geogrid (@h=1.8 m) (kN/m)	Design (FHWA2009) ΔTmax in upper geogrid (@h=1.8 m) (kN/m)	Measured Geogrid Stress Max Stresses (peak values) (kN/m)
wall 4 / El Centro 100%	0.41	0.72	1.26	0.87	3.73	1.07	0.87	0.87	2.18	2.31	0.36	0.87	1.17
wall 4 / El Centro 150%	0.61	0.94	1.51	1.05	4.76	1.41	1.05	1.05	2.88	3.05	0.43	1.05	1.65
wall 4 / El Centro 200%	0.75	0.98	1.55	1.07	7.17	1.47	1.07	1.07	4.97	3.18	0.44	1.07	3
wall 4 / Izmit 100%	0.2	0.39	0.74	0.51	1.71	0.58	0.51	0.51	0.92	1.24	0.21	0.51	0.46
wall 4 / Izmit 150%	0.29	0.54	0.99	0.69	2.38	0.80	0.69	0.69	1.28	1.71	0.28	0.69	0.63
wall 4 / Izmit 200%	0.34	0.62	1.11	0.77	2.8	0.92	0.77	0.77	1.51	1.97	0.32	0.77	0.8
wall 4 / Sakarya 100%	0.21	0.41	0.77	0.53	1.76	0.60	0.53	0.53	0.96	1.29	0.22	0.53	0.47
wall 4 / Sakarya 150%	0.31	0.57	1.04	0.72	2.47	0.85	0.72	0.72	1.33	1.81	0.30	0.72	0.66
wall 4 / Sakarya 200%	0.45	0.78	1.33	0.92	3.92	1.16	0.92	0.92	2.12	2.51	0.38	0.92	1.05
wall 4 / El Centro 250%	0.93	0.86	1.42	0.99	8	1.29	0.99	0.99	5.27	2.78	0.41	0.99	3.4
wall 4 / El Centro 275%	0.98	0.80	1.36	0.94	8.49	1.20	0.94	0.94	6.22	2.58	0.39	0.94	4

REFERENCES

AASHTO, 1996, "Standard specifications for highway bridges" American Association of State Highway and Transportation Officials, Washington, DC, USA.

AASHTO, 2002, *Standard Specifications for Highway Bridges*, 17th edition.

Barthust, R.J. and M.R. Simac, 1994, "Geosynthetic Reinforced Segmental Retaining Wall Structures in North America", *Proceedings of the 5th International Conference on Geotextiles*, Geomembranes and Related Materials, pp.1275-1298, Singapore.

Bathurst, R. J., and M. C. Alfaro, 2000, "Review of Seismic Design, Analysis and Performance of Geosynthetic Reinforced Walls, Slopes and Embankments", *EarthReinforcement, Ochiai, Yasufuku&Omine (eds)*, pp. 887-918, Balkema, Rotterdam.

Bathurst, R. J., M. El-Emman, M. M. Mashhour, 2002, "Shaking table model study on the dynamic response of reinforced soil walls.", *Proc., 7th Int. Conf. on Geosynthetics*, Delma, Gourc, and Girard, eds., 99–102, Swets and Zeitlinger, Lisse, The Netherlands.

Bathurst, R. J., Z. Cai, M. R. Simac, 1997, "Seismic performance chart for geosynthetic reinforced segmental walls." *Proc., Geosynthetics'97 Conference*, 1001–1014. Long Beach, California.

Bathurst, R.J. and M. C.Alfaro, 1997, "Review of seismic de- sign, analysis and performance of geosynthetic reinforced walls, slopes and embankments", *Earth Reinforcement*, Vol. 2, 887-918, Balkema.

Bathurst, R.J., 1998. Segmental Retaining Walls – Seismic Design Manual, first ed. National Concrete Masonry Association, Herndon, Virginia.

Bathurst, R.J., K. Hatami, M.C. Alfaro, 2002, “Geosynthetic-reinforced soil walls and slopes – seismic aspects.” In: Shukla, S.K. (Ed.), Geosynthetics and Their Applications, pp. 327–392. Thomas Telford, London.

Cai, Z. and R. J. Bathurst, 1996, “Seismic-induced Permanent Displacement of Geosynthetic-Reinforced Segmental Retaining Walls”, *Canadian GeotechnicalJournal*, Vol. 33, pp. 937-955.

Christopher, B.R. and R. R. Berg, 2001, *Mechanically Stabilized Earth Walls and Reinforced Soil Slopes Design and Construction Guidelines*, Elias, RFHWA NHI-00-043.

Claybourn, A. F. and J. T. H. Wu, 1993, “Geosynthetic-Reinforced Soil Wall Design”, Geotextiles and Geomembranes, Vol. 12, pp. 707 – 724.

Das, B. M., 2004, *Fundamentals of Geotechnical Engineering*, Thomson, U.S.A.

Ebeling, R. M. and E. E. Morrison, 1993, *The seismic design of waterfront retaining structures.* Naval Civil Engineering Laboratory Technical Report ITL-92-11 NCELTR-939, Port Huenene, California, USA.

El-Emam, M.M. and R.J. Bathurst, 2005.“Facing contribution to seismic response of reduced-scale reinforced soil walls”, Geosynthetics International 12 (3), 215–238.

El-Emam, M.M. and R.J. Bathurst, 2007.“Influence of reinforcement parameters on the seismic response of reduced-scale reinforced soil retaining walls”, Geotextiles and Geomembranes 25 (1), 33–49.

Elias, V., B. R. Christopher, and R. Berg, 2001, “Mechanically stabilized earth walls and reinforced soil slopes: Design and construction guidelines.” *Publication No.*FHWA-NHI-00- 043, Federal Highway Administration, Washington, U.S.A.

FHWA, 2009, “Design and Construction of Mechanically Stabilized Earth Walls and Reinforced Soil Slopes”, Federal Highway Administration (FHWA) Demonstration Project 82, Washington, DC, USA.

Futaki, M., N. Aoyama, K. Misawa, T. Konami, M. Sato, T. Tatsui, and K. Mikami, 2001, “Dynamic behavior of multi-anchored reinforced soil wall in large-scale shear box.”*Landmarks in earth reinforcement*, H. Ochiai, J. Otani, N. Yasufuku, and K. Omine, eds., Balkema, Rotterdam, The Netherlands.

Futaki, M., N. Ogawa, M. Sato, T. Kumada and S. Natsume, 1996, “Experiments about Seismic performance of Reinforced Earth Retaining Wall.” *Proc., 11th World Conf. on Earthquake Engineering*, Elsevier Science, New York.

Guler, E. and A. K. Enunlu, 2009, “Investigation of dynamic behavior of geosynthetic reinforced soil retaining structures under earthquake loads”, Bull, Earthquake Eng. 7:737-777.

Holtz, R. D. and W.F. Lee, 2002, “Internal Stability Analyses OfGeosynthetic Reinforced Retaining Walls”, Research Report, University of Washington, January, Washington

Iai, S. and T. Sugano, 1999, “Soil-structure interaction studies through Shaking table tests”, In: Séco e Pinto PS (ed), *Earthquake Geotechnical Engineering*. pp 927–940, Balkema, Rotterdam.

Jakrapiyanun, W. and S. A. Ashford, 2003, “Soil-foundation-structure-interaction study using the laminar container using One-g shake table testing”, *16th ASCE Engineering Mechanics Conference Proceedings,* University of Washington.

Jones, C. J.F.P., 1997, *Earth Reinforcement and Soil Structures*, p. 379, Thomas Telford,

Kadayıfçı, A., 2003, *Influence of Various Parameters on Seismic-Induced Permanent Displacement of Geosynthetic Reinforced Segmental Retaining Walls*, M.S.Thesis, Boğaziçi University.

Kasay, A., 2007, *Investigation Of Dynamic Behavior Of Geosynthetic Reinforced Soil Retaining Structures Under Earthquake Loads*, PhD. Dissertation, Boğaziçi University.

Kerisel, J., 1992, "History of Retaining Wall Designs", *Proceeding of Conference of Retaining Structures*, pp. 1-16, Cambridge, Balkema, Rotterdam.

Koseki, J., F. Tatsuoka, K. Watanabe, M. Tateyama, K. Kojima, Y. Munaf, 2003, "Model tests of seismic stability of several types of soil retaining walls", In: Ling, H., Leshchinsky, D., Tatsuoka, F. (Eds.), Reinforced Soil Engineering Advances in Research and Practice., pp. 378–385. Marcel Dekker, New York

Koseki, J., R. J. Bathurst, E. Guler, *et al.* ,2006, "Seismic stability of reinforced soil walls. Keynote Lecture", *8th International Conference on Geosynthetics*, Vol. 1.,pp 51–77, Yokohama, Japan,

Koseki, J., Y. Munaf,, F. Tatsuoka, M. Tateyama, K. Kojima, T. Sato, 1998, "Shaking and tilt table tests of geosynthetic-reinforced soil and conventional-type retaining walls." , *Geosynthetics International*, 5 (1–2), 73–96

Lee, K.L., B.D. Adams and J.M.J. Vagneron, 1973,"Reinforced Earth Retaining Walls", *Journal of the Soil Mechanics and Foundations Division*, Proceedings of the American Society of Civil Engineers, October 1973, Vol. 99, No. SM 10, pp. 745-764.

Leshchinsky, D., H. I. Ling, , J. P. Wang, 2008, "Equivalent seismic coefficient in geocell retention systems", *Geotextile Geomemembranes*, 27:9–18.

Ling, H. I., 2003, "Chapter 25. A critical review of full-scale shaking table tests conducted on reinforced soil retaining walls." *Reinforcedsoil engineering: Advances in research and practice*, Marcel Dekker, New York, 491–510

Ling, H. I., H. Liu and Y. Mohri, 2005, "Parametric Studies on the Behavior of Reinforced

Soil Retaining Walls under Earthquake Loading", *Journal of EngineeringMechanics*, Vol. 131, pp. 1056-1065, October 2005.

Ling, H. I., Y. Mohri, D. Leshchinsky, 2005, "Large-scale shaking table tests on modular block reinforced Soil retaining walls", *Journal of Geotechnical Geoenvironmental Engineering*, 131:465–476.

Ling, H. I., Y. Mohri, D. Leshchinsky, C. Burke, K. Matsushima, H. Liu, 2005, "Large-Scale Shaking Table Tests on Modular-BlockReinforced Soil Retaining Walls", Journal Of Geotechnical And Geoenvironmental Engineering, ASCE, pp. 1398-1404

Ling, H.I., H. Liu, V.N. Kaliakin, D. Leshchinsky, 2004, "Analyzing dynamic behavior of geosynehtic-reinforced soil retaining walls", *Journal of Engineering Mechanics*, ASCE 130 (8), 911–920.

Matsuo, O., T. Tsutsumi, K. Yokoyama, Y. Saito, 1998, "Shaking table tests and analyses of geosynthetic-reinforced soil retaining walls." *Geosynthet. Int.*, 51-52, 97–126.

Matsuo, O., T. Tsutsumi, K. Yokoyama, Y. Saito, 1998.,"Shaking table tests and analysis of geosynthetic-reinforced soil retaining walls" Geosynthetics International ,5 (1–2), 97–126.

Mitchell, J.K. and W.C.B.Villet, 1987, "Reinforcement of Earth Slopes and Embankments", National Cooperative Highway Research Program Report 290, Transportation Research Board, p. 323

Murata, O., M. Tateyama, F. Tatsuoka, 1994, "Shaking table tests on a large geosynthetic-reinforced soil retaining wall model." , *Recentcase histories of permanent geosynthetic-reinforced soil retainingwalls*, F. Tatsuoka and D. Leshchinsky, eds., pp. 259–264, Balkema, Rotterdam, The Netherlands

National Concrete Masonry Association (NCMA), 2010, *Seismic Design Of Segmental Retaining Walls*, TEK 15-9A, http://www.ncma.org.

National Concrete Masonry Association, 1997, Design Manual for Segmental Retaining Walls

National Concrete Masonry Association, 2002, Segmental Retaining Walls, http://www.ncma.org/use/srw.

Newmark, N.M., 1965,"Effects of earthquakes on damsandembankments",*Geotechnique* 15, 139–159.

Nova-Roessig, L. and N. Sitar, 2006, Centrifuge model studies of the seismic response of reinforced soil slopes. Journal of Geotechnical and Geoenvironmental Engineering, ASCE 132 (3), 388–400.

Prasad, S.K., I. Towhata, G. P. Chandradhara, P. Nanjundaswamy, 2004, "Shaking Table Tests In Earthquake Geotechnical Engineering", *Current Science*, Vol. 87, November, no. 10, Pp. 1398-1404.

Richardson, G. N., and K. L.Lee, 1975, "Seismic design of reinforced earth walls."*J. Geotech. Eng. Div., Am. Soc. Civ. Eng.*, 101-102, 167–188.

Richardson, G. N., D. Feger, A. Fong, and K. L. Lee, 1977, "Seismic testing of reinforced earth walls."*J. Geotech. Eng. Div., Am. Soc. Civ.Eng.*, 103-111, 1–17.

Rowe, R. K. and S. K. Ho, 1992, "Keynote lecture: A review of the behavior of reinforced soil walls", *Proceedings of the International Symposium on Earth Reinforcement Practice*, Kyushu-Japan, 11-13 November 1992, Vol. 2, pp. 801-829, Rotterdam.

Rowe, R. K. and S. K. Ho, 1993, "Keynote Lecture : A Review of the Behavior of Reinforced Soil Walls", *Earth Reinforcement Practice*, Ochiai, Hayashi&Otani (eds), pp.801-829, Balkema, Rotterdam

RSS-U.S. Department of Transportation FHA, 1990, "Reinforced Soil Structures", Publication No.FHWA-RD 89-043, November.

Sabermahani, M., Ghalandarzadeh, A., Fakher, A., 2009, “Experimental study on seismic deformation modes of reinforced-soil walls”, Geotextiles and Geomembranes 27 (2), 121–136.

Sarma, S.K., 1975,“Seismicstability of earthdamsandembankments”, *Geotechnique*, 25, 743–761.

Schmertmann, J.H., 1978, “Guidelines for cone test, performance and design", Federal Highway Administration, Report FHWA-TS-78209, Washington, USA.

Seed. H. B. and R. V. Whitman, 1970, “Design of earth remaining structures for dynamic Loads”. *Proceedings of the ASCE Specialty Conference. Lateral Stresses in theGround and Design of Earth Retaining Structures*, Ithaca, pp. 103-147, New York.

Segrestin, P. and M. J. Bastick, 1988, “Seismic design of reinforced earth retaining walls the contribution of finite element analysis”, *Theory and Practice of EarthReinforcement: Proceedings of the International Geotechnical Symposium onTheory and Practice of Earth Reinforcement. IS-Kyushu '88*. Fukuoka, Japan, pp. 577-582, Balkema, Rotterdam.

Selek, Ö., 2005, *Facing Stability of Geosynthetic Reinforced Soil Retaining Walls*, M.S.Thesis, Boğaziçi University.

Selek, Ö., 2011, *Earthquake Behavior of Geosynthetic-Reinforced Retaining Structures*, PhD.Thesis, Boğaziçi University.

State Of California Department Of Transportation Trenching and Shoring Manual, 1990 *Earth Pressure Theory and Application*, http://www.dot.ca.gov/hq/esc/construction/manuals/ TrenchingandShoring/.

Steedman, R.S., 1997, “Seismically Induced Displacement of Retaining Walls”, *Seismic Behaviour of Ground and Geotechnical Structures*, Seco e Pinto, pp. 351- 360, Balkema, Rotterdam.

Tatsuoka, F.T., 1993, “Keynote Lecture: Roles of Facing Rigidity in Soil Reinforcing”, *Earth Reinforcement Practice*, Ochiai, Hayashi &Otani (eds), pp. 830-869, Balkema, Rotterdam.

White, D. M., and R.D. Holtz, 1996, “Performance of geosynthetic-reinforced slopes and walls during the North- ridge”, California earthquake of 17 January 1994, Report, University of Washington, Seattle,

Wood, M. D., 2004, *Geotechnical Modelling*, Spon Press, United Kingdom

Wu, G. 1994, *Dynamic soil–structure interaction: Pile foundations and retaining structures*, Ph.D. thesis, Department of Civil Engineering, The University of British Columbia, Vancouver.

Zarnani, S. and R.J. Bathurst, 2007, “Experimental investigation of EPS geofoam seismic buffer using shaking table tests”, Geosynthetics International 14 (3), 165–177.